Chemical Thermodynamics:

Advanced Applications

by J. Bevan Ott, Juliana Boerio-Goates

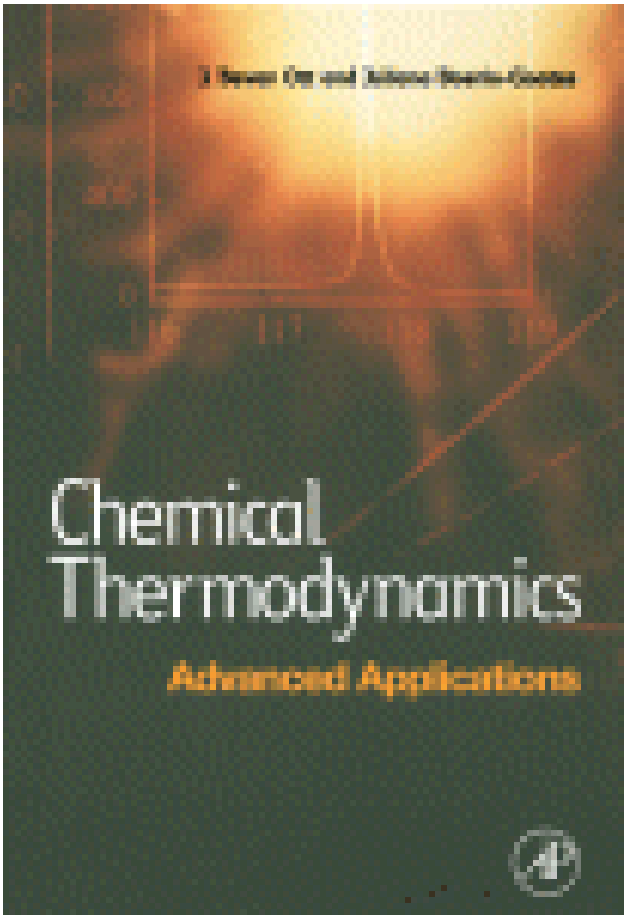

- ISBN: 0125309856
- Pub. Date: June 2000
- Publisher: Elsevier Science & Technology Books

Preface to the Two-Volume Series *Chemical Thermodynamics: Principles and Applications* and *Chemical Thermodynamics: Advanced Applications*

We recently completed the construction of a new chemistry building at Brigham Young University. The building is located just below a major geological fault line that runs parallel to the magnificent Wasatch Mountains. As a result, special care was taken to establish a firm foundation for the building to ensure that it would withstand a major earthquake. Massive blocks of concrete, extensively reinforced with metal bars, were poured deep in the earth, and the entire building was built upon these blocks. Resting on this foundation are the many classrooms, offices, and laboratories, with their wide variety of specialized functions. Each of the principal areas of chemistry is housed on a separate floor or wing in the building.

Thermodynamics is, in many ways, much like this modern science building. At the base of the science is a strong foundation. This foundation, which consists of the three laws, has withstood the probing and scrutiny of scientists for over a hundred and fifty years. It is still firm and secure and can be relied upon to support the many applications of the science. Relatively straightforward mathematical relationships based upon these laws tie together a myriad of applications in all branches of science and engineering. In this series, we will focus on chemical applications, but even with this limitation, the list is extensive.

Both our new chemistry building and the science of thermodynamics are functional, but beautiful. The building is a very modern combination of glass, steel, concrete, and brick, set on the edge of a hill, where it projects an image of strength, stability, and beauty. The aesthetic beauty of thermodynamics results from the rigor of the discipline. Thermodynamics is one of the pre-eminent

examples of an exact science. The simple mathematical relationships that are obtained from the laws enable one to derive a very large body of mathematical equations that can be used to describe and predict the outcome of the many processes of interest to chemists. One rests assured that if the laws are true, then the equations describing the applications are valid also.

Einstein recognized the fundamental significance of thermodynamics. He said,

> *A theory is the more impressive the greater the simplicity of its premises, the more different are the kinds of things it relates, and the more extended is its range of applicability. Therefore, the deep impression which classical thermodynamics made upon me. It is the only physical theory of universal content which I am convinced, that within the framework of applicability of its basic concepts, will never be overthrown.*[a]

A tension is always present in writing a thermodynamics book, between writing a textbook that the beginning serious student can easily follow, and writing a reference book that the established investigator on the cutting edge of the discipline can find useful. We do not think that the two goals are mutually exclusive and have tried very hard to address both audiences. The division into two volumes represents an attempt to organize material into two levels of sophistication and detail. To continue the metaphor of the chemistry building, we build the exterior and framework of the discipline in the first volume. In the second volume, we furnish the various floors of the "building" with applications of thermodynamic principles to a diverse set of specialized but broadly-defined problems involving chemical processes.

The first volume entitled *Chemical Thermodynamics: Principles and Applications* is appropriate for use as a textbook for an advanced undergraduate level or a beginning graduate level course in chemical thermodynamics. In the ten chapters of this volume, we develop the fundamental thermodynamic relationships for pure-component and variable-composition systems and apply them to a variety of chemical problems.

One does not learn thermodynamics without working problems and we have included an ample supply of exercises and problems at the end of each chapter. The exercises are usually straightforward calculations involving important equations. They are intended to move the reader into an active engagement with the equations so as to more fully grasp their significance. The problems often

---

[a] Taken from Albert Einstein, Autobiographical Notes, page 33 in The Library of Living Philosophers, Vol. VII; *Albert Einstein: Philosopher-Scientist*, edited by P. A. Schilpp, Evanston, Illinois, 1949.

involve more steps, and possibly data analysis and interpretation of the resulting calculations. Computer manipulation of the data for fitting and graphical representation is encouraged for these. Also, the chapters contain worked out examples within the body of the text. They illustrate problem-solving techniques in thermodynamics, as well as furthering the development of the topic at hand and expanding the discussion, and should be considered as an integral part of the presentation.

The intended audience of the second volume entitled *Chemical Thermodynamics: Advanced Applications* is the advanced student or research scientist. We have used it, independently of the first volume, as the text for an advanced topics graduate level course in chemical thermodynamics. It can also serve as an introduction to thermodynamic studies involving more specialized disciplines, including geology, chemical separations, and biochemistry, for the research scientist in or outside of those disciplines. We hope it will be especially helpful for non-thermodynamicists who might be unfamiliar with the power and utility of thermodynamics in diverse applications. Given the more advanced nature of the material covered here, only problems are provided at the end of the chapters in this volume. Taken together, the two volumes make an excellent reference source for chemical thermodynamics.

Even a thermodynamics book that contains much aqueous chemistry can be dry to read. We have tried to adopt a somewhat informal style of writing that will carry (rather than drag) the reader along through the derivations and reasoning processes. In the first volume, we have kept the beginner in mind by filling in the gaps in derivations to the point that they are easy to follow; as we move along, more and more is left to the reader to fill in the intermediate steps. It is a difficult line to tread — to give enough detail to be informative, but not so much that the discussion becomes repetitive. We hope we have succeeded in providing the proper balance. In order not to interrupt the flow of the dialogue, we have relegated some of the details and reminders to footnotes at the bottom of the pages.

As much as possible, we have used "real" examples in our discussions. We present many examples of contemporary scientific phenomena in which analysis along thermodynamic lines offers a unique and valuable perspective. Examples include laser cooling, properties of high temperature superconductors, theories of continuous phase transitions, theories of electrolyte solutions, and (fluid + fluid) phase equilibria. However, we have also chosen to feature some descriptions of the very old experiments that helped lay the foundation of the science. For example, Linhart's classic 1912 work on the determination of cell E° values is described, along with Haber's ammonia synthesis, and Giauque's 1930 study of the third law applied to glycerine. These are the result of exceptionally high quality investigations by investigators who worked under difficult circumstances. It is humbling to see the quality of the work

accomplished by these pioneers and reminds us that the field of thermodynamics has been built on the shoulders of giants.

A complete set of references to all sources of data are included, so that the reader can go to the original source if more detail is needed. We have also tried to include references to more advanced and specialized texts, monographs, reviews, and other compilations that the reader who is looking for more detail, can go to for supplementary reading.

We have generally used SI units throughout both volumes, and, as much as possible, have followed the recommendations of the IUPAC publication *Quantities, Units, and Symbols in Physical Chemistry*. An exception is the use of the bar in describing the standard state pressure for the gas. In our estimation the simplicity gained by using the bar more than compensates for the small compromise of SI units that this substitution entails. As we do this, we are careful to remind the reader continually of what we have done so that confusion can be avoided. It seems to us that IUPAC has set the precedent for such compromises of convenience by retaining the definition of the normal boiling point and normal freezing point as the temperature where the pressure is one atm. We have followed this convention also. In Chapter 10, we have used ω in cm^{-1} for energy in statistical thermodynamics calculations. Again, the simplicity introduced by this choice overshadows the advantages of going to SI units. Besides, we think it will be a long time before our spectroscopy friends stop using cm^{-1} as the unit for expressing energy. Since we are invading their discipline in this chapter, we feel inclined to go along.

With few exceptions, we have used SI notation throughout. One exception is in the use of γ_R (instead of f) for the activity coefficient with a Raoult's law standard state. It seems to us that using f would cause serious problems by confusing the activity coefficient with fugacity. We do not use the symbol K° (or K^θ) for what IUPAC describes as the "standard equilibrium constant". Such a choice of symbol and name seems confusing and redundant to us. Instead we use the symbol K for what we refer to as the "thermodynamic equilibrium constant", a choice that is acknowledged by IUPAC as acceptable. We have also chosen to keep the "free" in "free energy" while recognizing that many readers have grown up with free energy and would be confused by "Helmholtz energy" or "Gibbs energy".

Our science building at Brigham Young University is not complete. We are still adding equipment and modifying laboratories to accommodate the latest of experiments. In the same way, these two volumes do not represent a completed study of chemical thermodynamics. This is especially true in Chapters 15 and 16 where we have chosen to use the "case study" approach in which we introduce selected examples where we apply thermodynamics to the study of processes of an industrial, geological, and biological nature. It is impossible to cover these broad fields in one book. The examples that we have

chosen, some of which are of historical interest while others represent very recent applications, should allow the reader to see how the discipline applies in these areas and be able to extrapolate to other related problems.

Our hope is that the foundation has been built strong enough and the rooms completed to the point that new additions and changes can be easily accommodated and supported. It has been our experience that each time we have taught thermodynamics, we have found a new corridor to follow, leading to a new room to explore. This is one of the things that excites us most about studying thermodynamics. The science is old, but the applications (and implications) are endless.

The collaboration with many scientists over the years has had a major influence on the structure and content of this book. We are especially indebted to J. Rex Goates, who collaborated closely with one of the authors (JBO) for over thirty years, and has a close personal relationship with the other author (JBG). Two giants in the field of thermodynamics, W. F. Giauque and E. F. Westrum, Jr., served as our major professors in graduate school. Their passion for the discipline has been transmitted to us and we have tried in turn to pass it on to our students. One of us (JBG) also acknowledges Patrick A. G. O'Hare who introduced her to thermodynamics as a challenging research area and has served as a mentor and friend for more than twenty years.

We express appreciation to Brigham Young University for providing ongoing support for the thermodynamics related research that has served as the foundation for this project. It is significant that this has happened in an age when it is not fashionable to support research that involves making measurements with a calorimeter, densimeter, or thermometer. We especially appreciate the commitment and support of the university that has led directly to the creation of the two volumes that have resulted from this project. We recognize the help of Samuel Kennedy in composing many of the 137 figures, of Danielle Walker for help in preparing the manuscript, including composing over 1500 equations, and especially to Rebecca Wilford for continual support throughout the project. Finally, we recognize our spouses, RaNae Ott and Steven Goates, for their ongoing support and encouragement throughout what has become a long term project.

J. Bevan Ott and Juliana Boerio-Goates

Preface to the Second Volume *Chemical Thermodynamics: Advanced Applications*

This book is the second volume in a two-volume set that describes the principles of thermodynamics and its applications. In the first book: *Thermodynamics — Fundamentals and Applications*, we laid the foundation for the science through a rigorous development of the fundamental principles, and we illustrated how those principles lend themselves to applications in a variety of areas of study. The applications featured in that volume tended to be of a broad nature and often on a limited experimental scale.

In this second volume *Chemical Thermodynamics: Advanced Applications*, we illustrate in more depth, but with a narrower focus, applications of a more specialized nature. The book extends the range of a thermodynamics text to cover topics and applications that are not usually covered in the beginning text. In a sense, the book covers a "middle ground" between the basic principles developed in the beginning thermodynamics textbook and the very specialized applications that are a part of an ongoing research project. As such, it could prove invaluable to the practising scientist who needs to apply thermodynamic relationships to aid in the understanding of the chemical process under consideration. It would also be well suited for use as a text in a special topics course in thermodynamics that may be taught from time to time in the university. One of our major goals has been to write a comprehensive thermodynamics text that can serve as a major reference set that the student or the research scientist can use to learn or review thermodynamic principles. With this two volume set, we hope that we have accomplished this goal.

Thermodynamics is a broad subject, with applications in many areas, and there are many possible topics we could have chosen to emphasize in this book. Some of the areas chosen clearly reflect our own research interests and areas of expertise in solutions and solid-state properties. We happen to think that these are areas of broad interest to scientists. The book, of course, is broadly based,

and includes topics that cover a wide range of applications. We have enlisted the aid of experts in those fields to read and criticize these parts of the manuscript. We are indebted to Kenneth Breslauer from Rutgers University, Alexandra Navrotsky from the University of California at Davis, Guiseppe Arena from Catania University, and Earl Woolley, William Evenson, and Brian Woodfield from Brigham Young University for their assistance in this regard.

This volume begins as Chapter 11 in the two-volume set. This Chapter summarizes the fundamental relationships that form the basis of the discipline of chemical thermodynamics. This chapter can serve as a review of the fundamental thermodynamic equations that are necessary for the more sophisticated applications described in the remainder of this book. This level of review may be all that is necessary for the practising scientist who has been away from the field for some time. For those who need more, references are given to the sections in *Principles and Applications* where the equations are derived. This is the only place that this volume refers back to the earlier one.

The text is written in a somewhat informal style, although more technical than in the earlier volume, to make it more appealing to the reader and hopefully, dispense with the myth that the study of thermodynamics must be boring. Thermodynamics is an old science with modern applications and the authors give flavor to an old science by including and emphasizing modern applications that demonstrate that thermodynamics is an on-going and lively discipline, while at the same time, including examples that are of important historical interest. As much as possible "real" systems are used in the discussion and figures, in contrast to the "generic" examples that are often used in other textbooks. Examples of the "old" are the discussions of the Haber cycle, the synthesis of diamond, and the thermodynamic description of metabolism. Examples of the "new" include the use of critical exponents to describe continuous transitions, thermodynamic studies of oligonucleotides, and the use of Pitzer's equations to describe electrolyte solutions.

Problems are included at the end of each chapter that demonstrate the principles developed in the chapter. A complete set of references is included with each chapter that the reader can go to for obtaining more detail and understanding.

The remainder of this book applies thermodynamics to the description of a variety of systems that are of chemical interest. Chapter 12 uses thermodynamics to describe the effects of other variables such as gravitational field, centrifugal field, and surface area on the properties of the system. Most of the focus of the chapter is on surface effects. The surface properties of pure substances are described first, including the effect of curvature on the properties of the surface. For mixtures, the surface concentration is defined and its relationship to the surface properties is described.

Chapters 13 and 14 use thermodynamics to describe and predict phase equilibria. Chapter 13 limits the discussion to pure substances. Distinctions are made between first-order and continuous phase transitions, and examples are given of different types of continuous transitions, including the (liquid + gas) critical phase transition, order–disorder transitions involving position disorder, rotational disorder, and magnetic effects; the helium normal–superfluid transition; and conductor–superconductor transitions. Modern theories of phase transitions are described that show the parallel properties of the different types of continuous transitions, and demonstrate how these properties can be described with a general set of critical exponents. This discussion is an attempt to present to chemists the exciting advances made in the area of theories of phase transitions that is often relegated to physics tests.

Chapter 14 describes the phase behavior of binary mixtures. It begins with a discussion of (vapor + liquid) phase equilibria, followed by a description of (liquid + liquid) phase equilibria. (Fluid + fluid) phase equilibria extends this description into the supercritical region, where the five fundamental types of (fluid + fluid) phase diagrams are described. Examples of (solid + liquid) phase diagrams are presented that demonstrate the wide variety of systems that are observed. Of interest is the combination of (liquid + liquid) and (solid + liquid) equilibria into a single phase diagram, where a quadruple point is described.

Chapters 15 and 16 apply thermodynamics to a variety of chemical processes. A "case study" approach is used in these two chapters to demonstrate the application of thermodynamics to such diverse fields as biochemistry, geochemistry, and industrial chemistry. In these chapters, no attempt is made to be comprehensive in covering the field. Instead, examples have been chosen that demonstrate the thermodynamic principles as they apply to problems in different disciplines.

Chapter 15 begins with a description of the Haber process, a chemical reaction of great importance in industrial chemistry, followed by a discussion of a determination of the conditions that apply in the synthesis of diamond. Applications of thermodynamics to geological systems are described next, beginning with a discussion of the effect of temperature on the solubility of calcite, followed by a discussion of the energetics of ternary oxides of mineralogical significance. Finally, the thermodynamics of complexation with macrocyclic ligands, a system of interest in inorganic chemistry and chemical separations, is described.

Chapter 16 applies thermodynamics to problems of biological interest. The metabolic processes leading to mechanical work performed by a living organism are described first, followed by discussions of the role of thermodynamics as a tool for understanding the stabilities of biopolymers such as proteins, and oligonucleotides as model compounds for DNA.

Chapters 15 and 16 especially demonstrate the broad range of application of thermodynamics to chemical processes. In the discussions of the Haber cycle, synthesis of diamond, solubility of calcite, and the thermodynamics of metabolism, techniques are used to solve a specific problem for a particular substance. On the other hand, in the discussion of macrocyclic complexes, the description and interpretation involves the comparison of the properties of a number of complexes. This global approach is particularly helpful in the description of the energetics of ternary oxides in Chapter 15 and the stabilities of proteins and DNA in Chapter 16, where useful conclusions are obtained only after the comparison of a large amount of experimental data.

Thermodynamic measurements are often regarded by those who do not make them as being incapable of providing information about microscopic details. Spectroscopy or crystallography are proclaimed as the techniques of choice for such information. A common characteristic of the work of the scientists we have chosen to feature, especially in Chapters 15 and 16, is that the databases of thermodynamic information they have constructed by systematically varying chemical and/or physical properties and analyzing the effect on thermodynamic stabilities, enthalpies, and entropies, have provided valuable insights into microscopic factors that complement those provided by conventional structural techniques. The systematic studies of mineral energetics, for example, provide information concerning the relative contributions of various structural features like cation size to phase stabilities. As a second example, the pairing of NMR and optical spectroscopy with calorimetric measurements of the melting of small segments of synthetic DNA has made significant contributions to the understanding of the factors involved in mutations and drug binding in DNA.

Chapters 17 and 18 use thermodynamics to describe solutions, with nonelectrolyte solutions described in Chapter 17 and electrolyte solutions described in Chapter 18. Chapter 17 focuses on the excess thermodynamic properties, with the properties of the ideal and regular solution compared with the "real" solution. Deviations from ideal solution behavior are correlated with the type of interactions in the liquid mixture, and extensions are made to systems with (liquid + liquid) phase equilibrium, and (fluid + fluid) phase equilibrium when the mixture involves supercritical fluids.

Chapter 18 describes electrolyte solutions that are too concentrated for the Debye–Hückel theory to apply. Gugenheim's equations are presented and the Pitzer and Brewer tabulations, as a method for obtaining the thermodynamic properties of electrolyte solutions, are described. Next, the complete set of Pitzer's equations from which all the thermodynamic properties can be calculated, are presented. This discussion ends with an example of the extension of Pitzer's equations to high temperatures and high pressures. Three-dimensional figures show the change in the thermo-

dynamic properties with concentration, pressure, and temperature, for this representative system.

Also included in Chapter 18 is a discussion of ion association at high temperatures and the properties of surfactant solutions, which are described in terms of the pseudo-phase model and the mass action model.

The three appendices in this volume give selected sets of thermodynamic data (Appendix 5), review the statistical calculations covered in *Principles and Applications* (Appendix 6), and summarize the equations and parameters required to calculate the properties of electrolyte solutions, principally from Pitzer's equations (Appendix 7).

Chapter 11

Summary of Thermodynamic Relationships

This is the second of a two-volume series in which we continue the description of chemical thermodynamics. The first volume, titled *Chemical Thermodynamics: Principles and Applications*, contained ten chapters and four appendices, and presented the basic thermodynamic principles and applied these principles to systems of chemical interest. We will refer to that volume in this chapter as *Principles and Applications*. We begin this second volume that we have titled *Chemical Thermodynamics: Advanced Applications*, with Chapter 11 where we summarize and review the thermodynamic principles developed in the first volume, and then focus in subsequent chapters on a discussion of a variety of chemical processes in which we use thermodynamics as the basis of the description.

If you have had the opportunity to follow through the rigorous development of thermodynamic principles in a manner such as is presented in *Principles and Applications*, you can relate to the statement made very near the beginning of that volume.

> *Thermodynamics starts with two basic laws stated with elegant simplicity by Clausius.*
>
> - *Die Energie der Welt ist konstant*
> - *Die Entropie der Welt strebt einem Maximum zu*
>
> *These statements are "laws of experience". That is, no one has been able to find exceptions to them (although many have tried). If one assumes that these two laws are valid, then four fundamental equations, referred to as the Four Fundamental Equations of Gibbs, can be obtained. From these four, more than 50,000,000 equations relating the thermodynamic properties of the system can be derived using relatively simple mathematics. The derivations are rigorous. Thus, if the two laws are true,*

then the four equations are correct, and hence, the 50,000,000 equations are valid. These are the conditions ... that qualify a discipline as an exact science. By starting with a very few basic laws or postulates, a large body of rigorous mathematical relationships can be derived.

Most of the 50,000,000 equations have little use. However, a significant number are invaluable in describing and predicting the properties of chemical systems in terms of thermodynamic variables. They serve as the basis for deriving equations that apply under experimental conditions, some of which may be difficult to achieve in the laboratory. Their applications will form the focus of several chapters.

The derivation of the thermodynamic relationships ranks with similar developments in only a very limited number of other disciplines in its exactness. The idea that one can start with two fundamental "laws of experience" and rigorously derive a large body of mathematical relationships that must be true if the laws are true is almost unique in science.[a]

In this volume, we will apply the principles developed in *Principles and Applications* to the description of topics of interest to chemists, such as effects of surfaces and gravitational and centrifugal fields; phase equilibria of pure substances (first order and continuous transitions); (vapor + liquid), (liquid + liquid), (solid + liquid), and (fluid + fluid) phase equilibria of mixtures; chemical equilibria; and properties of both nonelectrolyte and electrolyte mixtures. But do not expect a detailed survey of these topics. This, of course, would require a volume of immense breadth and depth. Instead, representative examples are presented to develop general principles that can then be applied to a wide variety of systems.

We will not attempt to derive in this volume the thermodynamic principles and relationships that form the basis of our descriptions. These derivations can be obtained by referring to *Principles and Applications*, or to other elementary textbooks in thermodynamics.[1] Instead, we will simply summarize in this chapter most of the useful equations, and refer the reader to the appropriate sections of *Principles and Applications* for the details of the derivations.

11.1 Thermodynamic Relationships

The fundamental thermodynamic variables[b] are the pressure (p), temperature (T), internal energy (U), and entropy (S). Added to this list are the derived variables

---

[a] Newtonian mechanics is a discipline of equal rigor. There are few others.

[b] See Section 1.3 from Chapter 1 of the first volume of this series titled *Chemical Thermodynamics: Principles and Applications*, by J. B. Ott and J. Boerio-Goates. For the remainder of this chapter, we will refer to this volume as *Principles and Applications*.

enthalpy (H), Helmholtz free energy (A), and Gibbs free energy (G). These last three are defined in terms of the fundamental variables through the equations

$$H = U + pV, \tag{11.1}$$

$$A = U - TS, \tag{11.2}$$

and

$$G = U + pV - TS. \tag{11.3}$$

The first two (p and T) are intensive variables, while the others are extensive. The extensive properties can be made intensive by dividing by the number of moles (n) to give the molar quantities V_m, U_m, S_m, H_m, A_m, and G_m.

11.1a The Gibbs Equations

The laws of thermodynamics can be expressed mathematically by the equations that involve changes in the fundamental thermodynamic variables U and S:[c]

For the universe:

$$\sum \Delta U = 0 \tag{11.4}$$

$$\sum \Delta S \geqslant 0. \tag{11.5}$$

For the system:

$$\mathrm{d}U = \delta q + \delta w \tag{11.6}$$

$$\mathrm{d}S \geqslant \delta q/T, \tag{11.7}$$

where w is the work and q is the heat that flows in the process. For pressure–volume work,

$$\delta w = -p_{\text{ext}}\, \mathrm{d}V,$$

which in the reversible process becomes

$$\delta w = -p\, \mathrm{d}V. \tag{11.8}$$

[c] See Chapter 2, *Principles and Applications.*

For a temperature change, q is obtained from

$$\delta q = C\,\mathrm{d}T, \tag{11.9}$$

where C is the heat capacity. In equations (11.5) and (11.7), the equality applies to the reversible process and the inequality applies to the spontaneous process.

For the reversible process limited to pressure–volume work, the above equations can be combined to give the four fundamental equations of Gibbs[d]

$$\mathrm{d}U = T\,\mathrm{d}S - p\,\mathrm{d}V \tag{11.10}$$

$$\mathrm{d}H = T\,\mathrm{d}S + V\,\mathrm{d}p \tag{11.11}$$

$$\mathrm{d}A = -S\,\mathrm{d}T - p\,\mathrm{d}V \tag{11.12}$$

$$\mathrm{d}G = -S\,\mathrm{d}T + V\,\mathrm{d}p. \tag{11.13}$$

11.1b Differential Relationships

Starting with the above equations (principally the four fundamental equations of Gibbs), the variables U, S, H, A, and G can be related to p, T, V, and the heat capacity at constant volume (C_V) and at constant pressure (C_p) by the differential relationships[e] summarized in Table 11.1. We note that in some instances, such as the temperature derivative of the Gibbs free energy, S is also an independent variable. An alternate equation that expresses G as a function of H (instead of S) is known as the Gibbs–Helmholtz equation. It is given by equation (11.14)

$$\left(\frac{\partial(G/T)}{\partial T}\right)_p = -\frac{H}{T^2}. \tag{11.14}$$

Representing the dependent variables in Table 11.1 by Z, we find that the relationships apply to the molar quantities, Z_m, and to the differences ΔZ. For example,

$$\left(\frac{\partial H_m}{\partial p}\right)_T = V_m - T\left(\frac{\partial V_m}{\partial T}\right)_p, \tag{11.15}$$

---

[d] See Problem P11.1. For more details, see Section 3.1, Chapter 1, *Principles and Applications.*

[e] See Problem P11.2 For more details see Section 3.2, Chapter 3, *Principles and Applications.*

$$\left(\frac{\partial \Delta H}{\partial T}\right)_p = \Delta C_p, \tag{11.16}$$

and

$$\left(\frac{\partial (\Delta G/T)}{\partial T}\right)_p = -\frac{\Delta H}{T^2}. \tag{11.17}$$

Table 11.1 Thermodynamic relationships.

Z	$\left(\frac{\partial Z}{\partial T}\right)_V$	$\left(\frac{\partial Z}{\partial T}\right)_p$	$\left(\frac{\partial Z}{\partial V}\right)_T$	$\left(\frac{\partial Z}{\partial p}\right)_T$
S	$\frac{C_V}{T}$	$\frac{C_p}{T}$	$\left(\frac{\partial p}{\partial T}\right)_V$	$-\left(\frac{\partial V}{\partial T}\right)_p$
U	C_V	$C_p - p\left(\frac{\partial V}{\partial T}\right)_p$	$T\left(\frac{\partial p}{\partial T}\right)_V - p$	$-T\left(\frac{\partial V}{\partial T}\right)_p - p\left(\frac{\partial V}{\partial p}\right)_T$
H	$C_V + V\left(\frac{\partial p}{\partial T}\right)_V$	C_p	$T\left(\frac{\partial p}{\partial T}\right)_V + V\left(\frac{\partial p}{\partial V}\right)_T$	$V - T\left(\frac{\partial V}{\partial T}\right)_p$
A	$-S^*$	$-S - p\left(\frac{\partial V}{\partial T}\right)_p$	$-p$	$-p\left(\frac{\partial V}{\partial p}\right)_T$
G	$-S + V\left(\frac{\partial p}{\partial T}\right)_V$	$-S^*$	$V\left(\frac{\partial p}{\partial V}\right)_T$	V

* Alternative expressions are $\left(\frac{\partial (A/T)}{\partial T}\right)_V = -\frac{U}{T^2}$ and $\left(\frac{\partial (G/T)}{\partial T}\right)_p = -\frac{H}{T^2}$.

They also apply to the partial molar properties $\bar{Z}_i$, a quantity that we will define and describe next. For example, it can be shown that

$$\left(\frac{\partial G}{\partial p}\right)_T = V,$$

so that

$$\left(\frac{\partial \bar{G}_i}{\partial p}\right)_T = \bar{V}_i. \tag{11.18}$$

The partial molar property[f] $\bar{Z}_i$ referred to above is defined as

$$\bar{Z}_i = \left(\frac{\partial Z}{\partial n_i}\right)_{T,p,n_{j\neq i}}, \tag{11.19}$$

where Z is any of our extensive thermodynamic variables. It represents the contribution per mole of the component i in a solution to the thermodynamic property Z, so that

$$Z = \sum_i n_i \bar{Z}_i. \tag{11.20}$$

For a pure substance, the molar Gibbs free energy is also known as the chemical potential[g] μ. In a solution, the partial molar free energy is the chemical potential μ_i. Hence,

$$G = \sum_i n_i \mu_i. \tag{11.21}$$

The partial molar properties of the different components in a solution are related by the Gibbs–Duhem equation[h] given by

$$\sum_i n_i \, \mathrm{d}\bar{Z}_i = 0. \tag{11.22}$$

---

[f] See Section 5.3, Chapter 5, *Principles and Applications*.

[g] See Section 5.2, Chapter 5, *Principles and Applications*.

[h] See Problem P11.3. For more details see Section 5.4, Chapter 5, ***Principles and Applications***.

When applied to the chemical potential in a binary mixture, this equation becomes

$$n_1 d\mu_1 + n_2 d\mu_2 = 0. \tag{11.23}$$

11.2 Phase Equilibria Relationships

For a phase transition between two phases A and B of a pure substance represented by

$$A = B,$$

the condition for equilibrium[i] is

$$\Delta G = 0$$

or

$$\mu_A = \mu_B. \tag{11.24}$$

In a mixture, equilibrium is established when the chemical potential of each component is the same in each phase. That is,

$$\mu_{i,A} = \mu_{i,B}, \tag{11.25}$$

where i indicates the ith component.

Equation (11.25) is true for both first-order and a continuous (or second-order) phase transition. A first-order transition[j] is one for which the first and successive derivatives of ΔG are not equal to zero. That is,

$$\left(\frac{\partial \Delta G}{\partial T}\right)_p = -\Delta S \neq 0, \tag{11.26}$$

and

$$\left(\frac{\partial \Delta G}{\partial p}\right)_T = \Delta V \neq 0. \tag{11.27}$$

---

[i] See Section 5.6, Chapter 5, *Principles and Applications.*

[j] See Section 8.1e, Chapter 8, *Principles and Applications.*

An example of a second derivative equation is

$$\left(\frac{\partial^2 \Delta G}{\partial T^2}\right)_p = -\left(\frac{\partial \Delta S}{\partial T}\right)_p = -\frac{\Delta C_p}{T} \neq 0. \tag{11.28}$$

In a continuous (second-order) phase transition, the first derivatives of G {equations (11.26) and (11.27)} are equal to zero, but subsequent derivatives, such as the one represented by equation (11.28), are not zero at a critical temperature where the continuous transition is complete.[k]

The equality of chemical potentials in a first-order phase transition leads to two important relationships. The first is the Clapeyron equation[l]

$$\frac{dp}{dT} = \frac{\Delta S_m}{\Delta V_m}, \tag{11.29}$$

where ΔS_m and ΔV_m are the molar entropy and volume changes for the transition.[m] At equilibrium,

$$\Delta S_m = \frac{\Delta H_m}{T}, \tag{11.30}$$

so that the Clapeyron equation can also be written as

$$\frac{dp}{dT} = \frac{\Delta H_m}{T \Delta V_m}. \tag{11.31}$$

The Clausius–Clapeyron equation[n] is an integrated version of the Clapeyron equation that applies to equilibrium between an ideal gas vapor phase and a condensed phase, with the conditions that the volume of the

---

[k] In Section 8.1d, Chapter 8, *Principles and Applications*, we describe (vapor + liquid) equilibria in the region of the critical temperature as an example of a continuous transition. In Chapter 13 of this volume we will describe a number of other continuous transitions.

[l] See Section 5.6c, Chapter 5, *Principles and Applications*.

[m] In a solution, the partial molar quantities are involved. That is

$$\frac{dp}{dT} = \frac{\Delta \bar{S}_i}{\Delta \bar{V}_i}.$$

[n] See Problem P11.4. For more details see Section 8.1c, Chapter 8, *Principles and Applications*.

condensed phase is negligible in comparison to the volume of the gas phase and the enthalpy difference between the gas phase and the condensed phase is constant with temperature. When applied to (vapor + liquid) equilibrium, this equation is given by

$$\ln\frac{p_2}{p_1} = -\frac{\Delta_{vap}H_m}{R}\left(\frac{1}{T_2} - \frac{1}{T_1}\right) \tag{11.32}$$

or

$$\ln p = -\frac{\Delta_{vap}H_m}{R}\left(\frac{1}{T}\right) + \text{const}, \tag{11.33}$$

where $\Delta_{vap}H_m$ is the molar enthalpy of vaporization and p is the vapor pressure. For (vapor + solid) equilibrium, $\Delta_{vap}H_m$ in equations (11.32) and (11.33) is replaced by $\Delta_{sub}H_m$, the molar enthalpy of sublimation.

The second relationship that is useful in describing phase equilibria is the Gibbs phase rule[o]

$$f = C - P + 2, \tag{11.34}$$

where C is the number of components, P is the number of phases in equilibrium, and f is the number of degrees of freedom in the system.

The Clapeyron equation does not apply to a continuous transition, since both the entropy (or enthalpy) change and the volume change are zero. For such a transition, in the region of the critical point, the change in the thermodynamic variable given by the second derivative of G can be represented by an exponential equation. For example, in the region of the (vapor + liquid) critical point, ΔV_{vap} and T are related by[p]

$$(V_g - V_l) \sim \left(\frac{|T - T_c|}{T_c}\right)^{\beta}, \tag{11.35}$$

where T_c is the critical temperature and $\beta = 0.32$ is the critical exponent. In Chapter 13, we will show that β appears to have this same value for a variety of critical phenomena.

---

[o] See Section 5.6b, Chapter 5, *Principles and Applications.*

[p] See Section 8.1d, Chapter 8, *Principles and Applications.*

11.3 Fugacity

The fugacity f of a gas is defined by the relationships[q]

$$d\mu = RT\, d\ln f \tag{11.36}$$

and

$$\lim_{p\to 0} \frac{f}{p} = 1. \tag{11.37}$$

The ratio f/p is the fugacity coefficient ϕ, so that f and p are related by

$$f = \phi p. \tag{11.38}$$

Using equation (11.38), at low pressures, equation (11.37) becomes

$$\lim_{p\to 0} \phi = 1,$$

and f and p become equal.

For a mixtures of gases, equation (11.36) becomes

$$d\mu_i = RT\, d\ln f_i \tag{11.39}$$

for the ith component, and the total fugacity is given by

$$f = \sum f_i. \tag{11.40}$$

For condensed phases, it is the fugacity in the equilibrium vapor phase (vapor fugacity or very nearly vapor pressure) that gives the fugacity of the condensed phase. Equation (11.39) applies to relate this vapor fugacity to the chemical potential in the condensed phase.

11.3a Effect of Temperature and Pressure on the Fugacity

The effect of temperature on the fugacity[r] is given by equation (11.41)

$$\left(\frac{\partial \ln f}{\partial T}\right)_p = \frac{H_m^{\ddagger} - H_m}{RT^2}. \tag{11.41}$$

---

[q] See Problem P11.5. For more details see Section 6.1, Chapter 6, *Principles and Applications.*

[r] See Section 6.1d, Chapter 6, *Principles and Applications.*

For a gas, $H_m^{\ddagger} - H_m$ is the change in enthalpy as the gas at pressure, p, is expanded into a vacuum. For a liquid (or solid), $H_m^{\ddagger} - H_m$ is the enthalpy change as the liquid (or solid) is vaporized (or sublimed) into a vacuum. It has been called the **ideal enthalpy of vaporization (or sublimation)** since it represents the enthalpy change as the liquid (or solid) becomes an ideal gas.

The effect of pressure on f is given by[s]

$$\left(\frac{\partial \ln f}{\partial p}\right)_T = \frac{V_m}{RT}, \tag{11.42}$$

where V_m is the molar volume for a pure substance, or the partial molar volume for a component in solution. Equation (11.42) leads to the following equations for calculating the fugacity coefficient ϕ in the gas phase

$$\ln \phi = -\frac{1}{RT}\int_0^p \alpha \, dp \tag{11.43}$$

or

$$\ln \phi = -\int_0^p \frac{1-z}{p} \, dp, \tag{11.44}$$

where

$$\alpha = \frac{RT}{p} - V_m = V_m^{\text{ideal}} - V_m \tag{11.45}$$

and

$$z = \frac{pV_m}{RT}. \tag{11.46}$$

[s] See Section 6.1b, Chapter 6, *Principles and Applications*.

In a gaseous mixture, equation (11.43) becomes (for the ith component)[t]

$$\ln \phi_i = \int_0^p \left(\frac{\overline{V}_i}{RT} - \frac{1}{p} \right) dp, \tag{11.47}$$

where $\overline{V}_i$ is the partial molar volume. The simplest approximation for obtaining ϕ_i uses the Lewis and Randall rule given by

$$f_i = y_i f_i^*, \tag{11.48}$$

where f_i is the fugacity of the component in the mixture, y_i is the mole fraction in the gas, and f_i^* is the fugacity of the pure gaseous component at the same temperature and total pressure, p. The result of the Lewis and Randall rule is that ϕ_i has the same value as the pure gas would have at the same temperature and total pressure.

11.3b Raoult's Law, Henry's Law, and the Ideal Solution

Raoult's law and Henry's law are expressions[u] that relate the vapor fugacity of a component in a solution to composition. Raoult's law is given by

$$f_i = x_i f_i^*, \tag{11.49}$$

where f_i is the vapor fugacity of the component in the solution, x_i is the mole fraction, of i in the solution and f_i^* is the vapor fugacity of the pure substance.

Henry's law states that the vapor pressure of a solute in solution is proportional to the concentration (mole fraction x_2, molality m, or molarity c). That is,

$$f_2 = k_{\mathrm{H},x} x_2 \tag{11.50}$$

or

$$f_2 = k_{\mathrm{H},m} m \tag{11.51}$$

or

$$f_2 = k_{\mathrm{H},c} c, \tag{11.52}$$

---

[t] See Section 6.1e, Chapter 6, *Principles and Applications.*

[u] See Section 6.1e, Chapter 6, *Principles and Applications.*

where f_2 is the vapor fugacity and $k_{H,x}$, $k_{H,m}$ and $k_{H,c}$ are the Henry's law constants. They are related by

$$k_{H,m} = M_1 k_{H,x} \tag{11.53}$$

and

$$k_{H,c} = \frac{M_1 k_{H,x}}{10^{-3}\,\rho_1^*}, \tag{11.54}$$

where M_1 and ρ_1^* are the molecular weight and density of the solvent.

An **ideal solution** is one for which all components obey Raoult's law

$$f_i = x_i f_i^* \tag{11.49}$$

over the entire range of composition at all pressures and temperatures. In a **real solution**, Raoult's law and Henry's law are limiting laws that apply exactly only in the infinitely dilute solution. That is, if we designate component 1 as the solvent and component 2 as the solute, then $f_1 \longrightarrow x_1$ as $x_1 \longrightarrow 1$ and $f_2 \longrightarrow x_2$, m, or c as x_2, m, or $c \longrightarrow 0$.[v]

11.4 Activity and Standard States

The activity[w] a_i is defined as

$$a_i = \frac{f_i}{f_i^\circ}, \tag{11.55}$$

where f_i° is the fugacity in a reference or **standard state**. It is related to the chemical potential μ_i and the standard state chemical potential μ_i° by the relationship

$$\mu_i = \mu_i^\circ + RT \ln a_i. \tag{11.56}$$

---

[v] Henry's law applies only if the solute is a nonelectrolyte. For strong electrolyte solutes, Henry's law is replaced by expressions of the type

$$f_2 = km^\nu$$

where ν is the total number of ions resulting from the dissociation of the solute.

[w] See Section 6.2, Chapter 6, *Principles and Applications.*

11.4a Effect of Pressure and Temperature on the Activity

The effect of pressure on the activity[x] is given by

$$\left(\frac{\partial \ln a_i}{\partial p}\right)_T = \frac{\bar{V}_i}{RT}, \tag{11.57}$$

where $\bar{V}_i$ is the molar volume for a pure substance or the partial molar volume in solution. The effect of temperature on a_i is given by[y]

$$\left(\frac{\partial \ln a_i}{\partial T}\right)_p = -\frac{\bar{L}_i}{RT^2}, \tag{11.58}$$

where $\bar{L}_i = \bar{H}_i - \bar{H}_i^\circ$ is the **relative partial molar enthalpy**. That is, it is the enthalpy relative to the value in the standard state. We will describe it more fully in a following section.

11.4b Choice of Standard States

Standard states are usually chosen[z] so that the activity reduces to the pressure for gases at low pressures, and to concentrations in dilute solution. The choices are summarized in Table 11.2.[aa] We note that for a gas, the standard state is the ideal gas at a pressure of 1 bar (0.1 MPa), in which case, the activity differs from the pressure (expressed in bars) by the fugacity coefficient. That is,

$$a = \phi p.$$

For a pure substance, or for a solvent in solution, the standard state is the pure substance at 1 bar total pressure. This is known as a Raoult's law standard state. With this choice, $a = 1$ for the pure substance (including pure solvent) at a total pressure of one bar. For pressures other than one bar, a is give by

$$a = \Gamma(1), \tag{11.59}$$

---

[x] See Problem P11.6(a). For more details see Section 6.2a, Chapter 6, *Principles and Applications*.

[y] See Section 6.2b, Chapter 6, *Principles and Applications*.

[z] See Section 6.3a, Chapter 6, *Principles and Applications*.

[aa] The choices of standard states given in Table 11.2 for the solutes are only for nonelectrolyte solutes. We will summarize the choices for electrolyte solutes in the next section.

where the activity coefficient Γ can be obtained from

$$\ln \Gamma = \int_{1 \text{ bar}}^{p} \frac{V_m}{RT} \, dp. \tag{11.60}$$

Table 11.2 Choice of standard states ($a_i = f_i/f_i^\circ$)

State of matter	Standard state	Standard state fugacity	Activity coefficient	Limiting relationship
Gas	Ideal gas at $p = 1$ bar	$f^\circ = 1$ bar	$a = \phi p$	$\phi \rightarrow 1$ as $p \rightarrow 0$
Pure solid or pure liquid	Pure substance at $p = 1$ bar	$f^\circ = f^*$	$a = \Gamma$	$\Gamma \rightarrow 1$ as $p \rightarrow 1$
Solvent in a mixture	(Raoult's law) Pure substance at $p = 1$ bar	$f_1^\circ = f_1^*$	$a_1 = \gamma_{R,1} x_1$	$\gamma_{R,1} \rightarrow 1$ as $x_1 \rightarrow 1$
Solute* in a mixture	(Raoult's law)* Pure substance at $p = 1$ bar	$f_2^\circ = f_2^*$	$a_2 = \gamma_{R,2} x_2$	$\gamma_{R,2} \rightarrow 1$ as $x_2 \rightarrow 1$
	or (Henry's law) Hypothetical solution with $x_2 = 1$ that obeys Henry's law	$f_2^\circ = k_{H,x}$	$a_2 = \gamma_{H,x} x_2$	$\gamma_{H,x} \rightarrow 1$ as $x_2 \rightarrow 0$
	or (Henry's law) Hypothetical solution with $m = 1$ that obeys Henry's law	$f_2^\circ = k_{H,m}$	$a_1 = \gamma_{H,m} m$	$\gamma_{H,m} \rightarrow 1$ as $m \rightarrow 0$

*A Raoult's law standard state for the solute is often chosen for nonelectrolyte mixtures that cover the entire concentration range from $x_2 = 0$ to $x_2 = 1$.

It is easy to show that Γ differs little from one for a condensed phase unless the pressure differs significantly from one bar.

For a solvent in solution, the activity a_1 is related to the mole fraction x_1 through the activity coefficient $\gamma_{R,1}$, with $\gamma_{R,1} \rightarrow 1$ as $x_1 \rightarrow 1$. For nonelectrolyte solutes, a Henry's law standard state is often chosen so that activity a_2 is related to the mole fraction x_2 or the molality m by the activity coefficient $\gamma_{H,x}$ or $\gamma_{H,m}$, with ($\gamma_{H,x}$ or $\gamma_{H,m}$) $\rightarrow 1$ as (x_2 or m) $\rightarrow 0$.

11.4c Choice of Standard States for Strong Electrolyte Solutes

Strong electrolyte solutes[bb] follow a different limiting law than do nonelectrolyte solutes. For example, for a 1 : 1 electrolyte such as HCl, the limiting law is

$$f_2 = km^2.$$

With this limiting law, it is advantageous to consider the chemical potential to be the sum of the chemical potentials of the ions. That is,

$$\mu_2^\circ = \mu_+^\circ + \mu_-^\circ.$$

With this choice,

$$a_2 = a_+ a_- \tag{11.61}$$

$$= (\gamma_+ m_+)(\gamma_- m_-)$$

$$= \gamma_\pm^2 m^2. \tag{11.62}$$

where $m_+ = m_- = m$ and $\gamma_\pm$ is the geometric mean activity coefficient given by

$$\gamma_\pm = (\gamma_+ \gamma_-)^{1/2}. \tag{11.63}$$

Activity coefficient relationships for the different types of strong electrolyte solutions are summarized in Table 11.3.

11.4d Debye–Hückel Predictions of the Thermodynamic Properties of Strong Electrolyte Solutions[cc]

Debye–Hückel theory can be used to predict $\gamma_\pm$ for a solution containing a

[bb] See Section 6.5a, Chapter 6, *Principles and Applications*.

[cc] See Section 7.2, Chapter 7, *Principles and Applications*.

Table 11.3 Activity coefficient relationships for electrolyte solutions (single electrolyte)

Type example	Nonelectrolyte sucrose	1:1 NaCl $MgSO_4$	2:1 or 1:2 Na_2SO_4 $CaCl_2$	3:1 or 1:3 $AlCl_3$ Na_3PO_4	3:2 or 2:3 $La_2(SO_4)_3$ $Ca_3(PO_4)_2$	General $A_{\nu+}B_{\nu-}$
Limiting law $f_2 =$	km	km^2	km^3	km^4	km^5	$km^{(\nu_+ + \nu_-)}$
$a_2 =$	a	$(a_+)(a_-)$ or $[\gamma_\pm^2 m^2]$	$(a_+)^2(a_-)$ or $(a_+)(a_-)^2$ or $[4\gamma_\pm^3 m^3]$	$(a_+)(a_-)^3$ or $(a_+)^3(a_-)$ or $[27\gamma_\pm^4 m^4]$	$(a_+)^2(a_-)^3$ or $(a_+)^3(a_-)^2$ or $[108\gamma_\pm^5 m^5]$	$(a_+)^{\nu+}(a_-)^{\nu-}$ or $[(\nu_+)^{\nu+}(\nu_-)^{\nu-}][\gamma_\pm m]^{(\nu_+ + \nu_-)}$
$a_\pm =$	–	$[(a_+)(a_-)]^{1/2}$	$[(a_+)^2(a_-)]^{1/3}$ or $[(a_+)(a_-)^2]^{1/3}$	$[(a_+)(a_-)^3]^{1/4}$ or $[(a_+)^3(a_-)]^{1/4}$	$[(a_+)^2(a_-)^3]^{1/5}$ or $[(a_+)^3(a_-)^2]^{1/5}$	$[(a_+)^{\nu+}(a_-)^{\nu-}]^{1/(\nu_+ + \nu_-)}$
$m_\pm =$	-	m	$2^{2/3}m$	$3^{3/4}m$	$4^{4/5}m$	$[(\nu_+)^{\nu+}(\nu_-)^{\nu-}]^{1/(\nu_+ + \nu_-)}m$
$\gamma_\pm =$	-	$\frac{a_\pm}{m_\pm}$	$\frac{a_\pm}{m_\pm}$	$\frac{a_\pm}{m_\pm}$	$\frac{a_\pm}{m_\pm}$	$\frac{a_\pm}{m_\pm}$

strong electrolyte solute that dissociates according to the reaction[dd]

$$A_{\nu_+}B_{\nu_-} = \nu_+ A^{z+} + \nu_- B^{z-}. \tag{11.64}$$

The resulting equation is

$$\ln \gamma_\pm = -|z_+ z_-| \frac{C_\gamma I_m^{1/2}}{1 + B_\gamma a I_m^{1/2}}, \tag{11.65}$$

where I_m is the ionic strength given by

$$I_m = \tfrac{1}{2} \sum_j z_j^2 m_j, \tag{11.66}$$

with m as the molality and z the charge on each ion in the mixture. The constants C_γ and B_γ are given by

$$C_\gamma = (2\pi N_A \rho_A)^{1/2} \left(\frac{e^2}{4\pi\varepsilon_0 \varepsilon_A kT} \right)^{3/2}, \tag{11.67}$$

and

$$B_\gamma = e \left(\frac{2N_A \rho_A}{\varepsilon_0 \varepsilon_A kT} \right)^{1/2}. \tag{11.68}$$

In equations (11.67) and (11.68), N_A is Avogadro's number, k is the Boltzmann constant, T is the temperature, ρ_A is the density of the solvent (in $kg \cdot m^{-3}$), ε_0 is the permittivity of vacuum, and ε_A is the relative permittivity (dielectric constant) of the solvent. For aqueous solutions at $T = 298.15$ K, the values are

$$C_\gamma = 1.174 \text{ kg}^{1/2} \cdot \text{mol}^{-1/2}$$

$$B_\gamma = 3.32384 \times 10^9 \text{ kg}^{1/2} \cdot \text{mol}^{-1/2} \cdot \text{m}^{-1}.$$

The coefficients vary slowly with temperature. In water at 273.15 K, $C_\gamma = 1.133 \text{ kg}^{1/2} \cdot \text{mol}^{-1/2}$, while at 373.15 K, it has a value of $1.372 \text{ kg}^{1/2} \cdot \text{mol}^{-1/2}$.

[dd] See Section 7.2a, Chapter 7, *Principles and Applications.*

The a in equation (11.65) is the distance of closest approach between the ions in solution. It has a value that typically ranges from $(3 \times 10^{-10}$ to $8 \times 10^{-10})$ m, with most ions around 3×10^{-10} m. The product aB_γ has a value of $(3 \times 10^{-10})(3.3 \times 10^{9}) \approx 1$. Equation (11.65) is often simplified by letting $aB_\gamma = 1$ so that

$$\ln \gamma_{\pm} = -\frac{C_\gamma \mid z_+ z_- \mid I_m^{1/2}}{1 + I_m^{1/2}}. \tag{11.69}$$

A further simplification is made by noting that at low m, $I_m^{1/2} \ll 1$ and can be neglected in the denominator of equation (11.69). The resulting equation, valid only at very low m, is given by

$$\ln \gamma_{\pm} = -C_\gamma \mid z^+ z^- \mid I_m^{1/2}. \tag{11.70}$$

Values for C_γ as a function of temperature for aqueous solutions are tabulated in Appendix 7 of this volume.

Debye–Hückel theory also predicts other thermodynamic properties. The equation for the osmotic coefficient[ee] {equivalent to equation (11.69) for $\gamma_{\pm}$} is

$$1 - \phi = C_\phi \mid z_+ z_- \mid \frac{I_m^{1/2}}{1 + I_m^{1/2}}, \tag{11.71}$$

where $C_\phi = C_\gamma/3$, and the osmotic coefficient ϕ is given by

$$\phi = -\frac{\ln a_1}{M_1 \nu m}. \tag{11.72}$$

In equation (11.72), M_1 is the molecular weight of the solvent, m is the molality, and $\nu = \nu_+ + \nu_-$ is the total number of ions in the solution resulting from the dissociation. The limiting law equation for ϕ {equivalent to equation (11.70) for $\gamma_{\pm}$} is

$$1 - \phi = C_\phi \mid z_+ z_- \mid I_m^{1/2}. \tag{11.73}$$

[ee] See Section 7.2c, Chapter 7. *Principles and Applications.*

The Debye–Hückel limiting law prediction[ff] of the volumetric and thermal properties of the electrolyte solute are given by

$$\bar{V}_2 - \bar{V}_2^\circ = C_v \left(\frac{\nu}{2}\right) |z_+ z_-| I_m^{1/2}, \tag{11.74}$$

$$\bar{L}_2 = C_H \left(\frac{\nu}{2}\right) |z_+ z_-| I_m^{1/2}, \tag{11.75}$$

and

$$\bar{J}_2 = C_J \left(\frac{\nu}{2}\right) |z_+ z_-| I_m^{1/2}, \tag{11.76}$$

where $\bar{V}_2$ the partial molar volume, $\bar{L}_2$ is the relative partial molar enthalpy, and $\bar{J}_2$ is the relative partial molar heat capacity.

The Debye–Hückel equations work only in very dilute solution. In Chapter 18, we will extend the description to include the Guggenheim and Pitzer equations, which can be used in successively more concentrated solutions.

11.5 Thermodynamics of Mixtures

11.5a Change in the Thermodynamic Properties in Forming Nonelectrolyte Mixtures[gg]

We start by describing and calculating $\Delta_{mix}Z$, the change in the thermodynamic variable Z, when liquids (or solids) are mixed to form a solution. For the process

$$n_1\mathrm{A} + n_2\mathrm{B} + \cdots = \text{Solution} \tag{11.77}$$

the change in Gibbs free energy $\Delta_{\text{mix}}G$ is given by

$$\Delta_{\text{mix}}G = RT \sum_i n_i \ln a_i, \tag{11.78}$$

[ff] See Section 7.2d, Chapter 7, *Principles and Applications*.

[gg] See Section 7.1, Chapter 7, *Principles and Applications*.

where a_i is the activity in solution. With

$$a_i = \gamma_{R,i} x_i,$$

where $\gamma_{R,i}$ is the (Raoult's law) activity coefficient and x_i is the mole fraction, equation (11.78) becomes

$$\Delta_{mix} G = RT \sum_i (n_i \ln x_i + n_i \ln \gamma_{R,i}).$$

For a mole of solution, this equation becomes

$$\Delta_{mix} G_m = RT \sum_i (x_i \ln x_i + x_i \ln \gamma_{R,i}). \tag{11.79}$$

Thermodynamic Properties of Ideal Solutions: Equation (11.79) is the starting point for deriving equations for $\Delta_{mix} Z_m^{id}$, the change in Z_m for forming an ideal mixture.[hh] For the ideal solution, $\gamma_{R,i} = 1$ and equation (11.79) becomes

$$\Delta_{mix} G_m^{id} = RT \sum_i x_i \ln x_i. \tag{11.80}$$

The change in other thermodynamic properties to form the ideal mixture are easily obtained from equation (11.80). The results are

$$\Delta_{mix} S_m^{id} = -R \sum_i x_i \ln x_i, \tag{11.81}$$

$$\Delta_{mix} H_m^{id} = 0, \tag{11.82}$$

$$\Delta_{mix} U_m^{id} = 0, \tag{11.83}$$

and

$$\Delta_{mix} V_m^{id} = 0. \tag{11.84}$$

Effect of Temperature and Pressure on (Solid + Liquid) Equilibrium in an Ideal Solution: Useful relationships for the ideal solution are the equations that

[hh] See Problem P11.6(b) and P11.6(c). For more details see Section 7.1a, Chapter 7, *Principles and Applications*.

relate the equilibrium temperature T (melting temperature) and equilibrium pressure p (melting pressure) to the mole fraction x_i of the component that freezes from the solution to form a pure solid. This composition is often known as the **ideal solubility**, since it represents the composition of a saturated solution at a particular temperature and pressure. The equations that apply are[ii]

$$\left(\frac{\partial \ln x_i}{\partial T}\right)_p = \frac{\Delta_{\text{fus}} H_{\text{m},i}}{RT^2} \tag{11.85}$$

and

$$\left(\frac{\partial \ln x_i}{\partial p}\right)_T = -\frac{\Delta_{\text{fus}} V^*_{\text{m},i}}{RT}, \tag{11.86}$$

where the pure solid that freezes from solution has a molar enthalpy of fusion $\Delta_{\text{fus}} H_{\text{m},i}$ and a molar volume of fusion $\Delta_{\text{fus}} V_{\text{m},i}$.

Excess Thermodynamic Functions: The excess molar thermodynamic function[ij] Z^{E}_{m} is defined as the difference between $\Delta_{\text{mix}} Z_{\text{m}}$, the change in Z_{m} for mixing components to form a real solution, and $\Delta_{\text{mix}} Z^{\text{id}}_{\text{m}}$, the change in Z_{m} to form the ideal solution. Thus,

$$Z^{\text{E}}_{\text{m}} = \Delta_{\text{mix}} Z_{\text{m}} - \Delta_{\text{mix}} Z^{\text{id}}_{\text{m}}. \tag{11.87}$$

The combination of equation (11.87) with equations (11.79) to (11.84) gives

$$G^{\text{E}}_{\text{m}} = RT \sum x_i \ln \gamma_{\text{R},i}, \tag{11.88}$$

$$H^{\text{E}}_{\text{m}} = \Delta_{\text{mix}} H_{\text{m}}, \tag{11.89}$$

$$U^{\text{E}}_{\text{m}} = \Delta_{\text{mix}} U_{\text{m}}, \tag{11.90}$$

and

$$V^{\text{E}}_{\text{m}} = \Delta_{\text{mix}} V_{\text{m}}. \tag{11.91}$$

[ii] See Section 8.2c, Chapter 8, *Principles and Applications* where integrated forms of equations (11.85) and (11.86) can be found.

[ij] See Section 7.1b, Chapter 7, *Principles and Applications*.

The excess entropy is obtained from

$$S_m^E = \frac{H_m^E - G_m^E}{T}. \tag{11.92}$$

11.5b Relative Partial Molar Thermal Properties

The heat absorbed or evolved when liquids or solutions are mixed or diluted is obtained from the calculation of ΔH for the solution process.[kk] The calculation of ΔH is usually obtained from the relative partial molar enthalpy defined as

$$\bar{L}_i = \bar{H}_i - \bar{H}_i^\circ, \tag{11.93}$$

where $\bar{H}_i^\circ$ is the enthalpy in the standard state. The $\bar{L}_i$ can be combined to give the total relative enthalpy L in a solution

$$L = \sum n_i \bar{L}_i \tag{11.94}$$

from which ΔH can be calculated for the mixing process through the relationship

$$\Delta H = \Delta L. \tag{11.95}$$

Equation (11.95) can be applied to a variety of mixing processes. For mixing involving a solute B with a solvent A, the different types can be summarized as

Integral enthalpy of solution:

$$n_2\text{B} + n_1\text{A} = \text{Solution } (n_2\text{B} + n_1\text{A}).$$

Integral enthalpy of dilution:

$$n_1'\text{A} + \text{solution } (n_2\text{B} + n_1\text{A}) = \text{solution}' \; [n_2\text{B} + (n_1 + n_1')\text{A}].$$

Differential enthalpy of solution:

$$n_2'\text{B} + \text{solution } (n_1\text{A} + n_2\text{B}) = \text{solution } [n_1\text{A} + (n_2 + n_2')\text{B}].$$

In the differential process, n_1 and n_2 are much larger than n_2' so that the final solution does not differ significantly from the initial solution.

[kk] See Section 7.3, Chapter 7, *Principles and Applications.*

11.5c Relative Apparent Molar Properties

An apparent molar property ϕZ is defined as[ll]

$$\phi Z = \frac{Z - n_1 Z_1^*}{n_2}, \tag{11.96}$$

where Z is the total thermodynamic property, Z_1^* is the value for the pure solvent, and n_1 and n_2 are the moles of solvent and solute. For example,

$$\phi H = \frac{H - n_1 H_1^*}{n_2},$$

$$\phi V = \frac{V - n_1 V_1^*}{n_2},$$

and

$$\phi C_p = \frac{C_p - n_1 C_{p,1}^*}{n_2}.$$

The relative apparent molar enthalpy ϕL is given by[mm]

$$\phi L = \phi H - \phi H^\circ. \tag{11.97}$$

Thus, ϕL is the difference between the apparent molar enthalpy of the mixture, and the apparent molar enthalpy in the standard state. Relative apparent molar enthalpies can be used to calculate ΔH for a process through the relationship

$$\Delta H = \Delta L = n_2 \Delta \phi L. \tag{11.98}$$

11.6 Chemical Equilibrium

The generalized chemical reaction[nn]

$$\nu_1 A_1 + \nu_2 A_2 + \cdots = \nu_m A_m + \nu_{m+1} A_{m+1} + \cdots$$

[ll] See Problem P11.7. For more details see Section 5.5d, Chapter 5, *Principles and Applications.*

[mm] See Section 7.3c, Chapter 7, *Principles and Applications.*

[nn] See Problem P11.8. For more details see Section 9.1, Chapter 9, *Principles and Applications.*

can be written as

$$\sum_i \nu_i A_i = 0, \tag{11.99}$$

where the coefficients ν_i are positive for the products of the reaction and negative for the reactants.

The condition for equilibrium in a chemical reaction is given by

$$\sum_i \nu_i \mu_i = 0, \tag{11.100}$$

where the μ_i are the chemical potentials of the species in the reaction. The Gibbs free energy change in the chemical reaction is given by

$$\Delta_r G = \Delta_r G^\circ + RT \ln \prod_i a_i^{\nu_i} \tag{11.101}$$

where $\Delta_r G^\circ$ is the Gibbs free energy change with reactants in their standard states, and a_i is the activity.

11.6a The Equilibrium Constant

At equilibrium, equation (11.101) applies so that $\Delta_r G = 0$ and

$$\Delta_r G^\circ = -RT \ln K \tag{11.102}$$

with K, the thermodynamic equilibrium constant, equal to

$$K = \prod_i a_i^{\nu_i}. \tag{11.103}$$

The activities in equation (11.103) are now the equilibrium activities.

11.6b Alternate Forms of the Equilibrium Constant

For a gas-phase reaction, equation (11.103) can be written as

$$K = \prod_i f_i^{\nu_i} \tag{11.104}$$

where f_i is the fugacity, expressed in bars with the usual choice of standard states. Alternate forms of the equilibrium constant for the gas-phase reaction are[oo]

$$K_p = \prod_i p_i^{\nu_i}, \tag{11.105}$$

$$K_c = \prod_i c_i^{\nu_i}, \tag{11.106}$$

[oo] See Section 9.1a, Chapter 9, *Principles and Applications*.

and

$$K_x = \prod_i x_i^{\nu_i}. \tag{11.107}$$

In equations (11.105) to (11.107), p_i is the partial pressure, c_i is the molar concentration, and x_i is the mole fraction. These three equilibrium constants are related to the thermodynamic equilibrium constant K through the relationship

$$\frac{K}{J_\phi} = K_p = K_c \cdot (RT)^{\Sigma\nu_i} = K_x \cdot p^{\Sigma\nu_i}, \tag{11.108}$$

where J_ϕ is the fugacity coefficient ratio given by

$$J_\phi = \prod_i \phi_i^{\nu_i} \text{ and } p \text{ is the total pressure} \tag{11.109}$$

At low pressures $J_\phi \cong 1$ and equation (11.108) becomes

$$K = K_p = K_c \cdot (RT)^{\Sigma\nu_i} = K_x \cdot p^{\Sigma\nu_i}. \tag{11.110}$$

Alternate expressions can be written for reactions involving condensed phases. For example, for the ionization of water

$$H_2O(l) = H^+(aq) + OH^-(aq) \tag{11.111}$$

the thermodynamic equilibrium constant K is related to the ionization constant for water

$$K_w = a_{H^+} a_{OH^-} \tag{11.112}$$

through the relationship

$$K = \frac{a_{H^+} a_{OH^-}}{a_{H_2O}} = \frac{K_w}{a_{H_2O}}. \tag{11.113}$$

With the usual choice of standard states

$$a_{H_2O} = \Gamma_{H_2O}(l), \tag{11.114}$$

where Γ_{H_2O} is the activity coefficient for pure water. When the total pressure is 1 bar, Γ_{H_2O} becomes equal to one, in which case

$$K = K_w.$$

In a solution, a combination of equations (11.113) with (11.114) gives

$$K = \frac{\gamma_{\pm}^2 m_{H^+} m_{OH^-}}{\Gamma_{H_2O}}, \tag{11.115}$$

where $\gamma_{\pm}$ is the mean ionic activity coefficient in the solution.

11.6c Effect of Pressure and Temperature on the Equilibrium Constant

The Effect of Pressure: The thermodynamic equilibrium constant is independent of pressure. That is,

$$\left(\frac{\partial K}{\partial p}\right)_T = 0. \tag{11.116}$$

Alternate forms of the equilibrium constant do vary with pressure. For example,

$$\left(\frac{\partial \ln K_p}{\partial p}\right)_T = \frac{\Delta(V_i^{\text{ideal}} - \bar{V}_i)}{RT} \tag{11.117}$$

and

$$\left(\frac{\partial \ln K_w}{\partial p}\right)_T = \frac{V_m^*}{RT}, \tag{11.118}$$

where V_i^{ideal} is the molar volume of the ideal gas, $\bar{V}_i$ is the partial molar volume in the gaseous mixture, and V_m^* is the molar volume of the pure (liquid) water.

The Effect of Temperature: The effect of temperature on K is given by[pp]

$$\left(\frac{\partial \ln K}{\partial T}\right)_p = \frac{\Delta_r H^\circ}{RT^2}, \tag{11.119}$$

[pp] See Problem P11.8(b). For more details see Section 9.1b, Chapter 9, *Principles and Applications*.

where $\Delta_r H^\circ$ is the standard enthalpy change for the reaction. Over a small temperature range, $\Delta_r H^\circ$ can often be assumed as constant with temperature, in which case, equation (11.119) becomes

$$\ln \frac{K_2}{K_1} = -\frac{\Delta_r H^\circ}{R}\left(\frac{1}{T_2} - \frac{1}{T_1}\right). \tag{11.120}$$

Over extended temperature ranges, $\Delta_r H^\circ$ is expressed as a function of temperature by integrating the equation expressing $\Delta_r C_p^\circ$, the heat capacity change for the reaction as a function of temperature. The result is

$$\Delta_r H^\circ = \Delta H_I + \left(\sum_i \nu_i a_i\right) T + \frac{\left(\sum_i \nu_i b_i\right)}{2} T^2 - \frac{\left(\sum_i \nu_i c_i\right)}{T} + \frac{\left(\sum_i \nu_i d_i\right)}{3} T^3 + \cdots, \tag{11.121}$$

where ΔH_I is a constant of integration, and a_i, b_i, c_i, and d_i are constants of the heat capacity equation given by

$$C^\circ_{p,\mathrm{m},i} = a_i + b_i T + c_i T^{-2} + d_i T^2.$$

Values for a_i, b_i, c_i, and d_i can be found in tables.[qq]

Substitution of equation (11.121) into equation (11.119) and integrating gives an equation for $\ln K$ of the form

$$R \ln K = -I - \frac{(\Delta H_I)}{T} + \left(\sum_i \nu_i a_i\right) \ln T + \frac{\left(\sum_i \nu_i b_i\right)}{2} T + \frac{\left(\sum_i \nu_i c_i\right)}{2T^2} + \frac{\left(\sum_i \nu_i d_i\right)}{6} T^2 + \cdots \tag{11.122}$$

where I is a constant obtained from integration of equation (11.119).

[qq] See Table A5.5 of Appendix 5 to obtain values for the heat capacity coefficients needed for equation (11.122).

11.6d Enthalpies and Gibbs Free Energies of Formation

We represent $\Delta_f H°$ and $\Delta_f G°$ as the standard enthalpy and Gibbs free energy changes for the reaction in which the chemical substance is formed from the elements in their stable form, as they occur in nature at $T = 298.15$ K.[rr] For ions in solution, the values tabulated are relative to the standard enthalpy and Gibbs free energy of formation of the H^+ ion being set equal to zero.[ss]

The standard enthalpy and Gibbs free energy changes for a chemical reaction can be calculated from $\Delta_f H°$ and $\Delta_f G°$ data using the relationships

$$\Delta_r H° = \sum_i \nu_i \Delta_f H°_{m,i} \tag{11.123}$$

and

$$\Delta_r G° = \sum_i \nu_i \Delta_f G°_{m,i}. \tag{11.124}$$

11.7 Electrochemical Cells

For the cell reaction given by

$$\nu_1 A_1 + \nu_2 A_2 + \cdots = \nu_m A_m + \nu_{m+1} A_{m+1} + \cdots$$

or

$$\sum_i \nu_i A_i = 0,$$

the reversible voltage E of the cell is related to the Gibbs free energy change by[tt]

$$\Delta_r G = -nFE, \tag{11.125}$$

[rr] See Section 9.2, Chapter 9, *Principles and Applications*. Values for $\Delta_f H°$ and $\Delta_f G°$ at $T = 298.15$ K for selected substances and ions are tabulated in Tables A5.2 and A5.3 of Appendix 5 of this volume, with some $\Delta_f H°$ values also given in Table A5.1 of the same appendix.

[ss] See Section 9.2b, Chapter 9, *Principles and Applications*. Values for the standard enthalpies and Gibbs free energies of formation of selected ions at $T = 298.15$ K are summarized in Table A5.3 of Appendix 5 of this volume.

[tt] See Problem P11.9. For more details see Section 9.4, Chapter 9, *Principles and Applications*.

where n is the moles of electrons transferred in the cell reaction. Under the standard state conditions the relationship becomes

$$\Delta_r G^\circ = -nFE^\circ, \tag{11.126}$$

where E° is the voltage of the cell with reactants and products in their standard states. The relationship of E to the activities of the reactants and products in the cell reaction is given by the Nernst equation

$$E = E^\circ - \frac{RT}{nF} \ln \prod_i a_i^{\nu_i}. \tag{11.127}$$

Other thermodynamic variables can be related to the voltage E and its temperature and pressure derivatives. They are as follows:

$$\Delta_r S = nF \left(\frac{\partial E}{\partial T}\right)_p, \tag{11.128}$$

$$\Delta_r H = -nF \left[E - T\left(\frac{\partial E}{\partial T}\right)_p\right], \tag{11.129}$$

$$\Delta_r C_p = nFT \left(\frac{\partial^2 E}{\partial T^2}\right)_p, \tag{11.130}$$

and

$$\Delta_r V = -nF \left(\frac{\partial E}{\partial p}\right)_T. \tag{11.131}$$

The equilibrium constant K for the cell reaction can also be obtained from E° through the relationship

$$RT \ln K = nFE^\circ. \tag{11.132}$$

11.8 Calculations From Statistical Thermodynamics

11.8a The Boltzmann Distribution Equation

The calculation of the thermodynamic functions of a substance is based upon the[uu] Boltzmann distribution equation, which predicts the most probable distribution[vv] of molecules (or atoms) among a set of energy levels. The equation is

$$\frac{n_i}{g_i} = \frac{n_0}{g_0} \exp\left(-\frac{\epsilon_i}{kT}\right), \tag{11.133}$$

where n_i is the number of molecules in the energy level ϵ_i and g_i is the statistical weight factor (degeneracy) of that level, while n_0 and g_0 are the same quantities for the ground state.

In the calculation of the thermodynamic properties of the ideal gas, the approximation is made that the energies can be separated into independent contributions from the various degrees of freedom. Translational and electronic energy levels are present in the ideal monatomic gas.[ww] For the molecular gas, rotational and vibrational energy levels are added. For some molecules, internal rotational energy levels are also present. The equations that relate these energy levels to the mass, moments of inertia, and vibrational frequencies are summarized in Appendix 6.

11.8b The Partition Function

The partition function[xx] for a set of energy levels in an atom or molecule is given by

$$z = \sum g_i \exp\left(-\frac{\epsilon_i}{kT}\right). \tag{11.134}$$

[uu] See Section 10.3, Chapter 10, *Principles and Applications.*

[vv] For Avogadro's number of molecules, fluctuations from the most probable distribution are very small, and the Boltzmann distribution equation can be relied upon to predict the correct distribution.

[ww] The electronic energy levels contribute to the thermodynamic properties only at high temperatures, or if unpaired electrons are present.

[xx] See Section 10.4, Chapter 10, *Principles and Applications.*

Combining equation (11.134) with (11.133) gives

$$\frac{n_i}{N} = \frac{g_i \exp\left(-\dfrac{\epsilon_i}{kT}\right)}{z}. \tag{11.135}$$

The partition function tells us the fraction, n_i/N, of the molecules in energy state ϵ_i. It is a measure of the extent to which energy is partitioned among the different states. The partition function can be related to the thermodynamic properties U_m, H_m, $C_{V,m}$, $C_{p,m}$, S_m, A_m, and G_m. These relationships are summarized in Appendix 6.

11.8c Relationships for Calculating the Thermodynamic Functions of the Ideal Gas

Expressions for the partition function can be obtained for each type of energy level in an atom or molecule. These relationships can then be used to derive equations for calculating the thermodynamic functions of an ideal gas. Table 11.4 or Table A6.1 in Appendix 6 summarize the equations for calculating the translational, rotational, and vibrational contributions to the thermodynamic functions, assuming the molecule is a rigid rotator and harmonic oscillator.[yy] Moments of inertia and fundamental vibrational frequencies for a number of molecules are given in Tables A6.2 to A6.4 of Appendix 6. From these values, the thermodynamic functions can be calculated with the aid of Table 11.4.

For diatomic molecules, corrections can be made for the assumption used in the derivation of the rotational partition function that the rotational energy levels are so closely spaced that they can be considered to be continuous. The equations to be used in making these corrections are given in Appendix 6. Also given are the equations to use in correcting for vibrational anharmonicity and nonrigid rotator effects. These corrections are usually small.[zz]

11.8d Contributions of Internal Rotation to the Thermodynamic Functions of the Ideal Gas

For some (nonlinear) molecules, a vibrational degree of freedom may be replaced by a rotation of parts of the molecule about a bond. The contribution of this internal rotation to the thermodynamic functions is determined by the

---

[yy] See Problem P11.10. For more details see Section 10.7, Chapter 10, *Principles and Applications*.

[zz] We refer the reader to Section 10.7b of *Principles and Applications* for the procedures to follow and the information that is needed to make these corrections.

Table 11.4 Thermodynamic functions of an ideal gas (in $J \cdot K^{-1} \cdot mol^{-1}$)

(Use $R = 8.314510\ J \cdot K^{-1} \cdot mol^{-1}$ and SI units for pressure, temperature, and all molecular data)

Translation

$$S_{m,\,trans} = \frac{3}{2} R \ln M + \frac{5}{2} R \ln T - R \ln p + \underbrace{\left[\frac{5}{2} R + R \ln \left(\frac{(2\pi k)^{3/2}}{h^3 N^{5/2}}\right) + R \ln R\right]}_{+172.3005}$$

$$\left(\frac{G_m - H_{0,m}}{T}\right)_{trans} = -\frac{3}{2} R \ln M - \frac{5}{2} R \ln T + R \ln p + \underbrace{\left[-R \ln \left(\frac{2\pi k)^{3/2}}{h^3 N^{5/2}}\right) - R \ln R\right]}_{-151.5142}$$

$$\left(\frac{U_m - U_{0,m}}{T}\right)_{trans} = \frac{3}{2} R = (C_{V,m})_{trans}$$

$$\left(\frac{H_m - H_{0,m}}{T}\right)_{trans} = \frac{5}{2} R = (C_{p,m})_{trans}$$

Rotation

(Rigid Molecule Approximation)
Linear Polyatomic or Diatomic Molecules:

$$S_{m,\,rot.} = R \ln T + R \ln I - R \ln \sigma + \underbrace{\left[R \ln \left(\frac{8\pi^2 k}{h^2}\right) + R\right]}_{+877.3950}$$

$$\left(\frac{G_m - H_{0,m}}{T}\right)_{rot.} = -R \ln T - R \ln I + R \ln \sigma + \underbrace{\left[-R \ln \frac{8\pi^2 k}{h^2}\right]}_{-869.0805}$$

$$\left(\frac{U_m - U_{0,m}}{T}\right)_{rot.} = \left(\frac{H_m - H_{0,m}}{T}\right)_{rot.} = (C_m)_{rot.} = R$$

(continued)

Table 11.4 *Continued*

Nonlinear Polyatomic Molecules

$$S_{m,\,rot.} = \frac{3}{2} R \ln T + \frac{1}{2} R \ln I_A I_B I_C - R \ln \sigma + \underbrace{\left[R \ln \frac{8\pi^2 (2\pi k)^{3/2}}{h^3} + \frac{3}{2} R \right]}_{+1320.8515}$$

$$\left(\frac{U_m - U_{0,m}}{T} \right)_{rot.} = \left(\frac{H_m - H_{0,m}}{T} \right)_{rot.} = (C)_{rot.} = \frac{3}{2} R$$

$$\left(\frac{G_m - U_{0,m}}{T} \right)_{rot.} = -\frac{3}{2} R \ln T - \frac{1}{2} R \ln I_A I_B I_C + R \ln \sigma + \underbrace{\left[- R \ln \frac{8\pi^2 (2\pi k)^{3/2}}{h^3} \right]}_{-1308.3797}$$

Vibration (Harmonic Oscillator Approximation)

$$S_{m,\,vib} = R \sum_{i=1}^{n} \left[\frac{x_i}{\exp(x_i) - 1} - \ln(1 - \exp(-x_i)) \right]; \; x_i = \frac{hc\tilde{\omega}_i}{kT} = 1.43877 \frac{\tilde{\omega}_i}{T} (\text{use } \tilde{\omega}_i \text{ in cm}^{-1})$$

$$\left(\frac{G_m - H_{0,m}}{T} \right)_{vib} = \sum_{i=1}^{n} R \ln(1 - \exp(-x_i)) \approx \sum_{i=1}^{n} \left(- R \ln \frac{kT}{hc\tilde{\omega}_i} \right) \text{ (High temp. approx.)}$$

$$\left(\frac{U_m - U_{0,m}}{T} \right)_{vib} = \left(\frac{H_m - H_{0,m}}{T} \right)_{vib} = R \sum_{i=1}^{n} \frac{x_i}{\exp(x_i) - 1}$$

$$(C_m)_{vib} = R \sum_{i=1}^{n} \frac{x_i^2 \exp(x_i)}{[\exp(x_i) - 1]^2}$$

where $n = (3\eta - 6)$ or $(3\eta - 5)$, with η equal to the number of atoms in the molecule.

magnitude of kT, the energy available to thermally excite the molecule, relative to V_0, the height of the potential barrier.[aaa] For large V_0, the rotation becomes a torsional motion and is treated as a vibration.

The relationship between the internal rotational energy levels and internal moments of inertia in the molecule are given with the other energy level expressions in Appendix 6. Starting with the energy level equation, a partition function can be written and the contribution to the thermodynamic functions can be calculated.

For restricted rotation, the thermodynamic functions can be calculated as a function of the height of the potential barrier V_0. Pitzer has assumed a potential of the form

$$V_r = \frac{1}{2} V_0(1 - \cos n_f \phi), \tag{11.136}$$

where ϕ is the rotational angle, V_0 is the height of the potential barrier and n_f is the number of equivalent orientations. The resulting energy levels and hence the partition function, are complicated, but they can be evaluated. Pitzer[2] tabulated results for the various thermodynamic quantities as a function of two variables: V_0/RT and $1/z_f$, where z_f is the value the partition function would have for a free rotator ($V_0 = 0$). His table, which is reproduced as Table A6.6 of Appendix 6, can be used to calculate the internal rotation contribution to the thermodynamic properties.

11.8e The Debye Heat Capacity Equation

In deriving the Debye heat capacity equation, one assumes that the atoms in an atomic solid are vibrating with a range or frequencies ν varying from $\nu = 0$ to a maximum $\nu = \nu_m$. The resulting equation for calculating $C_{V,m}$ is

$$\frac{C_{V,m}}{3R} = \frac{3}{(\theta_D/T)^3} \int_0^{\theta_D/T} \frac{x^4 \exp(x)}{\{\exp(x) - 1\}^2} dx, \tag{11.137}$$

where

$$x = \frac{h\nu}{kT} \tag{11.138}$$

[aaa] See Section 10.7c, Chapter 10, *Principles and Applications.*

with k as the Boltzmann constant, h as Planck's constant, and θ_D as the Debye temperature given by

$$\theta_D = \frac{h\nu_m}{k}. \tag{11.139}$$

The integral in equation (11.137) must be evaluated numerically. Table A6.7 of Appendix 6 gives the heat capacity and other thermodynamic properties as a function of θ_D/T. It can be used to obtain values for the thermodynamic properties as a function of the temperature.

High-temperature and low-temperature limiting values can be obtained analytically. At high-temperatures, the limiting value is $C_{V,m} = 3R$. At low temperatures, the heat capacity varies with temperature according to the relationship

$$C_{V,m} = \frac{12\pi^4}{5}\left(\frac{T}{\theta_D}\right)^3. \tag{11.140}$$

We have now completed our summary of the thermodynamic relationships developed in the first volume of this series, *Chemical Thermodynamics: Principles and Applications*. We will use these relationships as we apply thermodynamics to the understanding and description of chemical processes. We refer those who are interested in the details of the principles leading to the derivations and descriptions of these relationships to the earlier volume. References to the appropriate sections are given in the footnotes of this chapter.

Problems

P11.1 The first of the four fundamental equations of Gibbs {equation (11.10)} is obtained by combining equation (11.6)}, the statement of the First Law applied to the system, with equation (11.7), the Second Law statement for a reversible process, again applied to the system, and equation (11.8) that calculates reversible pressure–volume work. Start with equation (11.10) and the defining equations for H, A, and G {equations (11.1), (11.2), and (11.3)}, and derive the other Gibbs equations {equations (11.11), (11.12), and (11.13)}.

P11.2 (a) Start with the Gibbs equations and the appropriate Maxwell relation[bbb] to show that

$$\left(\frac{\partial S}{\partial p}\right)_T = -\left(\frac{\partial V}{\partial T}\right)_p.$$

(b) Start with the appropriate Gibbs equations and the result in (a) to show[ccc] that

$$\left(\frac{\partial H}{\partial p}\right)_T = V - T\left(\frac{\partial V}{\partial T}\right)_p.$$

Most of the relationships summarized in Table 11.1 are obtained in this manner.

(c) Start with the relationship $G = H - TS$, divide by T, differentiate, and make substitutions as needed from Table 11.1 to derive the Gibbs–Helmholtz equation

$$\left(\frac{\partial (G/T)}{\partial T}\right)_p = -\frac{H}{T^2}.$$

[bbb] When a differential of the form $dZ = M\,dX + N\,dY$ is exact, the coefficients are related by

$$\left(\frac{\partial M}{\partial Y}\right)_X = \left(\frac{\partial N}{\partial X}\right)_Y.$$

This relationship is known as the Maxwell relation.

[ccc] To derive the equation that follows, you will need to make use of the relationship that a total derivative with a specified variable held constant is equal to the partial derivative. For example,

$$\left(\frac{dH}{dp}\right)_T = \left(\frac{\partial H}{\partial p}\right)_T.$$

(d) The Joule–Thomson coefficient $\mu_{J.T.}$ is defined as

$$\mu_{J.T.} = \left(\frac{\partial T}{\partial p}\right)_H.$$

Use the equations summarized in Table 11.1 to show[ddd] that

$$\mu_{J.T.} = -\frac{1}{C_{p,m}}\left[V_m - T\left(\frac{\partial V_m}{\partial T}\right)_p\right].$$

P11.3 (a) Start with the Gibbs–Duhem equation written in the form of equation (11.23)

$$n_1 d\mu_1 + n_2 d\mu_2 = 0,$$

and substitute vapor fugacity for chemical potential, using the relationship in equation (11.39), to obtain the Duhem–Margules equation

$$x_1\left(\frac{\partial \ln f_1}{\partial x_1}\right)_{p,T} = x_2\left(\frac{\partial \ln f_2}{\partial x_2}\right)_{p,T}.$$

(b) Start with the Duhem–Margules equation and show that if component 1 obeys Raoult's law over the entire composition range, then component 2 must do likewise. In other words, a sufficient condition for ideal solution behavior is that one of the components must obey Raoult's law over the entire range of composition.

[ddd] To derive this expression, you will need to make use of the following relationship between partial derivatives

$$\left(\frac{\partial X}{\partial Y}\right)_Z = -\frac{\left(\frac{\partial Z}{\partial Y}\right)_X}{\left(\frac{\partial Z}{\partial X}\right)_Y}.$$

P11.4 (a) Start with the condition for phase equilibrium for a pure substance given by equation (11.24), differentiate, and combine with the appropriate Gibbs equation, to derive the Clapeyron equation

$$\frac{dp}{dT} = \frac{\Delta S_m}{\Delta V_m} = \frac{\Delta H_m}{T \Delta V_m}.$$

(b) Start with the Clapeyron equation applied to (vapor + liquid) equilibrium and derive the Clausius–Clapeyron equation

$$\ln p = -\frac{\Delta_{vap} H_m}{R}\left(\frac{1}{T}\right) + \text{const.}$$

In making the derivation, you will need to assume that (i) the molar volume of the liquid is negligible when compared to that of the gas; (ii) the gas behaves ideally; and (iii) the molar enthalpy of vaporization is constant with temperature.

P11.5 Start with the defining equations for the fugacity f and the fugacity coefficient ϕ {equations (11.36), (11.37), and (11.38)}, along with the relationships given in Table 11.1, and show that ϕ is related to the compressibility factor z by equation (11.44)

$$\ln \phi = -\int_0^p \frac{1 - z}{p} dp.$$

P11.6 (a) Start with equation (11.56) relating chemical potential to activity, differentiate with respect to p with T held constant, and apply relationships given in Table 11.1 to show that activity varies with pressure according to the equation

$$\left(\frac{\partial \ln a_i}{\partial p}\right)_T = \frac{\bar{V}_i}{RT}.$$

(b) Assume a Raoult's law standard state and an ideal solution, and start with equation (11.56) to show that

$$\mu_i - \mu_i^* = RT \ln x_i.$$

(c) Start with the equation in (b) and show that for the mixing of components to form a mole of solution, the ideal Gibbs free energy change, ideal enthalpy change, and ideal entropy change are given by

$$\Delta_{\text{mix}} G_{\text{m}}^{\text{id}} = RT \sum_i x_i \ln x_i,$$

$$\Delta_{\text{mix}} H_{\text{m}}^{\text{id}} = 0,$$

and

$$\Delta_{\text{mix}} S_{\text{m}}^{\text{id}} = -R \sum_i x_i \ln x_i.$$

P11.7 Start with equation (11.96) applied to the apparent molar volume ϕV, solve for V, and differentiate to show that ϕV is related to the partial molar volume of the solute by

$$\overline{V}_2 = \phi V + m \left(\frac{\partial \phi V}{\partial m} \right)_{T,p,n_1},$$

where m is the molality (moles of solute per fixed amount of solvent).

P11.8 (a) Start with equations (11.56) and (11.99) and derive equation (11.101)

$$\Delta_{\text{r}} G = \Delta_{\text{r}} G^\circ + RT \ln \prod_i a_i^{\nu_i}.$$

(b) Apply the condition for chemical equilibrium {equation (11.100)} to equation (11.101) and show that

$$\Delta_{\text{r}} G^\circ = -RT \ln K,$$

where K is the equilibrium constant for the reaction. Divide this equation by T, differentiate with respect to T, and use the Gibbs–Helmholtz equation to show that

$$\left(\frac{\partial \ln K}{\partial T} \right)_p = \frac{\Delta_{\text{r}} H^\circ}{RT^2}.$$

P11.9 (a) Start with equation (11.101) and the relationship between $\Delta_r G$, the free energy change for a cell reaction, and the voltage E of the cell {equation (11.125)}, and derive the Nernst equation {(equation (11.127)}.

(b) Use equation (11.125) and the relationships in Table 11.1 to derive the following equations relating the cell voltage to the thermodynamic properties:

$$\Delta_r S = nF\left(\frac{\partial E}{\partial T}\right)_p,$$

$$\Delta_r H = -nF\left[E - T\left(\frac{\partial E}{\partial T}\right)_p\right],$$

$$\Delta_r C_p = nFT\left(\frac{\partial^2 E}{\partial T^2}\right)_p,$$

and

$$\Delta_r V = -nF\left(\frac{\partial E}{\partial p}\right)_T.$$

P11.10 Use the relationships in Table 11.4 and the molecular data in Tables A6.2 to A6.4 of Appendix 6 (along with a table of atomic weights) to calculate

(a) The entropy of ideal N_2 gas at $T = 298.15$ K and $p = 0.100$ MPa.

(b) The heat capacity of N_2O ideal gas at $T = 1000$ K and $p = 1.000$ MPa. (N_2O is a linear molecule.)

References

1. The equations summarized in this chapter follow directly from the derivations presented in the first volume of this series titled *Chemical Thermodynamics: Principles and Applications*, by J. B. Ott and J. Boerio-Goates, Academic Press, London, 2000. Much of the information is also contained in the following texts: K. S. Pitzer, *Thermodynamics*, Third Edition, McGraw-Hill, Inc., New York, 1995; J. M. Honig, *Thermodynamics*, Second Edition, Academic Press, San Diego, 1999; D. Kondepudo and I. Prigogine, *Modern Thermodynamics, From Heat*

Engines to Dissipative Structures, John Wiley and Sons, Chichester, UK, 1998; P. A. Rock, *Chemical Thermodynamics*, University Science Books, Mill Valley, California, 1983; I. M. Klotz and R. M. Rosenberg, *Chemical Thermodynamics, Basic Theory and Methods*, W. A. Benjamin, Menlo Park, California, 1972.

2. K. S. Pitzer, *Thermodynamics*, McGraw-Hill, New York, 1995.

Chapter 12

Thermodynamics of Other Variables

In Chapter 11 we summarized relationships among the thermodynamic variables[a] p, V, T, U, S, H, A, and G, along with the composition variables n_1, n_2 ... In this chapter we introduce additional variables to tie our thermodynamic equations to other types of processes. Consider as a simple example, the stretching of a rubber band[b] as shown in Figure 12.1. If one takes the rubber band and introduces a stress by hanging a weight on it as shown in Figure 12.1a, and then blows hot air on the rubber band, one discovers that with the constant force, the rubber band contracts with heating.[c]

Thermodynamics can be used to understand this effect. We start with the First Law relationship

$$\mathrm{d}U = \delta q + \delta w. \tag{12.1}$$

In the reversible process

$$\delta q = T\,\mathrm{d}S \tag{12.2}$$

and

$$\delta w = -p\,\mathrm{d}V + f\,\mathrm{d}l \tag{12.3}$$

where $-p\,\mathrm{d}V$ is the pressure–volume work and $f\,\mathrm{d}l$ is the work involved in using a force f to change the length of the rubber band by an amount $\mathrm{d}l$.

---

[a] We also included in the earlier discussion, the application of thermodynamics to electrochemical cells, for which we introduced into our thermodynamic equations the work involved when a quantity of electricity flows through a cell against an electrical potential or voltage.

[b] One must use natural rubber. A synthetic rubber band will not respond like the real thing.

[c] Intuitively, one would probably expect the rubber band to sag and stretch with heating. Thermodynamics predicts otherwise, a prediction that is realized.

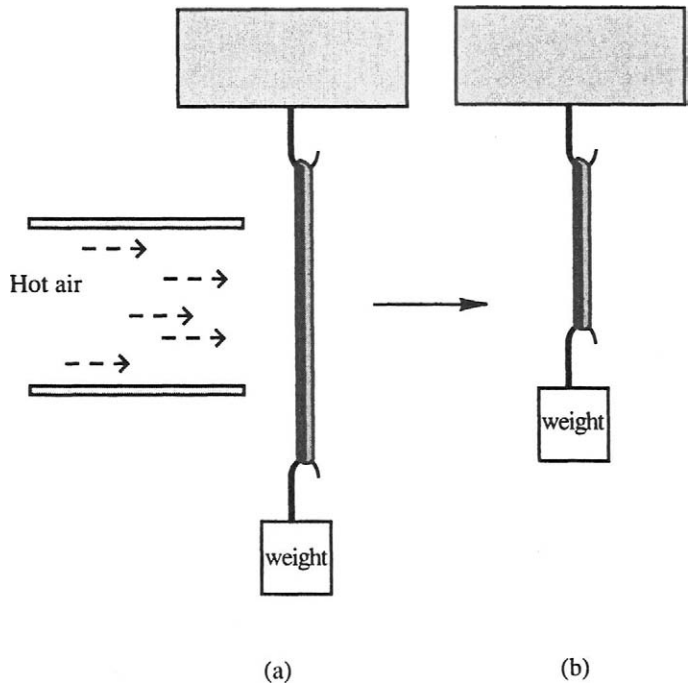

Figure 12.1 Heating a rubber band stretched by a weight causes the band to contract.

Substitution of equations (12.2) and (12.3) into equation (12.1) gives

$$dU = T\,dS - p\,dV + f\,dl. \tag{12.4}$$

We can add $d(pV)$ and subtract $d(TS)$ from both sides of equation (12.4) to get

$$dG = -S\,dT + V\,dP + f\,dl. \tag{12.5}$$

At constant T and p, equation (12.5) becomes

$$dG = f\,dl.$$

This equation is a specific example of a more general expression that relates the Gibbs free energy change to work,

$$dG = \delta w', \tag{12.6}$$

where $\delta w'$ is work other than pressure–volume work that occurs in a reversible constant temperature and constant pressure process.

Returning to equation (12.5), we can use the Maxwell relationships to write

$$\left(\frac{\partial S}{\partial l}\right)_{p,T} = -\left(\frac{\partial f}{\partial T}\right)_{p,l}. \tag{12.7}$$

But from the properties of the exact differential,

$$\left(\frac{\partial f}{\partial T}\right)_{l} = -\frac{\left(\frac{\partial l}{\partial T}\right)_{f}}{\left(\frac{\partial l}{\partial f}\right)_{T}}. \tag{12.8}$$

Substitution of equation (12.8) into (12.7) gives

$$\left(\frac{\partial S}{\partial l}\right)_{T} = \frac{\left(\frac{\partial l}{\partial T}\right)_{f}}{\left(\frac{\partial l}{\partial f}\right)_{T}}$$

$$= \left(\frac{\partial l}{\partial T}\right)_{f}\left(\frac{\partial f}{\partial l}\right)_{T}. \tag{12.9}$$

If one assumes that the rubber band obeys Hooke's law, we can write

$$f = kl$$

where k is a constant so that

$$\left(\frac{\partial f}{\partial l}\right)_{T} = k.$$

Substitution into equation (12.9) gives

$$\left(\frac{\partial S}{\partial l}\right)_T = k\left(\frac{\partial l}{\partial T}\right)_f . \tag{12.10}$$

From our experiment, we know that $(\partial l/\partial T)_f < 0$ since the length decreases as we increase the temperature. Hence, $(\partial S/\partial l)_T < 0$. This relationship can be understood from a molecular point of view. Rubber consists of long polymer molecules held together by sulfur crosslinking. Stretching the rubber lines up the strands of polymer, which increases the order and decreases the entropy. This decrease in entropy releases heat that increases the temperature of the rubber until the heat is removed.

Equation (12.4) can be generalized to include any type of work that may occur in a process. We can write

$$\mathrm{d}G = -S\,\mathrm{d}T + V\,\mathrm{d}p + \sum \phi_i\,\mathrm{d}\xi_i \tag{12.11}$$

where $\mathrm{d}\xi_i$ is a generalized displacement against a generalized force ϕ_i. When chemical work is involved, equation (12.11) becomes

$$\mathrm{d}G = -S\mathrm{d}T + V\mathrm{d}p + \sum \mu_i \mathrm{d}n_i$$

where $\mathrm{d}n_i$ is the displacement of moles in a chemical process resulting from a chemical potential μ_i.

Equation (12.11) can be derived in a different manner that helps in understanding the nature of ϕ_i. We start with

$$G = f(p, T, \xi_1, \xi_2, \ldots)$$

so that

$$\mathrm{d}G = \left(\frac{\partial G}{\partial T}\right)_{p,\xi} \mathrm{d}T + \left(\frac{\partial G}{\partial p}\right)_{T,\xi} \mathrm{d}p + \sum_i \left(\frac{\partial G}{\partial \xi_i}\right)_{p,T,\xi_{j\neq i}} \mathrm{d}\xi_i . \tag{12.12}$$

Comparing coefficients between equations (12.11) and (12.12) shows that

$$\left(\frac{\partial G}{\partial T}\right)_{p,\xi} = -S \tag{12.13}$$

$$\left(\frac{\partial G}{\partial p}\right)_{T,\xi} = V \tag{12.14}$$

$$\left(\frac{\partial G}{\partial \xi_i}\right)_{p,T,\xi_{j\neq i}} = \phi_i\,. \tag{12.15}$$

Thus, the generalized potential is the derivative of G with respect to the generalized displacement as given by equation (12.15).

Our plan is to apply equation (12.11) {or equation (12.12)} to a variety of processes. In each case, we will write an expression for $\phi_i\ \mathrm{d}\xi_i$ that is consistent with the work done in the process.

12.1 Effect Of Gravitational Fields

A gravitational field affects the chemical potential of a system. The work required to displace a sample vertically against the earth's gravitational field is given by

$$\delta w' = mg\ \mathrm{d}h,$$

where mg is the force, with m as the mass of the sample, g is the gravitational constant, and $\mathrm{d}h$ is the displacement against the force. Hence, $\mathrm{d}\xi = \mathrm{d}h$ and $\phi = mg$, and equation (12.11) for one mole of sample ($\mathrm{d}G = \mathrm{d}\mu, m = M$, the molecular weight) becomes

$$\mathrm{d}\mu = -S_\mathrm{m}\ \mathrm{d}T + V_\mathrm{m}\ \mathrm{d}p + Mg\ \mathrm{d}h. \tag{12.16}$$

12.1a Effect of Height on Atmospheric Pressure

Equation (12.16) can be used to derive an expression relating the change in atmospheric pressure to the distance above the surface of the earth. We will assume that temperature is constant ($\mathrm{d}T = 0$), and that equilibrium is present so that $\mathrm{d}\mu = 0$, in which case, equation (12.16) becomes

$$V_\mathrm{m}\ \mathrm{d}p + Mg\ \mathrm{d}h = 0.$$

If we assume the atmosphere is an ideal gas, we can write

$$V_m = \frac{RT}{p}.$$

Substituting into the above equation gives

$$\frac{RT}{p}\,dp + Mg\,dh = 0.$$

Integrating, assuming g does not change with h gives

$$\ln\frac{p}{p_\circ} = -\frac{Mgh}{RT}$$

or

$$p = p_\circ \exp(-Mgh/RT) \tag{12.17}$$

where $p_\circ$ is the pressure at the surface of the earth ($h = 0$). Equation (12.17) is known as the **barometric formula**. It predicts an exponential decrease in pressure with height. For example, at a height of 9 km (approximately the elevation at the top of Mount Everest), equation (12.17) calculates a value $p/p_\circ = 0.32$. In making this calculation,[d] we have assumed T is constant at 273.15 K and the average molecular weight of air is 0.029 kg · mol^{-1}.

12.1b Effect of Gravity on Composition

In a solution, the equilibrium concentration (mole fraction x_2) of solute is affected by the gravitational field and varies with height h. To find this effect we write

$$\mu_2 = f(p, T, h, x_2) \tag{12.18}$$

[d] The barometric formula is not very reliable for calculating the "actual" atmospheric pressure p, since T is far from constant with elevation, and M and g also vary. It gives a poor approximation at best. Experimental values for $p/p_\circ$ at the top of Mount Everest are approximately 0.31. The agreement with the value calculated above from the barometric formula is somewhat fortuitous.

where μ_2 is the chemical potential of the solute. Starting with equation (12.18), we can write

$$d\mu_2 = \left(\frac{\partial \mu_2}{\partial p}\right)_{T,h,x_2} dp + \left(\frac{\partial \mu_2}{\partial T}\right)_{p,h,x_2} dT + \left(\frac{\partial \mu_2}{\partial h}\right)_{p,T,x_2} dh + \left(\frac{\partial \mu_2}{\partial x_2}\right)_{p,T,h} dx_2 \tag{12.19}$$

where $d\mu_2$ is the change in chemical potential. At constant temperature, $dT = 0$, and at equilibrium, $d\mu_2 = 0$. Also, $(\partial \mu_2/\partial p)_{T,h,x_2} = \bar{V}_2$, the partial molar volume of the solute in the solution, and from equation (12.16), $(\partial \mu_2/\partial h)_{p,T,x_2} = M_2 g$, where M_2 is the molecular weight of the solute. Substitution of these relationships into equation (12.19) gives

$$\bar{V}_2\, dp + M_2 g\, dh + \left(\frac{\partial \mu_2}{\partial x_2}\right)_{T,p,h} dx_2 = 0. \tag{12.20}$$

Equation (12.20) can be applied to an ideal solution for which

$$\left(\frac{\partial \mu_2}{\partial x_2}\right)_{p,T,h} = \frac{RT}{x_2}$$

and

$$\bar{V}_2 = V^*_{m,2}.$$

The hydrostatic pressure in the solution is related to the height by

$$dp = -\rho g\, dh$$

where ρ is the density of the solution. In the ideal solution, ρ is given by

$$\rho = \frac{x_1 M_1 + x_2 M_2}{x_1 V^*_{m,1} + x_2 V^*_{m,2}}$$

where M_1 and M_2 are the molecular weights of the solvent and solute and $V^*_{m,1}$ and $V^*_{m,2}$ are the molar volumes. Substitution of these relationships into equation (12.20) gives an equation for the concentration gradient

$$\frac{dx_2}{dh} = \left(\frac{V^*_{m,1}M_1 - V^*_{m,2}M_2}{V^*_{m,1}x_1 + V^*_{m,2}x_2}\right) \cdot \left(\frac{gx_1x_2}{RT}\right). \tag{12.21}$$

Equation (12.21) can be integrated to relate x_2 to h. However, it will serve our purpose to calculate dx_2/dh to show that the effect of a gravitational field on concentration is usually negligibly small. For example, in an equimolar solution of ethanol (2) in water (1) at $T = 298.15$ K[e]

$$V^*_{m,1} = \frac{0.01802 \text{ kg} \cdot \text{mol}^{-1}}{0.9970 \times 10^3 \text{ kg} \cdot \text{m}^{-3}} = 1.807 \times 10^{-5} \text{ m}^3 \cdot \text{mol}^{-1}$$

$$V^*_{m,2} = \frac{0.04607 \text{ kg} \cdot \text{mol}^{-1}}{0.7851 \times 10^3 \text{ kg} \cdot \text{m}^{-3}} = 5.868 \times 10^{-5} \text{ m}^3 \cdot \text{mol}^{-1}$$

$$R = 8.314 \text{ J} \cdot \text{K}^{-1} \cdot \text{mol}^{-1}$$

$$g = 9.80 \text{ m} \cdot \text{sec}^{-1}$$

$$x_1 = x_2 = 0.500.$$

Substitution into equation (12.21) gives

$$\frac{dx_2}{dh} = -6.12 \times 10^{-5} \text{ m}^{-1}.$$

The interpretation of our answer is that the ethanol solute, which has a higher molecular weight than the water solvent, concentrates at the bottom of the solution (near $h = 0$), but the effect is very small. Qualitatively, this would be true for any solute, unless the height of the column of solution or the molecular weight of the solute becomes large. The height h does become large in the oceans, and concentration gradients could become significant there, although

[e] As we have seen earlier, the ideal solution approximation is not a very good one for (ethanol + water) mixtures. Thus, our quantitative calculation is only approximate, but the qualitative interpretation is valid, since the effect in a real solution will not differ greatly (certainly not orders of magnitude) from that in the ideal solution.

other problems occur, such as temperature variation with depth and non-equilibrium conditions, so that equation (12.21) only approximates the behavior. Significant concentration gradients could also result for large molecular weight solutes such as polymers or polypeptides.

A better approach to produce a significant concentration gradient in a solution involves increasing the force by substituting a centrifugal field for a gravitational field, an effect that we will now consider.

12.2 Effect Of Centrifugal Fields

In the ultracentrifuge, solutions can be rotated at speeds up to 80,000 revolutions per minute, which provides force fields larger than the force of gravity by a factor of 3×10^5. Under these conditions, much larger concentration gradients can be obtained.

The ultracentrifuge can be used to separate fractions of different molecular weights in a mixture of solutes and to determine the molecular weight of a solute. Two different approaches can be taken. In the sedimentation velocity approach, the change in the concentration profile with time is determined during the centrifugation process. This nonequilibrium process requires a knowledge of diffusion rates and is not based directly on thermodynamics. We will leave a discussion of this process to other texts.

In the sedimentation equilibrium method, the solution is allowed to come to equilibrium. When this happens, the analysis becomes very similar to that described in the previous section for gravitational fields, with the gravitational work $mg\mathrm{d}h$ replaced by $m\omega^2 r\mathrm{d}r$, where ω is the angular velocity of the centrifuge (in rad $\cdot$ sec^{-1}) and r is the distance from the center of the centrifuge. The final result is an equation similar to (12.21)

$$\frac{\mathrm{d}x_2}{\mathrm{d}r} = -\frac{M_2(1 - V^*_{\mathrm{m},1}\rho)\omega^2 r x_2}{RT}. \tag{12.22}$$

Integration gives

$$\ln\frac{c_2}{c_1} = -\frac{M_2(1 - V^*_{\mathrm{m},1}\rho)\omega^2(r_2^2 - r_1^2)}{2RT} \tag{12.23}$$

where r_1 and r_2 are the radial distances at which the concentrations of the solute are c_1 and c_2. In equation (12.23), c_1 and c_2 can be expressed in mol $\cdot$ dm^{-3} (or kg $\cdot$ dm^3) instead of mole fractions, since the ratio of molarities expressed in this manner and the mole fraction ratio are the same.

Equation (12.23) can be solved for M_2 to give a method for obtaining a (mass-average) molecular weight for the solute. The result is

$$M_2 = \frac{2\,RT\ln(c_1/c_2)}{(1 - V^*_{m,1}\rho)\omega^2(r_2^2 - r_1^2)}. \tag{12.24}$$

To employ equation (12.24), after running the centrifuge, the solution is sampled at the two distances r_1 and r_2, and the corresponding concentrations c_1 and c_2 are determined. A disadvantage of this method is that the time required to achieve equilibrium in the sample may be so long that the procedure is inconvenient to use, especially if the molecular weight of the solute is greater than 5×10^3 kg · mol^{-1}. This disadvantage can be overcome by sampling at the top meniscus and at the bottom of the cell, shortly after the centrifuge is brought to speed. Even though equilibrium has not been established throughout the cell, at the top and the bottom, changes in concentration cannot occur during the sedimentation process, so that the equilibrium condition is present in these sections immediately after the centrifuge is turned on.

12.2a Density-Gradient Centrifugation

A useful modification of equilibrium centrifugation involves spinning a concentrated salt solution in which the salt has a high molar mass, such as CsCl. A concentration gradient of the salt is generated, which in turn results in a density gradient in the solution.

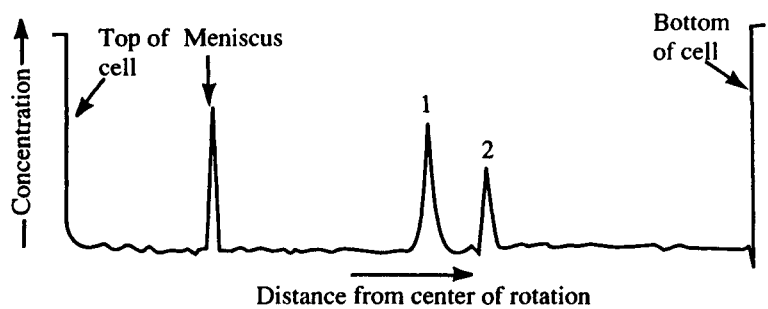

Figure 12.2 Separation of DNA samples by density-gradient centrifugation. Peak #1 is the DNA molecule containing ^{14}N, while peak #2 contains ^{15}N. Reprinted by permission from I. Tinoco, Jr., K. Sauer, and J. C. Wang, *Physical Chemistry. Principles and Applications in Biological Science*, Prentice Hall, Upper Saddle River, New Jersey, 1995, p. 292.

If a mixture of macromolecular species is also present in the solution, it will distribute itself in the centrifuge tube at r values where the density is right to make macromolecules of a certain mass "buoyant," and more dense macromolecules sink while those less dense float. The result is that macromolecules of a certain mass, initially uniformly distributed throughout the cell before sedimentation, will concentrate at a point. Macromolecules of a different density will collect at another position. The consequence is the separation of a mixture of macromolecular solutes of different molecular weights into a series of bands at different r values.

As an example, Figure 12.2 show the concentration of two DNA species in a CsCl solution. The initial solution had a density of 1.739 $g \cdot cm^3$. After spinning at 44,776 revolutions per minute at 298.15 K, the DNA species form two sharp bands. Species 1 is a bacterial virus DNA with a molecular weight of 2×10^4 $kg \cdot mol^{-1}$. Species 2 is the same DNA except that it contains the ^{15}N isotope rather than ^{14}N.

12.3 Thermodynamics Of Surfaces

When two phases such as (solid + liquid), (liquid + gas), (solid + gas), (solid + solid), or (liquid + liquid) are brought together, a boundary known as a surface or interface is present. To date we have used our thermodynamic relationships to describe only the bulk properties of a substance and considered the surface properties to be negligible.

The surface does have quite different properties than the bulk phases, and its effect can be disregarded only if the surface area A_s is small so that it makes only a negligible contribution to the properties of the system. This is usually the case. However, in some circumstances, A_s can become large, as for finely divided particles or droplets, and the effect of the surface cannot be ignored. As an example, Giauque and Archibald[1] measured the low-temperature heat capacities of crystalline MgO and finely divided MgO obtained from decomposing $Mg(OH)_2$. They found that heat capacity values for the powder were 6% higher at 90 K than for the crystals. They attributed this difference to surface effects resulting from the large surface area of the powdery sample.

We now want to use our thermodynamic relationships to describe this boundary or interface that we call the surface. As we do so, we should keep in mind that the change in properties in moving from one phase to another is not two-dimensional.[f] There is a small, but finite, thickness to the region in which the properties change from those on the interior of one phase to those on the interior of the other phase. There is every reason to believe that the thickness

[f] We will, however, define the position of the surface so that the surface volume is zero.

of the region is small — only a few molecular layers thick, but certainly not zero.[g,2]

12.3a A One-Component System

To start our discussion of the effect of surfaces, consider a pure substance in a closed system (n does not change) with a flat surface area A_s. If we change A_s by an amount dA_s, then the work done $\delta w'$ is given by

$$\delta w' = \gamma \, dA_s \tag{12.25}$$

where γ is the surface tension. As we saw earlier, $\delta w'$ is related to the Gibbs free energy by

$$dG = \delta w'. \tag{12.6}$$

Hence

$$dG_{T,p} = \gamma \, dA_s \tag{12.26}$$

or

$$\left(\frac{\partial G}{\partial A_s}\right)_{T,p,n} = \gamma. \tag{12.27}$$

We can also arrive at equation (12.27) by writing

$$G = f(p, T, A_s)$$

so that

$$dG = \left(\frac{\partial G}{\partial T}\right)_{p,A_s,n} dT + \left(\frac{\partial G}{\partial p}\right)_{T,A_s,n} dp + \left(\frac{\partial G}{\partial A_s}\right)_{p,T,n} dA_s. \tag{12.28}$$

But $(\partial G/\partial p)_{T,A_s,n} = V$ and $(\partial G/\partial T)_{p,A_s,n} = -S$ so that

$$dG = -S \, dT + V \, dp + \left(\frac{\partial G}{\partial A_s}\right)_{p,T,n} dA_s. \tag{12.29}$$

---

[g] For the (liquid + gas) interface, the thickness increases as one approaches the critical point, and may be significantly thicker near that temperature.

It is apparent in comparing[h] equations (12.26) and (12.29) that

$$\gamma = \left(\frac{\partial G}{\partial A_s}\right)_{T,p,n}.$$

---

[h] The surface tension can also be defined in terms of A, H, or U (here A is the Helmholtz free energy). One can start with

$$A = f(V, T, A_s)$$

to write

$$dA = \left(\frac{\partial A}{\partial T}\right)_{V,A_s,n} dT + \left(\frac{\partial A}{\partial p}\right)_{T,A_s,n} dp + \left(\frac{\partial A}{\partial A_s}\right)_{p,V,n} dA_s.$$

But $(\partial A/\partial T)_{V,A_s,n} = -S$ and $(\partial A/\partial V)_{T,A_s,n} = -p$. Hence

$$dA = -S\,dT - p\,dV + \left(\frac{\partial A}{\partial A_s}\right)_{p,V,n} dA_s. \tag{12.30}$$

Adding $d(pV)$ to both sides of equation (12.30) gives

$$dG = -S\,dT + V\,dp + \left(\frac{\partial A}{\partial A_s}\right)_{p,V,n} dA_s. \tag{12.31}$$

Comparing coefficients between equations (12.29) and (12.31) gives

$$\left(\frac{\partial A}{\partial A_s}\right)_{V,T,n} = \left(\frac{\partial G}{\partial A_s}\right)_{p,T,n} = \gamma.$$

Comparable expressions can be obtained involving H and U to show that

$$\gamma = \left(\frac{\partial G}{\partial A_s}\right)_{p,T,n} = \left(\frac{\partial A}{\partial A_s}\right)_{V,T,n} = \left(\frac{\partial H}{\partial A_s}\right)_{S,p,n} = \left(\frac{\partial U}{\partial A_s}\right)_{S,V,n}. \tag{12.32}$$

The situation is in many ways comparable to the alternate definitions for chemical potential μ_i given by

$$\mu_i = \left(\frac{\partial G}{\partial n_i}\right)_{T,p,n_{j\neq i}} = \left(\frac{\partial A}{\partial n_i}\right)_{T,V,n_{j\neq i}} = \left(\frac{\partial H}{\partial n_i}\right)_{S,p,n_{j\neq i}} = \left(\frac{\partial U}{\partial n_i}\right)_{S,V,n_{j\neq i}}.$$

For a pure substance, we will represent the surface free energy per unit surface area[i] as g^s and define it as $(\partial G/\partial A_s)_{T,p,n}$. Thus

$$g^s = \gamma \tag{12.33}$$

is the free energy per unit area. Applying the thermodynamic relationship $(\partial G/\partial T)_p = -S$ to the surface free energy gives

$$\left(\frac{\partial g^s}{\partial T}\right)_{p,n} = -s^s \tag{12.34}$$

or

$$\left(\frac{\partial \gamma}{\partial T}\right)_{p,n} = -s^s, \tag{12.35}$$

where S^s is the surface entropy.

The surface enthalpy h^s is then obtained from the relationship $G = H - TS$, so that

$$h^s = g^s + Ts^s. \tag{12.36}$$

Later, we will define the surface boundary so that the surface volume for a pure substance is zero, in which case, $h^s = u^s$, and equation (12.36) is often rewritten in terms of the surface energy

$$u^s = g^s + Ts^s \tag{12.37}$$

or

$$u^s = \gamma - T\left(\frac{\partial \gamma}{\partial T}\right)_{p,n}. \tag{12.38}$$

---

[i] We will follow the IUPAC recommendation that surface properties per unit surface area be represented by the lower case (g = Gibbs free energy, u = energy, h = enthalpy, etc.) with a superscript s designating that the property is for the surface. The quantities g^s, u^s, h^s ... for the surface are in many ways comparable to molar properties (or partial molar properties for mixtures) in the bulk phase.

As an example of the application of equation (12.38), Figure 12.3 shows a graph of γ against T for CCl_4, along with u^s calculated from this equation using the γ values and the slope of the γ against T curve. We note that both γ and u^s become zero at the critical point of CCl_4 where liquid and gas become indistinguishable.

The surface heat capacity can be obtained from

$$\left(\frac{\partial u^s}{\partial T}\right)_{V,p} = c_V^s. \tag{12.39}$$

Since $u^s = h^s$, distinctions are not made between c_V^s and c_p^s and

$$\left(\frac{\partial h^s}{\partial T}\right)_{p \text{ or } V} = \left(\frac{\partial u^s}{\partial T}\right)_{p \text{ or } V} = c_V^s = c_p^s. \tag{12.40}$$

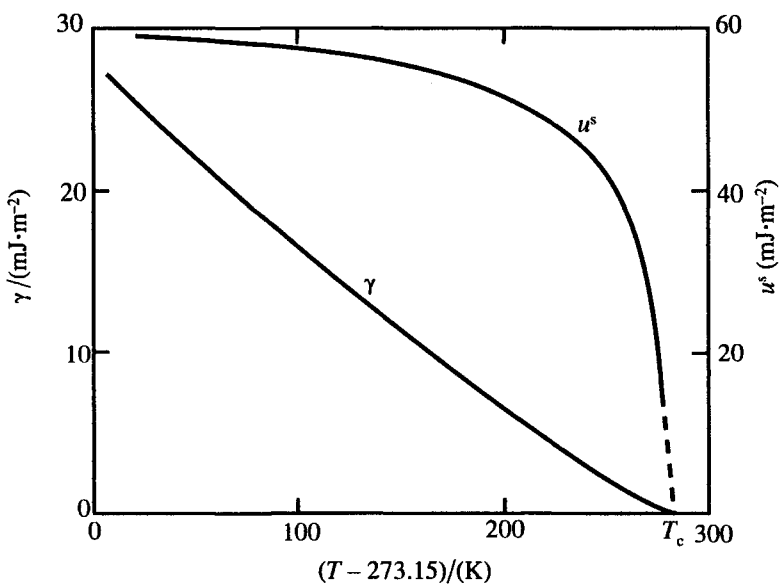

Figure 12.3 Variation of surface tension γ and total surface energy u^s with temperature for CCl_4. Both γ and u_s become zero at the critical temperature. Reprinted with permission from A. K. Adamson and A. P. Gast, *Physical Chemistry of Surfaces*. © by John Wiley and Sons, Inc., 1977.

Differentiating equation (12.38) gives

$$c_V^s = c_p^s = -T\left(\frac{\partial^2\gamma}{\partial T^2}\right)_p. \tag{12.41}$$

To calculate the surface thermodynamic properties from equations (12.33) to (12.41), we must know how γ changes with T. Equation (12.42) is a semi-empirical equation that has been used to relate γ and T. It is given by

$$\gamma = \gamma_0\left(1 - \frac{T}{T_c}\right)^n, \tag{12.42}$$

where n is an exponential factor and γ_0 is an empirical constant that may be thought of as the surface tension of a supercooled liquid at 0 Kelvin. This equation was first proposed by van der Waals in 1894 and developed further by Guggenheim.[3] The exponential coefficient n is 11/9 for many organic liquids, in which case, equation (12.42) becomes

$$\gamma = \gamma_0\left(1 - \frac{T}{T_c}\right)^{11/9}. \tag{12.43}$$

Using this equation, it is easy to show[j] that

$$s^s = \frac{11}{9}\frac{\gamma_0}{T_c}\left(1 - \frac{T}{T_c}\right)^{2/9}. \tag{12.44}$$

Equation (12.38) can then be used to show that

$$u^s = \gamma_0\left(1 - \frac{T}{T_c}\right)^{2/9}\left(1 + \frac{2}{9}\frac{T}{T_c}\right). \tag{12.45}$$

Other equations can be used. An old and well-known relationship attributed to Eötvös[4] is

$$\gamma V_m^{2/3} = k(T_c - T) \tag{12.46}$$

---

[j] See Problem P12.2 at the end of the chapter.

where V_m is the molar volume of the bulk phase and T_c is the critical temperature.[k] For many substances, the constant k has a value of 2.1×10^{-7} J · K^{-1}. A useful empirical equation that can be used for metals is

$$\gamma_m = \frac{3.6\ T_m}{V_m^{2/3}}$$

where m denotes the value at the melting temperature and γ_m is in mJ · cm^{-2}.

12.3b The Effect of Curvature On Surface Properties

To date we have limited our discussion to plane surfaces of pure substances. We now look at the effect of curvature on the properties of these surfaces. Specifically, we will derive relationships to obtain the difference in the thermodynamic properties of a flat surface or the bulk phase, and of small droplets. In doing so, we will assume γ is not affected by surface curvature. This assumption is justified as long as the radius of curvature is large compared with the thickness of the surface layer. We mentioned earlier that usually the surface has a thickness of only a few molecules; that is, it is of the order of a micrometer. Thus, curved surfaces with a radius greater than a few micrometers should follow the equations we derive.

We will first derive a relationship between the pressure p' within a drop and $p°$, the pressure outside, and show that p' is greater than $p°$. Consider a process in which a volume dV of liquid from a bulk phase (flat surface) is moved to the interior of a drop of radius r. The work of transfer is simply $(p' - p°)\ \mathrm{d}V$, which must equal the work of extending the surface by $\gamma \mathrm{d}A_s$. That is

$$(p' - p°)\ \mathrm{d}V = \gamma\ \mathrm{d}A_s. \tag{12.47}$$

For a sphere, $V = \frac{4}{3}\pi r^3$ and $A_s = 4\pi r^2$ so that $\mathrm{d}V = 4\pi r^2 \mathrm{d}r$ and $\mathrm{d}A_s = 8\pi r\ \mathrm{d}r$. Substitution into equation (12.47) gives

$$p' - p° = \frac{2\gamma}{r}. \tag{12.48}$$

---

[k] Equations (12.42) and (12.46) predict, as expected, that $\gamma \to 0$ as $T \to T_c$. Experimental evidence indicates that this begins to happen at a somewhat lower temperature than given by these equations. A modification to equation (12.46) suggested by W. Ramsay and J. Sheilds, *J. Chem. Soc.*, **63**, 1089 (1893) replaces T_c by $(T_c - 6)$. In either form the value of k is about the same.

Equation (12.48) is known as the Laplace equation.[l] The equation assumes a spherical drop. A more general form is

$$p' - p^\circ = \gamma\left(\frac{1}{r_1} + \frac{1}{r_2}\right) \tag{12.49}$$

where r_1 and r_2 are the principal radii of curvature.[m]

Equations (12.48) and (12.49) apply to a "filled" drop. The excess pressure within a bubble is twice this value because both the inner and outer surfaces of the thin liquid film make a contribution given by equation (12.48).[n]

We can also calculate the effect of droplet size on the vapor pressure of a liquid.[o] Consider the process shown in Figure 12.4 in which dn moles of fluid are transferred from a bulk phase where the chemical potential is μ_0 to a spherical drop of radius r where the chemical potential is μ. The work required for the

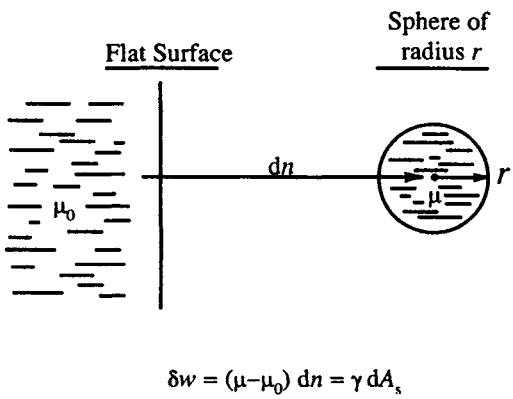

Figure 12.4 Work resulting from the transfer of dn moles from a flat surface where the chemical potential is μ_0 to a sphere of radius r where the chemical potential is μ.

---

[l] The beginning of the study of surface effects is old. Equation (12.48) was first reported in 1806 by P. S. Laplace in his celebrated *Mécanique céleste*, while W. Thomson (Lord Kelvin) reported equation (12.49) in *Proc. Roy. Soc. (London)*, **9**, 255 (1858).

[m] We refer the reader to a calculus text for the definition of radius of curvature. For a sphere, $r_1 = r_2$, and equation (12.49) reduces to equation (12.48). For a cylindrical surface, r_1 is the cylinder radius and $r_2 = \infty$. For a plane surface, $r_1 = r_2 = \infty$, in which case, $p' = p^\circ$.

[n] An interesting conclusion to be obtained from equation (12.48) applied to a bubble is that the smaller the bubble, the greater the pressure of the air inside relative to that outside.

[o] We are still considering only one component. Thus, the vapor pressure difference we calculate is for a pure substance.

transfer dn is $(\mu - \mu_0)\, dn$, and this must equal $\gamma\, dA_s$, the work of expansion of the drop. Thus,

$$(\mu - \mu_0)\, dn = \gamma dA_s. \tag{12.50}$$

The change in moles is related to a change in volume by

$$dV = V_m\, dn,$$

and from the geometry of a sphere

$$dA_s = \frac{2\, dV}{r}.$$

Combining equations gives

$$\mu - \mu_0 = \frac{2V_m\gamma}{r}. \tag{12.51}$$

The difference in chemical potential can be related to vapor fugacities by

$$\mu - \mu_0 = RT \ln \frac{f}{f_0} \tag{12.52}$$

where f_0 is the vapor fugacity of the bulk phase.

Combining gives

$$\ln \frac{f}{f_0} = \frac{2V_m\gamma}{RTr}. \tag{12.53}$$

With the approximation that vapor fugacity f or f_0 can be replaced by vapor pressure p or p_0, we get

$$\ln \frac{p}{p_0} = \frac{2V_m\gamma}{RTr}. \tag{12.54}$$

We note from equation (12.54) that p increases with decreasing r. For example, for water at $T = 298.15$ K, where $\gamma = 72.88\ \text{mJ} \cdot \text{m}^{-2}$ and $V_m = 1.80 \times 10^{-5}\ \text{m}^3 \cdot \text{mol}^{-1}$, a 10 nm droplet would have an increased vapor pressure

given by

$$\ln \frac{p}{p_0} = \frac{(2)(1.80 \times 10^{-5})(72.88 \times 10^{-3})}{(8.314)(293.15)(10 \text{ nm} \times 10^{-9}\text{m.nm}^{-1})}$$

$$= 1.08 \times 10^{-1},$$

or

$$\frac{p}{p_0} = 1.11.$$

The effect is not large, but helps explain why large droplets grow at the expense of small droplets in a system such as a fog.[p]

12.3c Surface Effects for Mixtures

We now want to consider the effect of multiple components on the thermodynamic properties of the interface. We will first generalize to any number of solutes, but eventually we will limit our treatment to binary mixtures.

Surface Concentration With mixtures, composition becomes a variable and we must first define and describe surface concentration. Then we will be ready to consider other thermodynamic properties. We will designate the surface concentration of the ith component in a mixture as Γ_i and note that Γ_i is the moles of component i per unit area (as contrasted to moles per unit volume in the bulk phases). To define Γ_i, let us take as our system, a region containing two phases I and II, along with a flat surface A_s that separates the two phases. The change in the bulk phase concentration as a function of distance perpendicular to the surface is shown schematically in Figure 12.5. We note that the higher concentration in phase I changes over a distance to a lower value in phase II. To separate the phases, let us imagine a plane at some location such as y' that is parallel to the surface. For the present, the location of this plane is arbitrary. With this plane as a boundary, we will designate the volume of phase I as V'_{I} while the volume of phase II will be V'_{II}. We note from the figure that the total volume V is given by $V = V'_{\text{I}} + V'_{\text{II}}$. Thus, the surface has no volume. Having established this division between the two phases, we can define and calculate the surface concentration of a component. The surface concentration Γ'_i for

[p] In a similar manner, solutes in solution show increased solubility with decreasing particle size. Coagulation of precipitates through digestion is aided by this effect.

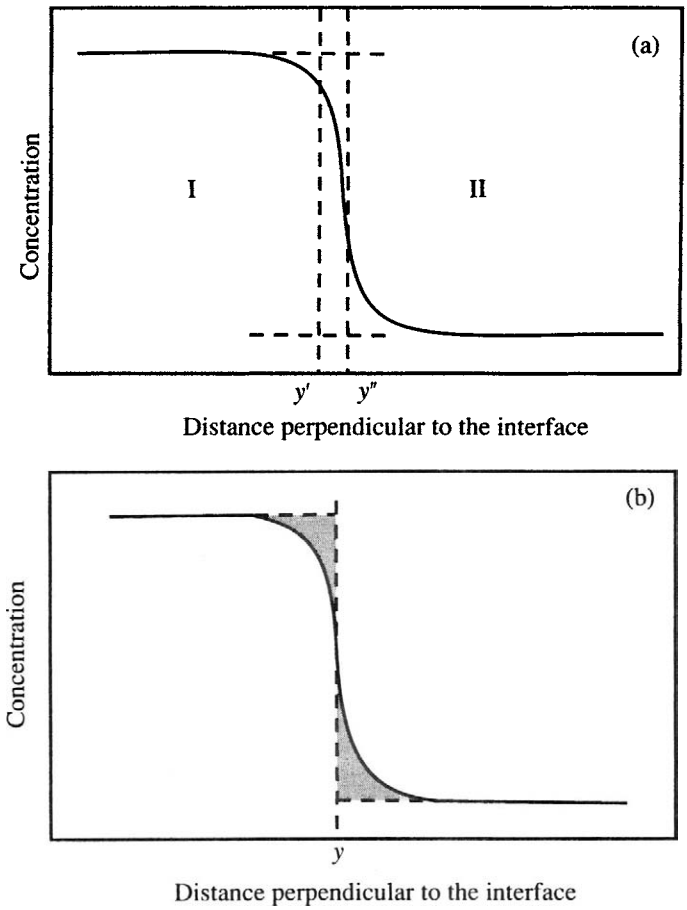

Figure 12.5 Concentration as a function of distance perpendicular to the surface is given by the solid curve. The surface concentration is the difference in area between the curve and the dashed rectangular path if the concentration is constant on each side of surfaces y' and y''. The surface plane at y corresponding to zero surface concentration is obtained by making the indicated areas equal.

component i is obtained from the excess in the number of moles of component i over that calculated for the bulk phases. That is

$$\Gamma'_i A_s = n_i - c_{\mathrm{I},i} V'_{\mathrm{I},i} - c_{\mathrm{II},i} V'_{\mathrm{II},i} \tag{12.55}$$

where n_i is the total number of moles[q] of component i and $c_{\mathrm{I},i}$ and $c_{\mathrm{II},i}$ are the molar concentrations of component i in the two bulk phases (moles $\cdot$ dm^{-3}).

[q] We will work with a closed system so that n_i does not change.

The surface concentration defined in this manner depends upon the location of the dividing plane y'. This can be seen by considering another dividing plane at position y''. Now the volume assigned to phase I is increased by $(y'' - y')A_s$ while the volume of phase II decreases by the same amount. Substitution into equation (12.55) shows that the surface concentration, now given by Γ_i'', differs from Γ_i' by the amount

$$(\Gamma_i'' - \Gamma_i') = (c_{\mathrm{II},i} - c_{\mathrm{I},i})(y'' - y'). \tag{12.56}$$

Thus, Γ_i depends upon the location of the dividing plane unless $c_{\mathrm{II},i} = c_{\mathrm{I},i}$.

In considering the thermodynamics properties associated with a surface, it is convenient to choose a position for the dividing plane that makes the surface concentration zero. For a single component (pure substance), it is possible to do this. From equation (12.55), we can show that this occurs when the two areas in Figure 12.5b are equal. This will be our choice for the phase boundary for a pure substance. With two or more components, in general it is not possible to make more than one Γ_i equal to zero. In this case, we usually choose the boundary to make Γ_1 the surface concentration of the solvent zero. With this choice, Γ_i for a solute will not be zero unless $c_{\mathrm{I},i} = c_{\mathrm{II},i}$.

Thermodynamic Properties of the Surface Consider two bulk phases I and II in equilibrium and separated by a surface of area A_s. For the thermodynamic variables $Z = U$, H, A or G, we define the surface quantity Z^s as the excess over the amount for the bulk phases. That is

$$U^s = U - U_{\mathrm{I}} - U_{\mathrm{II}} \tag{12.57}$$

$$H^s = H - H_{\mathrm{I}} - H_{\mathrm{II}} \tag{12.58}$$

$$S^s = S - S_{\mathrm{I}} - S_{\mathrm{II}} \tag{12.59}$$

$$A^s = A - A_{\mathrm{I}} - A_{\mathrm{II}} \tag{12.60}$$

$$G^s = G - G_{\mathrm{I}} - G_{\mathrm{II}} \tag{12.61}$$

$$n_1^s = n_1 - n_{\mathrm{II}1} - n_{\mathrm{III}} \tag{12.62}$$

$$n_2^s = n_2 - n_{\mathrm{I}2} - n_{\mathrm{II}2}$$

. . . .

$$n_i^s = n_i - n_{\mathrm{I}i} - n_{\mathrm{II}i} \tag{12.63}$$

. . . .

$$n_C^s = n_C - n_{\mathrm{I}C} - n_{\mathrm{II}C}$$

where C is the number of components. We have not written an equivalent expression for volume, since we have already shown that $V^s = 0$, since $(V = V_I + V_{II})$.

We can obtain equations relating Z to Γ and γ by starting with

$$U = f(S, V, A_s, n_1, n_2, \ldots),$$

$$H = f(S, p, A_s, n_1, n_2, \ldots),$$

$$A = f(V, T, A_s, n_1, n_2, \ldots),$$

$$G = f(p, T, A_s, n_1, n_2, \ldots),$$

and the defining equations for surface tension and chemical potential. The result is

$$dU = T\,dS - p\,dV + \gamma\,dA_s + \sum_i \mu_i\,dn_i \tag{12.64}$$

$$dH = T\,dS + V\,dp + \gamma\,dA_s + \sum_i \mu_i\,dn_i \tag{12.65}$$

$$dA = -S\,dT - p\,dV + \gamma\,dA_s + \sum_i \mu_i\,dn_i \tag{12.66}$$

$$dG = -S\,dT + V\,dp + \gamma\,dA_s + \sum_i \mu_i\,dn_i \tag{12.67}$$

where, as we have seen earlier [equation (12.32)],

$$\gamma = \left(\frac{\partial U}{\partial A_s}\right)_{S,V,n} = \left(\frac{\partial H}{\partial A_s}\right)_{S,p,n} = \left(\frac{\partial A}{\partial A_s}\right)_{T,V,n} = \left(\frac{\partial G}{\partial A_s}\right)_{T,p,n}. \tag{12.68}$$

Applying the conditions of exactness (Maxwell's relations) to equations (12.64) and (12.67) gives

$$\left(\frac{\partial S}{\partial A_s}\right)_{T,V,n} = -\left(\frac{\partial \gamma}{\partial T}\right)_{V,A_s,n} \tag{12.69}$$

$$\left(\frac{\partial p}{\partial A_s}\right)_{T,V,n} = -\left(\frac{\partial \gamma}{\partial V}\right)_{T,A_s,n} \tag{12.70}$$

$$\left(\frac{\partial \mu_i}{\partial A_s}\right)_{T,V,n} = -\left(\frac{\partial \gamma}{\partial n_i}\right)_{T,V,A_s,n} \tag{12.71}$$

$$\left(\frac{\partial S}{\partial A_s}\right)_{T,p,n} = -\left(\frac{\partial \gamma}{\partial T}\right)_{p,A_s,n} \tag{12.72}$$

$$\left(\frac{\partial V}{\partial A_s}\right)_{T,p,n} = -\left(\frac{\partial \gamma}{\partial p}\right)_{T,A_s,n} \tag{12.73}$$

$$\left(\frac{\partial \mu_i}{\partial A_s}\right)_{T,p,n} = -\left(\frac{\partial \gamma}{\partial n_i}\right)_{T,p,A_s,n} . \tag{12.74}$$

Similar relationships between surface tension and the change of U and H with surface area can also be obtained by dividing equations (12.64) and (12.65) by dA_s and specifying constant composition to get

$$\left(\frac{\partial U}{\partial A_s}\right)_{T,V,n} = T\left(\frac{\partial S}{\partial A_s}\right)_{T,V,n} + \gamma$$

and

$$\left(\frac{\partial H}{\partial A_s}\right)_{T,p,n} = T\left(\frac{\partial S}{\partial A_s}\right)_{T,p,n} + \gamma.$$

Combining with equations (12.69) and (12.72) gives

$$\left(\frac{\partial U}{\partial A_s}\right)_{T,V,n} = \gamma - T\left(\frac{\partial \gamma}{\partial T}\right)_{V,A_s,n} \tag{12.75}$$

$$\left(\frac{\partial H}{\partial A_s}\right)_{T,p,n} = \gamma - T\left(\frac{\partial \gamma}{\partial T}\right)_{p,A_s,n} . \tag{12.76}$$

The change of γ with T, V, p, and n_i can be evaluated. Hence, we have a means of determining the change of U, H, S, V, p, and μ_i with area under the

appropriate constant conditions. We should note, however, that these quantities are values for the entire system and not for the surface. For example, equation (12.70) involves the change of γ with the total volume of the system [$(V_{\mathrm{I}} + V_{\mathrm{II}})$, since $V^{\mathrm{s}} = 0$].

We use equations (12.69) to (12.75) when we want to calculate the effect of surface area on a total thermodynamic property. But we also want to know relationships between the different thermodynamic properties of the surface. With the aid of equations (12.57) to (12.63), in combination with equations (12.69) to (12.76), we can derive such relationships. For example, to obtain an equation for U^{s}, we differentiate equation (12.57) and get

$$\mathrm{d}U^{\mathrm{s}} = \mathrm{d}U - \mathrm{d}U_{\mathrm{I}} - \mathrm{d}U_{\mathrm{II}}. \tag{12.77}$$

We then substitute equation (12.64) for $\mathrm{d}U$ into equation (12.77), along with similar equations for $\mathrm{d}U_{\mathrm{I}}$ and $\mathrm{d}U_{\mathrm{II}}$, except that a term involving $\mathrm{d}A^{\mathrm{s}}$ is not included for these bulk phases. That is

$$\mathrm{d}U_{\mathrm{I}} = T\mathrm{d}S_{\mathrm{I}} - p\mathrm{d}V_{\mathrm{I}} + \sum_i \mu_{\mathrm{I},i}\,\mathrm{d}n_{\mathrm{I},i}$$

$$\mathrm{d}U_{\mathrm{II}} = T\mathrm{d}S_{\mathrm{II}} - p\mathrm{d}V_{\mathrm{II}} + \sum_i \mu_{\mathrm{II},i}\,\mathrm{d}n_{\mathrm{II},i}.$$

We also apply the equilibrium condition

$$\mathrm{d}\mu_i = \mathrm{d}\mu_{\mathrm{I},i} = \mathrm{d}\mu_{\mathrm{II},i}. \tag{12.78}$$

The result of these substitutions (after rearrangement) is

$$\mathrm{d}U^{\mathrm{s}} = T(\mathrm{d}S - \mathrm{d}S_{\mathrm{I}} - \mathrm{d}S_{\mathrm{II}}) - p(\mathrm{d}V - \mathrm{d}V_{\mathrm{I}} - \mathrm{d}V_{\mathrm{II}}) + \gamma\mathrm{d}A_{\mathrm{s}}$$

$$+ \sum_i \mu_i(\mathrm{d}n_i - \mathrm{d}n_{\mathrm{I},i} - \mathrm{d}n_{\mathrm{II},i}). \tag{12.79}$$

We now differentiate equations (12.59) and (12.63) to get

$$\mathrm{d}S^{\mathrm{s}} = \mathrm{d}S - \mathrm{d}S_{\mathrm{I}} - \mathrm{d}S_{\mathrm{II}}$$

$$\mathrm{d}n^{\mathrm{s}} = \mathrm{d}n - \mathrm{d}n_{\mathrm{I}} - \mathrm{d}n_{\mathrm{II}}.$$

Substitution of the above into equation (12.79), along with the fact that $dV - dV_I - dV_{II} = 0$ (since $V = V_I + V_{II}$) gives

$$dU^s = T\,dS^s + \gamma\,dA_s + \sum_i \mu_i\,dn_i^s. \tag{12.80}$$

A similar derivation involving H^s gives

$$dH^s = T\,dS^s + \gamma\,dA_s + \sum_i \mu_i\,dn_i^s. \tag{12.81}$$

Equations (12.80) and (12.81) are identical, from which we conclude that $U^s = H^s$. A comparable derivation involving A and G will show that

$$dA^s = dG^s = -S^s\,dT + \gamma\,dA_s + \sum_i \mu_i\,dn_i^s. \tag{12.82}$$

The surface energy U^s and surface enthalpy H^s are homogeneous functions of degree one in S^s, A_s, and n_i^s. Hence, we can use Euler's theorem to integrate equations (12.80) and (12.81) and obtain

$$H^s = U^s = TS^s + \gamma A_s + \sum_i n_i^s \mu_i. \tag{12.83}$$

Differentiating equation (12.83) and combining the results with equation (12.80) or (12.81) gives

$$S^s\,dT + A_s\,d\gamma + \sum_i n_i^s\,d\mu_i = 0, \tag{12.84}$$

which is an equation for the surface, equivalent to the Gibbs–Duhem equation {equation (11.22)} applied to the bulk phase.

Equation (12.84) can be divided by A_s to get

$$s^s\,dT + d\gamma + \sum_i \Gamma_i\,d\mu_i = 0 \tag{12.85}$$

where, as defined earlier, $s^s = S^s/A_s$ is the surface entropy per unit area (comparable to molar quantities in the bulk phases), and $\Gamma_i = n_i^s/A_s$ is the surface concentration.

Equation (12.85), written in the form

$$d\gamma = -s^s\, dT - \sum \Gamma_i\, d\mu_i \tag{12.86}$$

is the basic equation for surface tension that was first derived by Gibbs. It serves as the basis for the derivation of a number of relationships that apply to surfaces. For example, for a single component (with $\Gamma_1 = 0$), it becomes

$$d\gamma = -s^s\, dT$$

or

$$\left(\frac{\partial \gamma}{\partial T}\right)_{p,n} = -s^s. \tag{12.87}$$

Equation (12.87) is the same as equation (12.34), derived earlier for a single component and which led to equations for h^s and u^s.

The application of equation (12.86) to multicomponent systems is unduly complex for our discussion. We will limit our system to a binary mixture with $\Gamma_1 = 0$ (for the solvent), in which case, equation (12.86) becomes

$$d\gamma = -s^s\, dT - \Gamma_2\, d\mu_2. \tag{12.88}$$

For a (vapor + liquid) interface at constant temperature, $dT = 0$ and

$$d\mu_2 = RT\, d\ln f_2$$

where f_2 is the vapor fugacity. Combining gives

$$d\gamma = -\Gamma_2 RT\, d\ln f_2$$

or

$$\Gamma_2 = -\frac{1}{RT}\left(\frac{\partial \gamma}{\partial \ln f_2}\right)_T. \tag{12.89}$$

Equation (12.89) allows one to calculate the surface concentration of solute from the vapor fugacity.[r] It can be simplified more for the ideal solution where

$$\left(\frac{\partial \ln f_2}{\partial \ln x_2}\right)_T = 1$$

so that

$$\Gamma_2 = -\frac{1}{RT}\left(\frac{\partial \gamma}{\partial \ln x_2}\right)_T. \tag{12.90}$$

From equation (12.89) or (12.90), we see that a solute that lowers the surface tension is concentrated on the surface; that is, $\Gamma_2 > 0$. Conversely, a solute that raises surface tension is concentrated in the bulk phase.

Surfactants are perhaps the best examples of solutes that lower the surface tension of the solvent. From equation (12.90) we conclude that surfactant molecules are concentrated on the surface. A simpler example is provided by (alcohol + water) mixtures. Figure 12.6 shows the change of γ with x_2 for mixtures of $(x_1 H_2O + x_2 C_2H_5OH)$, according to the data of Butler and Wightman.[5] We note that $(\partial\gamma/\partial x_2) < 0$ so that $\Gamma_2 > 0$. Figure 12.7 is a graph of Γ_2 against x_2 obtained from equation (12.89), again using the data of Butler and Wightman.

We are not surprised from our general chemical knowledge to note that ethanol concentrates on the surface. We would expect that the OH groups would be oriented into the liquid where they hydrogen bond to the water molecules. This leaves the ethyl group on the surface. The minimum surface area per molecule is about 0.24 μm^2 in the $x_2 = 0.15$ solution. This is about the cross-sectional area of the ethyl group as found in n-paraffin crystals. Hence, the surface of the (ethanol + water) solution would have almost complete coverage with ethyl groups at $x_2 = 0.15$. In Figure 12.6, the initial steep decrease in γ with x_2 (below $x_2 = 0.15$), followed by a leveling off at higher x_2 at a value near that for ethanol, can be explained as being due to this concentration of ethanol molecules on the surface, with nearly complete coverage by $x_2 = 0.15$.[s]

---

[r] We can and will substitute vapor pressure for vapor fugacity without introducing significant error.

[s] This is another example of the application of thermodynamics to the understanding of phenomena on the molecular level. We emphasize once again that our conclusions are speculations and cannot be proved or disproved by thermodynamics.

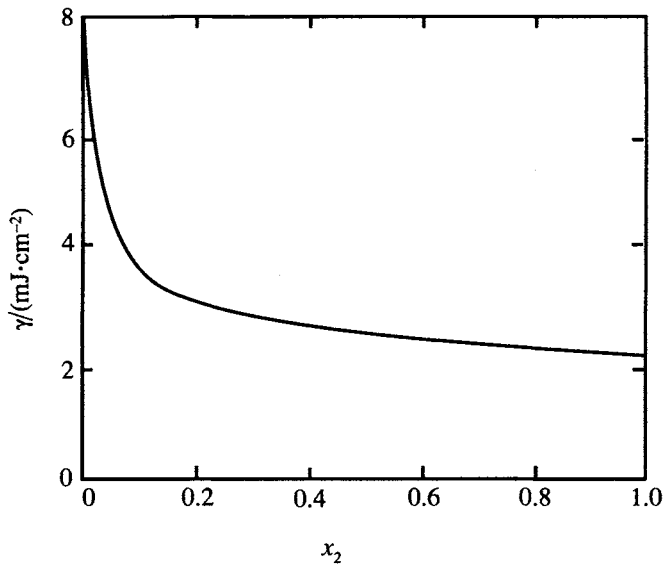

Figure 12.6 The surface tension of ($x_1H_2O + x_2C_2H_5OH$) mixtures at $T = 298.15$ K.

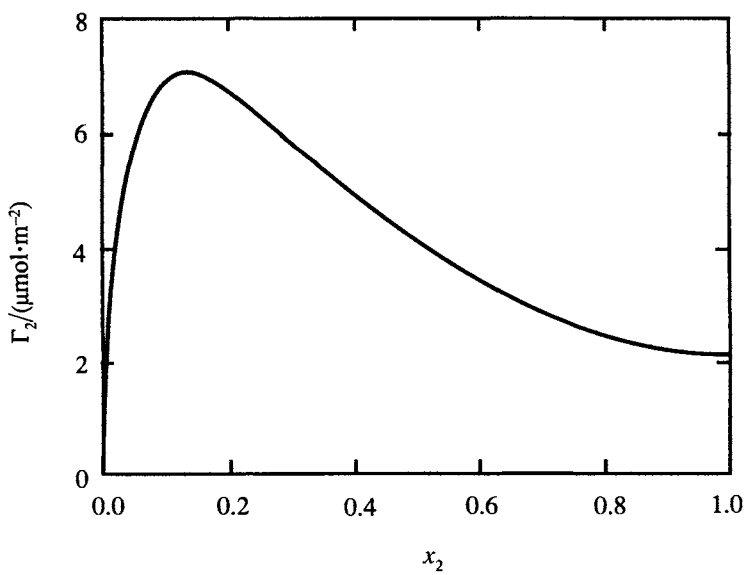

Figure 12.7 Surface concentration against mole fraction for ($x_1H_2O + x_2C_2H_5OH$) at $T = 298.15$ K.

Problems

P12.1 (a) Start with equations (12.1) to (12.3) and show that for the reversible stretching of a rubber band at constant pressure

$$dG = f\,dl - S\,dT,$$

and hence, that

$$f = \left(\frac{\partial G}{\partial l}\right)_T.$$

(b) Assume that the volume of the rubber band does not change during stretching and show that

$$\left(\frac{\partial U}{\partial l}\right)_T = f - T\left(\frac{\partial f}{\partial T}\right)_l.$$

(c) For an ideal gas with

$$\left(\frac{\partial U}{\partial V}\right)_T = 0, \text{ it can be shown that } \frac{1}{p}\left(\frac{\partial p}{\partial T}\right)_V = \frac{1}{T}.$$

In a similar manner, for an "ideal" rubber band with

$$\left(\frac{\partial U}{\partial l}\right)_T = 0, \text{ show that } \frac{1}{f}\left(\frac{\partial f}{\partial T}\right)_l = \frac{1}{T},$$

which raises the possibility of using a rubber band as the basis for an "absolute" temperature scale.

P12.2 Start with equations (12.35) and (12.38) and show that s^s and u^s are given by equations (12.44) and (12.45):

$$s^s = \frac{11}{9}\frac{\gamma_0}{T_c}\left(1 - \frac{T}{T_c}\right)^{2/9} \tag{12.44}$$

$$u^s = \gamma_0\left(1 - \frac{T}{T_c}\right)^{2/9}\left(1 + \frac{2}{9}\frac{T}{T_c}\right). \tag{12.45}$$

Assume that equation (12.42)

$$\gamma = \gamma_0 \left(1 - \frac{T}{T_c}\right)^{11/9} \tag{12.42}$$

can be used to represent the effect of temperature on the surface tension.

P12.3 Uranium can be enriched in ^{235}U by centrifuging UF_6 gas. What angular velocity is necessary to obtain enrichment of ^{235}U to 1% at $r = 3$ cm if its abundance is 0.7% at $r = 10$ cm?

P12.4 Calculate the vapor pressure at 298.15 K of 1.00×10^{-5} cm droplets of water. At this temperature, the vapor pressure of water in the bulk phase is 3.1672 kPa and the density is 0.9970 $g \cdot cm^{-3}$.

P12.5 The following data taken from the *Handbook of Chemistry and Physics* demonstrate how the surface tension at 323.15 K of (methanol + water) and (ethanol + water) solutions changes with composition

$(x_1H_2O + x_2CH_3OH)$		$(x_1H_2O + x_2C_2H_5OH)$	
x_2	$\gamma/(mJ \cdot cm^{-2})$	x_2	$\gamma/(mJ \cdot cm^{-2})$
0.000	6.79	0.000	6.79
0.034	5.62	0.016	5.34
0.046	5.50	0.033	4.68
0.126	4.32	0.087	3.43
0.303	3.30	0.135	3.07
0.394	3.08	0.218	2.82
0.635	2.50	0.312	2.55
0.796	2.26	0.437	2.41
1.000	1.95	0.547	2.26
		0.879	2.04
		1.000	1.99

Make a graph of x_2 against γ for the two systems and compare the results in terms of the discussion in the text of the covering of the surface of the liquid mixture by the alkyl group of the alkanol.

P12.6 A young man Horatio LeChatelier Smith devoted his leisure time to his hobby of stretching elastic bands. Once while stretching elastics, he quite by accident touched a freshly stretched band to his cleanly shaven face (Horatio was a nonconformist) and sensed that heat was being evolved

when the band was stretched. As he thought about the process being exothermic, he remembered LeChatelier's principle. Pausing only long enough to shout "serendipity!" he hastened to the laboratory, where he performed the following experiments:

(i) An elastic band was stretched by attaching one end to a solid support and the other to a 300 g weight that was freely suspended in the air. The length of the stretched band at room temperature was recorded as l_1. The stretched elastic was then warmed by the soothing rays of an infrared lamp, and the new length l_2 was recorded.

(a) Is l_2 longer or shorter than l_1? Explain.

(ii) Horatio then calorimetrically measured q by reversibly stretching (impossible) the elastic from l_0 to $2l_0$. During this reversible constant-temperature ($T = 300$ K) process, 1.50 J of heat was evolved. The elastic was then allowed to contract irreversibly back to l_0 without any restraining tension. The heat absorbed was 0.50 J ($T = 300$ K).

(a) How much work was required to stretch the elastic?

(b) Calculate the entropy change of the elastic for the stretching process.

(c) Calculate the entropy change for the contraction of the elastic.

(d) Calculate the entropy change of the universe for the two-step process of stretching and returning the elastic to its initial state.

References

1. W. F. Giauque and R. C. Archibald, "The Entropy of Water from the Third Law of Thermodynamics. The Dissociation Pressure and Calorimetric Heat of the Reaction $Mg(OH)_2 = MgO + H_2O$. The Heat Capacities of $Mg(OH)_2$ and MgO from 20 to 300 °K", *J. Am. Chem. Soc.*, **59**, 561–569 (1937).
2. See N. K. Adam, *The Physics and Chemistry of Surfaces*, 3rd edition, Oxford University Press, London, 1941, p. 5.
3. E. A. Guggenheim, "The Principle of Corresponding States", *J. Chem. Phys.*, **13**, 253–261 (1945).
4. R. Eötvös, "Uber den Zusammenhang der Oberflächenspannung mit dem Molecular-Volumen", *Ann. Phys. Chem.*, **27**, 448–459 (1886).
5. J. A. V. Butler and A. Wightman, "Absorption at the Surface of Solutions. Part I. The Surface Composition of Water–Alcohol Solutions", *J. Chem. Soc.*, **1932**, 2089–2097 (1932).

Chapter 13

Applications of Thermodynamics to Phase Equilibria Studies of Pure Substances

In the next two chapters, we use thermodynamic relationships summarized in Chapter 11[a] to delve further into the world of phase equilibria, using examples to describe some interesting effects. As we do so, we must keep in mind that our discussion still describes only relatively simple systems, with a much broader world available to those who study such subjects as critical phenomena, ceramics, metal alloys, purification processes, and geologic systems. In this chapter, we will limit our discussion to phase equilibria of pure substances. In Chapter 14, we will expand the discussion to describe systems containing more than one component.

13.1 Classification of Phase Transitions in Pure Materials

For any equilibrium phase change for a pure substance represented by

$$A = B$$

the chemical potentials, μ_A and μ_B, of the phases in equilibrium are related by[b]

$$\mu_A = \mu_B$$

so that

$$\Delta G_m = \mu_A - \mu_B = 0.$$

---

[a] The Gibbs phase rule and the Clapeyron equation will be especially useful.

[b] See Section 11.2 of Chapter 11 for a summary discussion of the equilibrium condition.

To differentiate between the variety of phase equilibria that occur, Ehrenfest proposed a classification of phase transitions based upon the behavior of the chemical potential of the system as it passed through the phase transition. He introduced the notion of an "*n*th order transition" as one in which the *n*th derivative of the chemical potential with respect to T or p showed a discontinuity at the transition temperature. While modern theories of phase transitions have shown that the classification scheme fails at orders higher than one, Ehrenfest's nomenclature is still widely used by many scientists. We will review it here and give a brief account of its limitations.

13.1a First- and Second-Order Transitions

In a first-order transition, the first derivative of G_m (chemical potential, μ) shows a discontinuity. Since

$$S_m = -\left(\frac{\partial \mu}{\partial T}\right)_p$$

and

$$V_m = \left(\frac{\partial \mu}{\partial p}\right)_T$$

one sees a discontinuity, a step-like function, in these two properties at a transition temperature T_t. The heat capacity and the compressibility are related to the first derivatives of S and V with respect to T and p, respectively, and thus, to the second derivatives of μ. These quantities approach infinity at T_t. Figure 13.1 shows the behavior of μ and its derivatives (or related quantities) at the transition temperature of first-order transitions. The enthalpy (not shown in Figure 13.1) will also show a discontinuity at T_t similar to the one for S.

According to Ehrenfest, a second-order transition occurs when μ and its first derivatives are continuous across the transition region, but the second derivatives, C_p and compressibility, κ are discontinuous. This behavior is illustrated in the second column of Figure 13.1. For these transitions, the enthalpy, in addition to the entropy and volume, is continuous across the transition.

Very few examples of heat capacity or compressibility behavior of the type shown in the second column have been observed experimentally, however. Instead, these two properties most often are observed to diverge to some very large number at T_t as shown in the third column of Figure 13.1.[1] The shapes of these curves bear some resemblance to the Greek letter, λ, and transitions that exhibit such behavior have historically been referred to as "lambda" transitions.

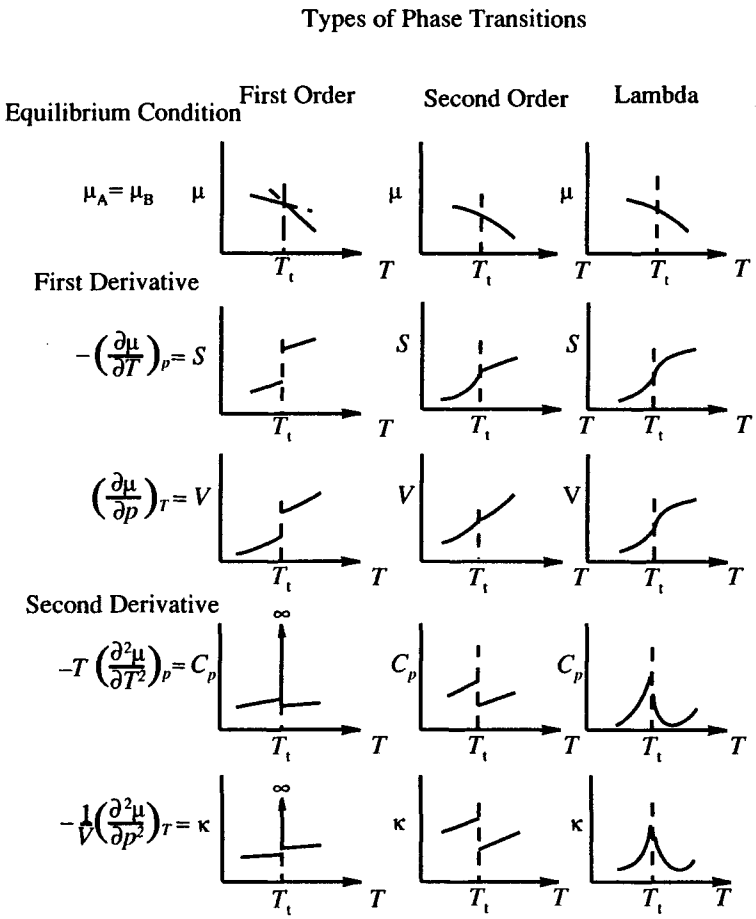

Figure 13.1 Changes in μ, S, V, C_p and κ for a first-order, second-order, and lambda transition.

Because these transitions are associated with a mechanism in which one phase gradually evolves into the other, they are also often referred to as continuous or cooperative transitions. The terms "second order", "lambda", and "continuous" transitions have often been used interchangeably to refer to the same transition even though a true Ehrenfest second-order heat capacity does not have a lambda shape. We shall use the designation "continuous transition" (in preference to second order or lambda) for all transitions in which the discontinuity occurs in the second derivative of G.

In a first order transition, two phases co-exist at the transition temperature. From the Gibbs phase rule, if thermodynamic equilibrium is maintained, these phases can only co-exist at a single temperature (for a fixed pressure). At that

temperature there are two values for the entropy, enthalpy, and volume. Many scientists who study phase transitions refer to this enthalpy difference (enthalpy of transition) as an **isothermal latent heat**. Experimentally, the latent heat is obtained from measurements in an adiabatic cryogenic calorimeter that measures heat capacities as a function of temperature, or by integration of the peak area under a differential scanning calorimetric trace. At a first-order transition temperature, the heat capacity rises very steeply and falls quickly, giving a sharp spike as shown in Figure 13.2a, the heat capacity in the region of the melting temperature of mercury.

By contrast, a continuous phase transition can be regarded as a single phase that evolves or changes gradually from one form to another. For example, in an order–disorder transition, at some low temperature, the phase is completely ordered; at some high temperature, the phase is completely disordered; and at intermediate temperatures, a single phase is present, with increasingly larger "patches" of disorder growing in as the temperature increases.

The transition temperature T_t in a continuous phase transition is defined as the temperature at which complete disorder is achieved.[c] Because infinitesimally small changes take place on either side of the transition temperature, the entropy, enthalpy and volumes of the two phases are equal at T_t in a continuous phase transition. There is no latent heat or volume change associated with such transitions, but there still is an **excess enthalpy or enthalpy of transition**, spread over a temperature range. As an example, Figure 13.2b shows the heat capacity of MnO as a function of temperature. Below about 50 K, the orientations of the magnetic dipoles of the Mn^{2+} ion are fixed. In the temperature region from 50 K to 117.7 K, increasing thermal energy allows the magnetic moments to overcome the stabilization inherent in their alignment, and the orientations of the moments become progressively more disordered as the temperature is increased. The magnetic moments absorb heat during this process, resulting in a contribution to the heat capacity in addition to that associated with the "normal" or lattice heat capacity of a solid. Once there is complete randomization in the orientation of the magnetic moments, the heat capacity drops down to some baseline value representative of this lattice heat capacity.

When one has a model or related data to estimate the normal or lattice heat capacity in the transition region, the enthalpy of transition for a continuous transition can be obtained as an integration of the excess heat capacity, defined as

$$C_p(\text{excess}) = [C_p(\text{measured}) - C_p(\text{lattice})]$$

[c] Later in the chapter, we will refer to these transition temperatures T_t as critical temperatures T_c, since they result from critical phenomena.

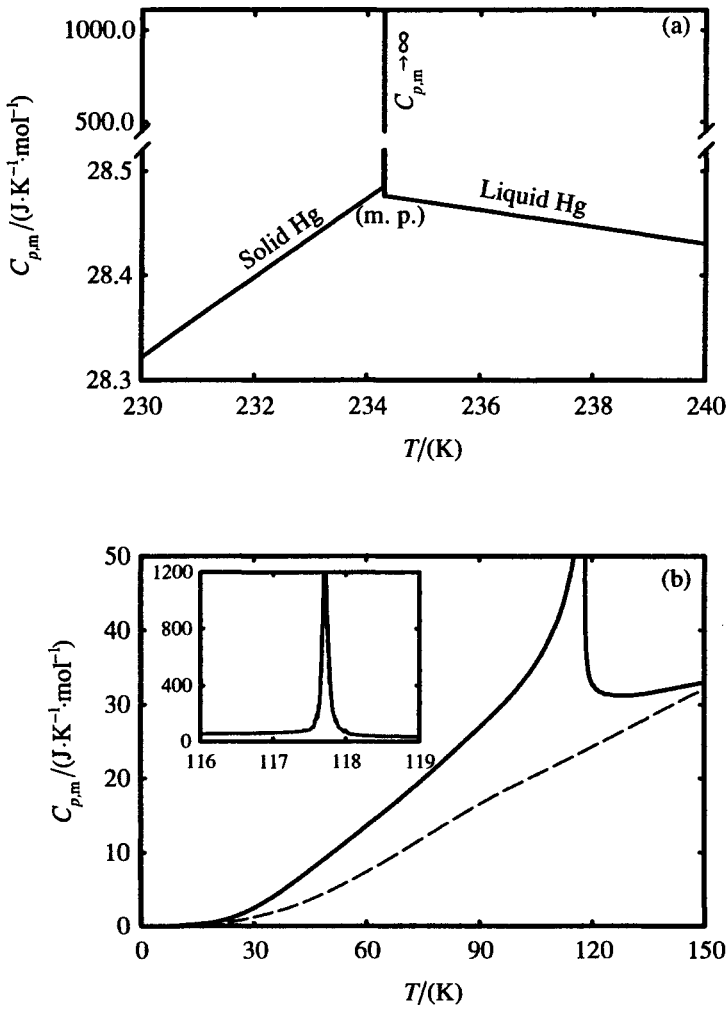

Figure 13.2 Heat capacities of (a), Hg near the melting temperature of 234.314 K showing the abrupt nature of the change in heat capacity for this first-order phase transition at this temperature [from R. H. Busey and W. F. Giauque, *J. Am. Chem. Soc.*, **75**, 61–64 (1953)]; and (b), MnO showing the continuous magnetic transition (note inset). (Data obtained from Professor Brian Woodfield and co-workers at Brigham Young University.) The dashed line is an estimate of the lattice heat capacity of MnO.

over the transition region. This difference in heat capacity is shown in Figure 13.2b for MnO. The entropy of transition can also be obtained as the integral of C_p(excess)/T, integrated over the transition region. Often, it can be related in a simple statistical way to the process involved.

A great deal of theoretical and experimental work has been conducted in trying to understand continuous phase transitions. After a brief discussion of first-order transitions that can be referred to for comparison, we will describe several continuous phase transitions that arise from very different physical phenomena (providing additional thermodynamic data of interest associated with these substances) and give a brief description of the current state of phase transition theory. We will see that thermodynamic properties associated with the phase transitions from these different phenomena behave in strikingly similar ways. The explanation of the mechanisms for such similarities is arguably one of the more interesting scientific advances in the 20th century.

13.1b First-Order Phase Transitions

Carbon dioxide and elemental tin are interesting examples of substances that have first-order phase transitions. The pressure against temperature phase diagrams for these substances are reproduced here as Figures 13.3 and 13.4. In Figure 13.3, (vapor + liquid) equilibria in the CO_2 occurs along line ab, (solid + liquid) equilibria is present along line bd, and (vapor + solid) equilibrium occurs along

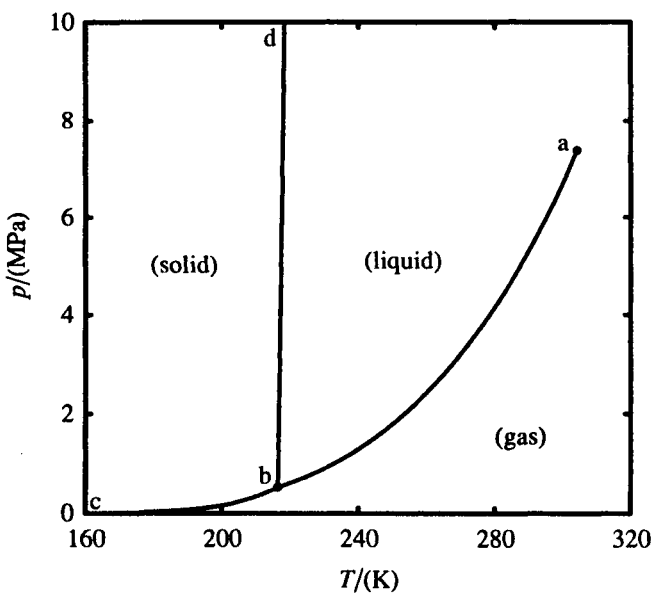

Figure 13.3 Phase diagram for CO_2. Point (a) is the critical point and point (b) is the triple point. Line ab gives the vapor pressure of the liquid, line bc gives the vapor pressure of the solid, and line bd gives the melting temperature as a function of pressure.

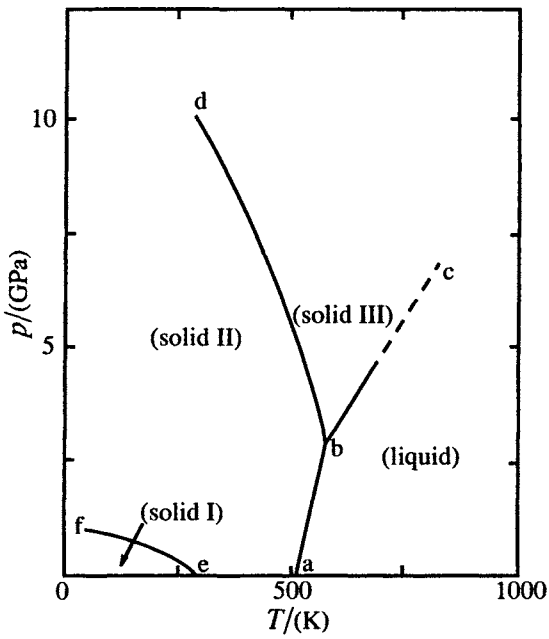

Figure 13.4 The phase diagram for Sn. The pressure is expressed in gigapascals (1 GPa = 10^9 Pa). The dashed line represents an extrapolation of the melting temperature to higher pressures.

line bc. The Clapeyron equation given in Chapter 11 applies. That is,[d]

$$\frac{dp}{dT} = \frac{\Delta H_m}{T\Delta V_m}. \tag{11.31}$$

In equation (11.31), ΔH_m and ΔV_m are the molar enthalpy and molar volume changes associated with the change in phase, and dp/dT gives the slope of the equilibrium lines. Point b is the triple point for CO_2. It is an invariant point, since, according to the Gibbs phase rule

$$f = C - P + 2, \tag{11.34}$$

$f = 0$ for a single component ($C = 1$) with three phases ($P = 3$) in equilibrium.

In Figure 13.4, (solid + liquid) phase equilibrium occurs in Sn at the pressure and temperature conditions given by line abc. In addition,

[d] The Clapeyron equation applies to first-order phase transitions, but not to second-order phase transitions where both $\Delta_{trans}S_m$ and $\Delta_{trans}V_m$ are zero.

(solid + solid) phase equilibrium is present, with (solid I + solid II) in equilibrium along line ef and (solid II + solid III) in equilibrium along line bd. Point b is again an invariant (triple) point, but in this case, two solids and a liquid are in equilibrium. Lines bd and ef differ in that the latter intersects the T axis at $p = 0$. Thus, the solid I = solid II transition can be made to occur by cooling at ambient pressure. As with many solid-phase transitions, the solid I = solid II transition is slow, and it usually takes considerable time for the change to occur.

We will not describe these systems in more detail here, but will describe two other systems to demonstrate the types of relationships that occur in first-order phase transitions. At $p = 0.1$ MPa, solid CsCl changes crystal structure at $T = 743$ K and melts at 918 K. Both are first-order phase transitions. Figure 13.5 demonstrates how G°_m, S°_m, and $C^\circ_{p,m}$ change with temperature for CsCl.[2] Note that the Gibbs free energy is continuous at the transition temperatures, but the temperature derivative of the free energy is discontinuous, leading to a value for $\Delta_{trans}S^\circ_m$ of 5.07 $J \cdot K^{-1} \cdot mol^{-1}$ at the transition temperature, and a $\Delta_{fus}S^\circ_m$ of 17.3 $J \cdot K^{-1} \cdot mol^{-1}$ at the melting point. The temperature derivative of entropy is also discontinuous, leading to a change in heat capacity that goes to infinity with an infinite slope at the transition and fusion temperatures. The heat capacity immediately assumes a new value, corresponding to the new state of the substance, once the transition temperature is exceeded.

Figure 13.6 shows the pressure against temperature phase diagram for CsCl.[3] X-ray diffraction studies made on CsCl show that solid α has the Cs and Cl in interpenetrating simple cubic lattices so that the coordination number around each ion is eight. In solid β, however, the ions are in a NaCl type of structure, with face-centered cubic interpenetrating lattices leading to a coordination number of six. The result of the change in structure is a significant expansion of the lattice when the solid changes from solid α to solid β, and a large ΔV_m for the transition occurs. Johnson, Agron, and Bredig[4] report a volume change of 8.0 $cm^3 \cdot mol^{-1}$ for the transition, which is an increase of 17.1%. The small slope for line ab in Figure 13.6 (the solid α = solid β transition line) results from this large $\Delta_{trans}V_m$. From the Clapeyron equation, we get

$$\frac{dp}{dT} = \frac{\Delta_{trans}S_m}{\Delta_{trans}V_m}$$

$$= 0.63 \text{ MPa} \cdot \text{K}^{-1}.$$

The reciprocal gives an increase in the transition temperature of 1.6 K for every 1 MPa increase in pressure.

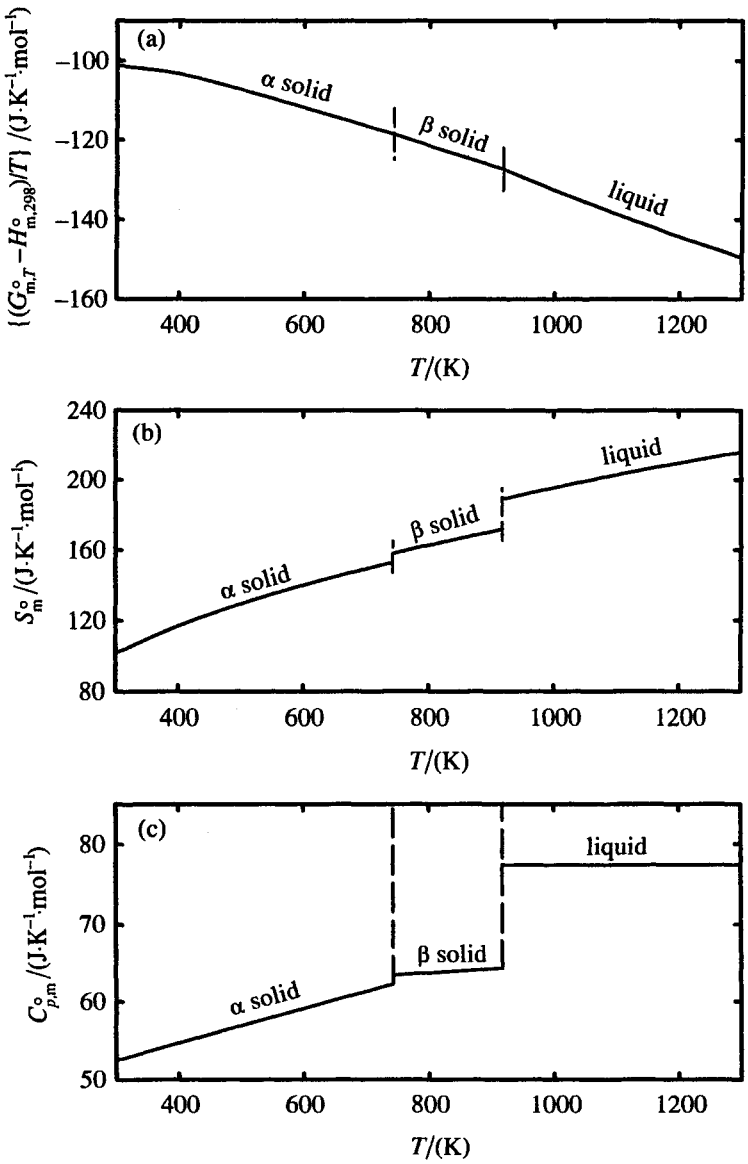

Figure 13.5 (a) Gibbs free energy function, (b) entropy, and (c) heat capacity at $p = 0.1$ MPa for CsCl through the phase transition at 743 K and the melting at 918 K. For these first-order phase changes, $\Delta_{trans}H^\circ_m = 3.77\ kJ \cdot mol^{-1}$ at $T = 743$ K, and $\Delta_{fus}H^\circ_m = 15.9\ kJ \cdot mol^{-1}$ at $T = 918$ K.

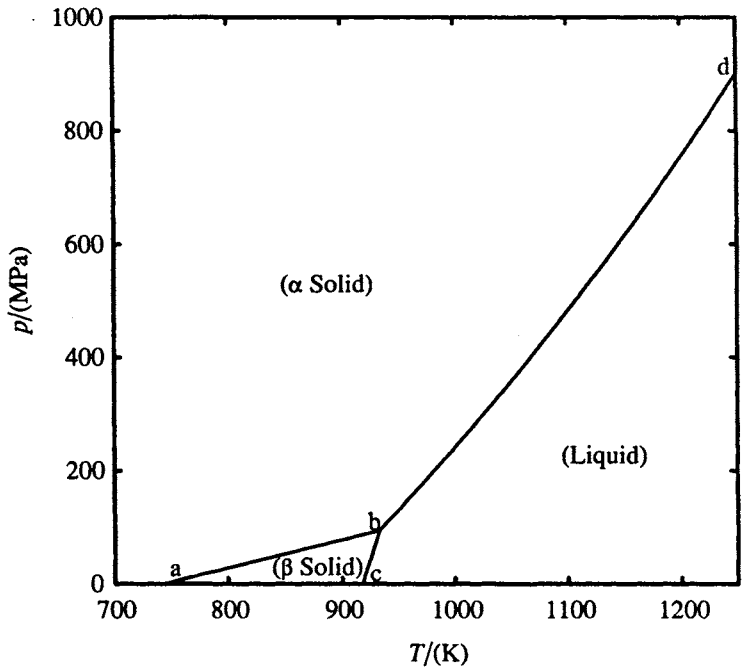

Figure 13.6 Phase diagram for CsCl showing the solid phase transition at low pressures.

Our description of first-order phase transitions would not be complete without describing the phase diagram for water shown in Figure 13.7. Gas, liquid, and seven different solid phases are shown.[c] Eight different triple points are present. At point a, gas, liquid and Ice I are in equilibrium. Two solids and a liquid are present at points b, d, f, and g; and three solids are present at points c, e, and h. Ice I is the only form of solid water that is less dense than the liquid so that $\Delta_{fus}V_m < 0$. Since $\Delta_{fus}H_m > 0$, the negative slope for line ab is in agreement with the Clapeyron equation prediction. Compressing liquid water at 373.15 K causes it to freeze to Ice VII at approximately 2.3 GPa. Compressing Ice I at 250 K causes it to melt, re-freeze to Ice III, change to Ice V, then to Ice VI, and finally to Ice VIII.

[c] Forms of ice designated as IV, IX, X, and XI have also been reported in the literature. See P. W. Hobbs, *Ice Physics*, Clarendon Press, Oxford, 1974, pp. 60–67; and C. Lobban, J. L. Finney, and W. F. Kuhs, "The Structure of a New Phase of Ice", *Nature*, **391**, 268–270 (1998). These phases are not shown in Figure 13.7, since they are metastable, not yet well-defined, or occur at pressure and temperature extremes beyond those given in the figure.

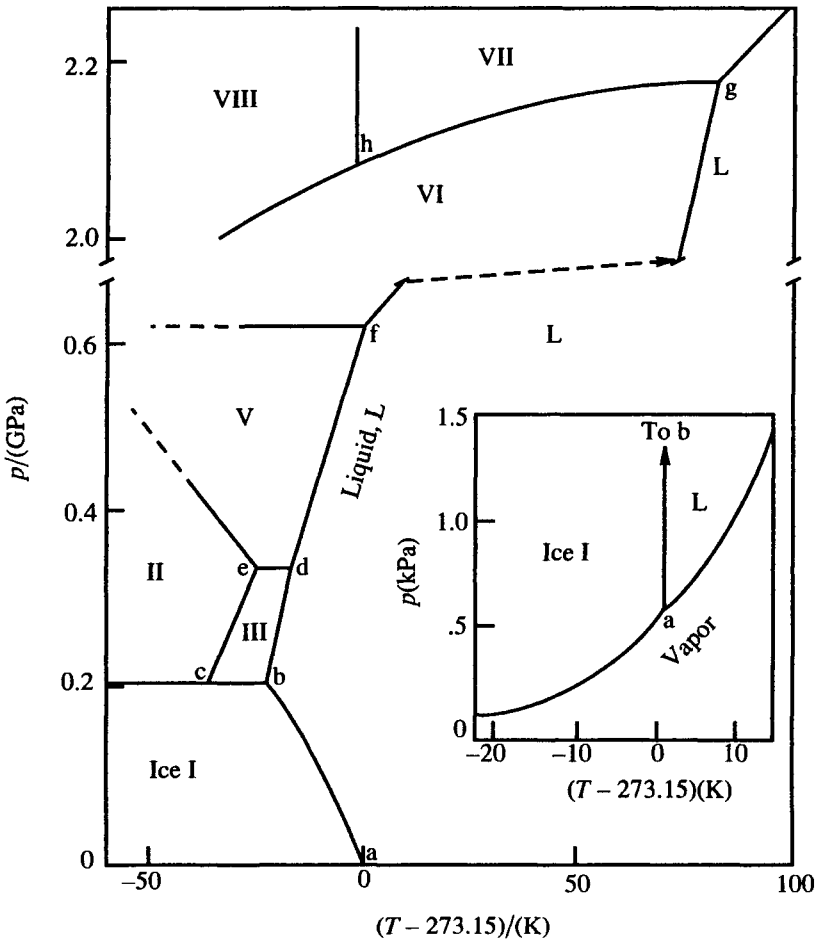

Figure 13.7 Phase diagram for H_2O. (Note the change in pressure scale above 0.7 GPa.) Ice IV, IX, X, and XI are not shown, since they are metastable, ill defined, or occur at pressure and temperature extremes beyond those given in the figure. (Adapted with permission from N. A. Gokcen and R. G. Reddy, *Thermodynamics, Second Edition*, Plenum Publishing Corp., New York, 1996, p. 127.)

13.1c Continuous Phase Transitions and Related Thermodynamic Information

Continuous phase transitions can result from many different types of effects, but they all have many common characteristics. We will describe these phase transitions and see the common behavior by giving examples of several different types.

(Liquid + Gas) Critical Phase Transition The liquid to gas transition at the critical temperature and pressure is an example of a continuous transition. At temperatures below the critical point, the two phases undergo a first-order transition. When this occurs, there is a single temperature for a given pressure at which the two phases are in equilibrium. The two phases have very different densities, and there is a latent heat or enthalpy change associated with the transition (the enthalpy of vaporization). As one approaches the critical point, however, the differences between most of the properties of the gas and the liquid approach zero. At the critical point, the transition is no longer first order, but the heat capacity or compressibility curves predicted by Ehrenfest's second-order transitions are not observed either. Rather, a divergent behavior like that shown in Figure 13.1 under lambda transitions is obtained. For example, Figure 13.8 shows the heat capacity of CO_2 at a pressure very nearly equal to the critical pressure, and in the temperature region spanning the critical temperature. The lambda shape of the curve is evident.

In the vicinity of the critical temperature, the density difference $(\rho_l - \rho_g)$ shows a temperature dependence similar to that given by equation (11.35)

$$(\rho_l - \rho_g) \sim \left(\frac{|T - T_c|}{T_c} \right)^{\beta}. \tag{13.1}$$

In a similar manner, heat capacity near the critical temperature can be expressed as

$$C \sim \left| \frac{T - T_c}{T_c} \right|^{-\alpha}. \tag{13.2}$$

The constants α and β are the critical exponents.[f] We will talk more about them later after we consider other types of continuous transitions involving critical phenomena.

Order – Disorder Transitions Involving Position, Orientation and Magnetic Moments

a. Position Disorder: In many solids, the molecules or atoms that make up the solid are arranged at points in the crystalline lattice in a regular, predictable way. Consider as an example, the binary metallic alloy β-brass, a nearly

[f] The critical exponents α and β are not to be confused with the coefficient of expansion and the pressure coefficient of a gas for which we use the same symbols.

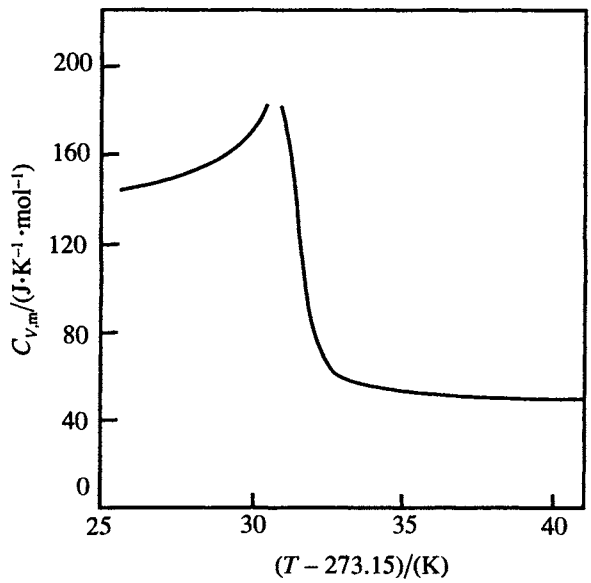

Figure 13.8 Heat capacity of CO_2 at temperatures near the critical temperature T_c. The line is at a density of 451.2 $kg \cdot m^{-3}$, which is very nearly the critical density. (The pressure is close to the critical pressure.)

equimolar mixture of Cu and Zn. In the solid, each atom can be thought of as being at the center of a cube with eight nearest neighbors, one at each of the corners of the cube.[g] At low temperatures, the crystalline structure of β-brass can be represented as two interpenetrating cubic lattices, with Cu atoms at the corners of each cube and Zn atoms at the center, or vice versa. If we distinguish between the two sites (corners vs centers) by labeling them as A and B sites, respectively, we can consider all of the Cu atoms to be on A sites and all of the Zn atoms to be on B sites at low temperatures. As the temperature is increased, the Cu and Zn atoms gain enough energy to move from one type of site to another. We can define a quantity called the **order parameter** η as the fraction of atoms that are on the "right" type of site. That is

$$\eta = \frac{(\text{no. of Cu atoms on A sites}) - (\text{no. of Cu atoms on B sites})}{(\text{no. of Cu atoms on A sites})}. \tag{13.3}$$

[g] The structure is the same as that for CsCl at ambient temperatures that we described earlier.

At low temperatures, η will be unity because all of the Cu atoms will be localized on A sites.[h] But the degree of disorder increases as the temperature increases until the Cu and Zn atoms are mixed randomly on the two sublattices and $\eta = 0$. This process, called a positional (order + disorder) transition, is often described as a cooperative phenomenon because it becomes easier to produce additional disorder once some disorder is generated. In the vicinity of a critical temperature, the order parameter η behaves like the density difference $(\rho_l - \rho_g)$ near the gas–liquid critical point. Thus,

$$\eta \sim \left| \frac{T - T_c}{T_c} \right|^{\beta} \tag{13.4}$$

and the heat capacity behaves like

$$C_p \sim \left(\frac{|T - T_c|}{T_c} \right)^{-\alpha}.$$

Figure 13.9 shows plots of this behavior for both the order parameter and the heat capacity of β-brass. Notice that the heat capacity tends to infinity at the critical transition temperature with the characteristic lambda shape. Above this temperature, further heating produces no more disorder, and the heat capacity falls back to a finite value.

b. Rotational Disorder: In molecular crystals, an orientational (order + disorder) transition is possible if the molecule can assume more than one distinguishable orientation at each site in the lattice. In some substances such as CO, N_2O, and H_2O, the disorder is not relieved by a phase transition as the temperature is lowered,[i] but the more common situation is a transition like that observed in the ordering of β-brass. One of the simplest molecules to undergo such a transition is methane, CH_4. At low temperatures, the molecules are situated in the solid with an ordered arrangement of the molecular axes. As the temperature is increased, the molecules begin to undergo a rotational motion which takes them into different orientations, thereby introducing disorder into the crystal. The onset of reorientational motion is also a cooperative phenomenon and the heat capacity, shown in Figure 13.10, diverges to infinity

[h] The Third Law demonstrates that solids go to a state of complete order (if possible) as $T \rightarrow 0$.

[i] The result is a discrepancy in the entropy calculated from heat capacity measurements using the Third Law for substances such as CO, N_2O, and H_2O.

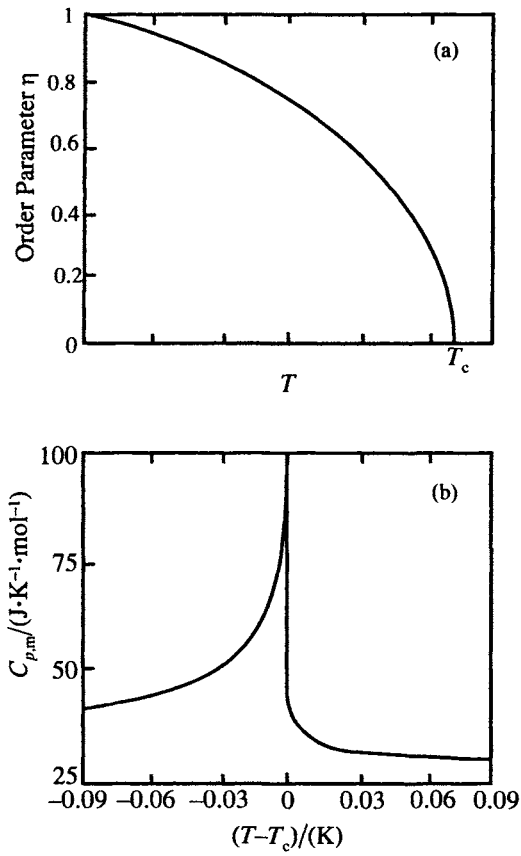

Figure 13.9 Properties of β-brass as a function of temperature; (a) the order parameter, and (b) the heat capacity.

at the critical temperature T_c. Above T_c the molecules rotate freely about their center of mass at each site in the lattice, and the heat capacity drops back to a finite value.

c. Magnetic Effects: In materials containing atoms with unpaired electrons, and therefore a magnetic moment, the magnetic moments can undergo an order–disorder transition as we have already described for MnO. In the ordered state, the magnetic moments are aligned in some regular fashion. In ferromagnets, the order is achieved by having all of the moments align parallel to one another and produce a net magnetization. In antiferromagnets, the ordered state has sublattices — the magnetic moments on one sublattice are parallel to each other, while those on a different sublattice are parallel to each other, but different from those on the first lattice. If the second sublattice has an

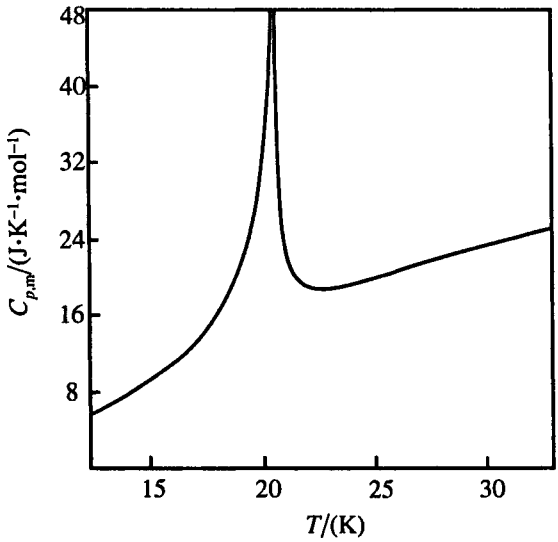

Figure 13.10 Heat capacity of CH_4 in the temperature region where the order–disorder transition results in complete rotation in the solid state.

arrangement that is completely antiparallel to the first, then there is no net magnetization. In all of these cases, one can define an order parameter that behaves, near the critical temperature, very much like the order parameter defined for the β-brass phase transition, and the heat capacity has a lambda-shaped peak in the heat capacity at a critical temperature, as shown in Figure 13.2 for MnO.

Helium-4 Normal–Superfluid Transition Liquid helium has some unique and interesting properties, including a transition into a phase described as a superfluid. Unlike most materials where the isotopic nature of the atoms has little influence on the phase behavior, ^{4}He and ^{3}He have a very different phase behavior at low temperatures, and so we will consider them separately.[j] Figure 13.11 shows the phase diagram for ^{4}He at low temperatures. The normal liquid phase of ^{4}He is called liquid I. Line ab is the vapor pressure line along which (gas + liquid I) equilibrium is maintained, and the (liquid + gas) phase transition is first order. Point a is the critical point of ^{4}He at $T = 5.20$ K and $p = 0.229$ MPa. At this point, the (liquid + gas) transition has become continuous. Line bc represents the transition between normal liquid (liquid I) and a superfluid phase referred to as liquid II. Along this line the transition

[j] Naturally-occurring He is 99.99986 atomic percent ^{4}He with the balance ^{3}He.

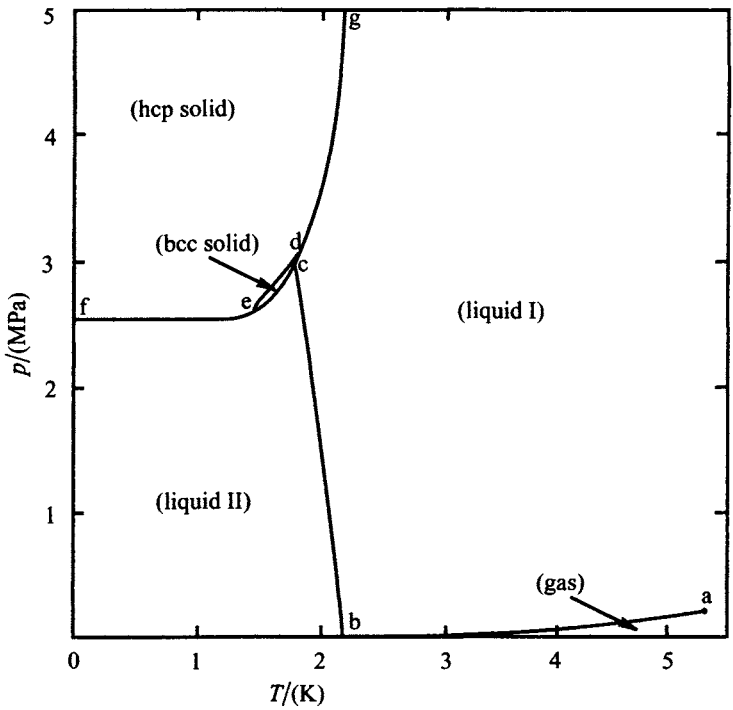

Figure 13.11 The ^{4}He phase diagram at low temperatures.

between the two phases is continuous rather than first order. Figure 13.12 shows the peak in the heat capacity of ^{4}He near the transition. Note from Figure 13.11 that helium remains liquid at the absolute zero of temperature; a pressure in excess of 2.5 MPa must be applied to solidify helium. He is the only known substance that does not solidify with cooling.[k]

The superfluid phase has no measurable viscosity (an extremely unusual property) and thus has very large mass-transfer characteristics. It passes through extremely small holes and flows up and over the sides of containers. This behavior has a quantum mechanical origin. Because the ^{4}He nucleus has zero spin, it follows Bose–Einstein quantum statistics. At low temperatures, these ^{4}He bosons condense to a state of nearly zero momentum with very large de Broglie wavelengths. Many atoms occupy this condensed state, and together they act as a coherent unit. The region in the phase diagram labeled liquid II

[k] Comparison of the entropy calculated from statistical considerations with that obtained by a Third Law integration of the heat capacities shows that the entropy of the superfluid helium is zero at zero Kelvin. Thus, at zero Kelvin, we have a liquid with zero viscosity that has perfect order — a most unusual combination.

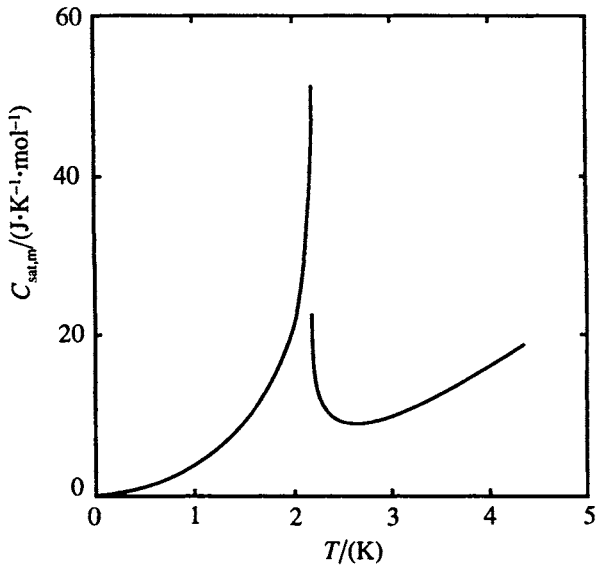

Figure 13.12 Heat capacity of liquid ^{4}He. The lambda transition temperature is 2.172 K.

corresponds to a mixture of normal ^{4}He atoms and those that are in the Bose "condensate" state. As the temperature is lowered, more and more of the atoms condense to the superfluid state in a manner analogous to the development of order below an (order + disorder) transition.[1] The order parameter associated with this transition is a quantum mechanical quantity whose explanation lies outside the scope of this text, but it, too, exhibits the power-law behavior observed for the (liquid + gas) critical transition and (order + disorder) transitions described above.

Other features of interest in the phase diagram of ^{4}He include triple points between various liquid and solid phases of the element. At point c in Figure 13.11, liquid I, liquid II and a body-centered cubic (bcc) solid phase are in equilibrium. The bcc solid exists over a narrow range of pressure and temperature. It converts by way of a first-order transition to a hexagonal close packed (hcp) solid, or to liquid I or liquid II. At point d, liquid I and the two solids (bcc and hcp) are in equilibrium; liquid II and the two solids are in equilibrium at point e.

Line cg is the freezing curve for liquid I while line cef gives the same for liquid II. Line cef has an extremely shallow minimum near 0.8 K. Because this is

[1] Predictions of the extent of conversion to the superfluid state at zero Kelvin vary from 10% to 100%, depending upon the theoretical assumptions employed in the predictions.

a first order transition, the Clapeyron equation

$$\frac{dp}{dT} = \frac{\Delta_{fus}S_m}{\Delta_{fus}V_m}$$

can be applied to gain an insight into the thermodynamic changes involved.[m] The volume change upon melting is fairly large, and it remains nearly constant to very low temperatures. The nearly horizontal slope of the cef line near 0 K indicates that $\Delta_{fus}S_m$ is very small, and it must be zero at the minimum near $T = 0.8$ K. The negative slope below this temperature indicates that $\Delta_{fus}S_m$ must be *negative* in this temperature region, and the solid has a slightly *higher* entropy than the liquid.[n]

a. Helium-3 Phase Properties: The nuclei of ^{3}He are of spin $\frac{1}{2}$ and therefore follow Fermi quantum statistics. A superfluid phase of the type found in ^{4}He is not observed in the phase diagram of ^{3}He, as shown in Figure 13.13. However, like ^{4}He, ^{3}He does not solidify except under pressure. Compression at temperatures below 3 K along line bc gives a solid with a bcc structure. Further compression converts the bcc structure into a solid with the atoms arranged in a hexagonal close-packed (hcp) structure at pressures given by line bd. At temperatures above 3 K, compression of the liquid gives the hcp solid directly. The (solid + solid) and (solid + liquid) transitions are all first order.

A pronounced minimum in the freezing curve bc occurs at approximately 0.3 K. As we have discussed earlier for ^{4}He, this leads to the conclusion that $\Delta_{fus}S_m = \Delta_{fus}H_m = 0$ at the pressure minimum, in this case, 2.98 MPa. Below 0.3 K, the liquid has a lower entropy than the solid, and both the enthalpy and entropy of fusion are negative. It is an interesting exercise to start with liquid ^{3}He at $T = 0.1$ K and $p = 3$ MPa and heat it isobarically. At about 0.6 K, the liquid solidifies with the absorption of heat. Heating the solid to 0.65 K causes it to melt, again with the absorption of heat!

Figure 13.14 shows the phase diagram for liquid ^{3}He in the very low (millikelvin) temperature region. Line abc gives the experimental conditions for equilibrium between the normal liquid and a superfluid designated as liquid A, and between the normal liquid and a different superfluid (liquid B). The transition between the normal liquid and either superfluid is a continuous

---

[m] We need to remember that the Clapeyron equation applies only to first-order phase transitions.

[n] Below 0.8 K, $\Delta_{fus}H_m = T\Delta_{fus}S_m$ is less than zero. Thus, heat must be added (while maintaining the pressure) to freeze liquid ^{4}He at temperatures less than 0.8 K. We will see the same effect in ^{3}He.

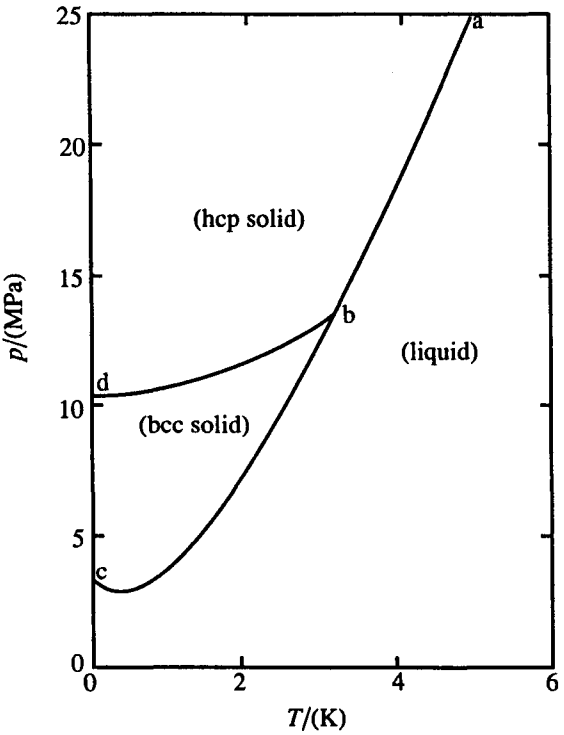

Figure 13.13 The ^{3}He phase diagram at low temperatures.

transition while that between the two superfluids is first order. The heat capacity for the transition from normal liquid into liquid A at $p = 3.34$ MPa is shown in Figure 13.15. The heat capacity behavior resembles that found for the normal to superconducting transition described in the next section, and is of the type designated as a second-order phase transition in Figure 13.1. An explanation for this behavior invokes the formation of bosons with spin = 1 from the coupling of two spin = $\frac{1}{2}$ ^{3}He nuclei as a result of the attractive portion of the van der Waals potential. The coupling also involves the onset of an orbital motion as the two particles rotate about each other. Thus, the particles have a spin angular momentum from the formation of the Bose pair, and an orbital angular momentum from the rotation of the particles within the pair. The spin and orbital momenta couple to give different total angular momentum states. These different states lead to the formation of different superfluid phases. Two superfluids (A and B) are present in zero field, but more can occur in the presence of an applied magnetic field, or if the container holding the fluid is allowed to rotate.

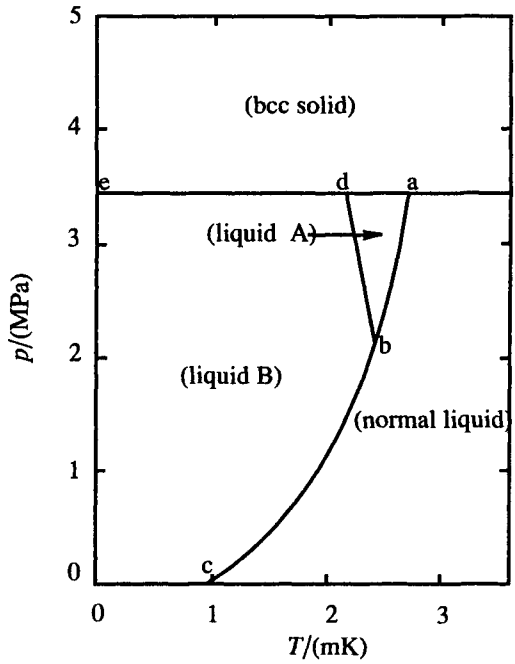

Figure 13.14 The ^{3}He phase diagram at very low temperatures.

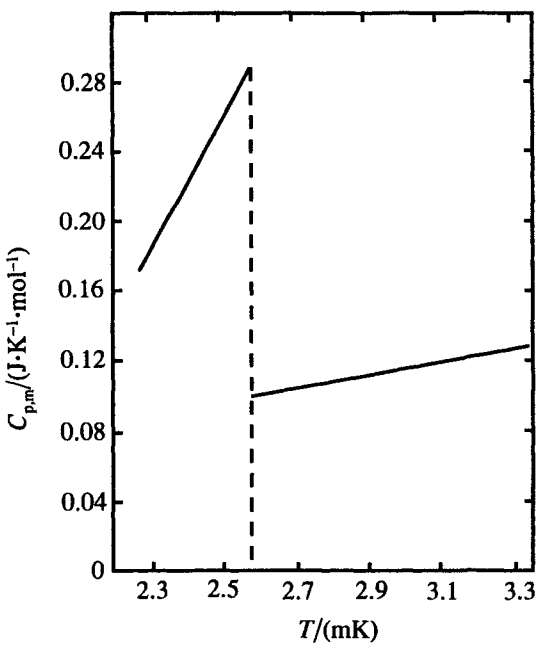

Figure 13.15 Molar heat capacity of ^{3}He at 3.34 MPa and temperatures near the continuous transition from normal liquid into superfluid A.

Conductor–Superconductor Transition: When some metals or compounds are cooled below a certain temperature, their electrical resistance drops abruptly to zero. This temperature is referred to as the superconducting transition temperature. These materials are classified into two categories, type I or type II superconductors, depending upon how a bulk sample behaves in an external magnetic field. In the absence of an external magnetic field, the (superconductor + normal) transition is continuous in both types of superconductors. When a magnetic field is applied, the transition becomes first order in type I superconductors, but remains continuous in the type II superconductors.

When a substance in a type I superconducting phase is placed in an external field, the magnetic flux lines do not penetrate the sample until a critical value of the field, $\mathcal{H}_c$ is reached.[o] This behavior is shown in Figure 13.16a where intensity of magnetization within the sample is plotted against the applied magnetic field. The magnetic field penetrating the sample is given by

$$\mathcal{H} = \mathcal{H}_A + 4\pi M$$

where $\mathcal{H}_A$ is the applied field and $4\pi M$ is the intensity of magnetization within the sample.

Below $\mathcal{H}_c$ in Figure 13.16a, $4\pi M$ is negative and, as can be seen, just balances $\mathcal{H}_A$. This effect (the Meissner effect) keeps the magnetic field at zero within the sample. At $\mathcal{H}_c$, the superconductivity is destroyed, $4\pi M$ becomes zero, and the material re-enters a normal state. The superconducting state can be regained in the magnetic field, however, by cooling to a new, lower, transition temperature. Thus, there exists a set of points ($\mathcal{H}_c$, T_c) that determine a phase line separating the normal and superconducting states. Figure 13.17a shows this relationship for a typical type I superconductor. Below the curve, the superconductor phase is the stable form of the material; above it the normal form is stable. We note that $\mathcal{H}_c$ reaches a maximum at $T = 0$ K. Thus, superconductivity will not occur in the sample at any temperature for magnetic field strengths exceeding this value. The critical magnetic fields as a function of temperature for a number of type I superconductors are plotted in Figure 13.17b.

The behavior of type II superconductors in an applied field is more complicated. This behavior is illustrated in Figure 13.16b. Below a certain field strength $\mathcal{H}_{c,1}$, the magnetic field lines are repelled, and the material is superconducting. From $\mathcal{H}_{c,1}$ to a second critical field strength $\mathcal{H}_{c,2}$, magnetic field lines are able to penetrate the type II material in its superconducting state

[o] The repulsive force of the expulsion of these field lines, known as the Meissner effect, leads to the phenomenon of levitation — a magnet placed above a superconductor floats suspended above the top of the superconductor.

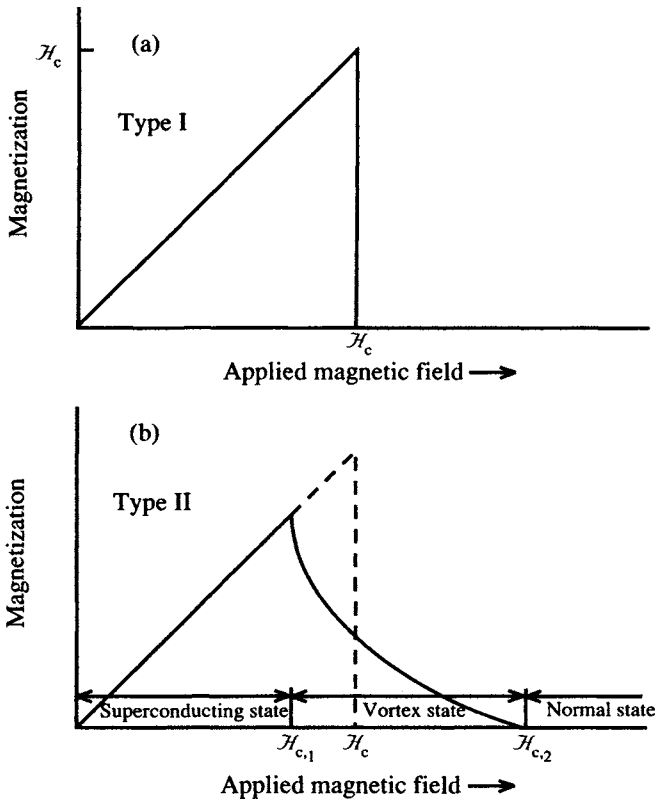

Figure 13.16 Magnetization verses applied magnetic field for (a) a type I superconductor and (b) a type II superconductor. For the type I superconductor, the magnetic flux does not penetrate the sample below $\mathcal{H}_c$ where the sample is a superconductor. Above $\mathcal{H}_c$, the sample is a normal conductor. For the type II superconductor, the magnetic field starts to penetrate the sample at $\mathcal{H}_{c,1}$, a magnetic field less than $\mathcal{H}_c$, the thermodynamic critical field. Superconductivity remains in the so-called vortex state between $\mathcal{H}_c$ and $\mathcal{H}_{c,2}$ until $\mathcal{H}_{c,2}$ is attained. At this magnetic field, complete penetration occurs, and the sample becomes a normal conductor.

without destroying the superconductivity. The material is said to be in a **vortex state** between these two values. At fields higher than $\mathcal{H}_{c,2}$, the superconductivity is lost and the substance returns to the normal state. In some superconductors, the range of the magnetic field in the vortex state may be very large, with $\mathcal{H}_{c,2}$ being as much as a hundred times larger than $\mathcal{H}_{c,1}$.[p]

[p] Type II superconductors find applications as the windings in superconducting magnets where high magnetic field strengths are the desired outcome.

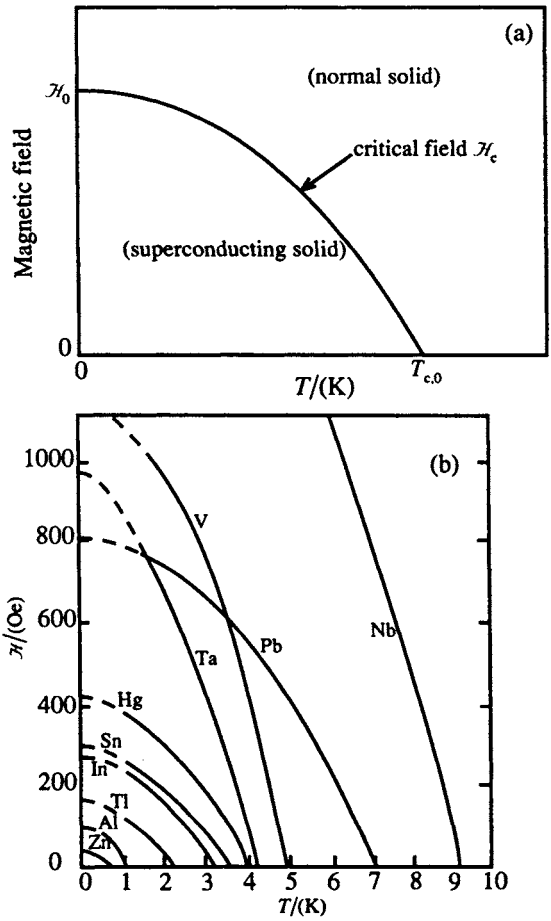

Figure 13.17 (a) Typical graph of critical magnetic field $\mathcal{H}_c$ as a function of temperature for a type I superconductor. Magnetic fields greater than $\mathcal{H}_c$ suppress the superconducting transition. (b) Critical magnetic fields for several type I superconductors.

Soft metallic elements such as Al, In, Pb, Hg, Sn, Zn, Tl, Ga, Cd, V and Nb are type I superconductors. Alloys and chemical compounds such as Nb_3Sn, V_3Ga, and $1La_3In$, and some transition elements, are type II superconductors. Type II substances generally have a higher T_c than do type I superconductors. The recently discovered transition metal oxide superconductors have generated intense interest because they are type II superconductors with very high transition temperatures. Table 13.1 summarizes T_c for selected superconductors.

Figure 13.18[5] illustrates the behavior of the entropy and heat capacity respectively of aluminum (a type I superconductor) in the vicinity of its (continuous) superconducting transition. Referring back to Figure 13.1, we

see that this continuous transition is of the type that we have designated as second order. As is required by the Ehrenfest definition of second-order transitions, the entropy of the normal and superconducting states are the same at the transition temperature,[q] and the heat capacity shows a finite

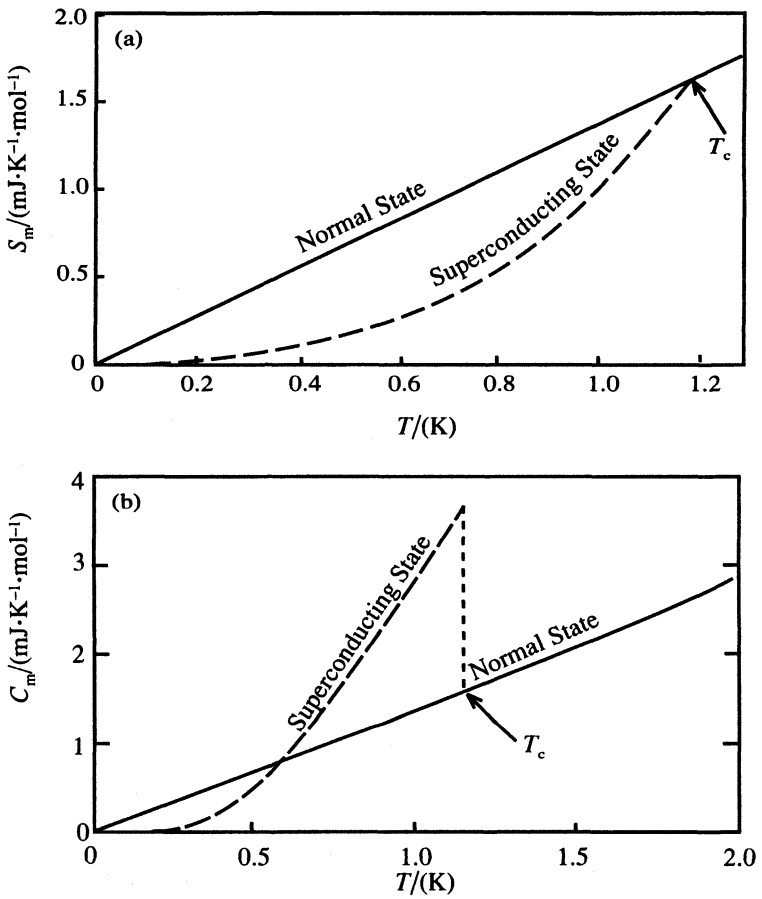

Figure 13.18 (a) Entropy S_m and (b) heat capacity C_m of Al in the normal and superconducting states as a function of temperature. The solid line represents the entropy or heat capacity of normal Al, while the dashed line represents values for the superconducting state. The results for normal Al below the superconducting transition temperature T_c of 1.1796 K were made in 0.03 Tesla magnetic field to suppress the superconduction transition.

[q] Note in Figure 13.18a that, in agreement with the Third Law, the entropy of both the normal and superconducting forms of Al becomes zero at the absolute zero of temperature.

discontinuity at T_c.[r] However, this heat capacity cannot be adequately represented by the form seen earlier for other continuous transitions. We will discuss an explanation for this later.

a. Effect of Pressure on Superconducting Transitions: In general, increasing pressure lowers the superconducting transition temperature for type I superconductors. Figure 13.19[6] shows how T_c varies with pressure for Al.[s] Table 13.1 gives a value of dT_c/dp of $-255\ \mu K \cdot MPa^{-1}$ for Al. Similar negative values are observed for other type I superconductors. The new high-temperature ceramic superconductors, which are non-stoichiometric oxides of copper mixed with other metallic elements, show a different behavior with pressure. Their transition temperatures tend to increase with pressure, at least over some initial pressure range, as shown in Figure 13.20.[7] The compound

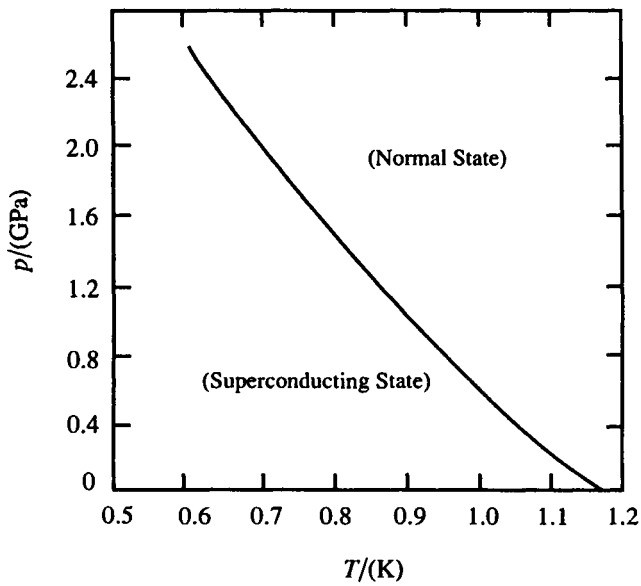

Figure 13.19 Effect of pressure on the superconducting transition in aluminum.

[r] The normal state was maintained below T_c by imposing an external field of 0.3 Tesla on the sample.

[s] In the paper reporting the p against T phase diagram for Al, Levy and Olsen explore the possibility that there exists a value of p above which the superconducting transition cannot occur, even at 0 K. The authors conclude that, in agreement with the theory of Bardeen, Cooper, and Schrieffer, which applies to type I superconductors, a critical p does not occur. That is, superconductivity cannot be destroyed simply by applying high pressure.

Table 13.1 Superconducting transition temperatures for selected substances

Element or compound	Type	$T_c/(K^*)$	$dT_c/dp/(\mu K \cdot MPa^{-1})$
Cd	I	0.519	−182
Zn	I	0.851	−247
Al	I	1.1796	−255
Tl	I	2.39	−230
In	I	3.4145	−391
Sn	I	3.72	−463
Hg(α)	I	4.15	−366
Ta	I	4.48	−260
La	II?	4.90	1900
V	II?	5.30	110
Pb	I	7.19	−386
Nb	I	9.5	0
La_3In	II	10.4	–
Nb_3Al	II	17.5	–
Nb_3Sn	II	18.05	–
K_3C_6O	II	19.2	–
Nb_3Ge	II	23.2	–
Rb_2CsC_{60}	II	31.3	–
$YBa_2Cu_3O_{6.9}$	II	95.5	–
$HgBa_2Ca_2Cu_3O_{8+\delta}$	II	138	–

* Value at zero magnetic field and at low pressures.

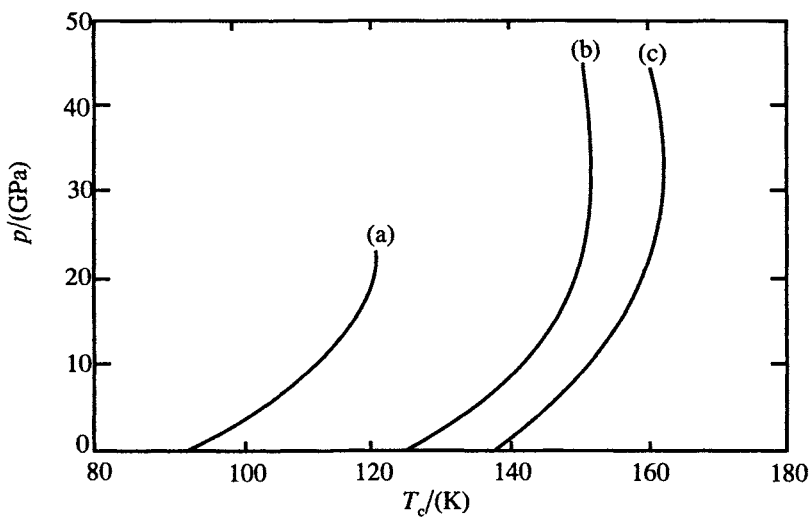

Figure 13.20 Effect of pressure on the superconducting transition temperature of the high-temperature superconductors: (a) $HgBa_2CuO_{4+\delta}$, (b) $HgBa_2CaCu_2O_{6+\delta}$, (c) $HgBa_2Ca_2Cu_3O_{8+\delta}$.

$HgBa_2Ca_2Cu_3O_{8+\delta}$ (known as Hg-1223) has a T_c value at ambient pressure of 138 K, which increases to 164 K at 31 GPa, then decreases slowly with increasing pressure.

13.2 Modern Theories of Phase Transformation

As we have illustrated above, properties associated with continuous or critical phase transitions behave similarly as one approaches the critical point. We have concentrated on two kinds of properties, the density or order parameter and the heat capacity, and have shown that they vary with temperature as given by equations (13.1), (13.2), and (13.4). That is,

$$\rho_l - \rho_g \sim \left| \frac{T - T_c}{T_c} \right|^{\beta} \tag{13.1}$$

or

$$\eta \sim \left| \frac{T - T_c}{T_c} \right|^{\beta} \tag{13.4}$$

and

$$C \sim \left| \frac{T - T_c}{T_c} \right|^{-\alpha}. \tag{13.2}$$

Other properties that behave in a similar fashion include the isothermal compressibility of fluids and the magnetic susceptibility for magnetic transitions.

Despite arising from a diverse set of intermolecular or interatomic forces, as seen by our examples in the previous section, these phenomena give rise to a very similar set of characteristics near the phase transition. The observation of this kind of behavior began more than a century ago, but the explanation of why this should be so has occurred only within the past 25 years. The details associated with the explanation are developed in renormalization group theory whose treatment lies outside the scope of this text. We will present only a qualitative survey of the results of the theory.

Equations of the form shown above as equations (13.1), (13.2) and (13.4) are said to be power-law relationships. This leads to a behavior that is in some ways similar to that discovered by van der Waals many years ago and

formulated as "the law of corresponding states". In the law of corresponding states, the reduced temperature is a ratio of absolute temperatures. However in critical phenomena, the reduced temperature is a temperature difference, relative to and scaled by the critical temperature. In the case of continuous phase transitions, there are several sets of curves that describe the different properties, each governed by a critical exponent, designated as α, β, γ, etc. Unlike the theory of corresponding states, power-law behavior is only observed in the limit as $T \rightarrow T_c$. The temperature interval over which the power law is followed depends on the particular property, and some other characteristics of the transition that we will discuss below. Table 13.2 defines the critical exponents we will consider here,[t] and Table 13.3 summarizes a number of transitions and systems for which these exponents have been measured.

Table 13.2 Some examples of power-law behavior and critical exponents

Critical exponent/related properties	Power-law definition
α Heat capacity, C	$C \sim \left\lvert \frac{T - T_c}{T_c} \right\rvert^{-\alpha}$
β Order parameter, η Magnetization, M Density difference, $\rho_l - \rho_g$ Site occupation	$\eta \sim \left\lvert \frac{T - T_c}{T_c} \right\rvert^{\beta}$
γ Isothermal compressibility, κ_T Magnetic susceptibility, $\chi_T = (\partial M/\partial \mathcal{H})_T$	$\kappa_T, \chi_T \sim \left\lvert \frac{T - T_c}{T_c} \right\rvert^{-\gamma}$
ν Correlation length, ξ	$\xi \sim \left\lvert \frac{T - T_c}{T_c} \right\rvert^{-\nu}$

[t] These critical exponents are often referred to as the static exponents because they are associated with equilibrium thermodynamic quantities. A second set, referred to as the dynamic exponents are associated with relaxation phenomena, e.g. correlation phenomena.

Table 13.3 Summary of critical exponents for various properties and transitions

Example and dimensionality		α	β	γ	ν	Reference*
Liquid–gas critical points						
SF_6	1		0.327 ± 0.006			GLD, p. 8
^3He	1		0.321 ± 0.006			GLD, p. 8
H_2O	1		0.35			BDFN, p. 8
Xe	1	<0.2	0.35 ± 0.015	1.3		BDFN, p. 22
H_2O	1			1.2		BDFN, p. 7
Binary fluid						
CH_3OH/C_6H_{12}	1	0.113 ± 0.005	0.322 ± 0.005	1.239 ± 0.002	0.625 ± 0.006	BDFN, p. 22
Magnetic critical points						
$DyAlO_3$	3		0.311 ± 0.005			GLD, p. 10
Fe	3	-0.03 ± 0.12	0.37 ± 0.01	1.33 ± 0.015	0.69 ± 0.02	BDFN, p. 22
Ni	3	0.04 ± 0.12	0.358 ± 0.003	1.33 ± 0.02	0.64 ± 0.1	BDFN, p. 22
Superfluid transition						
$(I \rightarrow II)$ in He^4	1	-0.014 ± 0.016	0.34 ± 0.01	1.33 ± 0.03	0.672 ± 0.001	BDFN, p. 22
Order–disorder transition						
β-brass	1	0.05 ± 0.06	0.305 ± 0.005	1.25 ± 0.02	0.65 ± 0.02	BDFN, p. 22

*GLD: Cited by N. Goldenfeld, *Lectures on Phase Transitions and the Renormalization Group*, Addison-Wesley, Reading, Mass., 1992.
BDFN: Adapted from tables by J. J. Binney, N. J. Dowrick, A. J. Fisher and M. E. J. Newman, *The Theory of Critical Phenomena, An Introduction to the Renormalization Group*, Clarendon Press, Oxford, 1992.

The power-law mathematical relationship leads to an interesting functional behavior as one approaches the critical temperature. Consider a general function $f(\varepsilon) \propto |\varepsilon|^{-1}$, where $\varepsilon = |(T - T_c)/T_c|$. Figure 13.21 shows that the function looks the same over various scales of ε. Figure 13.21a shows the region $-1 \leqslant \varepsilon < 0$ where $f(\varepsilon)$ goes from 0 to 100; Figure 13.21b expands the scale by three orders of magnitude: $-1 \times 10^{-3} \leqslant \varepsilon < 0$ and $f(\varepsilon)$ must be represented on a scale from 0 to $100 \times 10^{+3}$. Another reduction in the ε scale by a factor 10^2 as

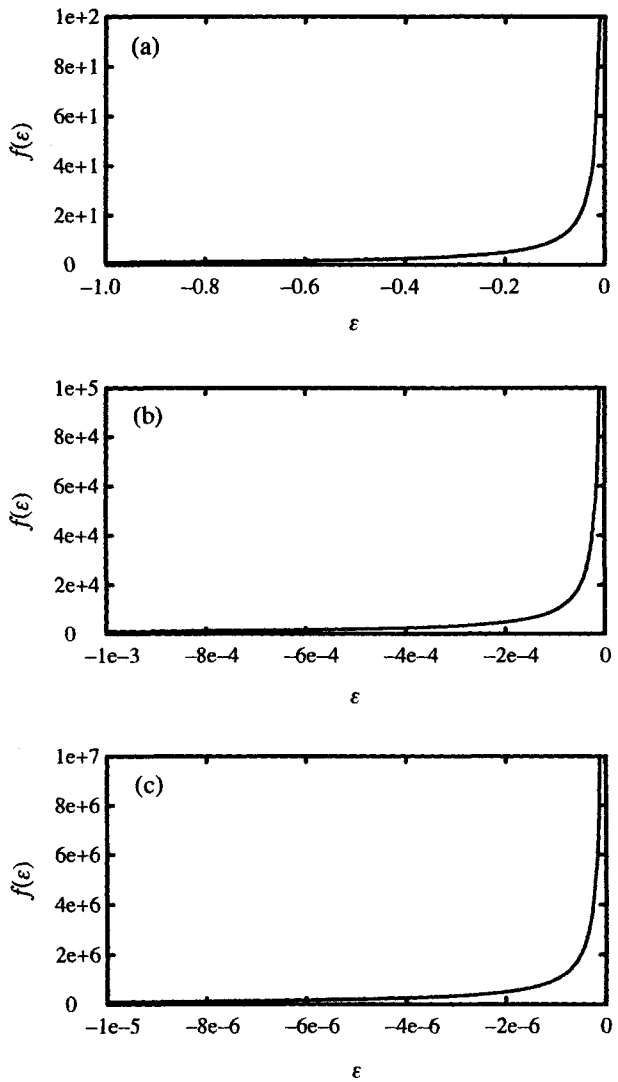

Figure 13.21 Graph of $f(\varepsilon)$ against different ranges of ε, where $f(\varepsilon) = |\varepsilon|^{-1}$.

shown in Figure 13.21c increases $f(\varepsilon)$ by 10^2. Thus, functions that follow a power-law behavior are invariant under a change of scale; they look the same as one increases the scale indefinitely!

Not only do the thermodynamic properties follow similar power laws near the critical temperatures, but the exponents measured for a given property, such as heat capacity or the order parameter, are found to be the same within experimental error in a wide variety of substances. This can be seen in Table 13.3. It has been shown that the same set of exponents (α, β, γ, ν, etc.) are obtained for phase transitions that have the same spatial (d) and order parameter (n) dimensionalities. For example, (order + disorder) transitions, magnetic transitions with a single axis about which the magnetization orients, and the (liquid + gas) critical point have $d = 3$ and $n = 1$, and all have the same values for the critical exponents. Superconductors and the superfluid transition in ^{4}He have $d = 3$ and $n = 2$, and they show different values for the set of exponents. Phase transitions are said to belong to different **universality classes** when their critical exponents belong to different sets.

Early attempts to develop theories that accounted for the power-law behavior and the actual magnitudes of the various critical exponents include those by van der Waals for the (liquid + gas) transition, and Weiss for the (ferromagnetic + paramagnetic) transition. These and a later effort called the Landau theory have come to be known as **mean field theories** because they were developed using the average or mean value of the order parameter. These theories invariably led to values of the exponents that differed significantly from the experimentally obtained values. For example, both van der Waals and Weiss obtained a value of 0.50 for β, while the observed value was closer to 0.35.

From thermodynamic considerations, early investigators were able to show that relationships, now called scaling laws, existed among sets of the critical exponents, with the same relationships holding for all universality classes. An example of these is the Rushbrooke scaling law, which was first proved as an inequality:

$$\alpha + 2\beta + \gamma \geqslant 2. \tag{13.5}$$

We will illustrate the proof of equation (13.5) as an example of the application of conventional thermodynamics to this problem. Let $C_{\mathcal{H}}$ be the heat capacity of a magnetic system at constant field strength, M be the magnetization, and $\chi_T = (\partial M/\partial \mathcal{H})_T$ be the magnetic susceptibility. From Table 13.2 we can see that just below the critical temperature:

$$C \sim (-\varepsilon)^{-\alpha},$$

$$M \sim (-\varepsilon)^{\beta},$$

and

$$\chi_T \sim (-\varepsilon)^{-\gamma}.$$

If $M \sim (-\varepsilon)^{\beta}$, then $(\partial M/\partial T)_{\mathcal{H}} \sim (-\varepsilon)^{\beta-1}$ since $[(\mathrm{d}(-\varepsilon^{\beta})/\mathrm{d}T)] = \beta \cdot (-\varepsilon)^{\beta-1}$. Therefore, $[(\partial M/\partial T)_{\mathcal{H}}]^2 \sim (-\varepsilon)^{2(\beta-1)}$. From thermodynamic derivations analogous to those which lead to

$$C_p - C_V = \alpha_p^2 VT/\kappa_T,$$

where $\alpha_p = (1/V)(\partial V/\partial T)_p$ and $\kappa_T = -(1/V)(\partial V/\partial p)_T$, one can show that

$$C_{\mathcal{H}} - C_M = T\alpha_{\mathcal{H}}^2/\chi_T,$$

where $\alpha_{\mathcal{H}} = (\partial M/\partial T)_{\mathcal{H}}$ and $\chi_T = (\partial M/\partial \mathcal{H})_T$. Since $C_{\mathcal{H}}$ and C_M are positive, $C > (C - C_M)$. One can substitute the power-law behavior of these functions to get

$$C_{\mathcal{H}} \geqslant \frac{T\alpha_{\mathcal{H}}^2}{\chi_T}$$

so that

$$(-\varepsilon)^{-\alpha} \geqslant T\frac{(-\varepsilon)^{2(\beta-1)}}{(-\varepsilon)^{-\gamma}} > (-\varepsilon)^{2(\beta-1)+\gamma}.$$

It can be shown that if two functions follow power-law relationships, $f(x) \sim x^{\lambda}$ and $g(x) \sim x^{\phi}$ and $f(x) \leqslant g(x)$ for sufficiently small positive x, then $\lambda \geqslant \phi$.[u] Thus,

$$2(\beta - 1) + \gamma \geqslant -\alpha$$

or

$$\alpha + 2\beta + \gamma \geqslant 2.$$

Other relationships among different combinations of critical exponents have been developed.[8]

---

[u] See H. E. Stanley, *Introductions to Phase Transitions and Critical Phenomena*, Oxford University Press, New York, 1971, p. 52 for the proof.

Widom[9] and others have tied down the relationships between the critical exponents still further. They proposed that the singular portion of the thermodynamic potential was a homogeneous function[v] of the reduced temperature and the other variables. This assumption leads to the observance of the power-law behavior for the various thermodynamic properties and produces the scaling laws as equalities rather than inequalities of the type developed above [equation (13.5)].

Certain experimental techniques, including neutron and optical scattering, show that properties like the order parameter fluctuate significantly about the average in a bulk sample as one approaches the critical temperature. Within a given microscopic region, the actual value of the order parameter (and related quantities such as magnetic susceptibility) may be very different from the average. The average spatial dimension associated with these fluctuating regions is called a **correlation length,** ξ. The phenomenon called critical opalescence that we have already discussed in regard to the (liquid + gas) critical point arises because the fluctuations in density occur in spatial regions that are on the order of the wavelength of visible light (400–750 nm).

One can rationalize the existence and behavior of these fluctuations near the critical point. As an example, let us consider an (order + disorder) transition. At high temperatures, entropic factors favor the disordered phase, and the free energy of the disordered phase is significantly lower than that of the ordered phase. However, as the temperature is lowered, the free energy of the two phases approach one another. It "costs" little free energy to create small regions in which there is more order than in the bulk phase, and there is not much driving force to eliminate such regions once they are formed. In fact, in such regions, the tendency to maximize entropy by increasing disorder is in competition with the tendency to minimize internal energy or enthalpy by ordering the interactions between particles. As the temperature gets closer to the critical temperature, free-energy differences between the two phases get even smaller, and larger and larger "ordered" regions can be tolerated within the bulk.

The correlation length is also found to scale in a power-law fashion, and it becomes very large at the transition temperature. One of the most significant results of renormalization group theory is to show that the behavior of the correlation length in the critical region is the basis of the power-law singularities observed in the other thermodynamic properties.

---

[v] For one variable, a homogeneous function is one for which $f(\lambda x) = \lambda^p f(x)$ where p is called the degree of homogeneity. The static scaling hypothesis actually is a more generalized form: $f(\lambda^a x, \lambda^b y) = \lambda f(x, y)$. The values of the two scaling parameters, a and b, are not specified in the scaling hypothesis but one can derive relationships involving a and b that yield the critical exponents. For example, for a magnetic system, if one takes the Gibbs free energy as $G(\lambda^a \epsilon, \lambda^b)$ where ϵ is the reduced temperature and, $\mathcal{H}$ is the field strength, then $\beta = (1 - b)/a$.

Another important outcome of modern theories is to show that within a critical temperature interval, $|T - T_c|/T_c$, the thermodynamic properties are generally dominated by the fluctuations, and it is insufficient to deal only with average values of the order parameter. The width of the critical temperature interval turns out to vary for different kinds of phase transitions. It can be shown to depend on the dimensionality of the system and the nature of the interparticle interactions. When the interactions extend over long distances, fluctuations are reduced and the critical region is narrowed. The interactions associated with phase transitions in magnetic systems, the (liquid + gas) critical point, the superfluid transition in ^{4}He, and (order + disorder) transitions, extend over distances on an interatomic scale. The critical intervals associated with these transitions are (very roughly) on the order of 1. That is, $\Delta T = |T - T_c| \approx T_c$. While this is a very broad estimate, it does indicate that the critical interval is experimentally accessible. For these systems, measurements made within a millikelvin, or even a few hundredths of a Kelvin, of T_c are well within the critical interval. Thus, properties like the heat capacity do not exhibit the Ehrenfest second-order discontinuity, but show instead the divergence that gives rise to the λ shape. In the case of the superconductors described earlier, however, the interactions extend over much longer distances, and the critical temperature interval is expected to be much smaller. Some estimates put it at the order of $(10^{-15})T_c$. Since it is not currently possible to make measurements this close to the transition temperature, experiments are made in the region where fluctuations of the order parameter are not significant and a mean-field discontinuous type behavior is observed.[w]

The inclusion of fluctuations severely complicates the mathematical analysis of physical models and only some simple models can be solved exactly. For these models, however, the results give critical exponents that agree with well-established experimental values.

Several paradoxes have become apparent from modern descriptions of phase transitions, and these have driven much of the research activity in this field. The intermolecular interactions that are responsible for the phase transition are relatively short-ranged, yet they serve to create very long-range order at the transition temperature. The quantum mechanical details of the interactions governing various transitions are very different, and the length scales over which they operate vary considerably, yet the observation of scaling laws and the equivalences of a given critical exponent value within a fixed dimensionality of the order parameter show that some additional principle not described by quantum mechanics must also be at work. Also, the partition

[w] The heat capacity for the superconducting transition shown in Figure 13.18 demonstrates this effect.

function, whose mathematical form is summarized in Chapter 11, is a smoothly varying function with temperature. How can such a function give rise to the singularities — that is, divergences in the thermodynamic functions — that are observed in the critical regions?

The answer to both questions reveals that unlike many physical situations where "the devil is in the details", the phenomenon which underlies the observed behavior follows from the laws of statistical mechanics. A simple argument by Kadanoff[10] illustrates in a physical way the process that underlies renormalization group theory. Consider a lattice of interacting magnetic spins. At the lowest level are the interactions of spins within the unit cell. However, when the system is near the critical temperature, its correlation length will be long enough that within each unit cell, one can treat the cell as having a single "effective spin". Its value can be obtained by a statistical averaging over the possible spin configurations within the cell. Then one can consider a block of neighboring cells, each cell being represented by the average spin of the intracellular components. The average spin from each block of cells can be obtained from an averaging over the block. The interaction between the average block spins should follow the same physics as that within the individual cells but with the coupling constants scaled by some factor. Again, if the correlation length is long relative to the dimensions of the block, a single average spin represents well the cells within each block.

One can continue to fashion larger and larger blocks made up of successive sets of smaller blocks. Each time, one expects the Hamiltonian that describes the physics to be of the same form, but with scaled interaction coefficients. This average and rescaling process continues as long as the actual correlation length is larger than the block size. For each process, however, the correlation length expressed on the new length scale becomes smaller, since the length scale increases with each round. Since the correlation length has been reduced, the system can be regarded as being farther from the critical point. This process is sometimes referred to as a **coarse-graining transformation** since it progressively smears out the details of the microscopic interactions under successive block spin transformations. The singular behavior that is observed in the thermodynamic properties arises after an infinite number of these transformations are performed.

The key aspects of the modern understanding of phase transitions and the development of renormalization group theory can be summarized as follows. First was the observation of power-law behavior and the realization that critical exponents were, to some extent, universal for all kinds of phase transitions. Then it became clear that theories that only treated the average value of the order parameter failed to account for the observed exponents. The recognition that power-law behavior could arise from functions that were homogeneous in the thermodynamic variables and the scale-invariant behavior of such functions

gave insights into the role of the diverging correlation length. Development of statistical processes to incorporate fluctuations showed how their role led to the existence of singularities and nonclassical exponents in the power laws. Connections between scaling laws for static and dynamic phenomena tied together formerly disparate areas of research. The conceptual insights of block transformations and the techniques for carrying out the transformations on the system Hamiltonians provide the ability to determine critical exponents for model systems that agree with experimental values.

Problems

P13.1 Compounds of magnesium, silicon and oxygen play an important role in the geochemistry of the earth's mantle. The phase behavior of one of these, magnesium silicate (Mg_2SiO_4), has been widely studied by geologists. In the following table are summarized the temperatures and pressures at which we have two-phase equilibrium among the three phases of this compound: olivine(s), β-phase(s), and the liquid.[11]

		β-phase		Olivine		Liquid	
T/(K)	p/(GPa)	V_T°/ ($cm^3 \cdot mol^{-1}$)	S_T°/ ($J \cdot K^{-1} \cdot mol^{-1}$)	V_T°/ ($cm^3 \cdot mol^{-1}$)	S_T°/ ($J \cdot K^{-1} \cdot mol^{-1}$)	V_T°/ ($cm^3 \cdot mol^{-1}$)	S_T°/ ($J \cdot K^{-1} \cdot mol^{-1}$)
1873	15.0	38.70	380.80	41.31	385.46		
2673	13.0			42.72	463.57	43.96	529.87
2873	18.4	38.49	463.70			42.18	549.20

(Note: The molar volumes of each phase are given for the specified p and T. However, the molar entropies are given for T, but at $p = 0.1$ MPa pressure.)

(a) Use this data to estimate the slopes (dp/dT) of the line for each two-phase equilibrium. (You may neglect the pressure dependence in S. This is not a bad assumption, although probably better for the β-olivine equilibrium than for the equilibria involving the liquid.)

(b) With the calculated slopes and a data point for each two-phase equilibria, construct an estimate of the phase diagram for Mg_2SiO_4 for pressures between 10 and 22 GPa and temperatures between 1673 and 3273 K. Identify the phases present in each region and comment on any problems with the diagram.

(c) Estimate a value for the triple point involving the β-phase, olivine and liquid from your diagram. Because of the assumptions (or errors in the data used to calculate the high-temperature and high-pressure thermodynamic quantities), the three lines probably will not intersect in a single point. Make a reasonable estimate based upon this graph.

(d) Comment on the possible sources of the errors that lead to this difficulty.

P13.2 The phase transition of ^{4}He into its superfluid phase from the normal liquid is continuous. The order parameter, η, of the transition has been found to vary as the square root of the ratio of the superfluid density, ρ_s, to the total density, ρ_t. Some data for η as a function of $(T_c - T)$ are given below. Obtain the critical exponent, β, for the order parameter from this data.

$(T_c - T)/(10^{-3}\ \mathrm{K})$	$\eta = (\rho_s/\rho_t)^{1/2}$
0.50	0.0943
1.00	0.1182
1.25	0.1280
2.00	0.1491
3.50	0.1806
5.00	0.2032
6.30	0.2192
8.02	0.2379
10.00	0.2563

P13.3 The following data are available for CCl_4. Determine

(a) The molar enthalpy of sublimation of solid CCl_4 at $T = 215$ K.

(b) The normal boiling point of CCl_4.

(c) The (p, T) phase diagram for CCl_4. Draw two separate diagrams showing (i) the (solid + liquid + vapor) diagram from 0 to 100 bar pressure and 0 to 600 K temperature and (ii) the (solid + liquid) diagram (leave out the gas phase, but be sure to include all three solid phases) from 0 to 13,000 bar and 200 to 500 K.

Data

$T_c = 556.3$ K

$p_c = 45.58$ bar

Melting point at 1 atm (1.01) bar pressure = 250.41 K

Solid I = Solid II = Solid III at 394 K and 8714 bar

Solid I = Solid II at 225.31 K and 1.01 bar
Solid II = Solid I; $\Delta_{trans}H^{\circ}_{m} = 38.74\ J \cdot g^{-1}$ at 225.31 K
Solid I = liquid; $\Delta_{fus}H^{\circ}_{m} = 21.28\ J \cdot g^{-1}$ at 250.41 K

Phase Equilibria for CCl_4

Solid II = Gas		Liquid = Gas		Solid I = Liquid	
T/(K)	$10^4\ p$/(bar)	T/(K)	p/(bar)	T/(K)	p/(bar)
203.4	1.94	253.1	0.01322	250.2	0.981
207.8	2.99	273.1	0.0441	257.9	214
213.5	5.12	293.1	0.1194	263.1	360
214.3	5.46	313.1	0.2812	268.1	503
216.3	6.72	333.1	0.5853	273.1	643
218.3	7.93	343.1	0.8183	278.1	780
223.0	12.33	363.1	1.482	280.6	849
		373.1	1.944	283.1	920
		393.1	3.188	318.7	1962
		413.1	4.966	382.7	3922
		433.1	7.385	429.6	5884
		453.1	10.53	468.3	7846
		473.1	14.58		
		493.1	19.73		
		513.1	26.17		
		533.1	34.04		
		553.1	43.76		
		556.3	45.58		

Solid I = Solid II		Solid II = Solid III		Solid I = Solid III	
T/(K)	p/(bar)	T/(K)	p/(bar)	T/(K)	p/(bar)
309.9	3922	299.5	6865	394.0	8714
331.5	4903	345.1	7846	398.7	8826
351.5	5884	394.0	8714	417.1	9806
367.5	6865			441.1	10287
382.7	7846			473.9	11768
394.0	8714				

References

1. See P. W. R. Bessonette and M. A. White, "Realistic Thermodynamic Curves Describing a Second-Order Phase Transition", *J. Chem. Ed.*, **76**, 220–223 (1999), for a discussion of the relationships among the different curves shown in Figure 13.1.
2. Data taken from M. W. Chase, Jr., C. A. Davies, J. R. Downey, Jr., D. J. Frurip, R. A. McDonald, and A. N. Syverud, "JANAF Thermochemical Tables, Third Edition," *J. Phys. Chem. Ref. Data*, **14**, Supplement No. 1, 1985.
3. Data to construct the phase diagram were taken from S. P. Clark, Jr., "Effect of Pressure on the Melting Points of Eight Alkali Halides," *J. Chem. Phys.*, **31**, 1526–1531 (1959).
4. J. W. Johnson, P. A. Agron, and M. A. Bredig, "Molar Volume and Structure of Solid and Molten Cesium Halides," *J. Am. Chem. Soc.*, **77**, 2734–2737 (1955).
5. N. E. Phillips, "Heat Capacity of Aluminum Between 0.1 °K and 4.0 °K", *Phys. Rev.*, **114**, 676–685 (1959).
6. M. Levy and J. L. Olsen, "Can Pressure Destroy Superconductivity in Aluminum?", *Solid State Commun.*, **2**, 137–139 (1964).
7. L. Gao, Y. Y. Xue, F. Chen, Q. Xiong, R. L. Meng, D. Ramirez, and C. W. Chu, "Superconductivity up to 164 K in $HgBa_2Ca_{m-1}Cu_mO_{2m+2+\delta}$ (m = 1, 2, and 3) under Quasihydrostatic Pressures", *Phys. Rev. B., Ser. 3*, **50**, 4260–4263 (1994).
8. See H. E. Stanley, *Introductions to Phase Transitions and Critical Phenomena*, Oxford University Press, New York, 1971, p. 52. for an excellent introduction to the early development of the current treatments of critical phase transitions. More modern texts that are helpful include two books in the "Frontiers in Physics" Series published by Addison-Wesley, Reading, MA: S. K. Ma, *Modern Theory of Critical Phenomena*, Vol. 64, 1976, and N. Goldenfeld, *Lectures on Phase Transitions and the Renormalization Group*, Vol. 85, 1992.
9. B. Widom, "Surface Tension and Molecular Correlations near the Critical Point", *J. Chem. Phys.*, **43**, 3892–3897 (1965).
10. L. P. Kadanoff, "Scaling Laws for ISING Models Near T_c", *Physics*, **2**, No. 6, 263–272 (1966).
11. The experimental data were taken from Y. Fei, S. K. Saxena, and A. Navrotsky, "Internally Consistent Thermodynamic Data and Equilibrium Phase Relations in the System $MgO–SiO_2$ at High Pressure and High Temperature", *J. Geophys. Res.*, **95**, 6913–6928 (1990).

Chapter 14

Applications of Thermodynamics to Phase Equilibria Studies of Mixtures

14.1 Phase Changes for Mixtures

We are now ready to expand our discussion of phase equilibria to consider composition as a variable. In doing so, we will usually hold temperature constant and see the effect of composition (usually mole fraction) on the equilibrium pressure (or pressure on the equilibrium mole fraction); or we will hold pressure constant and describe the relationship between temperature and mole fraction.

We will first describe (vapor + liquid) equilibria and (liquid + liquid) equilibria, with the extension to the critical region designated as (fluid + fluid) equilibria. Next we will describe (solid + liquid) equilibria, and then include systems in which several kinds of equilibria occur at the same time. For example, we will look at systems where (vapor + liquid) equilibria and (liquid + liquid) equilibria are present in the same phase diagram.[1]

The key to the study of phase equilibria is the phase diagram, interpreted by the phase rule and the Clapeyron equation. Such phase diagrams will serve as the basis for our discussion.

We intend to limit our discussion primarily to binary systems. Multicomponent systems are of interest and of value, but we will leave the discussion of such systems to more specialized texts. In considering binary systems, we may want to remind ourselves of what constitutes a component. For example, the system ($H_2SO_4 + H_2O$) is a binary system, although all of the following (and more) chemical species may be identified in the mixtures: $H^+(aq)$, $H_3O^+(aq)$, $HSO_4^-(aq)$, $SO_4^{2-}(aq)$, $H_2S_2O_7$, $H_2SO_4 \cdot H_2O(s)$, $H_2SO_4 \cdot 2H_2O(s)$, $H_2SO_4 \cdot 3H_2O(s)$, $H_2SO_4 \cdot 4H_2O(s)$, $H_2SO_4 \cdot 6.5H_2O(s)$, and $H_2SO_4 \cdot 8H_2O(s)$. All of these species are related

by chemical equations that limit the number of independent components to two.[a]

14.2 (Vapor + Liquid) Equilibria

Figure 14.1 summarizes the vapor pressure against composition, and boiling temperature against composition phase diagrams for {(x_1 or y_1) c-$C_6H_{11}CH_3$ + (x_2 or y_2) c-C_6H_{12}}. In Figure 14.1a, which is a graph of the (vapor) pressure p against composition at a fixed temperature, the upper curve is a graph of p against x_2, the mole fraction in the liquid phase. At pressures higher than this line, only liquid can be present in the system. The lower line is a graph of pressure p against y_2, the mole fraction in the vapor phase. At pressures lower than this line, only vapor can be present in the system. Liquid and vapor can exist together in equilibrium only at pressures and compositions corresponding to the region between the two curves. In this two-phase region, a horizontal line (constant pressure) known as a tie-line can be drawn. The intersection with the two curves of the tie-line drawn at a particular pressure, gives the compositions of the two phases in equilibrium at that pressure.

The Gibbs phase rule

$$f = C - P + 2 \tag{11.34}$$

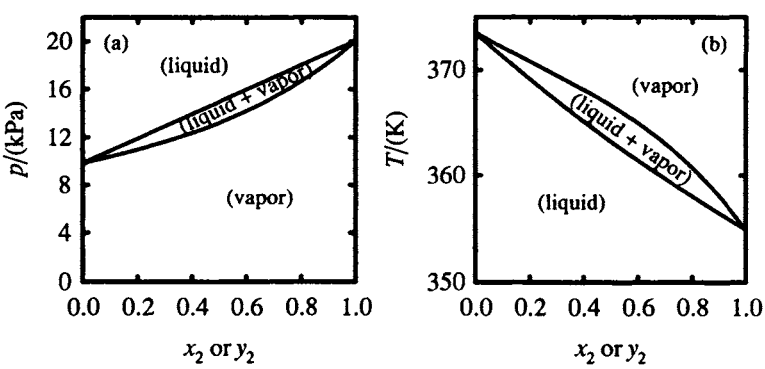

Figure 14.1 (a) Vapor pressures at $T = 308.15$ K; and (b) boiling temperatures at $p = 101.3$ kPa, for {(x_1 or y_1) c-$C_6H_{11}CH_3$ + (x_2 or y_2) c-C_6H_{12}}.

[a] We should remember that the choice of components is arbitrary, even though the number is not. Thus, we can describe ($H_2SO_4 + H_2O$) equally well as ($H_2S_2O_7 + H_2O$) {or even ($SO_3 + H_2O$)}, as well as ($H_2SO_4 \cdot H_2O + H_2O$), ($H_2SO_4 + H_2SO_4 \cdot H_2O$), etc.

can be used to predict the degrees of freedom f in the system. In the two-phase region where the number of phases, P, is equal to 2, $f = 1$ when the temperature is held constant, since for a binary system, $C = 2$. Thus, specifying the pressure p fixes the composition of the phases at equilibrium. Conversely, specifying the composition of one of the phases fixes the pressure and the composition of the other phase.

In Figure 14.1b, which is a graph of (boiling) temperature against composition at a fixed pressure, the equilibrium lines are reversed. That is, at temperatures above the upper curve, only vapor can be present in the system, and at temperatures below the lower curve, only liquid can be present. Vapor and liquid can exist together at equilibrium in the two-phase region between the two curves, where horizontal tie-lines (constant temperature) again give the compositions of the phases in equilibrium at the points where the tie-lines intersect the two curves. Again, in the two-phase region, one degree of freedom is present if the pressure is held constant. Specifying the temperature fixes the compositions of the phases in equilibrium, or specifying the composition of one of the phases, fixes the temperature and the composition of the other phase.

In a distillation, boiling the liquid results in a vapor sample that, when condensed, is richer in the more volatile component (in our example, component 2). In a fractional distillation, successive vaporizations followed by condensations can be used to separate the mixture into essentially pure components, with the more volatile component in the distillate and the less volatile component in the residue.[b]

The $\{(x_1 \text{ or } y_1)\ \text{c-}C_6H_{11}CH_3 + (x_2 \text{ or } y_2)\ \text{c-}C_6H_{12}\}$ system is an example of one that shows nearly ideal solution behavior.[c] Although the same general principles apply, most systems are not so well behaved. For example, Figure 14.2 compares the boiling temperatures for four systems that show deviations from ideal solution behavior. The (methanol + water) system[2] shown in Figure 14.2a shows positive deviations from Raoult's law. Thus, the vapor pressures are higher and the boiling temperatures are lower than expected for an ideal mixture of the two components.

The (pyridine + trichloromethane) system[3] shown in Figure 14.2b is an example of one with negative deviations from Raoult's law. That is, the vapor pressures are lower and the boiling temperatures are higher than for the ideal solution.

---

[b] For a detailed discussion of distillation procedures, see J. B. Ott and J. R. Goates, "Temperature Measurement With Application to Phase Equilibria Studies", Chapter 6 in *Determination of Thermodynamic Properties*, B. W. Rossiter and R. C. Baetzold, eds, Wiley Interscience, New York, 1992, pp. 508–549.

[c] See Section 11.3b of Chapter 11 for a summary of Raoult's law, Henry's law and ideal solutions.

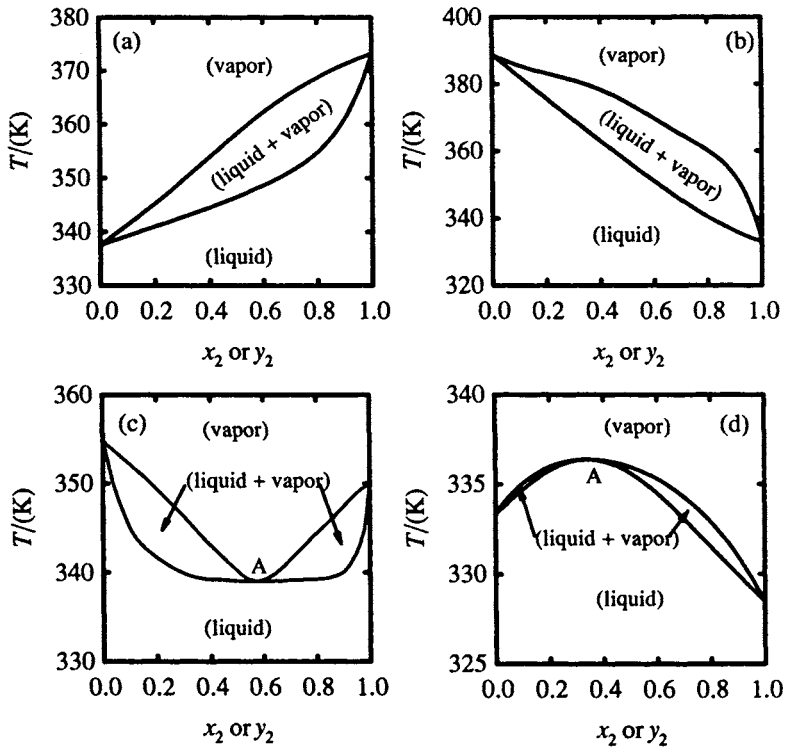

Figure 14.2 Boiling temperatures at $p = 101.3$ kPa for (a) $\{(x_1 \text{ or } y_1)\ CH_3OH + (x_2 \text{ or } y_2)\ H_2O\}$; (b) $\{(x_1 \text{ or } y_1)\ C_5H_5N + (x_2 \text{ or } y_2)\ CHCl_3\}$; (c) $\{(x_1 \text{ or } y_1)\ CH_3CN + (x_2 \text{ or } y_2)\ CCl_4\}$; (d) $\{(x_1 \text{ or } y_1)\ CHCl_3 + (x_2 \text{ or } y_2)\ (CH_3)_2CO\}$.

In Figure 14.2c, the positive deviations from Raoult's law for (acetonitrile + tetrachloromethane)[4] are so large that a maximum occurs in the vapor pressure curve and a corresponding minimum, given by point A, in the boiling temperature of the mixtures. At point A, the vapor and liquid have the same composition and the mixture forms an azeotrope. (Acetonitrile + tetrachloromethane) is an example of a system with a minimum boiling azeotrope. It is known as a positive azeotrope, since it results from positive deviations from Raoult's law. An azeotrope prevents the separation of components by distillation. Note that with the minimum boiling azeotrope, either distillation of mixtures rich in acetonitrile or mixtures rich in tetrachloromethane produce a distillate whose composition approaches that given by point A. Thus, a fractional distillation eventually produces a distillate of composition A.

The (trichloromethane + acetone) system[5] shown in Figure 14.2d has such large negative deviations from Raoult's law that a minimum occurs in the vapor

pressure curve, with a corresponding maximum in the boiling temperature curve. This maximum, shown as point A in Figure 14.2d, is a maximum boiling azeotrope, or a negative azeotrope since it results from negative deviations from Raoult's law.[d] As with the minimum boiling azeotrope, at the azeotropic composition given by point A, the vapor and liquid have the same composition. The maximum boiling azeotrope differs from the minimum boiling azeotrope, however, in that distillation of mixtures richer in component 2 (acetone) than point A produces a distillate that is richer in this component, while distillation of mixtures richer in component 1 (trichloromethane) than point A produce distillate richer in this component. Thus, a fractional distillation will eventually

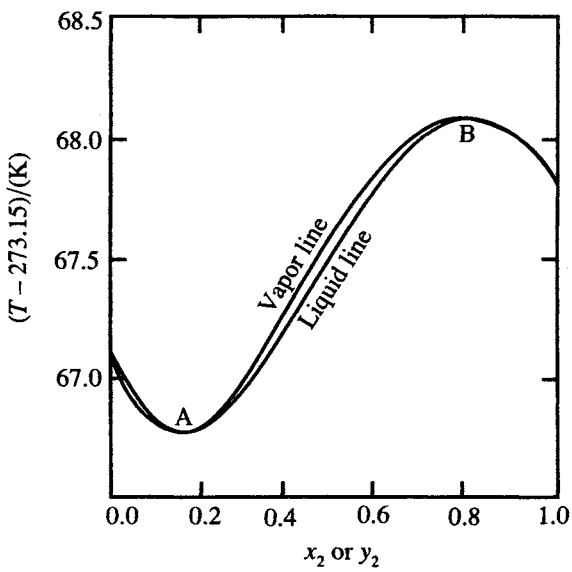

Figure 14.3 Boiling temperature against composition phase diagram for {(x_1 or y_1) C_6F_6 + (x_2 or y_2) C_6H_6} at a pressure of 0.664 MPa. Evident in the diagram is a minimum boiling azeotrope at point A and a maximum boiling azeotrope at point B. Reprinted with permission from W. J. Gaw and F. L. Swinton, "Occurrence of a Double Azeotrope in the Binary System Hexafluorobenzene + Benzene"; *Nature (London)*, **212**, 284 (1966). Copyright MacMillan Magazines Ltd.

[d] Mixtures such as those shown in Figure 14.2c and 14.2d are known more specifically as homoazeotropes. The homo- prefix indicates that phase separation does not occur in the liquid mixture, and (liquid + liquid) equilibrium is not present. Later we will describe azeotropy in systems where the liquids are not miscible. These systems are known as heteroazeotropic mixtures.

lead to pure component 1 or pure component 2 as the distillate, depending upon which side of the azeotropic composition we start from.[e]

The azeotropic composition will change with the total pressure. Also, more complicated effects can occur. For example, Figure 14.3 shows the boiling temperature against composition diagram for $\{(x_1 \text{ or } y_1)C_6F_6 + (x_2 \text{ or } y_2)C_6H_6\}$.[6] Both a minimum and a maximum boiling azeotrope are present in this system.

14.3 (Liquid + Liquid) Equilibrium

Figure 14.4 gives the (liquid + liquid) phase equilibrium diagram for the $(x_1\text{n-}C_6H_{14} + x_2CH_3OH)$ system. Two liquid phases L_1 and L_2 can exist in equilibrium in this system. Figure 14.4a is a graph of temperature against mole fraction with the pressure held constant, with the line giving the compositions of the phases in equilibrium. A horizontal tie-line in the two-phase region, such as the dotted line, gives the compositions of the two phases in equilibrium at this temperature as the points c and d where the tie-line intersects the equilibrium line. The Gibbs phase rule predicts that one degree of freedom is present in the two-phase region with pressure held constant. Thus, specifying the temperature gives the composition of the phases in equilibrium, or specifying the composition of

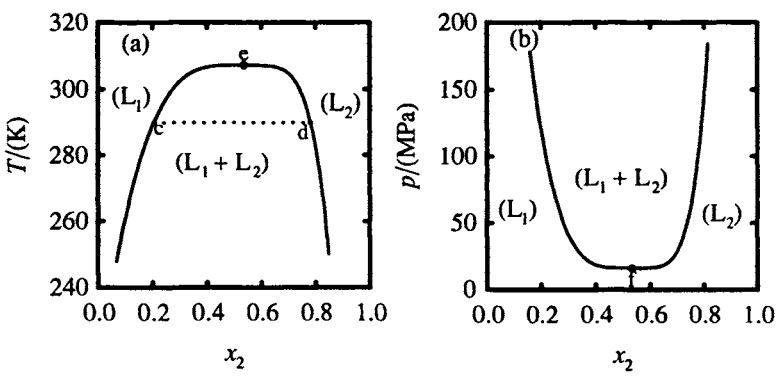

Figure 14.4 (Liquid + liquid) equilibria for $(x_1\text{n-}C_6H_{14} + x_2CH_3OH)$. (a) T against x_2 with $p = 0.10$ MPa; (b) p against x_2 with $T = 313.15$ K.

[e] If azeotropes are not present, a fractional distillation can eventually separate the mixture into the pure components, with the component with the higher vapor pressure ending up as the distillate and the less volatile component (known as the residue) left in the distillation pot. For a minimum boiling azeotrope, a fractional distillation can produce a distillate with the azeotropic composition and a residue that is one of the pure components, depending on the composition of the starting mixture. For a maximum boiling azeotrope a fractional distillation can produce one of the pure components as the distillate, and a residue with the azeotropic composition.

one of the phases gives the temperature and the composition of the other equilibrium phase. Outside the two-phase region, two degrees of freedom are present, and the temperature and composition can be varied independently.

This system is an example of one with an upper critical solution temperature (UCST). The UCST is the temperature at point e at the top of the curve. This point is known as the upper critical end point (UCEP). The temperature at the UCEP represents the highest temperature (at this pressure) where the liquid mixture will separate into two phases. If one starts with a liquid mixture at a temperature higher than the UCST, one liquid phase would be present. Upon cooling, separation into two phases occurs when the temperature given by the equilibrium curve is reached. With continued cooling, the compositions of the two phases change, as given by the intersections of the tie-line at that temperature with the curve. If the composition of the initial solution was that given by the UCEP, then separation upon cooling begins at the UCST.

Figure 14.4b is a graph for the same system of pressure against mole fraction with temperature held constant. Increasing pressure has the effect of decreasing the solubility so that a lower critical solution pressure (LCSP), shown by point f at the bottom of the curve, is present. Complete miscibility occurs in this system at $T = 313.15$ K and ambient pressure. If the pressure is increased while holding the temperature constant, a pressure is eventually reached (16.2 MPa at the LCSP) where separation into two phases occur. Again, with the temperature fixed, one degree of freedom is present in the two-phase region. Thus, specifying the pressure gives the composition of the two phases in equilibrium, or specifying the composition of one of the phases fixes the composition of the other phase and the pressure.

Phase equilibrium resulting in a UCST is the most common type of binary (liquid + liquid) equilibrium, but other types are also observed. For example, Figure 14.5 shows the (liquid + liquid) phase diagram for $\{x_1 H_2O + x_2(C_3H_7)_2NH\}$.[7] A lower critical solution temperature (LCST) occurs in this system.[f] That is, at temperatures below the LCST, the liquids are totally miscible, but with heating, the mixture separates into two phases.

Figure 14.6 shows the phase diagram for $\{x_1 H_2O + x_2 C_4H_8O\}$[g,8] It is an example of a system that has both a UCST and an LCST.[h] Mixtures of water and tetrahydrofuran (C_4H_8O) are miscible at low temperatures (at near-ambient

[f] Hydrogen-bonded systems provide the most common examples of an LCST.

[g] C_4H_8O is tetrahydrofuran.

[h] The normal boiling point of tetrahydrofuran (C_4H_8O) is 339.12 K. The (liquid + liquid) phase diagram shown in Figure 14.6 was determined at slightly elevated pressure to prevent the mixtures from boiling away.

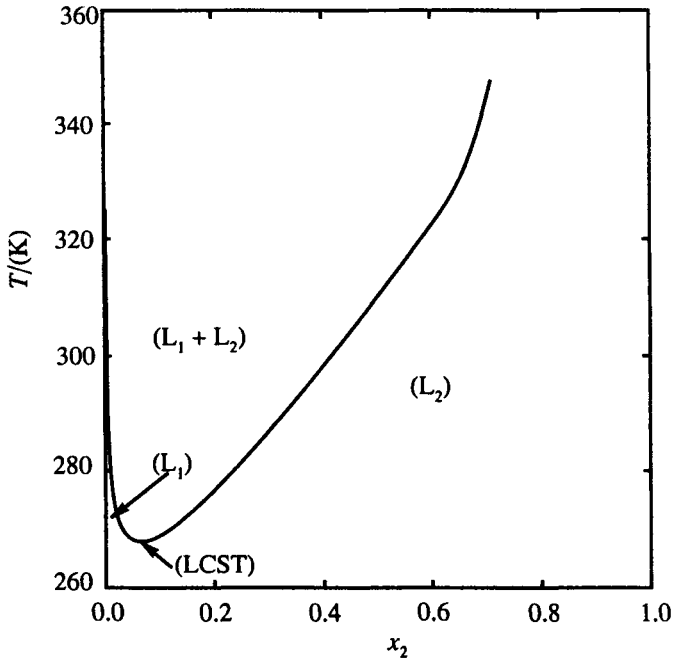

Figure 14.5 (Liquid + liquid) equilibria for $\{x_1H_2O + x_2(C_3H_7)_2NH\}$.

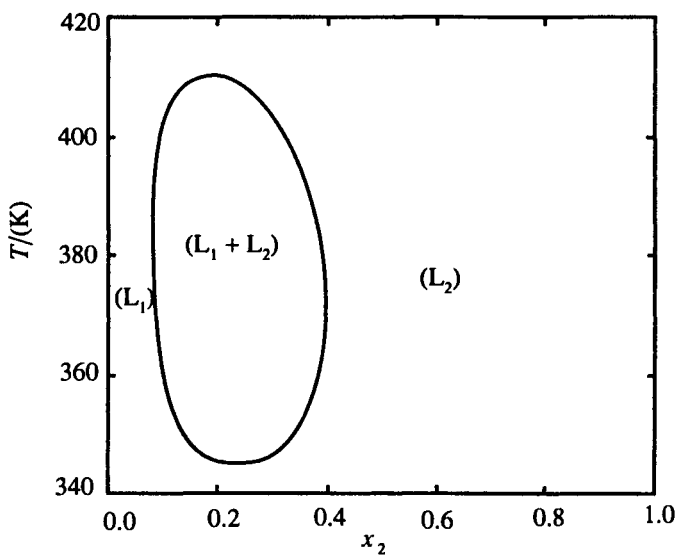

Figure 14.6 (Liquid + liquid) equilibria in the $\{x_1H_2O + x_2C_4H_8O\}$ system.

pressure, less than 345 K) and at high temperatures (at near-ambient pressure, greater than 410 K), with (liquid + liquid) phase separation and equilibrium occurring between these two temperature extremes.

Still other types of (liquid + liquid) equilibria are possible. Figure 14.7 schematically summarizes the possibilities. The effect of pressure is shown horizontally and the effect of temperature vertically. The shaded areas in (a) to (h) are cross-sections, either at constant pressure or at constant temperature, through the (p, T, x) volume where two phases are present. Figures 14.7i to 14.7v are representations of these (p, T, x) volumes, the boundaries of which give the compositions of the phases in equilibrium, and show how the (liquid + liquid) equilibrium changes with p, T, and x.[i] The designation T^c_U, T^c_L, p^c_U, and p^c_L indicate a UCST, LCST, UCSP or LCSP, respectively.

The (hexane + methanol) system shown earlier in Figure 14.4 is an example represented by Figures 14.7a and 14.7f. Figures 14.7i to 14.7l in the first horizontal row represent the cases where, with increasing pressure, a UCST either decreases (i), increases (j), goes through a temperature maximum (k), or goes through a temperature minimum (l). In the second row, Figures 14.7m through 14.7p represent cases where, with increasing pressure, an LCST increases (m), decreases (n), goes through a temperature minimum (o), or goes through a temperature maximum (p).

The third row {Figures 14.7q to 14.7t} represents cases where closed loops shrink with increasing pressure and disappear completely (q), appear at higher pressure (r), resemble elipsoids (s), or resemble hyperboloids (t). The final two cases are immiscibility surfaces of a saddle-like type as shown in Figures 14.7u and 14.7v. The designation p_{HC} or T_{HP} in Figure 14.7 is known as the **hypercritical pressure** or the **hypercritical temperature**. It indicates the pressure or temperature where those examples with ellipsoid or hyperboloid closed loops reduce to a point in the phase diagrams shown in Figure 14.7. Examples have been reported in the literature for all of the types[9] shown in Figure 14.7 except (k), (o), and (s) shown with question marks.

14.3a Combination of (Liquid + Liquid) and (Vapor + Liquid) Equilibrium

Under some circumstances, (liquid + liquid) equilibria occur under conditions where it is also important to consider the (vapor + liquid) effects. For example, Figure 14.8 shows the phase diagram for (water + 1-butanol) at $p = 101.3$ kPa. Lines ac and bc give the normal boiling temperatures for the mixtures. Since

[i] Of course, actual systems are not as symmetrical and aesthetically pleasing as the examples shown in Figure 14.7. The understanding of the dependence of p, T, and x on (liquid + liquid) equilibrium makes for an interesting study.

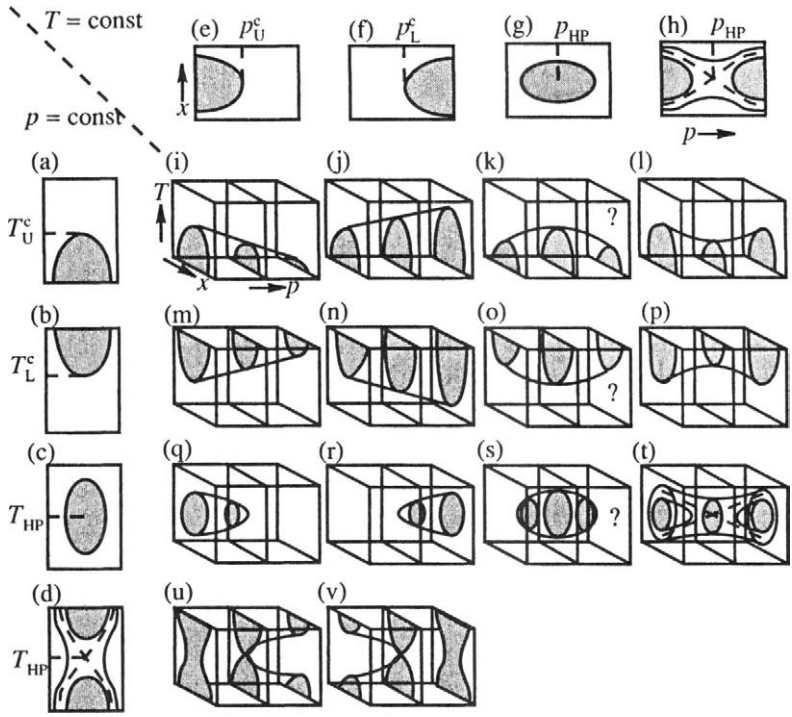

Figure 14.7 Schematic representation of the different types of binary (liquid + liquid) phase equilibria, showing the effect of p, T, and x on the two-phase volume. Examples are known for all except figures (k), (o), and (s). Reproduced with permission from G. M. Schneider, "High-pressure Phase Diagrams and Critical Properties of Fluid Mixtures", M. L. McGlashan, ed., Chapter 4 in *Chemical Thermodynamics*, Vol. 2, The Chemical Society, Burlington House, London, 1978.

point c represents a minimum boiling point, azeotropy[j] is present. It differs from the azeotropy described earlier in that the boiling occurs from two phases that are in equilibrium. If a mixture with overall composition within the $(L_1 + L_2)$ two-liquid phase region, enclosed by lines de and fg, is heated, boiling will begin at a temperature corresponding to line df. The phase rule predicts that point c, which is along this line, is invariant (at constant p), since three phases (L_1 with composition given by point f, L_2 with composition given by point d, and vapor with composition given by point c) are in equilibrium. Boiling will continue at this temperature until all of L_1 or L_2 (depending upon whether the overall composition is to the right or the left of point c) is used up. The temperature will then rise as the remaining liquid is boiled.

[j] We describe this process as heterazeotropy since two liquid phases are present.

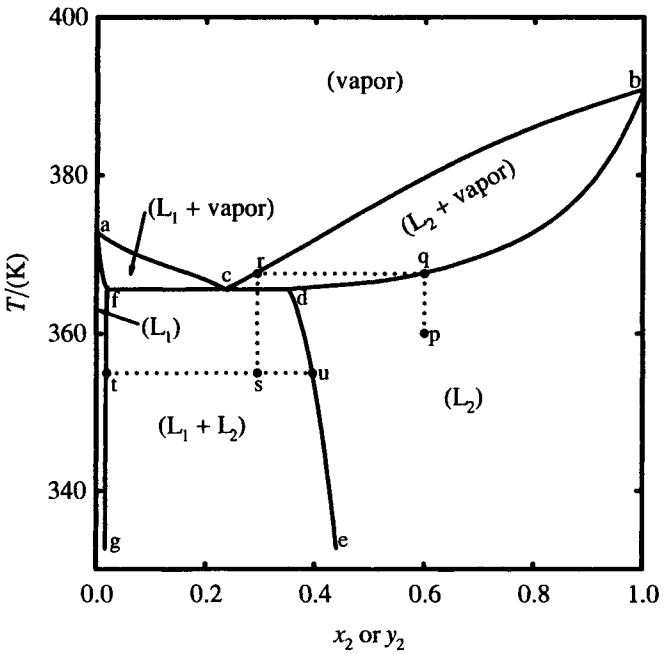

Figure 14.8 Boiling temperatures at $p = 101.3$ kPa for $\{(x_1 \text{ or } y_1)\ H_2O + (x_2 \text{ or } y_2)$ l-$C_4H_9OH\}$. L_1 and L_2 are liquid phases in equilibrium in the two-phase region.

Consider the changes that occur when liquid L_2 given by composition p is heated. Boiling will begin at a temperature corresponding to point q and the first distillate will have the composition given by point r. Cooling this distillate will cause it to condense into two liquids, which at a temperature corresponding to point s will have the compositions given by the points t and u, the ends of the tie-line.

14.4 (Fluid + Fluid) Equilibrium

Figure 14.9 is a three-dimensional graph that shows the extension of (vapor + liquid) equilibrium isotherms or isobars to the critical region. Line ab at $x_2 = 0$ is the vapor pressure line for pure component 1, with point b as the critical point. In a like manner, line cd at $x_2 = 1$ is the vapor pressure line for pure component 2, with point d as the critical point. Note that at temperatures and pressures below points b and d, the isotherms and isobars (shown as the shaded areas) intersect the vapor pressure curves.[k] However,

[k] These isotherms and isobars are similar to those shown in Figure 14.1.

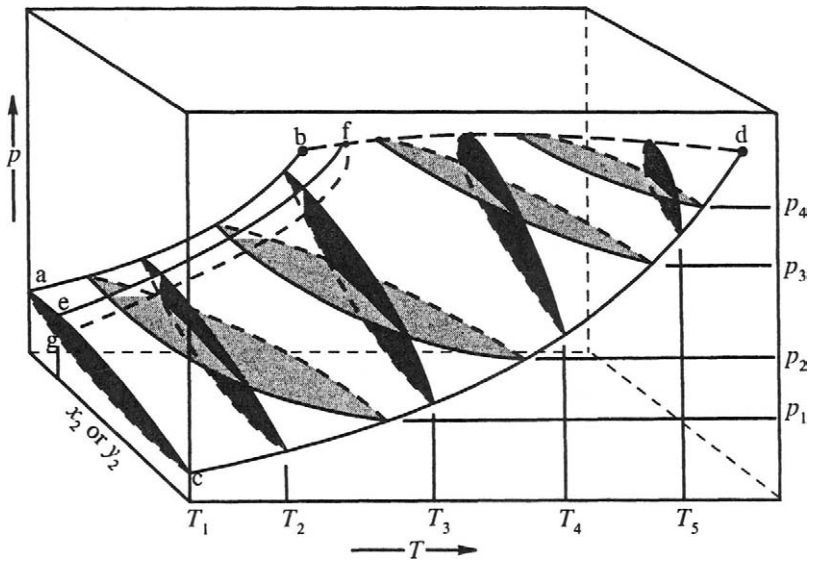

Figure 14.9 (Fluid + fluid) phase diagram for a type I system. Reproduced with permission from W. B. Streett, Chapter 1 in *Chemical Engineering at Supercritical Fluid Conditions*, M. E. Paulaitis, J. M. L. Penninger, R. D. Gray Jr., and P. Davidson, editors, Ann Arbor Science Press, 1983.

above point b (the lower of the two critical points), the intersection of the isotherms and isobars is not with line ab. Instead, it is with line bd, which connects the two critical points. Line bd is known as the **critical locus**. It can be thought of as the series of critical points of the mixture as the composition changes from $x_2 = 0$ to $x_2 = 1$.

14.4a Type I Systems

The critical locus shown in Figure 14.9 is only one (probably the simplest) of the types of critical loci that have been observed. Scott and van Konynenburg[10] have used the van der Waals equation to predict the types of critical loci that may occur in hydrocarbon mixtures. As a result of these predictions they developed a scheme that classifies the critical locus into one of five different types known as types I to type V.[1] A schematic representation of these five types of (fluid + fluid) phase equilibria is shown in Figure 14.10. In the figure, the solid lines represent the vapor pressure lines for the

[1] A sixth (type VI) occurs in systems when strong attractions, such as those resulting from hydrogen bonds, are present. It is more specialized in nature and will not be described here.

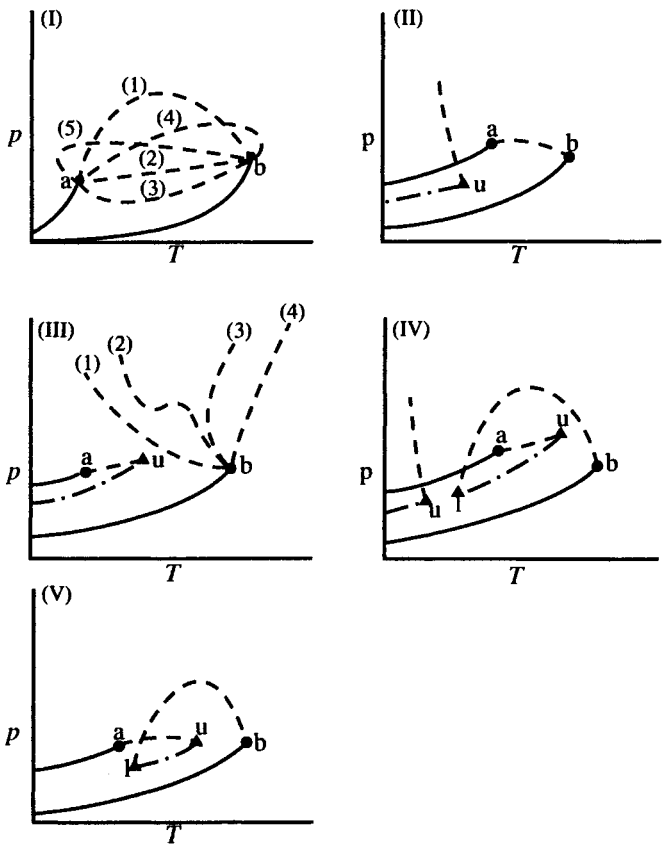

Figure 14.10 The five types of (fluid + fluid) phase diagrams according to the Scott and van Konynenburg classification. The circles represent the critical points of pure components, while the triangles represent an upper critical solution temperature (u) or a lower critical solution temperature (l). The solid lines represent the (vapor + liquid) equilibrium lines for the pure substances. The dashed lines represent different types of critical loci. (1):[Ar + CH_4], (2):[CO_2 + N_2O], (3):[C_3H_8 + H_2S], (4):[c-C_7H_{14} + $(CH_3)_4Si$], and (5):[$(CH_3)_2CO$ + n-C_5H_{12}] are examples of I; [CO_2 + C_8H_{18}] is an example of II; (1):[H_2 + CO], (2):[CH_4 + H_2S], (3):[H_2 + He], and (4):[He + CH_4], are examples of III; [CH_4 + C_2H_6] is an example of IV; and [C_2H_6 + C_2H_5OH] is an example of V. The dash-dot line represents the projection of a surface in which (liquid + liquid + gas) are in equilibrium.

pure components, while the dashed lines represent the critical loci for the mixture.[m]

From Figure 14.10, we see that the system represented by Figure 14.9 is of type I. Shown for this type of system are several possible projections of the critical locus that can occur. Mixtures represented by (1), in which the critical locus is convex upwards, are the most common, and occur when there are not large polarity differences between the molecules of the components, but moderately large differences between the critical temperatures.

Mixtures approximating curve (2), in which the critical locus is almost linear, usually are formed when the components have similar critical properties and form very nearly ideal mixtures. A minimum in the critical locus, as in curve (3), occurs when positive deviations from Raoult's law occur that are fairly large, but do not result in a (liquid + liquid) phase separation. Some (polar + nonpolar) mixtures and (aromatic + aliphatic) mixtures show this type of behavior.

Mixtures whose critical locus is represented by (4) are extremely rare. For these mixtures the critical locus extends to temperatures above the critical temperatures of both components. The phase separation that occurs along this critical locus is sometimes referred to as **(gas + gas) immiscibility**, since two phases are present at a temperature above the critical temperatures of both components.

The last type of critical locus, represented by (5), in which the critical line extends below both critical points is usually associated with the occurrence of a minimum boiling (maximum pressure) azeotrope that extends up to the critical line. Figure 14.11 shows an example of this type of behavior for the (cyclohexane + hexafluorobenzene) system. At the temperature corresponding to point c in Figure 14.11A, the azeotropic point intersects the critical locus. At higher temperatures, the (vapor + liquid) equilibrium line separates into two regions that come together at the critical locus. With increasing temperature, these regions move along the critical locus as shown in Figure 14.11B and disappear at the critical temperature of the less volatile pure component.

Retrograde Condensation: For near-ideal mixtures, the intersection of the $(p, x_2 \text{ or } y_2)$ isotherm with the critical locus occurs at the maximum in the (p, y_2) equilibrium line. For example, an enlargement of the two-phase $(p, x_2 \text{ or } y_2)$ section for $\{(x_1 \text{ or } y_1)\text{Ar} + (x_2 \text{ or } y_2)\text{Kr}\}$ at $T = 177.38$ K is shown in Figure 14.12. The point of intersection with the critical locus at point (c) gives rise to an

[m] In applying Figure 14.10, we must remember that this figure is a (p, T) projection of the critical locus, with the mole fraction variable, which is perpendicular to the (p, T) plane, not shown. Thus, a critical locus that connects the critical points a and b represents mixtures that change in composition from $x_2 = 0$ to $x_2 = 1$. Other critical loci shown in Figure 14.10 do not cover these extremes of composition, but do change with x.

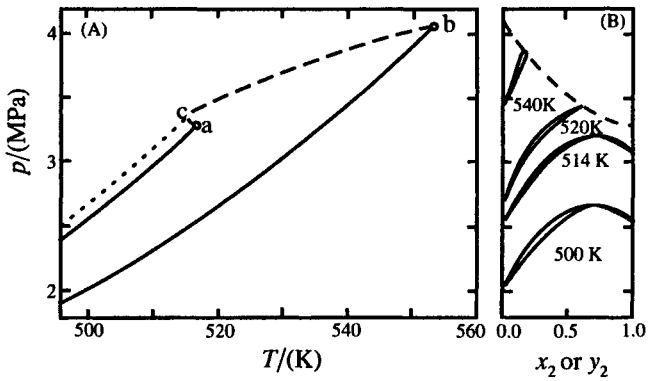

Figure 14.11 The critical locus for $(x_1C_6H_{12} + x_2C_6F_6)$, a system with a maximum boiling azeotrope. In (A), the circles represent the critical points (a and b) of pure components (1) and (2); the solid lines represent (vapor + liquid) equilibrium for the pure substances; the dashed line is the critical locus, and the short-dashed line represents the azeotrope composition, which intersects the critical locus at point c. (B) shows the intersection of the (vapor + liquid) equilibrium lines with the critical locus.

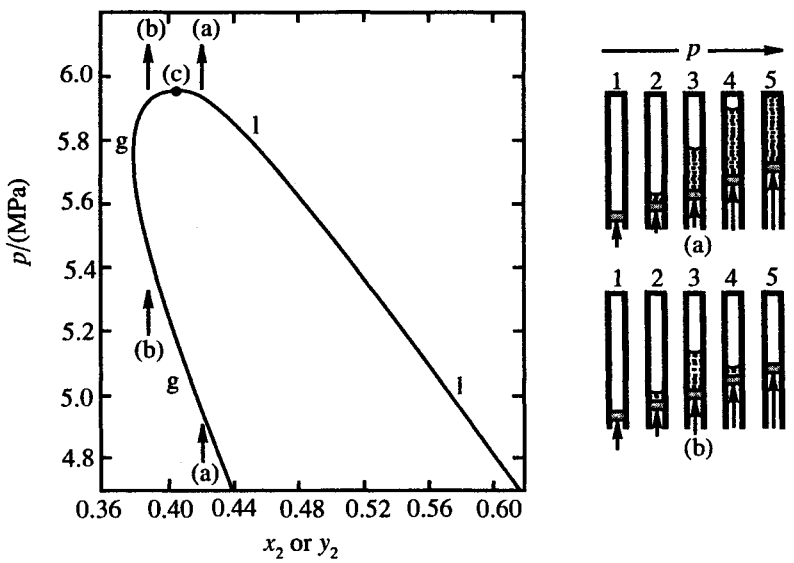

Figure 14.12 The top of the (vapor + liquid) isotherm for $(x_1Ar + x_2Kr)$ at $T = 177.38$ K. Point (c) is the intersection with the critical locus. The curve marked g gives the composition of the vapor phase in equilibrium with the liquid curve marked l. The tubes shown schematically to the right demonstrate the changes in phase when the fluid is compressed at a mole fraction given by (a), or at a mole fraction corresponding to (b) where retrograde condensation occurs. Reprinted with permission from M. L. McGlashan, *Chemical Thermodynamics*, Academic Press, London, 1979, p. 276.

interesting phenomena known as **retrograde condensation**. If a mixture with a composition given by point (a) that is to the right of (richer in Kr than) point (c) is compressed by a piston in a cylinder, condensation occurs as illustrated schematically in the cylinders designated as (a) to the right of the phase diagram. In (1) we are below the vapor line and only gas is present in the cylinder. In (2) we have crossed the vapor line and condensation from the vapor to liquid has begun. In (3) and (4), more condensation occurs as the pressure increases, until at (5) we cross the liquid line and all gas has disappeared.

With a mole fraction given by point (b) we repeat the process at a composition to the left of (richer in Ar than) point (c). The changes that occur can be followed by referring to the lower (b) set of cylinders. At (1) we are below the vapor line and only a gaseous mixture is present. In (2) we have intersected the vapor line and liquid is present. As the pressure increases, more condensation occurs as shown in (3). With continued compression, however, the liquid level shrinks as shown in (4) until we again intersect the vapor line where the liquid disappears and only a single vapor phase remains as shown in (5).[n]

Retrograde condensation is an example of phenomena that sometimes occur in science that appear to defy human intuition. To quote from M. L. McGlashan

> *It is easy to understand the bewilderment that must have greeted the first observation of this phenomena [retrograde condensation]. A gaseous mixture was expected to condense to a liquid when the pressure was increased at constant temperature or where the temperature was decreased at constant pressure. Moreover, at first sight the series of observations labeled (b) [on the right side of Figure 14.12] appear to the experimentalist to defy the rule that at a given temperature, an increase of pressure must result in a decrease in volume.*[11]

It is interesting observations such as this that keep science in general, and thermodynamics in particular, exciting, interesting, and challenging.

14.4b Type II Systems

Type II systems differ from type I in that (liquid + liquid) phase equilibrium occurs at a temperature lower than the critical temperatures of the pure components. This difference can be seen by referring again to Figure 14.10. The

---

[n] At (p, T, x) compositions this close to the critical locus, it is "stretching things" to talk about vapor and liquid phases. It would perhaps be more appropriate to describe the changes in terms of the more dense (we have designated as liquid) and the less dense (we have designated as vapor) phases.

UCST associated with the resulting (liquid + liquid) phase equilibria begins at point u where the two liquid phases are also in equilibrium with a gas phase.

The detail near the three phase region is shown in Figure 14.13. According to the phase rule, having three phases in equilibrium results in one degree of freedom. The surface shown in the figure gives the conditions where the three phases are in equilibrium. The parallel lines represent tie-lines connecting these three phases. Thus, if one specifies the temperature (or the pressure), then the pressure (or the temperature) is fixed, along with the compositions of all three phases. Also shown in Figure 14.13 is the projection of this surface on the (p, T) plane (line ab). This projection is the one shown as the dash-dot line in Figure 14.10(II).

With increasing pressure, the (liquid + liquid + gas) equilibrium plane ends at an upper critical end point u, where the gas phase disappears. At higher pressures, (liquid + liquid) equilibrium is present, ending at a UCST given by line uv. The projection of line uv is shown in Figure 14.10(II) as the near vertical dashed line. It is shown in the figure with an exaggerated negative slope, but it can also have a positive slope.

14.4c Type III Systems

Figure 14.14 shows the critical locus, along with some isothermal and isobaric (vapor + liquid) sections, for a type III system. Lines ab and cd are the vapor

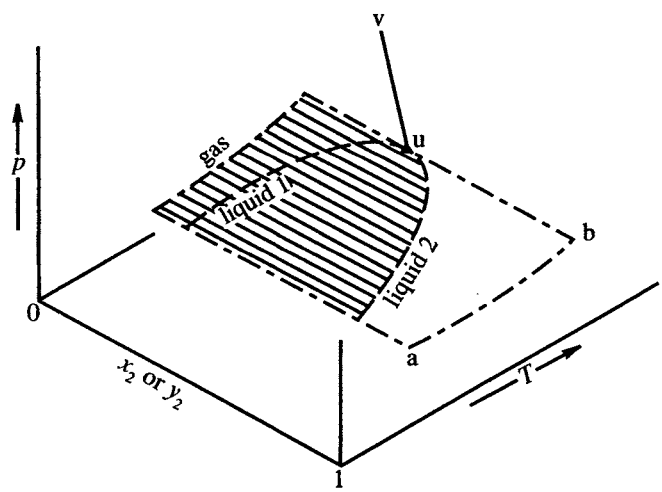

Figure 14.13 The three-phase (liquid + liquid + gas) region for a type II system. The shaded area represents the surface where three phases are in equilibrium. Reproduced with permission from W. B. Streett, Chapter 1 in *Chemical Engineering at Supercritical Fluid Conditions*, M. E. Paulaitis, J. M. L. Penninger, R. D. Gray Jr., and P. Davidson, editors, Ann Arbor Science Press, 1983.

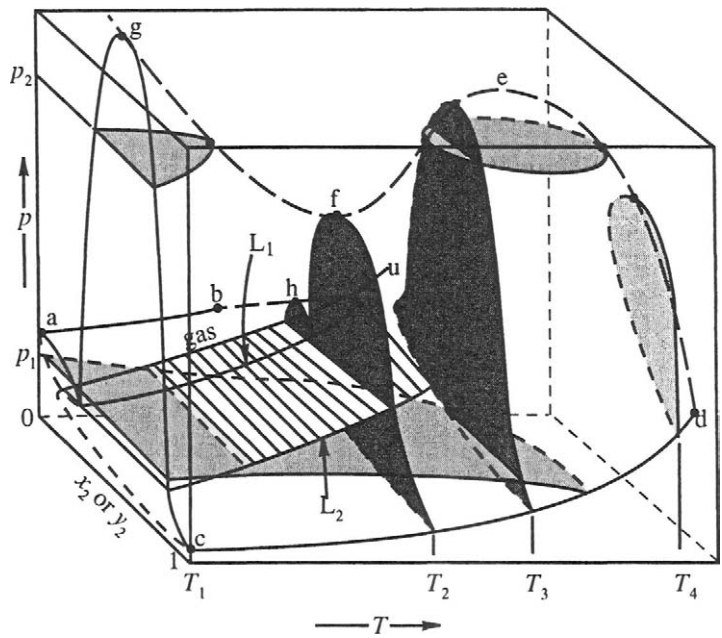

Figure 14.14 The (fluid + fluid) phase diagram for a type III system. Reproduced with permission from W. B. Streett, Chapter 1 in *Chemical Engineering at Supercritical Fluid Conditions*, M. E. Paulaitis, J. M. L. Penninger, R. D. Gray Jr., and P. Davidson, editors, Ann Arbor Science Press, 1983.

pressures of the pure components, with points b and d as the critical points. A ($L_1 + L_2 +$ gas) three-phase surface shown by the parallel tie-lines is again evident. Only one degree of freedom is present on this surface. Thus, specifying the pressure (or temperature) fixes the temperature (or pressure) and the composition of the three phases in equilibrium. The compositions of these three phases are given by the lines labeled L_1, L_2, and gas. This surface terminates at an upper critical solution temperature labeled as u.

A type III system is characterized by a discontinuity in the critical locus. The critical locus starting at point b (the critical point of the more volatile component) ends at u. In Figure 14.14, the critical locus beginning as point d (the critical point of the less volatile component) goes through a maximum at point e, a minimum at point f, and then increases indefinitely at pressures greater than those given by point g.[o] The shape of this critical locus is only one of several that can occur. Various possibilities are summarized in Figure

[o] There is no evidence that this critical locus ever turns around again, although it is usually terminated at some high pressure by the formation of a solid phase.

14.10(III), which we remember shows the projection of the critical loci in the (p, T) plane. Type III behavior usually occurs in systems with considerable differences in polarity between the two components, with the difference increasing as one goes from those represented by (1) to those given by (4). Examples (3) and (4) can once again give critical loci at a temperature higher than the critical points of either component. The result is (gas + gas) immiscibility. It is often referred to as (gas + gas) immiscibility of the second kind to distinguish it from the (gas + gas) immiscibility (of the first kind) described earlier for type I and type II systems.

Referring again to Figure 14.14, the isotherms at temperatures T_3 and T_4 are of the typical (gas + liquid) type, but at T_2, a temperature below u, two critical points occur, one at f and the other at h. The one at f is a typical (liquid + liquid) critical point while the one at h is better characterized as a (gas + liquid) critical point. In most systems with type III behavior, the critical locus bh occurs over a narrow temperature range, and the double critical points occur only over this small range of temperature.

14.4d Type IV and Type V Systems

Both type IV and type V systems have the phase behavior at high temperatures shown schematically in Figure 14.15. The difference between the two types can be seen by referring to Figure 14.10(IV) and (V). In type IV systems, (liquid + liquid) equilibrium, with the corresponding UCST, occurs at a lower temperature. Thus, types IV and V are related in a way similar to that for types I and II.

In Figure 14.15, lines ab and cd are the vapor pressure lines for the pure components, with points b and d as the critical points. Isotherms at temperatures T_1 to T_5 and isobars at pressures p_1 and p_2 are shown. A three phase ($L_1 + L_2 +$ gas) surface is present that begins at an LCST represented by point l, and ends at a UCST given by point u. Again, the parallel lines are tie-lines connecting the compositions of the phases in equilibrium, and only one degree of freedom is present on this surface. The temperature interval between points l and u is often short, resulting in a limited temperature range over which three phases are in equilibrium.

The critical locus has two parts, with the portion that begins at point b (the critical point of the more volatile component) ending at the UCST (point u), and the portion that starts at point d (the critical point of the less volatile component) ending at the LCST (point l). Although not shown in Figure 14.15, an isotherm at a temperature between T_2 and T_3 would show two critical points (similar to the one at T_2 in Figure 14.14). One critical point would be on the critical locus line bu while the other would be on the critical locus line dl.

In summary, (fluid + fluid) equilibria is often classified as one of five general classes. But we should keep in mind that the division is somewhat arbitrary and

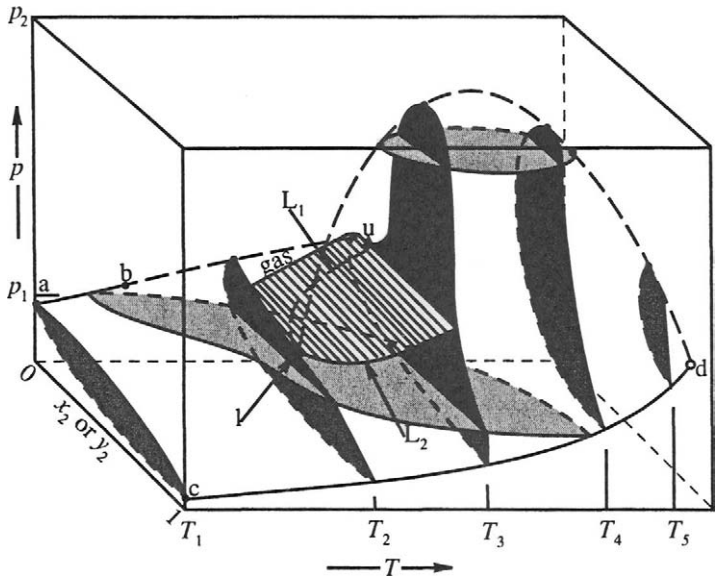

Figure 14.15 (Fluid + fluid) phase diagram for a type V system. Reproduced with permission from W. B. Streett, Chapter 1 in *Chemical Engineering at Supercritical Fluid Conditions*, M. E. Paulaitis, J. M. L. Penninger, R. D. Gray Jr., and P. Davidson, editors, Ann Arbor Science Press, 1983.

continuous transitions occur between the different types. We should also keep in mind that "actual" phase diagrams are often more complicated than the idealized diagrams shown in Figures 14.9 to 14.15.[p]

Azeotropes especially add complications. Excellent references can be found in the literature[12] that describe (fluid + fluid) phase equilibria in more detail than in our discussion and give many examples of actual systems.

14.5 (Solid + Liquid) Phase Equilibrium

The relationship between melting temperature T and mole fraction x_i when a pure solid freezes from an ideal solution is given by equation (11.85)

$$\left(\frac{\partial \ln x_i}{\partial T}\right)_p = \frac{\Delta_{\text{fus}} H_{\text{m},i}}{RT^2}. \tag{11.85}$$

[p] Work is underway to develop a more systematic nomenclature for describing (fluid + fluid) equilibria. It includes a finer differentiation so that more types are identified than the five proposed by Scott and van Konynenburg.

In a like manner, equation (11.86)

$$\left(\frac{\partial \ln x_i}{\partial p}\right)_T = -\frac{\Delta_{\text{fus}} V^*_{\text{m},i}}{RT} \tag{11.86}$$

gives the effect of pressure on the (solid + liquid) equilibrium of an ideal solution, where, once again, a pure solid freezes from the mixture. In equations (11.85) and (11.86), $\Delta_{\text{fus}} H_{\text{m},i}$ and $\Delta_{\text{fus}} V_{\text{m},i}$ are the molar enthalpy change and volume change for fusion of the pure solid that forms.

Figure 14.16 shows the (solid + liquid) phase diagram at $p = 0.1$ MPa for the (benzene + 1,4-dimethylbenzene) system,[13] which is an example of a very nearly ideal mixture where the equilibrium lines closely follow an integrated form of equation (11.85).[q] In Figure 14.16, line ac is the (solid + liquid) equilibrium line for solid benzene. A horizontal tie-line, such as the dotted line de in the two-phase region under this curve at a temperature T, gives point e as the composition of the liquid solution L_1 in equilibrium with the solid whose composition is given by point d. In a like manner, line bc is the (solid + liquid) equilibrium line for solid 1,4-dimethylbenzene. Tie-lines in the region under this curve, such as the dotted line fg, connect the composition of the liquid solution L_2 given by point f, in equilibrium with the pure solid 1,4-dimethylbenzene, whose composition is given by point g. With pressure held constant, the Gibbs phase rule {equation (11.34)} predicts one degree of freedom in either of the two-phase regions. Thus, specifying the temperature determines the composition, or specifying the composition sets the temperature. Point c is known as the eutectic point. Three phases are in equilibrium at this point, and it is invariant if the pressure is held constant.

Figure 14.17a summarizes the effect of pressure on the melting temperature, while Figure 14.17(b) shows the effect of temperature on the melting pressure, for the (benzene + 1,4-dimethylbenzene) system. The

---

[q] To integrate equation (11.85), we often assume $\Delta_{\text{fus}} H_{\text{m},i}$ is constant with temperature. A more accurate integration involves expressing $\Delta_{\text{fus}} H_{\text{m},i}$ as a function of temperature. This is done by expressing $\Delta_{\text{fus}} C_{p,\text{m}}$ as a function of temperature and integrating the relationship

$$\left(\frac{\partial \Delta_{\text{fus}} H_{\text{m},i}}{\partial T}\right)_p = \Delta_{\text{fus}} C_{p,\text{m},i}.$$

In the discussion of equation (11.85) in Chapter 11, references are given to sources that one may go to for this temperature dependence and the resulting integrated equation.

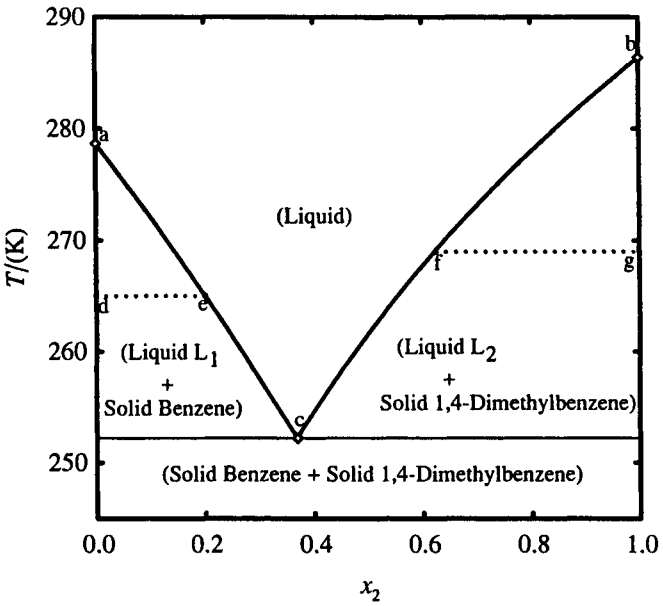

Figure 14.16 (Solid + liquid) phase equilibria for $\{x_1C_6H_6 + x_2 1,4\text{-}C_6H_4(CH_3)_2\}$ at $p = 0.1$ MPa, an example of a nearly ideal system.

predictions of the pressure effect were obtained by integrating equation (11.86) with the assumption that $\Delta_{fus}V_{m,i}$ is independent of pressure. Figure 14.17c shows schematically the (p, T, x) equilibrium surface for this system. From this surface, the isobaric sections in (a) and the isothermal sections in (b) can be obtained. For example, the intersection of the isothermal plane with the equilibrium surface gives one of the sets of lines shown in Figure 14.17b, while the intersection of the isobaric plane with the surface gives one of the sets of lines shown in Figure 14.17a. We note from Figure 14.17c that the eutectic, given by line ef, changes with pressure. This is to be expected, since one degree of freedom is present for this two-component system at the eutectic, where three phases are in equilibrium.

It is unusual to find systems that follow the ideal solution prediction as well as does (benzene + 1,4-dimethylbenzene). Significant deviations from ideal solution behavior are common. Solid-phase transitions, solid compound formation, and (liquid + liquid) equilibria often complicate the phase diagram. Solid solutions are also present in some systems, although limited solid phase solubility is not uncommon. Our intent is to look at more complicated examples. As we do so, we will see, once again, how useful the phase diagram is in summarizing a large amount of information.

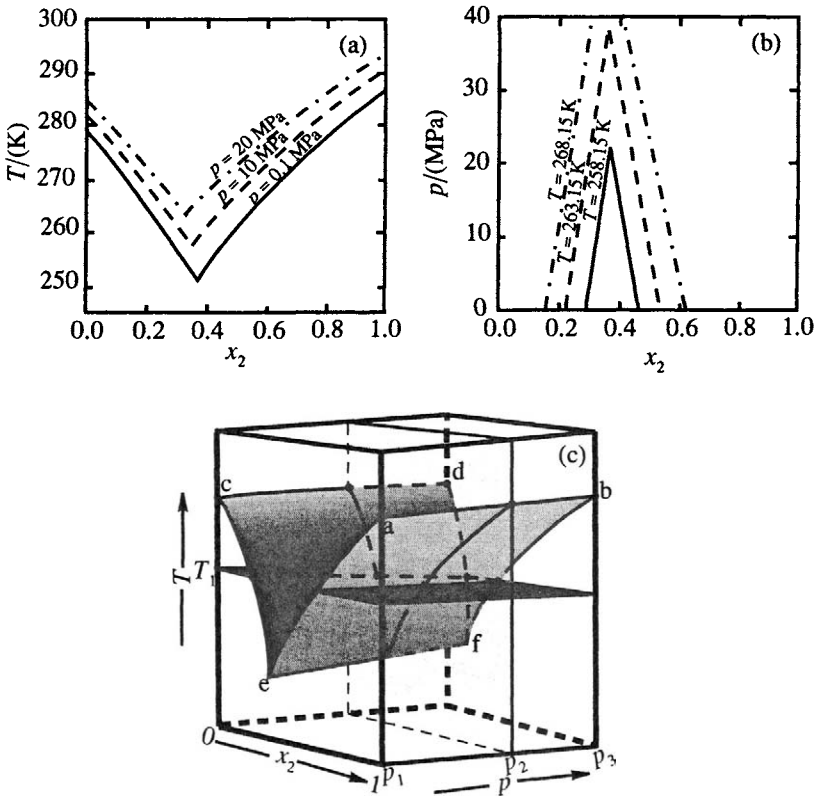

Figure 14.17 Ideal solution prediction of (a) the effect of pressure on the melting temperature, and (b) the effect of temperature on the melting pressure, for $\{x_1C_6H_6 + x_2\text{p-}C_6H_4(CH_3)_2\}$. The equilibrium curves to the left are for C_6H_6, while those to the right are for p-$C_6H_4(CH_3)_2$. (c) is a schematic representation of the (p, T, x) surface that leads to the isobaric sections shown in (a) and the isothermal sections shown in (b).

14.5a Simple Eutectic Systems with Large Deviations from Ideal Solution Behavior

Figure 14.18 shows the experimentally determined phase diagram for (1,4-dimethylbenzene + acetonitrile)[14] at ambient pressure, along with the diagram predicted by ideal solution behavior. The actual freezing point depressions are significantly less than those expected for ideal solutions.[r] We can interpret this

[r] We note from Figure 14.18 that ideal solution behavior is approached as the concentration approaches that of the pure material. This behavior is analogous to that for (vapor + liquid) equilibrium, where Raoult's law is approached for the solvent in dilute solution.

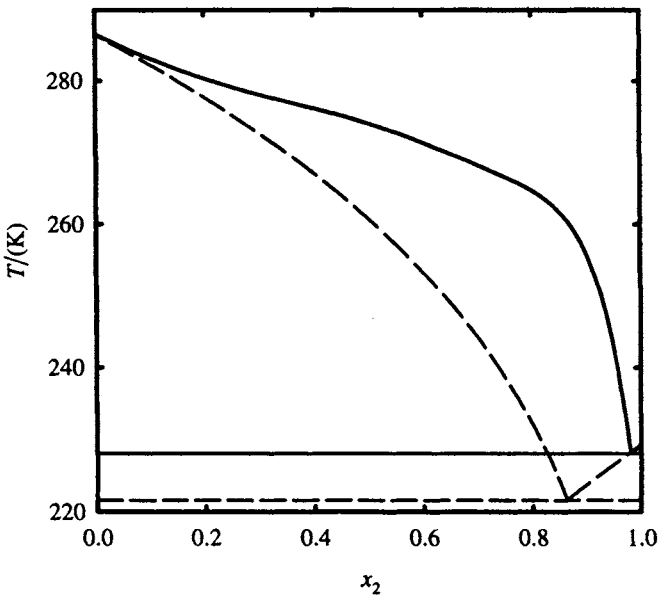

Figure 14.18 (Solid + liquid) equilibria for $\{x_1 1,4\text{-}C_6H_4(CH_3)_2 + x_2 CH_3CN\}$ at $p = 0.1$ MPa. The dashed line is the ideal solution prediction.

difference by expressing equation (11.85) in terms of the activity instead of mole fraction for the non-ideal mixture to get

$$R \ln a_1 = \int_{T_1^*}^{T_1} \frac{\Delta_{fus} H_{m,1}}{T^2} \, dT. \tag{14.1}$$

We see that the activity of the solvent is related to the integral of $\Delta_{fus} H_m / T^2$ over the temperature range from the melting of the pure solvent to that of the solution. For the real solution, T_1 is higher than for the ideal solution at the same composition. Thus, the integral in equation (14.1) is larger for the real solution than it would be for the ideal solution where $a_1 = x_1$. Therefore, a_1 in the real solution must be greater than in the ideal solution and $\gamma_{R,1} = a_1 / x_1$ is greater than 1, and these solutions show positive deviations from ideal solution behavior.

14.5b (Liquid + Liquid) with (Solid + Liquid) Equilibria

When the deviations from ideal behavior become large enough, the liquid mixture separates into two liquid phases. Cooling of this liquid mixture can result in the freezing of a solid, giving (liquid + liquid) and (solid + liquid)

equilibrium in the same phase diagram. An example at ambient pressure is shown in Figure 14.19a for mixtures of cyclohexane with methanol. A single liquid phase is present at point a. If the mixture is cooled along line aj, separation into two phases begins at point b. For example, when a temperature corresponding to point c is reached, two liquid phases are present with compositions given by points d and e, and their relative amounts given by the lever rule

$$\frac{\text{moles } L_1}{\text{moles } L_2} = \frac{ce}{dc}.$$

With continued cooling, the compositions change along line bdg (for L_1) and beh (for L_2). At temperatures and compositions corresponding to points g

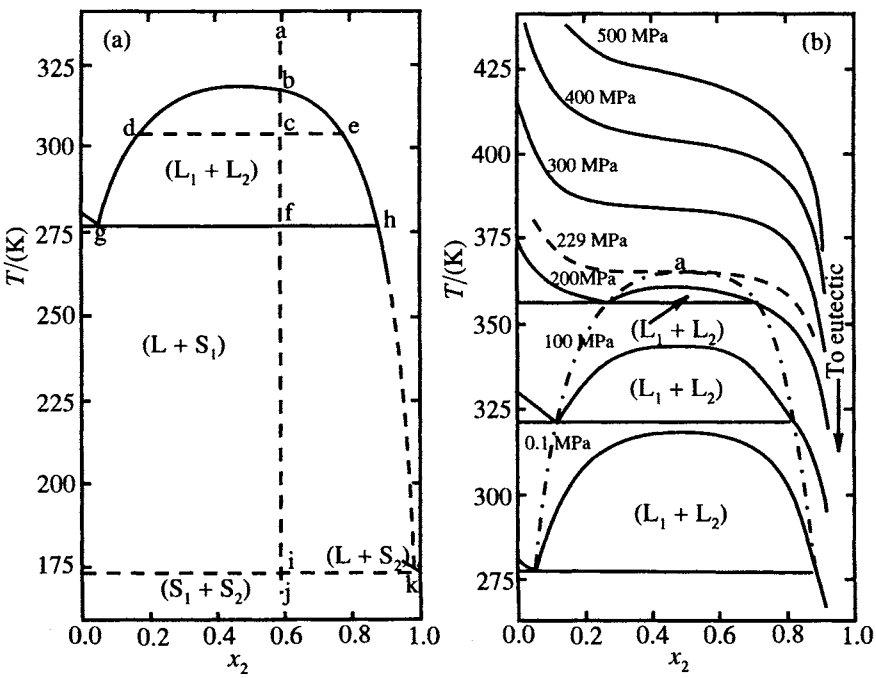

Figure 14.19 (Solid + liquid) and (liquid + liquid) phase diagram for (x_1c-C_6H_{12} + x_2CH_3OH) at (a) $p = 0.1$ MPa and (b) as a function of pressure. In (a), the freezing curve extending to the eutectic is estimated and is represented by a dashed line to reflect this uncertainty. In (b), the freezing line at $p = 229$ MPa is estimated and is represented by a dashed line. The dash-dot line in (b) is the envelope enclosing the region with two liquid phases.

and h, solid cyclohexane begins to freeze from solution. Three phases are in equilibrium, and the system is invariant since we have fixed the pressure at 0.1 MPa. The temperature will remain constant as cyclohexane freezes from solution. Solid forms at the expense of L_1, since it is the liquid phase that is rich in cyclohexane. The amount of L_1 will decrease and eventually disappear. After this happens, the temperature will fall and more cyclohexane (S_1) will freeze from a liquid solution whose composition follows line hk. At a temperature corresponding to i, the eutectic temperature is reached and solid methanol (S_2) begins to freeze from solution. Again, three phases are present (S_1, S_2, and L), the system is invariant, and the temperature stays at the eutectic temperature until all of the liquid is gone. Continued cooling lowers the temperature of the mixture of solids to point j.

Figure 14.19b summarizes the effect of pressure on the phase equilibrium in (cyclohexane + methanol).[15] The $p = 0.1$ MPa equilibrium lines shown at the bottom of the diagram are the same as those in Figure 14.19a. In Figure 14.19b at $p = 100$ MPa, we see that increasing the pressure increases both the melting temperature of the solid and the UCST for the (liquid + liquid) mixture, but the effect is more pronounced for the solid, and the temperature range over which two-liquid phases are present decreases. At $p = 229$ MPa, the two liquid phases disappear. Point a is a critical point ($T_c = 365.6$ K) where the (liquid + liquid) equilibria just disappears. At point a, the (solid + liquid) equilibrium (freezing) line has zero slope so that $(\partial T/\partial x_2)_p = 0$. Since it is a point of inflection $(\partial^2 T/\partial x_2^2)_p$ is also zero.

At higher pressures, (liquid + liquid) equilibrium is not present and the (solid + liquid) equilibria line shows large positive deviations from ideal behavior, but no phase separation. It is appropriate to describe the equilibrium at these pressures by saying that the (liquid + liquid) equilibrium curve has disappeared below the (solid + liquid) line.

A Quadruple Point: Figure 14.20 shows phase diagrams for (water + acetonitrile) at five different pressures.[16] The diagram in (a) at $p = 0.1$ MPa for this system is very similar to the (cyclohexane + methanol) diagram shown in Figure 14.19a that we described earlier, with a (liquid + liquid) equilibrium region present above the (solid + liquid) equilibrium curve for water.

Increasing the pressure lowers the melting temperature for ice[s] and raises the melting temperature of acetonitrile, and this causes a shift in the relative positions of the invariant points. In Figure 14.20b, the pressure is 100 MPa. The (liquid + liquid) region is still above the water freezing curve, but the freezing

[s] We remember that ice is less dense than liquid water. Thus, increasing the pressure lowers the melting temperature. For acetonitrile, the solid is more dense than the liquid so that increasing pressure raises the melting temperature.

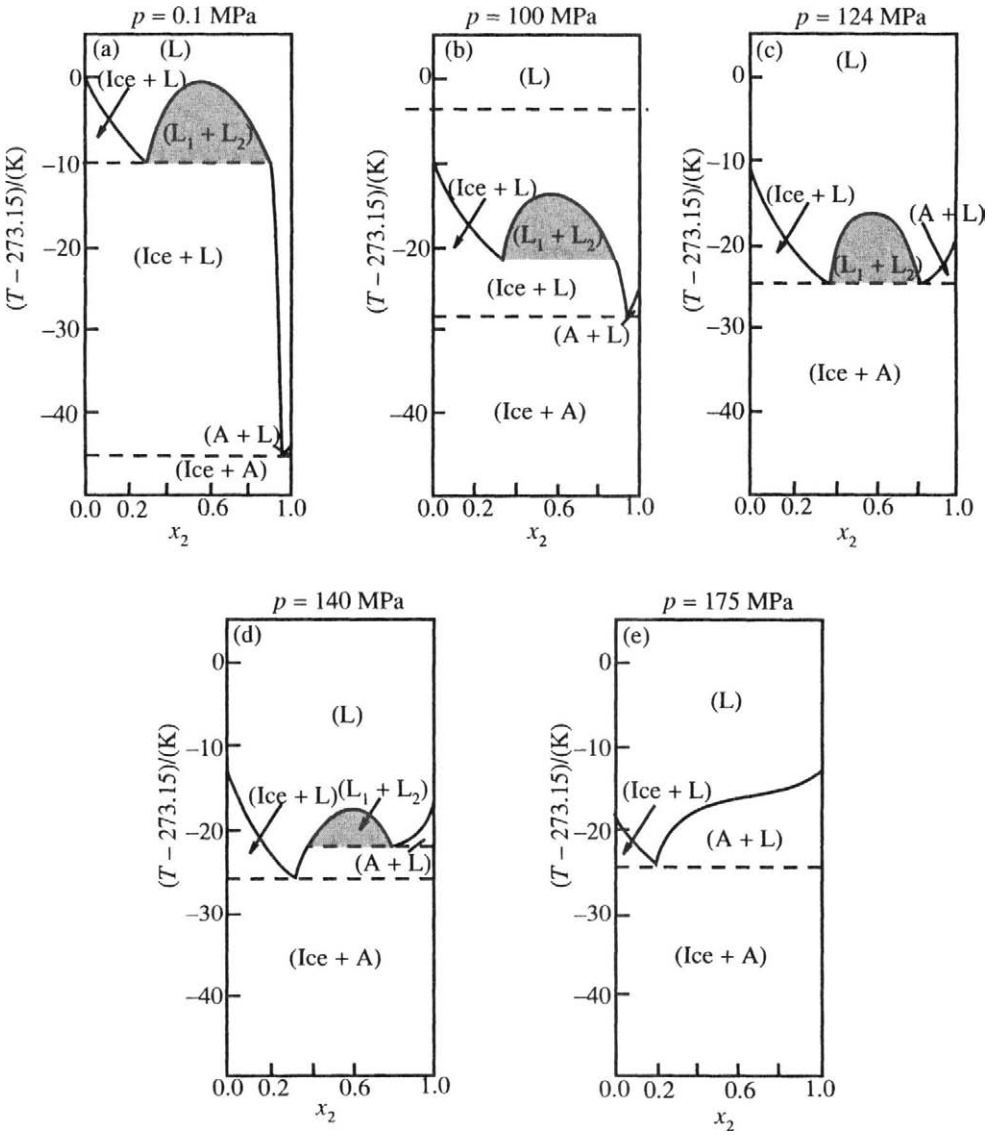

Figure 14.20 Effect of pressure on the (solid + liquid) and (liquid + liquid) phase equilibrium for ($x_1H_2O + x_2CH_3CN$). {L is liquid, ($L_1 + L_2$) gives the phases in equilibrium in a two-phase liquid region, and A is solid acetonitrile (CH_3CN).} Reprinted by permission from G. Schneider, *Z. Phys. Chem.*, **41**, 327–338 (1964). Copyright by R. Oldenbourg Verlag.

curves for the water and acetonitrile are much closer in temperature. The long very steep freezing curve for water in Figure 14.20a below the (liquid + liquid) region has shortened considerably in Figure 14.20b.

In Figure 14.20c, the pressure is 124 MPa. At this pressure the melting curves for water and for acetonitrile intersect the (liquid + liquid) curve at the same temperature. Thus, both ice and solid acetonitrile are in equilibrium with the two liquid phases. The temperature where this occurs is a **quadruple point**, with four phases in equilibrium. This quadruple point for a binary system, like the triple point for a pure substance, is invariant[t] with zero degrees of freedom. That is, it occurs only at a specific pressure and temperature, and the compositions of all four phases in equilibrium are fixed.

At $p = 140$ MPa (Figure 14.20d) the (liquid + liquid) equilibrium region has moved to the acetonitrile side of the eutectic. Increasing the pressure further decreases the (liquid + liquid) region, until at $p = 175$ MPa (Figure 14.20e), the (liquid + liquid) region has disappeared under a (solid + liquid) curve that shows significant positive deviations from ideal solution behavior.

14.5c (Solid + Solid) with (Solid + Liquid) Equilibria

Figure 14.21 summarizes the phase diagram for (n-octane + tetrachloromethane)[17]. A phase transition occurs in crystalline CCl_4 at 225.3 K.[u] Above this temperature, the highly-symmetrical CCl_4 molecules gain enough energy to exhibit free rotational motion at each point in the lattice. Because the molecules are already rotating, the fusion process liberates only translational motion, and consequently, $\Delta_{fus}H_m(CCl_4)$ is very small. Below this temperature, CCl_4 behaves like a normal solid with only small torsional oscillations about the equilibrium positions and $\Delta_{fus}H_m(CCl_4)$ is larger. The sharp break in the (solid + liquid) equilibrium curve at this temperature reflects the change in $\Delta_{fus}H_m(CCl_4)$ at the transition temperature. A rearrangement of equation (11.85) gives

$$\left(\frac{\partial T}{\partial x_2}\right)_p = \frac{RT^2}{x_2 \Delta_{fus}H_m}. \tag{14.2}$$

---

[t] A pure substance never has more than three phases together at equilibrium. Likewise, for a binary system, four phases in equilibrium (the quadruple point) is the maximum. To have more would result in negative degrees of freedom, a condition that is not thermodynamically possible.

[u] It is unclear whether the transition in CCl_4 is first order, or a sharp continuous transition. If it is continuous, the major part of the transition begins and ends over a narrow temperature range around 225 K, and the effect on the (solid + liquid) binary phase diagram is very nearly the same as for a first-order transition.

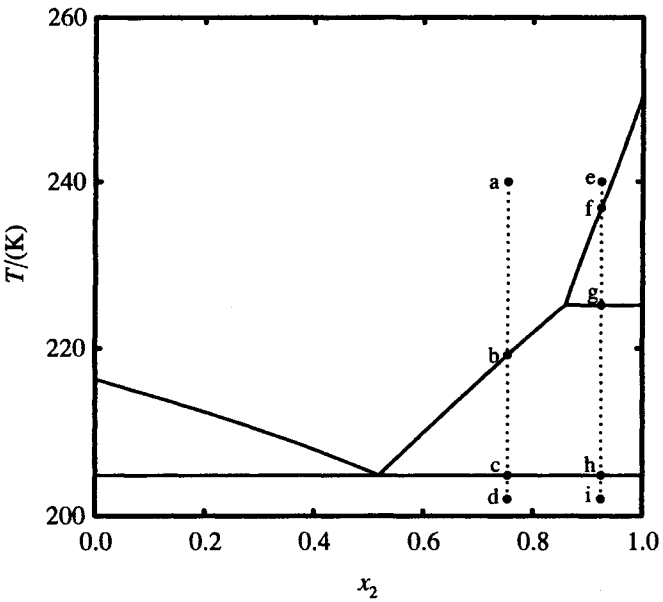

Figure 14.21 (Solid + liquid) phase equilibria for (x_1n-C_8H_{18} + x_2CCl_4). A solid-phase transition occurs in the CCl_4 at $T = 225$ K.

Since the (octane + tetrachloromethane) system is very nearly ideal, this equation can be used to describe the slope of the melting curve. The steep slope of the (solid + liquid) equilibrium line for CCl_4 above the transition temperature results from the very small enthalpy of fusion in the denominator of equation (14.2). Below the transition temperature, the enthalpy increases and the slope is significantly less steep.

If an (octane + tetrachloromethane) mixture with composition given by point a in Figure 14.21 is cooled along line abc, the low temperature form of CCl_4 freezes from solution at point b. As CCl_4 freezes from solution, the mixture becomes richer in n-C_8H_{18} and follows the (solid + liquid) equilibrium line. At the eutectic temperature, solid n-C_8H_{18} starts to crystallize from solution and an eutectic halt (in temperature) occurs (three phases in equilibrium) until all of the liquid is gone.

If a mixture with composition given by point e is cooled, the high-temperature form of CCl_4 starts to crystallize from solution at point f. This procedure continues until a temperature represented by g is reached. At this temperature, the high-temperature form converts to the low-temperature form. Three phases are present, the system is invariant, and the mixture stays at the transition temperature until all of the high-temperature form is converted to the low-temperature form. Continued cooling results in an

eutectic halt at the eutectic temperature h where the remaining mixture solidifies.

14.5d Metastable Equilibrium

Supercooling often accompanies the crystallization of solids from a liquid mixture, and not infrequently, a metastable solid is formed, which equilibrates with the liquid mixture to give a condition of metastable equilibrium. As an example, Figure 14.22 shows the (solid + liquid) phase diagram for (bromobenzene + mesitylene[v]).[18] Depending on the conditions, three different forms of mesitylene can be made to crystallize from the pure liquid or from solution.[w] The highest melting solid is, of course, the stable form, but the lower melting unstable forms do not easily convert to the stable form, and each can exist in equilibrium with the liquid mixture. The (solid + liquid) equilibrium curves for all three forms of mesitylene mixed with bromobenzene are shown in Figure 14.22. Dashed lines are used to represent the freezing lines for the metastable form. All three forms mix with bromobenzene to give simple eutectic systems. The three freezing lines are very nearly parallel, indicating that $\Delta_{fus}H_m$ is nearly the same for all three forms, so that $\Delta_{fus}H_m$, the enthalpy difference between the different solid forms, must be small[x] for these first-order phase transitions.

14.5e Congruently Melting Solid Addition Compounds

Figure 14.23 gives the (solid + liquid) phase diagram for (tetrachloromethane + 1,4-dimethylbenzene).[19] The maximum in the (solid + liquid) equilibrium curve at $x_2 = 0.5$ results from the formation of a solid addition compound with the formula $CCl_4 \cdot 1,4\text{-}C_6H_4(CH_3)_2$ that melts at the temperature corresponding

---

[v] Mesitylene is 1, 3, 5-trimethylbenzene.

[w] Cooling liquid mesitylene usually caused the lowest melting (and least stable) form of mesitylene to crystallize from solution. Alternate cooling and warming with stirring of a partially frozen sample at a temperature just below the melting temperature usually causes conversion to the intermediate (more stable) form. The highest temperature (stable) form is difficult to obtain. Crystals can usually be obtained by following a procedure described by Mair and Schicktanz {B. J. Mair and S. T. Schicktanz, *Bur. Standards J. Res.*, **11**, 665–680 (1933)}. This process involved cooling a brass rod (Mair and Schicktanz report that only brass would do) to liquid nitrogen temperatures, then plunging the rod into supercooled liquid mesitylene held at a temperature below the stable melting point, but above the metastable melting points. Almost always, this process will produce the stable solid. This procedure demonstrates that in studying phase changes, ingenuity, luck, and sometimes even a bit of black magic, seem to help in producing a desired result.

[x] In Figure 14.22, the metastable equilibrium involves metastable phases in one of the pure components. Metastable equilibria can also occur when addition compounds form. Later in this chapter, we will give an example of this type.

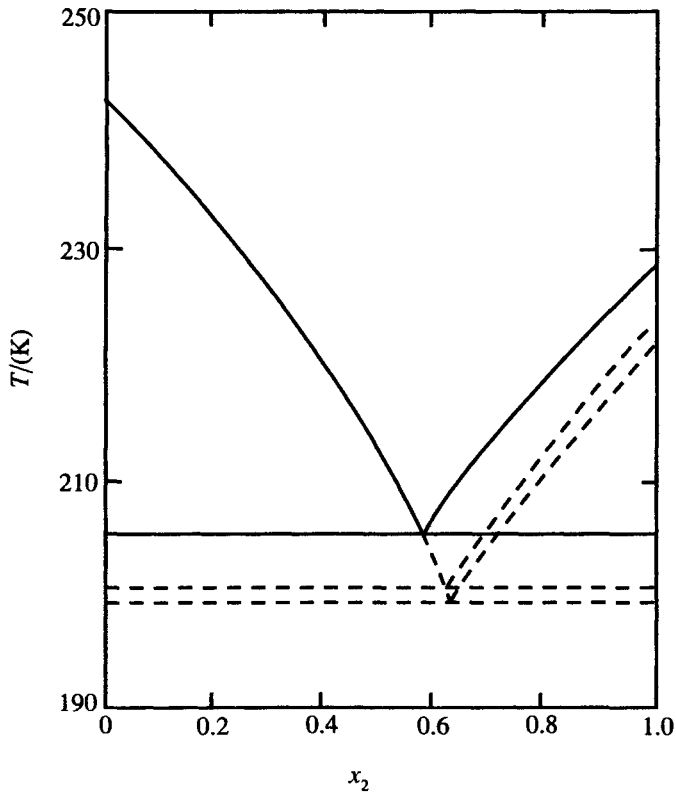

Figure 14.22 (Solid + liquid) phase equilibrium for $\{x_1C_6H_5Br + x_2 1,3,5\text{-}C_6H_3(CH_3)_3\}$. The dashed lines represent metastable equilibrium between the liquid solution and unstable forms of $1,3,5\text{-}C_6H_3(CH_3)_3$.

to the maximum, to form a liquid with the same composition. This type of melting is known as congruent melting. The phase diagram can be thought of as two simple eutectic phase diagrams placed side by side.[y] At the upper eutectic, e_u, $1,4\text{-}C_6H_4(CH_3)_2(s)$, $CCl_4 \cdot 1,4\text{-}C_6H_4(CH_3)_2(s)$ and liquid solution are in equilibrium, while at the lower eutectic, e_l, $CCl_4 \cdot 1,4\text{-}C_6H_4(CH_3)_2(s)$, $CCl_4(s)$, and liquid solution are in equilibrium. For the freezing curve between e_u and e_l, $CCl_4 \cdot 1,4\text{-}C_6H_4(CH_3)_2(s)$ and liquid are in equilibrium. If a mixture with a composition between e_u and e_l is cooled, the solid addition compound $CCl_4 \cdot 1,4\text{-}C_6H_4(CH_3)_2$ crystallizes from solution. If the composition is less than

[y] We will see in Section 14.5h that dissociation in the liquid phase rounds the top of the freezing curve at the stoichiometric composition so that an abrupt change in slope, similar to that obtained at the endpoints ($x_2 = 0$ and $x_2 = 1$) of the freezing curves for a simple eutectic system, does not occur. See this section for details.

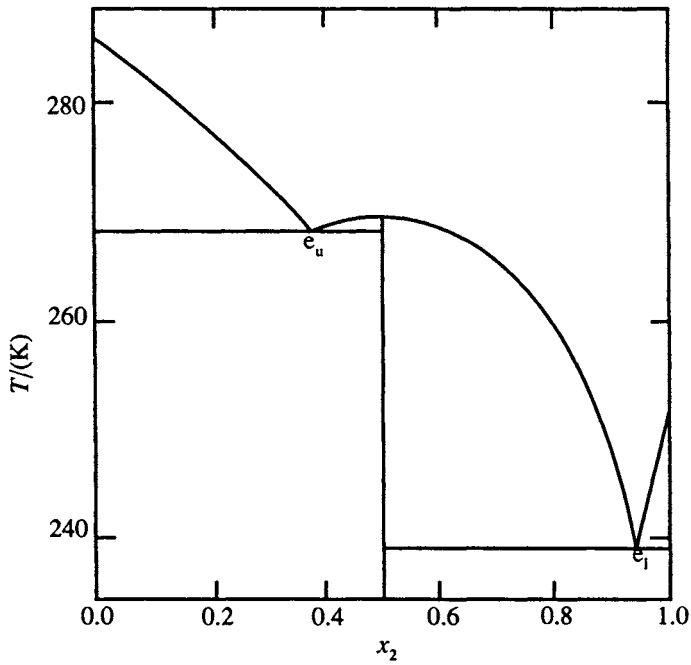

Figure 14.23 (Solid + liquid) phase diagram for $\{x_1 1,4\text{-}C_6H_4(CH_3)_2 + x_2 CCl_4\}$. A congruently melting addition compound with the formula $CCl_4 \cdot 1,4\text{-}C_6H_4(CH_3)_2(s)$ forms in this system.

$x_2 = 0.5$, but greater than e_u, cooling eventually leads to the upper eutectic, while cooling mixtures with x_2 greater than 0.5, but less than e_l, eventually leads to the lower eutectic. If mixtures with x_2 greater than e_l are cooled, $CCl_4(s)$ crystallizes from solution, while cooling mixtures with x_2 less than e_u results in the crystallization of $1,4\text{-}C_6H_4(CH_3)_2(s)$.

Figure 14.24 shows the (solid + liquid) phase diagram for $\{x_1 CHCl_3 + x_2(CH_3OCH_2)_2\}$.[20,z] It is an example of a system in which two congruently melting addition compounds form. The maxima in the melting curves occur at $x_2 = 0.333$ and $x_2 = 0.50$, indicating that the formulas of the addition compounds are $(CH_3OCH_2)_2 \cdot CHCl_3(s)$ and $(CH_3OCH_2)_2 \cdot 2CHCl_3(s)$. Figure 14.24 can be thought of as three simple eutectic systems placed side by side. One diagram is for the system $\{CHCl_3 + (CH_3OCH_2)_2 \cdot 2CHCl_3\}$, another for $\{(CH_3OCH_2)_2 \cdot 2CHCl_3 + (CH_3OCH_2)_2 \cdot CHCl_3\}$, and the third for $\{(CH_3OCH_2)_2 \cdot CHCl_3 + (CH_3OCH_2)_2\}$. For compositions less than those given by $e_{u,1}$, $CHCl_3(s)$ freezes from solution; for compositions between $e_{u,1}$

[z] $(CH_3OCH_2)_2$ is 1,2-dimethoxyethane.

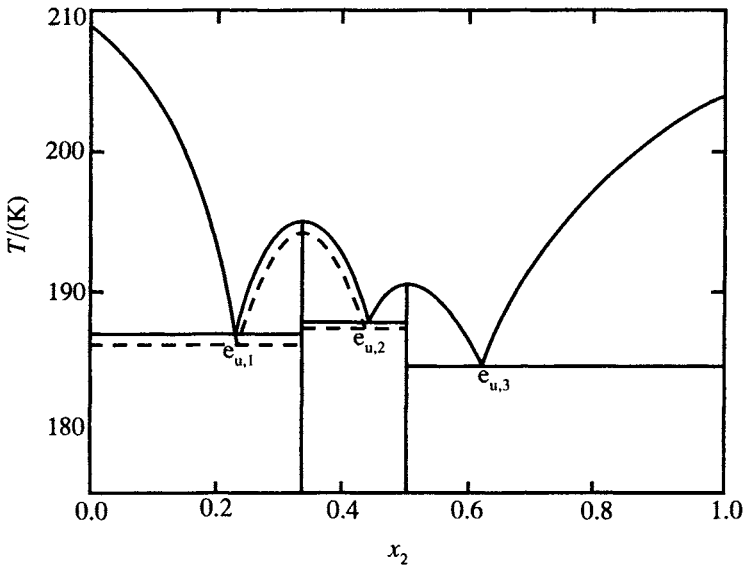

Figure 14.24 (Solid + liquid) phase diagram for $\{x_1CHCl_3 + x_2(CH_3OCH_2)_2\}$. The dashed lines represent the melting temperatures and the eutectics for a metastable form of $(CH_3OCH_2)_2{\cdot}2CHCl_3(s)$.

and $e_{u,2}$, $(CH_3OCH_2)_2{\cdot}2CHCl_3(s)$ forms, for compositions between $e_{u,2}$ and $e_{u,3}$, $(CH_3OCH_2)_2{\cdot}CHCl_3(s)$ forms, and for solutions with x_2 greater than $e_{u,3}$, $(CH_3OCH_2)_2(s)$ crystallizes from solution. A metastable form of $(CH_3OCH_2)_2{\cdot}2CHCl_3$ is also evident, with the dashed line representing the melting temperatures and the eutectic temperatures for this substance.

14.5f Incongruently Melting Solid Addition Compounds

Congruently melting addition compounds melt to directly form a liquid. The reaction can be represented as

$$m\text{A}{\cdot}n\text{B(s)} = \text{liquid solution} \tag{14.3}$$

where m and n are the moles of A and B in the addition compound, and the liquid has the same mole ratio m/n. In some instances, melting occurs by a decomposition reaction in which a solid addition compound melts to form a different solid plus a liquid mixture whose composition differs from that of either solid. This process is referred to as incongruent melting.

The incongruent melting reaction can be written as

$$m\text{A}{\cdot}n\text{B(s)} = q\text{A}{\cdot}r\text{B(s)} + \text{liquid solution.} \tag{14.4}$$

The (methanol + water) system,[21] whose phase diagram is shown in Figure 14.25, is an example. At low temperatures a mixture of H_2O and CH_3OH in an equimolar ratio combine to form a solid hydrate[aa] with the formula $CH_3OH{\cdot}H_2O(s)$. The vertical line at $x_2 = 0.5$ in Figure 14.25 is at the stoichiometric composition of this hydrate. To understand the nature of incongruent melting, let us start with a sample of the solid hydrate at a temperature given by point e and heat it along line edcba. No phase changes occur until point c is reached, at which temperature the hydrate melts incongruently (decomposes). The reaction is

$$CH_3OH{\cdot}H_2O(s) = H_2O(s) + \text{liquid solution.} \qquad (14.5)$$

Thus, in the melting process, the solid hydrate melts by decomposing to solid H_2O and a liquid solution. This liquid has the composition given by point p, known as the **peritectic point**. It is an invariant point, since three phases

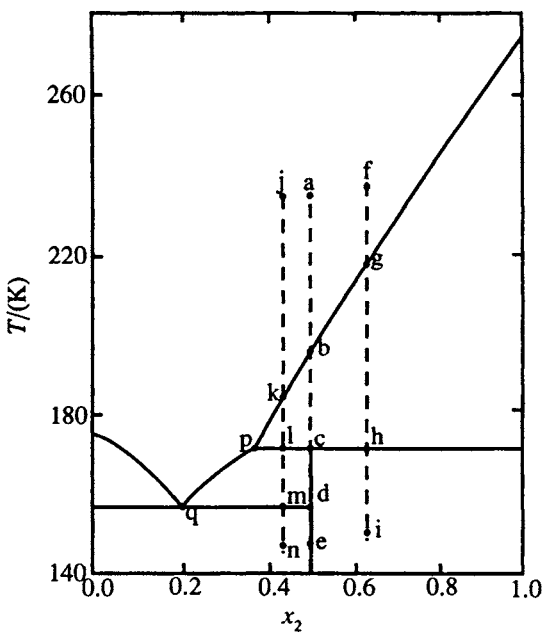

Figure 14.25 (Solid + liquid) phase diagram for $(x_1CH_3OH + x_2H_2O)$ at $p = 0.1$ MPa.

[aa] It is not unusual for alkanols to form solid hydrates. Examples of other alkanols that do so include ethanol, 2-propanal, 2-methyl-propan-2-ol (t-butyl alcohol), ethylene glycol, and 2,3-dimethyl- 2,3-butanediol (pinacol).

{$CH_3OH{\cdot}H_2O(s)$, $H_2O(s)$ and liquid solution} are in equilibrium. In the warming process, the temperature will stay at the peritectic temperature until all of the hydrate has melted (decomposed). Continued warming melts ice, with the composition of the liquid changing along line pb until point b is reached, at which temperature the last of the solid melts. Continued heating increases the temperature of the liquid ($x_2 = 0.5$) mixture to a temperature represented by point a.

It is instructive to compare the changes that occur when liquids with compositions given by points a, f, and j are cooled. Cooling along line abcde reverses the process described above. That is, ice freezes from the solution at point b. With continued cooling, more ice forms and the liquid follows line bp. At point c, the ice that has collected reacts with the liquid solution (composition given by p) to form hydrate

$$H_2O(s) + \text{liquid} = CH_3OH{\cdot}H_2O(s). \tag{14.6}$$

The temperature will stay at the value[bb] given by point p until all of the $H_2O(s)$ has reacted to form the hydrate. The stoichiometry of the reaction is just right so that the $H_2O(s)$ reacts with all of the liquid to form pure $CH_3OH{\cdot}H_2O(s)$. Cooling this solid to lower temperatures (point e) causes no further phase changes.

If a solution with composition and temperature given by point f is cooled, ice freezes from the mixture at point g. Further cooling produces more ice and the liquid changes composition along line gp until point p is reached. At this temperature the peritectic reaction occurs again, causing a peritectic halt. However, not enough liquid is present to react with all of the ice by reaction (14.6). As a result, when all of the liquid is used up, a heterogeneous mixture of $H_2O(s)$ and $CH_3OH{\cdot}H_2O(s)$ remains. Cooling this mixture to point i results in no further phase changes.

When a liquid mixture with composition and temperature given by point j is cooled, ice freezes from solution at point k. Continued cooling produces more ice, and the liquid follows line kp until point p is reached. At this temperature, the peritectic reaction {reverse of reaction (14.4)} again occurs, resulting in a peritectic halt. However, not enough ice has been formed to react with all of the liquid, and liquid is left when all of the ice is gone. With continued cooling, the liquid freezes to produce more $CH_3OH{\cdot}H_2O(s)$, and the composition of the liquid changes along line pq until q is reached. At this point solid CH_3OH freezes from solution, and three phases are present, resulting in a eutectic halt. The temperature will stay at the value given by point m until all of the liquid is

[bb] This temperature halt in the cooling process is known as a peritectic halt.

gone. Continued cooling takes the mixture of $CH_3OH(s)$ and $CH_3OH \cdot H_2O(s)$ to the temperature given by point n without any further temperature halts.[cc]

14.5g Solid Solution Formation

Partial Miscibility in the Solid State: So far, we have described (solid + liquid) phase equilibrium systems in which the solid phase that crystallizes is a pure compound, either as one of the original components or as a molecular addition compound. Sometimes solid solutions crystallize from solution instead of pure substances, and, depending on the system, the solubility can vary from small to complete miscibility over the entire range of concentration. Figure 14.26 shows the phase diagram for the (silver + copper) system.[22] It is one in which limited solubility occurs in the solid state. Line AE is the (solid + liquid) equilibrium line for Ag, but the solid that crystallizes from solution is not pure Ag. Instead it is a solid solution with composition given by line AC. If a liquid with composition and temperature given by point a is

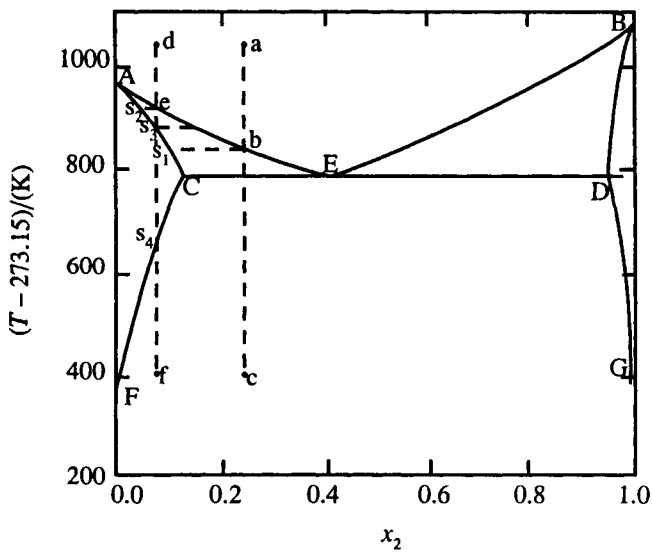

Figure 14.26 (Solid + liquid) phase diagram for $(x_1Ag + x_2Cu)$ at $p = 0.1$ MPa. Reprinted with permission from M. Hanson and K. Anderko, *Constitution of Binary Alloys*, 2nd ed., McGraw-Hill, New York, 1958, p. 18.

[cc] The changes we have described assume that equilibrium is maintained during cooling. Sometimes the reaction is sluggish, not all of the liquid reacts as the mixture is cooled along lines abcde or fghi, and a eutectic halt may occur, even though it should not.

cooled, solid solution S_1 crystallizes from the liquid melt at a temperature given by point b. With continued cooling, the solid in equilibrium with the solution changes composition along line AC, while the liquid changes composition along line AE. When the eutectic temperature is reached, the solid has a composition give by point C and the liquid a composition given by point E. Solid solution rich in Cu with a composition given by D will start to crystallize from the melt, and a eutectic halt will occur until all of the liquid is solidified. With further cooling, the solid solutions should change compositions, with concentrations given by lines CF and DG. In practice, it is difficult to get this to happen because the necessary diffusion from one solid phase to the other is slow.

A different sequence of phase changes occurs when a solution with temperature and mole fraction given by line def is cooled. Solid S_2 crystallizes from solution at point e. With continued cooling the composition of the solid that freezes out follows line AC while the composition of the liquid follows line AE. At point S_3 all of the liquid has solidified. With continued cooling, solid with composition given by S_3 is lowered in temperature. No phase changes occur until S_4 is reached. At this temperature, solid with composition given by line DG (connected by a tie-line with line CF) should crystallize from the solid S_4. With continued cooling, the compositions of the two solids should follow lines CF and DG, although, once again, this process would be slow. Note that with this mixture, a eutectic halt is not observed. The eutectic mixture is obtained only when we start with liquid mixtures with compositions between C and D.

Complete Miscibility in the Solid State: Figure 14.27 is the (solid + liquid) phase diagram for (silver + gold).[23] Complete miscibility in the liquid and solid states is present in this system. The upper line is known as the **liquidus line** and the lower line as the **solidus line**. Mixtures at temperatures above the liquidus line are liquid and mixtures below the solidus line are solid. In the region between the liquidus line and the solidus line, solid and liquid are in equilibrium, with compositions given by the horizontal tie-lines connecting the two curves. As an example, if a liquid with composition and temperature given by point a is cooled, solid with composition given by d will crystallize from the mixture when the temperature reaches point b. With cooling, the composition of the liquid follows the liquidus curve while the composition of the solid follows the solidus curve. Complete solidification occurs when the temperature reaches point c (the solidus line). Further cooling lowers the temperature of the single-phase solid solution, for example, to point e.[dd]

[dd] Continuous solid solution systems can be found in which the liquidus and solidus lines come together at a maxima or minima. The condition is analogous to azeotrope formation in (vapor + liquid) phase equilibria.

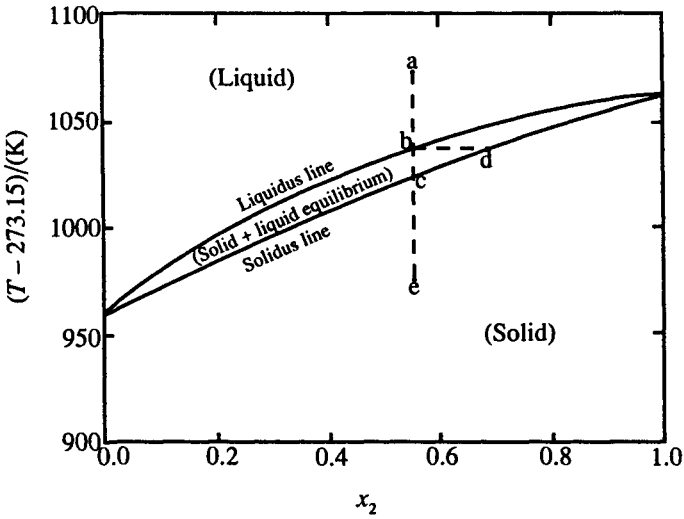

Figure 14.27 (Solid + liquid) phase diagram for $(x_1\text{Ag} + x_2\text{Au})$ at $p = 0.1$ MPa, an example of a system with complete miscibility in both the liquid and solid states.

Variable Composition in a Molecular Addition Compound: As a final example of solid solution behavior, Figure 14.28 shows the phase diagram for (tetrachloromethane + pyridine).[24] A congruently melting molecular addition compound with the formula $C_5H_5N{\cdot}2CCl_4(s)$ forms in this system. Solid solution formation is present, not only in solid tetrachloromethane and solid pyridine, but also in the molecular addition compound. The result is a molecular addition compound with variable composition. Thus, if one cools along line ab, the compound $C_5H_5N{\cdot}2CCl_4(s)$ is obtained. But cooling along line cd gives an addition compound with composition given by point e when the solidification process is complete, a composition that is much closer to $C_5H_5N{\cdot}CCl_4$ than to $C_5H_5N{\cdot}2CCl_4$.[ee]

As we end our discussion of (solid + liquid) phase diagrams we should keep in mind that the examples we have used represent only the simplest of systems. Combinations can be obtained that lead to much more complicated phase diagrams. For example, in the (sulfuric acid + water) system, congruently melting solid addition compounds form with the formulas $H_2SO_4{\cdot}H_2O$, $H_2SO_4{\cdot}2H_2O$, and $H_2SO_4{\cdot}4H_2O$. In addition the incongruently melting compounds $H_2SO_4{\cdot}3H_2O$, $H_2SO_4{\cdot}6.5H_2O$, and $H_2SO_4{\cdot}8H_2O$ are present, with the last of these occurring only as a result of metastable equilibrium.[25]

[ee] Solid-phase solubility leading to a variable composition for an addition compound is not uncommon in alloy systems and in mixed salts.

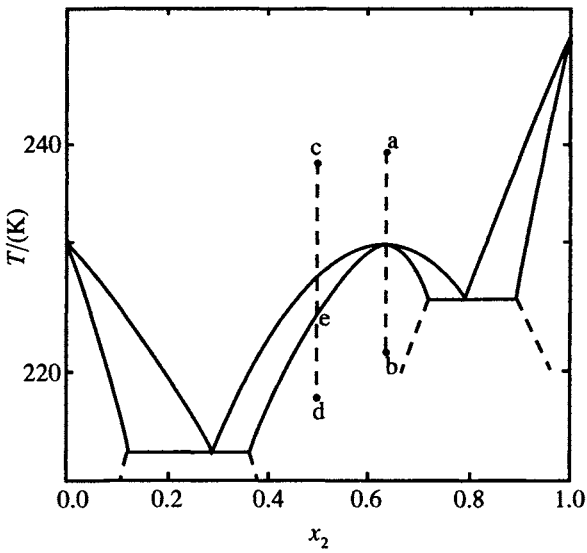

Figure 14.28 (Solid + liquid) phase diagram at $p = 0.1$ MPa for $(x_1C_5H_5N + x_2CCl_4)$.

14.5h The (Solid + Liquid) Equilibrium Curve for a Dissociable Solute

Figure 14.29 shows the (solid + liquid) phase diagram for (benzene + hexafluorobenzene). A congruently melting solid molecular addition compound with the formula $C_6H_6 \cdot C_6F_6(s)$ is evident in this system.[26] The rounded top of the freezing curve (solid line) for the addition compound results from almost complete dissociation of the addition compound in the liquid mixture. In other words, benzene and hexafluorobenzene act as independent molecular species in the liquid state and combine together as the addition compound only in the solid state.

The amount of rounding of the top of the freezing curve of the addition compound is determined by the degree of dissociation. The dashed lines with the sharp break at $x_2 = 0.5$ are what would be obtained if complete association occurs in the liquid state. Partial dissociation gives the curves represented by the dash-dot line.

The rounding of the top of the freezing curve results from the fact that, if dissociation occurs, addition of an infinitesimal amount of either of the two components to a mixture with the stoichiometric composition does not change the melting temperature. In other words, at the stoichiometric composition, the maximum is a continuous curve and not a cusp or a point of intersection of two curves. This may be seen as follows.

Although only two independent components are present in the solution, we may consider that three constituents are present, namely n_1 moles of C_6H_6 with chemical potential μ_1, n_2 moles of C_6F_6 with chemical potential μ_2, and n_3 moles

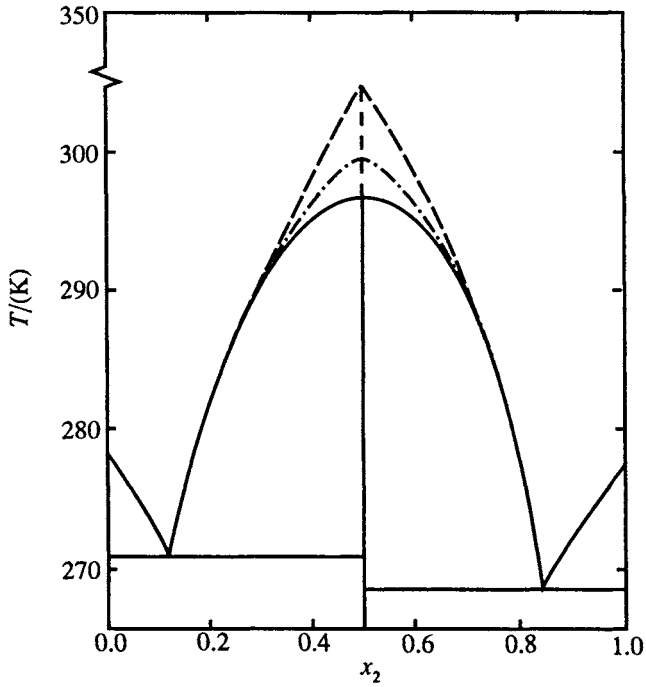

Figure 14.29 (Solid + liquid) phase diagram for $(x_1C_6H_6 + x_2C_6F_6)$. The dashed line represents expected melting points of the $C_6H_6{\cdot}C_6F_6$ solid addition compound if the addition compound did not dissociate in the liquid mixture, while the dash-dot line represents partial dissociation in the liquid mixture.

of $C_6H_6{\cdot}C_6F_6$ with chemical potential μ_3. These components are in equilibrium

$$C_6H_6 + C_6F_6 = C_6H_6{\cdot}C_6F_6 \tag{14.7}$$

so that

$$\Delta_r G^\circ_m = \mu_3 - \mu_2 - \mu_1 = 0. \tag{14.8}$$

Let us add dn_1 moles of C_6H_6 to the stoichiometric mixture. From the Gibbs–Duhem equation we can write

$$n_1\, d\mu_1 + n_2\, d\mu_2 + n_3\, d\mu_3 = 0. \tag{14.9}$$

But, at the stoichiometric composition, $n_1 = n_2$, since we have a 1 : 1 addition compound, and equation (14.9) becomes

$$n_2(d\mu_1 + d\mu_2) + n_3\, d\mu_3 = 0. \tag{14.10}$$

Differentiating equation (14.8) and combining with equation (14.10) gives

$$(n_2 + n_3)\, d\mu_3 = 0. \tag{14.11}$$

In equation (14.11), $(n_1 + n_2)$ cannot equal zero. Hence, $d\mu_3 = 0$. Thus, the chemical potential of the addition compound is not changed by adding an infinitesimal amount dn_1 of C_6H_6 (or dn_2 of C_6F_6), and equilibrium will be maintained without a change in the equilibrium temperature. The extent to which this statement is true depends upon the degree of dissociation. That is, the more the dissociation, the longer the mole fraction region over which the freezing maximum will remain flat.

Problems

P14.1 An azeotrope is a constant-boiling solution in which evaporation causes no change in the composition of the liquid. In other words, the composition of the liquid and gaseous phases must be identical. If the vapors may be assumed to be perfect gases, then the ratio of the two partial pressures is equal to the ratio of the mole fractions in the liquid. Use the Gibbs–Duhem equation to show that, at the azeotrope,

$$\frac{dp_1}{dx_1} + \frac{dp_2}{dx_1} = 0$$

and that the total vapor pressure $p = p_1 + p_2$ is a maximum or minimum.

x_2	T/(K)	x_2	T/(K)	x_2	T/(K)
0.0000	162.67	0.4997	187.79	0.7070	199.49
0.0045	162.55	0.5084	187.79	0.7289	200.41
0.0099	162.42	0.5188	187.74	0.7538	201.76
0.0182	167.1	0.5424	189.05	0.7765	202.87
0.0493	175.3	0.5796	191.81	0.8067	204.31
0.1371	181.06	0.5829	192.10	0.8460	206.01
0.2223	183.81	0.6145	194.12	0.9065	208.75
0.2755	185.17	0.6478	195.96	0.9492	210.61
0.3336	186.25	0.6667	197.04	1.0000	212.71
0.4048	187.27	0.6866	198.25		

Eutectics at T = 162.36 K and 187.66 K.
(Solid + Solid) transition in pure $HCON(CH_3)_2$ at 196.96 K.

P14.2 Given the following (solid + liquid) equilibrium temperatures for phase changes in the $\{x_1CFCl_3 + x_2HCON(CH_3)_2\}$ system[27]

(a) Construct the binary (solid + liquid) phase diagram. Label all the regions.

(b) Calculate the enthalpy of fusion of $HCON(CH_3)_2$ at its melting point.

P14.3 Draw time against temperature cooling curves showing the temperature halts that occur when liquid mixtures with $x_2 = 0.4$, 0.5, and 0.6, are cooled to a temperature where only solid remains for the systems shown in Figures 14.16, 14.23, 14.24, and 14.25.

P14.4 Draw time against temperature cooling curves showing the temperature halts when a liquid mixture of $(x_1H_2O + x_2CH_3CN)$ with $x_2 = 0.5$ is cooled from 273.15 K to 233.15 K at p = 100, 124, 140, and 175 MPa. (See Figure 14.20 for the phase diagram.)

At T = 333.15 K			At p = 101.32 kPa		
x_1	y_1	p/(kPa)	x_1	y_1	T/(K)
0.0000	0.0000	19.60	0.0000	0.0000	370.29
0.0250	0.0950	21.25	0.0421	0.1386	367.93
0.0500	0.1700	22.68	0.1220	0.2984	365.27
0.1000	0.2800	25.02	0.2202	0.4095	362.75
0.2000	0.4170	28.42	0.2437	0.4229	362.55
0.3000	0.4940	30.10	0.3661	0.5022	361.25
0.4000	0.5370	30.76	0.4626	0.5398	360.90
0.5000	0.5620	31.06	0.5359	0.5588	360.83
0.6000	0.5780	31.18	0.5686	0.5686	360.74
0.7000	0.5900	31.17	0.6039	0.5722	360.80
0.8000	0.5960	31.05	0.6406	0.5852	360.83
0.9000	0.6150	30.70	0.7193	0.5955	360.98
0.9500	0.6600	29.21	0.7979	0.5966	361.10
0.9750	0.7270	27.00	0.9105	0.6001	361.62
1.0000	1.0000	19.92	0.9344	0.6111	361.85
			0.9636	0.6466	363.01
			0.9780	0.6988	365.03
			0.9908	0.8436	369.03
			0.9939	0.8611	369.70
			1.0000	1.0000	373.15

P14.5 (a) Use thermodynamic data in Table A5.4 of Appendix 5 to determine if you would expect benzene (C_6H_6) to be more or less soluble in CS_2 than in n-octane (C_8H_{18}). Justify your choice.
(b) Benzene (C_6H_6) and n-octane (C_8H_{18}) form very nearly an ideal liquid solution, with no solid solutions and no solid addition compound formation. Use the thermodynamic data in Table A5.4 of Appendix 5 to construct the (solid + liquid) phase diagram for this system, and determine the eutectic composition.

P14.6 Given the following data for mixtures of $\{x_1H_2O + x_2CH_3(CH_2)_2OH\}$
(a) Construct the phase diagrams for p against x_1 and y_1 at $T = 333.15$ K, and T against x_1 and y_1 at $p = 101.32$ kPa. Label all the regions and compare the azeotropic composition obtained from the two diagrams.
(b) Assume ideal vapors and Raoult's law standard states and calculate the activity coefficients of H_2O ($\gamma_{R,1}$) and $CH_3(CH_2)_2OH$ ($\gamma_{R,2}$) at $T = 333.15$ K and each of the mole fractions given above. Make a graph of $\gamma_{R,1}$ and $\gamma_{R,2}$ against x_1.

References

1. Phase equilibria is a broad subject. We refer the reader to the following texts for extended discussion. Some are old "classic" texts while others are very recent. Some emphasize the theory of phase equilibria, while others take a very practical and applied approach. Some provide broadly based discussions of several types of phase equilibria, while others are more specifically focused. Some limit the discussion to binary systems, as we do, while others extend the description to include ternary systems, and more. (a) J. M. Prausnitz, R. N. Lichtenthaler, and E. G. de Azevedo, *Molecular Thermodynamics of Fluid-Phase Equilibria, Third Edition*, Prentice Hall PTR, Upper Saddle River, New Jersey, 1999; (b), J. S. Rowlinson and F. L. Swinton, *Liquids and Liquid Mixtures, Third Edition*, Butterworth Scientific, London, 1982; I. Prigogine and R. Defay, translated by D. H. Everett, *Chemical Thermodynamics*, Longmans Green and Co., London, 1954; A. W. Francis, *Liquid–Liquid Equilibriums*, Interscience Publishers, New York, 1963; J. E. Ricci, *The Phase Rule and Heterogeneous Equilibrium*, D. Van Nostrand Company, Inc., Toronto, 1951; A. Findlay and A. N. Campbell, *The Phase Rule and Its Applications, Eighth Edition*, Dover Publications, New York, 1945; S. M. Walas, *Phase Equilibria in Chemical Engineering*, Butterworth Publishers, Boston, 1985; G. Masig, translated by B. A. Rogers, *Ternary Systems: Introduction to the Theory of Three Component Systems*, Dover Publications, Inc., New York, 1944.
2. P. Dalager, "Vapor–Liquid Equilibria of Binary Systems of Water with Methanol and Ethanol at Extreme Dilution of the Alcohols", *J. Chem. Eng. Data*, **14**, 298–301 (1969).
3. V. S. Ezhov, S. N. Golovko, and E. M. Guseinov, "Determination of the Equilibrium Characteristics of Vapor–Liquid and the Liquid–Liquid Systems Applicable to Products of the Oxidative Ammonolysis of Toluene and Picolines", *Khim.-Farm. Zh.*, **10**, 77–79 (1976).
4. F. Mato and M. Sanchez, "Liquid–Vapor Equilibriums of Binary Mixtures of Acetonitrile", *An. Real. Soc. Espan. Fis. Quim. Ser. B*, **63**, 1–12 (1967).

5. C. R. Fordyce and D. R. Simonsen, "Cellulose Ester Solutions. Evaporation in Binary Solvent Mixtures", *Ind. Eng. Chem.* **41**, 104–111 (1949).
6. W. J. Gaw and F. L. Swinton, "Occurrence of a Double Azeotrope in the Binary System Hexafluorobenzene + Benzene", *Nature (London)*, **212**, 283–284 (1966).
7. R. W. Hobson, R. J. Hartman, and E. W. Kanning, "A Solubility Study of Di-n-propylamine", *J. Am. Chem. Soc.*, **63**, 2094–2095 (1941).
8. J. Matous, J. P. Novak, J. Sobr, and J. Pick, "Phase Equilibriums in the System Tetrahydrofuran(1)–Water(2)", *Collect. Czech. Chem. Commun.*, **37**, 2653–2663 (1972).
9. G. Schneider, "Phase Equilibriums in Liquid Systems at High Pressures", *Ber. Bunsenges. Physik. Chem.*, **70**, 497–520 (1966). G. M. Schneider, "Phase Equilibria in Fluid Mixtures at High Pressures", *Adv. Chem. Phys.* **17**, 1–42 (1970). G. M. Schneider, "Gas–Gas Equilibrium. Fluid Mixtures Under Pressure", *Fortschr. Chem. Forsch.* **13**, 559–600 (1970). G. M. Schneider, "Phase Behavior and Critical Phenomena in Fluid Mixtures Under Pressure", *Ber. Bunsenges. Physik. Chem.* **76**, 325–331 (1972). G. M. Schneider in *Water: A Comprehensive Treatise, Vol II*, F. Franks. ed., Plenum Press, New York, 1973, Ch. 6.
10. R. L. Scott and P. H. van Konynenburg, "Static Properties of Solutions. 2. Van der Waals and Related Models for Hydrocarbon Mixtures", *Discuss. Faraday Soc.*, **49**, 87–97 (1970).
11. M. L. McGlashan, *Chemical Thermodynamics*, Academic Press, London, 1979, p. 277.
12. A detailed discussion of (fluid + fluid) equilibrium can be found in (a) J. S. Rowlinson and F. L. Swinton, *Liquids and Liquid Mixtures, Third Edition*, Butterworths, London, 1982. This reference is especially good in summarizing references to many examples of systems that show the different types of phase equilibria behavior. (b) W. B. Streett, Chapter 1, "Phase Equilibria in Fluid and Solid Mixtures at High Pressure," in *Chemical Engineering at Supercritical Fluid Conditions*, M. E. Paulaitis, J. M. Penninger, R. D. Gray Jr. and P. Davidson, editors, Ann Arbor Science Press, 1983. This reference is the source for Figures 14.9, and 14.13 to 14.15. (c) G. M. Schneider, "High-pressure Phase Diagrams and Critical Properties of Fluid Mixtures," Chapter 4 of *Chemical Thermodynamics, Volume 2*, The Chemical Society, Burlington House, London, 1978.
13. J. R. Goates, J. B. Ott, J. F. Moellmer, and D. W. Farrell, "(Solid + Liquid) Phase Equilibrium in *n*-Hexane + Cyclohexane and Benzene + *p*–Xylene", *J. Chem. Thermodyn.*, **11**, 709–711 (1979).
14. J. R. Goates, J. B. Ott, and A. H. Budge, "Solid–Liquid Phase Equilibria and Solid Compound Formation in Acetonitrile–Aromatic Hydrocarbon Systems", *J. Phys. Chem.*, **65**, 2162–2165 (1961).
15. Taken from K. Roth, G. Schneider, and E. U. Franck, "Liquid–Liquid and Liquid–Solid Phase Equilibriums in Cyclohexane–Methanol and Phenol–Water Systems up to 6000 Bars", *Ber. Bunsenges. Physik. Chem.*, **70**, 5–10 (1966).
16. G. Schneider, "Druckeinfluß auf die Entmischung Flüssiger Systeme III. Das 4-Phasengleichgewicht Flüssig–Flüssig–Fest–Fest im System Acetonitril–H_2O bei – 24.2 °C und 1240 Bar", *Z. Phys. Chem. (Frankfurt)*, **41**, 327–338 (1964).
17. J. B. Ott and J. R. Goates, "(Solid + Liquid) Phase Equilibria in Binary Mixtures Containing Benzene, a Cycloalkane, an *n*-Alkane, or Tetrachloromethane: An Equation for Representing (Solid + Liquid) Phase Equilibria", *J. Chem. Thermodyn.*, **15**, 267–278 (1983).
18. J. R. Goates, J. B. Ott and J. F. Moellmer, "Solid + Liquid Phase Equilibria and Solid-Compound Formation in Halobenzenes + Aromatic Hydrocarbons", *J. Chem. Thermodyn.*, **8**, 217–224 (1976).
19. J. Boerio-Goates, S. R. Goates, J. B. Ott, and J. R. Goates, "Enthalpies of Formation of Molecular Addition Compounds in Tetrachloromethane + p-Xylene, + Toluene, and + Benzene from (Solid + Liquid) Phase Equilibria", *J. Chem. Thermodyn.*, **17**, 665–670 (1985).

20. C. Guanquan, J. B. Ott and J. R. Goates, "(Solid + Liquid) Phase Equilibria and Solid-Compound Formation in 1,2-Dimethoxyethane + Tetrachloromethane, + Trichlorofluoromethane, and + Trichloromethane", *J. Chem. Thermodyn.*, **18**, 31–37 (1986).
21. J. B. Ott, J. R. Goates and B. A. Waite, "(Solid + Liquid) Phase Equilibria and Solid-Hydrate Formation in Water + Methyl, + Ethyl, + Isopropyl, and + Tertiary Butyl Alcohols," *J. Chem. Thermodyn.*, **11**, 739–746 (1979).
22. M. Hansen and K. Anderko, *Constitution of Binary Alloys*, 2nd ed., McGraw-Hill, New York, 1958, p. 18.
23. M. Hansen and K. Anderko, *Constitution of Binary Alloys*, 2nd ed., McGraw-Hill, New York, 1958, p. 6.
24. C. Guanquan, J. B. Ott, and J. R. Goates, "(Solid + Liquid) Phase Equilibria and Solid Compound Formation in Tetrachloromethane + Furan, + Pyridine, and + N-Methylpyrrole", *J. Chem. Thermodyn.*, **18**, 603–608 (1986).
25. W. F. Giauque, E. W. Hornung, J. E. Kunzler, and T. R. Rubin, "The Thermodynamic Properties of Aqueous Sulfuric Acid Solutions and Hydrates from 15 to 300 °K", *J. Am. Chem. Soc.*, **82**, 62–70 (1960).
26. J. R. Goates, J. B. Ott, and J. Reeder, "Solid + Liquid Phase Equilibria and Solid Compound Formation in Hexafluorobenzene + Benzene, + Pyridine, + Furan, and + Thiophen", *J. Chem. Thermodyn.*, **5**, 135–141 (1973).
27. J. B. Ott, J. R. Goates, and D. E. Oyler, "Solid Compound Formation from Solutions of N, N-Dimethylformamide with Carbon Tetrachloride and Related Substances. A Solid Phase Transition in N,N-Dimethylformamide", *Trans. Faraday Soc.*, **62**, 1511–1518 (1966).

Chapter 15

Applications of Thermodynamics to Chemical Processes

In this chapter, we present a series of examples to show how thermodynamic concepts can be applied in a variety of processes across several scientific disciplines. We have selected examples that, in addition to being good chemistry, include the design of industrial processes, or have application to such diverse disciplines as materials science or geochemistry. In the next chapter, we will extend the discussion to include examples from biochemistry. In addition to a broad disciplinary coverage, the examples illustrate how thermodynamics can be targeted to solve narrowly focused problems such as the synthesis of ammonia and of diamond, while insights into problems of a larger scope require the systematic collection and analysis of many experiments. Some examples also illustrate how thermodynamic measurements can be coupled with structural and/or spectroscopic techniques to gain valuable perspectives on the problems.

We have had to be somewhat arbitrary in our choice of topics, and we apologize to the many fine thermodynamicists whose work is not featured here. Some of the examples are chosen to be of historical, as well as practical interest, and we have focused the discussion for these examples on "pioneers" in the field who made major contributions. Other examples, however, illustrate "cutting edge" research and demonstrate that thermodynamics, although a very old science, is still very much alive, and still a valuable tool for interpreting and solving "modern" chemical problems.

15.1 The Haber Cycle: Application to an Industrial Process

"Water water everywhere nor any drop to drink."

This quote from the *Rime of the Ancient Mariner*,[a] can be paraphrased to apply to the sources of so-called "fixed" nitrogen at the beginning of the twentieth century. An essentially inexhaustible supply of nitrogen was available as N_2 gas in the atmosphere, but the supplies of nitrogen in usable forms as a nitrate or ammonia were scarce, and fast being depleted. An ample supply of "fixed" nitrogen was critical to the world's economy. Sir William Crookes, an eminent English scientist of the time, warned "mankind" of approaching starvation. His forecast was based upon a growing world scarcity of nitrogen-containing fertilizer that was essential for plant growth.[b] The major sources of "fixed" nitrogen were animal waste and Chile saltpeter. Generation of the former could not keep up with the demand, and supplies of the latter, which originated mostly from "bird droppings", were fast being depleted.

With all of these concerns, there was considerable interest in developing reactions to synthesize ammonia or nitric acid. One such possibility is the direct reaction of hydrogen with nitrogen. The reaction is

$$3H_2(g) + N_2(g) = 2NH_3(g). \tag{15.1}$$

With the aid of the equations from statistical thermodynamics summarized in Chapter 11, we can investigate the possibility that ammonia can be produced from this process. We can obtain $\Delta_r G°$ and $\Delta_r H°$ for the reaction as a function of temperature using the relationships

$$\Delta_r G°_T = \Delta(G°_T - H°_{298}) + \Delta_r H°_{298} \tag{15.2}$$

$$\Delta_r H°_T = \Delta(H°_T - H°_{298}) + \Delta_r H°_{298}. \tag{15.3}$$

The necessary $(G°_T - H°_{298})$ and $(H°_T - H°_{298})$ functions can be calculated very accurately by statistical methods, using molecular parameters such as the molecular weight, moments of inertia, and vibrational frequencies. The equations needed to make the calculation, along with necessary molecular data, are summarized in Appendix 6, while values for the thermodynamic functions for a number of substances are given in Appendix

---

[a] Taken from *Rime of the Ancient Mariner* by Samuel Taylor Coleridge.

[b] Nitrogen as a nitrate or ammonia also finds many other uses, including being an important component in almost all explosives (until the advent of the atomic and hydrogen bombs). A scarcity of fixed nitrogen was especially worrisome to Germany as the First World War approached, with world opinion stacked against them and internal sources of nitrate almost nonexistent.

5. In equations (15.2) and (15.3), $\Delta_r H^\circ_{298}$ is the standard enthalpy change for the reaction at $T = 298.15$ K. It is twice the enthalpy of formation of $NH_3(g)$, a quantity that has been accurately measured[c] and is readily available (see Appendix 5).

Figure 15.1 summarizes calculated values of ΔG°_T, $\Delta_r H^\circ_T$, and $T\Delta_r S^\circ_T$ as a function of temperature for reaction (15.1). We note that $\Delta_r H^\circ_T$ is less than zero and almost constant with temperature. The main contribution to $\Delta_r H^\circ$ is the energy difference between the three H–H bonds and the $N \equiv N$ (triple) bond that are broken, and the six N–H bonds that form when reaction (15.1) occurs. The six bonds formed in the products release more energy than is required to break the six bonds (three single plus a triple) in the reactants, and the result is a lowering in energy for a negative $\Delta_r U^\circ$. The energy change is related to the enthalpy change by

$$\Delta_r H^\circ = \Delta_r U^\circ + p\Delta_r V^\circ, \tag{15.4}$$

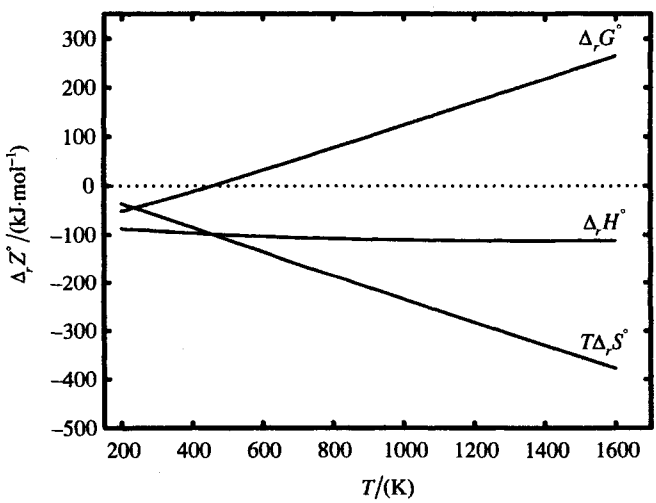

Figure 15.1 Standard enthalpy, Gibbs free energy, and entropy of formation as a function of temperature for the Haber reaction $3H_2(g) + N_2(g) = 2NH_3(g)$.

[c] Calorimetric techniques are used to measure $\Delta_r H_{298}$ for the formation of NH_3. The value would not be measured directly, since the reaction is very slow at ambient temperature. Instead, ΔH would be measured for a series of reactions that add together to give the formation reaction.

which becomes

$$\Delta_r H^\circ = \Delta_r U^\circ + RT \sum_i \nu_i \tag{15.5}$$

if the gases are ideal. The final term is small so that $\Delta_r H^\circ \approx \Delta_r U^\circ$.

The heat capacities of products and reactants are nearly equal so that $\Delta_r C_p^\circ \approx 0$. Since

$$\left(\frac{\partial \Delta_r H^\circ}{\partial T}\right)_p = \Delta_r C_p^\circ \approx \left(\frac{\partial \Delta_r U^\circ}{\partial T}\right)_p, \tag{15.6}$$

$\Delta_r H^\circ$ is almost constant with temperature.

The entropy change for reaction (15.1) is less than zero, the principal reason being that four moles of gaseous reactants are reduced to two moles of gaseous products, which is an ordering effect. The negative $T\Delta_r S^\circ$ that becomes more negative with increasing temperature is shown in Figure 15.1.[d] The difference between $\Delta_r H^\circ$ and $T\Delta_r S^\circ$ gives $\Delta_r G^\circ$. That is

$$\Delta_r G^\circ = \Delta_r H^\circ - T\Delta_r S^\circ. \tag{15.7}$$

As can be seen from Figure 15.1, $\Delta_r G^\circ$ is less than zero at low temperatures, but increases with temperature, becoming a large positive value at high temperatures. Since $\Delta_r G^\circ$ indicates the extent of the reaction, we see that at lower temperatures, products are favored, but as T increases, the reaction becomes less favorable, until at high temperatures, the extent of the reaction becomes small, with reactants favored at equilibrium.

The quantitative calculation of the extent of the reaction is obtained from the equilibrium constant K. Before proceeding, let us review the properties of K. In Chapter 11, we showed that for a chemical reaction written as

$$\sum_i \nu_i A_i = 0, \tag{11.99}$$

[d] The entropy change $\Delta_r S$ decreases with increasing temperature at low temperatures, but soon levels off at a relatively constant negative value. The continuing decrease in $T\Delta_r S$ shown in Figure 15.1 results from the product of a constant $\Delta_r S$ that is <0, with an increasing temperature. Since $\Delta_r G$ is given by the difference between $\Delta_r H$ and $T\Delta_r S$, it increases with increasing temperature.

the equilibrium condition is given by

$$\sum_i \nu_i \mu_i = 0, \tag{11.100}$$

where the ν_i, the coefficients in the reaction, are positive for products and negative for reactants.

In that chapter, we defined the thermodynamic equilibrium constant as

$$K = \prod_i a_i^{\nu_i} \tag{11.103}$$

where a_i is the activity. It is related to $\Delta_r G^\circ$ through the relationship

$$\Delta_r G^\circ = -RT \ln K = -2.3026\ RT \log K. \tag{11.102}$$

The equilibrium constant varies with temperature through the relationship

$$\left(\frac{\partial \ln K}{\partial T}\right)_p = \frac{\Delta_r H^\circ}{RT^2}. \tag{11.119}$$

Since $\Delta_r G^\circ$ is the standard state Gibbs free energy change, the pressure is specified. Hence, $(\partial \Delta_r G^\circ / \partial p)_T = 0$, and from equation (11.102) we get

$$\left(\frac{\partial \ln K}{\partial p}\right)_T = 0. \tag{11.116}$$

Equation (11.116) requires that the thermodynamic equilibrium constant cannot vary with pressure. There are, however, alternate expressions for the equilibrium constant that do change with pressure. For a gas-phase reaction such as the one that we are considering, the concentrations of species are often given in terms of their partial pressures, p_i. Then,

$$K = J_\phi K_p$$

where

$$K_p = \prod_i p_i^{\nu_i} \tag{11.105}$$

and J_ϕ is the fugacity coefficient ratio given by

$$J_\phi = \prod_i \phi_i^{\nu_i}, \tag{11.109}$$

with ϕ_i as the fugacity coefficient. Other equilibrium constants for the gas-phase reaction are the concentration (molarity) equilibrium constant K_c and the mole fraction equilibrium constant K_x. All are related through the expression

$$\frac{K}{J_\phi} = K_p = K_c \cdot (RT)^{\Sigma\nu_i} = K_x \cdot p^{\Sigma\nu_i}, \tag{11.108}$$

where p is the total pressure in the equilibrium mixture.

Although K does not vary with pressure, K_p, K_c and K_x do, since J_ϕ depends upon the pressure. For example, it is easy to show that

$$\left(\frac{\partial \ln K_p}{\partial p}\right)_T = \frac{\Delta(V_i^{\text{ideal}} - \bar{V}_i)}{RT}, \tag{11.117}$$

where V_i^{ideal} is the volume of the pure component acting as an ideal gas and $\bar{V}_i$ is the partial molar volume of the component in the mixture.

The equilibrium constant as a function of temperature can be calculated for reaction (15.1) using $\Delta_r G^\circ_T$ with equation (11.102)

$$\Delta_r G^\circ = -RT \ln K. \tag{11.102}$$

The result for reaction (15.1) is shown in Figure 15.2, where the logarithm of the thermodynamic equilibrium constant is plotted against $1/T$. With a constant $\Delta_r H^\circ$, the graph should be a straight line since the slope is given by

$$\left(\frac{\partial \log K}{\partial 1/T}\right)_p = \frac{\Delta_r H^\circ}{2.303\ R}. \tag{15.8}$$

Also shown in Figure 15.2 is a graph of an equation relating log K to $1/T$ derived by Walther Nernst. We will describe his contribution more fully in the next section.

Figure 15.3 shows even more directly the extent of the reaction as a function of temperature. In this figure the mole percent of NH_3 in a stoichiometric mixture of H_2 and N_2 is graphed against T. The mole percent of NH_3 is obtained from the mole fraction of NH_3, which is obtained from the mole

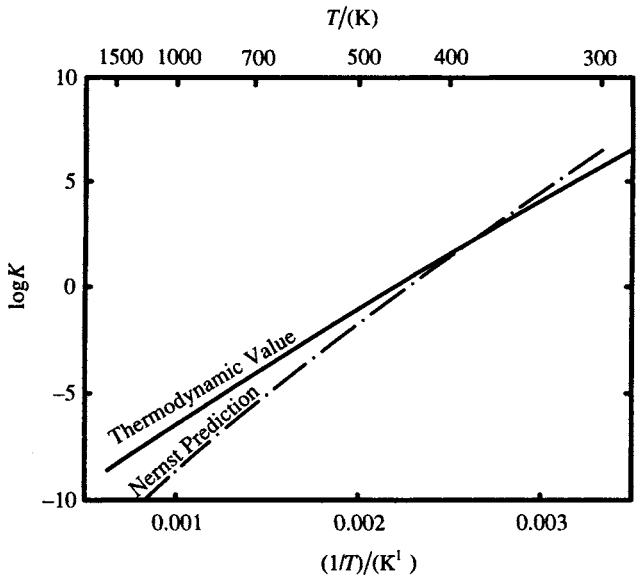

Figure 15.2 Graph of log K, the thermodynamic equilibrium constant calculated from molecular data (solid line), against $1/T$. Also shown is a prediction of log K obtained by Nernst (dashed-dotted line).

fraction equilibrium constant K_x, given by[e]

$$K_x = \frac{x_{NH_3}^2}{x_{H_2}^3 x_{N_2}}.$$

[e] It is easy to show that for the stoichiometric mixture,

$$K_x = \frac{256 x_{NH_3}^2}{27(1 - x_{NH_3})^4}, \tag{15.9}$$

which can be solved for x_{NH_3} to give the relationship

$$x_{NH_3} = \frac{b - \sqrt{b^2 - 4}}{2} \tag{15.10}$$

where

$$b = \frac{6\sqrt{3K_x} + 16}{3\sqrt{3K_x}}. \tag{15.11}$$

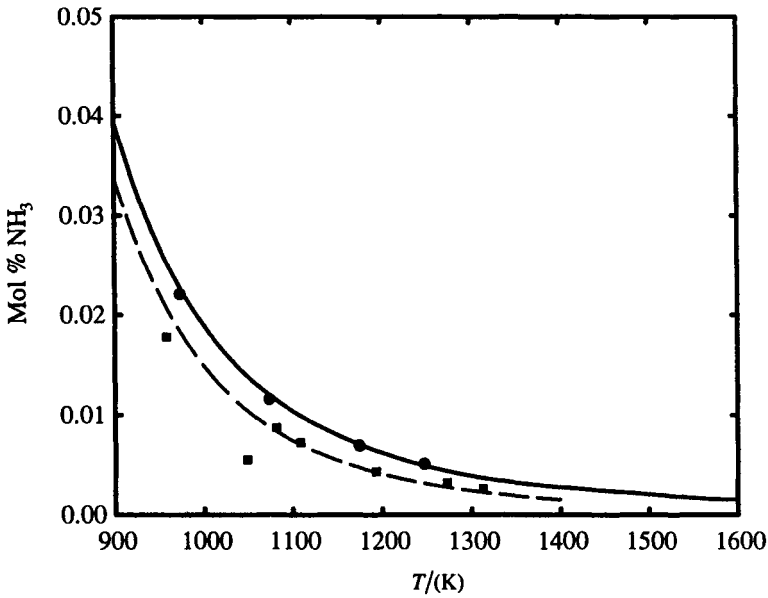

Figure 15.3 Comparison of the calculated mole % NH_3 with Haber and Nernst data. The solid line is the prediction at $p = 1$ atm calculated from the molecular parameters. ●, Haber's experimental results at $p = 1$ atm, which can be compared directly with the solid line. ■, Nernst's results at $p = 60$ atm; the dashed line is Nernst's prediction at $p = 60$ atm. Both Nernst's results and predictions are much lower than the values calculated from the molecular parameters at $p = 60$ atm (not shown).

As we noted earlier, the mole fraction equilibrium constant is obtained from the thermodynamic equilibrium constant by the relationship

$$K = K_x J_\phi p^{\Sigma\nu_i} \tag{11.108}$$

where p is the total pressure. For the ammonia reaction, $\Sigma\nu_i = -2$ so that

$$K = K_x J_\phi p^{-2}. \tag{15.12}$$

The fugacity coefficient ratio J_ϕ is

$$J_\phi = \frac{\phi^2_{NH_3}}{\phi^3_{H_2}\phi_{N_2}}. \tag{15.13}$$

The solid line in Figure 15.3 is calculated at a total pressure of 1 bar (0.1 MPa) where $p^{-2} = 1$ and, to a good approximation, $J_\phi = 1$.

Reaction (15.1) is known as the Haber reaction in recognition of the major role of Fritz Haber[f] in characterizing this process early in the twentieth century. At that time neither the molecular data nor the mathematical relationships were available for calculating the equilibrium condition, so that Haber had to rely upon experimental measurement. He determined the equilibrium concentration of NH_3 in the $(N_2 + 3H_2)$ mixture[g] as a function of temperature. His measurements, graphed as mole percent NH_3, were made at a total pressure of 1 atm (1.01 bar), and are also shown in Figure 15.3.[1] The agreement with the prediction from the thermodynamic equilibrium constant calculated from the molecular parameters (solid line) is excellent.

About the same time that Haber was making his measurements, Walther Nernst also studied the ammonia synthesis reaction at high temperatures and obtained results that differed significantly from those obtained by Haber.[2] Nernst's measurements were made at high pressures (approximately 60 atm). His results are also shown in Figure 15.3, and they do not appear to differ in a major way from those of Haber, until the effect of pressure is taken into account, as we will now see. From equation (15.12), we find that K_x is related to K by

$$K_x = \frac{Kp^2}{J_\phi}.$$

The fugacity coefficient ratio J_ϕ can be estimated by assuming that the Lewis and Randall rule[h] applies, at least approximately, for the mixture, so that each component has the same fugacity coefficient that it would have if it were a pure gas at the same total pressure. The Principle of Corresponding States can then be used to compare the fugacity coefficients of the three components. At $p = 60$ atm (61 bar) and in the temperature range from 900 to 1600 K, the reduced temperatures and pressures for the components of the equilibrium

---

[f] Fritz Haber was a Professor of Chemistry at several universities in Germany. He was born in Breslau (now Wroçlaw), Poland. He died in Switzerland, as a refugee from the Nazis. He received the Nobel Prize in Chemistry in 1918 for his work, mostly in characterizing the Haber reaction.

[g] It can be shown that the maximum conversion of nitrogen and hydrogen into ammonia occurs when the gases are mixed with the stoichiometric ratio. (See Problem P15.1.)

[h] See Section 11.3a of Chapter 11 for a discussion of the effect of pressure on the fugacity, including the Lewis and Randall rule.

mixture are

	$p_r = p/p_c$	$T_r = T/T_c$
H_2	4.70	27.3 – 48.5
N_2	1.79	7.1 – 12.7
NH_3	0.54	2.2 – 4.0

A correlation diagram would verify that at these high reduced temperatures, to a good approximation, $\phi = 1$ for all three components.[i] Thus $J_\phi = 1$ and $K_x = Kp^2$.

Using a K_x calculated from K at p = 61 bar, by using equation (15.12) with $J_\phi = 1$, we predict a value for the formation of NH_3 of 2.28 mole percent at 900 K, and 0.093 mole percent at 1600 K. These values are much higher than those obtained experimentally by Nernst. He approached the equilibrium condition from only one direction — by mixing N_2 and H_2.[j] Kinetics plays an important part in this reaction, and even with catalysts, the reaction is slow unless one goes to high temperatures. It seems probable that Nernst did not achieve equilibrium.

Again, we repeat that the statistical thermodynamic calculations from molecular parameters, whose predictions we rely on, were not known by Nernst, nor by Haber. Nernst obtained a theoretical equation for calculating the equilibrium constant based upon $\Delta_r G°$ and $\Delta_r H°$ at ambient temperature, and corrected to high temperatures using $\Delta_r C_p^\circ$ as a function of temperature. The heat capacity of NH_3 as a function of temperature was not known, but Nernst estimated a value, and derived an equation that gave K as a function of T. The result is shown as the broken line in Figures 15.2 and 15.3. Nernst's value of K differs from the statistical calculation, but agrees well with his experimental results shown in Figure 15.3, which gave him confidence in his measurements.

Haber and Nernst came together at the meeting of the Deutsche Bunsen Gesellschaft in 1907. Nernst was the eminent professor of the day. He presented his results, bolstered by his theory. He noted that Haber would need to heat his mixture to 1293 K to obtain the same results as he (Nernst) obtained at 893 K.

[i] Figure 6.4, of J. B. Ott and J. Boerio-Goates, *Chemical Thermodynamics: Principles and Applications*, Academic Press, London, 2000, shows such a diagram, as does almost any chemical thermodynamics textbook with an engineering emphasis.

[j] Haber, on the other hand, approached the equilibrium condition from both sides — by mixing H_2 and N_2 and by dissociating NH_3. He achieved the same final condition from either direction, giving credence to his results.

Nernst refused to accept Haber's results and called upon him to repeat his measurements under pressure, where higher concentrations could be obtained and measured more accurately.

Haber, on the other hand, was confident of his results and not overly pleased with Nernst's comments. Although he did have doubts about the feasibility of applying the ammonia synthesis reaction on an industrial scale, much of his concern was whether an apparatus could be constructed[k] to synthesize NH_3 at high temperatures and pressures on a large scale.

After the meeting, Haber began a series of experiments to measure equilibria at pressures as high as 30 bars. His results, using iron and manganese catalysts, were in good agreement with those he obtained at one atmosphere pressure.[3] Time and further study further verified Haber's conclusions. The result was a Nobel Prize for Haber in 1918. In his Nobel Address[4] he describes the process and his contributions. To quote from his lecture:

> *Es handelt sich um einen chemischen Vorgang der einfachsten Art. Gasförmiger Stickstoff bildet mit gasförmigem Wasserstoff nach einfachen Mengenverhältnissen gasförmiges Ammosiak. Die drei beteiligten Stoffe sind seit mehr als einem Jahrhundert dem Chemiker wohlbekannt. Jeder von ihnen ist in der zweiten Hälfte des vergangenen Jahrhunderts, in der uns ein Strom neuer chemischer Kenntnisse zufloß, hundertfältig in seinem Verhalten unter den verschiedensten Bedingungen studiert worden. Wenn es dennoch bis in unser Jahrhundert gedauert hat, ehe die Darstellung des Ammoniaks aus den Elementen gefunden wurde, so ist der Grund, daß ungewöhnliche Arbeitshilfsmittel benutzt und enge Bedingungen innegehalten werden müssen, wenn es gelingen soll, Stickstoff und Wasserstoff in erheblichem Maße zum freiwilligen Zusammentritt zu bringen und daß eine Verbindung experimenteller Erfolge mit thermodynamischen Überlegungen erforderlich war.*

A reasonable translation is as follows:

> *It is a chemical reaction of the simplest kind. Gaseous nitrogen and gaseous hydrogen form gaseous ammonia according to a simple stoichiometric relationship. The three materials involved have been well known to the chemist for more than a century. During the second half of the past century, during which time a stream of new chemical knowledge*

[k] Hydrogen gas embrittles high-carbon steel, especially under high pressure and temperature conditions, causing steel reaction vessels to fail. This problem needed to be solved before industrial synthesis of ammonia became feasible.

has poured forth, each one of [these materials] has been studied a hundred fold in its behavior under the most different conditions. None-the-less, it took until our century before the production of ammonia from the elements was found. The reason is that unusual catalysts have to be used and strict conditions have to be observed if nitrogen and hydrogen are to be brought together to yield considerable amounts in a successful spontaneous reaction. Furthermore, it was necessary to combine experimental successes with thermodynamic reasoning.

Haber goes on to summarize his measurements and discuss the differences between his results and those of Nernst. Figure 15.4 shows the mole percent conversion as a function of pressure and temperature as reported by Haber in this address, which demonstrated that pressure and temperature conditions could be found under which NH_3 could be produced in sizable amounts from H_2 and N_2.

Haber concludes his address with the following:

Das Ergebnis reicht anscheinend aus ... der Zukunftssorge zu entheben, die uns die drohende Erschöpfung der Salpeterlager vor zwanzig Jahren bereitet hat. Vielleicht ist diese Lösung keine endgültige. Die Stickstoff-baketerien lehren, daß die Natur in den verfeinerten Formen der

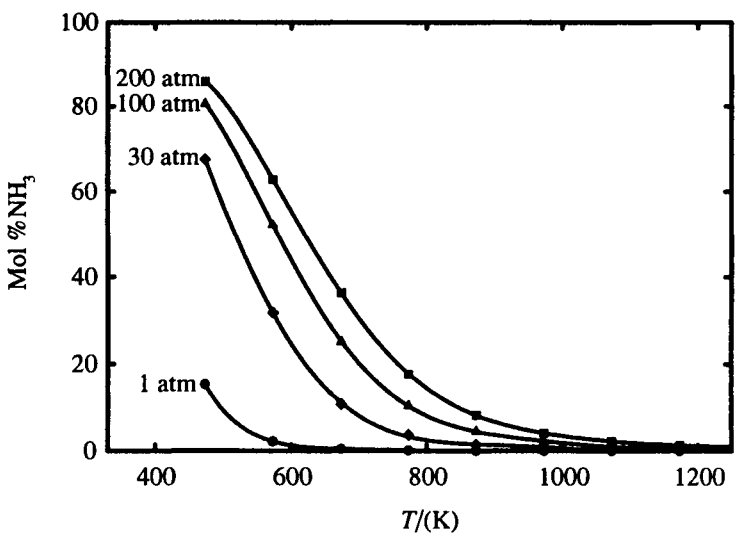

Figure 15.4 Equilibrium mol % NH_3 produced in the Haber process as a function of temperature at several different pressures, as reported by Haber in his Nobel Prize address (See F. Haber, *Naturwissenschaften*, **49**, 1041–1049 (1922).)

Lebenschemie noch Möglichkeiten kennt und verwirklicht, deren Nachahmung sich vorerst unserem Können entzieht. Genug, daß inzwishen neuer Reichtum an Nahrung der Menschheit aus reicherer Stickstoffdüngung des Bodens zufließt und die chemische Industrie dem Landmann zu Hilfe kommt, der auf der friedlichen Erde Stein in Brot verwandelt.

On translation his statement is:

This result seems to be sufficient to deliver us in the future from the worry of the past twenty years of the imminent depletion of saltpeter deposits.

Maybe this solution is not final. The nitrogen bacteria teach [us] that nature in the refined forms of the chemistry of life still knows and realizes possibilities, the imitation of which is at present beyond our ability. It suffices that in the meantime, a new abundance of food benefits mankind from a richer nitrogen fertilization of the soil, and that the chemical industry is coming to the aid of the farmer who changes stones into bread on this peaceful earth.[l]

Today ammonia is routinely synthesized by the Haber process. Pressures of 300 to 500 bar (or atm) and temperatures of 700 to 800 K are used. The usual catalyst contains about 95 wt% Fe_3O_4, along with some K_2O ($\sim$ 1 wt%), Al_2O_3 ($\sim$2 wt%), CaO ($\sim$2 wt%),[m] and smaller amounts of MgO and SiO_2. Containment is achieved using a steel reaction vessel to give strength, but lined with soft iron to prevent embrittlement of the steel due to contact with the H_2.[n] The procedure followed can be represented by the flow chart shown in Figure 15.5. A mixture of $N_2(g)$ and $H_2(g)$ is compressed, then put in the reaction vessel where it is heated over the catalyst. Reaction occurs to produce an equilibrium amount of NH_3. This equilibrium mixture then leaves the reaction vessel (and catalyst) and is cooled so that the ammonia condenses to liquid and is removed. The remaining $N_2(g)$ and $H_2(g)$ is then returned to the reaction mixture. The final result is an essentially complete conversion of the $(H_2 + N_2)$ gaseous mixture into NH_3.

---

[l] Haber's work was of great help to the German military in the First World War. Ammonia produced by this process was used to synthesize nitric acid, which was used to make explosives such as nitroglycerine and trinitrotoluene (TNT).

[m] The development of a catalyst was the result of an extensive investigation, in which amounts and kinds of impurities were varied and the effect observed. The final catalyst represents optimum conditions. In the Haber process, water must be carefully avoided since it poisons the catalyst.

[n] The soft iron becomes brittle, but holds together so that a pressure difference can be maintained between the liner and the walls of the vessel that allows any H_2 present at low pressures to escape without embrittling the reaction tube.

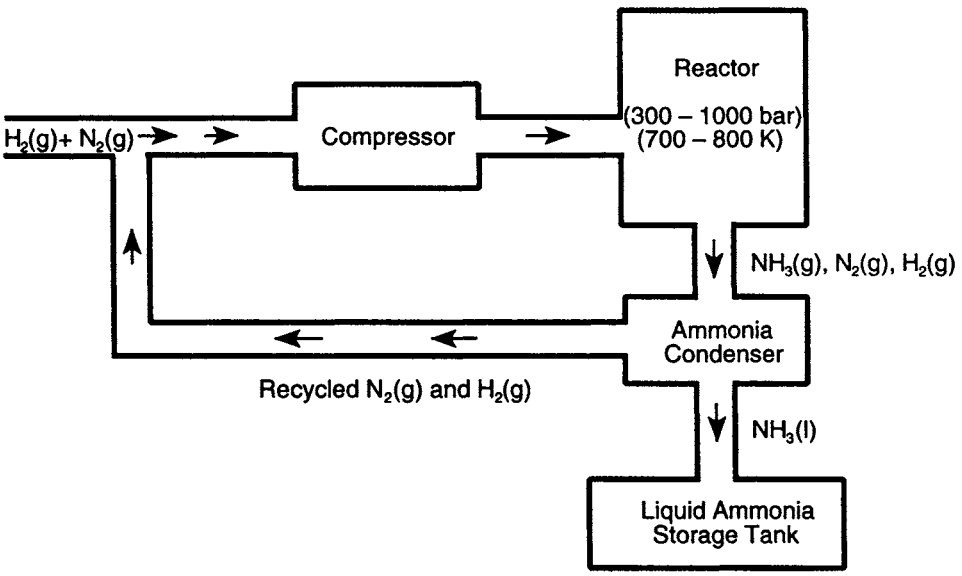

Figure 15.5 The Haber cycle used to produce liquid ammonia.

The importance of this reaction can be understood by recognizing that over 20 million tons of NH_3 were produced in the United States by this process in 1998. This amount can be compared with the production of sulfuric acid (48 million tons), the chemical that is produced in the largest amount.°

15.2 The Synthesis Of Diamond: Application to Phase Changes

Akin to the alchemist's dream of converting lead into gold has been the desire to convert graphite to diamond from the simple chemical process.

$$C\ (\text{graphite}) = C(\text{diamond}).$$

It is well known that graphite is the stable form of carbon at ambient conditions, and studies have been undertaken to find pressure and temperature conditions where diamond becomes stable, and as a consequence, graphite would convert spontaneously to diamond. The process is fraught with difficulty, and for many years the conversion was not successful. The

° For a chemical production report, see *Chemical and Engineering News*, **77**, June 28, 1999, page 36.

problems encountered have been summarized by H. Tracy Hall from whom we quote,[p5]

For the reaction C (graphite) → C (diamond), $\Delta G° = +692$ cal/g · atom at 25 °C and 1 atm pressure.[q] *This $\Delta G°$ is not obtained by direct measurement but, as is the case with most thermochemical data, is calculated from measurements of heats of combustion, specific heats, compressibility, thermal expansion, etc. The positive $\Delta G°$ indicates that diamond is thermodynamically unstable with respect to graphite. However, diamonds have not been known to transform into graphite by any observable amount over periods of hundreds of years under ordinary conditions. The rate of reaction (conversion) must, therefore, be extremely slow. Increased temperature will accelerate most reactions and this is also true for the conversion of diamond to graphite. This transformation begins to proceed at an observable rate at a temperature of 1200 °C at 1 atm. At this pressure and temperature, $\Delta G°$ has increased to about + 2400 cal, indicating that higher temperature decreases the thermodynamic stability of diamond. The $\Delta G°$ for the graphite–diamond transition assumes its lowest value at the absolute zero of temperature.*

$$\Delta G_0^\circ = +580 \text{ cal/g} \cdot \text{atom at 1 atm.}$$

In order to bring the graphite–diamond reaction into a region where $\Delta G°$ is negative, it is necessary to apply pressure. The pressure required depends on the temperature — the higher the temperature, the greater must be the pressure.

Equilibrium is established when the free energy difference between the two allotropes is zero, that is,

$$\Delta G = \Delta H - T\Delta S = 0.$$

The manner in which ΔG varies with pressure at a given temperature is given by

$$\left(\frac{\partial \Delta G}{\partial p}\right)_T = \Delta V,$$

---

[p] H. Tracy Hall is generally recognized as the first to successfully synthesize diamond. He accomplished this while an employee of the General Electric Company in the mid 1950s. He moved to Brigham Young University as Professor of Chemistry where he continued high-pressure research for many years. He is now Distinguished Professor of Chemistry Emeritus at that university.

[q] We have used modern terminology in expressing the thermodynamics properties. For example, H. Tracy Hall used ΔF instead of ΔG to represent the change in Gibbs free energy.

or by

$$\Delta G_T^p - \Delta G_T^\circ = \int_{p^\circ}^{p} \Delta V \, dp,$$

where ΔV is a function of both T and p and the integral is over the pressure interval from the standard state pressure p° to p. From these expressions, the free energy difference at any pressure and temperature may be expressed as

$$\Delta G_T^p = \Delta H_T^\circ - T\Delta S_T^\circ + \int_{p^\circ}^{p} \Delta V \, dP. \tag{15.14}$$

The (p, T) equilibrium line for the graphite–diamond transition is obtained from equation (15.14) by expressing $\Delta H°$ and $\Delta S°$ as a function of temperature and the integral term as a function of pressure and temperature. The free energy change ΔG_T^p is then set equal to zero (the equilibrium condition) and the resulting expression

$$\Delta H°(T) - T\Delta S°(T) + \int_{p^\circ}^{p} \Delta V(p, T) \, dp = 0 \tag{15.15}$$

is solved for the equilibrium pressure and temperature.

Berman[6] has summarized the procedure that is followed in making the calculations to obtain the equilibrium transition line, starting with equation (15.15). The effects of temperature on the standard enthalpy ($\Delta H°$) and entropy ($\Delta S°$) are obtained from the relationships[r]

$$\left(\frac{\partial \Delta H°}{\partial T}\right)_p = \Delta C_p^\circ \tag{15.16}$$

and

$$\left(\frac{\partial \Delta S°}{\partial T}\right)_p = \frac{\Delta C_p^\circ}{T}. \tag{15.17}$$

[r] See Table 11.1 in Chapter 11 for a summary of these relationships.

With these equations and one that gives ΔC_p° as a function of temperature, $\Delta H^\circ(T)$ and $\Delta S^\circ(T)$ can be obtained by integrating equations (15.16) and (15.17), using ΔH° (298K) and ΔS° (298K) to obtain the constant of integration.

The integral in equation (15.15) can be expressed as a function of temperature and pressure. We write [for one mole (g · atom) of reaction]

$$\int_{p^\circ}^{p} \Delta V_m(\mathrm{d}, T)p = \int_{p^\circ}^{p} V_m(\mathrm{d}, T)\,\mathrm{d}p - \int_{p^\circ}^{p} V_m(\mathrm{gr}, T)\,\mathrm{d}p \tag{15.18}$$

where $V_m(\mathrm{d}, T)$ and $V_m(\mathrm{gr}, T)$ are the molar volumes of diamond and graphite as a function of temperature T. Berman assumes that the bulk modulus[s] $B(\mathrm{d})$ for diamond is independent of pressure and temperature, and shows that this is a reasonable assumption. He is then able to relate the molar volume at a pressure p to the molar volume at $p = p^\circ$ by the equation

$$V_m^p(\mathrm{d}, T) = V_m^\circ(\mathrm{d}, T)[1 - p/B(\mathrm{d})]. \tag{15.19}$$

Integration gives

$$\int_{p^\circ}^{p} V_m(\mathrm{d}, T) = V_m^\circ(\mathrm{d}, T)[p - \tfrac{1}{2}p^2/B(\mathrm{d})]. \tag{15.20}$$

In equation (15.20), it is assumed that $p^\circ \ll p$ so that p° can be neglected when compared to p.

Graphite is much more compressible than diamond, and the variation of its bulk modulus with pressure must be taken into account. Berman assumes a linear relationship of B with p so that

$$B^p(\mathrm{gr}, T) = B^\circ(\mathrm{gr}, T) + np, \tag{15.21}$$

where n is a constant. He also assumes that $B(\mathrm{gr})$ is a function only of the molar volume, and hence independent of temperature, so that

$$\left(\frac{\partial B(\mathrm{gr})}{\partial T}\right)_{V_m} = 0. \tag{15.22}$$

[s] The bulk modulus B is the reciprocal of the average compressibility. Thus, $B = -V(\partial p/\partial V)_T$.

Values for $B°(\text{gr}, 298)$ and n can be obtained from measurements at room temperature. Equations (15.21) and (15.22) can then be used to show that

$$\frac{B°(\text{gr}, T)}{B°(\text{gr}, 298)} = \left[\frac{V°_{\text{m}}(\text{gr}, 298)}{V°_{\text{m}}(\text{gr}, T)}\right]^{n}. \tag{15.23}$$

The integral for graphite required for the equilibrium calculation is then

$$\int_{p°}^{p} V_{\text{m}}(\text{gr}, T)\, \text{d}p = \frac{V°_{\text{m}}(\text{gr}, T)B°(\text{gr}, \text{T})}{n-1}\left[\left\{\frac{np}{B°(\text{gr}, T)} + 1\right\}^{(n-1)/n} - 1\right]. \tag{15.24}$$

Substituting equations (15.20) and (15.24) into equation (15.18) and integrating gives the last term in equation (15.15) and the equilibrium (p, T) relationships.

Figure 15.6 shows the results of this calculation. A knowledge of the (p, T) equilibrium line shown in this figure does not guarantee an easy path for conversion of graphite to diamond. H. M. Strong[7] reports an energy of activation of at least 625 kJ · mol^{-1} that increases rapidly with increasing pressure. He describes a very early experiment performed by F. P. Bundy, one of the investigators at General Electric before the successful conversion of graphite to diamond. Strong reports that Bundy imbedded a small diamond crystal in graphite. He then packed the sample in a pipestone gasket, placed it in a Bridgeman-type anvil press, squeezed the sample to the anvil's limit of between 40 and 50 kbar (4 to 5 GPa), and then flash heated the sample by passing timed electrical current pulses through it from a spot welder. Upon the release of pressure, he recovered both the diamond and graphite unchanged. Strong's conclusion was that graphite was "nature's best spring".[t]

The successful conversion of graphite to diamond involves crystallizing the diamond from a liquid melt. The solvent most often used is nickel metal, or alloys of nickel with other ferrous metals. The reason for this success can be seen by referring to Figure 15.7, the binary (solid + liquid) phase diagram for (nickel + carbon).[u8] We note from the figure that (Ni + C) forms a simple

---

[t] An interesting report describing the developments leading to the successful conversion of graphite to diamond is given by K. Nassau and J. Nassau, "The History and Present Status of Synthetic Diamond, Part I and Part II", *The Lapidary Journal*, **32**, pp. 76–96 and pp. 490–508 (1978).

[u] This (T, x) phase diagram is for a pressure of 57 kbar (5.7 GPa), since this is about the pressure often employed to produce diamond. Similar diagrams would be obtained at other pressures, with the melting temperatures shifted to higher or lower values, depending upon the pressure.

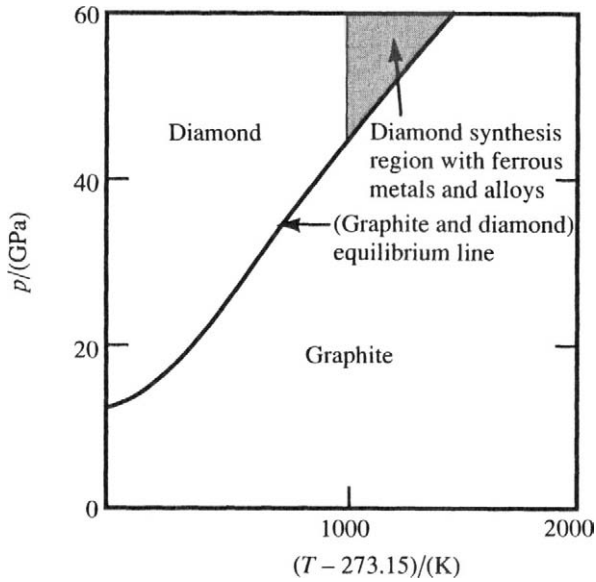

Figure 15.6 The (graphite + diamond) phase diagram, including the pressure–temperature region for diamond synthesis with ferrous metals and their alloys as solvent catalysts. Reproduced with permission from H. M. Strong, "Early Diamond Making at General Electric", *Am. J. Phys.*, **57**, 794–802 (1989). Published by the American Association of Physics Teachers.

eutectic system, with the (diamond + graphite) phase transition present on the carbon side of the diagram. At 5.7 GPa (57 kbar), the pressure that applies to Figure 15.7, the transition occurs at about $T = 1840$ K (1570 °C). In the temperature region between 1840 K and the (nickel + diamond) eutectic[v] at 1700 K (1430 °C), diamond is the stable solid phase that crystallizes from the melt. To obtain diamond, graphite and a strip of nickel foil are placed next to one another, pressure is applied, and the sample is heated to high temperatures to form a liquid melt. When the melt is cooled to a temperature between the transition temperature and the eutectic temperature (while maintaining the pressure), diamond crystallizes from the melt as graphite dissolves.

In the conversion process, graphite dissolves on one side of the nickel film and diamond deposits on the other. The shaded area in Figure 15.6 gives the (p, T) conditions where the conversion can be made at a reasonable rate (usually on the order of minutes) while still keeping the pressure at a value that is obtainable without too much difficulty. Quenching the mixture leaves

[v] Supercooling effects allow diamond to crystallize from the liquid at temperatures as low as 1675 K, the (approximate) temperature of the (nickel + graphite) eutectic.

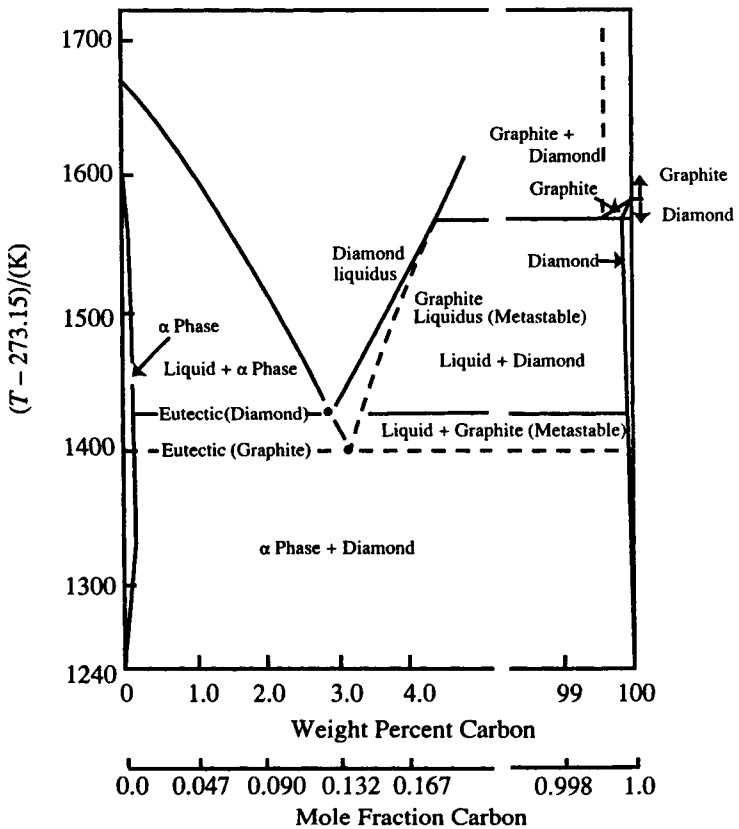

Figure 15.7 The (Ni + C) phase diagram at 5.7 GPa (57 kbar). Reproduced with permission from H. M. Strong and R. E. Hanneman, (1967), J. Chem. Phys., **46**, 3668. Modified by R. H. Wentorf, Jr., *Advances in High Pressure Research*, Vol. 4, R. H. Wentorf, Ed., Academic Press, London (1974).

diamond crystals. The sequence that must be followed to obtain diamond at ambient pressure and temperature involves (1) compressing the (graphite + nickel) sample, (2) heating under pressure to liquefy the nickel, dissolve graphite, and form diamonds, (3) cooling the converted sample to near-ambient temperature while maintaining the pressure, and (4) reducing the pressure to ambient.

We note from the phase diagram that some nickel remains dissolved in the diamond, but the amount is small, with mole fraction of carbon > 0.9998 at the eutectic temperature. Thus, diamond of reasonably high purity is obtained. At the present time, this and similar processes are used to produce large quantities of diamonds. The crystals are usually small and find most use in industrial grinding and cutting processes.

15.3 Applications Of Thermodynamics To Geological Systems

Temperature and pressure effects become important in chemical systems of geological interest. Also, the chemical nature of the system is often not well characterized. Nonstoichiometric compounds and solid solutions are often present, with complex silicates frequently playing an important part.

In spite of these complications, thermodynamic techniques can be very useful in understanding geological processes. We will consider an example involving a rather simple substance, followed by an example that demonstrates the usefulness of thermodynamic analysis in a more complex system.

15.3a Effect of Temperature on the Solubility of Calcite

The solubility of calcite ($CaCO_3$) can be represented by the equilibria

$$CaCO_3(s) = Ca^{2+}(aq) + CO_3^{2-}(aq) \tag{15.25}$$

for which the equilibrium constant is given by

$$K = \frac{a_{Ca^{2+}}\, a_{CO_3^{2-}}}{a_{CaCO_3}}. \tag{15.26}$$

The equilibrium constant can be calculated from thermodynamic data. Robie *et al.*[9] give the standard state thermodynamic data at $T = 298.15$ K, which we summarize in Table 15.1. The value of $\bar{C}^{\circ}_{p,m}$ for CO_3^{2-} (aq) has not been determined experimentally. Nordstrom and Munoz[10] used estimation techniques to obtain the value of $-403.3\ J \cdot K^{-1} \cdot mol^{-1}$ given in the table.

In calculating the solubility, Nordstrom and Munoz started with the equation

$$\left(\frac{\partial \ln K}{\partial T}\right)_p = \frac{\Delta_r H^{\circ}}{RT^2}, \tag{15.27}$$

assumed $\Delta_r C_p^{\circ} = 0$ for the reaction so that $\Delta_r H^{\circ}$ is constant with temperature, and obtained the equation

$$\ln K = \frac{1515}{T} - 24.26. \tag{15.28}$$

Table 15.1 Standard state thermodynamic values for the species involved in reaction (15.25) (for the species in solution, the values are partial molar quantities)

Species	$C^\circ_{p,\mathrm{m}}$ ($\mathrm{J \cdot K^{-1} \cdot mol^{-1}}$)	S°_{m} ($\mathrm{J \cdot K^{-1} \cdot mol^{-1}}$)	$\Delta_f H^\circ_{\mathrm{m}}$ ($\mathrm{kJ \cdot mol^{-1}}$)	$\Delta_f G^\circ_{\mathrm{m}}$ ($\mathrm{kJ \cdot mol^{-1}}$)
Calcite ($CaCO_3$)	83.47	91.71	−1207.37	−1128.842
Ca^{2+}(aq)	−27.61	−53.10	−542.83	−553.54
CO_3^{2-}(aq)	(−403.3)*	−56.90	−677.14	−527.90

* Value estimated by Nordstrom and Munoz.

They also did an extended treatment in which they assumed a constant $\Delta_r C^\circ_p$, so that $\Delta_r H^\circ$ varied linearly with $T/(\mathrm{K})$, and obtained the equation

$$\ln K = 390.12 - \frac{16930.9}{T} - 61.869 \ln T. \tag{15.29}$$

Figure 15.8 compares the prediction of $\ln K$ from equations (15.28) and (15.29). Also shown in the figure is a graph of the equation

$$\ln K = -395.829 - 0.17986T + \frac{6537.774}{T} + 71.595 \ln T. \tag{15.30}$$

Equation (15.30), which is of the form obtained by assuming that ΔC_p varies linearly with temperature, was obtained by Plummer and Busenberg[11] from a fit to their experimental measurements of the solubility over the temperature range from 278 to 363 K.

By comparing the results calculated from equations (15.28) and (15.29) with the experimental results represented by equation (15.30), we see from Figure 15.8 that the assumption of $\Delta_r C^\circ_p = 0$ is not a good one, since the $\ln K$ obtained experimentally does not vary linearly with $1/T$ [the behavior predicted by equation (15.28)]. Differences between the $\ln K$ results obtained from equation (15.29) assuming a constant $\Delta_r C^\circ_p$ and the experimental results are also significant. The differences could be due either to a poor estimate of $\overline{C}^\circ_{p,\mathrm{m}}$ for CO_3^{2-}(aq), to the assumption of constant $\Delta_r C^\circ_p$, or both.

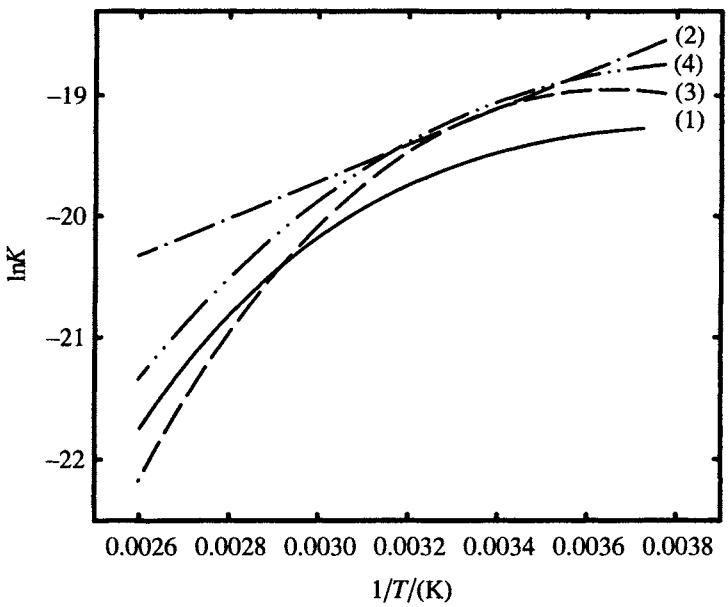

Figure 15.8 Equilibrium constant for the solubility of calcite [reaction (15.25)] as a function of temperature obtained from: Line 1: Measured solubility (fitting equation assumes ΔC_p is linear in temperature). Line 2: Thermodynamic data assuming ΔC_p equals zero. Line 3: Thermodynamic data assuming ΔC_p is constant. Line 4: Thermodynamic data assuming ΔC_p is constant with corrected $\overline{C}_p(CO_3^{2-})$.

Equation (15.30) can be used to check the estimated heat capacity of CO_3^{2-}(aq). The enthalpy change as a function of temperature for the reaction can be obtained by differentiating equation (15.30) and applying equation (15.27), as given above. The heat capacity difference is then obtained from

$$\left(\frac{\partial \Delta_r H^\circ}{\partial T}\right)_p = \Delta_r C_p^\circ.$$

The result is

$$\Delta_r C_p^\circ/(\mathrm{J \cdot K^{-1} \cdot mol^{-1}}) = 592.26 - 2.986\ T. \qquad (15.31)$$

Equation (15.31) gives a value for $\Delta_r C_p^\circ$ at $T = 298.15$ K of $-298.02\ \mathrm{J \cdot K^{-1} \cdot mol^{-1}}$. Combining this result with values for $C_{p,m}^\circ$ for $CaCO_3$(s) and $\overline{C}_{p,m}^\circ$ for Ca^{2+} (aq) from Table 15.1 gives a value for $\overline{C}_{p,m}^\circ$

of CO_3^{2-} (aq) of $-186.94\ J \cdot K^{-1} \cdot mol^{-1}$, a result that differs significantly from the estimated value ($-403.3\ J \cdot K^{-1} \cdot mol^{-1}$).

Equation (15.29) can be corrected by using the value of $-186.94\ J \cdot K^{-1} \cdot mol^{-1}$ as the heat capacity of CO_3^{2-} (aq). The result is

$$\ln K = 215.86 - \frac{9171.3}{T} - 35.843 \ln T. \tag{15.32}$$

A graph of equation (15.32) is shown in Figure 15.8.

From Figure 15.8, we conclude that the assumption that $\Delta C_p^\circ = 0$ is not a good one. (This is not unusual for reactions involving ionic species.) Correcting $\bar{C}_{p,m}^\circ(CO_3^{2-})$ and hence, changing ΔC_p° does change the $\ln K$ against T curve, although perhaps not as much as one would expect for a correction in $\bar{C}_{p,m}^\circ(CO_3^{2-})$ of over $200\ J \cdot K^{-1} \cdot mol^{-1}$.

15.3b Thermodynamic Insights into the Energetics of Ternary Oxides with Mineralogical Significance

Processes on the geologic scale are dictated by material properties on the atomic scale. Earthquakes and volcanic eruptions involve the ripping apart of strong chemical bonds such as Si–O linkages. One would like to understand geologic phenomena well enough to provide a quantitative framework that not only describes, but predicts, behavior. An important component in coming to a full understanding of such phenomena is a knowledge of the energetics leading to the characterization of chemical bond formation in minerals, and the effect these have on mineralogical processes.

In the previous example, (Section 15.3a) we considered a process that can be described as phase equilibria. Mineralogical processes may also be chemical reactions, such as

$$(Mg, Fe)_2SiO_4(\text{spinel}) = (Mg, Fe)SiO_3\ (\text{perovskite}) + (Mg, Fe)O\ (\text{rock salt})$$

where the names in parentheses refer to the crystallographic structure of the solid substance. This particular process, which involves a change in the Si coordination from tetrahedral to octahedral, is thought to occur at the 660 km deep seismic discontinuity that separates the transition zone from the lower mantle. We now want to look at examples of the use of thermodynamics to help in the description and understanding of chemical reactions that are of geological interest, such as the spinel decomposition shown above. In doing so, we will

focus on the thermochemical and thermophysical work of Alexandra Navrotsky of the University of California at Davis.[w]

Formation of Ternary Oxides[12]: Many compounds of mineralogical importance are ternary compounds of oxygen with a formula AB_aO_{1+b}, where A = Ca, Mg, Mn, Fe, Co, and Ni, and B = Si, W, C, and S. These compounds may be considered to be formed from the reaction of the binary oxides. That is

$$AO + B_aO_b = AB_aO_{1+b}. \tag{15.33}$$

Knowledge of the factors that determine the sign and magnitude of $\Delta_r G^\circ$ for reaction (15.33) contributes to an understanding of the range of stability of ternary oxides relative to binary oxides. In some cases, favorable enthalpy effects may tend to stabilize a material, while in other instances, a favorable entropy effect may dominate stability considerations.[x]

We will focus on looking for factors that determine the energy (or enthalpy) of formation of ternary oxide compounds. Oxides can be characterized on an acid/base scale. An acidic oxide, A_nO, is an oxide ion donor, while a basic oxide, B_nO, is one that accepts another oxide ion. The two reactions can be represented as

$$A_nO = nA^{(2/n)+} + O^{2-} \tag{15.34}$$

and

$$B_nO + O^{2-} = B_nO_2^{2-}. \tag{15.35}$$

An acidic oxide tends to undergo reaction (15.34) readily, while basic oxides show a preference for reaction (15.35). According to one scheme, oxides can be grouped into basic, amphoteric or acidic oxides on the basis of their ionic potential, defined as z/r, where z is the charge on the cation and r is its ionic radius as determined from the crystal structure of the oxide. Table 15.2 gives a representative listing of oxides and their ionic potentials.[1] The oxides have been sorted into columns separating main group element, transition metal, and

---

[w] Alexandra Navrotsky is the Interdisciplinary Professor of Ceramic, Earth, and Environmental Materials Chemistry at the University of California at Davis. The experiments and conclusions described here have been drawn primarily from two of her review articles, including her Presidential Address to the American Mineralogical Society. Additional sources are cited within those articles.

[x] We remember that $\Delta_r G$ determines the stability. Since $\Delta_r G = \Delta_r H - T\Delta_r S$, enthalpic effects or entropic effects dominate, depending upon the relative magnitude of $\Delta_r H$ and $T\Delta_r S$.

Table 15.2 Acid/base scales for Oxides[a]

Oxide			z/r of cation			Remarks
Main group	Transition metal	Lanthanide metal	Main group	Transition metal	Lanthanide metal	
K_2O			0.66			Strongly basic: $z/r < 2$
Na_2O			0.89			
BaO			1.45			
SrO			1.59			
CaO			2.00			
	MnO			2.41		Basic: $2 \leqslant z/r < 4$
	FeO			2.56		
		$\frac{1}{3}$ La_2O_3			2.58	
	CoO			2.68		
		$\frac{1}{3}$ Nd_2O_3			2.71	
	CuO			2.74		
MgO			2.77			
		$\frac{1}{3}$ Sm_2O_3			2.78	
		$\frac{1}{3}$ Eu_2O_3			2.81	
		$\frac{1}{3}$ Gd_2O_3			2.85	
	NiO			2.90		
		$\frac{1}{3}$ Dy_2O_3			2.92	
		$\frac{1}{3}$ Er_2O_3			2.99	
		$\frac{1}{3}$ Tm_2O_3			3.02	
	ZnO			3.33		
	$\frac{1}{2}$ ZrO_2			4.76		Amphoteric: $4 < z/r < 7$
$\frac{1}{3}$ Al_2O_3			5.60			
	$\frac{1}{3}$ WO_3			14.3		Acidic: $z/r < 7$
	$\frac{1}{2}$ SiO_2			15.4		

[a] The three columns under oxide and under z/r ratio separate the cations into main group elements, transition metals and lanthanides.

lanthanide element cations. A point to notice is the wide range of ionic potentials, with values ranging from <1 to >15. However, there are relatively small variations within the group of transition metal oxides, and even less variation within the lanthanide oxides. Within this ordering scheme, strongly basic oxides have z/r <2, basic oxides have z/r between 2 and 4, amphoteric oxides result from values of z/r between 4 and 7, and for acidic oxides, z/r exceeds 7.

A variety of experiments have been undertaken to look at the question of whether acid/base considerations explain the thermodynamic stability of processes involving ternary oxides. We will describe the results of several of these to illustrate the different kinds of information one can accumulate, and the range of perspectives and related questions to consider.

a. Enthalpies of Formation from the Oxides: The enthalpies of reaction for equation (15.33) (enthalpies of formation from the oxides) for a number of silicates, tungstates, carbonates and sulfates have been obtained using a variety of experimental techniques. These results have been compiled and plotted in Figure 15.9. All of the enthalpy changes are negative, with some as large in magnitude as $-350\ \text{kJ} \cdot \text{mol}^{-1}$.

The oxides are considered to be increasingly more acidic in the order: SiO_2, WO_3, CO_2, and SO_3. For a given B cation (and therefore a starting oxide of

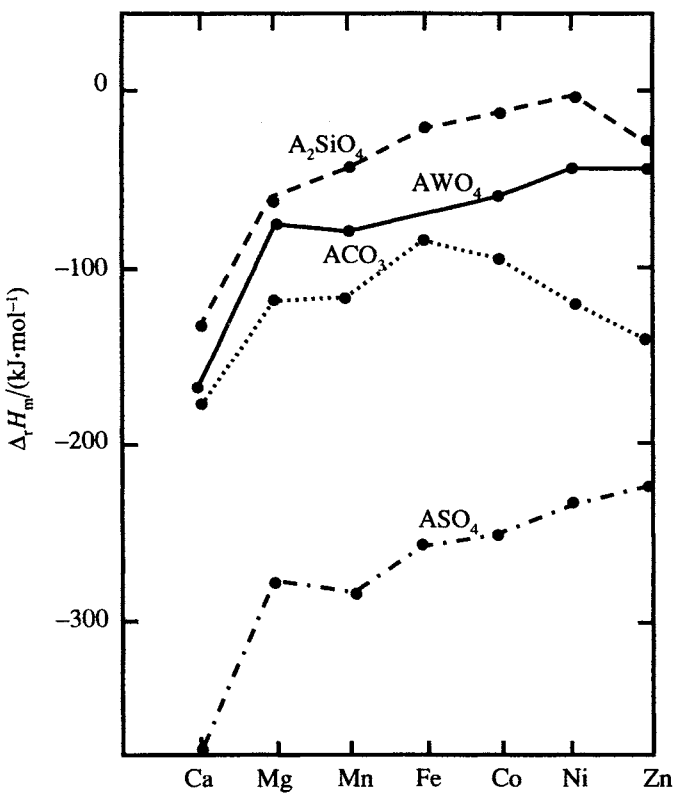

Figure 15.9 Enthalpy of formation of a series of silicates, tungstates, carbonates and sulfates from the oxides.

given basicity), there is a general trend toward greater exothermic $\Delta_r H$ values with increasing acidity of the other oxide. For example, the $\Delta_r H$ of calcium compounds become increasingly negative in the order Ca_2SiO_4, $CaWO_4$, $CaCO_3$ and $CaSO_4$. On the other hand, for a given A cation, the $\Delta_r H$ values get generally more exothermic as B becomes more basic. Thus, the largest negative enthalpies occur when a strong acid and a strong base react. In such reactions, an essentially complete transfer of an oxide ion from the base to the acid occurs, and the ternary structures contain well-defined covalently-bonded anions.

As the two binary compounds approach each other in acid/base character, the enthalpy of formation gets less negative. For ternary compounds formed from very similar binary oxides (for which the data are not shown), such as ($Al_2O_3 + SiO_2$), ($CuO + Fe_2O_3$), and ($Fe_2O_3 + TiO_2$), the $\Delta_r H$ values are, in fact, endothermic.

b. Entropies of Formation from the Oxides: The entropies of formation {equation (15.33)} for the ternary oxides show trends based upon the volatility of the oxides. For those ternary oxides derived from solid binary oxides, the entropy changes are quite small, ranging from about $(-15 \text{ to } +15)\ J \cdot K^{-1} \cdot mol^{-1}$. The $\Delta_r S$ for the reaction in which ternary oxides form from a gaseous oxide (CO_2 and SO_3) are quite large and negative because of the decrease in entropy associated with the confinement of the formerly gaseous molecules into the solid phase. Also, the entropy changes are positive when the primary coordination number increases with the reaction.

It is, of course, $\Delta_r G$ which actually determines the stability of the ternary compound relative to the binary oxides. Since it is determined by both $\Delta_r H$ and $\Delta_r S$, and since $\Delta_r S$ enters into the calculation as $T\Delta_r S$, the overall stabilities may show a change in behavior as the temperature is changed if $\Delta_r S$ is large in magnitude. The negative enthalpies of formation of ternary oxides arising from the most strongly acidic oxides (CO_2 and SO_3) are large enough at low temperatures to overcome the unfavorable entropies of formation also associated with these oxides. However, as the temperature is increased, the entropic term begins to dominate $\Delta_r G$, and the ternary oxides decompose by the evolution of gaseous oxide.

On the other hand, ternary compounds between similar binary oxides that have small negative enthalpies of formation, with some even endothermic, can increase their stabilities at high temperatures because of a favorable $\Delta_r S$. Mullite ($3Al_2O_3 \cdot 2SiO_2$), spinel ($CuFe_2O_4$) and pseudobrookite (Fe_2TiO_5) have positive entropies of formation arising from configurational or vibrational contributions. These compounds are found to be more stable at higher temperatures (or where they have positive enthalpies of formation) and are

stable above a certain temperature. Such compounds can be thought of as entropy stabilized.

Enthalpies of Formation of Orthosilicates: Orthosilicic acid has the formula H_4SiO_4. The corresponding anion is SiO_4^{4-}, which has a tetrahedral structure. Orthosilicate ions can polymerize to form more complex structures. Two SiO_4^{4-} ions can combine together by sharing a common oxygen atom to form the disilicate anion, $Si_2O_7^{6-}$. The structure of this anion can be described as the linking of a corner of two tetrahedra. This process can continue creating larger structures in which two or more oxygen atoms bridge silicon atoms to form chains, rings, or layers. For example, sharing of two oxygen atoms per SiO_4^{2-} tetrahedron gives cyclic anions such as $Si_6O_{18}^{12-}$, or extended chains with repeating $Si_2O_6^{4-}$ units. The mineral beryl ($Be_3Al_2Si_6O_{18}$) is an example of the first, while dropside ($CaMgSi_2O_6$) is of the second type. Additional sharing gives double stranded chain anions with the formula $(Si_4O_{11}^{6-})_n$ in asbestos minerals such as tremolite $\{Ca_2Mg_5(Si_4O_{11})_2(OH)_2\}$, or extended two-dimensional layered anions ($Si_4O_{10}^{4-}$) found in micas and talc. The latter has the formula $Mg_3(OH)_2(Si_4O_{10})$, with $Si_4O_{10}^{4-}$ as the repeating unit in the layered anion.

As a result of the ability to make these extended combinations, silicates usually exist as large polymeric structures, with metal ions of various amounts and types incorporated to maintain electrical neutrality. The energy or enthalpy change leading to the formation of these complex silicates involves the making (or breaking) of silicate linkages.

The enthalpies of formation (from the oxides) of one silicate family, the orthosilicates, with divalent cations have been measured for alkaline earth and transition metal elements. These $\Delta_r H$ are plotted in Figure 15.10 as a function of the ionic potential of the divalent cations. We note that the general trend is to have an increasingly more negative enthalpy of formation as the ionic potential decreases (the oxide becomes more basic). Some indications that factors other than the ionic potential are significant are evident from the observation that the enthalpies of formation of the transition metal ions, most of which have a value of z/r between Ca and Mg, do not lie on the same curve as these alkaline earths, but on one displaced towards less negative enthalpies. For a given ionic size and charge, transition metal ions are thought to have an increased tendency to bond covalently, instead of by a purely ionic interaction. Thus, one can consider the formation of the orthosilicate to be a competition between the two types of ions (Si^{4+} and M^{2+}) for the electron density of the O atom. Covalent interactions appear to affect the energetics of this competition and lead to reduced enthalpic stabilities relative to a purely ionic interaction.

Enthalpies of Mixing of (Metal Oxide + Silica) Systems: The thermodynamics of mixing of molten metal oxides (MO_x) with silica (SiO_2) can be

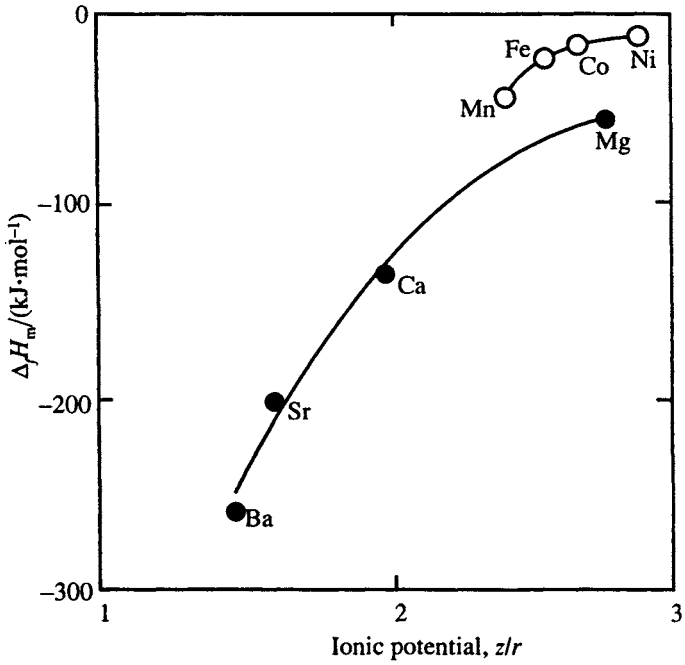

Figure 15.10 Enthalpies of formation of orthosilicates versus the ionic potential (z/r) of ●, alkaline earth, and O, transition metal cations.

represented by the process

$$x_2MO_x(l) + (1 - x_2)SiO_2(l) = \{\text{solution}\}, \tag{15.36}$$

where x_2 is the mole fraction of metal oxide.

If the mixing is viewed as an addition of the metal oxide to the molten silica, a viscous polymeric substance in which there are many Si–O–Si linkages, one can consider the process as one in which polymeric structures are broken apart into smaller units. Two nonbridging Si–O bonds are formed from one Si–O–Si linkage when the metal oxides are added. If, as suggested above, the trends in the enthalpies of formation reflect a competition for the O^{2-} electron density between the metal cation and Si^{4+}, then the enthalpies of mixing should show similar trends. Figure 15.11 shows the enthalpies of mixing of metal oxides with silica as a function of the mole fraction of the metal oxide. There is, indeed, a trend of increasingly negative enthalpies associated with the mixing process as the ionic potential of the metal cation decreases. Not enough data are available to see if trends within main group metals and within transition metals are parallel, but shifted. However, the curve involving PbO is considerably less exothermic than are those for the oxides of K, Na and Ca. The bonding in PbO is probably less ionic

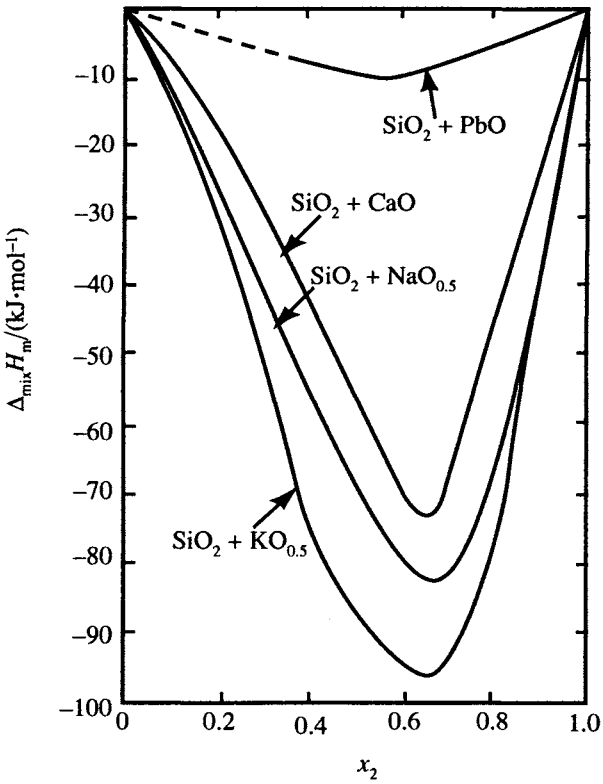

Figure 15.11 Enthalpies of mixing in binary molten silicates. Reproduced by permission from A. Navrotsky, *Am. Mineral.*, **79**, 589–605 (1994).

than in the alkaline and alkaline earth oxides, suggesting that the correlations described earlier for enthalpies of formation also apply to enthalpies of mixing.[y]

Enthalpies of Solution of Metal Oxides into a Molten "Oxide-buffered" Solution: Measurements have been made of the enthalpies of solution of many metal oxides into molten oxide solvents. The results for the solution of many of the oxides listed in Table 15.2 into a solvent consisting of molten $2PbO \cdot B_2O_3$ near 973 K are shown in Figure 15.12. The main group elements show the greatest range in ionic potentials; their enthalpies of solution go from being very exothermic for the strongly basic oxides, to slightly endothermic for the strongly acidic oxides. The lanthanides show modestly exothermic enthalpies of solution

[y] Data on viscosities of these melts show that for a given composition, the more basic the oxide, the less viscous (and by inference, the more depolymerized) the melt. This trend again supports the idea of a more complete oxide transfer from oxides with smaller z/r values.

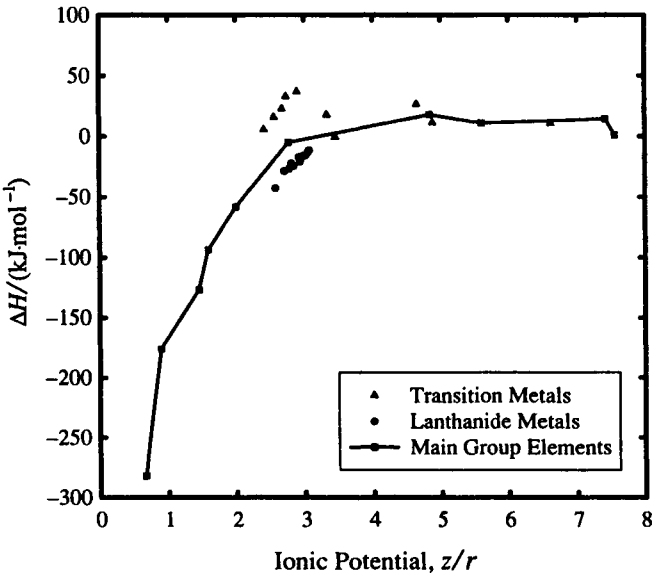

Figure 15.12 Enthalpies of solution (per mole of oxide ion) of crystalline metal oxides M_xO dissolved in molten $2PbO \cdot B_2O_3$ near 973 K. Data taken from A. Navrotsky, *Am. Mineral.*, **79**, 589–605 (1994).

that follow the trend of increasing exothermicity with decreasing ionic potential. In fact, the curve that describes their behavior in this region is approximately linear over the much smaller range of their ionic potentials, and is displaced only slightly from the results for the main group elements. The enthalpies of solution of the transition metal oxides, however, are more variable. They generally follow the established trend, but with more deviation. Their enthalpies of formation are also significantly less exothermic than are those of the main group compounds with similar ionic potentials. Enthalpies of solution in different mixed-oxide solvents of comparable acid/base strength show similar results.

Since lanthanide ions are generally considered to engage in significantly less covalent bonding than the transition metal ions, these results taken together support the idea that covalent interactions with the metal oxide reduce somewhat the enthalpic values of a process, relative to what might be expected from a metal ion that bonds through exclusively electrostatic interactions.

Conclusions These experiments support a hypothesis that acid/base considerations determine the energetics and stabilities of ternary oxide formation. The enthalpies of formation of the ternary oxides from the constituent binary oxides support this hypothesis, since the enthalpies get increasingly more exothermic with increasing strength of the acids and bases that react. Across the

whole range of ternary oxides, stabilities can be determined by entropic factors or enthalpic factors. Entropic factors are dominated by the phase state of the binary oxide, and the tendency of the strongest acidic oxides to be gases. If one considers only ternary oxides formed from solid oxides, then enthalpic factors dominate.

In a more detailed data set, where we considered separately the behavior of alkaline earth and divalent transition metal ions forming orthosilicates, trends that support the hypothesis were obtained, but a complicating factor arises in that the transition metals appear to lie on a different curve. This raises the question as to the effect of covalent interactions on the magnitude of the enthalpy change. Two sets of data, the enthalpies of mixing and the enthalpies of solution, suggest that transition metal ions, considered by themselves, follow a similar trend, but with less enthalpic stabilization. That the different behavior arises from covalent interactions is strengthened by the tendency of the lanthanides, which do not undergo extensive covalent bonding, to give values close to those of the main group elements.

It is important to note that the insights that we have described come from the consideration of the trends of a wide range of experiments on a variety of chemical substances. From a single measurement (for example, enthalpy of formation, solution, or mixing) one can say little. Rather, the analysis of trends is made possible from a variety of measurements on many materials. By carefully choosing the systems to include main group metals, transition metals, and lanthanides, one can probe the importance of contributions like covalent bonding. From the careful integration, compilation, and analysis of thermodynamic data on a number of systems, one can formulate useful generalizations and additional hypotheses to be tested. In addition, reasonable estimates of the thermodynamic properties of new materials can be made from these generalizations.

15.4 Thermodynamics of Complexation with Macrocyclic Ligands

Thermodynamics plays a major role in helping the inorganic chemist to understand the effects that are important in determining the stability of complex metal ions in aqueous solution, including the properties of the complexing ligand that affect its ability to form the complex ion. Within the last decade, macrocyclic compounds have been studied extensively,[z] in large part because of

[z] The interest in these compounds resulted in the awarding of the 1987 Nobel Prize in Chemistry to three prominent researchers in macrocyclic chemistry, C. J. Pedersen, D. J. Cram, and J.-M. Lehn.

their ability to selectively form complex ions. In this example, we will use our thermodynamic relationships to help in understanding the stability of these complexes. The systems we describe result principally from the work of R. M. Izatt and J. S. Bradshaw,[aa] in large part because of the extensive work they have done in this area. To begin our discussion, we quote from them:

> *Pedersen's publication in 1967*[13] *reporting synthesis and metal ion complexation properties of a large number of macrocyclic polyethers stimulated great interest by the scientific community in the unusual ligating properties of these compounds... Our research program has combined organic synthesis and various cation complexation properties of crown ethers and their derivatives in an effort to design and prepare macrocyles that will selectively bind specific cations. We have varied the ligands by changing the dimensions and rigidity of the macrocycle and have substituted sulfur and nitrogen atoms for part or all of the crown ether oxygen atoms.*

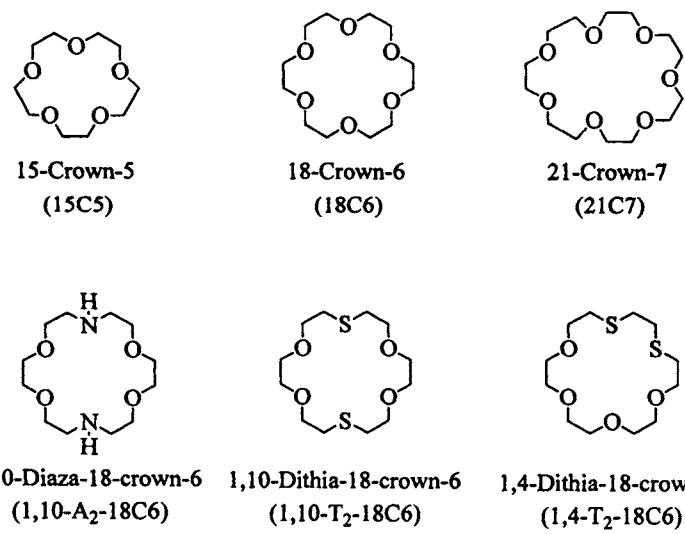

Figure 15.13 Macrocycles.

[aa] Reed M. Izatt is the Charles E. Maw Professor of Chemistry Emeritus at Brigham Young University, while Jerald S. Bradshaw is the Reed M. Izatt Professor of Chemistry, also at Brigham Young University. Jerald Bradshaw is an organic chemist who has supervised the synthesis of many macrocycles (crown compounds) while Reed Izatt is an inorganic chemist and calorimetrist who supervised the thermodynamic measurements made on these compounds.

The complexation reaction we will consider can be written as

$$M^{\nu+} + L = \{ML\}^{\nu+} \tag{15.37}$$

where $M^{\nu+}$ is a metal cation and L is a ligand. The reaction has been studied in a number of solvents and mixed solvents, but we will limit our discussion to aqueous solutions. The cation comes with various anions, which may influence the complexation, but in the examples we will consider, we will compare the different reactions at the same ionic strength and will assume that in the mixture of anions present, the effect of a specific anion will not be important.

The ligand L is a macrocycle. A large variety of sizes and shapes of macrocycle ligands have been studied for reaction (15.37). Izatt and his colleagues have summarized the thermodynamics of this reaction in several review papers.[14] The macrocycles that we have chosen as examples are summarized in Figure 15.13. They are all **Crown ethers**, which are among the simplest of macrocycles.[bb] We note that they all have a cyclic ring structure consisting of a heteroatom (in our examples, oxygen, nitrogen, or sulfur) separated by a two carbon (ethylenic) bridge. The result is a molecule with a "hole" or "cavity" in the middle. The name "macrocycle" is derived from this basic ring structure. The ring is not flat. The atoms have a staggered arrangement that resembles a crown; hence the alternate name "crown compounds". In a general way, the heteroatoms are directed toward the center of the crown. Complexation occurs as the macrocycle encircles the cation, and the heteroatoms of the macrocycle and the cation interact. With this type of interaction, one would expect the strength of the complex to depend upon the size of the cavity and/or the cation, as well as other factors. The result is a selectivity in complex formation that we now want to consider.

[bb] In naming Crown ether macrocycles, we give the total number of atoms in the ring followed by "Crown" and then the number of heteroatoms. For example, 18-Crown-6 (abbreviated 18C6) has a ring of 18 atoms of which 6 are oxygen. If the heteroatoms are all oxygen, nothing more is added to the name. Substitution with other heteroatoms requires that we give their position in the ring. For example, thia-18-Crown-6 (abbreviated T-18C6) has one of the oxygen atoms replaced with a sulfur (thia) atom. In Figure 15.13, 1, 10-dithia-18-Crown-6 (abbreviated 1, 10-T_2-18C6) has sulfur atoms at the 1 and 10 positions in the ring.

Additions to the ring are also named. For example, in dicyclohexano-18-Crown-6 the macrocyclic ring contains ethylenic carbon atoms that are also a part of cyclohexane rings, while dibenzo-18-Crown-6 has benzene rings at the same positions. In pyridino-18-Crown-6, the nitrogen from a pyridine ring replaces one of the oxygens.

The thermodynamic equilibrium constant for reaction (15.37) can be written as

$$K = \frac{a_{\{ML\}^{\nu+}}}{a_{M^{\nu+}} a_L} \tag{15.38}$$

where $a_{\{ML\}^{\nu+}}$ is the activity of the complex, a_L the activity of the ligand, and $a_{M^{\nu+}}$ the activity of the cation. The usual standard state chosen for these complexes involves Henry's law based on molarity, in which case

$$a_{\{ML\}^{\nu+}} = \gamma_{\{ML\}^{\nu+}} c_{\{ML\}^{\nu+}},$$

$$a_L = \gamma_L c_L,$$

and

$$a_{M^{\nu+}} = \gamma_{M^{\nu+}} c_{M^{\nu+}},$$

where $c_{\{ML\}^{\nu+}}$, $c_{M^{\nu+}}$, and c_L are molar concentrations. Substitution into equation (15.38) gives

$$K = K_c J_\gamma \tag{15.39}$$

where

$$K_c = \frac{c_{\{ML\}^{\nu+}}}{c_{M^{\nu+}} c_L} \tag{15.40}$$

and

$$J_\gamma = \frac{\gamma_{\{ML\}^{\nu+}}}{\gamma_{M^{\nu+}} \gamma_L}. \tag{15.41}$$

Reaction (15.37) is usually studied in dilute solution (ionic strength $\leqslant 0.1$). If, as in our examples, the ligand is a nonelectrolyte, then it is a reasonable approximation to assume that $\gamma_L \approx 1$. It is also not unreasonable to expect $\gamma_{\{ML\}^{\nu+}} \approx \gamma_{M^{\nu+}}$ in these dilute solutions, since ions with the same charge behave in a somewhat similar manner, as suggested by the Debye–Hückel theory. Hence, $J_\gamma \approx 1$ and $K = K_c$. Because we will not be overly concerned with quantitative results of high accuracy in this discussion, we will assume this approximation is sufficient and use K for K_c. It is not absolutely necessary that we do so, however, since corrections can be made for J_γ.

The measurement of an equilibrium constant requires the assumption of a non-thermodynamic measuring technique. Procedures that have been employed to measure K for reaction (15.37) include calorimetric, potentiometric, conductimetric, NMR, light absorption, and polarographic methods. The calorimetric measurements are especially useful, because they give $\Delta_r H°$ for the reaction in addition to K. Since

$$\Delta G° = -RT \ln K \tag{11.102}$$

and

$$\Delta S° = (\Delta H° - \Delta G°)/T, \tag{15.43}$$

the calorimetric measurements result in the determination of all three of these thermodynamic quantities.

15.4a Thermodynamic Properties of Macrocycle–Metal Ion Complexes

We will first consider the complexation of alkali metal and alkaline earth metal ions with the oxygen macrocycles 15-Crown-5 (15C5), 18-Crown-6 (18C6), and 21-Crown-7 (21C7). We will then expand our discussion to include other metal ions and the nitrogen- and sulfur-substituted ligands 1,10-diaza-18-Crown-6 (1,10-A_2-18C6) and 1,10-dithia-18-Crown-6 (1,10-T_2-18C6).

Complexes with Oxygen Macrocycles: Figure 15.14 summarizes log K values for the complexes of the 15C5 macrocycle with alkali metal cations, and the 18C6 macrocycle with both alkali metal and alkaline earth metal cations.[cc] The log K results for these systems were determined from calorimetric measurements. Values are plotted against the ratio of the cation crystal radius to the radius of the hole in the center of the macrocycle.[dd]

For the complexes of 18C6 with the alkali metal cations, log K is largest for the K^+ ion. It is interesting to note that the radius ratio for K^+ with 18C6 is very nearly one. Thus, the K^+ ion fits snugly in the hole. This seems to give the highest complex stability, with the log K values for the smaller Na^+ ion (which would not completely fill the hole) and the larger Rb^+ and Cs^+ ions (which are too big for the hole) smaller than for K^+.

[cc] Original references to the results given in Figure 15.14, along with other systems described in this section can be found in the review articles referenced earlier.

[dd] From X-ray diffraction studies the hole is estimated to be between 0.086–0.092 nm for 15C5 and 0.134–0.143 nm for 18C6. We have used values of 0.089 nm and 0.138 nm for the two macrocycles. Izatt has used Carey–Pauling–Kolting models to give an estimate of the radius of the hole in 21C7 as 0.17 nm.

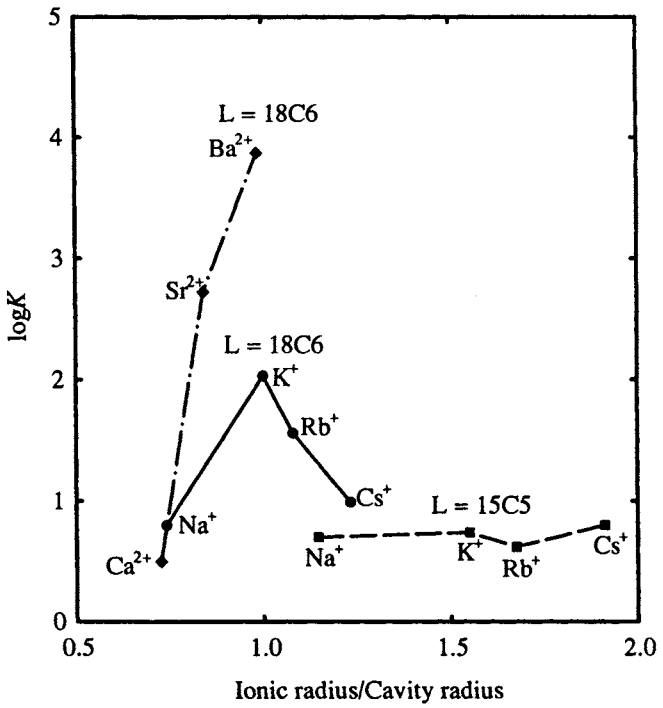

Figure 15.14 Comparison of log K for the reaction $M^{\nu+} + L = \{ML\}^{\nu+}$ for macrocyclic ligands $L = 18C6$ or 15C5 with alkali or alkaline earth metal ions $M^{\nu+}$. The comparison is made as a function of the ratio of the radius of the ion to the radius of the cavity in the macrocycle.

A similar trend is observed for the alkaline earth cation complexes with 18C6, with Ba^{2+} (where the radius ratio is approximately one) forming the strongest complex.[ee] We note that the alkaline earth complexes have a log K that is several times as large as for the corresponding alkali metal complexes. This difference is not surprising, since the alkaline earth cations have twice the electronic charge of the alkali metal cations. We will discuss this effect in more detail later.

Also shown in Figure 15.14 are log K values for the alkali metal cation complexes of 15C5. We note that all of the alkali metal cations are too large to fit into the 15C5 hole. All of the 15C6 complexes have approximately the same log K values as for Cs^+ with 18C6, which has a radius ratio with that macrocycle that overlaps the range of radius ratios of the alkali metal cations with 15C5.

[ee] It would be interesting to see if log K would decrease for Ra^{2+}. Unfortunately (but understandably), data are not available for this system.

It would be interesting to compare the 15C5 and 18C6 results with those for 21C7, but the alkali metal cations complexed with 21C7 have not been studied in aqueous solution. Measurements for these systems have been studied in methanol solvent, and log K values in aqueous solutions can be estimated from these results. As a basis for the estimations, we can compare log K values for the alkali metal cations with 18C6 in water solvent and methanol solvent. We find that the log K values in methanol are displaced by almost a constant amount for all four cations. The displacement is 3.80 ± 0.25 log K units. If we assume this same displacement for the 21C7 complexes, we get aqueous solution log K values of 1.21 for Cs^+ (radius ratio = 1.0), 1.06 for Rb^+ (radius ratio = 0.88), and 0.42 for K^+ (radius ratio = 0.81).[ff] Again, we see that the most favorable complex formation (when the other conditions are the same) occurs when the radius ratio is nearly one.[gg]

As we described earlier, the calorimetric determination of log K allows one to also get $\Delta_r H$ for reaction (15.37). The values reported by Izatt and his colleagues were obtained in an aqueous solution with an ionic strength of 0.1. Izatt reports that enough measurements were made in more dilute solutions to show that the enthalpy of dilution to the infinitely dilute solution (the standard state) is small and can be ignored. Hence, we will assume that the $\Delta_r H$ values reported are the standard state $\Delta_r H^\circ$ values. Thus we have available, $\Delta_r G^\circ$, obtained from equation (15.42), and $\Delta_r S^\circ$ obtained from equation (15.43).

The results for reaction (15.37) for the alkali metal cations complexed with 18C6 and 15C5 are shown in Figure 15.15. As with log K, the $\Delta_r Z^\circ$ values ($\Delta_r G^\circ$, $\Delta_r H^\circ$, and $T\Delta_r S^\circ$) are plotted against the radius ratio.

It is interesting to compare $\Delta_r Z^\circ$ in Figure 15.15 for the interaction of each cation with 18C6 and with 15C5. First we note that $\Delta_r S^\circ$ (expressed as $T\Delta_r S^\circ$) is very nearly the same for a specific cation with each of the ligands. For example, $T\Delta_r S^\circ$ is most negative for the K^+ complexes, and is nearly the same for $\{K18C6\}^+$ and $\{K15C5\}^+$.

In comparing $\Delta_r H^\circ$, we note that the values are more negative than are the $T\Delta_r S^\circ$ values. The result is a negative $\Delta_r G^\circ$ for reaction (15.37), resulting in a stable complex for all four alkali metals with both macrocycles. We describe the formation of these complexes as energy (or enthalpy) driven. That is, the favorable $\Delta_r H^\circ$ more than compensates for the unfavorable $T\Delta_r S^\circ$ to give a $\Delta_r G^\circ < 0$, and hence, a favorable equilibrium constant K.

[ff] For Na^+, correcting the log K value in methanol to an aqueous solution value by subtracting 3.80 gives a negative log K. Given the uncertainty of the displacement, we are inclined to think that the subtraction over corrects for the Na^+ ion.

[gg] It would be interesting to compare the above with results for Fr^+ with 21C7. Presumably, the radius ratio would be too large and log K would decrease to a value less than that for Cs^+.

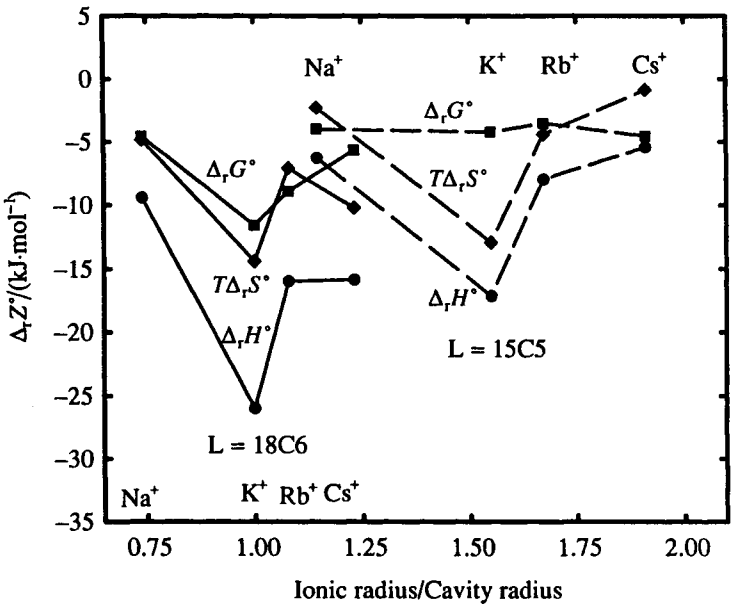

Figure 15.15 Comparison of the thermodynamic properties for the reaction $M^{\nu+} + L = \{ML\}^{\nu+}$ as a function of the ratio of the ionic radius to the radius of the cavity in the macrocycle. The macrocycle L is 18C6 (results indicated by solid lines) or 15C5 (results indicated by dashed lines), and $M^{\nu+}$ is an alkali metal ion as indicated in the figure.

We note the especially large negative $\Delta_r H°$ for the formation of the $\{K18C6\}^+$ complex. The result is an extra large stability for this complex, as shown by the maximum log K value for that alkali metal complex observed in Figure 15.14. We also see from Figure 15.15 that for the (alkali metal + 15C5) complexes, $\Delta_r H°$ is most negative for the $\{K15C5\}^+$ complex, but with that ligand, the $\Delta_r H°$ values are displaced from the $T\Delta_r S°$ values by a constant small difference. The result is the small (but still favorable) log K values shown in Figure 15.14.

Complexes with Macrocycles Containing Heteroatoms other than Oxygen: Figure 15.16 compares log K values[hh] (again in aqueous solution)

[hh] See the review articles referenced earlier for the original sources for the values plotted in Figure 15.16. The log K for the aza-complexes were obtained from potentiometric measurements. For the thia-complexes, the log K were obtained from calorimetric measurements, except for the mercury complex, where log K was obtained from polarographic measurements.

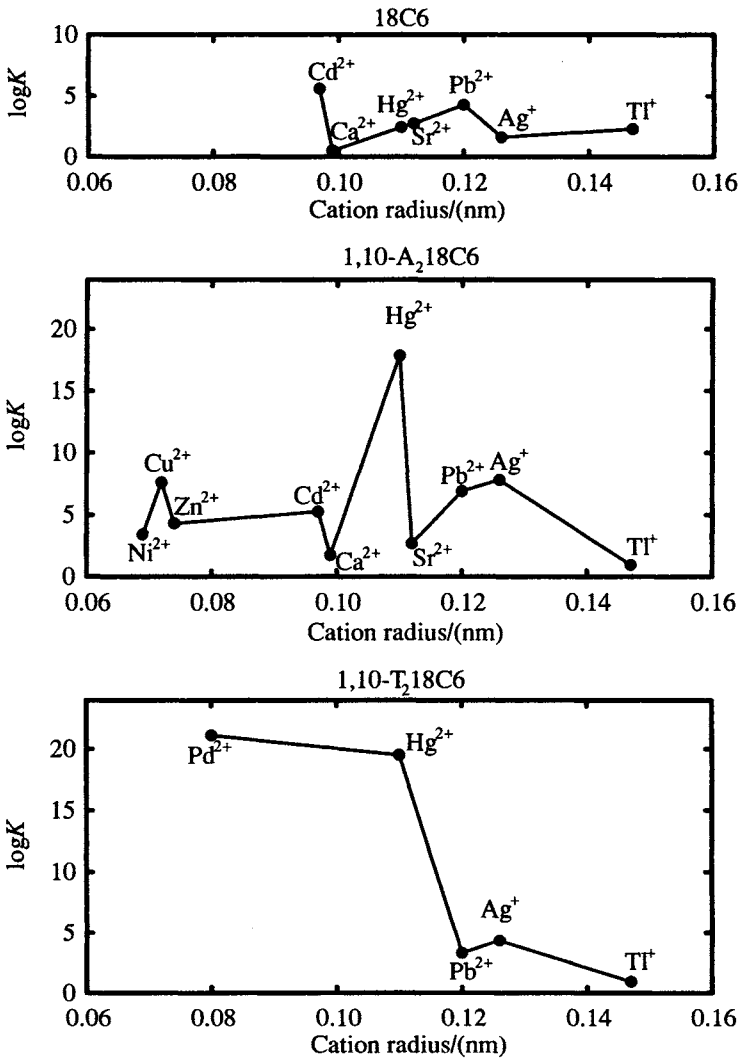

Figure 15.16 Graph of log K for the reaction $M^{\nu+} + L = \{ML\}^{\nu+}$, against the radius of the cation, for three different macrocycles. All are plotted on the same scale so that the log K values can be compared.

for reaction (15.37), of metal cations complexing with 1,10-A_2-18C6 and 1,10-T_2-18C6.[ii] Also shown for comparison on the same scale are log K values for the 18C6 complexes. The log K values are plotted against the ionic crystal

[ii] See Figure 15.13 for the structure of these macrocycles.

radii of the metal cations. We recall that the radius of the cavity in 18C6 is approximately 0.139 nm. The C–N bond length is very nearly the same as the C–O bond length so that we would expect the cavity to be about the same size in 1,10-A_2-18C6 as in 18C6. The C–S bond length is about 25% longer than the C–O bond length. Hence, the cavity in 1,10-T_2-18C6 is perhaps somewhat larger than in 18C6, although the sulfur may allow the 1,10-T_2-18C6 molecule to be more flexible so that it can more easily fold back upon itself to better accommodate a smaller cation. In any event, for all three macrocycles, the radius of the cavity is probably larger than the radius of the cation for nearly all of the examples shown, so that the radius ratio is less than one.

It is apparent from Figure 15.16 that 1,10-A_2-18C6 and 1,10-T_2-18C6 complex much more strongly, especially for certain elements, than does 18C6. For the 1,10-A_2-18C6 complexes we note the increased strength of the Cu^{2+} complex compared to the Ni^{2+} and Zn^{2+} complexes. This trend is similar to that for the $Cu(NH_3)_4^{2+}$, $Ni(NH_3)_4^{2+}$ and $Zn(NH_3)_4^{2+}$ complex ions.[jj] The Ag^+ complex is also strong,[kk] which is in agreement with the high stability of the $Ag(NH_3)_2^+$ complex ion.

We note in Figure 15.16, the exceptional stability of the Hg^{2+} complex of 1,10-A_2-18C6, and of 1,10-T_2-18C6. The thermodynamic reasons for this can be understood better by referring to Figure 15.17 where we graph $\Delta_r G°$, $\Delta_r H°$, and $T\Delta_r S°$ for the formation of the Sr^{2+}, Ag^+, and Hg^{2+} complexes with the three macrocycles.[ll] The thermodynamic differences $\Delta_r Z°$ for the three cations are plotted on the same scale so that comparisons can easily be made. The alkaline earth cation Sr^{2+} was chosen for comparison since it has nearly the same ionic radius as Hg^{2+} and Ag^+.

From Figure 15.17, we see that the Sr^{2+} complexes of both 18C6 and 1,10-A_2-18C6 are relatively weak and almost completely energy stabilized. For Ag^+, the 18C6 complex is again weak and energy stabilized. The 1,10-A_2-18C6 complex is fairly strong, and it is almost completely energy stabilized. For the 1,10-T_2-18C6 complex with Ag^+, the entropy effect works against the enthalpy effect so that $\Delta_r G°$ is smaller and the complex is weaker than for the corresponding 1,10-A_2-18C6 complex.

The Hg^{2+} complex of 18C6, is again weak, with a small entropy effect working against the enthalpy stabilization. For the Hg^{2+} complexes with

---

[jj] The trend is in agreement with the Irving–Williams order for the strength of complex ion formation for metal ions. That is, $Ni^{2+} < Cu^{2+} > Zn^{2+}$.

[kk] We remember that in 18C6 the M^+ complexes are considerably weaker than the M^{2+} complexes. That this is not true for Ag^+ complexes compared with the M^{2+} complexes attests to the increased tendency of Ag^+ to form amine complexes.

[ll] Thermodynamic data are not available in aqueous solution for Sr^{2+} with 1,10-T_2-18C6. Hence, only complexes of the other two macrocycles are compared.

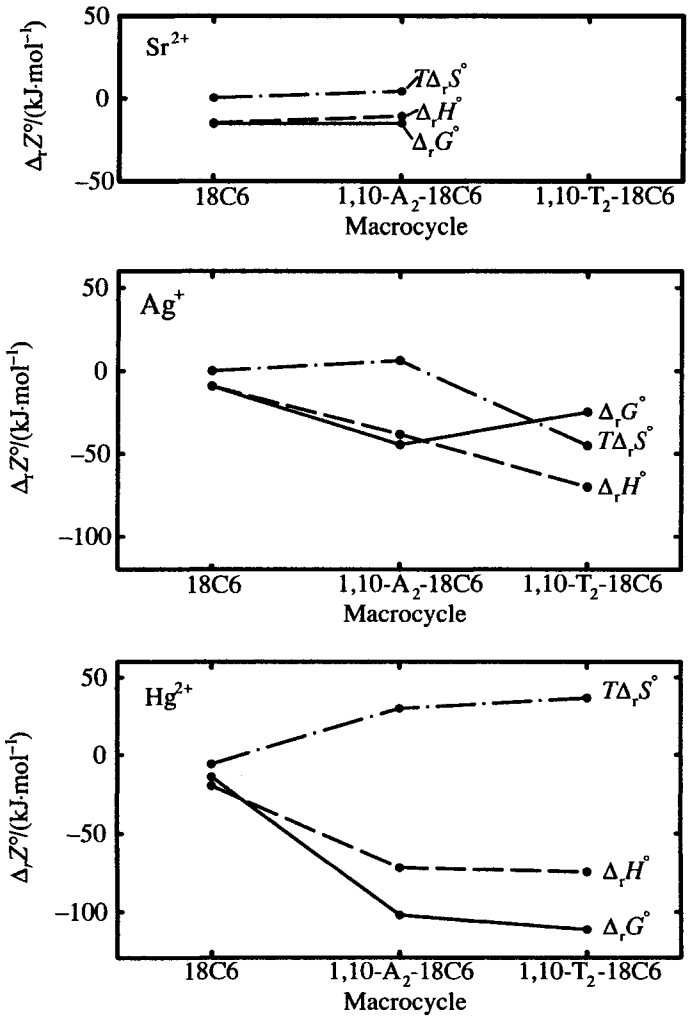

Figure 15.17 Thermodynamic change $\Delta_r Z°$ for the reaction $M^{\nu+} + L = \{ML\}^{\nu+}$, where $M^{\nu+}$ is the metal ion Sr^{2+}, Ag^+, and Hg^{2+}, and L is the ligand 18C6, 1,10-A_2-18C6, or 1,10-T_2-18C6. The solid line gives $\Delta_r G°$, the dashed line gives $\Delta_r H°$, and the dashed-dotted line gives $T\Delta_r S°$.

1,10-A_2-18C6 and 1,10-T_2-18C6, however, large entropy, as well as enthalpy, stabilizations are present. The result is a large negative $\Delta_r G°$ and very stable complexes, especially for $\{Hg\text{-}1,10\text{-}T_2\text{-}18C6\}^{2+}$. The stability of this last complex is not unexpected, especially in light of the known tendency for Hg and S to form very stable bonds. We note, however, that both energy and entropy stabilization contribute to the large K for the formation of the mercury

aza- and thia-complexes. We will return to these complexes later as we attempt to explain and better understand the nature of the bonding in the macrocycle complexes that we are describing.

We note from Figure 15.16 that Pd^{2+} also forms a very stable complex with 1,10-T_2-18C6. Again, the stability of the complex results from both strong enthalpy ($\Delta_r H° = -82.4$ kJ) and entropy ($T\Delta_r S° = 38.1$ kJ) stabilizations, so that $\Delta_r G° = -120.5$ kJ, and hence, log $K = 21.1$.[mm]

Because the Pd^{2+} ion is much too small to fill the cavity in the 1,10-T_2-18C6 macrocycle, the requirement that the metal ion "just fill the hole in the macrocycle" must not make an important contribution to the stability of this complex. Izatt and coworkers[15] have studied this complex in detail. They have determined the crystal structure of solid Pd (1,10-T_2-18C6)$(NO_3)_2$ from X-ray crystallography studies. The results show that Pd^{2+} forms a distorted square-planar complex, with the two NO_3^- ions at adjacent corners and the two sulfur atoms of the macrocycle at the other two corners. To bring the sulfur atoms in position to bond, the molecule assumes a cupping shape. As a result, the oxygen atoms move away from the Pd^{2+} and do not participate significantly in the bonding.[nn]

15.4b Interpretation of the Results to Explain Complex Stability Involving "Hard" and "Soft" Metal Ions

We see that for the (alkali metal + oxygen macrocycle) complexes, charge and relative size of the ion play an important part in determining the stability of the complex. However, for the (transition metal + aza- or thia-substituted macrocycle) complexes, the nature of the bonding seems to be the important effect. Sten Ahrland[16] has used a classification scheme for metal ion acceptors that helps us understand this difference. He designates the metal ion as either *hard* or *soft*. The characteristics that determine the assignment are as follows.

Hard ions: These have high charge and/or a small radius. They usually have a low polarizability, participate principally in electrostatic bonding, and are structure breakers or formers in a polar solvent.

[mm] A useful property of macrocyclic ligands is the ability to tailor the size, shape, and make-up of the macrocycle to selectively complex a particular metal ion (or other species), while complexing very little with other ions that are similar chemically, and thus difficult to separate by most techniques. Excellent examples are the Hg^{2+} and Pd^{2+} complexes of 1,10-T_2-18C6. Because of the strong complexes formed, procedures can be devised to extract Hg^{2+} or Pd^{2+} to extremely low concentrations from an aqueous solution containing a variety of ionic species. These procedures have been developed commercially to effect large-scale separations and purifications.

[nn] It is interesting to note that 1,4-T_2-18C6 forms a 2:1 complex with Pd. That is, the formula would be $\{Pd(1,4\text{-}T_2\text{-}18C6)_2\}^{2+}$. In this complex, the four sulfur atoms form a stable square-planar complex around the Pd^{2+} ion. Again the oxygens are not significantly involved in the complex formation. (See Izatt reference for details.)

Soft ions: These have high polarizability. They usually have a large number of d electrons in the outer electronic shells. As a result, they form covalent bonds with the water molecules in the solvent to form hydrates, and with the ligand to form complexes. Beyond the formation of covalently bonded hydrates, they do not have a large effect on the structure of a polar solvent.

Using these criteria, Ahrland classifies the alkali and alkaline earth metal ions as hard ions, with the hardness decreasing as the radius of the ion increases. The transition metal ions, Ag^+, Pd^{2+}, and Hg^{2+}, on the other hand, are soft, with the softness increasing in that order, so that the Hg^{2+} ion is an especially soft ion.

The donor atoms in ligands can also be classified as hard or soft using the same criteria. Ahrland does not include macrocyclic ligands in his classification, but one would expect all three to be soft ligands, with 15C5, 18C6, and 21C7 as moderately soft, 1,10-A_2-18C6 as softer, and 1,10-T_2-18C6 as very soft.

The complexation represented by reaction (15.37) can be thought of as consisting of two parts:

1. Formation of a chemical bond between the metal ion and the macrocyclic ligand. We will designate ΔH_1 and ΔS_1 as the enthalpy and entropy changes for this process.
2. Rearrangement and restructuring of the solvent during the formation of the complex. For aqueous solutions, this change involves dehydrating the metal ion, hydrating the complex ion, and making or breaking hydrogen bonds in the solvent as water is removed or added to the hydration sphere around the ion. We will designate ΔH_2 and ΔS_2 as the enthalpy and entropy changes for this process.

The ΔH and ΔS for these steps, and the combination to give $\Delta_r H°$ and $\Delta_r S°$ for the overall reaction, depends upon the hardness and softness of the ions and ligands involved in the process. To see how the concept of hard and soft ions and ligands helps to explain the observed values for $\Delta_r H°$ and $\Delta_r S°$, let us consider two examples:

(Hard Ion + Soft Ligand Complexes): This combination characterizes the complexing of alkali or alkaline earth metals with any of the macrocycles. Bond formation is primarily electrostatic, with $\Delta H_1 < 0$ and of moderate size. The better the ion fits in the cavity, the larger the attraction between the positive ion and the negative oxygen atoms of the macrocycle. The result is that ΔH_1 is most negative for the ion that just fits in the cavity. Increasing the charge on the ion also increases the electrostatic attraction and lowers the energy. As a result, the alkaline earth metal ions would give a more negative ΔH_1 in the complexation reaction than would the alkali metals.

The entropy change $\Delta S_1 < 0$ and of moderate size, since the bonding process involves the condensation of two species into one.

For the second process, $\Delta H_2 < 0$ and $\Delta S_2 < 0$, but both effects should be small, since the (dehydration of the metal ion + the breaking of hydrogen bonds in the solvent) should largely be compensated for by the formation of the larger, and still charged, complex ion. By comparing ΔH and ΔS for the two processes, we see that the complexation reaction is dominated by the bonding, with the overall $\Delta_r H° < 0$ and $\Delta_r S° < 0$, and this effect is the largest when the metal ion fits well into the cavity of the macrocycle.[oo] $\Delta_r H°$ is larger in magnitude than $\Delta_r S°$ but the two effects largely cancel to give a $\Delta_r G° < 0$, but small in magnitude.[pp]

(Soft Ion + Soft Ligand Complexes): This combination of metal ion + ligand occurs when the 18C6 unsubstituted and substituted (thia- and aza-) ligands complex with the Pd^{2+}, Ag^+, and Hg^{2+} ions. The metal ion and macrocycle bond covalently, so that $\Delta H_1 \ll 0$. The strongest covalent bond forms between Pd^{2+} (the softest ion) and 1,10-T_2-18C6 (the softest ligand) so that ΔH_1 is the most negative for the complex formation in this reaction. On the other hand, the covalent bonding is the weakest and ΔH_1 is the smallest when the unsubstituted 18C6 is involved, since this macrocycle is the least soft (hardest) of the three. Said another way, oxygen does not covalently bond as well with metal ions such as Pd^{2+}, Ag^+, and Hg^{2+} as does nitrogen or sulfur.

For the entropy change, the important thing is that once again, the bonding reaction involves the combination of two species into one. Thus $\Delta S_1 < 0$ for all of the complexes, but is of moderate size.

Soft metal ions also form coordinate bonds with the water molecules from the solvent. As a result, the metal ions are hydrated. This coordination partially breaks down when the complex forms. As a result, $\Delta H_2 > 0$, but of moderate size. The complex formation is a disordering process in the solvent as the hydration of the metal ion breaks down. Hence, $\Delta S_2 > 0$. The magnitude of ΔH_1 is larger than that of ΔH_2, while the magnitude of ΔS_2 is larger than the

---

[oo] When the cation is too large to fit into the cavity, extra hydration effects and reactions involving more than one ligand per metal ion can occur. This can complicate the resulting $\Delta_r H°$ (and $T\Delta_r S°$), and trends can be affected. It appears that this may be happening in the formation of either $\{Rb18C6\}^+$ or $\{Cs18C6\}^+$. Further investigation of these systems would be interesting and worthwhile.

[pp] The increased stability of the Cu^{2+} (a soft ion) complex with 1,10-A_2-18C6, as compared to similar complexes with Ni^{2+} and Zn^{2+} (both of which are also soft ions), is probably related to the stronger covalent bonding (and more negative ΔH_1) in the Cu^{2+} complex. We leave it to the inorganic chemists to explore this difference in bonding in more detail.

magnitude of ΔS_1. The net effect is that $\Delta_r H° < 0$, while $\Delta_r S° > 0$. The $\Delta_r H°$ and $\Delta_r S°$ reinforce one other to give a $\Delta_r G° < 0$ and large in magnitude.[qq] A study of Figure 15.17 shows that the results shown there are in agreement with the conclusions given above.

Problems

P15.1 Show that in reaction (15.1), assuming ideal behavior of the gases, the maximum (equilibrium) conversion of nitrogen and hydrogen into ammonia at a given temperature and total pressure, is obtained when the reacting gases are in the proportion of 1 to 3. (To do so, suppose that the N_2 and H_2 molecules are present in the ratio of 1 to r, with x as the mole fraction of NH_3 present at equilibrium. Then express K_p in terms of mole fractions and the total pressure, and find the condition that makes dx/dr equal to zero.)

P15.2 Use the thermodynamic data from Table A5.1 of Appendix 5 to show that the dissociation of H_2 into H is not a complication that needs to be considered in calculating the equilibrium mole fraction of NH_3 in the Haber reaction at 800 K and 0.1 MPa. Assume J_γ is one for the H_2 dissociation at these conditions of pressure and temperature.

P15.3 Use the thermodynamic data summarized in Table A5.1 of Appendix 5 to calculate the mole percent NH_3 in an equilibrium stoichiometric mixture of $N_2 + H_2$ at a total pressure of 60 atm (6.06 MPa), and in the temperature range from 900 K to 1400 K. Make a graph of the results and compare them with the experimental values reported by Nernst as summarized in Figure 15.3. As we saw in the text, we can assume $J_\gamma = 1$ for the reaction under these experimental conditions.

P15.4 (a) Use the $\Delta_f H°_{298}$ and $\Delta_f G°_{298}$ data from Table A5.2 of Appendix 5 and the heat capacity data from Table A5.5 from the same appendix to derive an expression for the Haber reaction of ln K as a function of temperature (valid in the temperature range from 298 K to 1500 K).

(b) Make the same calculation of ln K at a series of temperatures over the same temperature range using thermodynamic functions from Table A5.1 of Appendix 5. Graph ln K against $1/T$ in a manner similar to that shown in Figure 15.2 to compare the calculations in (a) and (b).

(c) Use the results calculated in (b) to reproduce Haber's results of the mole percent NH_3 as a function of T as shown in Figure 15.3.

[qq] We thank Professor Giuseppe Arena of the Dipartimento di Scienze Chimiche, Università di Catania, in Catania, Italy, for many helpful discussions that led to the interpretation of the experimental results described here.

P15.5 In the water gas reaction, $H_2O(g)$ is passed over hot charcoal at 1250 K. The reaction is

$$C(s) + H_2O(g) = CO(g) + H_2(g).$$

(a) Assume the charcoal is graphitic carbon and use thermodynamic data from Table A5.1 of Appendix 5 to determine the equilibrium partial pressure of all three gases when hot steam is passed over charcoal at a (final) pressure of 0.100 MPa and a temperature of 1250 K.

(b) For this reaction, calculate the equilibrium mole fraction of $H_2O(g)$ as a function of temperature and a total pressure of 0.100 MPa, and determine at what temperature 99 mole percent of the $H_2O(g)$ will be converted to $H_2(g) + CO(g)$. Repeat the calculation at a pressure of 10.0 MPa and compare the results. You may assume J_γ is one for the reaction at both pressures.

P15.6 Given the following thermodynamic data for the complexation of Pb^{2+} (a soft ion) at 298.15 K according to the reaction

$$Pb^{2+} + 1,10\text{-}T_2\text{-}18C6 = \{Pb\text{-}1,10\text{-}T_2\text{-}18C6\}^{2+}$$

Solvent	$\Delta_r H°/(kJ \cdot mol^{-1})$	log K
Water	−75.0	3.31
Methanol	−34.5	4.76

Use the table to calculate $\Delta_r S°$ and $\Delta_r G°$ for the reaction in each of the solvents and explain the results, including the differences observed in the two solvents, in terms of the contributions from covalent bonding of the ion by the ligand, and changes in the structure of the solvent.

P15.7 For the two reactions in aqueous solution at 298.15 K

$$K^+ + 18C6 = \{K18C6\}^+, \qquad \log K = 2.03$$

$$Na^+ + 18C6 = \{Na18C6\}^+, \qquad \log K = 0.80$$

(a) Calculate the equilibrium molar concentration of K^+ when equal volumes of 0.020 M K^+ and 0.20 M 18C6 are mixed. You may assume J_γ is one for the reaction.

(b) Repeat the calculation using the same macrocycle ligand with a Na^+ solution instead of a K^+ solution. Use the results to decide if 18C6 could be used to effectively separate the two ions in solution.

P15.8 Start with equation (15.30) in the text

$$\ln K = -395.829 - 0.17986T + \frac{6537.774}{T} + 71.595 \ln T$$

for representing the solubility of calcite as a function of $T/(\mathrm{K})$.

(a) Calculate $\Delta_r G^\circ_{298}$, $\Delta_r H^\circ_{298}$, and $\Delta_r S^\circ_{298}$ for the solubility reaction

$$CaCO_3(s) = Ca^{2+}(aq) + CO_3^{2-}(aq).$$

(b) On an average day, Mammoth Hot Springs in Yellowstone National Park releases approximately 500 gallons per minute of water that has been heated underground to 75 °C. Assume this hot water is saturated with $CaCO_3$ and calculate how many kg of solid $CaCO_3$ is deposited per year in the area around the hot springs as the water cools to 20 °C.

P15.9 Boron nitride (BN) is isoelectronic with carbon and the B, C, and N atoms are about the same size. The result is that BN forms crystal structures similar to those of carbon, in that it crystallizes in a hexagonal (graphite-like hBN) and a cubic (diamond like cBN) structure. The data summarized at the end of the problem are available for the two forms of BN.[17]

(a) Use the heat capacity data and the Third Law of Thermodynamics to calculate $\Delta_{tr} S^\circ_m$ at $T = 298.15$ K and $p = 0.1$ MPa for the transition

$$\mathrm{hBN} = \mathrm{cBN}.$$

(b) Fluorine bomb calorimetry has been used to determine the standard enthalpies of formation at 298.15 K for the different forms of BN. The values obtained are $-250.6\ \mathrm{kJ \cdot mol^{-1}}$ for hBN and $-247.6\ \mathrm{kJ \cdot mol^{-1}}$ for cBN. At $T = 298.15$ K and $p = 0.10$ MPa, calculate $\Delta_{tr} H^\circ_m$ for the transition, combine this result with $\Delta_{tr} S^\circ_m$ from part (a) to obtain $\Delta_{tr} G^\circ_m$, and determine which form of BN is stable at this temperature and pressure.

(c) Use the high-temperature enthalpy data given in the table that follows to calculate the transition temperature at $p = 0.1$ MPa.
Note: Two other crystalline modifications of BN are known at high pressures, one with a wurtzite structure (wBN), and another with a rhombohedral structure (rBN). Although some of the phase relationships are known, a reliable prediction of the pressure against

temperature phase diagram for this substance awaits the determination of more accurate thermodynamic data for all four allotropic forms.

Heat capacity data for BN

T/(K)	$C_{p,m}$/ ($J \cdot K \cdot mol^{-1}$)		T/(K)	$C_{p,m}$/ ($J \cdot K \cdot mol^{-1}$)		T/(K)	$C_{p,m}$/ ($J \cdot K \cdot mol^{-1}$)	
	hBN	cBN		hBN	cBN		hBN	cBN
4		0.00005	80	3.556	0.3749	210	13.20	7.524
6		0.0007	90	4.221	0.5578	220	13.97	8.425
10		0.0033	100	4.900	0.8021	230	14.71	9.346
15	0.1473	0.0056	110	5.602	1.104	240	15.50	10.29
20	0.2501	0.0078	120	6.323	1.474	250	16.26	11.23
25	0.3914	0.0158	130	7.060	1.913	260	17.02	12.19
30	0.5632	0.0215	140	7.809	2.415	270	17.71	13.14
35	0.7635	0.0306	150	8.567	2.977	280	18.51	14.09
40	0.9906	0.0456	160	9.332	3.603	290	19.25	15.03
45	1.242	0.0644	170	10.10	4.291	298.15	19.85	15.79
50	1.517	0.0873	180	10.88	5.034	300	19.99	15.97
60	2.129	0.1487	190	11.65	5.823			
70	2.813	0.2412	200	12.43	6.655			

High-temperature enthalpy data for BN
Coefficients for the equation:

$$(H^\circ_T - H^\circ_{298})/(J \cdot mol^{-1}) = aT + bT^2 + cT^3 + dT^4 + eT^{-1} + f$$

	a	$b \times 10^2$	$c \times 10^5$	$d \times 10^9$	$e \times 10^{-5}$	f
hBN	2.0579	4.1285	−1.6977	2.7542	2.2932	−4621.505
cBN	6.2507	4.0024	−1.9353	−3.7362	8.4850	−7781.667

References

1. Report of the experimental procedure and the experimental results obtained is given in F. Haber and R. LeRossignol, "On the Ammonia-Equilibrium", *Ber. Bunsenges. Phys. Chem.*, **40**, 2144–2154 (1907). The report of the final results is found in F. Haber and R. LeRossignol, "The Ammonia Equilibrium under Pressure", *Z. Elektrochem.* **14**, 181–196 (1908).

2. W. Nernst and F. Jost, "Ammonia Equilibrium", *Z. Elektrochem.*, **13**, 521–524 (1907).
3. See F. Haber and R. LeRossignol, "The Ammonia Equilibrium under Pressure", *Z. Elektrochem.*, **14**, 181–196 (1908).
4. F. Haber, "The Production of Ammonia from Nitrogen and Hydrogen", *Naturwissenschaften*, **10**, 1041–1049 (1922).
5. H. T. Hall, "The Synthesis of Diamond", *J. Chem. Ed.*, **38**, 484–489 (1961).
6. R. Berman, "Thermal Properties", Chapter 1 from R. Berman, editor, *Physical Properties of Diamond*, Clarendon Press, Oxford, 1965.
7. H. M. Strong, "Early Diamond Making at General Electric", *Am. J. Phys.*, **57**, 794–802 (1989).
8. Figure 15.7 is reproduced with permission from R. H. Wentorf Jr., "Diamond Formation at High Pressures", taken from *Advances in High-Pressure Research, Vol. 4*, R. H. Wentorf, Jr., editor, Academic Press, London, 1974, pp. 249–281.
9. R. A. Robie, B. S. Hemingway, and J. R. Fisher, "Thermodynamic Properties of Minerals and Related Substances at 298.15 K and 1 bar (10^5 Pascals) Pressure and at Higher Temperatures", *U.S. Geol. Sur. V. Bull.*, **1452**, 456 pp. (1978).
10. D. K. Nordstrom and J. L. Munoz, *Geochemical Thermodynamics, Second Edition*, Blackwell Scientific Publications, Boston, 1994.
11. L. N. Plummer and E. Busenberg, "The Solubilities of Calcite, Aragonite, and Valerite in Carbon Dioxide–Water Solutions Between 0 and 90 °C, and an Evaluation of the Aqueous Model for the System Calcium Carbonate–Carbon Dioxide–Water", *Geochim. Cosmochim. Acta.*, **46**, 1011–1040 (1982).
12. The examples described are taken from Alexandra Navrotsky's Presidential Address given at the annual meeting of the Mineralogical Society of America, October 26, 1993, in Boston, Massachusetts. The address entitled "Repeating Patterns in Mineral Energetics", was published in *American Mineralogist*, **79**, 589–605 (1994). A second source is A. Navrotsky, "Thermodynamic Aspects of Inorganic Solid-State Chemistry", Ch. 10 of *Solid State Chemistry*, A. K. Cheetham and P. Day eds., Oxford Science Publications, 1988.
13. C. J. Pedersen, "Cyclic Polyethers and their Complexes with Metal Salts", *J. Am. Chem. Soc.*, **89**, 7017–7036 (1967).
14. The review articles summarizing the thermodynamics of cation–macrocycle complexes are: R. M. Izatt, J. S. Bradshaw, S. A. Nielsen, J. D. Lamb, and J. J. Christensen, "Thermodynamic and Kinetic Data for Cation–Macrocycle Interaction", *Chem. Rev.*, **85**, 271–339 (1985). R. M. Izatt, K. Pawlak, and J. S. Bradshaw, "Thermodynamic and Kinetic Data for Macrocycle Interaction with Cations and Anions", *Chem. Rev.*, **91**, 1721–2085 (1991).
15. R. M. Izatt, G. Wu, W. Jiang, and N. K. Dalley, "Interactions in Aqueous Solution at 25 °C of Palladium (II) and Mercury (II) with 1,4-Dithia-18-Crown-6 and 1,10-Dithia-18-Crown-6. A Thermodynamic, Spectral, and X-ray Crystallographic Study", *Inorg. Chem.*, **29**, 3828–3832 (1990).
16. See S. Ahrland, "Enthalpy and Entropy Changes by Formation of Different Types of Complexes", *Helv. Chim. Acta*, **50**, 306–318 (1967); and S. Ahrland, "Thermodynamics of Complex Formation Between Hard and Soft Acceptors and Donors", in *Structure and Bonding, Volume 5*, C. K. Jørgensen, J. B. Neilands, R. S. Nyholm, D. Reinen, and R. J. P. Williams, eds, Springer-Verlag, New York, 1968, pp. 118–149.
17. For a summary of the thermodynamic properties of BN, see: J. H. Edgar, "1.2 Crystal Structure, Mechanical Properties and Thermal Properties of BN", pp. 7–21; and V. L. Solozhenko, "2.1 Phase Diagram of BN", pp. 43–70; taken from J. H. Edgar, Editor, *Properties of Group III Nitrides*, INSPEC, 1994.

Chapter 16

Applications of Thermodynamics to Biological Processes

In this chapter, we continue the discussion begun in the last chapter of applying thermodynamics to chemical processes. We will focus our discussion here on two examples of biological interest. The principles are the same — all of our thermodynamic relationships work. But biochemists have their own vocabulary, and sometimes apply unique conditions to their systems. For example, as we shall see, unusual standard states are sometimes chosen. There is nothing wrong with this, since the choice of standard states is completely arbitrary as long as we keep track of what is done. Standard states are usually chosen in a way that makes the results most useful. That is true in this case.

Living cells undergo a variety of cyclic processes. An important part of metabolism is to generate the energy that drives these processes. This energy is converted into work, with heat as a byproduct. Cycles, heat, work, and energy are the framework upon which thermodynamics is built. Therefore, it should not be surprising that the study of biological systems from a thermodynamics perspective has yielded valuable insights into the forces that dictate the structures of organisms and the functioning of their various cellular components.

Initially, biologists were not convinced that the various processes associated with living organisms could be understood in terms of a series of chemical reactions. The tools to isolate and identify the chemical composition and structures of cellular components began to be developed near the end of the 19th century. Over the next few decades, the chemical structures of increasing numbers of biomolecules became known, and there came a growing acceptance that chemistry was associated with the functioning of cellular components.

We will focus our attention in this chapter on an overview of the thermodynamic analysis of metabolism and of the stabilities of two types of biomolecules, proteins and nucleic acids. Rather than provide a comprehensive account of thermodynamic applications to biological systems, we have chosen these two key areas where, historically, thermodynamic measurements have

provided important quantitative data that gave insights into fundamental biological processes. In the course of these discussions, we will also point out several conclusions about the nature of biological systems that arise from thermodynamic considerations.

16.1 Metabolism And Work

The study of metabolism is a study of energy; where does the energy to create complex biomolecules — lipids, proteins, and nucleic acids — come from? Where does the energy to enable a living organism to do mechanical work come from? How is energy stored in the cell and made available when and where it needs to be?

It is now well established that the formation and subsequent hydrolysis of certain kinds of phosphate bonds are fundamentally involved in this process. Before we consider the historical development from which this knowledge has evolved, let us think about some important implications drawn from the Second Law of Thermodynamics that give insights into the structure and performance of living organisms. From one of the classical statements of the Second Law of Thermodynamics, we find that heat cannot be used in an isothermal cyclic process to generate work. The Carnot analysis of heat engines showed that a temperature differential between two reservoirs is required to enable the engine to work. However, living cells are essentially isothermal. Thus, the heat generated in metabolic processes cannot be used to perform the work of the cells.

The Gibbs free energy change during a reaction is a measure of the reversible work (other than pressure–volume work) that can be obtained from the process at constant T and p. Since cellular processes are isothermal and isobaric, free energies are the quantities of choice in studying metabolic processes with respect to their ability to carry out the work of cells.

The free energy change associated with a reaction that occurs at constant temperature and pressure has significance in addition to its relationship to an ability to do work. Because living organisms are not closed systems, nor are they at equilibrium, the net process representing the sum of all the activities of the cell must be considered to be a spontaneous process. The sign of the free energy change for an isothermal, isobaric reaction allows us to determine the direction of spontaneity. A negative $\Delta_r G$ indicates a spontaneous process, while a positive $\Delta_r G$ indicates that spontaneity is achieved in the reverse direction.

Consideration of many individual biologically important reactions with respect to their $\Delta_r G$ shows that the direction in which the reaction is observed to go is not what is predicted by thermodynamics when only the one reaction is considered. In general, anabolic processes in which complex biomolecules are synthesized *in situ* from simpler substrate molecules have $\Delta_r G$ values that are

positive. For example, the synthesis of proteins from a series of amino acids is not a spontaneous process. It requires free energy. (Biochemists use the term ***exergonic*** and ***endergonic*** to represent reactions that have a negative $\Delta_r G$ or a positive $\Delta_r G$, respectively.)

As we have seen in mechanical and purely chemical systems, the requirement for spontaneity must be met in a global sense.[a] Individual endergonic reactions can take place as long as some other process associated with them is more strongly exergonic so that $\Delta_r G$ for the total process is negative. Biologists speak of a ***coupling*** between endergonic reactions and the more strongly exergonic reactions that "drive" them.

Respiration and ***fermentation*** are two complex biological processes whose net $\Delta_r G°$ values are negative and thus both represent spontaneous processes that can provide energy for cells to do work. Respiration is the reaction of glucose with O_2 to form CO_2 and H_2O. The net reaction can be represented as

$$C_6H_{12}O_6(aq) + 6O_2(g) = 6CO_2(g) + 6H_2O(l), \tag{16.1}$$

and thermochemical and thermophysical measurements (e.g. combustion, solution, and adiabatic heat capacity calorimetric measurements) yield a value of $-686\ kJ \cdot mol^{-1}$ of glucose for $\Delta_r G°$ under the conventions summarized in Chapter 11 for the various thermodynamic standard states.[b] The magnitude of $\Delta_r G°$ and its negative sign indicates that the process is spontaneous with a large driving force; hence its usefulness to cells looking for an energy source.

---

[a] Earlier, when we had only the entropy as a criterion for spontaneity, we saw an example of what is meant here by the term "global sense". The freezing of liquid water at temperatures below 273.15 K occurs with a negative entropy change, but the overall ΔS ($\Delta S_{universe}$) is positive when the effect of the process on the surroundings is included. The free energy was developed to allow us to predict spontaneity without needing information about the surroundings, but the principle of a net process governing spontaneity is the same.

[b] A word should be said here about the standard state conventions adopted by those who work in biological systems. For pure solids and liquids, the pure substances under 1 bar (often 1 atm instead) pressure are assigned unit activities. Because most biological systems are considered to be dilute aqueous solutions, the activity of water is usually taken as 1, and the activity of solute species are approximated by their concentrations (usually molarities), except for the activity of the proton. Thus, unit activity is taken as a 1 molar solution for solutes other than H^+. A unit activity for the proton ion concentration is taken to occur at pH = 7, a value close to the physiologically-observed concentration. The standard state reaction can be summarized as one in which the pH is 7, and all other solute species are present at 1 molar concentrations. To distinguish between this definition and the more formal definition in terms of hypothetical solutions that follow Henry's law, biothermodynamicists use the symbol, $\Delta_r G°'$ where the ' indicates the different convention with respect to pH. Occasionally in specialized problems, other standard states may be useful, so that it is important to understand what conventions have been adopted when comparing thermodynamic values from various sources.

Fermentation occurs in both mammals and anaerobic organisms under conditions where oxygen is absent. In this process, a molecule of glucose, a six-carbon sugar, can be converted into two molecules of lactate acid, each containing three carbons. The net reaction

$$C_6H_{12}O_6(aq) = 2CH_3CHOHCOOH(aq) \tag{16.2}$$

has a $\Delta G°$ of -197 kJ·mol^{-1} of glucose under the conventional (nonbiological) standard state conditions.

Some of the free energy released in respiration and fermentation is used to generate "high-energy" molecules. These molecules store the excess free energy by using it to form anhydride bonds involving phosphate groups. These bonds can be hydrolyzed at some later stage to provide free energy to an endergonic process. Perhaps the most important of the high-energy molecules[c] associated with reactions involving mechanical and electrical work output of the cells is adenosine triphosphate, ATP, whose structure is shown in Figure 16.1. The hydrolysis of ATP to give adenosine diphosphate (ADP) and a phosphate ion, often referred to as inorganic phosphate and designated as P_i, is an exergonic reaction that fuels many endergonic biological processes. In fact, the use of this hydrolysis reaction to power biological processes is so ubiquitous that ATP is often referred to as the free-energy currency of the cell.

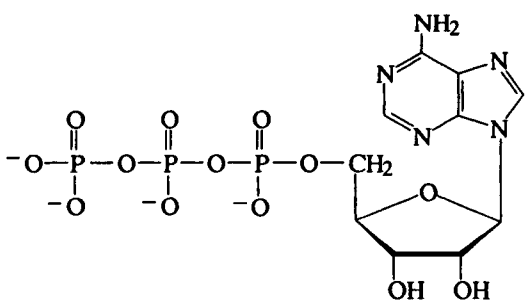

Figure 16.1 The structure of adenosine triphosphate (ATP). The lower ring is a ribose sugar, the upper molecule is the base, adenine. Adenosine diphosphate (ADP) differs from ATP by having two phosphate groups attached instead of three.

[c] Biological systems have evolved over time to utilize other nucleoside (ribose sugar plus cyclic nitrogen-containing bases) triphosphates in the synthetic aspects of metabolism. For example, the triphosphates of guanosine, cytidine and uridine are associated with the synthesis of proteins, lipids, and carbohydrates, respectively.

Glycolysis is the name given to the first segment of the fermentation process in which glucose is converted into two molecules of pyruvic acid. The pyruvic acid molecules generated in gylcolysis can be consumed in the remaining steps of fermentation to yield lactic acid, or be used in other metabolic or synthetic pathways. The steps in the glycolytic pathway illustrate the various strategies employed in biological systems to satisfy thermodynamic constraints on free energy. This pathway contains steps that are strongly exergonic, ones that are endergonic and must be coupled enzymatically with exergonic processes, as well as ones in which the $\Delta_r G°$ is small and positive. For these steps, where the system is near equilibrium at all times, the direction of spontaneity can be altered by changes in the relative activities of reactants and products since, as shown in equation (11.101),

$$\Delta_r G = \Delta_r G° + RT \ln \prod_i a_i^{\nu_i}, \tag{16.3}$$

where the a_i values are the activities and the ν_i values are the stoichiometric factors. In such steps, the activities can be altered by selective binding to enzymes, or through concentration fluctuations that arise from demands of the system. We will detail key steps in the glycolytic pathway to illustrate the variety of ways in which the biological system meets the requirement for negative $\Delta_r G$.

Step 1. Phosphorylation of Glucose The initial reaction in the glycolytic pathway can be represented by the following reaction:

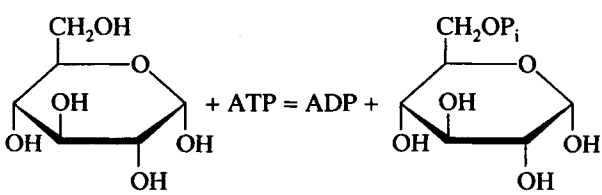

(16.4)

It actually arises from two parts. The first is a phosphorylation (addition of phosphate, P_i) of glucose at the carbon-6 position (top carbon shown above):

$$\text{glucose} + P_i = \text{glucose-6-phosphate} + \text{water}. \tag{16.5}$$

The second is the hydrolysis of ATP to regenerate phosphate:

$$ATP + H_2O = ADP + P_i. \tag{16.6}$$

The glucose phosphorylation reaction (16.5) has a large positive $\Delta_r G°'$ of 13.8 $kJ \cdot mol^{-1}$ of glucose. This $\Delta_r G°'$ is large enough that the relative

concentrations of glucose and glucose-6-phosphate would have to differ by more than a factor of 1000 (e.g. concentrations of glucose $\sim 10^{-1}$ M and glucose-6-phosphate $\sim 10^{-4}$ M) in order to make the reaction spontaneous. Instead, reaction (16.5) is driven by an enzymatic coupling to the hydrolysis of ATP {reaction (16.6)}, whose more negative $\Delta_r G°'$ of hydrolysis (-31 kJ·mol^{-1} of ATP), yields a net $\Delta_r G°'$ of -17.2 kJ·mol^{-1}. The coupling occurs via the formation of a complex in which glucose and ATP are bound to an enzyme, hexokinase.

It is instructive to consider how structural aspects of the enzyme–substrate binding produce thermodynamic conditions that drive the reaction to completion. As we have noted, the $\Delta_r G°'$ for the glucose phosphorylation reaction (16.5) is quite positive, and the relative activities (concentrations) of the reactant (a_G) and product (a_{G6P}) glucose species needed to make $\Delta_r G$ negative are not observed physiologically. However, the activities of the phosphate ion (a_{P_i}) and water (a_{H_2O}) also enter into the determination of the actual $\Delta_r G$ as given by the equation

$$\Delta_r G = \Delta_r G° + RT \ln \frac{a_{G6P} a_{H_2O}}{a_G a_{P_i}}. \tag{16.7}$$

Decreasing the a_{H_2O} and increasing the a_{P_i} tends to drive the reaction in the forward direction. Lowering a_{H_2O} also has the effect of reducing the tendency of the ATP hydrolysis to proceed independently.

These changes in the relative activities are brought about in the enzyme–glucose–ATP complex. When glucose binds to the hexokinase, a conformational change occurs in the enzyme. The structural rearrangement causes parts of the enzyme to close in around the binding site, with the result that water is excluded from the vicinity of the bound glucose molecule. The conformational change also increases the affinity of ATP binding for a second site on hexokinase. Once bound, the terminal phosphate group of the ATP is in an excellent orientation for the phosphoryl transfer to take place directly to the hydroxyl on the glucose. Since water, the thermodynamically favored recipient of the ATP phosphate group, is excluded from the active sites, the phosphoryl transfer to the glucose hydroxyl is an acceptable alternative.

Step 2. The Isomerization of Glucose-6-Phosphate into Fructose-6-Phosphate: The reaction is

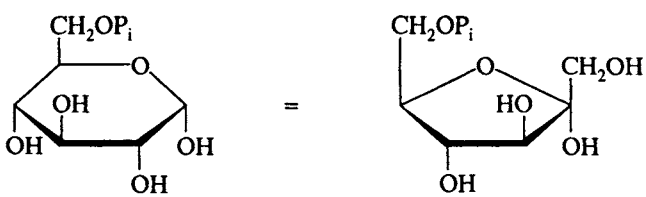

(16.8)

It has a relatively small positive standard free energy change of $+1.7\ \text{kJ}\cdot\text{mol}^{-1}$, but the $\Delta_r G$ can be made negative by small changes in the activities of the reactant and product species. These changes are accomplished through the differential binding affinities of the two isomers to the enzyme.

How a preferential binding of a reactant species over a product species affects the thermodynamic activities is influenced by the nature of the reaction. For reactions that occur on the surface of the enzyme, the preferential binding of reactant species causes its activity to be increased relative to that of the product and the conversion to products on the binding surface is favored. When the reaction takes place in the bulk solution, a preferential binding of the reactant species to the surface lowers its activity relative to that of the product, and the reverse reaction becomes favored. The hexakinase–glucose–ATP reaction is an example of the first type.

Step 3. Phosphorylation of Fructose-6-Phosphate: The reaction is

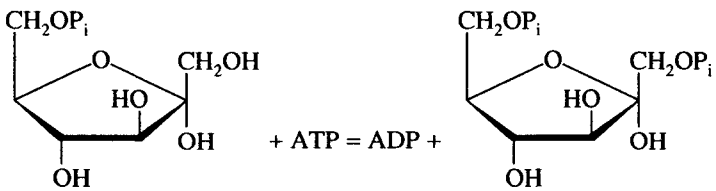

(16.9)

In vitro,[d] an uncoupled phosphorylation of fructose-6-phosphate to form the fructose-1,6-bisphosphate has a positive $\Delta_r G°'$, but *in vivo*, it is coupled with the ATP–ADP hydrolysis through the enzyme, phosphofructokinase, to yield an overall negative reaction free energy.

Step 4. Cleavage of Fructose-1,6-Bisphosphate into Three-Carbon Phosphates: The reaction is

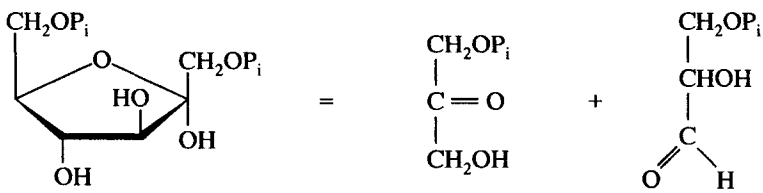

(16.10)

[d] "In vitro" is a term used by biochemists indicating a reaction that takes place in an artificial environment. Conversely, 'in vivo' indicates that the reaction takes place in a living cell or organism.

The cleavage, which yields two three-carbon fragments, one a ketone and the other an aldehyde, has a very large positive $\Delta_r G°'$. Unlike the two previous examples that had large positive $\Delta_r G°'$, this one is not coupled with an exergonic reaction. Rather, it proceeds in the forward direction because the products are removed continuously in the next steps of the pathway so that their concentrations are kept exceedingly small. One product, dihydroxyacetone phosphate, is readily converted into the other, glyceraldehyde-3-phosphate, through a rapid, reversible process in which $\Delta_r G \approx 0$. The equilibrium actually favors the dihydroxyacetone phosphate, but the glyceraldehyde-3-phosphate is removed quickly in subsequent steps so that the reaction is pulled to the direction of aldehyde formation.

Step 5. Oxidative Phosphorylation of Glyceraldehyde-3-Phosphate: There are two aspects to this process: (a) the oxidation and subsequent phosphorylation of glyceraldehyde-3-phosphate (G3P) to 1,3-bisphosphoglycerate (1,3-BGP), and (b) the reduction of nicotinamide adenine dinucleotide (NAD^+) to its reduced form designated as NADH. The net reaction can be written as

$$\text{glyceraldehyde-3-phosphate} + P_i + NAD^+ = \text{1,3-bisphosphoglycerate} + NADH + H^+. \quad (16.11)$$

Inspection of the three-carbon reactant (G3P) and product species (1,3-BGP) given below shows that the phosphate group is present in the reactant, G3P, as an ester of an alcoholic oxygen, while in the product, 1,3-BGP, it is involved in an anhydride linkage with an acyl group.

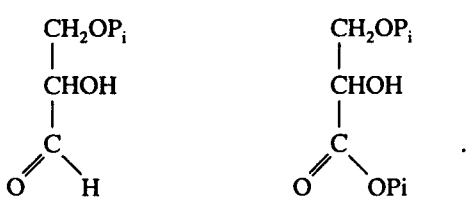

G3P 1,3-BGP

The acyl-phosphate linkage in 1,3-BGP is an example of a high-energy bond of the type found in ATP. Its formation is a free-energy requiring step, but its hydrolysis in a later step will be free-energy releasing. The required free energy for the formation comes from the oxidation of the aldehyde to the carboxylate by the NAD^+/NADH redox couple.

The oxidation and reduction steps are coupled through the binding of G3P to a sulfhydryl group on an enzyme that already has bound a NAD^+ molecule. The enzyme facilitates a H^- (hydride ion) shift from G3P to reduce the NAD^+ to NADH. The oxidation of G3P results in the formation of a high-energy thioester bond that is subsequently replaced by an orthophosphate group to yield the 1,3-BGP.

In later steps, the high-energy acyl phosphate group is transferred to ADP to regenerate one molecule of ATP. This process is made possible because the free energy stored in the acyl-phosphate group of 1,3-BGP is larger than that needed to form the anhydride phosphate bond in ATP. In still later steps, an even higher free-energy phosphate bond is formed in the generation of phosphoenolpyruvate. A second ATP molecule is generated from a coupled phosphoryl transfer as the phosphoenolpyruvate is converted into pyruvate. The reaction is

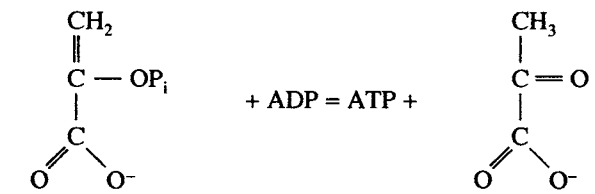

Phosphoenol-pyruvate Pyruvate (16.12)

Because one glucose molecule yields two three-carbon fragments, each of which goes on to become pyruvate, there is a net synthesis of two ATP molecules for each glucose molecule consumed.

The steps of this pathway illustrate some of the key roles that enzymes play in improving the thermodynamic favorability of processes. The conformational change in hexokinase upon binding of glucose closes up the environment around the glucose molecule and brings the reactive portion of the molecule in close vicinity to the terminal phosphate group of a bound ATP, thereby altering the activities of water and phosphate relative to glucose and tipping the balance in favor of phosphorylation. In a later stage, an enzyme couples the oxidation of glyceraldehyde-3-phosphate with the reduction of NAD^+ and stores the free energy released in the spontaneous process through the formation of a thioester linkage that is ultimately replaced by the formation of another high-energy phosphate bond. As we will detail next, enzymes also provide the coupling to convert this stored free energy into mechanical work.

Living organisms use the energy generated in metabolic processes like glycolysis to perform many kinds of work, including chemical, electrical and mechanical, that are essential to the growth and sustenance of the organism. Cells perform chemical work in the biosynthesis of complex molecules like

lipids, proteins and nucleic acids. Mitochondria do electrical work to bring about electron transfers in various redox reactions, while muscle cells generate mechanical work to cause the contractions and relaxations that drive motion within the organism. In order to better understand this last process, we will take a short excursion in our treatment of the energetics of metabolism to consider the mechanism by which muscle cells perform mechanical work.

Heat and work can be distinguished in terms of random molecular motion versus directed or coordinated motion. In muscle cells, from organisms as simple as yeast to those as complex as humans, the hydrolysis of ATP provides the driving force for the interactions and conformation of two cellular proteins, myosin and actin. Conformational changes associated with the binding and release of ATP and ADP provide the means by which a coordinated movement of these muscle cells is possible to do mechanical work.

A longitudinal section of a muscle cell is illustrated in Figure 16.2a along with the labels that have been attached to its characteristic features. A schematic

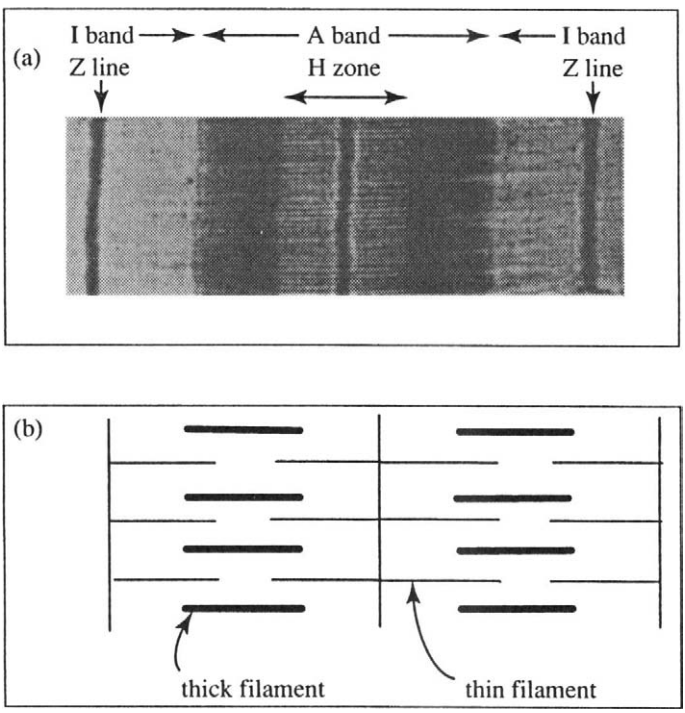

Figure 16.2 (a) An electron micrograph of a longitudinal section of a striated muscle cell and (b) a schematic drawing of the structures observed within the cell. From *Biochemistry*, 4th Edition, by Stryer, pp 392 and 393. © 1995, 1988, 1981, and 1975, by W. H. Freeman and Company.

representation of the structure is shown in Figure 16.2b. There are two kinds of interpenetrating protein filaments observable in the structure. A cross-section of the cell shows that one of the filaments has a diameter of about 15 nm while the other has a diameter of about 9 nm. Not surprisingly, these are referred to as the *thick* and *thin* filaments, respectively. The thick filaments are primarily myosin while the thin filaments contain primarily actin.

Myosin is a large protein composed of two heavy chains and two pairs of lighter chains. Its structure is represented schematically in Figure 16.3. The two heavy chains are aligned in a parallel sense. At the amino terminus ends of these

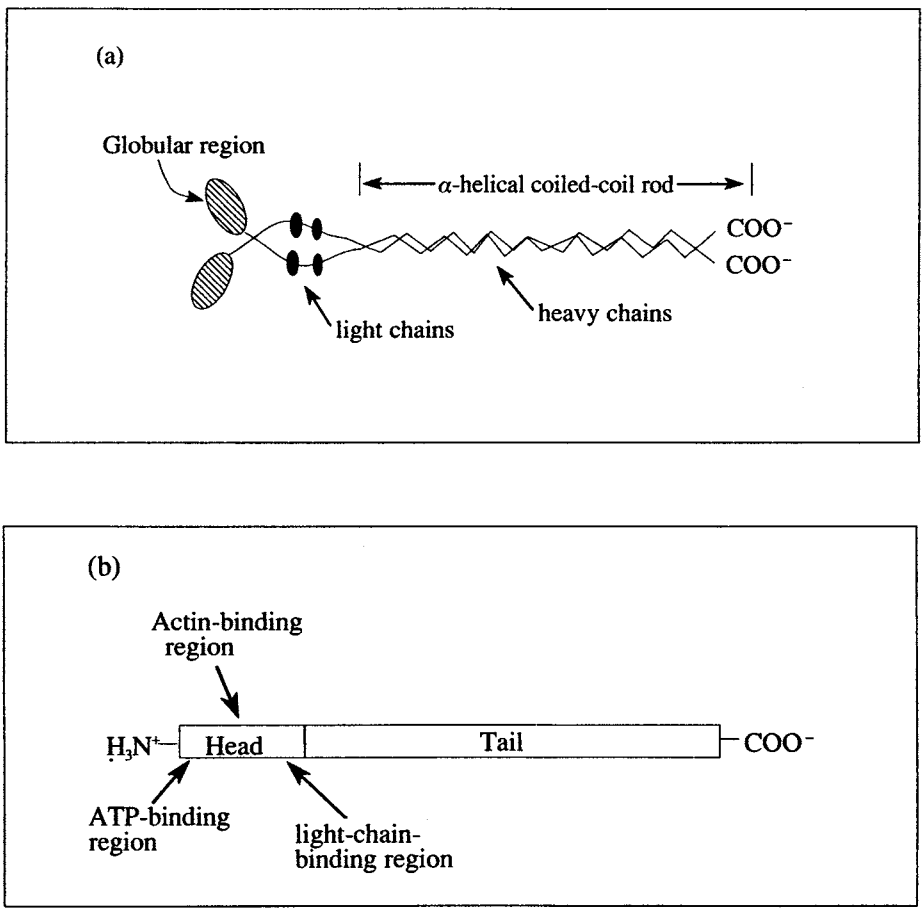

Figure 16.3 A schematic of the myosin protein. (a) Representation of the different structural regions in the myosin and (b) a representation of the localities where the various activities of the enzyme are found. From *Biochemistry*, 4th Edition, by Stryer, p. 395. © 1995, 1988, 1981, and 1975, by Lubert Stryer. Used with permission by W. H. Freeman and Company.

chains are found globular regions referred to as the "head" of the protein, while the 170 nm tail is a two-stranded coil of α-helices that form a rod. A regularly-repeating structure of seven-residue units permits the two α-helices to interact. Two light chains wrap themselves around a segment near the head–tail intersection, and the region near the amino end of the head is found to exhibit the ATP hydrolysis activity. The light chains serve a regulatory function associated with phosphate binding.

Actin is a protein that polymerizes at physiologic ionic strength levels into thin filaments. The monomers in actin are oriented to one another by a rotation of 166° and a translation of 275 nm. This gives an assembly that resembles a double-stranded string of beads.

Myosin and actin interact through the formation of crossbridges extending at regular intervals from the myosin to the actin. These crossbridges are formed and broken during a cyclic process that consists of (a), the binding of ATP by the myosin head groups; (b), hydrolysis of ATP; (c), binding of actin and ejection of P_i; (d), release of ADP; and (e), the rebinding of new ATP to restart the cycle. Conformational changes in the myosin head group during the complexation of ATP, binding of actin, and release of ADP and P_i are responsible for the sliding of the thick and thin filaments past one another. This cycle is represented in Figure 16.4. The steps are as follows:

(A) In resting muscle, ATP has been bound to myosin, then hydrolyzed to ADP and P_i.
(B) The hydrolysis products remain bound to myosin, and actin is prevented from binding due to the action of one of the light-chain proteins called tropomyosin, which is bound around the myosin. When muscle is stimulated, tropomyosin shifts position, the phosphate group is released, and the head groups on myosin can now reach out to form crossbridges with actin monomers.
(C) The binding of actin lowers the affinity of myosin for the bound ADP so that it can now be released. A conformational change in the head group of myosin occurs prior to the release of the ADP and alters the relative orientation of the actin and myosin head group. Because the actin is tightly bound to the myosin head group, the conformational change that snaps the myosin head group around moves the bound actin by about 10 nm. This step is often referred to as the power stroke. ADP is released at the end of this step.
(D) ATP is bound again to the myosin, and actin is rapidly released by the breaking of the cross-bridge.
(E) The bound ATP is hydrolyzed to await the next stimulation signal.

The overall effect is that the conformational change in myosin and the attendant motion of the actin, when coordinated through many cells, gets amplified to move organisms on a macroscopic scale.

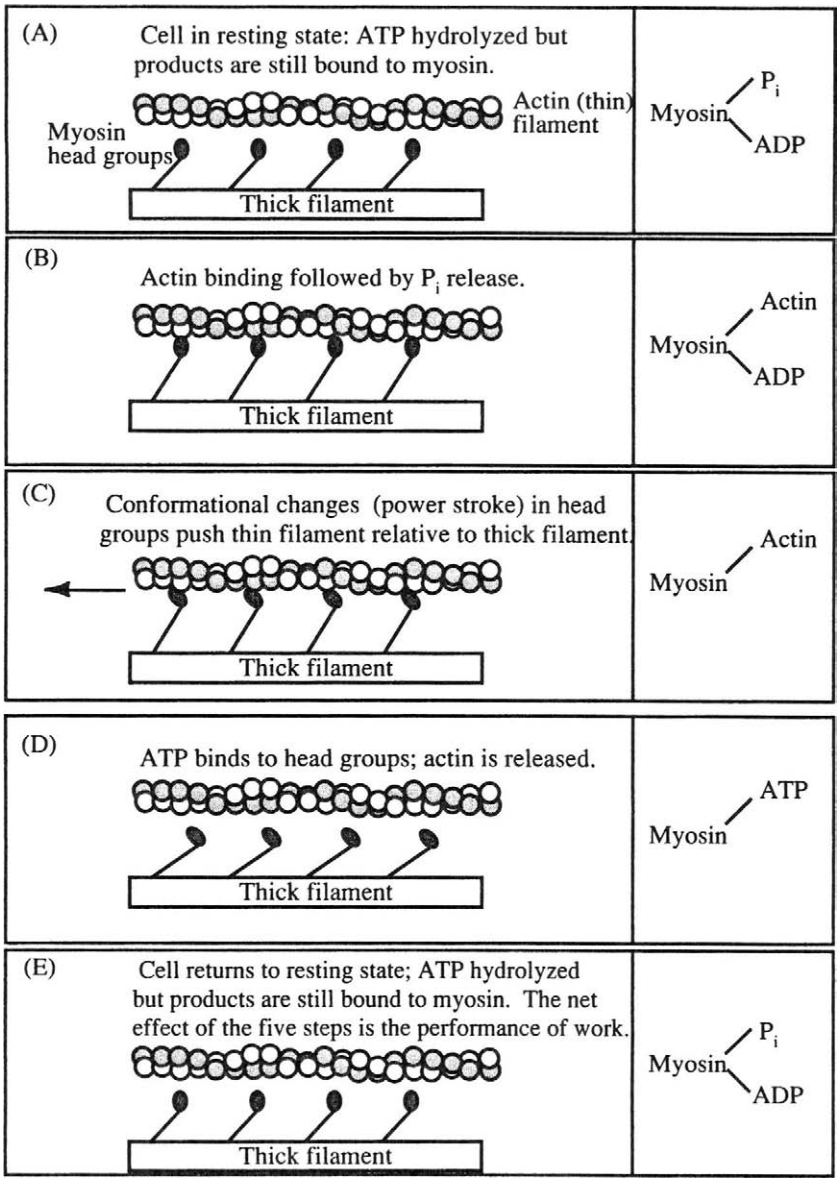

Figure 16.4 Schematic representation of the stages in muscle contraction. The box on the right indicates the species bound to the myosin at each stage of the cycle. From *Biochemistry*, 4th Edition, by Stryer, p. 399. © 1995, 1988, 1981, and 1975 by Lubert Stryer. Used with permission by W. H. Freeman and Company.

As long as the products of ATP hydrolysis remain bound to myosin, the free energy released from the hydrolysis (31 $kJ \cdot mol^{-1}$ at standard biological conditions) remains stored, essentially intact, within the protein. Upon the release of P_i, energy is made available to effect the conformational change that provides the motion.

When the cell is activated for a long period of time, the relatively small supply of ATP present in the muscle cell may be depleted. A reservoir of another phosphorylated compound, phosphocreatine, capable of transferring its phosphoryl compound to ADP, is available to replenish the ATP supply. The reaction is

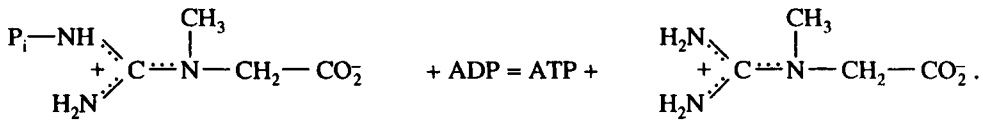

(16.13)

Using some clever experimental designs, investigators[1] have recently measured the average distance traveled by a single myosin molecule and the average force it exerts on a bound actin molecule during the power stroke of a cycle in which one ATP molecule is hydrolyzed. The distance was found to be 11 nm, and the average force measured as 4 pN. A differential quantity of work, δw, can be calculated as

$$\delta w = f\,dx$$

where f is the net force and dx is the distance over which the force is acting. From the force and distance values measured in these experiments, we can calculate that about 4×10^{-20} J of work are performed on a myosin molecule during the power stroke. This corresponds to about 26 $kJ \cdot mol^{-1}$ of myosin molecules, a value that is well within the range released by the hydrolysis (31 $kJ \cdot mol^{-1}$ of ATP under standard conditions).

16.1a Historical Perspective on Metabolic Energy and the Thermodynamics of Phosphate Compounds

We have seen instances in the various biochemical examples that we have cited of a close coupling between an exergonic and an endergonic process. The need for such couplings to account for the observed appearances of the products of endergonic processes (for example, the synthesis of complex biological molecules from simple ones) was recognized for some time before the details

were understood. Various coupling mechanisms were suggested but none proved satisfactory until Fritz Lipmann proposed the transfer of phosphoryl units between compounds. Given the current recognition that phosphorylation and dephosphorylation reactions are essential processes of metabolic energetics, it is perhaps surprising to learn that phosphorylation processes were initially regarded as a minor aspect, or even aberrant side effect, of *in vitro* experiments. A later hypothesis was proposed that phosphate bonds were introduced into compounds merely to facilitate their decomposition. However, as more and more phosphorylation reactions were observed in diverse processes associated with metabolism, the recognition that they must play some significant role grew.

Lipmann published a paper[2] in 1941 in which he argued that the anhydride or acyl phosphate bond might, in fact, be a "carrier" or storage repository of free energy. He arrived at this hypothesis in a manner that illustrates the benefits of having a wide variety of scientific experiences. His early training was as a physician at a time that biochemistry was not an integral part of a medical education. He became interested in biochemistry while completing a fellowship in pharmacology, and he pursued graduate work in this area, but in a laboratory with a strong biological approach. In this laboratory, that of Carl Meyerhoff, he began to study phosphate chemistry and glycolysis. Fortuitously, also ongoing in this laboratory were the calorimetric measurements that established the unusual energetics of phosphate hydrolysis in compounds like phosphocreatine. Lipmann pursued additional studies with problems associated with phosphorylated proteins. He investigated metabolic processes in various tissue cultures and dabbled in a myriad of other biological areas in laboratories around the world. He brought much of this background to bear as he assembled information obtained from a wide range of physiological experiments concerned with metabolic processes. He noticed the association of one or another phosphorylated compound with each of these processes. When he tabulated standard free energies for the hydrolysis reactions of these compounds, he observed that they fell into two main groups as shown in Table 16.1.[e] Simple esters of alcoholic hydrogens, such as the glucose- and fructose-6-phosphates found in the early stages of the glycolytic pathway, exhibited relatively small negative free energies, while those associated with acyl groups or anhydride linkages were considerably more negative. The free energy of hydrolysis of ATP to either ADP or AMP (adenosine monophosphate) resulted in a $\Delta_r G°'$ that was in the middle of the two main groups.

[e] Note that these are free energies using the biological standard state. That is, the activity of H^+ is 1 at pH = 7, the activity of liquid water is taken as 1, and activities of other species are approximated by their molar concentrations.

Table 16.1 The free energies of hydrolysis of phosphate compounds at 298.15 K

Compound/process	Structure	$\Delta_r G°'$(kJ·mol^{-1})
Phosphoenolpyruvic acid	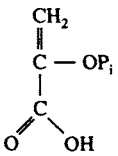	−61.9
1,3-Bisphosphoglycerate	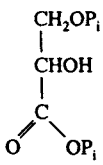	−49.4
Phosphocreatine	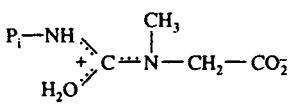	−45.2
Acetyl phosphate	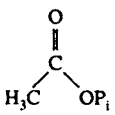	−43.1
PP_i	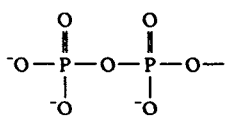	−33.5
$ATP \rightarrow AMP + PP_i$		−32.2
$ATP \rightarrow ADP + P_i$		−30.5
Glucose-1-phosphate	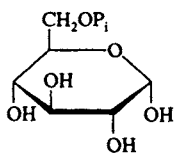	−20.9
Fructose-6-phosphate	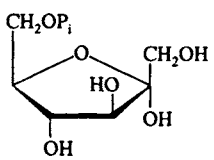	−13.8
Glucose-6-phosphate	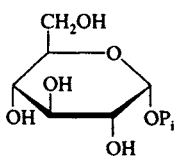	−13.8

Lipmann recognized that the ordering based upon the free energy of hydrolysis provided information similar to that given by the oxidation (or reduction) potential for the transfer of electrons. He coined the term "group potential" as a measure of the tendency of the phosphate groups to be transferred from one species to another. Compounds with a higher group potential (more negative Gibbs free energy of hydrolysis) could transfer a phosphate group to one below it in a spontaneous process. Examples of this behavior are found in both the glycolytic pathway and the process of muscle contraction. ATP donates a phosphate group to molecules in the initial stages of glycolysis, but then ADP is phosphorylated by phosphoenolpyruvate at the end of the pathway. Phosphocreatine is able to phosphorylate ADP in muscle cells when ATP stores are low.

From a perspective of group potentials, Lipmann was able to see that phosphoryl transfers among compounds belonging to the same class provided a mechanism to preserve and store free energy. He also recognized that these high-energy transfer processes constituted a mechanism by which nonspontaneous reactions could be coupled to spontaneous ones. The degradation of a substrate proceeds by way of reactions in which part of the free-energy change is retained in these acyl or anhydride phosphate bonds. For example, some of the energy made available from the oxidation of glucose becomes incorporated in the high-energy phosphoenolpyruvate molecule.

The middle position that the ATP/ADP couple occupies in the potential ranking explains why it is so useful in cellular metabolism. There are numerous compounds lower on the potential scale to which the transfer of P_i represents a spontaneous process, and yet there are also a few cellular compounds with higher potentials that can in turn phosphorylate ADP to regenerate ATP.

Herman Kalckar, also credited with significant discoveries leading to the acceptance of the significance of phosphorylation in metabolism and energy transfer, describes Lipmann[3] in a "*festschrift*" issue as "preaching the gospel of phosphorylation." Kalckar[f] says that Lipmann recognized the need to express

---

[f] Kalckar himself spent a year at Cal Tech in "the orbit of the great G. N. Lewis school of thermodynamics" where he was careful to stay away from "frivolous" thermodynamic expressions. He 'volunteered for Hugh Huffman's so-called "crematory" where one was supposed to obtain the ΔH of combustion of benzoic acid or naphthalene ... with a precision within 8 decimal places.' Kalckar says that he was unable to get farther than six places and was never "advanced to the point of doing Huffman's elegant heat capacity measurements." He attributes his education in the Cal Tech "crematorium" with his ability to follow Lipmann's analysis of the relative energetics of the phosphate bond in phosphopyruvate and phosphoglycerate.

Hugh Huffman left Cal Tech during the Second World War and was an important scientist at a national laboratory set up to provide technical information to support the war effort. He left a legacy of high precision experimental techniques that yielded high-quality thermodynamic data on a wide variety of substances, including simple biological molecules.

this gospel in a clever language that avoided the "purity and austerity of classic thermodynamics" if he was going to get it accepted.

As part of this effort, Lipmann introduced the "squiggle" notation, ~P and used the terms "bond energy" and "high-energy bonds" to represent the amount of potential energy that could be stored in these bonds. In his book, *Wanderings of a Biochemist*, he says,

> *My paper caused a stir when it appeared, although at first it was given what one might call a mixed reception. The talk of energy-rich bonds aroused forceful, sometimes virulent antagonism. Unwittingly, I had stepped into a hornet's nest by using "bond energy" to express the potential energy derivable from a bond ... Many organic chemists were outraged by what they felt was a misuse of the term bond energy. This antagonism surprised me because I felt that organic synthesis as much as biosynthesis dealt largely with group activation and group transfer. I thought, therefore, that the new terminology I was forced to create should also have relevance to organic synthesis. It has made me happy recently to see the squiggle (~) ... creep into borderline organic literature. But the antagonism of the professional physiochemists still remains ...*[4]

He concludes this section of his reminiscing with an observation made by a good friend and colleague:

> *You always have to see that your union card is in good order.*

A perusal of current biochemistry texts suggests that the use of the squiggle has largely died out, but the concept of a group potential and the importance of these phosphate anhydride bonds in energy storage and transfer is universally accepted. Lipmann shared the Nobel Prize in Physiology/Medicine in 1953 with Hans Krebs of the Krebs (citric acid) cycle. His Nobel citation read in part,

> *Doctor Lipmann. You are a fighter. Your opponent, and everybody knows you have only one, is an impersonal opponent, namely the complexity of biochemical processes. Your keen wish to make things understandable and distinct has been rewarded in the form of a clear-cut and far-reaching discovery ... You have removed an obstructive confusion by the clear demonstration of a widespread reaction and have discovered simultaneously a new way for the transmission of energy in the cell.*[5]

16.2 Biopolymer Stabilities

Proteins and nucleic acids (e.g. DNA and RNA) are two classes of biopolymers that have been studied extensively by thermodynamic techniques. These two

classes of molecules share some significant characteristics. Both consist of a backbone made of small repetitive units with variations in the nature of the species that extend out from the backbone. They form three-dimensional structures that are essential to their biological function. Both types of molecules also undergo thermally-induced structural changes that significantly alter their three-dimensional structures and biological activity.

The factors that are responsible for the formation and stabilities of these structures are of great interest in order to create "designer" genes and proteins. From a more theoretical point of view, these molecules are interesting because they exhibit a regularity associated with the repeat of the peptide (protein) or the phosphate-pentose ester (nucleic acid) linkage that is typically associated with crystals, yet, unlike crystals, they are aperiodic. That is, the translational symmetry observed in a crystal is broken by the variation in the side chains of the protein or the bases along the nucleic acid. The extent to which regularity but not symmetry is responsible for the stabilization of these materials must be understood if scientists are to design new materials that improve upon the favorable properties of natural biopolymers.

The stabilization energetics associated with both types of molecules have been probed by looking at factors, including temperature, that disrupt their three-dimensional structures, but do not break the bonds that keep their primary structure intact. It is believed that much information about the nature of the forces that hold the molecule in its three-dimensional structure can be gained by understanding under what conditions these forces can be overcome.

In the simplest case, the thermally-induced structural change in the biopolymer can be represented as a change between two macrostates. The macrostates associated with the transition in proteins are represented in Figure 16.5a. The native structure is very compact, with portions of the protein winding around itself. As the temperature is increased, the molecule's thermal energy becomes large enough to overcome the forces holding it in its compact state, and the molecule opens up in a process referred to as unfolding. When this process occurs in enzymes, catalytic activity is lost, and the process is often referred to as **denaturation**. We will refer interchangeably to denaturation and unfolding when describing the process, although apparently there is still some question about the extent to which the protein completely unfolds in a thermal process.[g] In large complex proteins, the denaturation might be expected to take

[g] P. L. Privalov [P. L. Privalov, "Stability of Proteins — Small Globular Proteins", *Adv. Prot. Chem.*, **33**, 167–241 (1979)], whose work we will discuss later, makes a formal distinction between a denatured state and a completely unfolded state, but he suggests that the thermally denatured state is a good approximation to the completely unfolded state. This is apparently still a matter of some debate as discussed in O. B. Ptitsyn, 'Molten Globule and Protein Folding', *Adv. Prot. Chem.*, **47**, 83–230 (1995).

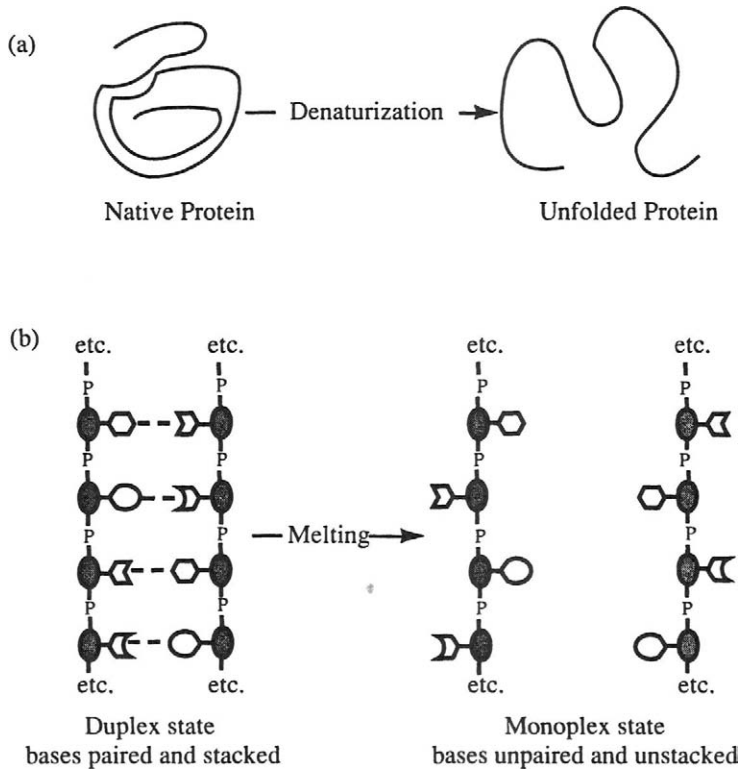

Figure 16.5 (a) The native folded state of the protein and the unfolded, denatured state following the thermally-induced structural change; (b) the duplex state of nucleic acids, stable at low temperatures, in which the bases are paired and stacked, and the monomer states following the thermal disruption in which the bases are unpaired and randomly arranged along the backbone.

place in multiple steps as various parts of the protein unfold separately. As we will see, thermodynamic measurements have provided direct evidence for multidomain unfolding and the degree of independence associated with melting in a given domain.

Nucleic acids exist in their normal state as paired strands. Hydrogen bonds formed between heterocyclic amine bases bonded to the phosphate-pentose backbone assist in the formation of the paired or duplex structure. There is a specificity in the pairing because of the structural capability to form hydrogen bonds only between adenine (A) and thymine (T) or uracil (U); and only between guanine (G) and cytosine (C). This specificity is illustrated in the duplex states shown in Figure 16.5b where the different shaped polygons represent the four different bases found in DNA, and their shapes suggest why AG or TC pairing would not be generally observed without perturbation of the duplex. In

the simplest case, increasing the temperature of a dilute solution of a nucleic acid disrupts its duplex structure by breaking the hydrogen bonds between base-pairs and generates two monoplexes.

In addition to the base-pairing disruption, this "melting" also destroys the stacking of bases in fixed orientations relative to one another that is observed in the duplex. Later, we will present an argument based upon thermodynamic measurements of the stabilities of synthetic ***oligonucleotides*** (small pieces of synthetic nucleic acids) that the next-nearest neighbor interactions observed in the base stacking sequence are a major contributor to the relative stabilities of duplexes.

Many of the same models and techniques have been used to study the transitions in these two types of biopolymers, and we will present some common background information first. Then we will specialize and present the results of important thermodynamic studies in proteins and nucleic acids separately. However, common to both reports is the observation that the application of thermodynamic measurements and a thermodynamic analysis to carefully but widely chosen systems allows one to gain insights into structural details that complement molecular structure determinations obtained from instrumental techniques such as spectroscopy and X-ray crystallography.

16.2a The Thermodynamics of the Two-State Model

Both the denaturation process in proteins and the melting transition (also referred to as the helix-to-coil transition) in nucleic acids have been modeled as a two-state transition, often referred to as the "all-or-none" or "cooperative" model. That is, the protein exists either in a completely folded or completely unfolded state, and the nucleic acid exists either as a fully ordered duplex or a fully dissociated monoplex. In both systems, the conformational flexibility, particularly in the high-temperature form, is great, so that numerous "microstates" associated with different conformers of the biopolymer are expected. However, the distinctions between the microstates are ignored and only the macrostates described earlier are considered. For small globular proteins and for some nucleic acid dissociation processes,[h] the equilibrium between the two states can be represented as

$$A = B \tag{16.14}$$

where A represents one macrostate and B the other. If α represents the fraction of molecules in the B state, then $1 - \alpha$ is the fraction in the A state. In the dilute

[h] The exact nature of the expression for the duplex–monoplex equilibrium in oligonucleotides depends upon the structure of the monomer strand(s) and the nature of the possible base-pairing that this structure permits. We will give some explicit examples shortly.

solution limit[i] where activities can be represented as molar concentrations c_A and c_B, the equilibrium constant K for the reaction is given by

$$K = \frac{c_B}{c_A} = \frac{\alpha}{1-\alpha}. \tag{16.15}$$

Many physical properties of the system vary monotonically as α goes from 0 to 1. Such properties include the NMR shifts of peak positions associated with different atoms in the molecule, the ultraviolet absorbance at particular wavelengths, and the enthalpy of transition. By monitoring the change in one or more of these properties, one can follow the evolution of α as the temperature changes, and obtain values for K. Equation (11.119) given in Chapter 11, which relates the temperature variation of the equilibrium constant for a reaction to the enthalpy change, can be solved for ΔH to obtain equation (16.16)

$$\Delta H_{\nu H} = RT^2 \left(\frac{\partial \ln K}{\partial T} \right)_p. \tag{16.16}$$

Biochemists often refer to enthalpies obtained in this manner as van't Hoff enthalpies[j] and attach the subscript νH to the ΔH to distinguish it from an enthalpy obtained directly from calorimetric measurements. In practice, one need not actually obtain the K values to extract the enthalpy change. Rather, there is a relationship between $d\alpha/dT$ and $d\ln K/dT$. For the equilibrium of equation (16.15) (at constant pressure so that the partial derivative can be replaced by the total derivative),

$$\frac{d \ln K}{dT} = \frac{1}{K} \frac{dK}{dT} = \frac{1-\alpha}{\alpha} \left[\frac{1}{1-\alpha} \frac{d\alpha}{dT} + \frac{\alpha}{(1-\alpha)^2} \frac{d\alpha}{dT} \right] = \frac{1}{\alpha(1-\alpha)} \frac{d\alpha}{dT}. \tag{16.17}$$

The expression for $d \ln K/dT$ developed in equation (16.17) can be substituted into equation (16.16) to obtain the enthalpy. The van't Hoff enthalpy is often

[i] Dilute solutions are used experimentally because one is interested in studying the intramolecular interactions responsible for the stabilization of the structure rather than any interactions between different molecules. Other factors, such as aggregation and reduced solubility of the protein in the denatured state, also make this the concentration region of choice.

[j] Other scientists sometimes refer to it as a "second-law" enthalpy.

obtained at a temperature, T_m, where $\alpha = 0.5$. Substitution of $\alpha = 0.5$ and the observed value of $d\alpha/dT$ at T_m into equation (16.17) yields the enthalpy for the process:

$$\Delta H_{\nu H} = 4RT_m^2 \left(\frac{d\alpha}{dT}\right)_{T=T_m} . \tag{16.18}$$

The magnitude of $(d\alpha/dT)$ at $T = T_m$ can be obtained as the slope of the tangent line to the curve of α vs T, drawn at the mid-point, $\alpha = 0.5$.

We use optical (spectroscopic) measurements below to illustrate the specific details of this method. Such measurements were the first source of information about these temperature-induced changes in biopolymer structure because of their great sensitivity and the ease with which they can be made. Later, as instrumentation and the techniques for protein and oligonucleotide synthesis improved, calorimetric experiments were designed to measure directly the enthalpy and heat capacity changes associated with these processes. Consideration of the agreement between the results obtained from the two types of measurements has yielded great insights into the details of the processes, as we will now see.

Optical Methods and the van't Hoff Enthalpy: The optical method relies upon the change in the UV absorption of both proteins and nucleic acids as the transformation from one molecular state to the other takes place. For example, the absorbance A at 260 nm of a solution containing a nucleic acid duplex is found to increase significantly from some baseline value as the duplex melts until it reaches a second baseline where the nucleic acid is completely melted.

The curve representing the change in UV absorption of a nucleic acid solution during the melting transition where we go from the double helix to coiled polymers is illustrated in Figure 16.6a. Such curves are often referred to as UV melting curves. If the change in absorption is linearly related to the change in the composition of the system from A to B, then α can be determined as a function of temperature by measuring the ratio $y/(x + y)$ at various stages in the process. A plot of α obtained in this manner against T is shown in Figure 16.6b. From this graph, one could calculate the values of K as a function of temperature and get a value for $\Delta H_{\nu H}$ at T_m.

Should the process take place with some number of intermediate steps, such as the unfolding of only part of the protein chain or an incomplete unzipping of the duplex, then the fractional change in the absorbance will not be linearly related to the composition of the mixture A + B. Under these circumstances, the melting curve is often broader and spread out over a larger temperature interval than would occur for the simple two-state process. The broadening leads to a

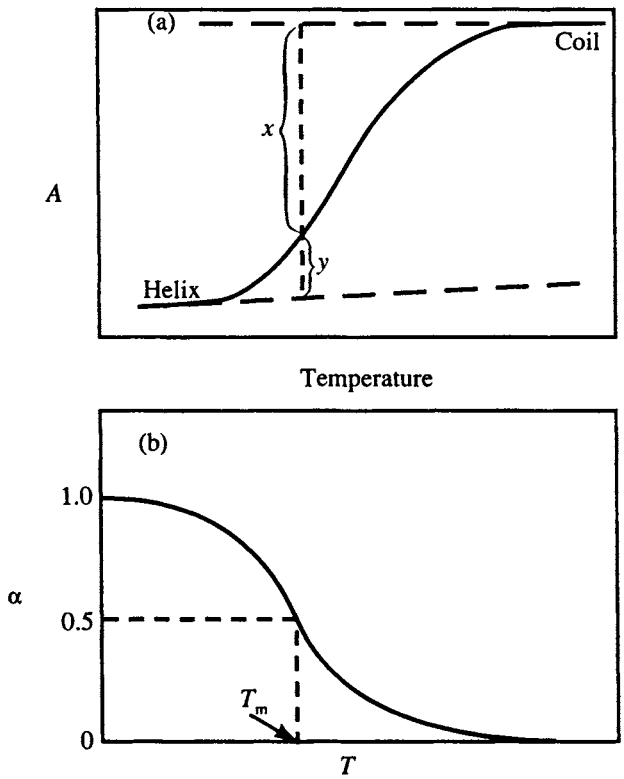

Figure 16.6 (a) The temperature-dependent change observed in the optical absorbance A (at $\lambda = 260$ nm) of a nucleic acid during its structural change, and the quantities, x and y used to calculate α from the curve; (b) the temperature-dependent change in α as the reaction proceeds. T_m is the temperature at which the mid-point of the reaction is observed.

lower value for the slope of the tangent at T_m, and thus yields a lower value of the van't Hoff enthalpy. Thus, a van't Hoff analysis of a multistate process gives erroneous results for ΔH_{vH}. Unfortunately, it is not generally possible to tell from the inspection of the α versus T plot whether the process occurs in two stages or in multistages.

The large UV absorptions of nucleic acids and proteins make the optical method a highly sensitive technique, and very small amounts of sample in very dilute solutions can be used. However, the selection of baselines between which the fractional change in absorption is evaluated must be made carefully to avoid error. The best agreement with values obtained from calorimetric measurements is observed when the slopes of both baselines are extended into the transition region, and the determination of x and y are made between the extrapolated lines as shown in Figure 16.6a.

Calorimetric Studies: For several reasons, the application of calorimetric techniques to the study of biopolymers developed at a time significantly after the establishment of the optical methods. The requirement that the experiments be conducted in dilute solutions meant that the heat effects associated with changes in a relatively few molecules were small, plus they had to be resolved against a large background heat capacity of the solvent. Also, significant sample volumes and sample sizes were required to achieve desirable signal to noise ratios. With the increase in electronics technology and the development of automated synthesizers for proteins and nucleic acids, both problems have eventually been overcome. The calorimetric experiments on biological systems to be described here have been performed using some variation of a differential scanning calorimeter. Reviews that provide additional experimental details, descriptions of other calorimetric techniques, and other applications to biological problems have been published.[6,7]

In the differential scanning calorimetric (DSC) technique, matched cells containing equal volumes of a dilute solution of the protein in a buffer (sample cell) and of the buffer alone (reference cell) are scanned through a controlled temperature program, and the differential power needed to keep the two cells at the same temperature is recorded. During an endothermic transition in the protein or nucleic acid, additional power must be supplied to the sample cell to maintain the same temperature as the reference cell. An example of the DSC output obtained from a solution of the protein lysozyme is shown in Figure 16.7. The line at zero differential power represents the electronic signal level that would be obtained if the two solutions had the same heat capacity. The DSC instrument can be calibrated to relate the differential power output to the excess heat capacity C_p^{excess} of the protein or nucleic acid solution, where

$$C_p^{\text{excess}} = C_p(\text{solute} + \text{buffer}) - C_p(\text{buffer}).$$

The result is shown in Figure 16.8. From these results, one can directly obtain the enthalpy of the transition. The procedure, like that for the analysis of the optical data, requires the estimation of a pre- and post-transitional baseline. For relatively short temperature intervals, the baselines are often assumed to be linear and are extrapolated to the mid-temperature as shown in Figure 16.8. The area under the curve in Figure 16.8 is the enthalpy of the transition. That is,

$$\Delta H = \int \Delta C_p \, dT,$$

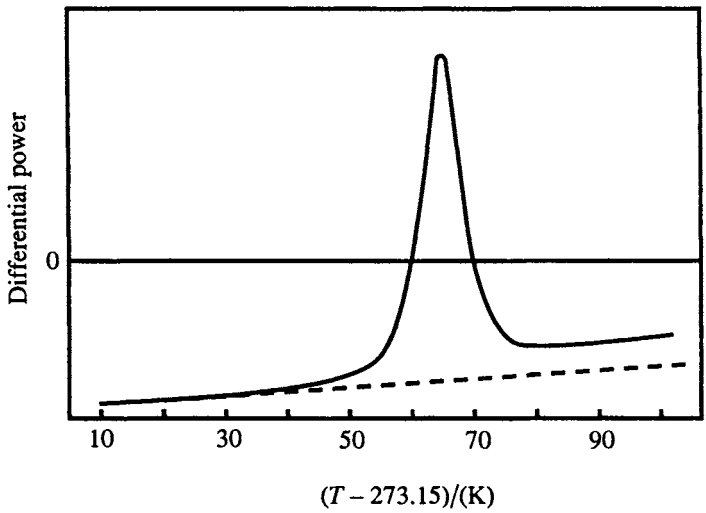

Figure 16.7 The differential power output obtained from a DSC containing a dilute buffered solution of lysozyme in the sample cell and the buffer in the reference cell during the denaturation process. Adapted from P. L. Privalov, *Adv. Prot. Chem.*, **33**, 179 (1979).

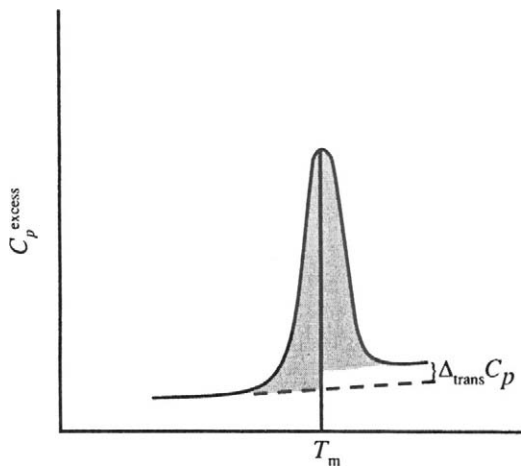

Figure 16.8 The excess heat capacity, $C_p^{excess} = C_p$ (protein + buffer) $- C_p$(buffer), as a function of temperature, obtained from a differential scanning calorimeter. The shaded area is intergrated to yield the enthalpy of the transition. $\Delta_{trans}C_p$ is the difference in the baseline heat capacity at T_m.

where $\Delta C_p(T)$ is the height of the segment between C_p^{excess} and the extrapolated baseline at temperature T. It is calculated as

$$\Delta C_p(T) = C_p^{\text{excess}}(T) - C_p^{\text{baseline}}(T).$$

The entropy of transition, ΔS can also be obtained directly from an integration of $\int (\Delta C_p/T)\, dT$. As shown in Figure 16.8, the calorimetric method also provides a direct measure of the change in the heat capacity, $\Delta_{\text{trans}} C_p$, of the two macrostates at T_m. That is

$$\Delta_{\text{trans}} C_p = C_p^{\text{excess}}(\text{high temperature state}) - C_p^{\text{excess}}(\text{low temperature state}).$$

With additional information, including the heat capacity of the buffer solvent, the partial specific volumes (volume per gram of the solute), and the specific volume of the solvent, one can extract the partial specific heat capacity ($J \cdot K^{-1} \cdot g^{-1}$) of the solute. Privalov has summarized these calculations.[8] Because the solutions are studied at very low concentrations, it is assumed that the contribution to the total heat capacity from the solvent cancels out when one calculates the excess heat capacity. With only minor exceptions, the procedures used to calculate parameters associated with the transformations in nucleic acids and in proteins are the same and yield quantities that are interpreted in similar ways, although researchers in these two fields may use a different notation for the same quantity.

16.2b Thermodynamic Studies of Protein Stabilities

Experimental studies of protein stabilities are numerous and there are still points of serious disagreement concerning the conclusions to be drawn from these studies. Areas of discord include the extent to which thermal denaturation corresponds to denaturation by chemical agents and the extent to which hydrophobic, van der Waals, and/or hydrogen bonds stabilize the native state. In this discussion, we will focus on the work of Peter L. Privalov.[k] Privalov has developed much of the microcalorimetric instrumentation that has made the calorimetric studies of proteins feasible. He has also published numerous review articles that summarize experimental data and formulate general observations concerning protein denaturation. His 1995 paper in *Advances in Protein Chemistry*[9] presents a recent, comprehensive, review of the experimental results

[k] P. L. Privalov is formerly of the Institute of Protein Research at the Academy of Sciences of the USSR. He is now a Professor of Biology at Johns Hopkins University.

available on many proteins. The preceding article by Lazaridis, Archontis, and Karplus in this same volume[10] presents the results of quantum and statistical mechanical calculations on models related to those developed by Privalov and his colleagues. Each paper contains an Epilogue in which the authors respond to the other's article. Taken together, they present an interesting perspective on the continuing dialogue concerning this important topic.

We will present only a brief description of Privalov's work here. We begin with the derivation of some additional techniques for the analysis of the calorimetric data that Privalov and others have developed and applied to the study of protein unfolding. We end with a summary of the observations and conclusions that have resulted from his work.

The Calorimetrically Obtained van't Hoff Enthalpy: In a manner analogous to that used to obtain the van't Hoff enthalpy from the fractional change in the optical absorbance, one can use the temperature dependence of the fractional enthalpy as a function of temperature to determine an "effective" enthalpy. We will adopt the notation $\Delta_N^D H$ to represent the total enthalpy associated with the denaturation transition. It can be obtained from an integration of the excess heat capacity, corrected for the baselines, as discussed before:

$$\Delta_N^D H = \int_{T_i}^{T_f} \Delta C_p \, dT$$

where T_i and T_f represent the initial and final temperatures over which the denaturation transition takes place. Then, we can define

$$\Delta H(T) = \int_{T_i}^{T} \Delta C_p \, dT$$

where $T_i \leqslant T \leqslant T_f$. Thus, $\Delta H(T)$ is the integrated enthalpy up to some temperature T while $\Delta_N^D H$ is the same integral taken over the entire temperature interval. If we define $\xi(T)$ by the relationship

$$\xi(T) = \Delta H(T)/\Delta_N^D H,$$

then $\xi(T)$ is a direct measure of the progress of the reaction, analogous to α obtained from optical measurements. If the reaction is a simple two-state process and the equilibrium is given by equation (16.14), one can show that a van't Hoff enthalpy can be obtained from the temperature dependence of ξ in a manner exactly analogous to the derivation of equation (16.17) from equation

(16.16) to yield

$$\Delta H_{\text{eff}} = \frac{RT^2}{\xi(1-\xi)} \frac{\mathrm{d}\xi}{\mathrm{d}T}, \tag{16.19}$$

where we use the notation, ΔH_{eff}, to represent the van't Hoff enthalpy obtained from the calorimetric measurements.

The calorimetric heat capacity measurements have an advantage over spectroscopic measurements in the application of equations (16.18) or (16.19). In the analysis of spectroscopic data, the temperature derivative must be determined numerically from a differentiation of the α versus T curve. The heat capacity measurements provide this derivative directly as we show below:

$$\frac{\mathrm{d}\xi}{\mathrm{d}T} = \frac{1}{\Delta_{\text{N}}^{\text{D}}H} \frac{\mathrm{d}\Delta H}{\mathrm{d}T} = \frac{\Delta C_p(T)}{\Delta_{\text{N}}^{\text{D}}H}. \tag{16.20}$$

Thus, the derivative can be evaluated at any temperature by dividing the baseline-corrected excess heat capacity, $\Delta C_p(T)$, by the integrated enthalpy $\Delta_{\text{N}}^{\text{D}}H$. By substituting this result into equation (16.19) one obtains

$$\Delta H_{\text{eff}}(T) = \frac{RT^2}{\xi(1-\xi)} \frac{\Delta C_p(T)}{\Delta_{\text{N}}^{\text{D}}H}. \tag{16.21}$$

For the specific temperature, T_{d} where $\xi = 0.5$, the result is

$$\Delta H_{\text{eff}} = 4RT_{\text{d}}^2 \frac{\Delta C_p(T_{\text{d}})}{\Delta_{\text{N}}^{\text{D}}H}. \tag{16.22}$$

If the process follows the two-state model, then the calorimetric enthalpy, $\Delta_{\text{N}}^{\text{D}}H$, the calorimetrically obtained van't Hoff enthalpy, ΔH_{eff}, and, where optical measurements have been made, the optical van't Hoff enthalpy, $\Delta H_{\nu\text{H}}$, should agree. Figure 16.9 shows the ratio, $\Delta H_{\text{eff}}/\Delta H_{\nu\text{H}}$ obtained from denaturation studies of five globular proteins under various conditions, plotted against the corresponding denaturation temperature. This plot shows that the ratio is very close to unity. Similar results for numerous other small globular proteins have been obtained and most show a similar relationship. It is clear, however, that the ratio is closer to 1.05 than to 1. Freire and Biltonen[11] have shown from a consideration of the partition functions associated with the native and the denatured state that this relative excess is

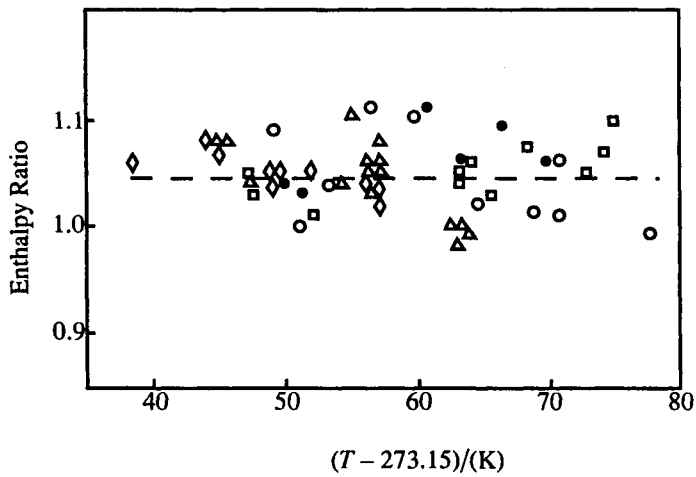

Figure 16.9 The ratio of the effective calorimetric enthalpy to the enthalpy calculated by the van't Hoff method from optical measurements, plotted against the temperature of denaturation. The symbols represent the following proteins: ●, metmyoglobin; △, ribonuclease; ○, cytochrome c; ◇, α-chymotrypsin; □, lysozyme. Reproduced by permission from P. L. Privalov, *Adv. Prot. Chem.*, **33**, 167 (1979).

related to the presence of intermediates. Since the excess in these proteins is <5%, the conclusion is reached that such proteins melt in a cooperative fashion, with the entire protein acting as a single unit, and that the intermediates can be neglected. Not all small globular proteins exhibit such cooperative melting, however. Papain and the Bence–Jones proteins, both in the molecular weight range of typical globular proteins, show ratios of 1.80 and 1.90, respectively. It has been proposed that these proteins consist of two subunits that melt independently. Structural studies show that papain has a deep cleft that bisects the protein into two nearly equal domains, while the Bence–Jones protein consists of four domains.

On the other hand, the ratio obtained for pancreatic trypsin inhibitor calculated per mole of monomer unit is near 0.5, suggesting that the cooperative unit of this protein is a dimer. Thus, we see that it is not possible to generalize completely about the size of a cooperative unit from a knowledge of the protein structure, but that the comparison of these two enthalpy measurements provides insights into the presence of discrete units within the protein domain.

An extreme example of this is the protein plasminogen, which denatures in at least seven steps. The DSC trace of successive scans obtained from heating a solution of plasminogen is shown in Figure 16.10. Using statistical mechanical techniques, Privalov and his colleagues were able to deconvolute the observed

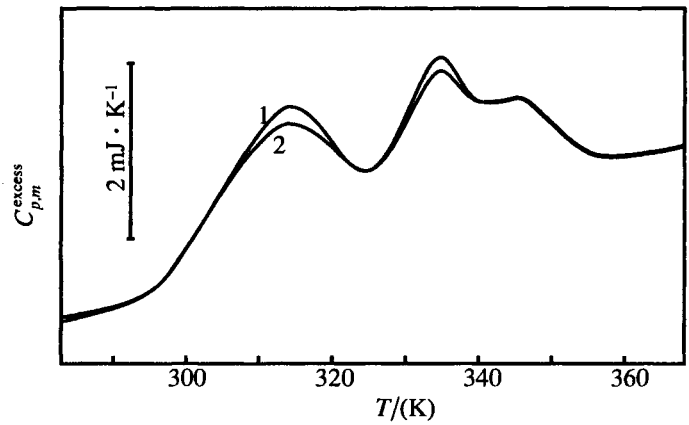

Figure 16.10 The DSC output of successive scans through the denaturation region of plasminogen. Reprinted with permission from P. L. Privalov, *Ann. Rev. Biophys. Chem.*, **18**, 47 (1989). © 1989, by Annual Reviews http://www.AnnualReviews.org

heat capacity curve into seven peaks. The sum of these seven peaks reproduced the observed curve remarkably well as shown in Figure 16.11a. Melting studies of fragments of the plasminogen molecule are presented in Figures 16.11b to 16.11e. These fragments gave melting curves that could be deconvoluted independently to yield the curves obtained in part (a). An important conclusion drawn from these results is that the various domains of the protein melt independently of one another. The domains in this protein contain about 100 amino acid residues so that they resemble small globular proteins in size.

Calorimetric studies have established several general features of protein denaturation.[12,13,14] For small globular proteins, the denaturation process is well represented by a two-state process,

$$\text{Native} = \text{Denatured}.$$

The populations of other intermediate states are very small and can be neglected. For larger more complex proteins made up of multiple subunits, and in many fibrous proteins, this conclusion cannot be supported. Complex globular proteins appear to melt cooperatively in domains in which the smaller units melt independently, and the melting in fibrous proteins is even more complex. While the molar quantities for the heat capacity are dependent upon the size of the protein, the partial specific heat capacities of many proteins are very nearly the same.

In all globular proteins studied, a significant increase in the heat capacity of the denatured protein relative to the native state has been observed in the vicinity of the denaturation transition. (This quantity is represented in

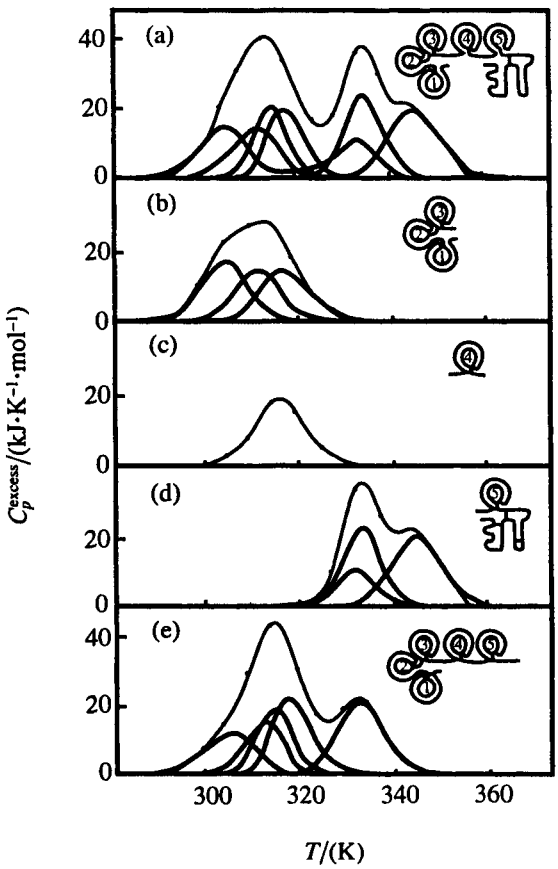

Figure 16.11 The deconvolution of the multistage melting of plasminogen into single-stage melting of various protein domains. Each figure represents the observed melting and calculated curves of the protein fragment shown in the right-hand corner. Reproduced with permission from P. L. Privalov, *Ann. Rev. Biophys. Chem.*, **18**, 47 (1989). © 1989, by Annual Reviews http://www.AnnualReviews.org

Figure 16.8 by $\Delta_{trans}C_p$, but Privalov uses the notation $\Delta_N^D C_p$, which we will adopt here.) That is, near T_d, $\Delta_N^D C_p = C_{p,D} - C_{p,N} > 0$.[1] As the temperature interval over which proteins have been studied has increased, it has become clear that $\Delta_N^D C_p$ is not constant over extended temperatures. The observed trend suggests that the value for $\Delta_N^D C_p$ decreases to zero at about 415 K for all the proteins studied. A consequence of the decreasing $\Delta_N^D C_p$ is that the enthalpy and entropy of denaturation approach constant values as T approaches 415 K,

[1]This behavior is not observed in nucleic acids where $\Delta_{trans}C_p \approx 0$ and is usually neglected.

since the temperature-dependent relationships for enthalpy and entropy changes derived earlier will hold for this specific process:

$$\Delta_N^D H(T_2) = \Delta_N^D H(T_1) + \int_{T_1}^{T_2} \Delta_N^D C_p \, dT$$

$$\Delta_N^D S(T_2) = \Delta_N^D S(T_1) + \int_{T_1}^{T_2} \frac{\Delta_N^D C_p}{T} \, dT$$

Figure 16.12 shows the behavior expected in the enthalpy and entropy of denaturation as a function of temperature for two proteins under the

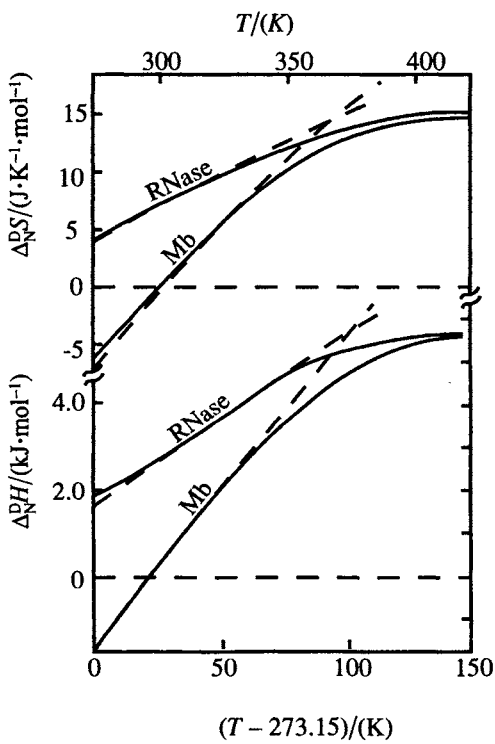

Figure 16.12 The temperature-dependent behavior of the denaturation enthalpy and entropy of ribonuclease (RNase) and myoglobin (Mb) under the assumption that $\Delta_N^D C_p$ is constant (dashed line) or decreasing with increasing temperature (solid line). Reproduced with permission from P. L. Privalov, *Ann. Rev. Biophys. Chem.* **18**, 47 (1989). © 1989, by Annual Reviews http://www.AnnualReviews.org

assumptions that (a), $\Delta_N^D C_p$ is constant; and (b), that it is decreasing with temperature. In Figure 16.13 the free energy of denaturation, $\Delta_N^D G$, that results from the combination of the enthalpic and entropic denaturation quantities with the assumption of a decreasing $\Delta_N^D C_p$ is presented. This figure shows that the stabilities of small globular proteins do not differ greatly from each other, and that their stabilities near physiological temperatures are not large, being in the range of 50 ± 20 kJ·mol^{-1}. It also shows that for each protein there exists a temperature at which the native structure has a maximum stability. A surprising conclusion from the assumption of a nonconstant $\Delta_N^D C_p$ is that the native form will undergo a second denaturation at low temperatures when $\Delta_N^D G$ again becomes negative. An unusual aspect of this low-temperature denaturation is that it is predicted to occur in an exothermic process as indicated by the trend in the enthalpy curve at low temperatures as shown in Figure 16.12. There is some experimental evidence on supercooled protein solutions that such behavior is actually observed.[15]

16.2c Thermodynamic and Spectroscopic Studies of Synthetic Oligonucleotides as Model Compounds for DNA

In this section, we describe the combined use of spectroscopic and calorimetric experiments to gain insights into the structure and stability of DNA. The results

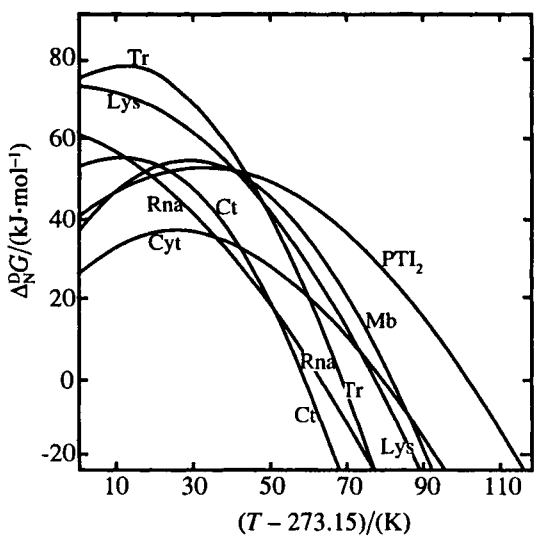

Figure 16.13 The free energy of denaturation $\Delta_N^D G$ as a function of temperature for a number of proteins: Lys = lysozyme; Rna = ribonuclease A; Ct = α-chymotrypsin; Cyt = cytochrome c; Mb = metmyoglobin; Tr = Trypsin and PTI_2 = the dimer of pancreatic trypsin inhibitor. Reprinted with permission from P. L. Privalov, "Stability of Proteins — Small Globular Proteins," *Adv. Prot. Chem.*, **33**, 167 (1979).

we discuss come principally from the work of Kenneth Breslauer[m] of Rutgers University and his colleagues. For more than a decade, Dr. Breslauer's group has studied synthetic deoxyribose oligonucleotides using temperature-dependent optical and NMR spectroscopic techniques in conjunction with differential scanning calorimetry (DSC) measurements. The particular oligonucleotides were chosen to carefully, and in a controlled fashion, introduce structural features similar to those observed in naturally occurring or mutant DNA. The study of duplex structures that differ by only a single structural alteration allows the energetic contribution associated with that modification to be elucidated. In addition, the systematic study of the thermodynamic properties of many oligonucleotides has enabled the generation of a database from which one can make predictions about the conformational preference, stability and melting properties of new oligonucleotides, or portions of polynucleotides, for which the base sequence is known. From that database, structural features that are known or hypothesized to be involved in ligand binding, control mechanisms, and/or mutations can be correlated with the base sequence and their related energetics. With this database, one can predict the structures and their stability from a knowledge of the primary base sequence.

In the discussion that follows, we will not attempt to give an exhaustive account of the research efforts of the Breslauer group with oligonucleotides, but rather to present enough of a picture that the reader will grasp the flow of their experiments, the analysis of the results, and the correlation and synthesis of the data from the various techniques.

Perhaps a short introduction to the chemistry of nucleic acids and the nomenclature used in the study of the oligonucleotides is in order before we address the Breslauer research efforts. Our comments in this regard will focus essentially on DNA oligonucleotides, but there are many similarities to those of RNA. A ***nucleoside*** is composed of a heterocyclic amine base, either a purine (adenine or guanine) or a pyrimidine {thymine (DNA only), uracil (RNA only), or cytosine}, that is attached through a N-glycosidic linkage to a hydroxyl group on the C1 position in a five-carbon sugar (ribose in RNA and deoxyribose in DNA). ***Nucleotides***, the basic building blocks of nucleic acids (or oligonucleotides), consist of a nucleoside plus a phosphate ester formed at the hydroxyl group on the C5 of the sugar. Each strand in the duplex nucleic acid molecule (the familiar double helix of DNA being a macromolecular example) is built up from a sequence of nucleotides linked through a phosphate ester as shown in the schematic of a dinucleotide shown in Figure 16.14. Larger oligonucleotides are formed by the sequential addition of new nucleotides, with each new linkage coming from the 3′ end of the strand to the 5′ position on the new nucleotide.

---

[m] Kenneth Breslauer is the Linus C. Pauling Professor of Chemistry at Rutgers University.

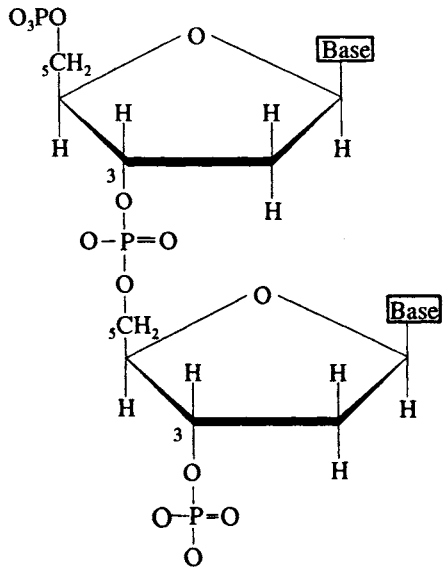

Figure 16.14 A dinucleotide of deoxyribose showing the free phosphate group at the 5′ carbon end of the first sugar and the free phosphate group at the 3′ carbon of the second sugar.

An oligonucleotide strand is named by starting first with the sugar moiety that is involved in the backbone, with either a "d" for deoxyribose or an "r" for ribose, then enclosing in parentheses the sequence of bases, named starting with the 5′ end of the molecule and progressing to the 3′ end. For example, the notation d(GAATTC) designates a six-member oligonucleotide constructed with deoxyribose in the phosphodiester backbone. Guanine (G) is the base on the first nucleotide at the 5′ end, molecules of adenine (A) are the second and third bases, thymine (T) are the fourth and fifth, and cytosine (C) is the sixth base at the 3′ end. The monomer strand is sometimes referred to as a "*n*"-mer where *n* is the number of nucleotides in the strand. Thus, the oligonucleotide d(GAATTC) can be referred to as a 6-mer or hexamer. A duplex formed by the association of two molecules of this oligonucleotide is indicated by $d(GAATTC)_2$.

In Figure 16.15 we show a schematic representation of the duplex formed from d(GAATTC). Bases from one monomer pair with those from a second to form the duplex. G forms **base-pairs** with C, and A with T through hydrogen bonding. These base-pairs are referred to as Watson–Crick base-pairs, and they make up the "rungs of the ladder" associated with the familiar double helix of DNA.

The oligonucleotide, d(GAATTC), is said to be **self-complementary** because the duplex is formed by joining two strands of the **same** monomer in such a way that the free 5′ end of one strand forms a Watson–Crick base-pair with the free

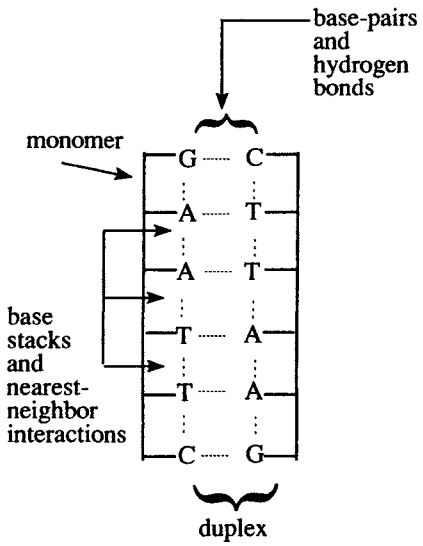

Figure 16.15 A schematic representation of a duplex formed from the self-complementary monomer, d(GAATTC), that illustrates base-pairing and nearest-neighbor stacking interactions.

3′ end of the second, and all intermediate bases along the first strand pair with the corresponding bases on the second. The two strands in such a duplex structure are said to be **antiparallel** since, in a reading from one end of the duplex to the other, one strand goes from the 5′ to the 3′ end, while the complementary strand goes from the 3′ to the 5′ end.

The hydrogen-bonded interactions associated with duplex formation are not the only stabilizing forces present in these molecules. Within a monomeric strand, **base-stacking** interactions are possible between the heterocyclic aromatic rings of the nucleotides of nearest neighbors. More specifically, these interactions originate from $\pi - \pi$ electronic interactions through the partial overlap of adjacent purine and pyrimidine bases along the phosphodiester backbone of the monomer. Interstrand base-stacking interactions also contribute to the overall stability of a DNA duplex.

Because d(GAATTC) is self-complementary, the intrastrand base-stacking interactions between nearest neighbors are the same on each strand in the duplex. Starting from the 5′ end of each strand, the intrastrand base stacks are G-A, A-A, A-T, T-T and T-C. Because of the directionality of the bonding along the phosphodiester backbone and the twist associated with the helical structure, the overlap, within a strand, of two adjacent bases of the same identity, can be different. For example, G-A and A-G represent two different base-stacking interactions within a strand. Upon association with two

complementary strands, the resulting duplex is stabilized by inter- as well as intrastrand base-stacking interactions.

16.2d Description of Procedures and Techniques Associated with Duplex Melting

The Breslauer group has investigated a number of types of duplex melting to probe the energetics of, and structural changes occurring in, the disruption of the duplex. While base-pair and interstrand base-stacking interactions are broken during duplex melting, intrastrand stacking interactions may or may not be fully disrupted upon duplex melting, depending upon the final temperature of the melt and the sequence in the single strand.

The particular combination of spectroscopic and calorimetric techniques used in these studies illustrates how the strength of one technique can be used to overcome the weaknesses of another, and to ultimately give a multidimensional picture of a complex problem. In the early stages of this work, optical studies were used to provide information about the extent of base stacking because these interactions influence the absorption of the oligonucleotide at 260 nm. In later studies, NMR was used as the spectroscopic technique of choice. It, too, can provide information about the extent of $\pi - \pi$ stacking interactions from the change in chemical shift of protons on the bases, but it can also signal the presence or absence of hydrogen bonding from base-pairing, and changes in the phosphodiester backbone imposed by chemical or temperature-induced modifications in the oligonucleotide.

In addition, because one can study the melting phenomena with NMR from protons associated with different parts of the oligonucleotides, very specific information about the extent to which different base-pairs are involved in the melting process can be determined. For example, NMR studies of duplexes containing terminal AT base-pairs showed that there was a considerable disruption of AT base-pairs at the ends of the molecule below the melting temperature. This phenomenon is referred to as "end effects". Calorimetric measurements suggested that these terminal base-pairs were not energetically involved in the cooperative melting transition. This information could then be used in the design of additional oligonucleotides for study and to adjust the enthalpy measurements of other melting processes with terminal AT base-pairs.

Calorimetric (DSC) measurements yield thermodynamic properties of duplex melting in these oligonucleotides independent of any assumptions concerning the model of melting, such as a cooperative all-or-none process versus a noncooperative, multiple-stage melting process. Comparison of calorimetric enthalpies with van't Hoff enthalpies obtained either from the manipulation of heat capacity curves outlined in equations (16.19) to (16.22), or from optical or NMR measurements [equations (16.14) to (16.17)] allows conclusions to be drawn concerning the size of the cooperative unit. If the two

enthalpies agree within experimental error, one can conclude that the process is cooperative. That is, it proceeds in an all-or-none (two state) manner. When the two enthalpies differ significantly, the most common observation is that the van't Hoff enthalpy is lower, consistent with a multistate transition in which intermediate states are significantly populated. The ratio of the two, taken as $\Delta H_{\nu H}/\Delta H_{cal}$ gives a measure of the fraction of the molecule that melts cooperatively, the so-called cooperative unit.

It is sometimes more convenient to analyze the melting process in reverse, that is, the association of monomers to form the duplex. If the process is truly an equilibrium one, then either direction should give an equivalent analysis. We will switch back and forth in our discussion if one direction is more convenient, although most experimental measurements have been of the melting process (rather than the formation reaction), and all thermodynamic properties will be reported for melting.

The most common type of oligonucleotides studied in the early work of the Breslauer research group involved self-complementary sequences. For example, the sequence d(GCGCGC) can form a duplex in a process according to

$$2\ \text{GCGCGC} = \begin{matrix}\text{GCGCGC}\\ \vdots\vdots\vdots\vdots\vdots\vdots\\ \text{CGCGCG}\end{matrix} \quad . \tag{16.23}$$

(We will drop the designation for the deoxyribose portion to simplify the representation of equilibria.)

Similarly, the longer, but still self-complementary oligonucleotide d(CGCGAATTCGCG) has been observed to form a duplex via the dimerization/association reaction

$$2\ \text{CGCGAATTCGCG} = \begin{matrix}\text{CGCGAATTCGCG}\\ \vdots\vdots\vdots\vdots\vdots\vdots\vdots\vdots\vdots\vdots\vdots\vdots\\ \text{GCGCTTAAGCGC}\end{matrix} \quad . \tag{16.24}$$

but it can also form an alternative secondary structure via an intramolecular rearrangement:

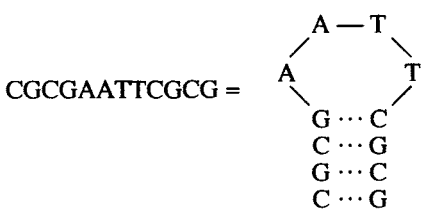

(16.25)

This structure is referred to as a DNA "hairpin".

The duplex formation in reaction (16.24) involves two molecules and is described as a bimolecular process, or one that occurs with a molecularity of two. The formation of the hairpin structure in reaction (16.25), however, involves only a single molecule and the reaction is said to be unimolecular and has a molecularity of one.

Duplexes can also be formed from monomers that are not self-complementary. In that case, the duplex, AB, contains two different oligonucleotide strands, A and B. The formation of this type of duplex can be represented as

$$A + B = AB. \tag{16.26}$$

One such example would be the antiparallel association of d(GGAATCG) with d(CGATTCC) to form the duplex

GGAATCG
⋮⋮⋮⋮⋮⋮⋮ .
CCTTAGC

We have written the processes represented by reactions (16.24) to (16.26) as formation reactions, because the designations of molecularity and complementarity are easier to see in this direction. However, the thermodynamic measurements we will discuss are all for the reverse (melting) process, and we will proceed with our derivations applied to that process.

Let us consider a general melting process. If one defines α as the concentration of monomer strands in the duplex and c_{TOT} as the total monomer strand concentration, then one can derive relationships between the van't Hoff enthalpy and the temperature derivative of α at T_m to show that there is a concentration dependence of T_m for the melting of some duplexes and not others.

As an example, let us consider the derivation for the melting of a duplex into two identical self-complementary monomers

$$A_2 = 2A.$$

For this reaction, the total concentration of oligonucleotide can be given in terms of the concentration of duplex and monomer, $c_{TOT} = 2c_{A_2} + c_A$, and a relationship for α can be obtained: $\alpha = 2c_{A_2}/c_{TOT}$. From these definitions, one obtains that $c_{A_2} = \frac{1}{2}\alpha c_{TOT}$ and $c_A = (1 - \alpha)c_{TOT}$, and the equilibrium constant for the melting process (assuming activity coefficients are one) is given by

$$K = \frac{2(1 - \alpha)^2 c_{TOT}}{\alpha}. \tag{16.27}$$

Similar analyses have been performed to obtain expressions for K in terms of α and c_{TOT} for other melting schemes that arise from the dissociation of more complicated structures.

From the temperature derivative of K and the corresponding derivative of α, one can get a relationship for the van't Hoff enthalpy at T_m as a function of $d\alpha/dT$. These relationships are summarized in Table 16.2. For the specific case of a reaction like (16.26) involving two different types of strands, the table gives only the case where $c_A = c_B$.

Note that the self-complementary and nonself-complementary processes of the same molecularity (n) give identical expressions for the van't Hoff enthalpy of the melting process, but not for the equilibrium constant. The factors in the expressions for K arise from the indistinguishability of 2A monomers in a process like $A_2 = 2A$, while the A and B monomers in an $AB = A + B$ process are distinguishable.

When T_m is concentration dependent, an additional method[n] can be used to determine the thermodynamic quantities associated with melting. For example, consider the dissociation of a duplex that is formed from a self-complementary bimolecular process. {The reverse reactions to those given in reactions (16.23) or (16.24) are specific examples of such processes.} As Table 16.2 shows, the equilibrium constant for such a dissociation process is given by

$$K = \frac{2(1-\alpha)^2 c_{TOT}}{\alpha}.$$

At T_m, where $\alpha = 0.5$, $K = c_{TOT}$ and

$$\Delta G^\circ = -RT_m \ln c_{TOT} = \Delta H^\circ - T_m \Delta S^\circ.$$

This can be rearranged to give

$$\frac{1}{T_m} = \frac{R \ln c_{TOT}}{\Delta H^\circ} + \frac{\Delta S^\circ}{\Delta H^\circ}. \tag{16.28}$$

If ΔH° and ΔS° are assumed to be constant with the temperature, then graphs of $1/T_m$ versus $\ln c_{TOT}$ should be linear for self-complementary bimolecular

[n] This method has some advantages over the derivative method outlined earlier in Section 16.2a because it reduces the dependence of the T_m on the choice of baseline. It is used frequently by Breslauer as well as others. See Marky and Breslauer, *Biopolymers*, **26**, 1601–1620 (1987) for additional details.

Table 16.2 A summary of expressions for the equilibrium constant and van't Hoff enthalpies for duplex meltings of various molecularities

Process	$A = B$	$A_2 = 2A$	$AB = A + B$	$A_n = nA$	$A_1A_2A_3 \ldots A_n = A_1 + A_2 + A_3 + \cdots + A_n$
Molecularity	1	2	2	n	n
K	$\dfrac{(1-\alpha)}{\alpha}$	$\dfrac{2(1-\alpha)^2 c_{TOT}}{\alpha}$	$\dfrac{(1-\alpha)^2 c_{TOT}}{\alpha}$	$\dfrac{n(1-\alpha)^n c_{TOT}^{n-1}}{\alpha}$	$\dfrac{(1-\alpha)^n c_{TOT}^{n-1}}{n^{n-1}\alpha}$
$\Delta H_{\nu H}$ at T_m	$4RT_m^2(d\alpha/dT)_{T=T_m}$	$6RT_m^2(d\alpha/dT)_{T=T_m}$	$6RT_m^2(d\alpha/dT)_{T=T_m}$	$(2+2n)RT_m^2(d\alpha/dT)_{T=T_m}$	$(2+2n)RT_m^2(d\alpha/dT)_{T=T_m}$

Adapted from L. A. Marky and K. J. Breslauer, *Biopolymers*, **26**, 1601–1620 (1987).

processes, with a slope that is inversely proportional to $\Delta H°$ and an intercept that yields $\Delta S°$.

Inspection of Table 16.2 shows that only a unimolecular process has an equilibrium constant, and, therefore a T_m, that shows no concentration dependence. Reaction (16.25) is such a process. Thus, one can identify a unimolecular process from experiments that show T_m to be independent of concentration.

With the description of the additional thermodynamic analysis techniques employed by the Breslauer group, we can now describe their results for selected systems and illustrate how they have used these results to generate a database that allows one to predict the energetics of duplex melting based upon nearest neighbor interactions and predict structural features from these.

Observance of Equilibria Between Two Oligonucleotide Conformations

Reactions (16.24) and (16.25) show the two possible duplex structures associated with the oligonucleotide, d(CGCGAATTCGCG). Optical and calorimetric studies of the melting of this duplex were conducted at various salt (NaCl) and oligonucleotide concentrations to gain information about the relative stabilities of the two structures. The results of these studies are summarized in Table 16.3.

From UV absorbance studies of solutions of d(CGCGAATTCGCG), it was clear that the melting behavior was dependent upon the concentrations of NaCl and oligonucleotide. Two melting transitions were observed at all the oligonucleotide concentrations studied (10.5×10^{-6} to 97.0×10^{-6} mol·dm^{-3}) when the NaCl concentration was very low ($c_{NaCl} < 0.010$ mol·dm^{-3}), but at higher salt concentrations ($c_{NaCl} \geq 0.010$ mol·dm^{-3}), only a single transition could be observed at any strand concentration. When biphasic behavior (two transitions) was observed, the higher of the two T_m values was found to be independent of oligonucleotide concentration, but the lower one was observed to increase with increasing concentrations of oligonucleotide. Increasing salt concentration was also found to increase both T_m values.

The calorimetric studies required strand concentrations in the range of 10^{-3} mol·dm^{-3} to achieve acceptable signal-to-noise levels. At these high strand concentrations, only one concentration-independent transition was observed.

The optical results at low salt concentration have been interpreted in terms of the presence of the two conformations given by reactions (16.24) and (16.25). The latter structure is only partially double-stranded and incorporates the "hairpin" loop region in which four bases are not paired. The lower transition temperature, which is concentration-dependent, with the larger melting enthalpy is ascribed to the disruption of the full duplex structure, which is a bimolecular process. The higher temperature transition (with a lower transition enthalpy) is attributed to the disruption of the hairpin structure, which is a

Table 16.3 Summary of optical and calorimetric data for the duplex melting of d(CGCGAATTCGCG) at different salt and strand concentrations

Obtained from absorption methods						Obtained from calorimetric methods			
c_{NaCl}/ (mol·dm^{-3})	c_{TOT}/ (μmol·dm^{-3})	T_m/(K)		$\Delta H_{\nu H}$/(kJ·mol^{-1})		c_{NaCl}/ (mol·dm^{-3})	T_m/ (K)	ΔH_{cal}/ (kJ·mol^{-1} of duplex)	$\Delta H_{\nu H}$/ (kJ·mol^{-1} of duplex)
		Transition 1	Transition 2	Transition 1	Transition 2				
0.001	10.5	304.2	335.4	586	159				
	20.8	305.5	335.9						
	50.6	306.5	335.6						
	97.0	307.4	335.4						
0.010	7.43	307.6	339.1	377	151	0.01	338.3	377	393*
	14.3	309.6							
	34.5	312.8							
	70.1	316.1							
0.10	8.62	326.2		176		0.10	344.5	427	310*
	19.2	329.2							
	49.4	334.1							
	97.3	335.4							
1.00	8.2	337.9		272		1.00	351.7	565	318*
	18.1	339.5							
	45.3	343.6							
	88.6	345.6							

*This van't Hoff enthalpy was obtained by an analysis based on the shape of the DSC curve. See the reference for details.
(Data from L. A. Marky, K. S. Blumenfeld, S. Kozlowski, and K. J. Breslauer, *Biopolymers*, **22**, 1247–1257 (1983).

monomolecular process, and, therefore expected to have a concentration-independent T_m. The lower melting enthalpy of the hairpin structure is attributed to the disruption of fewer base-pairs and base stacks in the melting of this structure than occurs in the full duplex structure. At the concentrations of monomer employed for the calorimetric measurements, only a single melting transition can be observed, but it is expected that both conformations are present below the observed melting temperature.

16.2e Studies of Synthetic Oligonucleotides to Generate Information About the Energetics of Structural Features

Table 16.4 summarizes the results from spectroscopic and calorimetric studies of duplex melting of selected oligonucleotides. These particular oligonucleotides were selected to illustrate how information can be extracted to relate structural features with the energetics of duplex melting. The table heading gives the nucleotide sequence of the particular oligonucleotide, then shows the structure of the duplex formed by the oligonucleotide. The vertical direction gives the next-neighbor stacking interactions along the oligonucleotide strand while the horizontal pairing shows the hydrogen-bonded base-pairs in the duplex. Melting is assumed to disrupt the base-pair and base-stacking interactions that are present in the duplex.

The first four oligonucleotides given in the table are self-complementary, and they form full duplex structures in biomolecular processes that are the reverse of melting. The last two oligonucleotides are only partially self-complementary. However, they share a common self-complementary core with the previous two entries in the table. The common core of these four oligonucleotides is given in bold letters in the table.

The d(GCGCGC)$_2$ Duplex. The d(GCGCGC)$_2$ duplex was the first oligonucleotide melting process for which a comparison was made of the calorimetrically-determined enthalpy with the spectroscopically-determined van't Hoff enthalpy. This study showed that good agreement could be obtained between the two calculations, if appropriate baselines were established in the optical measurements. It also provided information about the energetics of GC base-pairing and base-stacking interactions.

The d(ATGCAT)$_2$ Duplex. From NMR studies of the d(ATGCAT)$_2$ duplex, it was known that, even at the lowest temperature studied, the terminal AT base-pairs were partially open or "frayed". By partitioning the calorimetrically measured enthalpy into contributions from the internal AT and GC pairs using data from the d(GCGCGC)$_2$ duplex and other measurements on AT pairs (not reproduced here), Breslauer and colleagues were able to show that what the NMR spectra interpreted as "open pairs" were also energetically ruptured.

Table 16.4 Results of duplex melting obtained from spectroscopic and calorimetric studies of selected deoxyribose oligonucleotides

Name of oligonucleotide:	d(GCGC-GC)		d(ATGCAT)		d(CGCGAA-TTCGCG)		d(GGAAT-TCC)		d(GAATTC-GCG)		d(CGTGAATTCG-CG)	
Duplex structure:	GC CG GC CG GC CG		AT TA GC CG AT TA		CG GC CG **GC** **AT** **AT** **TA** **TA** **CG** GC CG GC		GC **GC** **AT** **AT** **TA** **TA** **CG** CG		G C G **GC** **AT** **AT** **TA** **TA** **CG** **G** C G		CG GC TG* **GC** **AT** **AT** **TA** **TA** **CG** GT* CG GC	
Technique:	Calor	*v*H	Calor	*v*H	Calor	*v*H	Calor	*v*H	Calor	*v*H	Calor	*v*H
ΔH/(kJ·mol^{-1} of duplex):	238	240	141	164[a] 163[b] 146[c]	376 427	393[a] 310[a]	247	247	251	146	441	320[c]
T_m/(K)	NR	NR	NR	NR	344	345[d]	326	NR	319	310	324	324–326[d]
Reference:	(1)		(2)		(3)		(4)		(5)		(6)	

Abbreviations: calor = ΔH obtained from integration of the integrated DSC curve; *v*H = a van't Hoff enthalpy obtained from UV absorbance or NMR chemical shift measurements unless otherwise noted; NR indicates that results were not reported.

[a] Evaluated from the slope of $d\alpha/dT$ at T_m.

[b] Evaluated from the slope of $1/T_m$ vs $\ln c_{TOT}$.

[c] Evaluated from the shape of the calorimetric curve.

[d] Obtained from the midpoint of temperature-dependent NMR chemical shifts of nonexchangeable GC and AT protons.

(1) D. D. Albergo, L. A. Marky, K. J. Breslauer, and D. H. Turner, *Biochemistry*, **20**, 1409 (1981).
(2) L. A. Marky, L. Canuel, R. A. Jones, and K. J. Breslauer, *Biophys. Chem.*, **13**, 141 (1981).
(3) D. J. Patel, S. A. Kozlowski, L. A. Marky, C. Broka, J. A. Rice, K. Itakura, and K. J. Breslauer, *Biochemistry*, **21**, 428 (1982).
(4) D. J. Patel and L. Canuel, *Eur. J. Biochem.*, **96**, 267 (1979).
(5) D. J. Patel, S. A. Kozlowski, L. A. Marky, C. Broka, J. A. Rice, K. Itakura, and K. J. Breslauer, *Biochemistry*, **21**, 451 (1982).
(6) D. J. Patel, S. A. Kozlowski, L. A. Marky, J. A. Rice, C. Broka, J. Dalla, K. Itakura, and K. J. Breslauer, *Biochemistry*, **21**, 437 (1982).

Since a comparison of various van't Hoff enthalpies (calculated by analysis of $d\alpha/dT$ at T_m, the slope of $1/T_m$ vs ln c_{TOT}, and the shape of the calorimetric curve)[o] with the calorimetric enthalpy shows that $\Delta H_{\nu H} \approx \Delta H_{cal}$, it was concluded that the melting transition in this duplex is cooperative and well represented by a two-state model.

The d(CGCGAATTCGCG)$_2$ Duplex. When studied at comparable salt (NaCl) and duplex concentrations, the duplex of d(CGCGAATTCGCG) was found to have about the same T_m by DSC measurements (344 K) and by the temperature-dependent changes in the NMR chemical shifts of nonexchangeable GC and AT protons (345 K). At 0.01 M NaCl, the calorimetric enthalpy was 376 kJ·mol^{-1} of duplex, while the van't Hoff enthalpy evaluated from equation (16.28) was found to be 393 kJ·mol^{-1} of duplex. At a 10-fold higher salt concentration, the calorimetric enthalpy was 427 kJ·mol^{-1} of duplex, while the van't Hoff enthalpy was 310 kJ·mol^{-1} of duplex. From the ratio of the van't Hoff enthalpy to the calorimetric enthalpy at the higher salt concentration, it was estimated that 9 out of 12 base-pairs melt together in the cooperative unit, while all melt simultaneously at the low salt concentrations.

The d(GGAATTCC)$_2$ and d(GAATTCGCG)$_2$ Duplexes. Comparison of the duplex formed by d(GGAATTCC), which is fully self-complementary, with the partially self-complementary d(GAATTCGCG)$_2$ duplex allows one to consider the effect of dangling (unpaired) ends on duplex stability. In NaCl solutions with a concentration of 1 mol·dm^{-3}, the calorimetric evidence shows that the melting enthalpies of the two duplexes are essentially equal (247 kJ·mol^{-1} of d(GGAATTCC)$_2$ versus 251 kJ·mol^{-1} of d(GAATTCGCG)$_2$), even though the fully self-complementary duplex has a significantly higher T_m (326 K versus 319 K). At low temperatures, the NMR results suggest that aggregation takes place between molecules of the d(GAATTCGCG)$_2$ duplex. It is hypothesized that the single ends of one duplex pair up with the ends of other duplexes. There is also evidence from the NMR studies that the terminal GC ends, even though unpaired, still stack. Comparison of the van't Hoff enthalpies with the calorimetric enthalpies indicates that the 8-mer melts cooperatively {247 kJ·mol^{-1} of d(GGAATTCC)$_2$ from both techniques} while the d(GAATTCGCG)$_2$ duplex does not melt as a single unit (calorimetric enthalpy of 251 kJ·mol^{-1} of duplex versus a van't Hoff enthalpy of 146 kJ·mol^{-1} of duplex). The 146 kJ·mol^{-1} of duplex, observed in the van't Hoff melting of the d(GAATTCGCG)$_2$ duplex, is approximately what might be calculated for the melting of the d(GAATTC)$_2$ core fragment using the estimation methods

[o] See Breslauer's work for details of this more involved process.

outlined below. Thus, the remaining 105 kJ can be attributed to stacking effects in the single-stranded ends and/or higher-order polymers caused by loose pairings between the sticky ends of the duplexes.

Wobble Base-Pairs The stability and energetic effects of replacing a normal Watson–Crick base-pair with a different combination have been investigated by a study of the duplex melting of $d(CGTGAATTCGCG)_2$. Because of the nucleotide sequence in this oligonucleotide, a GT base-pair is formed at the third nucleotide in from each end of the duplex. The bases G and T are not as well suited to form hydrogen bond pairs as are G and C, but base-pairing between them has been observed, and it is suspected of being the source of some naturally occurring mutations. Interactions like that found in the GT base-pair have been referred to as ***wobble base-pairs*** because the mismatching of the species involved in hydrogen bond formation leads to a less rigid arrangement of the base-pairs relative to one another.

This duplex contains the same hexameric core of nucleotides, GAATTC, described in (c) and (d). It differs from the $d(CGCGAATTCGCG)_2$ discussed in (c) by the substitution of the two G-T base-pairs for the conventional G-C pairing. The G-T pairs are marked in Table 16.4 with an asterisk*. The substitution of one T for a C also introduces differences in the nearest-neighbor stacking interactions. At the end of the duplex described in (c) the sequence CGCG/GCGC leads to the following stacking interactions: CG/GC followed by GC/CG and CG/GC. The notation here is AB/A′B′ where A and B are stacked bases on one monomer and A′ and B′ are stacked bases on the second monomer; A and A′ are base-paired as are B and B′. In the modified duplex, $d(CGTGAATTCGCG)_2$, the initial sequence CGTG/GCGC leads to CG/GC, GT/CG, and TG/GC nearest-neighbor interactions.

From the NMR results, base-pair formation between G and T is established, and increased fraying of the terminal GC ends relative to those in the normal duplex is observed, but this technique is not able to provide complete information about the changes in the stacking between GTG stacking relative to the GCG stacking in the normal duplex. Interior base-pairs distant from the wobble pair show similar NMR behavior, indicating that the duplex can localize the conformational distortions resulting from the GT mismatch. It is interesting to note that the two base-pair mismatches have little effect on the calorimetric enthalpy (427 vs 441 $kJ \cdot mol^{-1}$ of duplex) nor the van't Hoff enthalpy (310 vs 320 $kJ \cdot mol^{-1}$ of duplex), but they change the melting temperature by 20 K. This suggests that unfavorable entropic interactions on the duplex might be imposed by the geometric constraints associated with the mismatch. Neither the GTG duplex nor the GCG duplex melt in a fully cooperative manner, as indicated by the discrepancies between the calorimetric and van't Hoff enthalpies (310/427 versus 320/441), but the size of the

cooperative unit remains the same, with about 9 of the 12 base-pairs that make up each oligonucleotide duplex involved.

16.2f Generation of a Thermodynamic Database to Estimate Melting Parameters of Oligonucleotides and Portions of Nucleic Acids

Table 16.5 list the results from calorimetric melting studies of some synthetic deoxyribose oligonucleotides designed by the Breslauer research group to obtain thermodynamic information concerning the effect of next-neighbor interactions on duplex stability. The observed calorimetric enthalpies of melting of oligonucleotides of chain length n have been divided by the number of base stacks, which is equal to $n - 1$, to obtain an average enthalpy for a stacking interaction reported as ΔH_{cal} near the bottom of the table.

Table 16.5 Enthalpy and melting temperature results from calorimetric studies of oligonucleotides used to generate data for nearest-neighbor base-stacking interactions. The poly designates a strand of base-pairs of undetermined length.

Parameter	d(GCGCGC)	poly(dA)·poly(dT)	poly[(dAT)]	poly[d(AC)]·poly[d(TG)]
Duplex structure (base-pairs — horizontal; base stacks — vertical)	GC CG GC CG GC CG	AT AT AT AT AT ·	AT TA AT TA AT TA ·	AT CG AT CG AT CG ·
Base stack energetics probed	GC/CG and CG/GC	AA/TT	AT/TA and TA/AT	AC/TG and CA/GT
Molecularity/ Complementarity	2 SC*	2 NonSC*	2 SC	2 NonSC*
ΔH_{cal}/(kJ·mol^{-1} of stack pairs)	49.8	36.0	29.7	23.4
T_m/(K) c_{NaCl}/(mol·dm^3)	338 (1.0)	329 (0.01)	322 348 (0.01) (1.0)	350 (0.01)

Data from L.A. Marky and K.J. Breslauer, *Biopolymers*, **21**, 2185–2194 (1982).
*SC indicates that the strand is self-complementary, while NonSC indicates that the strand is not self-complementary.

Estimation of a Duplex Melting Enthalpy. From the average enthalpies given in Table 16.5, one can estimate the melting enthalpies of an oligonucleotide duplex based on its nucleotide sequence. For example, the oligonucleotide duplex $d(ATGCAT)_2$ has the structure

A—T—G—C—A—T
⋮ ⋮ ⋮ ⋮ ⋮ ⋮
T—A—C—G—T—A

and it contains two AT/TA overlaps (assuming AT and TA are the same), two TG/AC overlaps (TG/AC is assumed to be equivalent to CA/GT) and one GC/CG overlap. Using values in Table 16.5, and assuming the equivalence of the pairs of stacking interactions, the melting enthalpy is estimated to be $2 \times 29.7 + 2 \times 23.4 + 1 \times 49.8 = 156$ kJ·mol^{-1} of duplex. Comparison with the reported value of 140 kJ·mol^{-1} of duplex shows reasonable agreement. Since the terminal AT base-pairs in this duplex were shown to be partially frayed, the disagreement is in the right direction, since one might expect that the terminal AT stacking interactions would also be diminished.

The model compounds used in this early study did not differentiate between the orientational differences and therefore, possible stacking energetic differences, between two adjacent bases, X and Y stacked next to each other through X(5′) – (3′)Y stacking versus a Y(5′) – (3′)X stacking. In later publications, enough model compounds were studied to differentiate between these isomers. The final results for all ten possible nearest neighbors assuming Watson–Crick base-pairings are given in Table 16.6. Because this early calorimetric work showed that the change in C_p upon melting is insignificant, these quantities were considered to be relatively temperature-independent. Just recently, Breslauer and coworkers[16] have taken advantage of a new generation of more sensitive DSC instruments to detect and quantify an average heat capacity change, ΔC_p, of 270 J·K^{-1}·mol^{-1}. When this ΔC_p value is used to extrapolate the thermodynamic data to a common reference temperature (e.g. 298.15 K) one finds the thermodynamic parameters to be far less dependent on duplex composition and sequence than previously assumed. Nevertheless, the analyses and the predictive capacities described here remain valid whether or not the average heat-capacity term is used to extrapolate the data to a common reference temperature.

Breslauer and his colleagues have been able to use this database to predict the energetics associated with the melting of a wide variety of duplexes based on the nucleotide sequence in the oligonucleotide. Conversely, from the known nucleotide sequence and the melting energetics obtained from Table 16.6, they have been able to predict the likelihood that structural features like the hairpin loop of reaction (16.25) would be observed.

Table 16.6 Thermodynamic database for the effect of nearest-neighbor interactions on duplex stability

Interaction	ΔH/(kJ·mol^{-1} of base stacks)	ΔS/(J·K^{-1}·mol^{-1} of base stacks)	ΔG/(kJ·mol^{-1} of base stacks)
AT/TT	38.1	100.4	7.9
AT/TA	36.0	100.0	6.3
TA/AT	25.1	70.7	3.8
CA/GT	24.3	54.0	7.9
GT/CA	27.2	72.4	5.4
CT/GA	32.6	87.0	7.0
GA/CT	23.5	56.5	7.0
CG/GC	49.8	116.3	15.1
GC/CG	46.4	111.7	13.0
GG/CC	46.0	111.3	13.0

Data from K. J. Breslauer, R. Frank, H. Blöcker, and L. A. Marky, *Proc. Natl. Acad. Sci. USA*, **83**, 3746–3750 (1986).

One implication of the ability of the database to make reasonable predictions about the thermodynamics of duplex melting is that base sequence, rather than total base composition, determines duplex stability. This conclusion is supported by the observation that the second and third entries in Table 16.6, which involve only A and T, have the same base composition but yield significantly different melting thermodynamics.

16.2g Ligand Binding of Cisplatin

We will conclude with a description of how the database can be used to provide "baseline" values for normal duplexes against which to compare the melting thermodynamics observed in duplexes that have been altered by ligand binding, crosslinking, or other effects.

The drug cisplatin (*cis*-diamminedichloroplatinum II) produces its anti-tumor effects by binding and crosslinking DNA. The platinum binds principally at sites where two adjacent guanine molecules occur, as shown in Figure 16.16. Structural studies, including those by crystallography and NMR, suggest that the binding of the cisplatin partially unwinds the DNA duplex and introduces a bend in the phosphodiester backbone around the site. Calorimetric and UV studies similar to those used to create the database have been made of a synthetic oligonucleotide bound and unbound by cisplatin.[17] The structure of the oligonucleotide is shown in Figure 16.17. The thermodynamic results from the calorimetric and UV experiments are summarized in Table 16.7. These

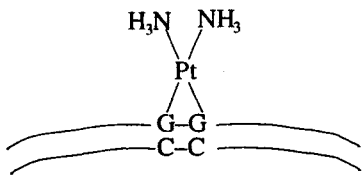

Figure 16.16 A schematic representation of the binding of cisplatin to a DNA duplex.

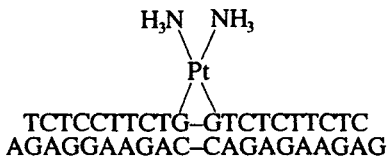

Figure 16.17 The cisplatin-bound synthetic oligonucleotide used in the Breslauer study.

results show that the binding of cisplatin affects both the temperature and thermodynamic stability of the duplex. The thermal stability of the bound duplex is seen to be reduced by more than 8 K relative to the unbound GG20 duplex. The binding also introduces an enthalpic destabilization since the cisplatin-bound duplex melting requires 71 $kJ \cdot mol^{-1}$ of duplex less enthalpy than the unbound GG20 duplex. On the other hand, the binding introduces an entropic stabilization factor. The combination of the unfavorable enthalpic and favorable entropic contributions yields a destabilization in the free energy that is reflected in the decreased T_m of the duplex.

While the binding represents an energetic change in the duplex, it is interesting to note that it does not affect the mechanism of melting. Comparison of the calorimetric and van't Hoff enthalpies shows good agreement in both the bound and unbound duplex, indicating that both melt cooperatively. This result is not necessarily what might be expected. Since conventional base-stacking interactions are already disrupted in the affected sequence, DNA damage induced by mutagens and/or drugs such as cisplatin could act as a nucleation site for melting. Hence, one could envision melting to originate at the site of the DNA damage and to radiate outwards from there. This apparently is not observed in the GG20 oligonucleotides studied here.

The NMR studies show that the binding does introduce conformational changes in the duplex, however. These changes do not disrupt the base-pairing interactions, but do affect the base-stacking interactions between bases near the binding site. The database in Table 16.6 provides a means to calculate the maximum effect if the base-stacking interaction is completely destroyed. The most likely interactions to be disrupted are those involving the G—G binding

Table 16.7 Thermodynamic results from the study of the effects of cisplatin binding on the melting of the GG20 duplex

Duplex	T_m/(K)	ΔH/(kJ·mol^{-1} of duplex)		ΔS/(J·K^{-1}·mol^{-1} of duplex)		ΔG_{298}/(kJ·mol^{-1} of duplex)	
		Calorimetric	UV absorption	Calorimetric	UV absorption	Calorimetric	UV absorption
GG20	343.4	636	632	1841	1753	87.4	109
Cisplatin-GG20	335.0	565	569	1690	1602	61.1	89.1
Change in property (GG20–cisplatinGG20)	8.4	71	63	151	151	26.4	20.1

Data taken from N. Poklar, D. S. Pilch, S. J. Lippard, E. A. Redding, S. U. Dunham, and K. J. Breslauer, "Influence of Cisplatin Intrastrand Crosslinking on the Conformation, Thermal Stability and Energetics of a 20-mer DNA Duplex," *Proc. Natl. Acad. Sci. USA*, **93**, 7606–7611 (1996).

site and the ones on either side of it, in this case TG/AC and GT/CA interactions. Summing up the enthalpic contributions from the GG/CC, TG/AC and GT/CA interactions given in Table 16.6 gives $46.0 + 24.3 + 27.2 = 97.5$ kJ·mol^{-1} of duplex. That is, complete disruption of these three base-stacking interactions would enthalpically destabilize the duplex by 97.5 kJ·mol^{-1} of duplex. Because of the uncertainty in the experimental calorimetric measurements on the GG20 and cisplatin-GG20 duplex melting, it is difficult to assess how significant is the difference between the observed (71 kJ·mol^{-1} of duplex) and calculated (97 kJ·mol^{-1} of duplex) enthalpic destabilization, but the results are certainly comparable. Also, calorimetric measurements on oligonucleotides showing similar changes in the phosphodiester helix suggest that there might be an enthalpic contribution not included in the base-stacking interactions table that could account for the difference.

Thermodynamic studies performed on a number of other guanosine adducts show some examples where binding represents an enthalpic destabilized, but entropy stabilized, process and others that are enthalpically stabilized, but entropically destabilized. The net thermodynamic result, however, appears to be a relatively modest localized free-energy destabilization that could form the basis for some recognition mechanism.

We end our discussion of biological thermodynamics with a quote from Kenneth Breslauer.[18]

> *As calorimeters are instruments that permit the direct and quantitative measurement of heat, it should not be surprising to learn that many of the giants of science ... were the first to build calorimeters, thereby establishing the field of calorimetry ... For the most part, the early calorimeters were used to measure heat changes accompanying simple, well-defined processes (e.g. ice melting and radioactive decay). However, it is of interest to note that some of the earliest calorimetric studies were conducted on more complex "biological" systems ... For example, in 1780, Lavoisier and Laplace built an "ice calorimeter" in which they placed a guinea pig. They measured the amount of ice melted and CO_2 produced by the animal over a 10-hour period and compared this with the heat produced in 10 hours on combustion of the equivalent amount of carbon. The experiment was inspired by their notion that animal respiration could be equated to simple combustion, so that the heat produced on exhalation of a specific amount of CO_2 should equal the heat produced by oxidation of the corresponding amount of carbon. In some sense, the measurements of Lavoisier and Laplace heralded the beginning of the field of biocalorimetry.*
>
> *... during the first half of the twentieth century the field of biocalorimetry was not widely embraced by the scientific community. However, during the 1960s, 1970s, and 1980s, biocalorimetry has experienced an explosive*

rebirth. This renewed interest can be attributed to four important factors. First, major advances in electronics have vastly improved the sensitivity of modern calorimetric instrumentation. Second, improvements in synthetic methodologies and biochemical separations/purifications now make available samples of sufficient purity and quantity for calorimetric measurements. Third, the development of a theoretical formalism coupled with advancements in computer technology now makes it possible to extract the maximum amount of information inherent in the raw calorimetric data. Finally, commercialization has made highly sensitive microcalorimeters more generally available to the scientific community so that the field of biocalorimetry no longer is restricted to those laboratories capable of building their own instruments.

Problems

P16.1 The reaction by which plants convert CO_2 into glucose by photosynthesis can be written as

$$6CO_2(g) + 6H_2O(l) = C_6H_{12}O_6(aq) + 6O_2(g)$$

Estimate how many 500 nm photons (in the green region of the spectrum) are needed to produce one mole of aqueous glucose, if the standard free-energy change for the reaction can be taken as a measure of the chemical work performed in the process.

P16.2 Derive the results for the self-complementary and nonself-complementary processes of molecularity n in Table 16.2.

P16.3 The protein, bovine pancreatic trypsin inhibitor (BPTI), contains a disulfide bond between cystine amino acids located at positions 30 and 51. This bond is buried deep within the hydrophobic core of the protein. Using spectroscopy and calorimetry, Breslauer *et al.*[19] have studied the effects on the stability of this protein when the disulfide bond is eliminated through the substitution of different amino acids at these two positions. Some of their results are summarized below:

Parameter	Protein			
	BPTI	C30V/C51A	C30T/C51A	C30A/C51S
$T_m/(K)$	377.6	345.1 ± 0.5	335.1 ± 0.5	329.1 ± 0.5
$\Delta H_{cal}/(kJ \cdot mol^{-1})$	312	249 ± 17	219 ± 17	211 ± 17
$\Delta H_{\nu H}/(kJ \cdot mol^{-1})$	324	58.9 ± 20	226 ± 20	240 ± 20
$\Delta S_{cal}/(J \cdot K^{-1} \cdot mol^{-1})$	778	720 ± 50	653 ± 50	640 ± 50

The following notation is used to name the mutant proteins: CpositionX where C = cystine position (either 30 or 51) and X represents the substituted amino acid. The following abbreviations are used to represent the amino acid substitutions: A = alanine, G = glycine, T = threonine, and S = serine.

(a) If the melting temperature is a measure of the overall stability, what effect does the elimination of the disulfide bond have on the stability of the mutant proteins?

(b) Is there a predominant contributor (enthalpic or entropic) to the change in stability of the mutant proteins relative to the native protein?

(c) Is the nature (cooperative versus noncooperative) of the melting transition affected by the substitutions?

P16.4 The tetramethylammonium ion (Me_4N^+) has been reported to stabilize oligonucleotides. Marky *et al.*[20] have studied its effect on the helix-to-coil transition in poly(dA-dT). They compared their results with similar studies conducted in solutions containing the sodium ion of the same concentration. The results are summarized below:

Salt	T_m/(K)		ΔH_{cal}/(kJ·mol^{-1} of base-pairs)	Cooperative unit
	UV optical	DSC		
1 M NaCl	348.5	347.6	28	27
1 M Me_4NCl	354.4	354.1	29	32

The cooperative unit as expressed here is the number of base-pairs in a given oligonucleotide duplex that melt together as a unit. Consider that the uncertainties of the melting temperatures are about ±1 K, and for the calorimetric enthalpies, about ±1kJ·mol^{-1} of base-pairs.

(a) What do the melting temperatures say about the stability of the duplex in the two salt solutions, and does this change in stability arise from enthalpic effects associated with the melting of the duplex?

(b) The size of the cooperative unit has been calculated from the ratio of the van't Hoff enthalpy to the calorimetric enthalpy and the known size of the oligonucleotide chain. Do these results support a claim that the Me_4N^+ ion stabilizes A-T base-pairings and prevents them from opening prematurely before the melting temperature?

References

1. J. T. Finer, R. M. Simmons, and J. A. Spudich, "Single Myosin Molecule Mechanics: Piconewton Forces and Nanometre Steps", *Nature*, **368**, 113–119 (1994).
2. F. Lipmann, "Metabolic Generation and Utilization of Phosphate Bond Energy", *Adv. Enzymol.*, **1**, 99–162 (1941).
3. H. Kalckar, "Lipmann and the Squiggle", in *Current Aspects of Biochemical Energetics*, N. O. Kaplan and E. P. Kennedy, eds., Academic Press, New York, 1966, pp. 1–8.
4. F. Lipmann, *Wanderings of a Biochemist*, Wiley-Interscience, New York, 1971, p. 37.
5. Quote taken from Internet at http://www.nobel.se/laureates/medicine-1953-press.html
6. P. L. Privalov and V. V. Plotnikov, "Three Generations of Scanning Microcalorimeters for Liquids", *Thermochim. Acta*, **139**, 257–277 (1989).
7. K. J. Breslauer, E. Freire, and M. Straume, "Calorimetry: A Tool for DNA and Ligand–DNA Studies", in *Methods in Enzymology*, D. M. J. Lilley and J. E. Dahlberg, Eds., Vol. **211**, pp. 533–567, Academic Press, San Diego (1992).
8. P. L. Privalov, "Scanning Microcalorimeters for Studying Macromolecules", *Pure Appl. Chem.*, **52**, 479–497 (1980).
9. G. I. Makhatadze and P. L. Privalov, "Energetics of Protein Structure", *Adv. Protein Chem.*, **47**, 307–425 (1995).
10. T. Lazaridis, G. Archontis, and M. Karplus, "Enthalpic Contribution to Protein Stability: Insights from Atom-based Calculations and Statistical Mechanics", *Adv. Protein Chem.*, **47**, 231–306 (1995).
11. E. Freire and R. L. Biltonen, "Statistical Mechanical Deconvolution of Thermal Transitions in Macromolecules. I. Theory and Application to Homogeneous Systems", *Biopolymers*, **17**, 463–479 (1978).
12. P. L. Privalov, "Stability of Proteins", *Adv. Protein Chem.*, **33**, 167–241 (1979).
13. P. L. Privalov and S. J. Gill, "Stability of Protein Structure and Hydrophobic Interaction", *Adv. Protein Chem.*, **39**, 191–234 (1988).
14. G. I. Makhatadze and P. L. Privalov, "Energetics of Protein Structure", *Adv. Protein Chem.*, **47**, 307–425 (1995).
15. P. L. Privalov, "Thermodynamic Problems of Protein Structure", *Ann. Rev. Biophys. Chem.*, **18**, 47–69 (1989).
16. T. V. Chalikian, J. Volker, G. E. Plum, and K. J. Breslauer, "A More Unified Picture for the Thermodynamics of Nucleic Acid Duplex Melting: A Characterization by Calorimetric and Volumetric Techniques", *Proc. Natl Acad. Sci. USA*, **96**, 7853–7858 (1999).
17. N. Poklar, D. S. Pilch, S. J. Lippard, E. A. Redding, S. U. Dunham, and K. J. Breslauer, "Influence of Cisplatin Intrastrand Crosslinking on the Conformation, Thermal Stability, and Energetics of a 20-mer DNA Duplex", *Proc. Natl Acad. Sci. USA*, **93**, 7606–7611 (1996).
18. K. J. Breslauer, E. Freire, and M. Straume, "Calorimetry: A Tool for DNA and Ligand–DNA Studies", *Methods Enzymol.*, **211**, 533–567 (1992).
19. Y. Liu, K. Breslauer, and S. Anderson, "'Designing' Out Disulfide Bonds: Thermodynamic Properties of 30–51 Cystine Substitution Mutants of Bovine Pancreatic Trypsin Inhibitor", *Biochemistry*, **36**, 5323–5335 (1997).
20. L.A. Marky, D. Patel, and K. J. Breslauer, "Effect of Tetramethylammonium Ion on the Helix-to-Coil Transition of Poly(deoxyadenylylthymidine): A Nuclear Magnetic Resonance and Calorimetric Investigation", *Biochemistry*, **20**, 1427–1431 (1981).

Chapter 17

Applications of Thermodynamics to Nonelectrolyte Solutions

It has been said "chemists have solutions!"[a] Solutions are involved in so many chemical processes[b] that we must have the mathematical tools to comfortably work with them, and thermodynamics provides many of these tools. Thermodynamic properties such as the chemical potential, partial molar properties, fugacities, and activities, provide the keys to unlock the description of mixtures.

Solutions are usually classified as "nonelectrolyte" or "electrolyte" depending upon whether one or more of the components dissociates in the mixture. The two types of solutions are often treated differently. In electrolyte solutions properties like the activity coefficients and the osmotic coefficients are emphasized, with the dilute solution standard state chosen for the solute.[c] With nonelectrolyte solutions we often choose a Raoult's law standard state for both components, and we are more interested in the changes in the thermodynamic properties with mixing, $\Delta_{mix}Z$. In this chapter, we will restrict our discussion to nonelectrolyte mixtures and use the change $\Delta_{mix}Z$ to help us understand the nature of the interactions that are occurring in the mixture. In the next chapter, we will describe the properties of electrolyte solutions.

---

[a] This phrase comes from a popular bumper sticker promoted by the American Chemical Society.

[b] What could possibly be a more important chemical reaction than

$$H^+(aq) + OH(aq) = H_2O(l).$$

[c] See Sections 11.4b and 11.4c of Chapter 11 for a discussion of standard states.

17.1 Excess Thermodynamic Properties

In Section 11.5a of Chapter 11, we indicated that for the mixing process, represented by

$$n_1\mathrm{A} + n_2\mathrm{B} + \cdots = \text{Solution}, \tag{17.1}$$

the change in Gibbs free energy $\Delta_{\text{mix}}G$ is given by

$$\Delta_{\text{mix}}G = RT \sum_i n_i \ln a_i, \tag{17.2}$$

where a_i, the activity in solution with a Raoult's law standard state, is given by

$$a_i = \gamma_{\text{R},i} x_i, \tag{17.3}$$

with $\gamma_{\text{R},i}$ as the activity coefficient and x_i the mole fraction. Substitution of equation (17.3) into (17.2) gives

$$\Delta_{\text{mix}}G = RT \sum_i (n_i \ln x_i + n_i \ln \gamma_{\text{R},i}). \tag{17.4}$$

For a mole of solution, equation (17.4) becomes

$$\Delta_{\text{mix}}G_{\text{m}} = RT \sum_i (x_i \ln x_i + x_i \ln \gamma_{\text{R},i}). \tag{17.5}$$

17.1a Thermodynamic Properties of Ideal Solutions

Equation (17.5) is the starting point for deriving equations for $\Delta_{\text{mix}}Z^{\text{id}}_{\text{m}}$, the change in Z_{m} to form an ideal mixture. For the ideal solution, $\gamma_{\text{R},i} = 1$ and equation (17.5) becomes

$$\Delta_{\text{mix}}G^{\text{id}}_{\text{m}} = RT \sum_i x_i \ln x_i. \tag{17.6}$$

The change in other thermodynamic properties to form the ideal mixture is easily obtained from equation (17.6). Differentiating equation (17.6) with respect to T and with respect to p gives

$$\Delta_{\text{mix}}S^{\text{id}}_{\text{m}} = -R \sum_i x_i \ln x_i \tag{17.7}$$

and

$$\Delta_{\text{mix}} V_{\text{m}}^{\text{id}} = 0. \tag{17.8}$$

Applying the relationships

$$\Delta_{\text{mix}} H_{\text{m}}^{\text{id}} = \Delta_{\text{mix}} G_{\text{m}}^{\text{id}} + T\Delta_{\text{mix}} S_{\text{m}}^{\text{id}} \tag{17.9}$$

and

$$\Delta_{\text{mix}} U_{\text{m}}^{\text{id}} = \Delta_{\text{mix}} H_{\text{m}}^{\text{id}} + p\Delta_{\text{mix}} V_{\text{m}}^{\text{id}} \tag{17.10}$$

gives

$$\Delta_{\text{mix}} H_{\text{m}}^{\text{id}} = 0 \tag{17.11}$$

and

$$\Delta_{\text{mix}} U_{\text{m}}^{\text{id}} = 0. \tag{17.12}$$

In real solutions, we describe the excess thermodynamic property Z_{m}^{E}. It is the excess in Z over that for the ideal solution. That is,

$$Z_{\text{m}}^{\text{E}} = \Delta_{\text{mix}} Z_{\text{m}} - \Delta_{\text{mix}} Z_{\text{m}}^{\text{id}}. \tag{17.13}$$

Applying equation (17.13) to equations (17.6) through (17.8), and (17.11) to (17.12) gives

$$G_{\text{m}}^{\text{E}} = RT \sum_i x_i \ln \gamma_{\text{R},i}, \tag{17.14}$$

$$H_{\text{m}}^{\text{E}} = \Delta_{\text{mix}} H_{\text{m}}, \tag{17.15}$$

$$U_{\text{m}}^{\text{E}} = \Delta_{\text{mix}} U_{\text{m}}, \tag{17.16}$$

and

$$V_{\text{m}}^{\text{E}} = \Delta_{\text{mix}} V_{\text{m}}. \tag{17.17}$$

The excess entropy is obtained from

$$S_{\text{m}}^{\text{E}} = \frac{H_{\text{m}}^{\text{E}} - G_{\text{m}}^{\text{E}}}{T}. \tag{17.18}$$

17.1b Thermodynamic Properties of Regular Solutions

On the molecular level, the mixing process can be thought of as the breaking of A–A types of interactions in component A and B–B types of interactions in component B, and replacing them with A–B interactions. In the ideal solution, the molecules A and B are of similar size, and the A–A, B–B, and A–B interactions are of the same strength and same energy. The result is that $\Delta_{mix}U_m^{id}$, $\Delta_{mix}H_m^{id}$, and $\Delta_{mix}V_m^{id}$, and hence, U_m^E, H_m^E and V_m^E are equal to zero. In the ideal solution, $\Delta_{mix}G_m^{id}$ is not zero, since work is required to separate this mixture into components, and $\Delta_{mix}G_m^{id}$ would equal this work,[d] but the equality of the interactions causes G_m^E to be zero.

In the regular solution, specific interactions such as hydrogen bonding, acid–base association, and charge transfer do not occur, but the intermolecular forces are no longer equal. That is, the energies associated with A–A and B–B interactions are not equal to the A–B interactions. Under these conditions, if the molecules are about the same size, it can be shown[e] that G_m^E is given by

$$G_m^E = x_1 x_2 w \tag{17.19}$$

where w is independent of composition, but may depend upon the temperature.

Starting with equation (17.19), equations for the activity coefficients can be derived. For $n = (n_1 + n_2)$ total moles, equation (17.19) becomes

$$G^E = (n_1 + n_2)x_1 x_2 w. \tag{17.20}$$

Differentiating equation (17.20) with respect to n_1 while holding n_2 constant and remembering that x_1 and x_2 are functions of n_1 gives, after some manipulation, the following relationship for $\ln \gamma_1$

$$\ln \gamma_1 = x_2^2 \frac{w}{RT}. \tag{17.21}$$

A similar derivation for $\ln \gamma_2$ gives

$$\ln \gamma_2 = x_1^2 \frac{w}{RT}. \tag{17.22}$$

---

[d] We recall that in a constant temperature and pressure process, ΔG is the work, other than pressure–volume work, associated with the process.

[e] For systems in which the molecules differ significantly in size, volume fractions replace mole fractions. For a detailed discussion, see J. H. Hildebrand and R. L. Scott, *Regular Solutions*, Prentice-Hall, Inc., Englewood Cliffs, New Jersey, 1962.

Equations for the other excess properties can also be obtained. Starting with

$$\left(\frac{\partial G_m^E}{\partial T}\right)_{p,n} = -S_m^E \tag{17.23}$$

and differentiating equation (17.19) gives

$$S_m^E = -x_1 x_2 \frac{\partial w}{\partial T}. \tag{17.24}$$

A combination of equations (17.19) and (17.24) then gives

$$H_m^E = x_1 x_2 \left(w - T\frac{\partial w}{\partial T}\right). \tag{17.25}$$

Equations (17.19) and (17.25) predict that a graph of G_m^E or H_m^E against x_2 should be of a parabolic shape and symmetric about $x_2 = 0.5$. As examples, Figure 17.1 shows graphs of G_m^E and H_m^E for the liquid (cyclohexane + 2,3-dimethylbutane), ($N_2 + O_2$), and (cyclohexane + methylcyclohexane) systems.[1] In each instance, the lines are the fit of equations (17.19) and (17.25) to the experimental data points. We note that the experimental G_m^E agree reasonably well with equation (17.19) for all three systems. In the case of H_m^E, deviations occur with the last of these systems, and it is the system where the largest differences in size and shape of the two types of molecules occur. It is often the case that G_m^E is more symmetrical with mole fraction than is H_m^E.

As an example of the failure of regular solution theory to correctly represent the properties of real systems, Figure 17.2 summarizes G_m^E and H_m^E at $T = 298.15$ K for binary mixtures of the four cycloalkanes: cyclopentane, cyclohexane, cycloheptane, and cyclooctane.[2] These are systems where one may expect that regular solution theory would work reasonably well, and yet major deviations from the symmetrical (and positive) G_m^E and H_m^E that are predicted for regular solutions are present. G_m^E is small in magnitude for all these systems. Symmetrical G_m^E curves are obtained for (cyclohexane + cycloheptane) and (cyclohexane + cyclooctane), but highly asymmetrical curves are obtained for other combinations, including the (cyclopentane + cyclooctane) system, where an "s"-shaped curve is obtained. Once again, H_m^E seems to show larger deviations from the regular solution prediction than does G_m^E. None of the H_m^E curves are highly symmetrical, with "s"-shaped curves obtained for two of the systems. Ewing and Marsh,[3] suggest that the unusually large (in magnitude) values for H_m^E

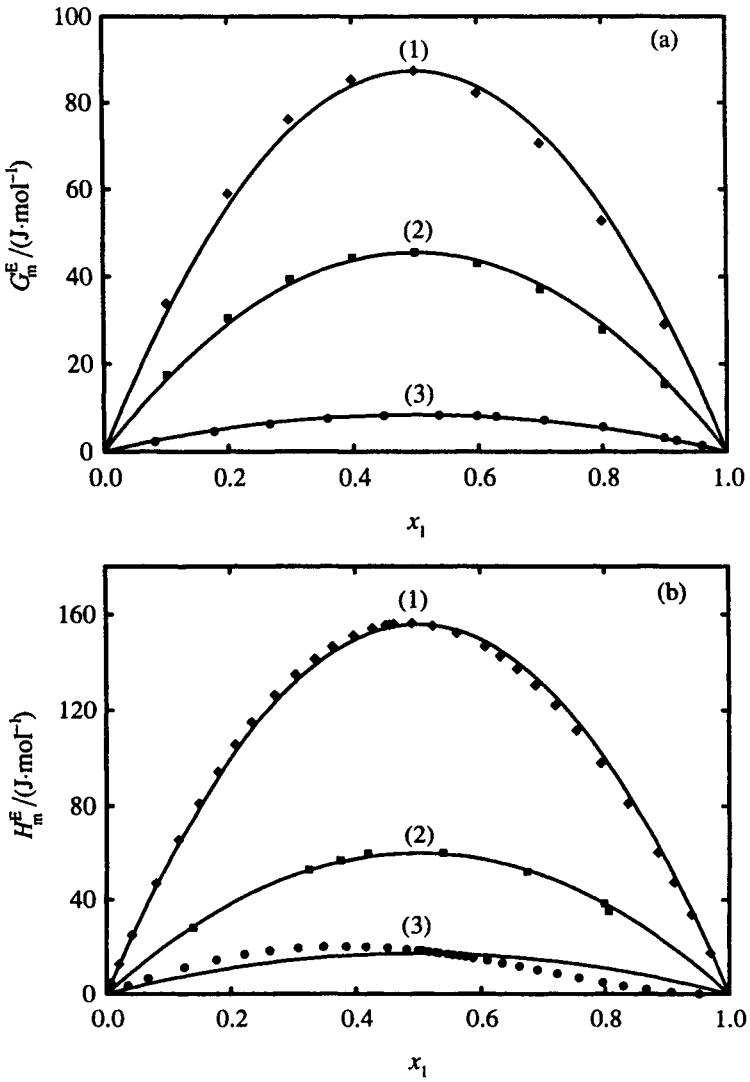

Figure 17.1 (a), Excess molar Gibbs free energies and (b) excess molar enthalpies for (1) (cyclohexane + 2,3-dimethylbutane); (2) (liquid) ($N_2 + O_2$); and (3) (cyclohexane + methylcyclohexane), with x_1 as the mole fraction of the cyclohexane or N_2. The lines are the predictions assuming regular solution behavior. The temperatures are 298.15 K in the cyclohexane systems, and 63.14 K (for G_m^E) and 80.3 K (for H_m^E) in the ($N_2 + O_2$) system.

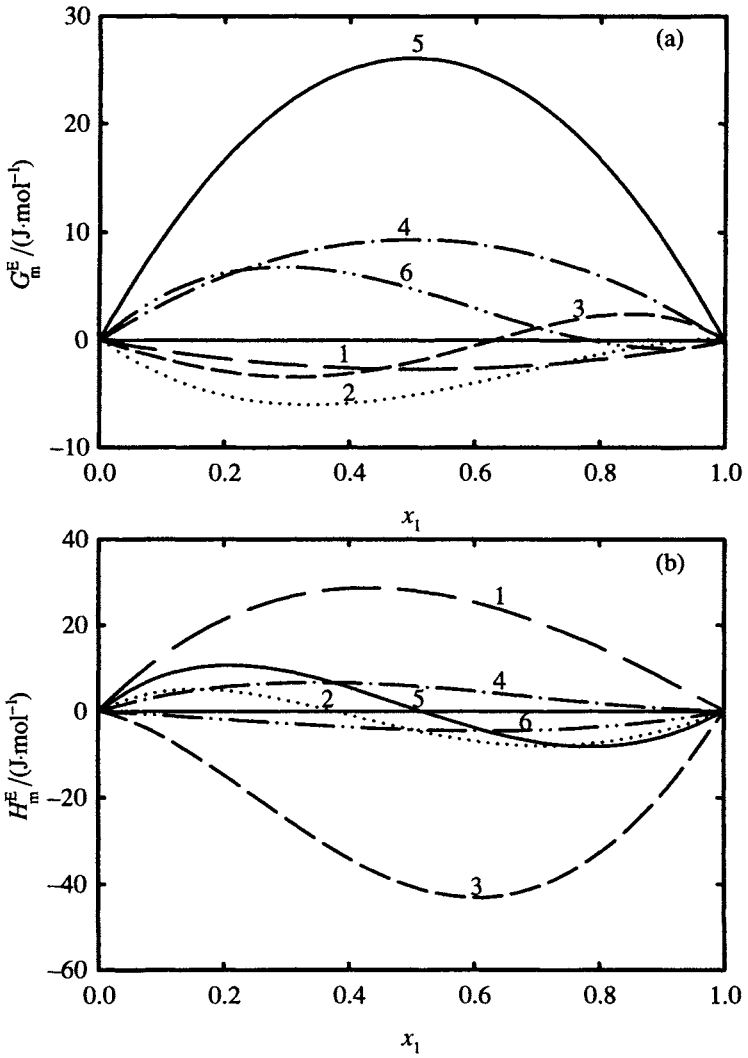

Figure 17.2 Comparison of (a) G_m^E and (b) H_m^E at $T = 298.15$ K for (x_1c-C_mH_{2m} + x_2c-C_nH_{2n}) with m less than n. The values of m and n are as follows: (1) $m = 5$, $n = 6$; (2) $m = 5$, $n = 7$; (3) $m = 5$, $n = 8$; (4) $m = 6$, $n = 7$; (5) $m = 6$, $n = 8$; (6) $m = 7$, $n = 8$.[2]

in the (cyclopentane + cyclohexane) and (cyclopentane + cyclooctane)[f] systems are due to the lack of flexibility (hindered conformational changes) of the cyclopentane ring, but a theoretical quantitative calculation has not been made that will verify this conclusion.

17.1c Examples of Thermodynamic Properties of Real Solutions

It should not be surprising to find out that most nonelectrolyte solutions are not ideal, nor are they regular.[g] Equations such as (17.19) or (17.25) do not adequately describe the functional dependence of G^E_m, H^E_m, or V^E_m on concentration. Extended forms are often used. A common one is the Redlick–Kister equation given by

$$Z^E_m = x_1 x_2 \sum_{j=0}^{m} a_j (1 - 2x_2)^j. \tag{17.26}$$

In equation (17.26), Z^E_m is G^E_m, H^E_m, or V^E_m, while x_1 and x_2 are the mole fractions and the A_i values are fitting coefficients, with as many chosen as needed to properly represent the experimental results.[h]

We now extend the discussion of excess properties to examples that help us to better understand the nature of interactions in a variety of nonelectrolyte mixtures. We will give examples showing temperature and pressure effects, including an example of solutions near the critical locus of the mixture and into the supercritical fluid region.

Nonpolar + Nonpolar mixtures[i]: Figure 17.3 summarizes the excess thermodynamic properties for (cyclohexane + hexane) mixtures.[j,4] We have chosen this

---

[f] Among the four cycloalkanes, cyclopentane is the most different in size and shape. It should not be surprising that the cyclopentane mixtures deviate most from the regular solution description.

[g] Regular solution theory is more of historical interest than of practical value. More sophisticated methods are now used to represent G^E_m and H^E_m. See, for example, J. J. Christensen, R. L. Rowley, and R. M. Izatt, *Handbook of Heats of Mixing: Supplementary Volume*, Wiley Interscience. New York, 1988, pp. 28–107.

[h] Note that equation (17.26) reduces to the regular solution equations [equation (17.19), (17.24), and (17.25)] when only one term is included. Extended forms of equation (17.26) can be found in the literature that include skewing factors in the denominator to shift the maximum to low- or high-mole fractions, and switching factors that change from one Redlick–Kister type of equation at low-mole fractions to a different one at high-mole fractions.

[i] Alkanes that we will use as examples in this section may have a small dipole moment. We may instead have appropriately titled this section as "Almost (Nonpolar + Nonpolar) Mixtures".

[j] The mixtures we describe first are at ambient pressure ($p \approx 0.1$ MPa). Later we will describe the effect of pressure on the excess thermodynamic properties.

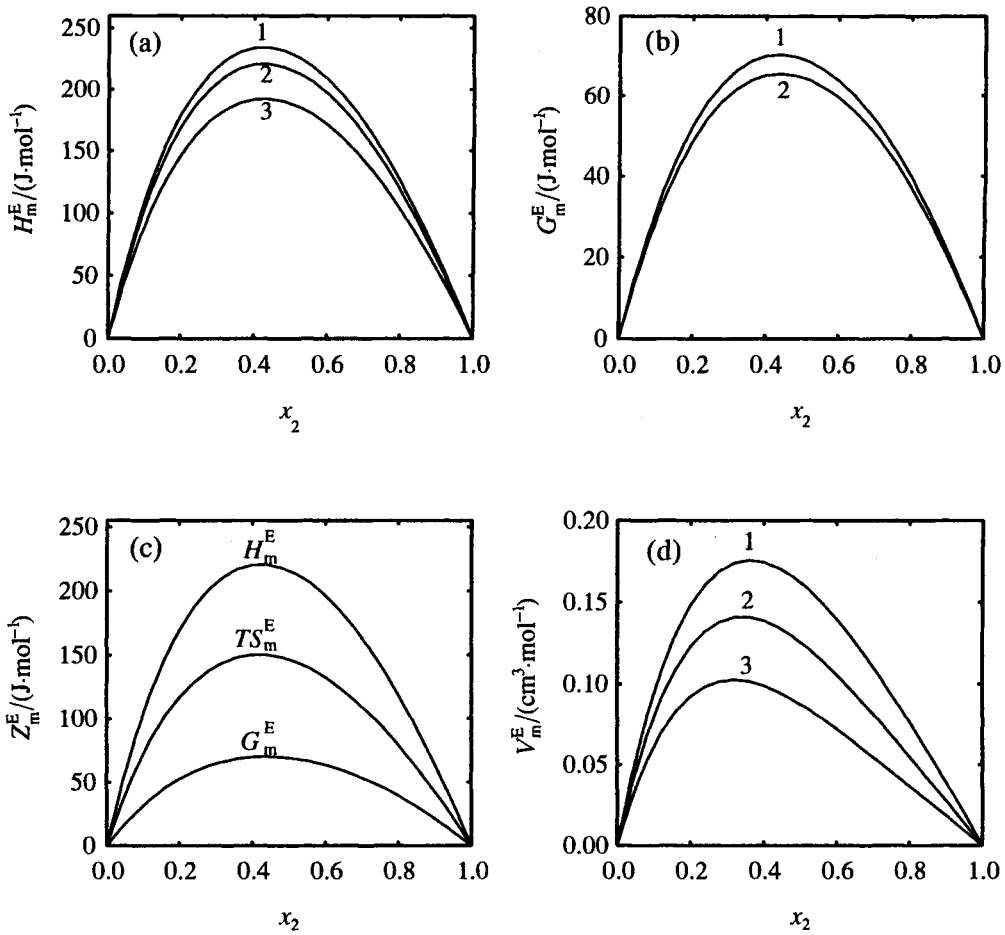

Figure 17.3 Excess molar properties at $p = 0.1$ MPa for $(x_1\text{c-}C_6H_{12} + x_2\text{n-}C_6H_{14})$.
(a) Excess molar enthalpies at (1), $T = 288.15$ K; (2) $T = 298.15$ K; and (3) $T = 318.15$ K.
(b) Excess molar Gibbs free energies at (1) $T = 298.15$ K; and (2) $T = 308.15$ K.
(c) Comparison of excess molar properties at $T = 298.15$ K.
(d) Excess molar volumes at (1) $T = 283.15$ K; (2) $T = 298.15$ K; and (c) $T = 313.15$ K.

system as representative of mixtures of nonpolar (or slightly polar) molecules, since it is often used as a reference system for checking and calibrating instruments that measure excess properties. The thermodynamic properties for this system are not unusual, but the results will serve as a point of reference as we look at other more varied systems. We will also use this system to review the

relationships among the various thermodynamic properties that must be followed for thermodynamic consistency.

Figure 17.3a compares H_m^E for (cyclohexane + hexane) at three temperatures. The curves are not symmetrical with mole fraction (as required for regular solution behavior), with maximum values of approximately 200 J·mol^{-1}, skewed toward the mole fraction of cyclohexane. As with previous examples, on the molecular level, we can think of the mixing process as one in which we replace A–A interactions (in cyclohexane) and B–B interactions (in hexane) with A–B interactions (between hexane and cyclohexane). The energy difference for this process is the major contributor to H_m^E. We will find this simplified qualitative description useful as we compare systems that contain different types of interactions.[k]

With an H_m^E of 200 J·mol^{-1}, the energy difference for the (cycloalkane + alkane) interactions is significant, when compared to the (alkane + alkane) and (cycloalkane + cycloalkane) interactions. For example, the maximum H_m^E for mixing (hexane + decane)[5] at 298.15 K is 14.5 J·mol^{-1}, while the maximum for mixing (cyclohexane–cycloheptane)[6] at 298.15 K is 6.8 J·mol^{-1}.

Figure 17.3b compares G_m^E at two temperatures for the (cyclohexane + hexane) system. The positive G_m^E indicates positive deviations from Raoult's law. The effect of temperature on G_m^E is related to the H_m^E results through the equation[l]

$$\left(\frac{\partial G_m^E/T}{\partial T}\right)_p = -\frac{H_m^E}{T^2}. \tag{17.27}$$

In fact, the G_m^E results in Figure 17.3b at $T = 308.15$ K were obtained from vapor pressure measurements and corrected to $T = 298.15$ K using equation (17.27).

Figure 17.3c compares H_m^E, G_m^E and TS_m^E with the entropy change calculated from

$$TS_m^E = H_m^E - G_m^E. \tag{17.28}$$

---

[k] A quantitative description would require much more specific information about the sizes, shapes, and energy surfaces of the molecules. Several different procedures have been used, including group contribution methods, equations of state, and volumetric methods. We leave such a discussion to sources that focus on the quantitative prediction of the excess properties. For a summary, see J. J. Christensen, R. L. Rowley, and R. M. Izatt, *Handbook of Heats of Mixing: Supplementary Volume*, Wiley-Interscience, New York, 1988.

[l] See equation (11.14) in Chapter 11.

The positive S^E_m indicates increased disorder in the mixture (over that for an ideal solution) as the alkane chain-like molecules are mixed with the almost spherical cycloalkane molecules.

Figure 17.3d compares V^E_m at three temperatures for (cyclohexane + hexane). The implication from these results is that chains and spheres do not pack as efficiently as do chains with chains, or spheres with spheres. This difference can better be seen by referring to Figure 17.4. In Figure 17.4a, we compare V^E_m for mixing cyclohexane with a series of n-alkanes.[7] We see that the bigger the chain, the less efficient the packing. This is in contrast to the mixing of hexane with other n-alkanes as shown in Figure 17.4b,[8] in which the negative V^E_m indicates that packing two alkanes of differing chain lengths is efficient, and becomes more so, the bigger the difference in chain length.

Figure 17.5 summarizes temperatures and pressure derivatives of H^E_m and V^E_m for (cyclohexane + hexane). Figure 17.5a gives $C^E_{p,m}$, the temperature derivative of H^E_m. That is,

$$C^E_{p,m} = \left(\frac{\partial H^E_m}{\partial T}\right)_p . \tag{17.29}$$

The values shown were obtained by numerically differentiating the H^E_m results given in Figure 17.3a. We note that $C^E_{p,m}$ is negative, reflecting the decrease in H^E_m with increasing temperature. The minimum (maximum absolute value of)

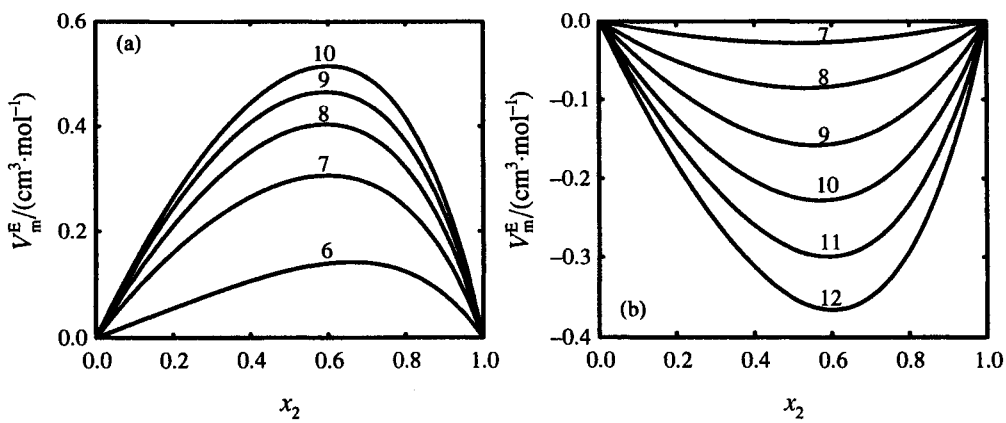

Figure 17.4 Excess molar volumes at $T = 298.15$ K and $p = 0.1$ MPa for (a) $(x_1C_mH_{2m+2} + x_2\text{c-}C_6H_{12})$; and (b) $(x_1C_mH_{2m+2} + x_2\text{n-}C_6H_{14})$. The numbers on the graph give m, the number of carbon atoms in the n-alkane.

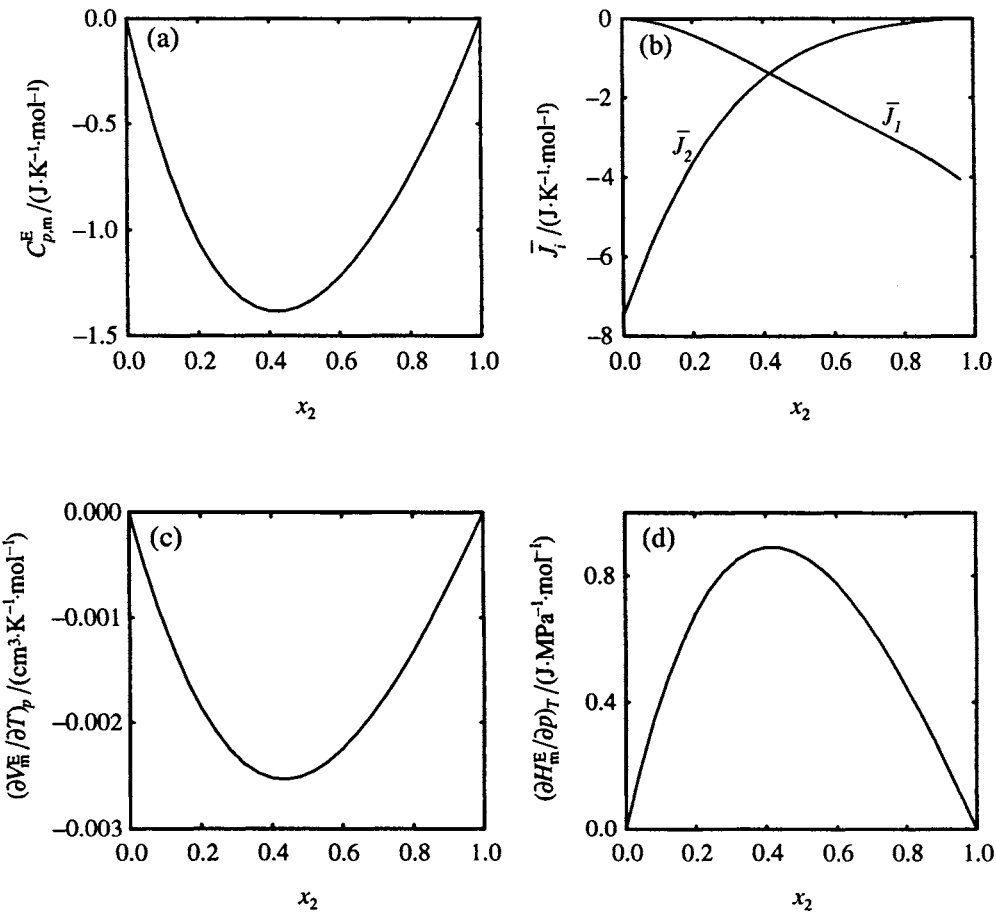

Figure 17.5 Derived thermodynamic properties at $T = 298.15$ K and $p = 0.1$ MPa for $(x_1\text{c-C}_6\text{H}_{12} + x_2\text{n-C}_6\text{H}_{14})$: (a) excess molar heat capacities obtained from the excess molar enthalpies; (b) relative partial molar heat capacities obtained from the excess molar heat capacities; (c) change of the excess molar volume with temperature obtained from the excess molar volumes; and (d) change of the excess molar enthalpies with pressure obtained from the excess molar volumes.

$C^{E}_{p,m}$ of $-1.4\ \text{J}\cdot\text{K}^{-1}\cdot\text{mol}^{-1}$ is again of moderate size. Figure 17.5b summarizes the relative partial molar heat capacity $\bar{J}_i = (\bar{C}_{p,m,i} - \bar{C}^{*}_{p,m,i})$. We note that the molar heat capacity of hexane in the infinitely dilute solution is $7.4\ \text{J}\cdot\text{K}^{-1}\cdot\text{mol}^{-1}$ less than the molar heat capacity of pure hexane.

Figure 17.5c summarizes the temperature derivative of the excess volume. The negative values reflect the fact that V^{E}_m as shown in Figure 17.3d decreases with increasing temperature. Apparently, with increasing temperature, the spheres and chains fit together better.

Figure 17.5d shows the effect of pressure on H^E_m as obtained from the equation[m]

$$\left(\frac{\partial H^E_m}{\partial p}\right)_T = V^E_m - T\left(\frac{\partial V^E_m}{\partial T}\right)_p. \tag{17.30}$$

The effect is small so that it takes large pressures to change H^E_m significantly. At the maximum $(\partial H^E_m/\partial p)_T$ at $x_2 \approx 0.4$, a pressure increase of 2.5 MPa changes H^E_m by approximately 1%. The major contribution to $(\partial H^E_m/\partial p)_T$ in equation (17.30) often comes from the $T(\partial V^E_m/\partial T)_p$ term. For the (n-hexane + cyclohexane) system at $x_2 = 0.4$ (a composition near the maximum value), approximately 85% of $(\partial H^E_m/\partial p)_T$ comes from this term at $T = 298.15$ K.

Polar + Nonpolar Mixtures Figure 17.6 summarizes H^E_m, $C^E_{p,m}$, and V^E_m for mixtures of 1-chlorobutane with heptane.[9] We note that H^E_m for this system is significantly larger than for any of the (nonpolar + nonpolar) systems described previously. A major contribution to H^E_m is the energy required to break apart the (dipole + dipole) interaction between the polar 1-chlorobutane molecules. Thus, if A–A represents (heptane + heptane) interactions and B–B represents (1-chlorobutane + 1-chlorobutane) interactions, with A–B representing (1-chlorobutane + heptane) interactions, then energy is required to break apart A–A that is not recovered when A–B forms, and H^E_m is positive.

Both $C^E_{p,m}$ and V^E_m are small for this system. The strength of (dipole + dipole) interactions is nearly temperature independent, and it is typical for H^E_m in systems of this type to change very little with temperature. Shown in Figure 17.6a are H^E_m at $T = 298.15$ K and 323.15 K, demonstrating the small temperature coefficient ($C^E_{p,m}$) for this system shown in Figure 17.6b. The small V^E_m shown in Figure 17.6c suggests that the chain-like heptane molecules pack well with the chain-like 1-chlorobutane molecules.

Another example of a system with (polar + nonpolar) interactions is shown in Figure 17.7, where curve 1 shows H^E_m for mixing non-polar tetrachloromethane molecules with polar acetonitrile molecules.[10] The breaking of (dipole + dipole) interactions in the acetonitrile when mixed with tetrachloromethane results in a large positive H^E_m.

An interesting comparison is made in Figure 17.7 between H^E_m for (tetrachloromethane + acetonitrile) (curve 1), and for (trichloromethane + acetonitrile) (curve 3), where fairly large negative H^E_m are obtained. These negative H^E_m are attributed to hydrogen bonding. The hydrogen in $CHCl_3$ has a

[m] See Table 11.1 for this and other differential relationships.

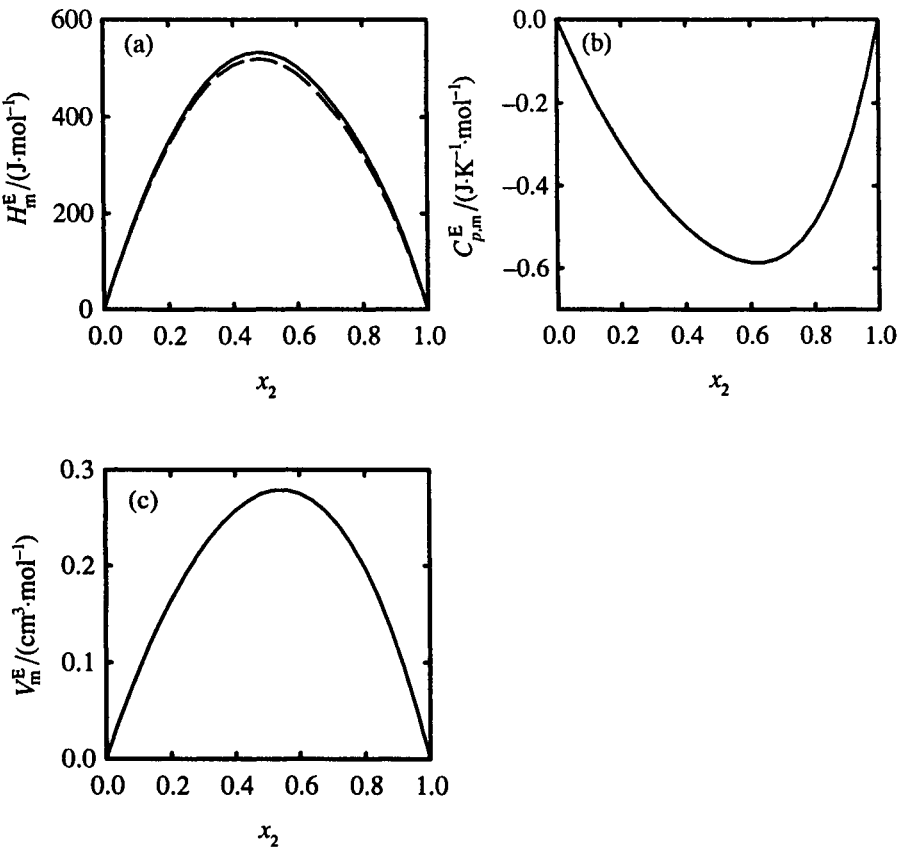

Figure 17.6 Excess molar properties at $p = 0.1$ MPa for $(x_1\text{n-}C_7H_{16} + x_2\text{1-}C_4H_9Cl)$; (a) gives the excess molar enthalpies. The solid line represents values at $T = 298.15$ K, while the dashed line gives values changed to $T = 323.15$ K, using the excess molar heat capacities at $T = 298.15$ K shown in (b). The excess molar volumes at $T = 298.15$ K are shown in (c).

high positive charge due to the three electronegative chlorines, and it is capable of hydrogen bonding. But strong hydrogen bonds form only with oxygen, fluorine, and nitrogen. Hence, strong hydrogen bonds are not present in liquid trichloromethane, but do form between the acetonitrile and the trichloromethane. When the liquids are mixed, an important result is the replacement of A–A (nonpolar + nonpolar) and B–B (dipole + dipole) interactions with A–B hydrogen bonds. In the process, the energy decreases, and H_m^E is negative.

Also shown as curve 2 in Figure 17.7 is H_m^E for the (dichloromethane + acetonitrile) system. Hydrogen bonds similar to those in the (trichloromethane + acetonitrile) system can occur, but are weaker because the hydrogen is polarized by

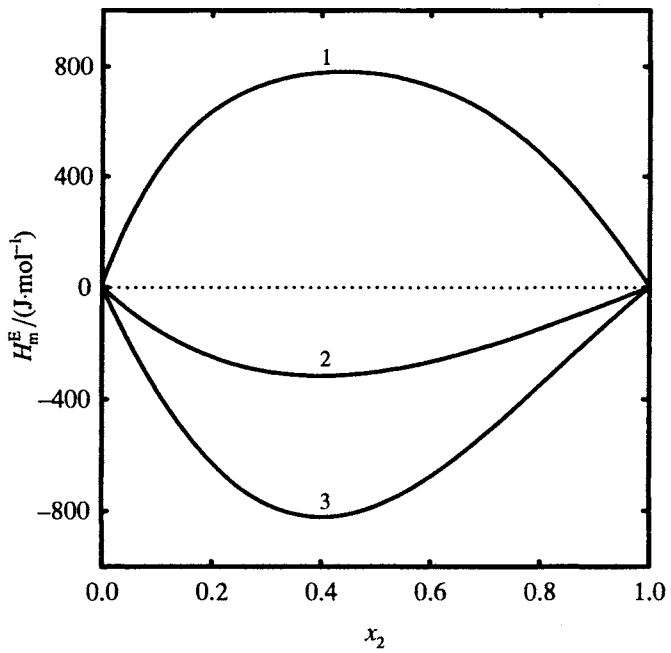

Figure 17.7 Excess enthalpies at $T = 298.15$ K for (1) $(x_1CCl_4 + x_2CH_3CN)$; (2) $(x_1CH_2Cl_2 + x_2CH_3CN)$; and (3) $(x_1CHCl_3 + x_2CH_3CN)$.

two (instead of three) chlorines in the CH_2Cl_2 molecule. These weaker hydrogen bonds release less energy (or enthalpy) than in the (trichloromethane + acetonitrile) system, and the H^E_m, although still less than zero, are smaller in magnitude.

Figure 17.8 summarizes H^E_m, $C^E_{p,m}$ and V^E_m for mixtures of cyclohexane with 1,4-dioxane (a cyclic diether, $C_4H_8O_2$) (curve 1), and oxane[11] (a cyclic ether, $C_5H_{10}O$) (curve 2). The values of H^E_m, V^E_m and $C^E_{p,m}$ for the oxane system are typical of those for a (polar + nonpolar) mixture, with a maximum H^E_m of approximately 450 J·mol^{-1} and small $C^E_{p,m}$, and V^E_m. For the 1,4-dioxane system, however, H^E_m and G^E_m are very large, with maxima in excess of 1600 J·mol^{-1} for H^E_m and 1000 J·mol^{-1} for G^E_m. V^E_m is also large, with a maximum of nearly 1 cm^3·mol^{-1}. Of special interest is the double minimum in $C^E_{p,m}$ as a function of x_2 for this system, as shown in Figure 17.10d. These so-called "W" heat capacity curves are unusual, but not uncommon. They occur in mixtures of a normal or cycloalkane with certain chemically dissimilar liquids. Saint-Victor and Patterson[12] have summarized a number of these systems, which include as the second component (in addition to 1,4-dioxane), trioxanonane, 2-butanone, 3-pentanone, 1,2-dichloroethane, 1,4-dichlorobutane, and tetraoxadodecane. Associated with each "W"-shaped $C^E_{p,m}$ curve are large H^E_m, G^E_m and V^E_m maximum values.

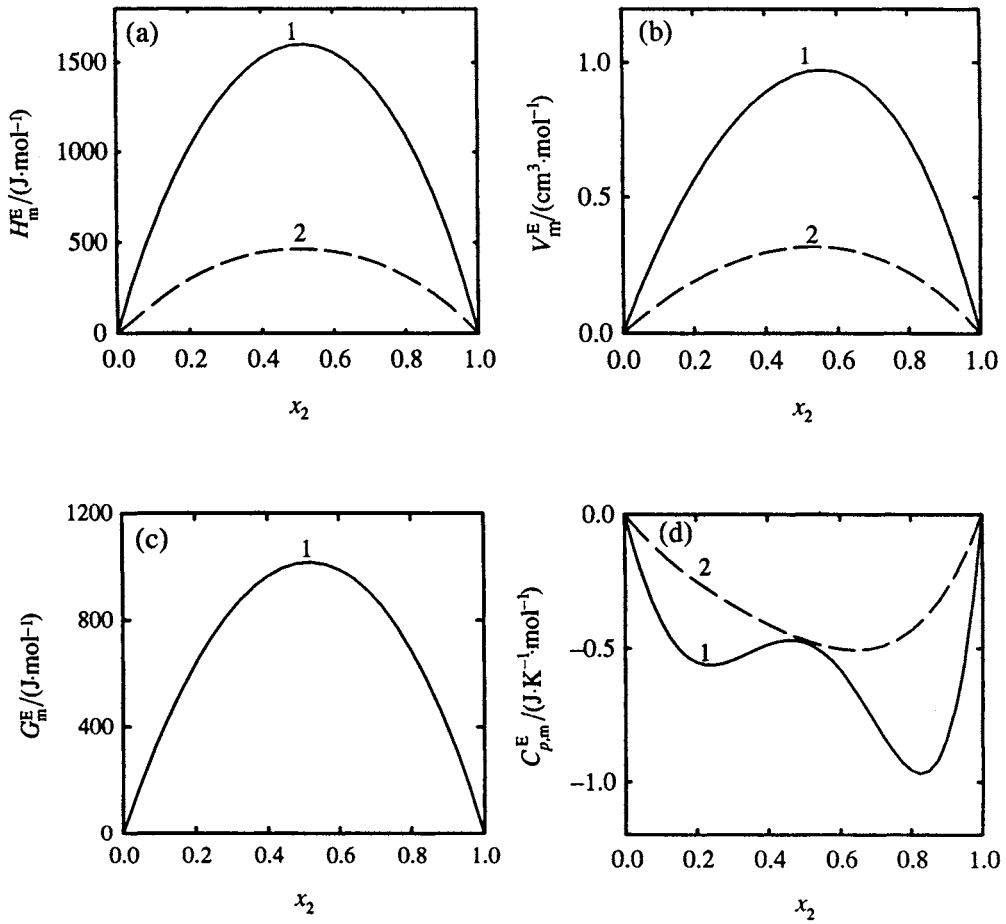

Figure 17.8 (a) Excess molar heat enthalpies; (b) excess molar volumes; (c) excess molar Gibbs free energies; and (d) excess molar heat capacities at $T = 298.15$ K and $p = 0.1$ MPa for cyclohexane (C_6H_{12}) with 1,4-dioxane ($C_4H_8O_2$), and with oxane ($C_5H_{10}O$). The curves are (1) (x_1c-$C_4H_8O_2 + x_2$c-C_6H_{12}), and (2) (x_1c-$C_5H_{10}O + x_2$c-C_6H_{12}).

Patterson, Wilhelm, and others[13] have proposed an explanation for this behavior. They suggest that a random contribution to $C^E_{p,m}$ is present of the type we observed in Figures 17.5, 17.6, and for the (oxane + cyclohexane) system as shown in Figure 17.8. This contribution would be negative and approximately parabolic in shape. In addition, a nonrandom contribution is present that is nonparabolic in form and concave upwards with the major contribution in the mid-mole fraction range. This contribution results from concentration fluctuations in the solution. The sum of these two contributions

would result in a "W"-shaped $C^{E}_{p,m}$ curve as a function of x_2. Concentration fluctuations should result in concentration and density gradients in the solution and cause light scattering. This scattering has been observed, which lends support to this explanation.[14]

Polar + Polar Mixtures When molecules with large dipole moments are mixed, the magnitude and sign of H^{E}_{m} depends upon the relative strength of the A–A, B–B and A–B interactions. For example, Figure 17.9 compares H^{E}_{m} for mixtures of (dimethylsulfoxide + acetone)[15] (curve 1), (nitromethane + acetonitrile)[16] (curve 2), and (acetone + acetonitrile)[17] (curve 3). For (nitromethane + acetonitrile), apparently the A–A, B–B, and A–B interactions are of very nearly the same strength, leading to an H^{E}_{m} very close to zero over the entire composition range. On the other hand, A–B interactions are weaker than A–A and B–B interactions in (dimethylsulfoxide + acetone), leading to a positive H^{E}_{m}, while the reverse is true in the (acetone + acetonitrile) system.

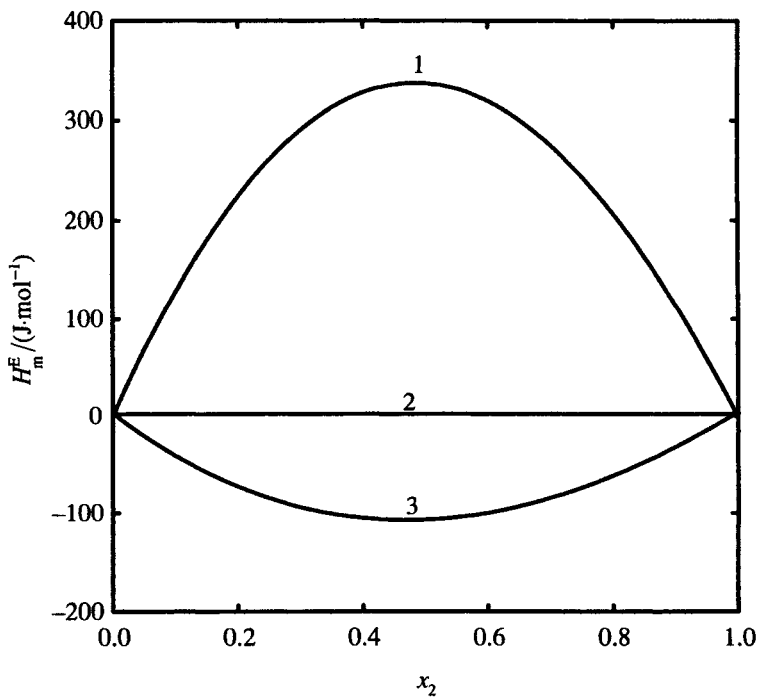

Figure 17.9 Excess enthalpies at $T = 298.15$ K and $p = 0.1$ MPa for mixtures of polar fluids. The symbols designating the system are: (1) $\{x_1(CH_3)_2SO + x_2(CH_3)_2CO\}$; (2) $\{x_1CH_3NO_2 + x_2CH_3CN\}$; (3) $\{x_1(CH_3)_2CO + x_2CH_3CN\}$.

Mixtures With Complex Formation: In some instances, mixing of two liquids causes the formation of a chemically bonded complex in the mixture. One would expect that the formation of the complex should result in a significant lowering in energy and hence, a large negative H_m^E. Examples are shown in Figure 17.10[18] for mixtures of tetrachloromethane with N,N-dimethylformamide (DMF) and with 1,4-dioxane.

The excess Gibbs free energies are positive for these systems, indicating positive deviations from Raoult's law as these polar and nonpolar molecules are mixed. But H_m^E is negative over most of the concentration range for the first of these systems and over the entire concentration range for the second, indicating

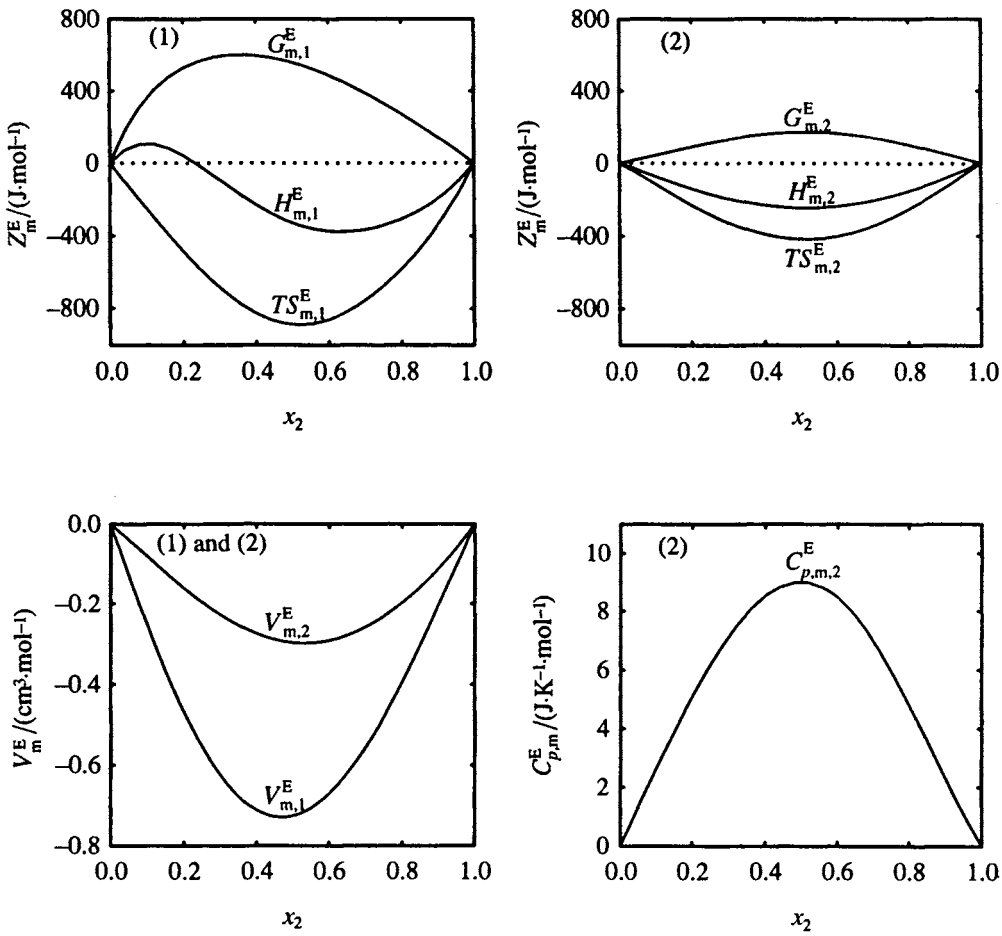

Figure 17.10 Excess molar thermodynamic functions at $T = 298.15$ K and $p = 0.1$ MPa for (1) $\{x_1CCl_4 + x_2HCON(CH_3)_2\}$ and (2) $\{x_1CCl_4 + x_2p\text{-}C_4H_8O_2\}$.

a lowering in energy. Even more significant is the large negative S^E_m, indicating structure in the mixtures. These effects suggest complex formation that can be represented by an equilibrium reaction of the type

$$A(l) + B(l) = AB \text{ (in solution)}.$$

The negative V^E_m support this conclusion, since one would expect the formation of a complex to shrink the volume of the system. Temperature should have a significant effect on the formation of the complex by shifting the point of equilibrium in the reaction. Thus H^E_m and S^E_m should be very temperature-dependent. This is verified by the large positive $C^E_{p,m}$ for the (dioxane + tetrachloromethane) system as shown in Figure 17.10d.[n]

(Solid + liquid) phase studies can be found in the literature for both (tetrachloromethane + DMF)[19] and (tetrachloromethane + 1,4 dioxane).[20] Solid molecular addition compounds form in both systems. The formation of these compounds has been attributed to a charge-transfer interaction in which electrons from the nitrogen in DMF, or the oxygen in 1,4-dioxane, are transferred to the chlorines in the tetrachloromethane. A similar process could account for the complex formation in the liquid mixture. The DMF·CCl_4(s) addition compound is an especially strong one, with an enthalpy of formation from the solid components[21] of -11.11 kJ·mol^{-1}. One would expect the nitrogen in DMF to be a better electron donor than the oxygens in 1,4-dioxane. The relative size of the H^E_m, S^E_m and V^E_m shown in Figure 17.10 when (DMF + tetrachloromethane) (1) is compared to (1,4 dioxane + tetrachloromethane) (2) agrees with this expectation.

Hydrogen-Bonded Systems: In Figure 17.7, we explained the negative H^E_m for mixtures of acetonitrile with trichloromethane and with dichloromethane as resulting from the formation of a hydrogen bond between the hydrogen of the chlorinated methane and the nitrogen of the acetonitrile. A more common occurrence is the mixing of a liquid containing hydrogen bonds, such as water or an alkanol, with a second component that cannot hydrogen bond. In such a case, the net effect is the breaking of hydrogen bonds. The A–B interactions are much weaker than the A–A hydrogen-bond interactions, and H^E_m is large and positive. An example is shown in Figure 17.11 for mixtures of n-butane with 1-butanol.[22] In Figure 17.11a, we note the large positive H^E_m resulting from the breaking of hydrogen bonds as the 1-butanol is diluted with butane. Also shown in Figure 17.11a is the large temperature effect on H^E_m,[o] giving rise to the large

---

[n] The $C^E_{p,m}$ shown in Figure 17.10 (for tetrachloromethane + 1,4-dioxane) were obtained from the change in H^E_m with T. H^E_m results at several temperatures are not available for (tetrachloromethane + DMF) and a similar $C^E_{p,m}$ curve could not be obtained for this system.

[o] The large $C^E_{p,m}$ is in contrast to that for mixtures of alkanes with polar molecules. See Figure 17.6.

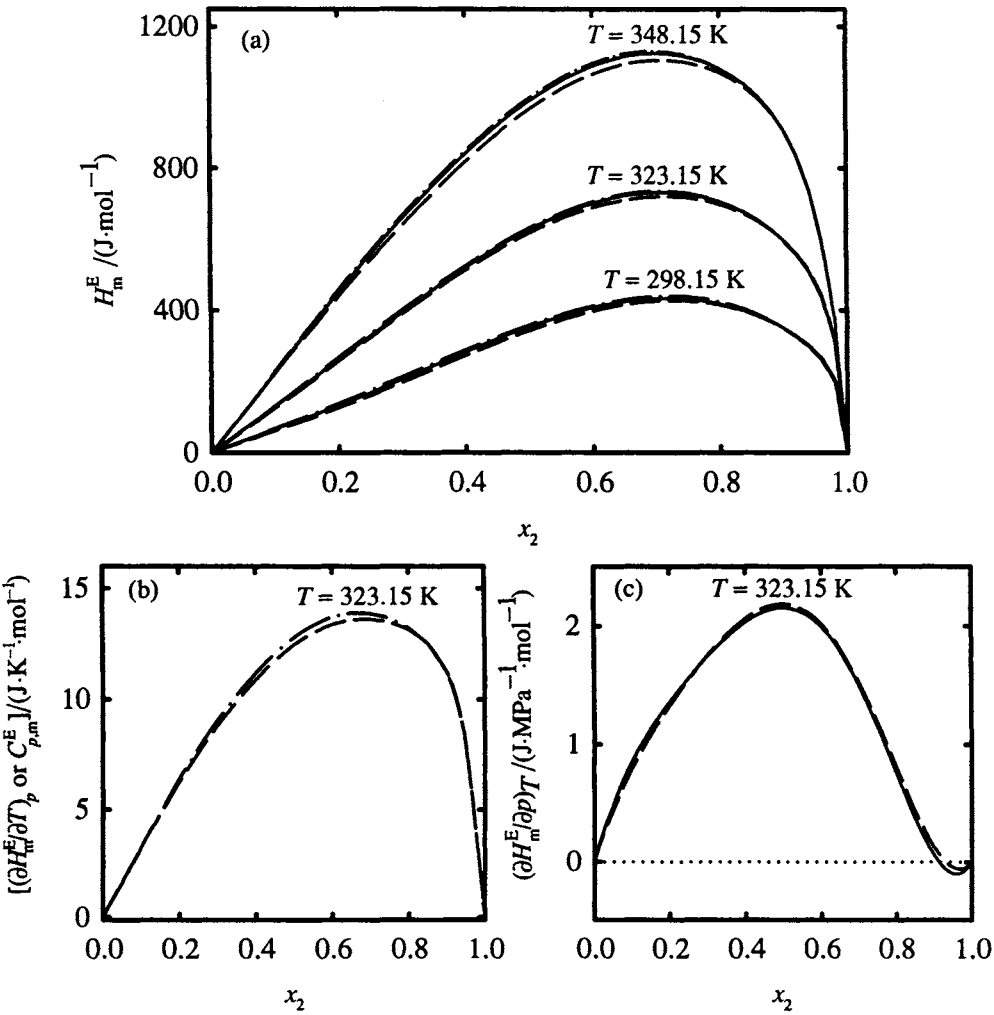

Figure 17.11 Graph of (a) H^E_m; (b) $(\partial H^E_m/\partial T)_p$; and (c) $(\partial H^E_m/\partial p)_T$ for ($x_1$1-$C_4H_9OH + x_2$n-C_4H_{10}). In (a), the pressures are $p = 5$ MPa (dashed line), $p = 10$ MPa (solid line), and $p = 15$ MPa (dash-dot line). In (b), $p = 5$ MPa (dashed line); and $p = 15$ MPa (dash-dot line). In (c), $p = 10$ MPa, with the solid line giving the calculation from V^E_m results and the dashed line giving the calculation from H^E_m.

positive $C^E_{p,m}$ shown in Figure 17.11b. This temperature effect is usually explained as being due to the fact that as the temperature increases, hydrogen bonds break more easily, so that more break during mixing at higher temperatures, and more energy is required in the mixing process, leading to a larger H^E_m.

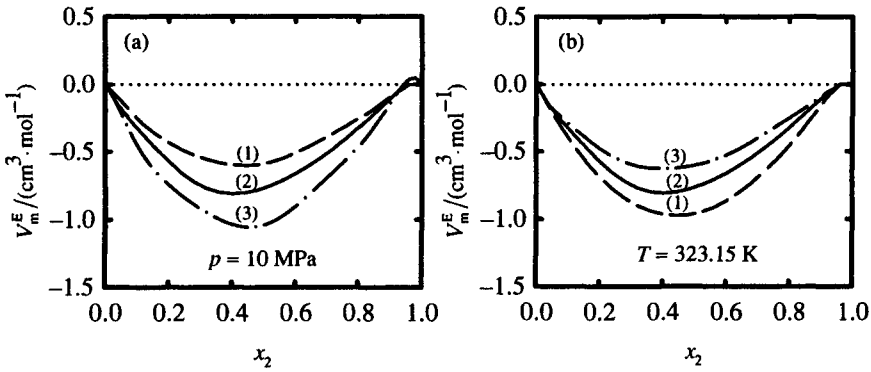

Figure 17.12 Excess molar volumes for ($x_1$1-C_4H_9OH + x_2n-C_4H_{10}) as a function of temperature and pressure. In (a), $p = 10$ MPa with (1) $T = 298.15$ K, (2) $T = 323.15$ K, and (3) $T = 348.15$ K. In (b), $T = 323.15$ K with (1) $p = 5$ MPa, (2) $p = 10$ MPa, and (3) $p = 15$ MPa.

Figure 17.12 summarizes V_m^E for the same (butane + 1-butanol) system, with the effect of temperature on V_m^E shown in Figure 17.12a and the effect of pressure in Figure 17.12b. Breaking hydrogen bonds causes the system to contract so that V_m^E is negative. This contraction increases with increasing temperature as more bonds are broken, and V_m^E becomes more negative with increasing temperature (Figure 17.12a). On the other hand, increasing the pressure suppresses the breaking of hydrogen bonds, so that V_m^E decreases with increasing pressure (Figure 17.12b).

Figure 17.11a shows the effect of pressure on H_m^E, with the measurements made at $p = 5$, 10 and 15 MPa. From these results, the pressure coefficient $(\partial H_m^E/\partial p)_T$ can be calculated. It can also be calculated from the V_m^E results using equation (17.30). Figure 17.11c compares $(\partial H_m^E/\partial p)_T$ calculated by the two methods. The excellent agreement is an example of thermodynamic consistency, and is verification of the reliability of the measurements.

17.2 The Excess Thermodynamic Properties and (Liquid + Liquid) Phase Equilibrium

Figure 17.13a shows H_m^E for the (cyclohexane + acetonitrile) system at (1), $T = 348.15$ K and (2), $T = 323.15$ K. At the higher temperature, a large positive H_m^E is obtained, as expected for a (nonpolar + polar) mixture. At the lower temperature, (liquid + liquid) phase equilibrium with phase separation is present and a break occurs in the H_m^E curve. The breaks at points (i) and (ii) are at compositions corresponding to the solubilities given by the (liquid + liquid) phase diagram shown in Figure 17.13b. Breaks in H_m^E curves such as at (i) and

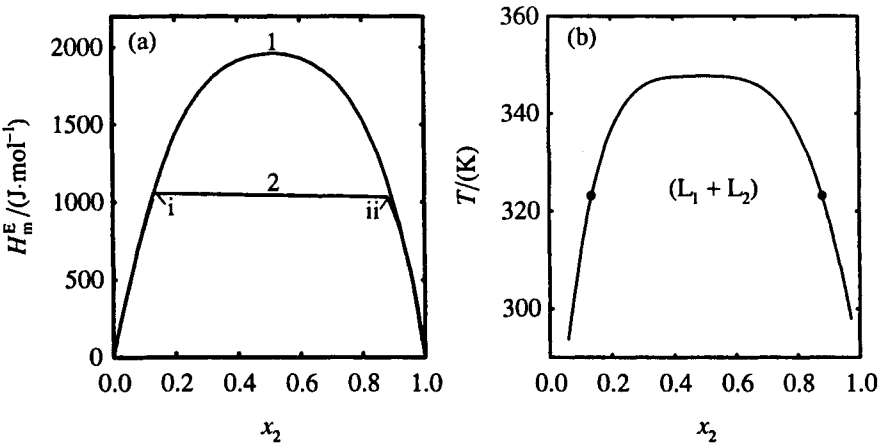

Figure 17.13 (a), Excess molar enthalpies; and (b) (liquid + liquid) equilibria at $p = 0.1$ MPa for $(x_1CH_3CN + x_2c\text{-}C_6H_{12})$. The temperatures in (a) are (1) 348.15 K and (2) 323.15 K. The data points (•) in (b) correspond to the breaks in the H^E_m curve at 323.15 K in (a).

(ii) can be used to construct (liquid + liquid) equilibrium curves,[23] although usually not as easily as can be done using other techniques.

We can use thermodynamics to predict the arithmetic sign of the excess molar properties above above the temperature (UCST) of the upper critical end point (UCEP), and below the temperature (LCST) of a lower critical end point (LCEP). At an (UCEP), the chemical potential goes through a point of inflection. The result is that

$$\left(\frac{\partial \mu_2}{\partial x_2}\right)_{p,T} = \left(\frac{\partial^2 \mu_2}{\partial x_2^2}\right)_{p,T} = 0. \tag{17.31}$$

Equation (17.31) applies equally well at a lower critical end point (LCEP). Furthermore, the Gibbs–Duhem equation {equation (11.22)} requires that if these equations are valid for component 2, then the same must be so for component 1. That is

$$\left(\frac{\partial \mu_1}{\partial x_2}\right)_{p,T} = \left(\frac{\partial^2 \mu_1}{\partial x_2^2}\right)_{p,T} = 0. \tag{17.32}$$

Equations (17.31) and (17.32) can be used to derive equations describing the behavior of G^E_m, H^E_m, and S^E_m at the UCEP and the LCEP. We start with the

relationship

$$G_m^E = H_m^E - TS_m^E. \tag{17.33}$$

Differentiating twice with (p and T) held constant gives

$$\left(\frac{\partial^2 G_m^E}{\partial x_2^2}\right)_{p,T} = \left(\frac{\partial^2 H_m^E}{\partial x_2^2}\right)_{p,T} - T\left(\frac{\partial^2 S_m^E}{\partial x_2^2}\right)_{p,T}. \tag{17.34}$$

The total molar Gibbs free energy in a mixture is given by

$$G_m = x_1\mu_1 + x_2\mu_2.$$

Substituting (with a Raoult's law standard state) the relationship between μ and mole fraction

$$\mu_1 = \mu_1^* + RT\ln\gamma_{R,1}x_1$$

$$\mu_2 = \mu_2^* + RT\ln\gamma_{R,2}x_2$$

gives

$$G_m = x_1(\mu_1^* + RT\ln x_1) + x_2(\mu_2^* + RT\ln x_2) + G_m^E \tag{17.35}$$

where

$$G_m^E = RT(x_1\ln\gamma_{R,1} + x_2\ln\gamma_{R,2}).$$

Differentiating equation (17.35), again with p and T held constant, rearranging, and making use of equations (17.31) and (17.32) gives

$$\left(\frac{\partial^2 G_m}{\partial x_2^2}\right)_{p,T} = \frac{RT}{x_1x_2} + \left(\frac{\partial^2 G_m^E}{\partial x_2^2}\right)_{p,T} = 0. \tag{17.36}$$

Combining equations (17.34) and (17.36) gives

$$T\left(\frac{\partial^2 S_m^E}{\partial x_2^2}\right)_{p,T} - \left(\frac{\partial^2 H_m^E}{\partial x_2^2}\right)_{p,T} = \frac{RT}{x_1x_2}. \tag{17.37}$$

Since RT/x_1x_2 is everywhere positive, equation (17.37) becomes

$$T\left(\frac{\partial^2 S_m^E}{\partial x_2^2}\right)_{p,T} - \left(\frac{\partial^2 H_m^E}{\partial x_2^2}\right)_{p,T} > 0. \tag{17.38}$$

By starting with the above equations and doing a Taylor series expansion of G_m^E and H_m^E around the critical end point, one can show the following:

For an UCEP

$$\left(\frac{\partial^2 G_m^E}{\partial x_2^2}\right)_{p,T} = -\frac{RT}{x_1x_2}; \quad \left(\frac{\partial^2 H_m^E}{\partial x_2^2}\right)_{p,T} < 0; \quad \left(\frac{\partial^2 S_m^E}{\partial x_2^2}\right)_{p,T} \leqslant \frac{R}{x_1x_2}. \tag{17.39}$$

For a LCEP

$$\left(\frac{\partial^2 G_m^E}{\partial x_2^2}\right)_{p,T} = -\frac{RT}{x_1x_2}; \quad \left(\frac{\partial^2 H_m^E}{\partial x_2^2}\right)_{p,T} > 0; \quad \left(\frac{\partial^2 S_m^E}{\partial x_2^2}\right)_{p,T} \geqslant \frac{R}{x_1x_2}. \tag{17.40}$$

Furthermore, if $G_m^E(x_2)$, $H_m^E(x_2)$ and $S_m^E(x_2)$ maintain the same arithmetic sign for all x_2[p], it follows that:

For an UCEP

$$G_m^E > 0; \; H_m^E > 0, \; S_m^E \geqslant 0 \text{ or } < 0, \quad \text{but satisfying equation (17.39).} \tag{17.41}$$

For a LCEP

$$G_m^E > 0, \; H_m^E \leqslant 0, \; S_m^E < 0, \quad \text{but satisfying equation (17.40).} \tag{17.42}$$

The derivation of the equation leading to the above conclusions is straightforward, but somewhat lengthy, and we leave it to others.[q]

---

[p] That is, the excess function remains either > 0 (convex upward) or < 0 (convex downward) over the entire composition range.

[q] For a derivation of the relationships expressed in equations (17.39) to (17.42) see I. Prigogine and R. Defay (translated by D. H. Everett), *Chemical Thermodynamics*, John Wiley and Sons, Inc., New York, 1962, pp. 284–288.

These equations lead to some interesting conclusions. At an UCEP, equation (17.38) is satisfied even if S_m^E is zero since $(\partial^2 H_m^E/\partial x_2^2) < 0$. Thus, the formation of an UCEP is controlled by an enthalpy (or energy) effect. On the other hand, for a LCEP, $(\partial^2 H_m^E/\partial x_2^2)_{p,T} > 0$. To satisfy equation (17.38), $(\partial^2 S_m^E/\partial x_2^2)_{p,T}$ must be greater than zero, and large enough to exceed the contribution from H_m^E. Thus, we can say that the formation of a LCEP is controlled by an entropy effect. That is, the LCEP is related to a large deviation of the entropy of mixing from the ideal value.

On the molecular level, an UCEP often occurs when polar molecules are mixed with nonpolar molecules, with energy required to separate the polar molecules when diluted with nonpolar molecules. A LCEP happens when interactions between molecules result in complex formation and a resultant large entropy stabilization. This is not a very common occurrence. The hydrogen bond can cause the formation of such complexes, and a LCEP, when it forms, often involves mixtures of components that can hydrogen bond.

Our analysis above applies at the UCEP or the LCEP, but we can extend it to include the one-phase region in the neighborhood of, but above the UCEP; or near, but below, the LCEP. Figure 17.14 schematically summarizes these relationships.

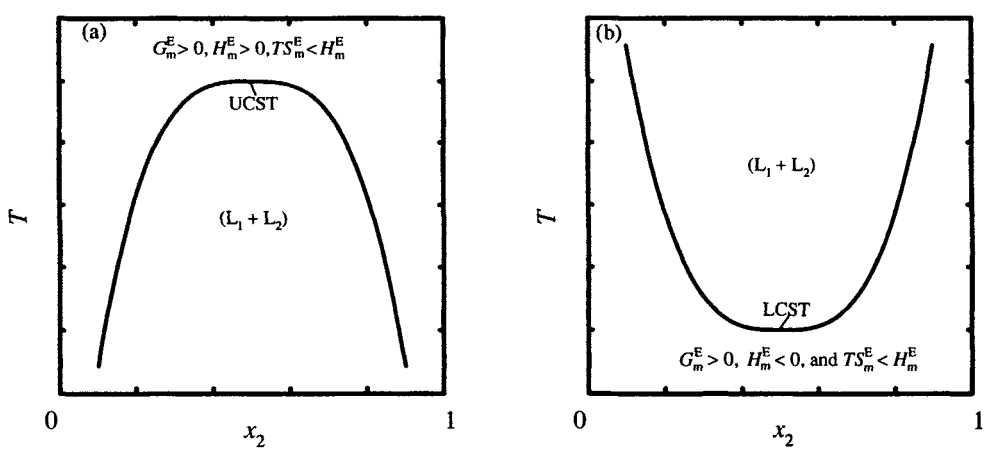

Figure 17.14 Schematic (liquid + liquid) phase diagrams showing the expected arithmetic sign of the excess molar properties at (a) just above the UCST and (b) just below the LCST.

As an example, Figure 17.15a shows the (liquid + liquid) phase diagram (a system with an UCST) for the (cyclohexane + methanol) system and Figure 17.15b gives G^E_m, H^E_m, and TS^E_m for this system at a temperature near, but above, the UCST.[24] The arithmetic signs of the results are in agreement with those

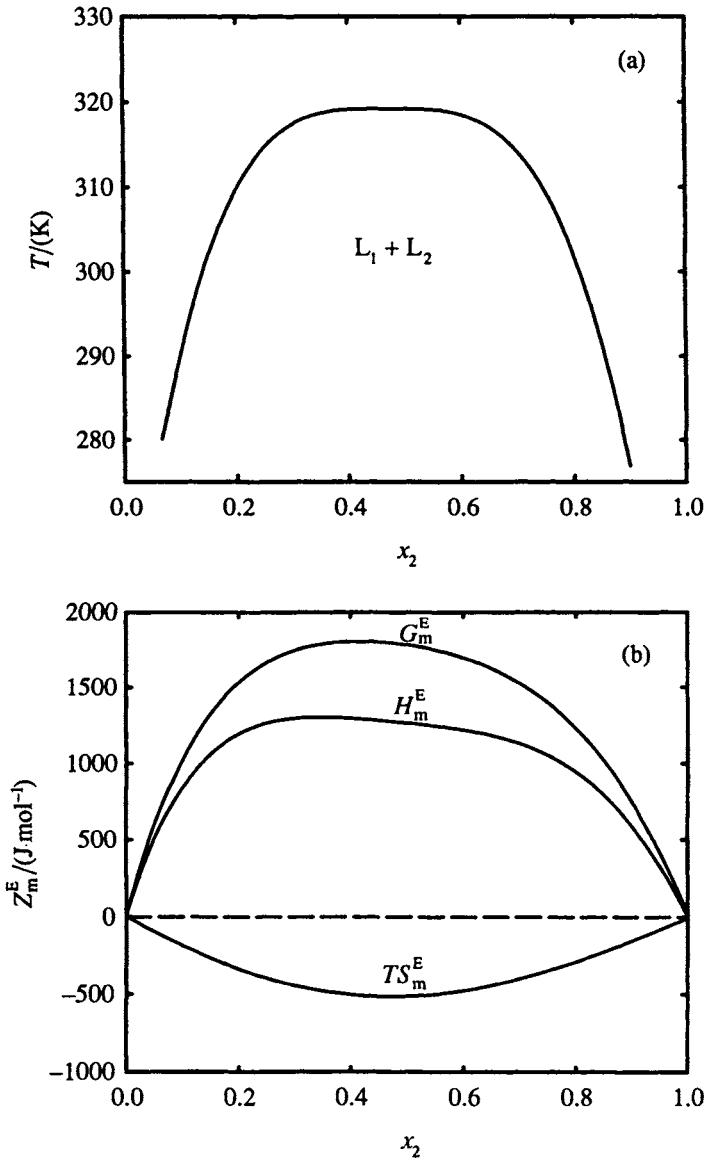

Figure 17.15 (a) (Liquid + liquid) phase equilibria and (b) excess thermodynamic functions at $T = 323.15$ K, for (x_1c-C_6H_{12} + x_2CH_3OH).

summarized in Figure 17.14a. Figure 17.16a shows the (liquid + liquid) phase diagram for the (water + triethylamine) system.[25] Evident is the LCEP[r] with $T_c \approx 292$ K and $x_{2,c} \approx 0.09$. Figure 17.16b gives G^E_m, H^E_m, and TS^E_m for this system[26] at $T = 283.15$ K, a temperature just below the LCST. The results

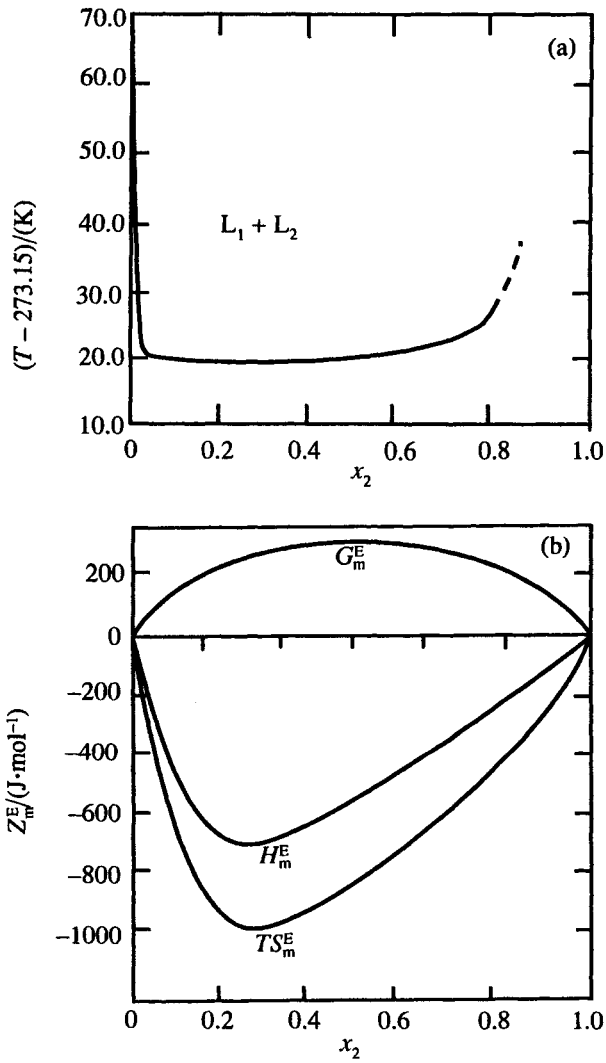

Figure 17.16 (a) (Liquid + liquid) phase equilibia and (b) excess thermodynamic functions at 283.15 K for $\{x_1H_2O + x_2(C_2H_5)_3N\}$.

[r] The $x_{2,c}$ at a LCEP and the minimum in H^E_m are often significantly displaced from $x_2 = 0.5$ as a result of the nonsymmetrical stoichiometry of the complexes that form in the system.

(especially the large negative TS_m^E) are in agreement with the expectation summarized in Figure 17.14b.

It is interesting to extend this analysis to predict the change in G_m^E, H_m^E, and TS_m^E in systems for which more involved types of (liquid + liquid) phase equilibria are present. For example, Figure 17.17 schematically summarizes how

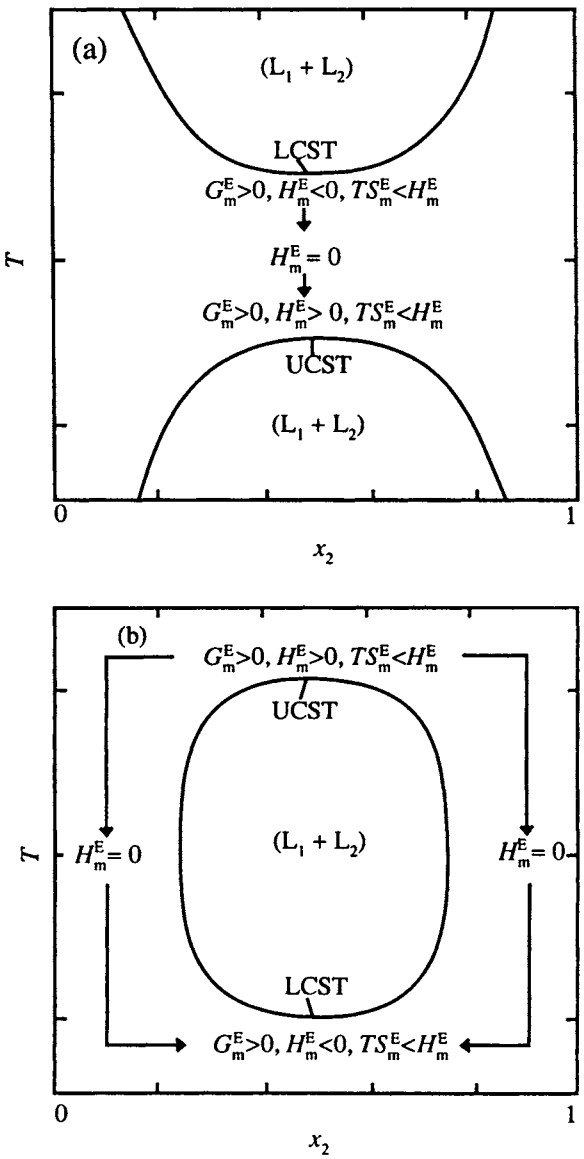

Figure 17.17 Schematic (liquid + liquid) phase diagrams having both an UCST and a LCST, showing the expected arithmetic sign of the excess molar properties.

these quantities should change for (liquid + liquid) equilibria systems of types (c) and (d) shown in Figure 14.7, in which both an UCEP and a LCEP are present. We note that $G_m^E > 0$ over the entire temperature region. However, above the UCEP, $H_m^E > 0$, while below the LCEP, $H_m^E < 0$. Because of this change in sign, we would predict that intermediate between the UCST and the LCST is a temperature where $H_m^E = 0$.[s] We cannot predict whether or not S_m^E will change in sign for this same temperature change, but we do know that $S_m^E < 0$ below the LCST, and smaller (more negative) there than above the UCST.

17.3 The Excess Thermodynamic Properties and (Fluid + Fluid) Phase Equilibrium

We will now extend the description of the excess thermodynamic properties to temperatures and pressures near the critical locus so that supercritical fluids are involved and (fluid + fluid) phase equilibrium is present. For example, Figure 17.18 summarizes the properties of (ethanol + ethane), a type V system similar to that shown in Figure 14.15. Figure 17.18a shows the pressure against temperature projection of the critical loci for this system.[t] The + signs give the experimental conditions where the excess molar enthalpy measurements shown in Figure 17.18b (at $T = 298.15$ K) and in Figure 17.18c (at $T = 348.15$ K) were taken.

Curve (1) in Figure 17.18b gives H_m^E results just below the LCST and, as expected, H_m^E is negative.[u] For curve (2), H_m^E is obtained at a higher pressure ($p = 10$ MPa), and we have moved far enough away from the LCST so that the negative component of H_m^E is almost gone. At $p = 15$ MPa {curve (3)}, H_m^E is positive over the entire mole fraction range, although the extreme skew of the curve suggests a negative contribution to H_m^E at low x_2.

In Figure 17.18c, the temperature (348.15 K) is above the critical temperature of ethane, so that it is supercritical fluid. At $p = 15$ MPa {curve (3)}, the ethane is compressed to the point that it behaves much like a liquid, and an H_m^E curve is obtained that is similar in shape to the H_m^E curve at $p = 15$ MPa and $T = 298.15$ K, except that the size of H_m^E is much larger at the higher temperature.

---

[s] Because of the asymmetry of $G_m^E(x)$, $H_m^E(x)$, and $TS_m^E(x)$, the values may show an "s" shaped behavior as a function of x as they get small in magnitude (instead of becoming zero for all x at a single temperature and pressure).

[t] The relationship between the LCEP and UCEP, and the pressure and temperature conditions where the experimental measurements were made, can be visualized better by indicating the experimental conditions in the three-dimensional representation shown in Figure 14.15.

[u] See Section 17.2, especially Figure 17.14.

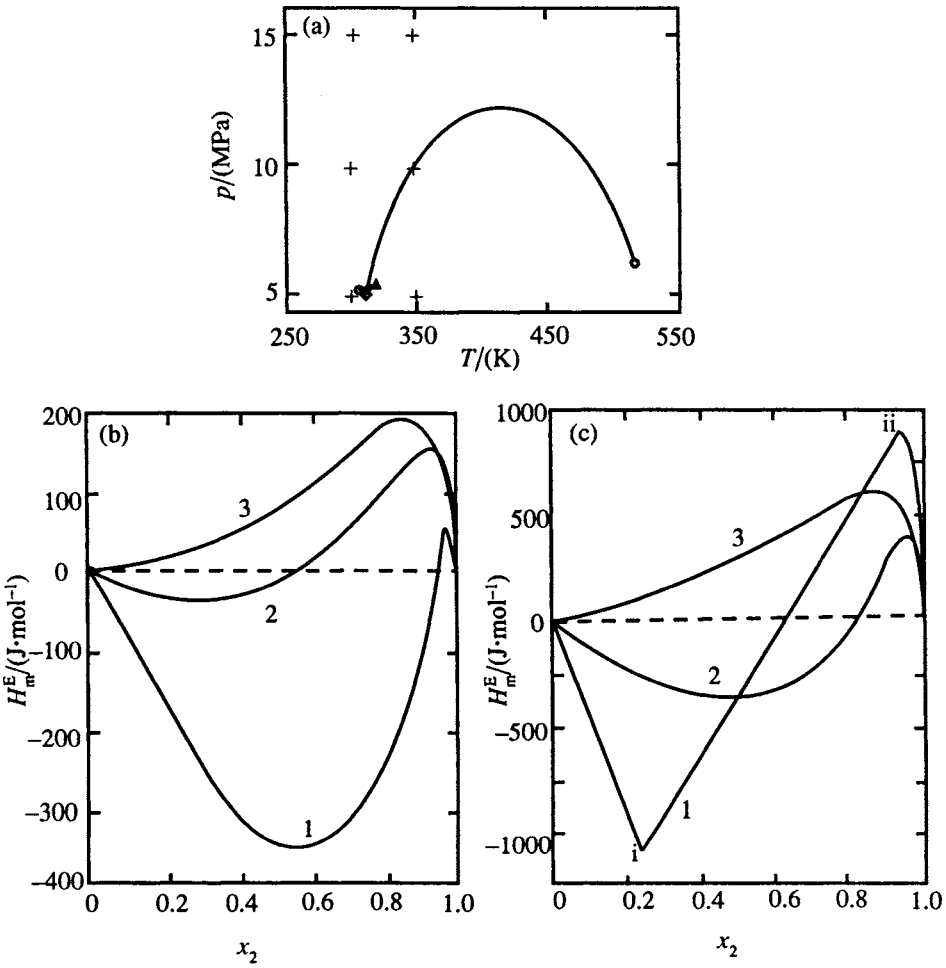

Figure 17.18 (a) (Fluid + fluid) equilibria for ($x_1C_2H_5OH + x_2C_2H_6$) with (○) critical points of the pure components; (△) UCEP; (◇) LCEP. The + signs indicate the pressure and temperature conditions where the H_m^E measurements were made. In (b) the H_m^E measurements are at $T = 298.15$ K, while in (c) $T = 348.15$ K. In (b) and (c), the pressures are as follows: (1) $p = 5$ MPa; (2) $p = 10$ MPa; (3) $p = 15$ MPa.

At $p = 5$ MPa and $T = 348.15$ K (curve 1 in Figure 17.18c), the measurements were made at a pressure and temperature condition where phase separation occurs, and (fluid + fluid) phase equilibria is present. Under these conditions, an H_m^E curve is obtained with a straight-line region analogous to the straight-line region shown in Figure 17.13. The breaks in the curve at points (i) and (ii) give the composition of the two fluid phases in equilibrium.

Compositions and temperatures corresponding to these points can be used to construct the (fluid + fluid) phase diagram if measurements are made at a sufficiently large number of pressures and temperatures to establish the equilibrium lines.

A major difference between the H_m^E curves in Figures 17.13 and 17.18 at temperatures where phase separation is occurring, is the change in the linear region in the latter from large negative values to large positive values. This change can be explained by the properties of the supercritical ethane at this temperature and pressure. At $p = 5$ MPa, ethane is at a low density and behaves like a gas. Referring again to curve (1) in Figure 17.18c, if one starts with pure liquid ethanol ($x_2 = 0$) and adds ethane, the gaseous ethane condenses into the ethanol and releases its enthalpy of condensation. The result is a negative H_m^E. This process continues until point (i) is reached where phase separation occurs.

If, instead, one starts with pure ethane ($x_2 = 1$) and adds ethanol, the liquid alkanol vaporizes into the gas-like ethane and the enthalpy of vaporization of the ethanol must be absorbed. The result is a large positive H_m^E. This process continues until point (ii) is reached, where phase separation to produce the liquid phase occurs.

If ethane is added to change the overall composition from points (i) to (ii) no changes occur in the composition of the fluid phases. Instead, the amount of the phase represented by (ii) grows, while the amount of the phase represented by (i) diminishes, and the overall H_m^E is an average of H_m^E at points (i) and (ii), weighted by the amounts of the two phases that are present. A linear H_m^E is the result of this averaging.

If one holds the temperature constant and measures H_m^E at increasingly higher pressures, a series of H_m^E curves will be obtained, each of which will have a straight-line region resulting from phase separation, but the magnitude of the maximum and minimum values will decrease and the length of the straight line will shorten until a pressure corresponding to the critical locus is reached, where the straight-line region will disappear. At $T = 348.15$ K, this occurs very nearly at $p = 10$ MPa. Curve (2) in Figure 17.18c gives H_m^E for this condition. Here, an "s"-shaped H_m^E curve is obtained, with smaller (in magnitude) maximum and minimum values than at $p = 5$ MPa, and without a straight-line region.

Problems

P17.1 At $T = 315$ K, the enthalpy of mixing of 1 mole of water with 1 mole of ethanol is -343 J·mol^{-1}. For this solution at this temperature, the vapor pressure of the water is $0.821 p_1^*$ and that of the ethanol is $0.509 p_2^*$, where p_1^* and p_2^* are the vapor pressures of the pure liquids. Assume the vapors are ideal and calculate S_m^E for the mixing process.

P17.2 (a) Use equations in the chapter to show that for a regular solution, the activities are given by

$$\ln a_1 = \ln x_1 + x_2^2 \frac{w}{RT}$$

$$\ln a_2 = \ln x_2 + x_1^2 \frac{w}{RT}.$$

(b) Start with the criteria that, since an UCEP is a point of inflection, the first and second derivatives of $\ln a_1$ and $\ln a_2$ with respect to x_2 are zero, and show that at this point (for a regular solution),

$$x_{1,c} = x_{2,c} = 0.5$$

and

$$T_c = \frac{w}{2R}.$$

The result is that at this point, for either component, $\gamma = 1.65$ and $a = 0.82$ so that $p = 0.82(p_1^* + p_2^*)$. This result may be compared with the two extreme cases. An equimolar ideal solution would have $p = 0.50(p_1^* + p_2^*)$, while two liquids that are completely immiscible would have a total pressure given by $p = p_1^* + p_2^*$.

P17.3 Given the following equations for calculating H_m^E, G_m^E, and V_m^E for $\{x_1 C_{12}H_{26} + x_2 C_6H_{14}\}$ at 308.15 K and 0.1 MPa

$$H_m^E/(\text{J·mol}^{-1}) = x_1 x_2[102.05 + 22.96(1 - 2x_2) - 13.34(1 - 2x_2)^2 + 7.49(1 - 2x_2)^3]$$

$$G_m^E/(\text{J·mol}^{-1}) = x_1 x_2[-101.37 - 0.56(1 - 2x_2) + 5.33(1 - 2x_2)^2 - 7.83(1 - 2x_2)^3 + 4.62(1 - 2x_2)^4]$$

$$V_m^E/(\text{cm}^3\text{·mol}^{-1}) = x_1 x_2[-1.6588 + 0.6623(1 - 2x_2) - 0.2445(1 - 2x_2)^2 + 0.0697(1 - 2x_2)^3]$$

(a) Make a graph of H_m^E, G_m^E and TS_m^E at $T = 308.15$ K and $p = 0.1$ MPa over the entire composition range and compare the values.
(b) Assume V_m^E and H_m^E are constant with temperature and pressure and calculate G_m^E at $x_2 = 0.5$ with $T = 298.15$ K and $p = 1.0$ MPa.

P17.4 At $T = 333.15$ K, the excess chemical potentials in the {2-butanol (component 1) + n-hexane (component 2)} system are given by the expressions

$$\frac{\mu_1^E}{RT} = x_2^2[1.5448 - 0.229(3x_1 - x_2) + 0.275(5x_1 - x_2)(x_1 - x_2)$$

$$- 0.179(7x_1 - x_2)(x_1 - x_2)^2]$$

and

$$\frac{\mu_2^E}{RT} = x_1^2[1.5448 - 0.229(x_1 - 3x_2) + 0.275(x_1 - 5x_2)(x_1 - x_2)$$

$$- 0.179(x_1 - 7x_2)(x_1 - x_2)^2].$$

At this temperature, the vapor pressures of the pure components are $p_1^* = 18.15$ kPa and $p_2^* = 76.45$ kPa.

(a) Calculate G_m^E at every 0.1 mole fraction unit and make a graph of G_m^E against x_2.
(b) Assume the vapors are ideal gases and calculate p_1, p_2, and $p = p_1 + p_2$ at every 0.1 mole fraction unit. Make a graph of these three pressures against x_2. Also show on the graph the ideal solution prediction for each of the three pressures.
(c) Construct the (vapor + liquid) phase diagram by making a graph of p against x_2, and against y_2, the mole fraction in the vapor phase, and look for the presence of an azeotrope. Again, you may assume the vapors are ideal gases.

P17.5 (Ethane + propane) forms a type I system. Figure 17.19a shows the critical locus for this system. Figures 17.19b and 17.19c show how the density of ethane and propane change with pressure over the temperature range extending above and below the critical temperatures of 305.50 K for ethane and 369.82 K for propane. Figure 17.20 summarizes H_m^E results for this system at the pressure and temperature conditions indicated in Figure 17.19a. Use the density information summarized in Figure 17.19b and 17.19c to explain the effect of

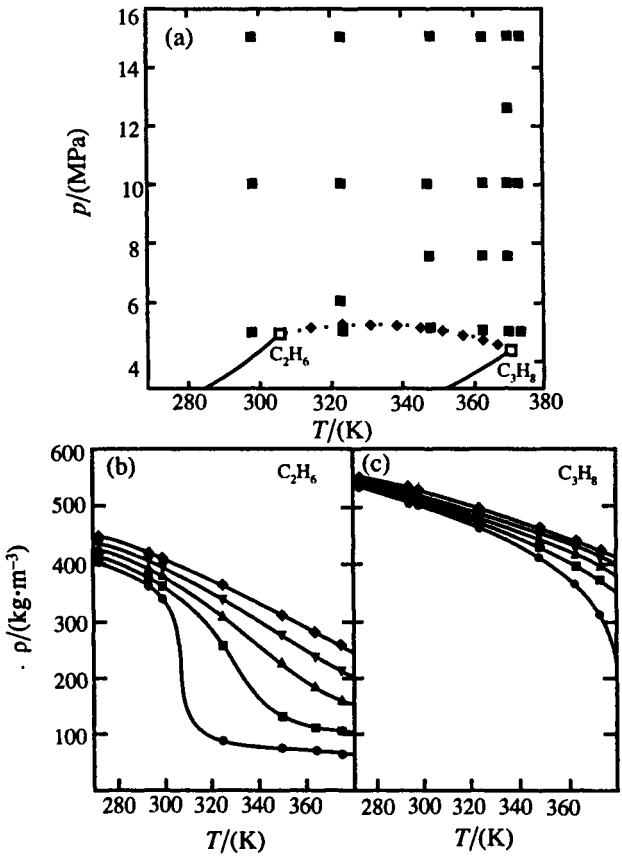

Figure 17.19 (a), Critical locus (···◆···) for the (propane + ethane) system: (□), critical points of pure ethane and pure propane; (■) pressure and temperature conditions where H_m^E measurements were made. Solid lines give vapor pressures of the pure materials. (b) density of ethane and (c) density of propane as a function of temperature and pressure. The pressures in (b) and (c) are: (●) 5 MPa; (■) 7.5 MPa; (▲) 10 MPa; (▼) 12.5 MPa; (◆) 15 MPa.

temperature and pressure on H_m^E for this system. The discussion will be similar to that given in Section 17.3 for the (ethane + ethanol) system. The following observations should help with the explanation:

(a) At $T = 298.15$ K, both the ethane and propane are liquids.

(b) At and above $T = 323.15$ K, but below $T = 369.82$ K, propane is liquid while ethane is a supercritical fluid. At $p = 5$ MPa, the measurements in this temperature range closely follow the critical locus (and actually drop below the locus into the two-phase region at $T = 323.15$ K). In this pressure and temperature region, the ethane

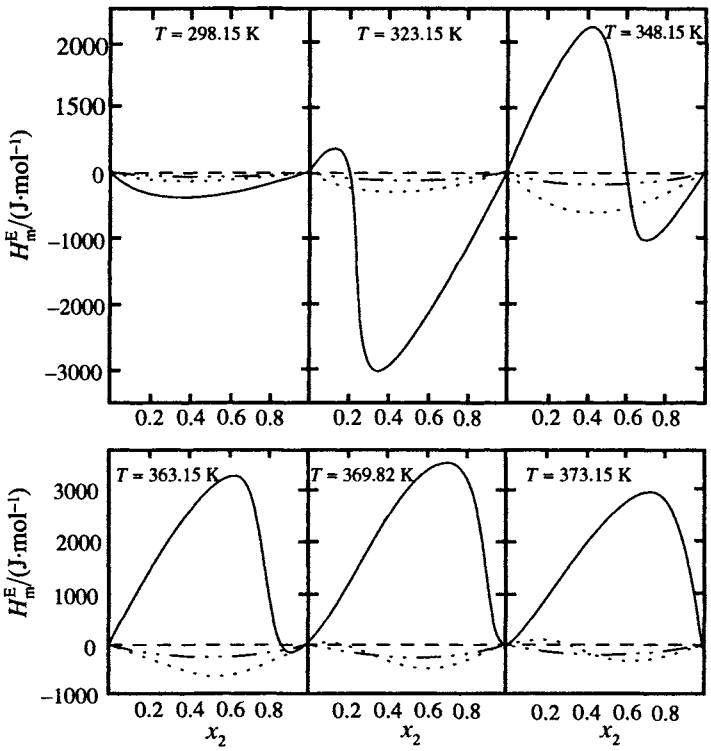

Figure 17.20 Excess enthalpies for $(x_1C_2H_6 + x_2C_3H_8)$. The pressures are: ————, 5 MPa; · · · · · · ·, 10 MPa; and — · · —, 15 MPa.

has a gas-like density, while the propane has a liquid density. At $p = 15$ MPa, the density of the ethane in this temperature range has increased until it is more like that of a liquid. At $p = 10$ MPa, the density is intermediate between that of a liquid and of a gas.

(c) Above $T = 369.82$ K, both the ethane and propane are supercritical fluids, but the propane continues to have a relative high density up to the high-temperature limit of the measurements at $T = 373.15$ K, even at $p = 5$ MPa.

References

1. The data show in Figure 17.1 were obtained from the following sources:
A. G. Duncan and L. A. K. Staveley, "Thermodynamic Functions for the Liquid Systems Argon + Carbon Monoxide, Oxygen + Nitrogen, and Carbon Monoxide + Nitrogen", *Trans. Faraday Soc.*, **62**, 548–552 (1966). K. L. Lewis, G. Saville, and L. A. K. Staveley, "Excess Enthalpies of Liquid Oxygen + Argon, Oxygen + Nitrogen, and Argon + Methane", *J. Chem. Thermodyn.*, **7**, 389–400 (1975). M. B. Ewing and K. N. Marsh, "Excess Gibbs Free

Energies, Excess Enthalpies, Excess Volumes, and Isothermal Compressibilities of Cyclohexane + 2,3-Dimethylbutane", *J. Chem. Thermodyn.*, **6**, 35–41 (1974). J. B. Ott, K. N. Marsh, and R. H. Stokes, "Excess Enthalpies, Excess Gibbs Free Energies, and Excess Volumes for (Cyclohexane + n-Hexane), and Excess Gibbs Free Energies and Excess Volumes for (Cyclohexane + Methylcyclohexane) at 298.15 and 308.15 K", *J. Chem. Thermodyn.*, **12**, 1139–1148 (1980).

2. Figure 17.2 is described in J. B. Ott and J. T. Sipowska, "Applications of Calorimetry to Nonelectrolyte Solutions", *J. Chem. Eng. Data*, **41**, 987–1004 (1996). The original papers by M. J. Ewing, K. N. Marsh, and R. H. Stokes reporting the measurements that lead to this figure are given in this reference.
3. The references to the original work are summarized in J. B. Ott and J. T. Sipowska, "Applications of Calorimetry to Nonelectrolyte Solutions", *J. Chem. Eng. Data*, **41**, 987–1004 (1996).
4. The excess thermodynamic properties for (cyclohexane + hexane) were obtained from the following sources: Excess enthalpies come from K. N. Marsh and R. H. Stokes, "Enthalpies of Mixing of n-Hexane + Cyclohexane at 25 °C", *J. Chem. Thermodyn.*, **1**, 223–225 (1969); and M. B. Ewing and K. N. Marsh, "The Enthalpy of Mixing of n-Hexane + Cyclohexane at 288.15 and 318.15 K", *J. Chem. Thermodyn.*, **2**, 295–296 (1970). Excess volumes and excess Gibbs free energies come from J. B. Ott, K. N. Marsh, and R. H. Stokes, "Excess Enthalpies, Excess Gibbs Free Energies and Excess Volumes for (Cyclohexane + n-Hexane), and Excess Gibbs Free Energies and Excess Volumes for (Cyclohexane + Methylcyclohexane) at 298.15 and 308.15 K", *J. Chem. Thermodyn.*, **12**, 1139–1148 (1980).
5. K. N. Marsh, J. B. Ott, and M. J. Costigan, "Excess Enthalpies, Excess Volumes, and Excess Gibbs Free Energies for (n-Hexane + n-Decane) at 298.15 and 308.15 K", *J.Chem. Thermodyn.*, **12**, 343–348 (1980).
6. M. B. Ewing and K. N. Marsh, "Excess Functions for Cyclohexane + Cycloheptane and Cycloheptane + Cyclooctane", *J. Chem. Thermodyn.*, **6**, 1087–1096 (1974).
7. J. R. Goates, J. B. Ott, and R. B. Grigg, "Excess Volumes of Cyclohexane + n-Hexane, + n-Heptane, + n-Octane, + n-Nonane, and + n-Decane", *J. Chem. Thermodyn.*, **11**, 497–506 (1979).
8. J. R. Goates, J. B. Ott and R. B. Grigg, "Excess Volumes of n-Hexane + n-Heptane, + n-Octane, + n-Nonane, and + n-Decane at 283.15, 295.15, and 313.15 K", *J. Chem. Thermodyn.*, **13**, 907–913 (1981). References to V_m^E for n-hexane + n-undecane and + n-dodecane are given in this paper.
9. Excess enthalpies were obtained from J.-P. E. Grolier, K. Sosnkowska-Kehiaian, and H. V. Kehiaian, "Enthalpies of Mixing of Organic Chlorides with Hydrocarbons", *J. Chim. Phys. Physicochim. Biol.*, **70**, 367–373 (1973). Excess volumes and excess heat capacities were obtained from A. Lainez, E. Wilhelm, G. Roux-Desgranges and J.-P. E. Grolier, "Excess Molar Quantities of (a Halogenated n-Alkane + an n-Alkane). A comparative Study of Mixtures Containing Either 1-Chlorobutane or 1,4 -Dichlorobutane", *J. Chem. Thermodyn.*, **17**, 1153–1161 (1985).
10. I. Nagata, K. Tarmura, and S. Tokuriki, "Excess Enthalpies for the Systems Acetonitrile–Benzene–Tetrachloromethane and Acetonitrile–Dichloromethane–Tetrachloromethane at 298.15 K", *Fluid Phase Equilib.*, **8**, 75–86 (1982); I. Nagata and Y. Kawamura, "Excess Thermodynamic Functions and Complex Formation in Binary Liquid Mixtures Containing Acetonitrile", *Fluid Phase Equilib.*, **3**, 1–11 (1979).
11. The results shown in Figure 17.8 were obtained from the following sources:
S. Cabani and N. Ceccanti, "Thermodynamic Properties of Binary Mixtures of Cyclohexane with Cyclic Amines or Cyclic Ethers at 298.15 K", *J. Chem. Thermodyn.*, **5**, 9–20 (1973);

A. W. Andrews and K. W. Morcom, "Thermodynamic Properties of Some Hydrocarbon + Cyclic Ether Mixtures. 2. Enthalpies of Mixing", *J. Chem. Thermodyn.*, **3**, 519–525 (1971); A. Inglese, J.-P. E. Grolier, and E. Wilhelm, "Excess Volumes and Excess Heat Capacities of Oxane + Cyclohexane and 1, 4-Dioxane + Cyclohexane", *Fluid Phase Equilib.*, **15**, 287–294 (1984); and D. D. Deshpande and S. L. Oswal, "Thermodynamics of Mixtures Containing p-Dioxan or Tetrahydrofuran. 1. Excess Gibbs Free Energies and Excess Volumes", *J. Chem. Thermodyn.*, **7**, 155–159 (1975).

12. M.-E. Saint-Victor and D. Patterson, "The W-Shape Concentration Dependence on C_p^E and Solution Non-randomness: Ketones + Normal and Branched Alkanes", *Fluid Phase Equilib.*, **35**, 237–252 (1987).
13. See M.-E. Saint-Victor and D. Patterson, "The W-Shape Concentration Dependence on C_p^E and Solution Non-randomness: Ketones + Normal and Branched Alkanes", *Fluid Phase Equilib.*, **35**, 237–252 (1982). Also, see E. Wilhelm, "Thermodynamics of Solutions: Selected Aspects", *Thermochim. Acta*, **162**, 43–57 (1990).
14. See for example R. G. Rubio, M. Cáceres, R. M. Masegosa, L. Andreolli-Ball, M. Costas, and D. Patterson, "Mixtures with 'W-Shape' C_p^E Curves. A Light Scattering Study", *Ber. Bunsenges. Phys. Chem.*, **93**, 48–56 (1989); and A. Lainez, M. R. Lopez, M. Cáceres, J. Nuñez, and R. G. Rubio, "Heat Capacities and Concentration Fluctuations in Mixtures of 1,2-Dibromoethane with Alkanes", *J. Chem. Soc. Faraday Trans. 1*, **91**, 1941–1947 (1995).
15. H. L. Clever and S. P. Pigott, "Enthalpies of Mixing of Dimethylsulfoxide with Water and with Several Ketones at 298.15 K", *J. Chem. Thermodyn.*, **3**, 221–225 (1971).
16. I. Brown and W. Foch, "Heats of Mixing. II. Acetonitrile and Nitromethane Systems", *Aust. J. Chem.*, **9**, 180–183 (1956).
17. I. Nagata, K. Tamura, and S. Tokuriki, "Excess Enthalpies and Complex Formation of Acetonitrile with Acetone, Chloroform, and Benzene", *Thermochim. Acta*, **47**, 315–331 (1981).
18. The papers reporting the results shown in Figure 17.10 are as follows:
K. Quitzsch, "Studien zur Thermodynamik Binärer Flüssigkeitsgemische mit Homologen Formamiden", *Z. Phys. Chem. Leipzig*, **233**, 321–332 (1966); D. D. Deshpande and S. L. Oswal, "Vapour–Liquid Equilibrium and Excess Free Energies for Benzene + Dioxan and Carbon Tetrachloride + Dioxan Systems", *J. Chem. Soc. Faraday Trans. 1*, **68**, 1059–1064 (1972); M. J. Costigan, L. J. Hodges, K. N. Marsh, R. H. Stokes, and C. W. Tuxford, "The Isothermal Displacement Calorimeter: Design Modifications for Measuring Exothermic Enthalpies of Mixing", *Aust. J. Chem.*, **33**, 2103–2119 (1980); M. D. Guillen and C. Gutierrez-Losa, "Excess Enthalpies and Excess Volumes of n-Hexane + and of Tetrachloromethane + Furan, + 1,4-Dioxane, + Tetrahydrofuran, and + Tetrahydropyran", *J. Chem. Thermodyn.*, **10**, 567–576 (1978); R. B. Grigg, J. R. Goates, and J. B. Ott, "Excess Volumes for Tetrachloromethane + N,N-Dimethylformamide, + N,N-Dimethylacetamide, + p-Dioxane, and + Dimethylsulfoxide", *J. Chem. Thermodyn.*, **11**, 703–708 (1979).
19. J. R. Goates, J. B. Ott, and D. E. Oyler, "Intermolecular Compound Formation in Solutions of N,N-Dimethylformamide with Carbon Tetrachloride and Several Related Substances. A Solid Phase Transition in N,N-Dimethylformamide," *Trans. Faraday Soc.*, **62**, 1511–1518 (1966).
20. J. B. Ott, J. R. Goates, and N. F. Mangelson, "Solid–Liquid Phase Equilibria in Binary Mixtures of p-Dioxane with CCl_4, $CBrCl_3$, and $CFCl_3$. Solid Compound Formation in the CCl_4 and $CFCl_3$ Systems", *J. Chem. Eng. Data*, **9**, 203–206 (1964).
21. S. R. Goates, J. Boerio-Goates, J. R. Goates, and J. B. Ott, "The Thermodynamic Stability of Solid Intermolecular Compounds", *J. Chem. Soc. Faraday Trans. 1*, **83**, 1553–1558 (1987).
22. J. T. Sipowska, L. R. Lemon, J. B. Ott, P. R. Brown, and B. G. Marchant, "Excess Enthalpies and Excess Volumes for (Butane + Butan-1-ol) at the Temperatures 298.15,

323.15, and 348.15 K and Pressures 5, 10, and 15 MPa", *J. Chem. Thermodyn.*, **26**, 1275–1286 (1994).

23. For examples of the use of this technique, see C. G. Savini, D. R. Winterhalter, and H. C. Van Ness, "Heats of Mixing for Partially Miscible Systems: Methanol–*n*-Hexane and Methanol–*n*-Heptane", *J. Chem. Eng. Data*, **10**, 171–172 (1965); J. B. Ott, J. T. Sipowska, and R. M. Izatt, "Excess Enthalpies for (Propane + Acetonitrile) at the Temperatures 298.15, 313.15, 323.15, 333.15, 338.15, and 348.15 K and at the Pressures 5, 10, and 15 MPa. Determination of (Liquid + Liquid) Equilibria from the Calorimetric Results", *J. Chem. Thermodyn.*, **23**, 687–698 (1991).
24. The (liquid + liquid) equilibria diagram for (cyclohexane + methanol) was taken from D. C. Jones and S. Amstell, "The Critical Solution Temperature of the System Methyl Alcohol–Cyclohexane as a Means of Detecting and Estimating Water in Methyl Alcohol", *J. Chem. Soc.*, **1930**, 1316–1323 (1930). The G_m^E results were calculated from the (vapor + liquid) results of K. Strubl, V. Svoboda, R. Holub, and J. Pick, "Liquid–Vapour Equilibrium. XIV. Isothermal Equilibrium and Calculation of Excess Functions in the Systems Methanol–Cyclohexane and Cyclohexane–Propanol", *Collect. Czech. Chem. Commun.*, **35**, 3004–3019 (1970). The H_m^E results are from M. Dai and J.-P.Chao, "Studies on Thermodynamic Properties of Binary Systems Containing Alcohols. II. Excess Enthalpies of C_1 to C_5 Normal Alcohols + 1,4-Dioxane", *Fluid Phase Equilib.*, **23**, 321–326 (1985).
25. V. Rothmund, "Die Gegenseitige Löslichkeit von Flüssigkeiten und der Kritische Lösungspunkt", *Z. Phys. Chem.* (*Leipzig*) **26**, 433–492 (1898).
26. Reproduced from the figures given by J. L. Copp and D. H. Everett, "Thermodynamics of Binary Mixtures Containing Amines", *Discuss. Faraday Soc.*, **15**, 174–188 (1953).

Chapter 18

Applications of Thermodynamics to Solutions Containing Electrolyte Solutes

18.1 Electrolyte Solutions

In the previous chapter, we described the thermodynamic properties of nonelectrolyte solutions. In this chapter, we focus on electrolytes as solutes. Electrolytes behave quite differently in solution than do nonelectrolytes. In Chapter 11, we described the strong electrolyte standard state and summarized relationships between the activity of the solute a_2, the mean activity coefficient $\gamma_\pm$, and the molality m in Table 11.3.

The "special properties" of electrolyte solutions present both advantages and disadvantages as we attempt to describe these mixtures. A disadvantage is that significant deviations from limiting law solution behavior occur at much lower concentrations for electrolyte solutes than for nonelectrolyte solutes. An advantage is that the coulombic attractions and repulsions in the electrolyte solution dominate other types of interactions. The result is that theoretical descriptions of electrolyte solutions can concentrate on the coulombic interactions.

The Debye–Hückel theory that we summarized in Chapter 11 is based on this assumption. In that chapter we gave the following equations that apply to limiting law behavior

$$\ln \gamma_\pm = -C_\gamma \mid z_+ z_- \mid I^{1/2} \tag{18.1}$$

$$1 - \phi = C_\phi \mid z_+ z_- \mid I^{1/2} \tag{18.2}$$

$$C_\gamma = 3C_\phi \tag{18.3}$$

$$\overline{L}_2 = C_H \left(\frac{\nu}{2}\right) \mid z_+ z_- \mid I^{1/2} \tag{18.4}$$

$$\bar{J}_2 = C_J\left(\frac{\nu}{2}\right) \mid z_+ z_- \mid I^{1/2} \tag{18.5}$$

$$\bar{V}_2 - \bar{V}_2^\circ = C_v\left(\frac{\nu}{2}\right) \mid z_+ z_- \mid I^{1/2} \tag{18.6}$$

where $\gamma_\pm$ is the mean ionic activity coefficient and ϕ is the osmotic coefficient given by

$$\phi = -\frac{\ln a_1}{M_1 \sum_k \nu_k m_k}, \tag{18.7}$$

with ν_k as the number of moles of ions produced by a solute whose molality is m_k, and M_1 as the molecular weight of the solvent in kg·mol^{-1}. For a single symmetrical electrolyte, ϕ becomes

$$\phi = -\frac{\ln a_1}{M_1 m}. \tag{18.8}$$

In these equations I is the molal-based ionic strength[a] given by

$$I = \frac{1}{2}\sum_i m_i z_i^2 \tag{18.9}$$

with z_+ and z_- as the ionic charges, and $\nu = \nu_+ + \nu_-$ is the total number of ions per molecular unit.

The constants C_γ, C_ϕ, C_H, C_J and C_v are related to fundamental constants and properties of the solvent. The relationships are given in Chapter 11. Values for these constants for aqueous solutions are given as a function of temperature and pressure in Table 18.1.[b] Below $T = 373.15$ K, the constants are the values at

[a] In Chapter 11, we used I_m as the symbol for molal-based ionic strength. In this chapter, we will use I. This simplifies the notation and corresponds to that used later in the chapter.

[b] Table 18.1 actually gives values for A_γ, A_ϕ, A_L, A_J and A_v, the constants in the Pitzer equations that we will summarize in the next section. The heading of the table relates C_γ to A_γ, C_ϕ to A_ϕ, etc.

Table 18.1 Debye–Hückel parameters for the osmotic coefficient, volume, enthalpy, and heat capacity

$(T-273.15)/$ (K)	$A_\phi = C_\phi = A_\gamma/3/$ $[(\text{kg·mol})^{1/2}]$	$A_v = \frac{2}{3}C_v/$ $(\text{cm}^3\cdot\text{kg}^{1/2}\cdot\text{mol}^{-3/2})$	$A_L/RT = \frac{2}{3}C_H/RT/$ $[(\text{kg·mol})^{1/2}]$	$A_J/R = \frac{2}{3}C_J/R/$ $[(\text{kg·mol})^{3/2}]$
0.0	0.3767	1.504	0.556	2.95
10.0	0.3821	1.643	0.649	3.39
20.0	0.3882	1.793	0.749	3.76
25.0	0.3915	1.875	0.801	3.94
30.0	0.3949	1.962	0.854	4.13
40.0	0.4023	2.153	0.965	4.51
50.0	0.4103	2.372	1.081	4.92
60.0	0.4190	2.622	1.203	5.37
70.0	0.4283	2.909	1.331	5.86
80.0	0.4384	3.238	1.467	6.40
90.0	0.4491	3.615	1.611	7.00
100.0	0.4606	4.050	1.764	7.66
110.0	0.4727	4.550	1.927	8.40
120.0	0.4857	5.127	2.102	9.24
130.0	0.4994	5.795	2.290	10.17
140.0	0.5140	6.572	2.492	11.23
150.0	0.5295	7.477	2.712	12.45
160.0	0.5460	8.536	2.951	13.84
170.0	0.5634	9.779	3.213	15.47
180.0	0.5820	11.25	3.500	17.38
190.0	0.6017	12.99	3.819	19.65
200.0	0.6228	15.07	4.175	22.38
210.0	0.6453	17.6	4.576	25.72
220.0	0.6694	20.6	5.032	29.85
230.0	0.6953	24.3	5.556	35.05
240.0	0.7232	28.8	6.165	41.73
250.0	0.7535	34.4	6.885	50.46
260.0	0.7865	41.5	7.749	62.15
270.0	0.823	50.5	8.806	78.18
280.0	0.863	62.3	10.13	100.8
290.0	0.908	77.8	11.82	133.7
300.0	0.960	98.7	14.05	183.4
310.0	1.02	127	17.1	261
320.0	1.09	169	21.4	391
330.0	1.18	231	28.0	622
340.0	1.29	330	38.6	1060
350.0	1.44	493	57.3	1920

the standard pressure of 1 bar (10^5 Pa). Above 373.15 K, the values apply to water at a pressure equal to its own vapor pressure (the saturation pressure).

18.1a Thermodynamics of More Concentrated Electrolyte Solutions

The limiting law expression for $\ln \gamma_\pm$ [equation (18.1)] is applicable to molalities less than 0.01 moles·kg^{-1}. Extensive deviations occur at higher concentrations, as can be seen in Figure 18.1 in which $\ln \gamma_\pm$ is graphed against $I^{1/2}$ to high molalities. Shown as dashed straight lines are the Debye–Hückel limiting law predictions, which obviously apply only at small I.

The range can be extended by equation (18.10)

$$\ln \gamma_\pm = -C_\gamma \, | z_+ z_- | \frac{I^{1/2}}{1 + I^{1/2}}. \tag{18.10}$$

Similar equations can be written for other thermodynamic functions. For example,

$$1 - \phi = C_\phi \, | z_+ z_- | \frac{I^{1/2}}{1 + I^{1/2}}. \tag{18.11}$$

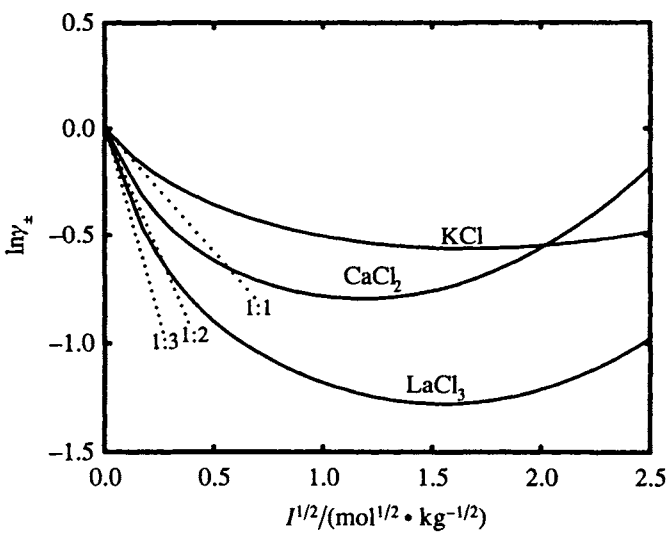

Figure 18.1 $\ln \gamma_\pm$ as a function of the ionic strength ($I^{1/2}$) at $p = 0.1$ MPa and $T = 298.15$ K, for KCl, $CaCl_2$, and $LaCl_3$. The dotted lines at low I are the Debye–Hückel limiting-law predictions for the three electrolytes.

But equations of this type do not extend the range to much higher concentrations.

18.1b Guggenheim's Equations

As early as 1922, Brønsted[1] proposed equations of the type

$$\ln \gamma_{\pm} = -\alpha m^{1/2} - 2\beta m$$

$$1 - \phi = \left(\frac{\alpha}{3}\right) m^{1/2} + \beta m$$

for electrolytes. In these equations, α is a general constant[c] while β is specific for the particular solute. Guggenheim[2] extended the work of Brønsted to multivalent electrolytes and to mixtures and incorporated the Debye–Hückel equation to obtain an equation that takes the form for a single electrolyte

$$\ln \gamma_{\pm} = -C_{\gamma} \mid z_{+}z_{-} \mid \frac{I^{1/2}}{1 + I^{1/2}} + 2\frac{\nu_{+}\nu_{-}}{\nu}(2\beta)m. \tag{18.12}$$

A transformation through the Gibbs–Duhem equation gives the comparable equation for the osmotic coefficient

$$1 - \phi = C_{\phi} \mid z_{+}z_{-} \mid \frac{I^{1/2}}{1 + I^{1/2}} \sigma(I^{1/2}) - \frac{2\nu_{+}\nu_{-}}{\nu} \beta_{m} \tag{18.13}$$

where $\sigma(I^{1/2})$ is a function of the form

$$\sigma(y) = \frac{3}{y^3}[1 + y - (1 + y)^{-1} - 2\ln(1 + y)] \tag{18.14}$$

Guggenheim and Turgeon[3] published a tabulation of the coefficient β for a number of electrolytes. They state that equations (18.12) and (18.13) represent the facts with a useful degree of accuracy, at least for uni-univalent, bi-univalent, and uni-bivalent electrolytes, up to an ionic strength of about 0.1. Table 18.2 summarizes values for Guggenheim's β at $T = 273.15$ and 298.15 K

[c] α is, of course, the Debye–Hückel constant. Brønsted's work preceded the Debye–Hückel derivation.

obtained from Guggenheim and Turgeon's tabulation. These constants can be used with equations (18.12) and (18.13) to calculate $\gamma_\pm$ and ϕ.

Example 18.1: Use Table 18.2 to calculate $\gamma_\pm$ for a 0.050 molal solution of KCl at $T = 298.15$ K.

Solution: From Table 18.2, $\beta = 0.10$ for KCl at $T = 298.15$ K. For a 1:1 electrolyte, $I = m = 0.050$:

From equation (18.12)

$$\ln \gamma_\pm = -(1.174)\frac{(0.050)^{1/2}}{[1+(0.050)^{1/2}]} + \frac{(2)(1)(1)}{(2)}(2)(0.10)(0.050)$$

$$= 0.815.$$

The experimental value is 0.816.

Table 18.2 Specific ion interaction constants for the Guggenheim equation

Salt	β(273.15 K)	β(298.15 K)
HCl	0.25	0.27
HBr	–	0.33
HI	–	0.36
$HClO_4$	–	0.30
HNO_3	0.16	–
LiCl	0.20	0.22
LiBr	0.30	0.26
$LiNO_3$	0.23	0.21
LiOAc	0.19	0.18
NaCl	0.11	0.15
NaBr	0.20	0.17
NaOAc	0.26	0.23
$AgNO_3$	–	−0.14
KCl	0.04	0.10
KBr	0.06	0.11
KNO_3	−0.26	−0.11
KOAc	0.30	0.26
CsCl	–	0
$CsNO_3$	–	−0.15

From E. A. Guggenheim and J. C. Turgeon, "Specific Interaction of Ions", *Trans. Faraday Soc.*, **51**, 747–761 (1955).

18.1c Pitzer and Brewer Tabulations

K. S. Pitzer and L. Brewer used equation (18.12) as the base for tabulating a summary of the thermodynamic properties of aqueous electrolyte solutions at 298.15 K. They wrote equation (18.12) in the form that involves base 10 logarithms

$$\log \gamma_{\pm} = -\frac{C_{\gamma}}{2.303} | z_+ z_- | \frac{I^{1/2}}{1 + I^{1/2}} + \frac{2\nu_+\nu_-}{\nu} B^{\bullet} m, \tag{18.15}$$

where

$$B^{\bullet} = \frac{2\beta}{2.303}.$$

They chose a reference system (KCl for a 1 : 1 electrolyte and $CaCl_2$ for a 2 : 1 electrolyte) for which they tabulated detailed values of ϕ, $\gamma_{\pm}$, ϕL, $\bar{L}_2$, ϕC_p, and $\bar{J}_2$. For this reference system

$$\log(\gamma_{\pm})_{\text{ref}} = -\frac{C_{\gamma} | z_+ z_- |}{2.303} \left(\frac{I^{1/2}}{1 + I^{1/2}} \right) + \frac{2\nu_+\nu_-}{\nu} B^{\bullet}_{\text{ref}} m. \tag{18.16}$$

Subtracting equation (18.16) from (18.15) gives

$$\log \frac{\gamma_{\pm}}{(\gamma_{\pm})_{\text{ref}}} = \frac{2\nu_+\nu_-}{\nu} \Delta B^{\bullet} m. \tag{18.17}$$

Values of $\Delta B^{\bullet}$ are tabulated by Pitzer and Brewer[4] for a number of 1 : 1, 2 : 1, and 1 : 2 electrolytes from which $\gamma_{\pm}$ can be calculated.

Example 18.2: Use the Pitzer and Brewer tabulation to obtain $\gamma_{\pm}$ for CsCl at $m = 3.0$ mol·kg^{-1} and $T = 298.15$ K.

Solution: From Pitzer and Brewer's tables, at $T = 298.15$ K and $m = 3.0$ mol·kg^{-1}, $\gamma_{\pm} = 0.568$ for KCl and $\Delta B^{\bullet} = -0.025$ for CsCl. For a

1 : 1 electrolyte, $2\nu_+\nu_-/\nu = 1$. Using equation (18.17), we get

$$\log\frac{\gamma_\pm}{0.568} = -(0.0251)(3.0)$$

so that

$$\gamma_\pm = 0.478.$$

Similar relationships can be used to obtain the other thermodynamic properties. The reader is referred to the Pitzer and Brewer reference for details. This procedure provides a good method for determining the thermodynamic properties because of the nature of $B^\bullet$. Figure 18.2 shows a graph of $B^\bullet$ as a function of molality for several electrolytes. We note that $B^\bullet$ changes slowly with molality (except at low m where more rapid changes are not as important in the calculation). Thus, it is easy to interpolate in a table of $\Delta B^\bullet$ values, and an extensive table is not needed to obtain accurate values for the thermodynamic properties.

18.1d Pitzer's Equations

The procedure described in the previous section provides an excellent method for quickly obtaining thermodynamic data for electrolyte solutes and is recommended as a method to use by the scientist who occasionally needs an

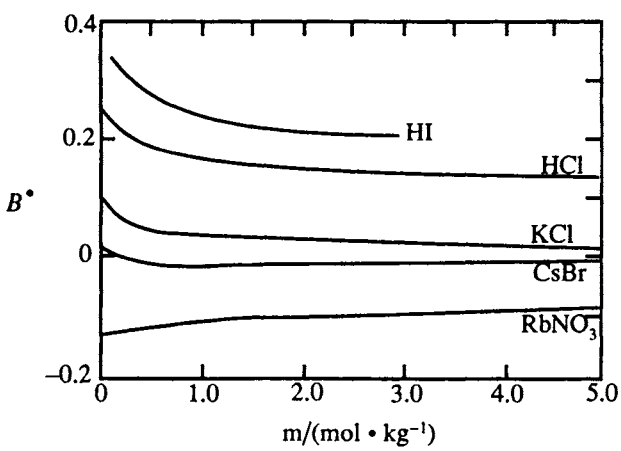

Figure 18.2 Variation of $B^\bullet$ with molality. Reproduced with permission from G.N. Lewis, M. Randall, K. S. Pitzer, and L. Brewer, *Thermodynamics, Second Edition*, McGraw-Hill Book Company, New York, 1961.

activity coefficient, osmotic coefficient, relative partial molar enthalpy, or partial molar heat capacity. The problem with the method is that analytical expressions are not available that express the effect of concentration on $B^{\bullet}$. To quote Pitzer[5]

> *once the $B^{\bullet}$ (or β's) are dependent on concentration, many of the advantages of these equations are lost since rigorous thermodynamic transformation now becomes complex.*

Pitzer's solution to the problem was the development of a set of analytical equations that are thermodynamically consistent after transformations through the Gibbs–Duhem equation. These equations are known as the Pitzer equations, in recognition of the major role that he played in developing them and the major contributions he made in the understanding of electrolyte solutions through a lifetime of work. We will now summarize these equations and describe their usefulness. For details of the derivation we refer the reader to Pitzer's original paper.[6]

The Osmotic Coefficient and Activity Coefficient: Equations for calculating the osmotic coefficient have the form[d]

$$\phi - 1 = |z_M z_X| f^{\phi} + m(2\nu_M\nu_X/\nu)B^{\phi}_{MX} + m^2[2(\nu_M\nu_X)^{3/2}/\nu]C^{\phi}_{MX} \quad (18.18)$$

where

$$f^{\phi} = -A_{\phi} I^{1/2}/(1 + bI^{1/2}) \quad (18.19)$$

$$B^{\phi}_{MX} = \beta^{(0)}_{MX} + \beta^{(1)}_{MX} \exp(-\alpha I^{1/2}). \quad (18.20)$$

In applying these equations to a range of electrolytes, it is found that a satisfactory fit can be obtained using the values $b = 1.2$ kg$^{1/2}$·mol$^{-1/2}$ and $\alpha = 2.0$ kg$^{1/2}$·mol$^{-1/2}$ for all electrolytes. The 2:2 salts (such as $MgSO_4$, $ZnSO_4$...) are an exception, presumably due to ion pairing. For 2:2 salts, an extra term must be included in B^{ϕ}_{MX} to give

$$B^{\phi}_{MX} = \beta^{(0)}_{MX} + \beta^{(1)}_{MX} \exp(-\alpha_1 I^{1/2}) + \beta^{(2)}_{MX} \exp(-\alpha_2 I^{1/2}) \quad (18.21)$$

---

[d] We will use Pitzer's notation as we summarize his equations. Note that the equations reduce to the Debye–Hückel limiting law at low m and are extensions of the Guggenheim equation at higher m, with an m^2 term added.

with $\alpha_1 = 1.4\ \text{kg}^{1/2}\cdot\text{mol}^{-1/2}$ and $\alpha_2 = 12\ \text{kg}^{1/2}\cdot\text{mol}^{-1/2}$. A_ϕ is the Debye–Hückel constant given in Table 18.1 and $\nu = \nu_+ + \nu_-$ is the total number of ions in the formula. Although these equations are not simple expressions, they do an exceptional job of fitting ϕ for a large number of electrolytes with only three parameters ($\beta^{(0)}$, $\beta^{(1)}$ and C^ϕ) that are specific to the electrolyte.[e] Furthermore, the equation reduces to the Debye–Hückel limiting law expression at low ionic strengths. Values for the Pitzer parameters for a number of electrolyte solutes are given in Appendix 7, along with the concentration range over which the parameters are valid. Figure 18.3 shows how well equations (18.18) to (18.20) fit the experimental results over the molality range from 0 to 5 $\text{mol}\cdot\text{kg}^{-1}$ for KCl and $CaCl_2$ and 0 to 3.8 $\text{mol}\cdot\text{kg}^{-1}$ for $LaCl_3$.[7] This example demonstrates that the equations work well for 1:1, 2:1 and 3:1 electrolytes.

Equations (18.18) to (18.21) can be transformed through the Gibbs–Duhem equation to obtain a comparable set of equations for $\ln\gamma_\pm$. The results are as follows:

$$\ln\gamma_\pm = |z_M z_X| f^\gamma + m(2\nu_M\nu_X/\nu)B^\gamma_{MX} + m^2[2(\nu_M\gamma_X)^{3/2}/\nu]C^\gamma_{MX} \quad (18.22)$$

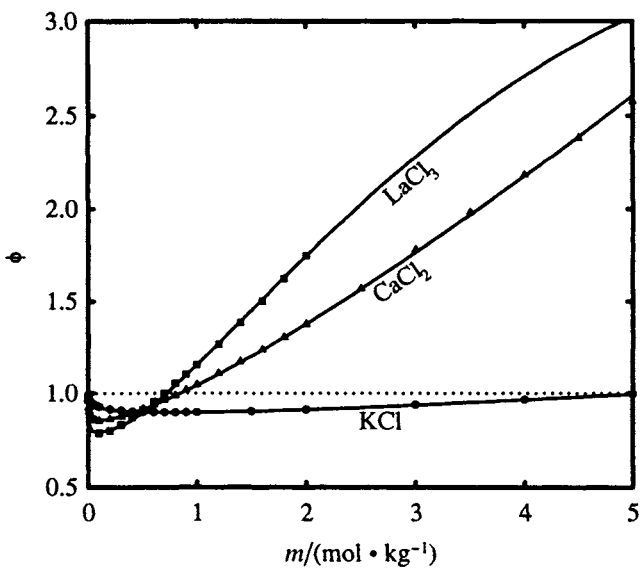

Figure 18.3 Comparison of osmotic coefficients at $T = 298.15$ K for three different electrolytes as calculated from Pitzer's equations (solid lines) with the experimental results (symbols).

[e] Four parameters are required for the 2:2 electrolytes.

where

$$f^{\gamma} = -A_{\phi}\left[I^{1/2}/(1 + bI^{1/2}) + \left(\frac{2}{b}\right)\ln(1 + bI^{1/2})\right] \tag{18.23}$$

$$B^{\gamma}_{MX} = B_{MX} + B^{\phi}_{MX} \tag{18.24}$$

$$C^{\gamma}_{MX} = \frac{3}{2} C^{\phi}_{MX} \tag{18.25}$$

with

$$B_{MX} = \beta^{(0)}_{MX} + \beta^{(1)}_{MX} g(\alpha_1 I^{1/2}) + \beta^{(2)}_{MX} g(\alpha_2 I^{1/2}) \tag{18.26}$$

where the $\beta^{(2)}_{MX}$ is included only for 2:2 electrolytes. The term $g(\alpha I^{(1/2)})$ is of the form

$$g(x) = 2[1 - (1 + x)\exp(-x)]/x^2 \tag{18.27}$$

with[f]

$$x = \alpha I^{1/2}. \tag{18.28}$$

The values of b and α are the same as were used in equations (18.18) to (18.21). That is, $\alpha_1 = 2.0$ kg$^{1/2}$·mol$^{-1/2}$ and $\alpha_2 = 0$ for all except the 2:2 electrolytes, where $\alpha_1 = 1.4$ kg$^{1/2}$·mol$^{-1/2}$ and $\alpha_2 = 12$ kg$^{1/2}$·mol$^{-1/2}$. Note that the same set of three (or four) parameters gives the values for $\ln \gamma_{\pm}$ and for ϕ. Figure 18.4 shows how well the set of parameters used to obtain ϕ for KCl, $CaCl_2$, and $LaCl_3$ represent the experimental $\gamma_{\pm}$ for the same three electrolytes.

Thermal Properties: Pitzer's equations for $\ln \gamma_{\pm}$ and ϕ [equations (18.18) to (18.26)] can be used to obtain relative partial molar enthalpies $\bar{L}_1$ and $\bar{L}_2$, and relative partial molar heat capacities[g] $\bar{J}_1$ and $\bar{J}_2$, by taking derivatives. For

[f] For a 2:2 electrolyte, $x = \alpha_1 I^{1/2}$ or $x = \alpha_2 I^{1/2}$, depending upon the value of $g(x)$ to be used in equation (18.27).

[g] $\bar{L}_1$, $\bar{L}_2$, $\bar{J}_1$, and $\bar{J}_2$ are enthalpy and heat capacity values relative to the standard state. That is $\bar{L}_i = \bar{H}_i - \bar{H}^{\circ}_i$ and $\bar{J}_i = C_{p,i} - \bar{C}^{\circ}_{p,i}$. The total relative enthalpy L is given by $L = n_1\bar{L}_1 + n_2\bar{L}_2$. See Section 11.5b of Chapter 11 for a discussion of these quantities.

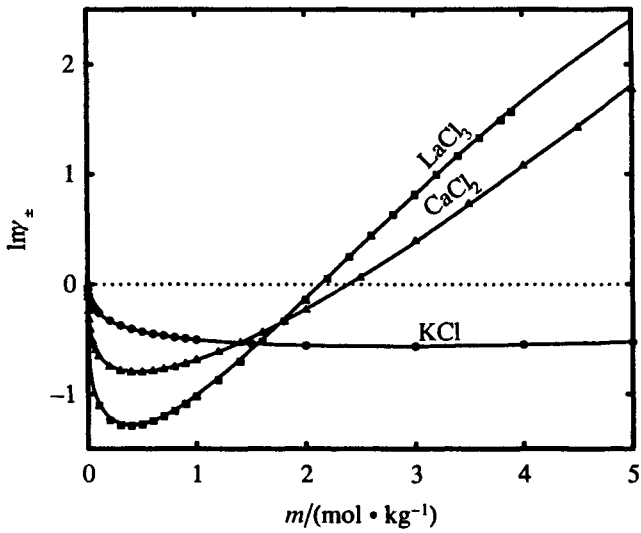

Figure 18.4 Comparison of activity coefficients at $T = 298.15$ K for three different electrolytes as calculated from Pitzer's equations (solid lines) with the experimental results (symbols).

example, $\bar{L}_2$ and $\bar{J}_2$ are obtained from

$$\bar{L}_2 = -\nu RT^2 \left(\frac{\partial \ln \gamma_\pm}{\partial T} \right)_p$$

$$\bar{J}_2 = \left(\frac{\partial \bar{L}_2}{\partial T} \right)_p .$$

Apparent values, defined as[h]

$$\phi Z = \frac{Z - n_1 Z_1^*}{n_2} \tag{18.29}$$

can also be calculated. In equation (18.29), Z_1^* is the value of the thermodynamic quantity Z for the pure solvent, with n_1 and n_2 as the moles of solvent and solute in the solution. Applied to enthalpies and heat capacities,

[h] See Section 11.5c of Chapter 11 for a discussion of these quantities.

equation (18.29) becomes

$$\phi H = \frac{H - n_1 H_1^*}{n_2}$$

and

$$\phi C_p = \frac{C_p - n_1 C_{p,1}^*}{n_2},$$

with

$$\phi L = \phi H - \phi H^\circ. \tag{18.30}$$

The Pitzer equations that apply to ϕL and ϕC_p are[i]

$$\phi L = \nu \mid z_M z_X \mid \left(\frac{A_L}{2b}\right) \ln(1 + bI^{1/2})$$

$$- 2\nu_M \nu_X RT^2 [mB_{MX}^L + m^2(\nu_M z_M) C_{MX}^L] \tag{18.31}$$

where

$$B_{MX}^L = \left(\frac{\partial B_{MX}}{\partial T}\right)_{p,I}$$

$$= \beta^{(0)L} + \beta^{(1)L} g(\alpha_1 I^{1/2}) + \beta^{(2)L} g(\alpha_2 I^{1/2}) \tag{18.32}$$

with

$$\beta^{(i)L} = \left(\frac{\partial \beta^{(i)}}{\partial T}\right)_p, \quad i = 0, 1, 2 \tag{18.33}$$

[i] The apparent partial molar quantities are often used in electrolyte solutions, and, in fact, are usually preferred over the partial molar properties by thermodynamicists who specialize in the treatment of electrolyte solutions.

and

$$C_{MX}^{L} = \frac{|z_M z_X|^{1/2}}{2} \left(\frac{\partial C_{MX}^{\phi}}{\partial T} \right)_p . \tag{18.34}$$

In a similar manner

$$\phi C_p - \bar{C}_{p,2}^{\circ} = \left(\frac{\partial \phi L}{\partial T} \right)_{p,I}$$

$$= \nu |z_M z_X| \left(\frac{A_J}{2b} \right) \ln(1 + bI^{1/2})$$

$$- 2\nu_M \nu_X RT^2 [mB_{MX}^{J} + m^2 (\nu_M z_M) C_{MX}^{J}] \tag{18.35}$$

where

$$B_{MX}^{J} = \left(\frac{\partial^2 B_{MX}}{\partial T^2} \right)_{p,I} + \frac{2}{T} \left(\frac{\partial B_{MX}}{\partial T} \right)_{p,I} \tag{18.36}$$

$$C_{MX}^{J} = \left(\frac{\partial^2 C_{MX}}{\partial T^2} \right)_{p} + \frac{2}{T} \left(\frac{\partial C_{MX}}{\partial T} \right)_{p} . \tag{18.37}$$

The relative partial molar enthalpy and relative partial molar heat capacity are obtained from[8]

$$\frac{\bar{L}_1}{RT} = M_w \left\{ -\frac{A_H}{2RT} \left[\frac{I^{3/2}}{1 + bI^{1/2}} \right] \right.$$

$$\left. + 2\nu_M \nu_X Tm^2 [\beta_{MX}^{(0)L} + \beta_{MX}^{(1)L} \exp(-\alpha I^{1/2}) + 2\nu_M z_M m C_{MX}^{L}] \right\}, \tag{18.38}$$

$$\frac{\bar{L}_2}{RT} = \frac{\nu \mid z_M z_X \mid A_H}{4RT}\left[\frac{I^{1/2}}{1+bI^{1/2}} + \left(\frac{2}{b}\right)\ln(1+bI^{1/2})\right]$$

$$-2\nu_M\nu_X Tm\left[2\beta^{(0)L}_{MX} + \frac{2\beta^{(1)L}_{MX}}{\alpha^2 I}\right.$$

$$\times\left\{1-\left(1+\alpha\, I^{1/2}-\frac{\alpha^2 I}{2}\right)\exp(-\alpha I^{1/2})\right\}$$

$$\left.+\,3\nu_M z_M m C^L_{MX}\right], \tag{18.39}$$

$$\frac{\bar{J}_1}{R} = M_w\left\{-\frac{A_J}{2R}\left[\frac{I^{3/2}}{1+bI^{1/2}}\right]\right.$$

$$\left.+\,2\nu_M\nu_X T^2 m^2[\beta^{(0)J}_{MX} + \beta^{(1)J}_{MX}\exp(-\alpha I^{1/2}) + 2\nu_M z_m m C^J_{MX}]\right\}, \tag{18.40}$$

$$\frac{\bar{J}_2}{R} = \frac{\nu \mid z_M z_X \mid A_J}{4R}\left[\frac{I^{1/2}}{1+bI^{1/2}} + \frac{2}{b}\ln(1+bI^{1/2})\right]$$

$$-2\nu_M\nu_X T^2 m\left[2\beta^{(0)J}_{MX} + \frac{2\beta^{(1)J}_{MX}}{\alpha^2 I}\right.$$

$$\times\left\{1-\left(1+\alpha I^{1/2}-\frac{\alpha^2 I}{2}\right)\exp(-\alpha I^{1/2})\right\}$$

$$\left.+\,3\nu_M z_M m C^J_{MX}\right]. \tag{18.41}$$

Volumetric Properties: Equations for ϕV, the apparent molar volume, can also be obtained. They are as follows

$$\phi V = \overline{V}_2^{\circ} + \nu \mid z_M z_X \mid \left(\frac{A_v}{2b}\right) \ln(1 + bI^{1/2}) + 2\nu_M \nu_X RT[mB^v_{MX} + m^2(\nu_m z_m)C^v_{MX}] \tag{18.42}$$

where

$$B^v_{MX} = \beta^{(0)v} + \beta^{(1)v} g(\alpha_1 I^{1/2}) + \beta^{(2)v} g(\alpha_2 I^{1/2}) \tag{18.43}$$

$$\beta^{(i)v} = \left(\frac{\partial \beta^{(i)}}{\partial p}\right)_T, \quad i = 0, 1, 2 \tag{18.44}$$

$$C^v_{MX} = \frac{\mid z_M z_X \mid^{1/2}}{2} \left(\frac{\partial C^{\phi}_{MX}}{\partial p}\right)_T. \tag{18.45}$$

In equations (18.29) to (18.43), the terms are the same as defined in equations (18.18) to (18.26) with A_H, A_J, and A_v as the Debye–Hückel parameters. In addition, T is the temperature and M_w is the molecular weight of the solvent (water) in kg·mol^{-1}. Values for these coefficients for a number of electrolytes are given in Appendix 7, and can be used to calculate the appropriate quantity.[j]

18.1e Pitzer's Equations at Elevated Temperatures

We have applied Pitzer's equations at $T = 298.15$ K, but they are not limited to that temperature and can be applied at any temperature where the coefficients are known.[k] Table 18.1 (and Table A7.1 of Appendix 7) gives the Debye–Hückel coefficients A_ϕ, A_γ, A_H, and A_J as a function of temperature, but the coefficients specific to the electrolyte are tabulated in Appendix 7 only at $T = 298.15$ K. The usual solution to this problem is to express the coefficients as

---

[j] We have limited our discussion to electrolyte solutions involving a single solute. As one could imagine, the already complicated equations become even more so when more than one solute is present. Pitzer has treated mixed electrolytes in the publication K. S. Pitzer, editor, *Activity Coefficients in Solutions*, 2nd Edition, Chapter 3, pp. 88–91, CRC Press, Boca Raton, Florida, (1991); and in the textbook K. S. Pitzer, *Thermodynamics*, McGraw-Hill, Inc., New York, 1995, Chapter 17. The equations for mixed electrolytes include expressions with coefficients involving each solute, plus cross-interaction terms. Some simplification occurs when two solutes have a common anion or cation. We refer the reader to the original references for more details.

[k] At high temperatures the effect of pressure must also be considered, since the (saturated) vapor pressure above the solution can be much larger than 1 bar (10^5 Pa).

a function of temperature. For example, the coefficients $\beta^{(0)}$, $\beta^{(1)}$, and C^{ϕ} for aqueous NaCl solutions have been expressed as a function of temperature by Silvester and Pitzer by the equations[9]

$$\beta^{(0)} = q_1 + q_2\left(\frac{1}{T} - \frac{1}{T_r}\right) + q_3 \ln\left(\frac{T}{T_r}\right) + q_4(T - T_r) + q_5(T^2 - T_r^2) \tag{18.46}$$

$$\beta^{(1)} = q_6 + q_9(T - T_r) + q_{10}(T^2 - T_r^2) \tag{18.47}$$

$$C^{\phi} = q_{11} + q_{12}\left(\frac{1}{T} - \frac{1}{T_r}\right) + q_{13} \ln\left(\frac{T}{T_r}\right) + q_{14}(T - T_r), \tag{18.48}$$

where the q_i are constant specifics for the electrolyte and T_r is the reference temperature (298.15 K).

Using the values of the coefficients given by Silvester and Pitzer while holding b and α constant at the $T = 298.15$ K values, the thermodynamic properties of NaCl solutions as a function of molality are reproduced within experimental error over the temperature range from 273.15 K to 573.15 K.

The problem with this procedure is that it adds more parameters, although not as many as might be expected, since derivatives of equations (18.46) to (18.48) using equations (18.33), (18.36), and (18.37) give the thermal coefficients $\beta^{(0)L}$, $\beta^{(1)L}$, B^{J}_{MX}, and C^{J}_{MX}. Silvester and Pitzer use a total of 16 parameters to represent the thermodynamic properties of NaCl(aq) as a function of the temperature from 273.15 to 573.15 K and molalities from 0 to that of the saturated solution at $p = 0.1$ MPa (or the saturation vapor pressure).

Figure 18.5 gives the osmotic coefficient and the activity for NaCl(aq) as a function of temperature and molality as predicted by the equation of Silvester and Pitzer. Note that both ϕ and $\gamma_{\pm}$ increase as T changes from 273.15 K to 323.15 K, and then decrease in a regular manner with increasing temperature. At $T = 523.15$ K, $\gamma_{\pm}$ has become a small value at high m.

18.1f Generalized Equations

Starting with Pitzer's equations, internally consistent generalized equations can be written to express the thermodynamic properties of aqueous electrolytes as a function of pressure, as well as temperature and molality. For example, Archer[10] gives the equations for calculating $\gamma_{\pm}$, ϕ, ϕL, ϕC_p, ϕV, ϕK and ϕE for aqueous NaCl solutions[1] as a function of p, T, and m over the temperature range from

[1] K and E are $(\partial V_m/\partial p)_T$ and $(\partial V_m/\partial T)_p$. As with the other apparent variables, ϕK and ϕE are differences in K and E, compared to the pure solvent.

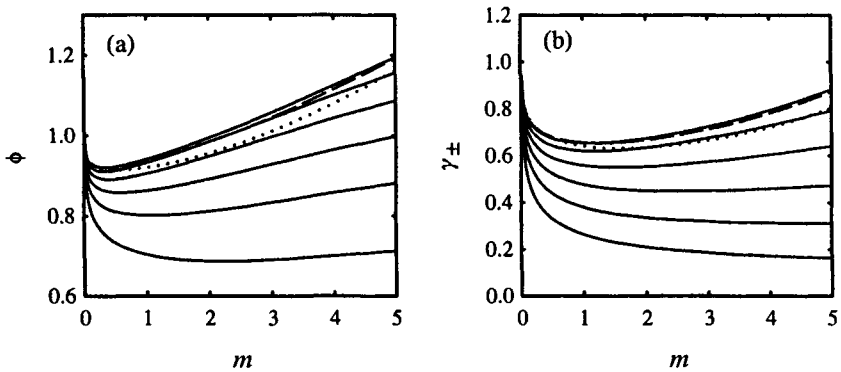

Figure 18.5 Graph of (a) the osmotic coefficient and (b) the activity coefficient for NaCl(aqueous) at $p = 0.1$ MPa as a function of temperature. The curves were obtained by using temperature-dependent coefficients in Pitzer's equations. The dotted line is for $T = 273.15$ K and the dashed line is for $T = 298.15$ K. The solid lines are for $T = 323.15$, 373.15, 423.15, 473.15, 523.15, and 573.15 K, with both ϕ and $\gamma_\pm$ decreasing with increasing temperature.

250 to 600 K and the pressure range from 0.1 MPa, or the saturated vapor pressure, to 100 MPa. The molality range varies with temperature, but as a minimum, it goes from zero to 5 mol·kg^{-1}.

We will not attempt to reproduce Archer's equations here. A total of 108 coefficients are present in the equations. Fortunately, many of these coefficients are not needed to fit the data and are set equal to zero. Archer, in his analysis of NaCl solutions, used 54 of the coefficients in his fit. He shows in his paper that his equations with these coefficients accurately summarize the properties of NaCl solutions over the pressure, temperature, and molality range given above.

By assuming that NaCl is a representative example, Archer's equations provide an opportunity to explore the effect of p, T, and m on the thermodynamic properties of an aqueous 1 : 1 electrolyte. Figures 18.6 and 18.7 summarize these effects.[m] In Figure 18.6, graphs are shown as isobaric surfaces as a function of T and m for the thermal properties $\gamma_\pm$, ϕ, ϕL, and ϕC_p. The volumetric properties ϕV, ϕK (apparent molar compressibility) and ϕE (apparent molar expansibility) are shown, again as isobaric surfaces, in Figure 18.7. The following observations can be made from the figures:

---

[m] Graphs and numerical values generated from Archer's equations were provided by E. M. Woolley of Brigham Young University. We appreciate his assistance in formulating these graphs and for much counsel and input into the discussions of the thermodynamics of electrolyte mixtures.

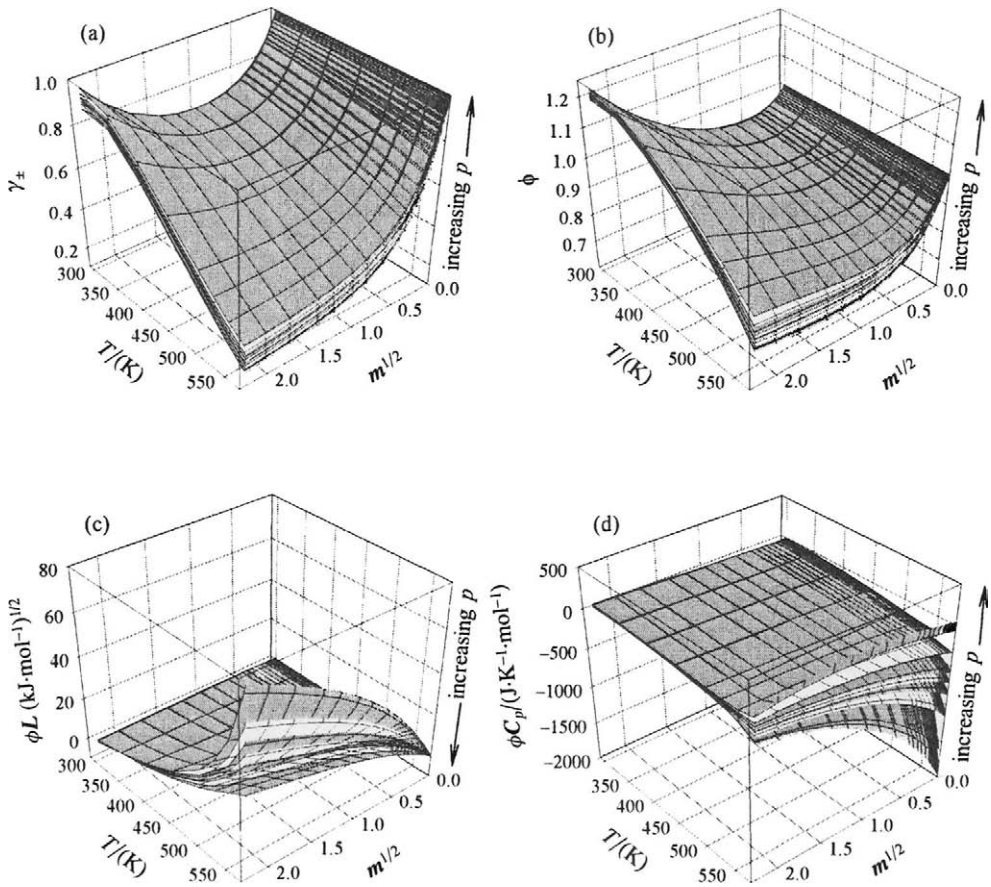

Figure 18.6 Thermal properties of aqueous NaCl solutions as a function of temperature, pressure and concentration. (a) activity coefficient; (b) osmotic coefficient; (c) relative apparent molar enthalpy; and (d) apparent molar heat capacity. The effect of pressure is shown as alternating grey and white isobaric surfaces of $\gamma_\pm$, ϕ, ϕL, and ϕC_p at $p = 0.1$ or saturation, 20, 30, 40, 50, 70, and 100 MPa, that increase with increasing p in (a), (b), and (d), and decrease with increasing p in (c).

1. Figures 18.6a and 18.6b show in more detail than in Figure 18.5, the major effect of temperature on $\gamma_\pm$ and ϕ. Pressure, on the other hand, has only a small effect on $\gamma_\pm$ and although the effect does increase at high temperatures and high molality. The equations that give the pressure

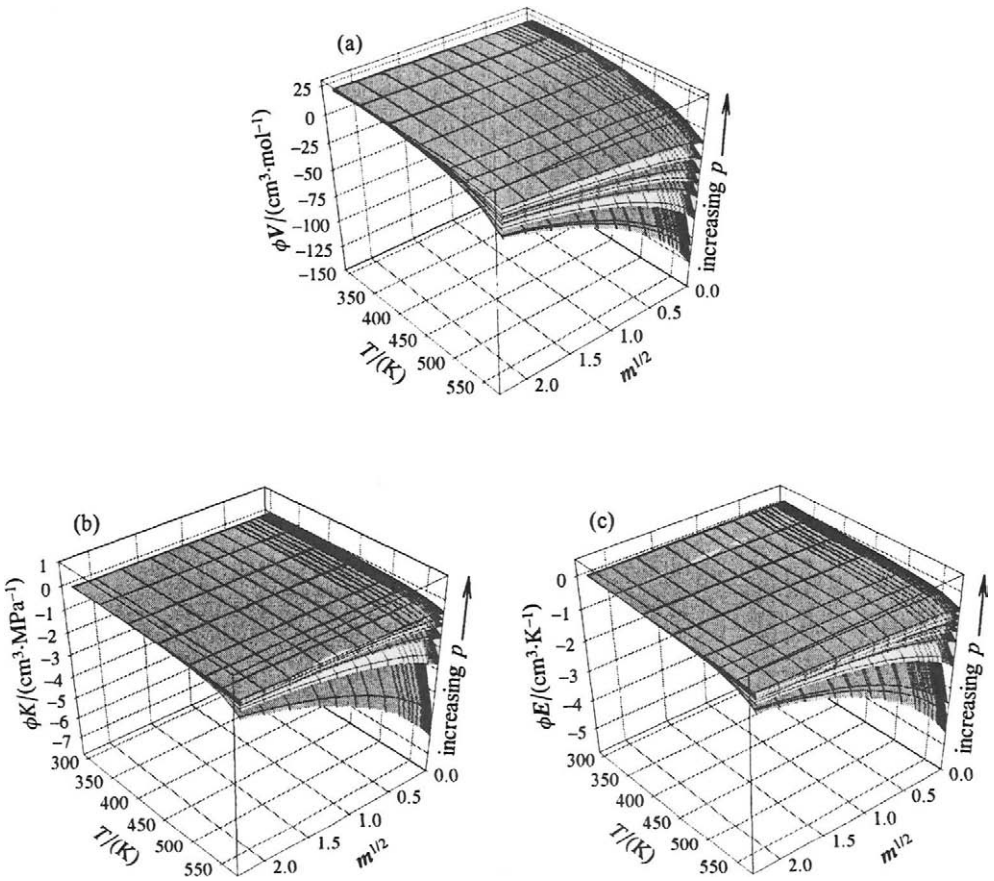

Figure 18.7 Volumetric properties of aqueous NaCl solutions as a function of temperature, pressure, and concentration. (a) apparent molar volume; (b) apparent molar compressibility; and (c) apparent molar expansibility. The effect of pressure is shown as alternating grey and white surfaces of ϕV, ϕK, and ϕE at $p = 0.1$ or saturation, 20, 30, 40, 50, 70, and 100 MPa. In all three instances, the surfaces increase with increasing pressure.

coefficient for $\ln \gamma_{\pm}$ and ϕ are

$$\left(\frac{\partial \ln \gamma_{\pm}}{\partial p}\right)_T = \frac{\bar{V}_2 - \bar{V}_2^{\circ}}{\nu RT} \tag{18.49}$$

$$\left(\frac{\partial \phi}{\partial p}\right)_T = -\frac{(\bar{V}_1 - V_1^*)}{\nu m M_1 RT}, \tag{18.50}$$

where M_1 is the molecular weight of the solvent in kg·mol^{-1} and V_1^* is the molar volume of the pure solvent (assuming a Raoult's law standard state). The small effect of p on $\gamma_\pm$ and ϕ results from the small differences $\bar{V}_2 - \bar{V}_2^\circ$ and $\bar{V}_1 - V_1^*$.

2. Figure 18.6c shows that ϕL is very dependent upon pressure at high temperatures and high molalities, with the effect increasing with decreasing pressure. The pressure coefficient for ϕL is given by[n]

$$\left(\frac{\partial \phi L}{\partial p}\right)_T = (\phi V - \phi V^\circ) - T\left[\left(\frac{\partial \phi V}{\partial T}\right)_p - \left(\frac{\partial \phi V^\circ}{\partial T}\right)_p\right]$$

or

$$\left(\frac{\partial \phi L}{\partial p}\right)_T = (\phi V - \phi V^\circ) - T(\phi E - \phi E^\circ) \tag{18.51}$$

where ϕE, the apparent molar expansibility, is given by

$$\left(\frac{\partial \phi V}{\partial T}\right)_p = \phi E.$$

---

[n] It can be shown by starting with the definition of the apparent molar property and differentiating that the apparent molar quantities are related by the same equations as the molar quantities. Thus if,

$$\left(\frac{\partial \bar{L}_2}{\partial p}\right)_T = (\bar{V}_2 - \bar{V}_2^\circ) - T\left[\left(\frac{\partial \bar{V}_2}{\partial T}\right)_p - \left(\frac{\partial \bar{V}_2^\circ}{\partial T}\right)_p\right]$$

then

$$\left(\frac{\partial \phi L}{\partial p}\right)_T = (\phi V - \phi V^\circ) - T\left[\left(\frac{\partial \phi V}{\partial T}\right)_p - \left(\frac{\partial \phi V^\circ}{\partial T}\right)_p\right].$$

The differences $(\phi V - \phi V^\circ)$ and $(\phi E - \phi E^\circ)$ are small, except at low pressures and high temperatures, where they become significant.

3. Figure 18.6d shows the effect of temperature and pressure on ϕC_p. The effect of both temperature and pressure are small, except at very high temperatures and low molalities. The pressure coefficient $(\partial \phi C_p / \partial p)_T$ at each m is positive at all temperatures. This positive $(\partial \phi C_p / \partial p)_T$ is in agreement with the ϕE data shown in Figure 18.7c since[o]

$$\left(\frac{\partial \phi C_p}{\partial p}\right)_T = -T\left(\frac{\partial^2 \phi V}{\partial T^2}\right)_p$$

$$= -T\left(\frac{\partial \phi E}{\partial T}\right)_p. \tag{18.52}$$

From Figure 18.7(c), we see that $(\partial \phi E / \partial p)_T$ is negative, which results in a positive $(\partial \phi C_p / \partial p)_T$ when substituted into equation (18.52).

The sudden increase in ϕC_p with temperature at the highest pressure and high temperatures is interesting, although care should be taken in relying too heavily on this result, since it represents a prediction of the third derivative of the chemical potential near both the pressure and temperature limits of the reliability of the equations.

4. As a final observation, we note from Figure 18.7 that the effect of pressure on ϕV and its derivatives is small at all except the highest temperatures and low molalities. These results are not unexpected, since condensed phases are not very compressible. At the temperature and molality conditions where pressure effects are significant, the solutions are dilute and the temperatures approach the critical temperature of water ($T_c = 647.3$ K). When liquids are at temperatures near their critical temperature, they become more compressible, and pressure will have a larger effect on quantities such as ϕV and its derivatives.

---

[o] Equation (18.52) is obtained from the relationship

$$\left(\frac{\partial C_p}{\partial p}\right)_T = -T\left(\frac{\partial^2 V}{\partial T^2}\right)_p.$$

18.2 Ion Association

The thermodynamic properties for electrolyte solutions that we have described so far in this chapter assume complete dissociation in the solution. The activity coefficient $\gamma_{\pm}$, for example, that we calculate from the Debye–Hückel, Guggenheim, or Pitzer equations assumes the strong electrolyte standard state. For most electrolyte solutions at near ambient temperatures, this choice of standard state seems to be the best to use, although there are exceptions. For example, Pitzer's equations require extra terms to calculate the properties of 2:2 electrolytes such as $MgSO_4$, $ZnSO_4$, etc. Debye–Hückel theory also shows deviation from the limiting law expression in more dilute solutions for 2:2 electrolytes than for other types. The reason usually given for these deviations is that the electrolyte is not completely dissociated in solution. Expressed in another way, ion association for the 2:2 electrolyte, given by the reaction

$$M^{2+} + X^{2-} = MX \tag{18.53}$$

occurs.

It is important to remember that reactions such as the above do not invalidate our choice of a strong electrolyte standard state. We repeat that thermodynamics does not tell us what is happening in solution on a molecular (ionic) level. The observation we make is that $\gamma_{\pm}$ deviates more for mixtures of 2:2 electrolytes than for solutions of 1:1, 1:2, and 1:3 electrolytes, and we attribute this deviation to ion association. But we can handle these deviations perfectly well in our treatment without assuming ion association. We can stay with our strong electrolyte standard state and accept as a fact of life that, at a given low concentration, $\gamma_{\pm}$ deviates more from unity than for other mixtures.

An analogy can be made with nonelectrolyte mixtures. For (nonpolar + nonpolar) mixtures, near-ideal solution behavior occurs and activity coefficients given by

$$a_i = \gamma_{R,i} x_i$$

are nearly one. Activity coefficients greater than one occur for (polar + nonpolar) mixtures where we break up attractions between the polar molecules, and we describe this in terms of positive deviations from Raoult's law. When complex formation (including hydrogen bonding) is present, deviations occur that result in $\gamma_{R,i}$ that are less than one, and we describe these solutions as having negative deviations from Raoult's law. The point is that to apply our thermodynamics, we do not need to know about breaking apart dipole interactions or forming complexes. We simply absorb whatever is happening on a molecular level into the activity coefficient. We can, however, choose standard states that, for example, recognize complex formation in the mixture. When we do so, we end up with

activity coefficients that deviate less from unity. But at the same time we must find some method for measuring the extent of complex formation, and this usually requires a nonthermodynamic technique.

In a similar manner, standard states can be chosen for electrolytes that take into account molecular association. We call this the weak electrolyte standard state, and some method must be employed to determine the extent of association. As an example, we usually treat nitric acid HNO_3 as a strong electrolyte so that in solution

$$a_2 = \gamma_{\pm}^2 m^2. \tag{18.54}$$

But there is evidence that, at least in more concentrated solutions, ion association occurs. That is

$$H^+(aq) + NO_3^-(aq) = HNO_3(aq).$$

For example, Raman spectroscopy techniques show vibrational transitions that can be attributed to the HNO_3 molecule as well as to the NO_3^- ion.[11] By using the intensities of the Raman bands to measure the concentrations of the species in solution, an equilibrium constant K_c can be written

$$K_c = \frac{c_{HNO_3}}{c_{H^+} c_{NO_3^-}} \tag{18.55}$$

that is related to the thermodynamic equilibrium constant by[p]

$$K = \frac{a_{HNO_3}}{a_{H^+} a_{NO_3^-}} = K_c \frac{\gamma_{HNO_3}}{\gamma_{\pm,c}^2}. \tag{18.56}$$

Using this method, Redlich reports[q] an association constant K_c at $T = 298.15$ K of 0.048, implying a significant level of ion association in concentrated solution.

---

[p] Note that molar concentrations are used in equations (18.54) and (18.55). The activity coefficient $\gamma_{\pm,c}$ is the value that converts c to a_2. Thus

$$a_{H^+} \cdot a_{NO_3^-} = \gamma_{\pm,c}^2 c_{H^+} \cdot c_{NO_3^-}.$$

In dilute aqueous solutions, $c \approx m$ and $\gamma_{\pm,c} \approx \gamma_{\pm}$. Calculations can be made to change from one type of activity coefficient to the other, but the differences are small in aqueous solution.

[q] Redlich actually reports a constant of 21 for the dissociation reaction. He compares this result with values obtained for the reaction by other methods and shows that the results are in reasonably good agreement.

We can summarize the difference between the two standard states for HNO_3 as follows

Strong electrolyte:

$$K = \frac{a_{HNO_3}}{a_{H^+} a_{NO_3^-}} = 1$$

$$= \frac{1}{\gamma_{\pm}^2 m^2}$$

Weak electrolyte:

$$K = \frac{a_{HNO_3}}{a_{H^+} a_{NO_3^-}}$$

$$= \frac{\gamma_{HNO_3} c_{HNO_3}}{\gamma_{\pm,c}^2 c_{H^+} c_{NO_3^-}}$$

$$= \frac{\gamma_{HNO_3}}{\gamma_{\pm,c}^2} K_c$$

where K_c is the association constant.[r]

For HNO_3, Raman spectroscopy was used to determine concentrations, and hence equilibrium constants, in HNO_3(aq) solutions. But this technique is often not possible in other systems because vibrational or electronic transitions that can be used to differentiate between the ion and the molecule are not present, and other techniques must be used. As we do so, we must keep in mind that the different techniques are based upon assumptions that lead to the measurement of the equilibrium concentration. For example, a light-scattering technique such as Raman spectroscopy usually relies on the assumption that the concentration of the species in solution is proportional to the intensity of the observed band.

Different assumptions for measuring concentration can lead to different values for the equilibrium concentrations, and hence, to different equilibrium

[r] The free energy of formation of HNO_3 would not be the same with the different choices of standard states. They differ by $RT \ln K_c$ (assuming the molality and molarity based equilibrium constants are the same). The activity coefficients $\gamma_{\pm}$ and $\gamma_{\pm,c}$ also differ slightly from one another.

constants. It is reassuring that when different kinds of measurements can be made on the same system, the agreement is often good.

In Section 11.7 of Chapter 11, we summarized equations that can be used with electrochemical cell measurements to determine K_a and K_w for the dissociation (reverse of association) of an acid and of water, assuming a weak electrolyte standard state. If care is taken to obtain reversible conditions, this method, which does involve thermodynamic measurements, is a good one for determining K. Another method often employed involves using conductance measurements. The assumption is made that α, the degree of ionization or dissociation of an electrolyte is given by the ratio Λ/Λ'. That is,

$$\alpha = \frac{\Lambda}{\Lambda'} \tag{18.57}$$

where Λ is the molar conductance obtained from electrical resistance measurements on the solution. The quantity Λ' is the hypothetical conductance that would be obtained in a solution of completely dissociated solute. The assumption is made that the solute obeys the Onsager relationship in dilute solution

$$\Lambda' = \Lambda_o - (A + B\Lambda_o)c^{1/2} \tag{18.58}$$

where Λ_o is the limiting equivalent conductance, c is the molar concentration, and A and B are theoretical constants that can be calculated from values for the viscosity, relative permittivity (dielectic constant), temperature, and ionic charge of the solvent.

When association occurs, the Onsager equation must be modified to include only the free ions. Assuming the ion pair makes no contribution to the conductance, equation (18.58) becomes

$$\Lambda = \alpha[\Lambda_o - (A + B\Lambda_o)]c^{1/2}. \tag{18.59}$$

Once α is obtained, the association constant can be calculated from

$$K = \frac{(1-\alpha)}{\alpha^2 c \gamma_{\pm,c}^2}. \tag{18.60}$$

To obtain K, Λ is measured for a series of solutions of different concentration. Equation (18.59) is then used to get α, which can be substituted into equation (18.60) to get K. The activity coefficient $\gamma_{\pm,c}$ is usually approximated by the

extended Debye–Hückel relationship. Alternatively, K and Λ_o can be obtained from the Shedlovsky equation, which is a combination of the above.

$$\frac{1}{\Lambda S(z)} = \frac{1}{\Lambda_o} + \frac{c\Lambda S(z)\gamma_{\pm,c}^2}{K\Lambda_o^2}. \tag{18.61}$$

In applying equation (18.61), $S(z)$ is treated as an empirical parameter, and Λ_o and K are solved for simultaneously.

As an example of the application of this procedure, Davies[12] has given Λ values for $MgSO_4(aq)$ at $T = 298.15$ K and a range of c. He obtains an equilibrium constant for the reaction

$$Mg^{2+}(aq) + SO_4^{2-}(aq) = MgSO_4(aq)$$

of 175. This corresponds to an α (after correction for $\gamma_{\pm,c}$ using the Debye–Hückel limiting law)[s] of 0.989 at $c = 1.62 \times 10^{-4}$ mol·dm^{-3}. Thus, $MgSO_4$ is associated (ion-paired) even in this very dilute solution.

18.2a Ion Association at High Temperatures

In most instances, ion association increases with increasing temperature.[t] For example, Mesmer[13] and co-workers at the Oak Ridge National Laboratories have determined K for the association reactions shown[u] in Figure 18.8. Both conductivity and cell EMF measurements were used to determine the values. The EMF measurements were based on the concentration cell

$$H_2(g),\ Pt \mid \underset{\{\text{test solution}\}}{NaCl(m_1),\ HA(0.01m),\ NaA(0.01m)} \mid\mid \underset{\{\text{reference solution}\}}{NaCl(m_1),\ HCl(0.01m)} \mid Pt,\ H_2(g)$$

where HA represents a weak monoprotic acid and m is the molality. The EMF for the cell is given by

$$E = \frac{RT}{F} \ln \frac{(m_{H^+})_r \gamma_r}{(m_{H^+})_t \gamma_t} + \text{ELJ} \tag{18.62}$$

---

[s] We assume $\gamma_{MgSO_4} = 1$ in this dilute solution ($MgSO_4$ is a nonelectrolyte).

[t] Association, even in NaCl solutions, contributes to the decrease in $\gamma_\pm$ (based on the strong electrolyte standard state) with increasing temperature shown in Figures 18.5 and 18.6.

[u] The equilibrium constants were obtained at the saturation vapor pressure, that is, at a pressure equal to the vapor pressure of water over the solution.

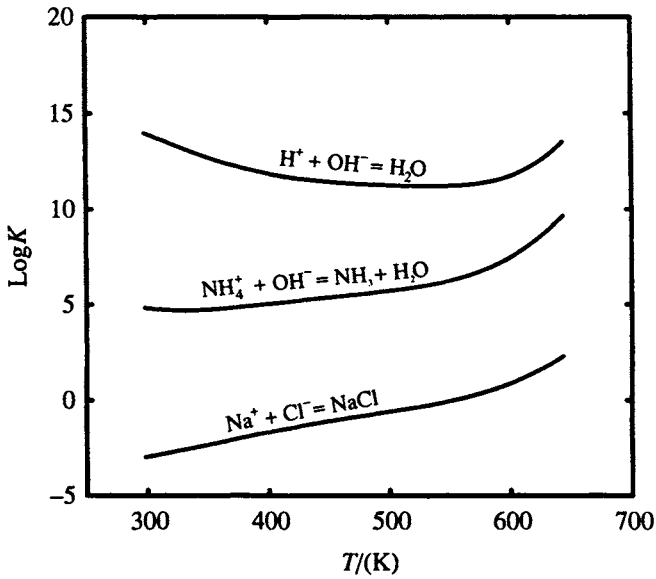

Figure 18.8 Equilibrium constants for several association reactions as a function of temperature at a pressure equal to the saturation vapor pressure. Results courtesy of R. E. Mesmer, Oak Ridge National Laboratories.

where r refers to the reference half cell and t to the test solution. The double line indicates that a salt bridge is present in the cell with a resulting junction potential ELJ. The cell is run with high (and equal) concentrations of NaCl in the reference and test sides. The NaCl effectively swamps out all other sources of ions so that $\gamma_r = \gamma_t$. Also, the junction potential becomes small under these conditions and can be accurately corrected for.

In Figure 18.8, K for the acid-base reactions (the first two) were determined by both cell EMF and conductivity measurements. Only conductivity measurements could be used to get K for the ion-pairing in NaCl. We note from this figure that association, even in NaCl, becomes appreciable at high temperatures. It has been said that it is difficult to find ionic solutions where ion-pairing is not important at high temperatures.

The effect of temperature on the equilibrium constant for the association reaction for water is interesting. This reaction has the value $K = 1/K_w$, which at 298.15 K is 1.0×10^{14} so that $\log K = 14$. With increasing temperature, $\log K$ (and hence, K) first decreases and then increases. The effect of temperature on K is given by

$$\left(\frac{\partial \ln K}{\partial T}\right)_p = \frac{\Delta_r H^\circ}{RT^2}. \tag{18.63}$$

Figure 18.9 summarizes $\Delta_r H°$ for this reaction.[14] We see that at near-ambient temperatures $\Delta_r H < 0$ so that $(\partial \ln K/\partial T)_p < 0$ and K decreases with increasing T. At approximately 500 K, $\Delta_r H°$ becomes zero and log K goes through a minimum. Above this temperature, $\Delta_r H > 0$, and equation (18.63) requires that $(\partial \ln K/\partial T)_p > 0$, an effect that is apparent in Figure 18.8.

Shown in Figure 18.9 is a comparison of $\Delta_r H°$ obtained from calorimetric measurements (solid line) and $\Delta_r H°$ obtained from the Marshall-Frank equation,[15] which is an expression relating K to T that gives $\Delta_r H°$ from $(\partial \ln K/\partial T)_p$. The agreement between the two methods is another example of thermodynamic consistency.

18.2b Ion Association from Flow Calorimetry

Flow calorimetry provides another method for measuring ion association at high temperatures. For example, the equilibrium constants for the reactions shown in Figure 18.10 were determined in this manner. In the procedure followed, an aqueous H_2SO_4 solution was mixed in a flow calorimeter with an aqueous Na_2SO_4 solution, and the heat of mixing was measured under the condition where the flow rate of the H_2SO_4 solution was held constant while the flow rate of the Na_2SO_4 solution (and hence, the total flow) was varied. From

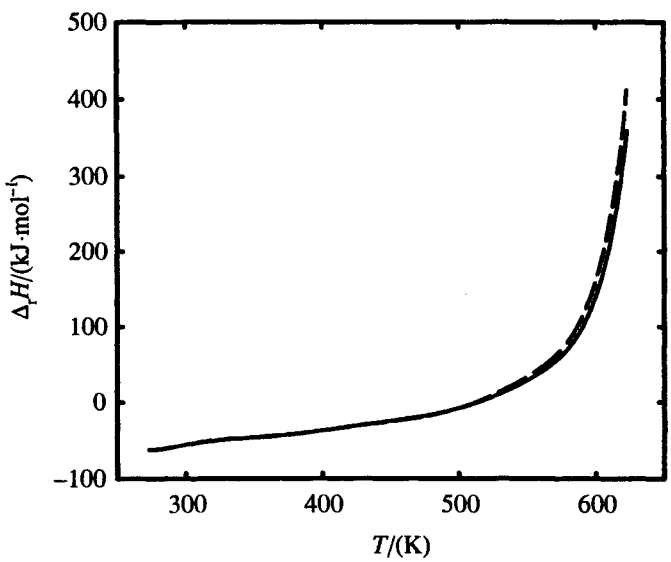

Figure 18.9 $\Delta_r H$ as a function of temperature for the association reaction $H^+(aq) + OH^-(aq) = H_2O(l)$. The solid line gives the values obtained from calorimetric measurements and the dashed line gives the values obtained from the Marshall–Frank equation.

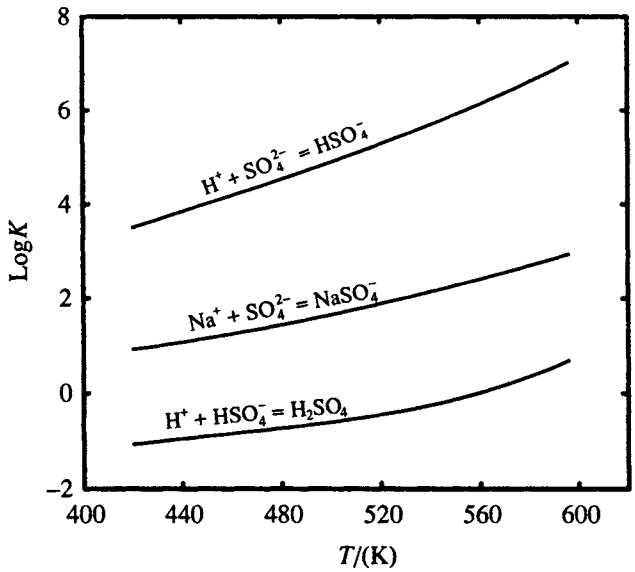

Figure 18.10 Equilibrium constants as a function of temperature for several association reactions. The constants were obtained from flow calorimetric measurements at a pressure equal to the saturation vapor pressure.

the results of these measurements with different concentrations of reactants and at a series of temperatures, equilibrium constants are calculated from the effect of the initial concentration and temperature on the heat of mixing.

In the reacting mixture, possible association reactions are

$$H^+ + SO_4^{2-} = HSO_4^- \qquad (1)$$

$$H^+ + HSO_4^- = H_2SO_4 \qquad (2)$$

$$Na^+ + SO_4^{2-} = NaSO_4^- \qquad (3)$$

$$Na^+ + HSO_4^- = NaHSO_4 \qquad (4)$$

$$H^+ + NaSO_4^- = NaHSO_4 \qquad (5)$$

$$Na^+ + NaSO_4^- = Na_2SO_4 \qquad (6)$$

For any of these reactions, the equilibrium constant can be written as

$$K = J_\gamma K_m \qquad (18.64)$$

where K_m is the molality ratio and J_γ is the activity coefficient ratio. For example, for reaction (1)

$$J_\gamma = \frac{\gamma_{HSO_4^-}}{\gamma_{H^+}\gamma_{SO_4^{2-}}} \tag{18.65}$$

$$K_m = \frac{m_{HSO_4^-}}{m_{H^+}m_{SO_4^{2-}}}. \tag{18.66}$$

The log K values shown in Figure 18.10 are the values that best reproduce all of the heat of mixing curves.[v] The J_γ values are obtained by estimating initial values using the activity coefficients for NaCl(aq).[16] These initial values of J_γ are then readjusted, as the value for K_m is optimized, by adjusting the coefficients of Pitzer's equations, whose form is described in the previous section. Pitzer's equations are, of course, internally consistent so that adjustments to the activity or osmotic coefficient parameters result in adjustments to the thermal parameters (ϕL, $\bar{L}_2$, ϕJ, or $\bar{J}_2$), and hence, to the heat effects.

Details of the optimization procedure used to calculate the equilibrium constants can be found in the literature[17]. In this procedure, reactions are excluded that do not change the fit to the heat effect. In our example, only reactions (1) to (3) are important so that reactions (4), (5), and (6) are excluded. This is equivalent to saying that ion association in reactions (4), (5), and (6) is negligible compared to that in the other three reactions.

The procedure described would not be possible without high-speed computers that can simultaneously look at all the relationships and optimize the fit while keeping in mind the thermodynamic relationships between the different parameters. For example,

$$\left(\frac{\partial \ln K}{\partial T}\right)_p = \frac{\Delta_r H^\circ}{RT^2}$$

$$\left(\frac{\partial \Delta_r H^\circ}{\partial T}\right)_p = \Delta_r C_p^\circ$$

$$\left(\frac{\partial \ln \gamma}{\partial T}\right)_p = -\frac{\bar{L}_2}{RT^2}.$$

[v] With this method, we use the heat of the reaction (rather than the optical absorbance or the electrical conductivity as described earlier) to determine the extent of the reaction. A bonus of the method is that $\Delta_r H$, $\Delta_r C_p$ and J_γ are obtained directly, along with log K.

The calorimetric method gives equilibrium constants that agree reasonably well with values obtained from other methods, such as conductance measurements or cell EMF measurements. The reliability is increased when a combination of calorimetric measurements with conductivity or cell EMF measurements is used in establishing the equilibrium conditions, especially when more than one reaction is significant.

Some interesting observations can be made from the K values shown in Figures 18.8 and 18.10. First, we see that, as a general trend, association increases with increasing temperature, and becomes an important effect at high temperatures even for solutes that we consider to be strong electrolytes (completely dissociated) at ambient temperature. For example, we note that at high temperatures, H_2SO_4 should no longer be thought of as a strong acid, and NaCl and $NaSO_4^-$ are not strong electrolytes.

The increase in K with temperature requires that $\Delta_r H^\circ > 0$ for the association reaction that we can write in a general form as

$$M^+(H_2O)_m + X^-(H_2O)_n = MX(H_2O)_p + (m + n - p)H_2O.$$

Furthermore, $T\Delta S^\circ$ must also be greater than zero at high temperatures for this reaction so that ΔG° given by

$$\Delta_r G^\circ = \Delta_r H^\circ - T\Delta_r S^\circ$$

becomes less than zero at these temperatures. Mesmer and coworkers[18] compare $\Delta_r G$ for several association reactions in terms of $\Delta_r H^\circ$ and $T\Delta_r S^\circ$. They show that $T\Delta_r S^\circ > \Delta_r H^\circ$ and increases more rapidly than does $\Delta_r H^\circ$. Hence, $\Delta_r S^\circ$ is the driving force for the reaction.

In an attempt to understand the observed trend, Mesmer and his coworkers divide this overall process into three steps: (1) the formation of the MX bond; (2) the liberation of $(m + n - p)$ waters of hydration from around the ions; and (3) the bonding of the liberated water with the solvent. For step (1), ΔH° and ΔS° are both expected to be negative. For step (2), both are expected to be positive as bonds and structure are lost, while in step (3), both are expected to be negative, since bonds and structure form. The conclusion that can be reached is that since all the quantities are positive only in step (2), ΔH° and ΔS° for this step must be predominant at high temperatures. That is, association occurs principally as a result of the breakdown of the hydration sphere around the ions at high temperatures. The large decrease in the relative permittivity (dielectric constant) of the solvent with temperature makes a major contribution to the positive ΔH° and ΔS° for step (2) of the association reaction at high temperatures, since the ion–solvent hydration interactions become less important as the permittivity decreases, resulting in a breakdown of the hydration sphere around the ions.

18.3 Surfactant Solutions

Surfactants are molecular or ionic species that have a polar (hydrophilic) moiety (head) attached to a long nonpolar (hydrophobic) moiety (tail). Examples are

$H(CH_2)_n-COO^-Na^+$	(sodium carboxylates)
$H(CH_2)_n-SO_4^-Na^+$	(sodium alkyl sulfates)
$H(CH_2)_n-NH_3^+Cl^-$	(alkylammonium chlorides)
$H(CH_2)_n-NC_5H_5^+Cl^-$	(alkylpyridinium chlorides)
$H(CH_2)_n-N(CH_3)_2$	(alkylamines)

where n typically has values ranging from 6 to 16. Many surfactants are electrolytes, but some, such as the alkylamines, are non-ionic.

18.3a Thermodynamic Properties of Surfactant Solutions

Mixtures of these surfactants with water result in solutions with unique properties that we want to consider. We will use the alkylpyridinium chlorides as examples. Figure 18.11 compares the osmotic coefficient ϕ, apparent relative molar enthalpy ϕL, apparent molar heat capacity ϕC_p, and apparent molar volumes ϕV as a function of molality for two alkylpyridinium chlorides in water.[w 19]

The abrupt changes in the slope of the lines at low m result from the formation of aggregates called micelles in the solution. A schematic representation of a micelle can be seen in Figure 18.12. The surfactant is represented by the long "snake-like" structure,[x] with the enlarged area representing the polar hydrophilic head and the remainder representing the hydrophobic hydrocarbon tail. If the head is ionic, then counterions of opposite charge are scattered throughout the solution to maintain electrical neutrality.

At low concentrations the surfactant is present principally as individual ions. With increasing concentration, some association can occur, and dimers or larger structures can form. Finally, a concentration is reached, known as the critical micelle concentration or CMC, where the micelle forms more or less cooperatively. In the micelle, the molecules (or ions) can group themselves in

---

[w] The scatter of the experimental data points reflects the difficulty of measuring thermodynamic quantities in these dilute solutions. The origin of the fitting lines will become apparent as we describe the mass action model later in this section.

[x] The micelle is not flat. Instead, it is approximately spherical in shape. With increasing concentration, the structure changes to a cylindrical shape, and eventually to a laminar structure.

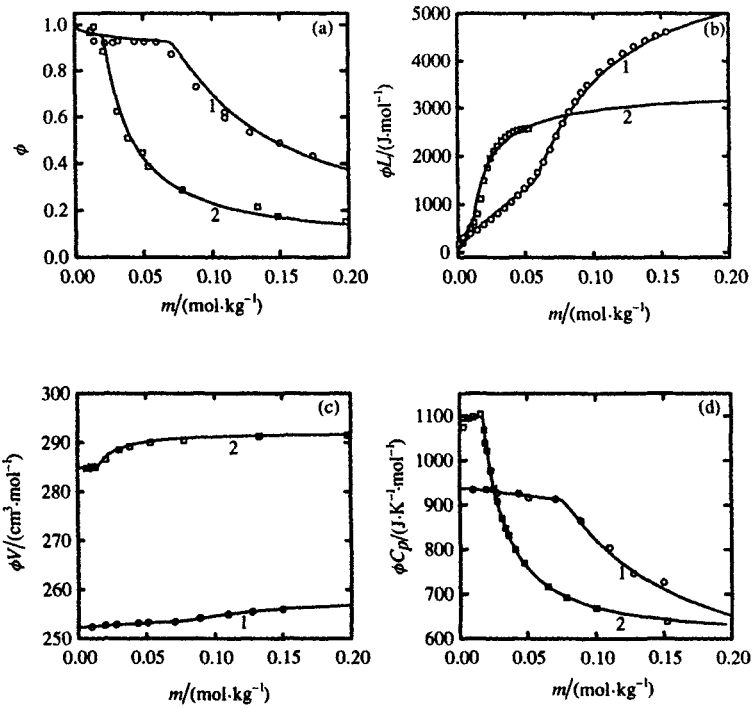

Figure 18.11 (a) Osmotic coefficient; (b) apparent relative molar enthalpy; (c) apparent molar volume; and (d) apparent molar heat capacity, at $T = 298.15$ K and $p = 0.1$ MPa, for (1) n-decylpyridinium chloride and (2) n-dodecylpyridinium chloride.

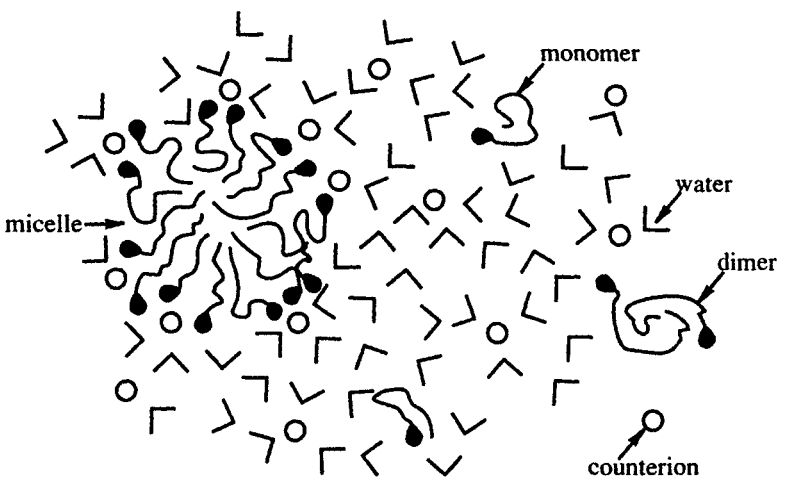

Figure 18.12 Two-dimensional representation of an aqueous surfactant solution showing the presence of a micelle. Drawing courtesy of E. M. Woolley, Brigham Young University.

an almost spherical structure, with the hydrocarbon chains on the interior of the sphere, enclosed by the polar heads on the surface of the micelle in contact with the solvent water molecules. Structural measurements such as neutron scattering, X-ray diffraction, diffusion, and electrical conductivity indicate that a typical ionic micelle may have 20–90 surfactant monomers in the aggregate. Much of the electrical charge on the micelle is neutralized by counterions that pair with ions on the surface, so that the micelle has a net charge of perhaps 5 to 20. The size of the micelle depends upon the length of the hydrocarbon chain and upon the temperature. The shorter the chain, the fewer the number of molecules that are required to form the micelle. Thus, at a given temperature, as can be seen in Figure 18.11 where n-decylpyridinium chloride and n-dodecylpyridinium chloride are compared, the CMC, which occurs at the abrupt change in slope, shifts to lower molality with increasing length of the chain.

The effect of temperature on the thermodynamic properties and the CMC is shown in Figure 18.13, where ϕL, ϕC_p and ϕV at three temperatures are graphed as a function of the molality m for n-dodecylpyridinium chloride. We can interpolate the results in Figure 18.13a to determine that ϕL at the CMC is near zero for this surfactant at a temperature near, but just above, 298.15 K. When $\phi L = 0$, the CMC is at its minimum value. We will better understand why as we consider theories for describing the curves shown in Figures 18.11 and 18.13.

18.3b Theoretical Description of Surfactant Solutions

Two principal approaches have been used to describe the thermodynamics of surfactant solutions — the **pseudo-phase model** and the **mass action model**.

The Pseudo-Phase Model: Consider a process in which surfactant is added to water that is acting as a solvent. Initially the surfactant dissolves as monomer species, either as molecules for a non-ionic surfactant or as monomeric ions for an ionic surfactant. When the concentration of surfactant reaches the CMC, a micelle separates from solution. In the pseudo-phase model,[20] the assumption is made that this micelle is a separate pure phase that is in equilibrium with the dissolved monomeric surfactant. To maintain equilibrium, continued addition of surfactant causes the micellar phase to grow, with the concentration of the monomer staying constant at the CMC value. This relationship is shown in Figure 18.14 in which we plot m, the stoichiometric molality,[y] against m_2, the molality of the monomer in the solution. Below the CMC, $m = m_2$, while above the CMC, $m_2 =$ CMC and the fraction α of the surfactant present as monomer

[y] The stoichiometric molality is the calculated concentration that does not take into account the nature of the species in solution.

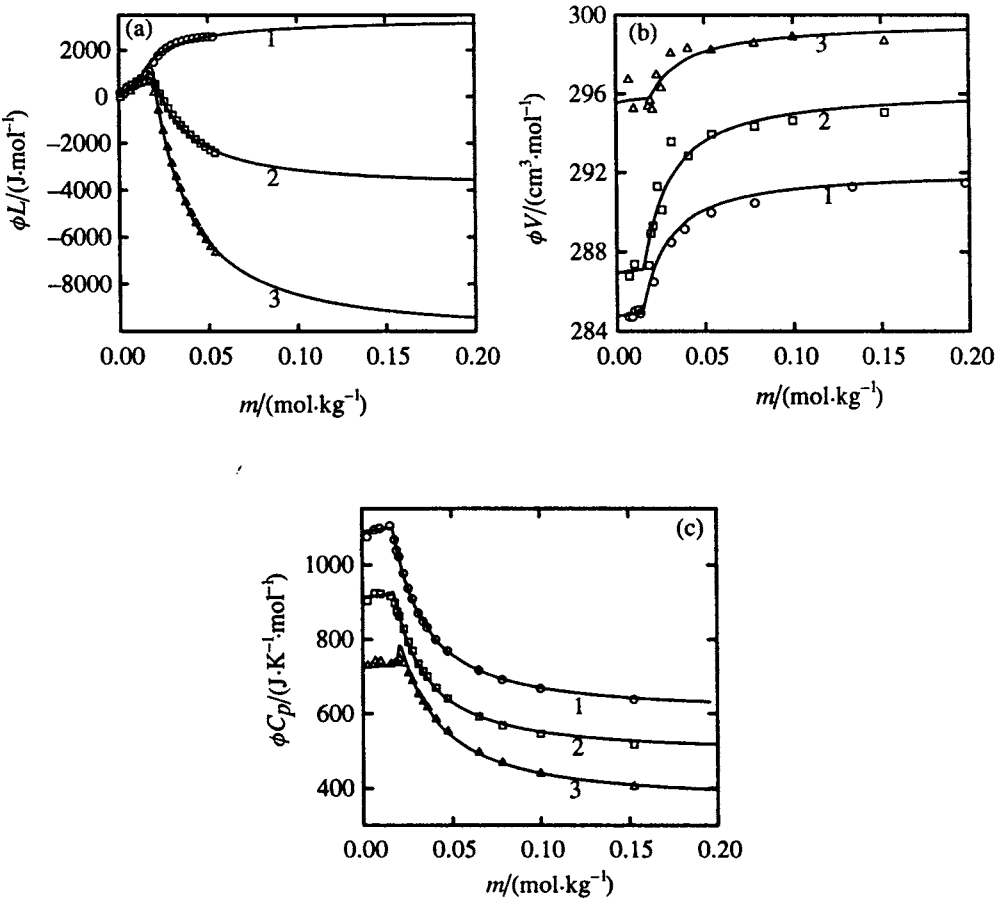

Figure 18.13 Effect of temperature on (a) apparent relative molar enthalpies; (b) apparent molar volumes; and (c) apparent molar heat capacities, for n-dodecylpyridinium chloride. The temperatures are (1) 298.15 K; (2) 313.15 K; and (3) 328.15 K.

is given by

$$\alpha = \frac{m_2}{m} = \frac{\text{CMC}}{m}. \tag{18.67}$$

We assume that the micelle is a pure surfactant phase with a chemical potential given by μ_A^*. If the chemical potential of the monomer is μ_2, then the condition of phase equilibrium is given by

$$\mu_A^* = \mu_2. \tag{18.68}$$

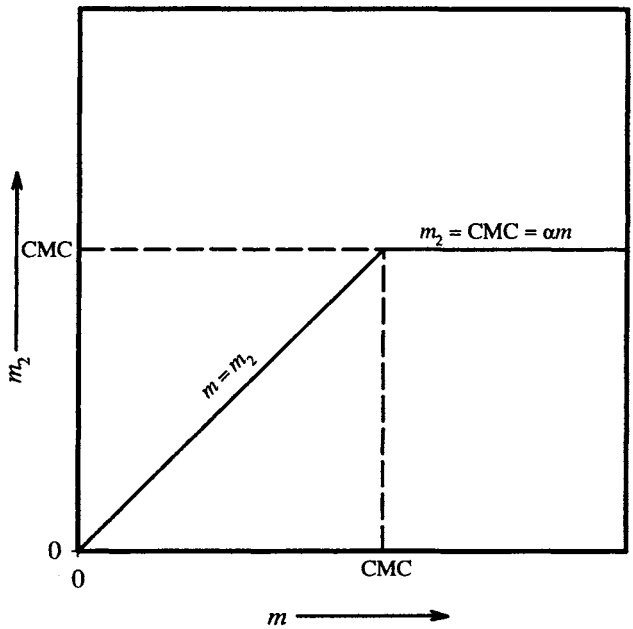

Figure 18.14 Comparison of the stoichiometric molality m and the molality of the monomer m_2 in a surfactant solution, according to the pseudo-phase model.

But μ_2 is related to the activity a_2 of the monomer in the aqueous phase by the equation

$$\mu_2 = \mu_2^\circ + RT \ln a_2 \tag{18.69}$$

where μ_2° is the chemical potential of the monomer in the standard state. The activity a_2 is related to m_2 by

$$\begin{aligned} a_2 &= \gamma_2 m_2 \\ &= \gamma_2 \alpha m. \end{aligned} \tag{18.70}$$

In the pseudo-phase model, ideal solutions are assumed[z] so that $\gamma_2 = 1$ and

$$a_2 = \alpha m. \tag{18.71}$$

[z] The solutions are usually very dilute at the CMC (critical micelle concentration). Hence, the assumption of ideal solution behavior is not unreasonable.

Combining equations (18.68), (18.69), and (18.70) gives

$$\frac{\mu_A^* - \mu_2^\circ}{RT} = \ln \alpha m \tag{18.72}$$

or

$$\frac{\Delta G_{A,m}^\circ}{RT} = \ln \alpha m \tag{18.73}$$

where $\Delta G_{A,m}^\circ$ is the difference in molar Gibbs free energy between the pure surfactant and the monomer in the standard state. With the ideal solution approximation, it also represents the same difference in molar Gibbs free energy in the solution.

By using equation (18.72), equations can be obtained for relating the other thermodynamic properties to m. The total Gibbs free energy G of the surfactant solution is the sum of the contributions from the solvent, the monomer, and the micelle. That is,

$$G = G \text{ (solvent)} + G \text{ (monomer)} + G \text{ (surfactant)}.$$

In terms of number of moles and chemical potentials, this relationship can be written as

$$G = n_1\mu_1 + n_2\mu_2 + n_A\mu_A \tag{18.74}$$

where the subscripts are (1) for the solvent, (2) for the monomer, and (A) for the micelle.

If we take enough solution so that G is the Gibbs free energy for an amount of solution containing 1 kg of solvent, then $n_2 = m_2 = \alpha m$ and $n_A = (1 - \alpha)m$. With the ideal solution approximation, $\mu_1 = \mu_1^*$, $\mu_A = \mu_A^*$, and $\mu_2 = \mu_2^\circ + RT \ln \alpha m$. Substitution into equation (18.74) gives

$$G = n_1\mu_1^* + \alpha m(\mu_2^\circ + RT \ln \alpha m) + (1 - \alpha)m\mu_A^*. \tag{18.75}$$

Differentiating equations (18.72) and (18.75) with respect to pressure and with respect to temperature, and combining while making use of the relationships

$$\left(\frac{\partial G}{\partial p}\right)_T = V$$

$$\left(\frac{\partial G/T}{\partial T}\right)_p = -\frac{H}{T^2}$$

gives

$$Z = n_1 Z^*_{1,m} + \alpha m Z^\circ_2 + (1-\alpha) m Z^*_{A,m} \tag{18.76}$$

where Z is V or H. Equation (18.76) is easily converted to an equation involving apparent molar quantities using equation (11.96) to give

$$\phi Z = \alpha Z^\circ_2 + (1-\alpha) Z^*_{A,m} \tag{18.77}$$

where $\phi Z = \phi V$, ϕH, or ϕL. Substituting for α from equation (18.67) gives

$$\phi Z = Z^*_{A,m} - \frac{\text{CMC}}{m} \Delta Z_{A,m} \tag{18.78}$$

where $\Delta Z_{A,m} = Z^*_{A,m} - Z^\circ_2$.

The apparent molar heat capacity ϕC_p is obtained from a temperature derivative of equation (18.77) applied to ϕH.[aa] The result is

$$\left(\frac{\partial \phi H}{\partial T}\right)_p = \alpha \left(\frac{\partial H^\circ_2}{\partial T}\right)_p + (1-\alpha)\left(\frac{\partial H^*_{A,m}}{\partial T}\right)_p - \Delta H_{A,m}\left(\frac{\partial \alpha}{\partial T}\right)_p, \tag{18.79}$$

where $H_{A,m} = H^*_{A,m} - H^\circ_2$. We obtain $(\partial\alpha/\partial T)_p$ by differentiating equation (18.73). The result is

$$\left(\frac{\partial \alpha}{\partial T}\right)_p = \alpha \left(\frac{\partial \Delta G_{A,m}/RT}{\partial T}\right)_p$$

$$= -\alpha \frac{\Delta H_{A,m}}{RT^2}.$$

[aa] In like manner, a pressure derivative of equation (18.77) applied to ϕV gives the apparent expansivity.

Substituting this equation, along with heat capacities for the enthalpy derivatives, into equation (18.79) gives

$$\phi C_p = C^*_{p,\mathrm{A},m} - \frac{\mathrm{CMC}}{m}\left[\Delta C_{p,\mathrm{A},m} - \frac{(\Delta H_{\mathrm{A},m})^2}{RT^2}\right]. \tag{18.80}$$

Equation (18.78) applied to ϕV and equation (18.80) predict that a graph of ϕV or ϕC_p against $1/m$ should be a straight line with an intercept at $1/m = 0$ of $V^*_{\mathrm{A},m}$ or $C^*_{p,\mathrm{A},m}$. Figure 18.15 shows a schematic representation of the results predicted by these equations. The straight-line graph applies only at molalities above the CMC ($1/m < 1/\mathrm{CMC}$). For $1/m > 1/\mathrm{CMC}$, ϕV and ϕC_p are constant at the standard state values for the monomer. Thus, a break in the curve occurs at $1/m = 1/\mathrm{CMC}$ that can be used to determine the CMC. The $\Delta H^2_{\mathrm{A}}/RT$ term in equation (18.80) shifts the line at the CMC. This displacement is the pseudo-phase model prediction of the relaxation effect observed experimentally in ϕC_p.

The pseudo-phase model is an idealization of results that are obtained for real systems. Figure 18.16, for example, shows ϕV and ϕC_p for sodium dodecylsulfate[21] graphed as a function of $1/m$. The circles represent the experimental results. Note that a sharp break is not obtained at $1/m = 1/\mathrm{CMC}$, but the intersection of the lines extrapolated from before and after the CMC gives a value of $1/\mathrm{CMC} = 120$ or $\mathrm{CMC} = 0.0083$[bb] $\mathrm{mol \cdot kg^{-1}}$.

The insets in Figure 18.16 demonstrate that a break (that shows up better in the ϕC_p graph) occurs at approximately $1/m = 5\ \mathrm{kg \cdot mol^{-1}}$ or $m = 0.2\ \mathrm{mol \cdot kg^{-1}}$. This break is attributed to a change in the micelle known as the second transition. At this molality, the micelle apparently changes from a spherical to a cylindrical structure.[cc]

Extrapolation to $1/m = 0$ gives values of $\bar{V}^\circ_2 = 238.2\ \mathrm{cm^3 \cdot mol^{-1}}$ and $V^*_{\mathrm{A},m} = 250.0\ \mathrm{cm^3 \cdot mol^{-1}}$ and $250.5\ \mathrm{cm^3 \cdot mol^{-1}}$ for the spherical and cylindrical micelle. Because of the many approximations inherent in the pseudo-phase

---

[bb] The CMC for sodium dodecylsulfate occurs at a very low value of m and it is difficult to obtain precise data below this concentration. The result is the scattering shown in Figure 18.16.

[cc] This change in structure is not surprising. According to the pseudo-phase model, the size of the micelle continues to grow with increasing concentration. Eventually a size is obtained where the spherical structure becomes unstable, and it is replaced by a cylinder, with the hydrophobic tails of the micelle directed toward the axis of the cylinder. Adding more surfactant causes the cylinder to lengthen to accommodate the extra surfactant molecules. Continued addition of surfactant can cause other transitions that form a hexagonal grouping of cylinders, and then a laminar structure of sheets that are two micelles thick, with the hydrophobic tails directed toward the center of the sheet. Eventually a reverse micelle forms with water molecules in the center of a grouping of surfactant molecules with the hydrophilic ends directed inward and the hydrophobic tails directed outward.

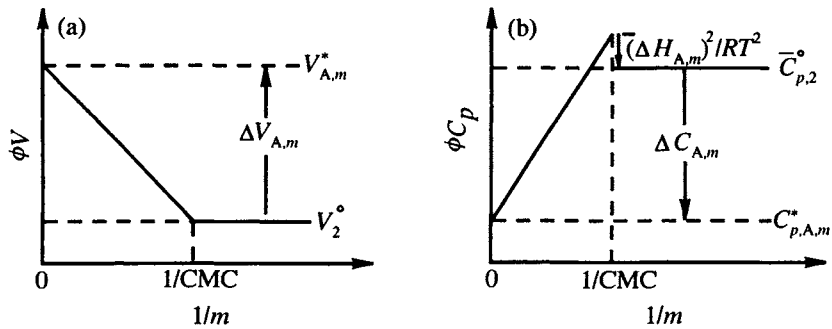

Figure 18.15 Surfactant pseudo-phase model prediction for (a) the apparent molar volume and (b) the apparent molar heat capacity. Drawing courtesy of K. Ballerat-Busserolles from the Institut de Chemie des Surfaces et Interfaces, Mulhouse, France.

model, these values must be considered as only approximate, although they do agree reasonably well with experimental values obtained from other methods.

The Mass Action Model: The mass action model represents a very different approach to the interpretation of the thermodynamic properties of a surfactant solution than does the pseudo-phase model presented in the previous section. A chemical equilibrium is assumed to exist between the monomer and the micelle. For this reaction an equilibrium constant can be written to relate the activity (concentrations) of monomer and micelle present. The most comprehensive treatment of this process is due to Burchfield and Woolley.[22] We will now describe the procedure followed, although we will not attempt to fill in all the steps of the derivation. The aggregation of an anionic surfactant MA is approximated by a simple equilibrium in which the monomeric anion and cation combine to form one aggregate species (micelle) having an aggregation number n, with a fraction of "bound" counterions, β. The reaction is[dd]

$$(n\beta)\mathrm{M}^+ + n\mathrm{A}^- = \mathrm{M}_{n\beta}\mathrm{A}_n^{-n(1-\beta)}. \tag{18.81}$$

A surfactant solution having a concentration greater than the CMC can be considered to be a mixture containing m_A mol·kg^{-1} of the 1:1 electrolyte [M^+A^-] and m_B mole·kg^{-1} of the $1:n(1-\beta)$ electrolyte micelle. The equilibrium molalities m_A and m_B are related to the stoichiometric molality m by

$$m = m_A + nm_B. \tag{18.82}$$

[dd] Although we are deriving the equations for an anionic surfactant A^- with counterions M^+, identical equations are obtained for a cationic surfactant A^+ with counterions M^-.

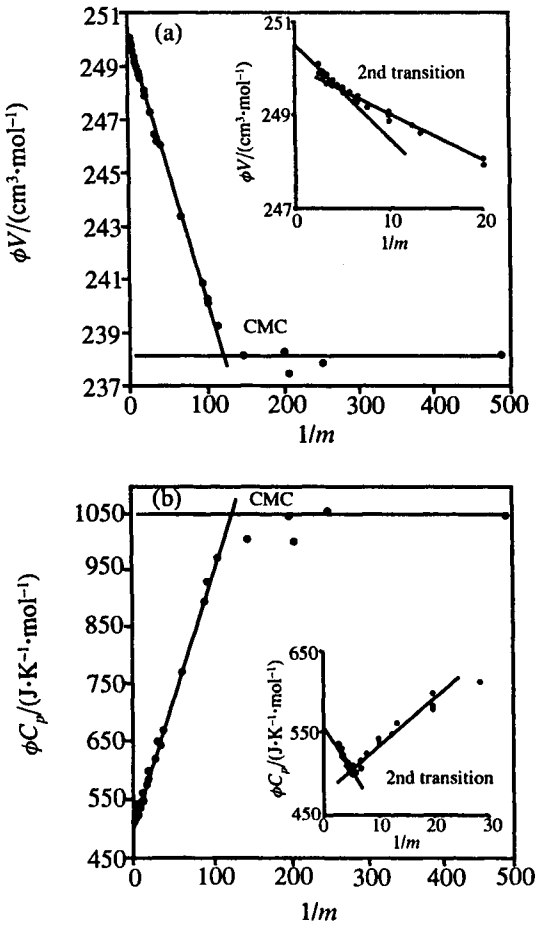

Figure 18.16 (a) Apparent molar volume and (b) apparent molar heat capacities for aqueous sodium dodecylsulfate at $T = 298.15$ K and $p = 0.1$ MPa, graphed as a function of $1/m$. The insets give the values at low m where a second transition occurs in the micelle.

The mole fraction of surfactant combined as a micelle is defined as

$$\alpha = \frac{n m_B}{m}. \tag{18.83}$$

The equilibrium constant for reaction (18.81) is then given by

$$K = [\alpha/\{n(1 - \beta\alpha)^{n\beta}(1 - \alpha)^n m^{(n\beta + n - 1)}\}](\gamma_B/\gamma_M^{n\beta}\gamma_A^n) \tag{18.84}$$

where the activity coefficients for the species M^+, A^-, and $M_{n\beta}A_n^{-n(1-\beta)}$ are γ_M, γ_A, and γ_B, respectively.

The Guggenheim extensions of the Debye–Hückel equations (see Section 18.1b) are used to obtain expressions for the activity coefficients. The result is

$$\ln \gamma_{\pm} = -A_\gamma I^{1/2}/(1 + bI^{1/2}) + \tfrac{1}{2} \ln(1 - \alpha) + \tfrac{1}{2} \ln(1 - \beta\alpha)$$
$$+ [\ln(10)]B_{1\gamma}[m(2 - \alpha - \beta\alpha)/2] + [\ln(10)]B_{n\gamma}(m\alpha/2n) \qquad (18.85)$$

where $\gamma_{\pm}$ is the mean activity coefficient of the ions in solution; A_γ is the Debye–Hückel constant, b is the ion-size parameter, and $B_{1\gamma}$ and $B_{n\gamma}$ are the Guggenheim specific ion–ion interaction parameters (expressed in terms of $\log_{10}$) for the (monomer + cation) and (micelle + cation) interactions, respectively. The ionic strength I is given by

$$I = \tfrac{1}{2}[2(1 - \alpha) + n\delta^2(1 - \beta)^2\alpha + (1 - \beta)\alpha]m, \qquad (18.86)$$

where the "effective charge" on the micelle is $n(\beta - 1)\delta$. The parameter δ is a screening constant that has a value less than one. It is introduced into equation (18.86) in recognition of the fact that the large micelle has an effective charge in the solution that is less than the charge $n(\beta - 1)$ that is expected for a"normal"-sized ion, and it is this effective charge that should be used in calculating the ionic strength.

Starting with equation (18.85), equations can be derived for ϕ, ϕL, ϕC_p, and ϕV. The osmotic coefficient is obtained from a transformation using the Gibbs–Duhem equation. The result is

$$(1 - \phi) = \alpha(1 + \beta - 1/n)/2 + A_\gamma I^{3/2}\sigma(bI^{1/2})/3m$$
$$- B_{1\gamma}[(1 - \alpha)(1 - \beta\alpha)m[\ln(10)]/2] - B_{n\gamma}[\alpha(1 - \beta\alpha)m[\ln(10)]/2n] \qquad (18.87)$$

where[ee]

$$\sigma(y) = 3[1 + y - 1/(1 + y) - 2\ln(1 + y)]/y^3. \qquad (18.88)$$

[ee] Note the similarity between this term and the one obtained in Pitzer's equations for simpler electrolytes.

The equation for ϕL is obtained by relating the free energy to $\gamma_\pm$ and ϕ and differentiating as follows:

$$\frac{G - G^\circ}{2mRT} = \ln \gamma_\pm + \ln m - \phi \left[\left(\frac{\partial (G - G^\circ)/T}{\partial T} \right) \right]_p$$

$$= -\frac{\Delta H}{T^2} = -m\phi L/T^2 \tag{18.89}$$

so that

$$\phi L = -2RT^2 \left(\frac{\partial \ln \gamma_\pm}{\partial T} \right)_p + 2RT^2 \left(\frac{\partial \phi}{\partial T} \right)_p . \tag{18.90}$$

Differentiating equation (18.90), again with respect to T, gives

$$\phi C_p - \bar{C}^\circ_{p,2} = -4RT \left(\frac{\partial \ln \gamma_\pm}{\partial T} \right)_p - 2RT^2 \left(\frac{\partial^2 \ln \gamma_\pm}{\partial T^2} \right)_p$$

$$+ 4RT \left(\frac{\partial \phi}{\partial T} \right)_p + 2RT^2 \left(\frac{\partial^2 \phi}{\partial T^2} \right)_p . \tag{18.91}$$

Differentiation of equation (18.89) with respect to p gives ϕV

$$\phi V - \bar{V}^\circ_2 = 2RT \left(\frac{\partial \ln \gamma_\pm}{\partial p} \right)_T - 2RT \left(\frac{\partial \phi}{\partial p} \right)_T . \tag{18.92}$$

In equations (18.91) and (18.92), $\bar{C}^\circ_{p,2}$ and $\bar{V}^\circ_2$ are the partial molar heat capacity and partial molar volume of the surfactant in the infinitely dilute solution (standard state values).

The fit of equations (18.87), (18.90), (18.91) and (18.92) to experimental results of ϕ, ϕL, ϕC_p, and ϕV as a function of the stoichiometric molality and temperature, requires known values of b, n, β, δ, A_γ, $B_{1\gamma}$, $B_{n\gamma}$, $\ln K$ (or α), $\bar{C}^\circ_{p,2}$, and $\bar{V}^\circ_2$. The first four coefficients are assumed to be independent of pressure

and temperature. They are obtained as follows:

- b is set equal to one to give the equations the same form as the extended Debye–Hückel and the Guggenheim equations.
- n and β are obtained from nonthermodynamic structural information on micellar solutions.
- δ has a value of approximately 0.5. A precise value is obtained by optimizing the fit to activity coefficient or osmotic coefficient data.
- A_γ and its derivatives are the Debye–Hückel parameters.

The other parameters are obtained from fits to experimental values. $B_{1\gamma}$, $B_{n\gamma}$, and ln K are obtained from fitting experimental $\gamma_\pm$ or ϕ results.[ff] Derivatives of these three parameters are obtained from ϕL, ϕC_p and ϕV results.[gg]

The lines through the data points in Figures 18.11 and 18.13 are fits of the mass action model to the experimental results. The agreement is excellent when we consider that only three variable parameters are required to fit each of the thermodynamic properties.[hh]

In comparing the two models for describing surfactant solutions, the pseudo-phase model has the advantage of simplicity in that graphical extrapolations are used to apply it to experimental data. It is a model that can be effectively used to understand, from a qualitative point of view, the properties of the mixtures. An advantage of the mass action model is the quantitative fit to the experimental results that it provides, including the change in property at the CMC and the nature of the results in the concentration region below the CMC, which is a concentration region where the pseudo-phase model does not apply and does not provide any information.

Problems

P18.1 Given the following information:

The molality of a saturated solution of $Al(NO_3)_3 \cdot 9H_2O(s)$ at $T = 298.15$ K is 3.161 mol·kg^{-1}, in which the mean ionic activity coefficient, $\gamma_\pm$, is 1.16 and the vapor pressure is 1.9158 kPa. At this temperature, pure water has a vapor pressure of 3.167 kPa.

(a) Calculate the osmotic coefficient of a saturated solution of $Al(NO_3)_3 \cdot 9H_2O$.

[ff] The break at the CMC determines the value of ln K.

[gg] Extrapolation of ϕC_p and ϕV results to infinite dilution gives $\overline{C}^\circ_{p,2}$ and $\overline{V}^\circ_2$.

[hh] $B_{n\gamma}$ and its derivatives are covariant with other parameters and normally are not needed to fit results that do not go to high molalities.

(b) Calculate the free energy difference

$$\Delta\mu^\circ = \mu^\circ[Al(NO_3)_3(aq)] - \mu^\circ[Al(NO_3)_3 \cdot 9H_2O(s)]$$

at 298.15 K.

P18.2 Given that the osmotic coefficient for an electrolyte solution has the form

$$1 - \phi = a_1 m^{1/2} + a_2 m + a_3 m^{3/2}.$$

What is the mean ionic activity coefficient of the solute?

P18.3 Information for $\gamma_\pm(KCl)$ and $\gamma_\pm(KNO_3)$ at 298.15 K are given below. The $\Delta B^\bullet$ values in the table are $B^\bullet_{KNO_3} - B^\bullet_{KCl}$ obtained from the Pitzer and Brewer tabulations.

$m/(\text{mol}\cdot\text{kg}^{-1})$	$\gamma_\pm(KNO_3)$	$\gamma_\pm(KCl)$	$\Delta B^\bullet(KNO_3)$
0.1	0.733	0.769	−0.18
0.2	0.659	0.718	
0.3	0.607	0.687	
0.5	0.542	0.649	−0.15
0.7	0.494	0.626	
1.0	0.441	0.603	−0.135
1.5	0.378	0.582	
2.0	0.327	0.572	−0.118
2.5	0.293		
3.0	0.266	0.568	−0.108
3.5	0.244		−0.101
4.0		0.576	

Make a graph of $\ln\gamma_\pm$ against $m^{1/2}$ for KNO_3 at 298.15 K. Compare these experimental results with $\ln\gamma_\pm$ for KNO_3 calculated using the $\Delta B^\bullet$ values obtained from the Pitzer and Brewer tabulation, and with $\ln\gamma_\pm$ calculated from the Debye–Hückel limiting law, the extended form of the Debye–Hückel equation, Guggenheim's equation, and Pitzer's equations. Values in Tables 18.1 and 18.2 and in Table A7.2 of Appendix 7 will be of value in making the calculations.

P18.4 Given the following thermodynamic properties[23] at 298.15 K for aqueous solutions of the surfactant hexyldimethylphosphine oxide (C_6DPO):

$m/(\text{mol}\cdot\text{kg}^{-1})$	$\phi V/(\text{cm}^3\cdot\text{mol}^{-1})$	$\phi C_p/(\text{J}\cdot\text{K}^{-1}\cdot\text{mol}^{-1})$	$\phi L/(\text{J}\cdot\text{mol}^{-1})$
0.023976	168.97	735.6	184.9
0.040256	169.03	731.5	311.4
0.059946	168.87	730.5	465.6
0.080627	168.76	729.5	628.7
0.10040	168.73	730.6	785.9
0.15782	168.48	730.6	1249
0.18618	168.46	729.8	1487
0.20647	168.42	730.5	1657
0.24159	168.35	732.8	1970
0.28638	168.27	735.9	2385
0.29926	168.23	737.1	2506
0.33762	168.21	741.2	2885
0.35476	168.20	743.5	3058
0.38114	168.20	748.5	3366
0.41193	168.23	753.5	3982
0.45030	168.29	757.0	4265
0.50729	168.45	752.5	5043
0.56161	168.65	740.0	5773
0.60714	168.82	724.8	6220
0.65404	168.98	709.8	6828
0.71062	169.19	692.0	7295
0.80686	169.50	663.0	8009
0.89629	169.74	640.0	–
0.99721	169.98	619.1	9012
1.1759	170.32	586.9	9694
1.3972	170.64	558.9	–
1.6349	170.91	535.0	–
1.8086	171.06	522.0	11427
2.0117	171.21	510.0	11704
3.2187	171.70	486.6	–
4.1725	171.89	453.4	–

(a) Compare the pseudo-phase model and the mass action model for interpretation of the results by making graphs of ϕV, ϕC_p and ϕL against m and against $1/m$. Obtain the CMC concentrations from each of the graphs and tabulate your results. Compare the effectiveness of the two different models and the three different thermodynamic quantities in determining the CMC.

(b) The break in ϕL at the CMC is small at 298.15 K because the enthalpy of micellization is small at this temperature. Assume ϕC_p is

constant with temperature and calculate ϕL at $T = 283.15$ K and $T = 313.15$ K. Make a graph of ϕL against m and $1/m$ at the three temperatures and compare the effect observed at the CMC.

P18.5 Sea water contains approximately 26,000 parts per million of dissolved NaCl, plus smaller amounts of other solutes, principally in the form of salts containing Mg^{2+}, K^+, Cl^-, Br^-, SO_4^{2-}, and CO_3^{2-}. In a water purification procedure, a reverse-osmosis process is used, in which half of the water is removed as pure water, leaving a concentrate that has twice the concentration of NaCl. Calculate the minimum work required to obtain a metric ton (10^3 kg) of pure water. Ignoring the impurities, the process is

$$\text{Sea water } (2 \times 10^3 \text{ kg } H_2O + 52 \text{ kg NaCl}) =$$
$$\text{Concentrate } (10^3 \text{ kg } H_2O + 52 \text{ kgNaCl}) + \text{Pure water } (10^3 \text{ kg}).$$

Calculating the minimum work requires a knowledge of ΔG for the above process, which requires that we know the activities in the various solutions. Decide which equations (Pitzer, Guggenheim, and Debye–Hückel) can be used to accurately calculate the activities at the concentrations and use these equations to calculate ΔG.

References

1 J. N. Brønsted, "Calculation of the Osmotic and Activity Functions in Solutions of Uni-univalent Salts", *J. Am. Chem. Soc.*, **44**, 938–948 (1922).

2. E. A. Guggenheim, "Specific Thermodynamic Properties of Aqueous Solutions of Strong Electrolytes", *Phil. Mag.*, **19**, 588–643 (1935).
3. E. A. Guggenheim and J. C. Turgeon, "Specific Interaction of Ions", *Trans. Faraday Soc.*, **51**, 747–761 (1955).
4. G. N. Lewis, M. Randall, K. S. Pitzer, and L. Brewer, *Thermodynamics, Second Edition*, McGraw-Hill Book Company, New York, 1961, Appendix 4, p. 640.
5. K. S. Pitzer, "Ion Interaction Approach: Theory and Data Correlation", Chapter 3 of *Activity Coefficients in Electrolyte Solutions*, 2nd Edition, K. S. Pitzer, Editor, CRC Press, Boca Raton, 1991, p. 82.
6. K. S. Pitzer, "Ion Interaction Approach: Theory and Data Correlation", Chapter 3 of *Activity Coefficients in Electrolyte Solutions*, 2nd Edition, K. S. Pitzer, Editor, CRC Press, Boca Raton, 1991. Parameters for many electrolytes are summarized in this reference. The equations and parameters can also be found in K. S. Pitzer, *Thermodynamics, Third Edition*, McGraw-Hill, Inc., New York, 1995.
7. Osmotic coefficients for KCl and $CaCl_2$ were obtained from Appendix 4 of G. N. Lewis, M. Randall, K. S. Pitzer, and L. Brewer, *Thermodynamics, Second Edition*, McGraw-Hill Book Company, New York, 1961. Values for $LaCl_3$ were obtained from F. H. Spedding, H. O. Weber, V. W. Saeger, H. H. Petheram, J. A. Rard, and A. Habenschuss, "Isopiestic Determination of the Activity Coefficients of Some Aqueous Rare Earth Electrolyte Solutions at 25 °C 1. The Rare Earth Chlorides", *J. Chem. Eng. Data*, **21**, 341–360 (1976).

8. Equations used to calculate ϕL and ϕC_p are taken from K. S. Pitzer, "Ion interaction approach: theory and data correlation", Chapter 3 in *Activity Coefficients in Electrolyte Solutions, 2nd Edition*, K. S. Pitzer, Editor, CRC Press, Boca Raton, Florida, 1991. Equations for calculating $\bar{L}_1$, $\bar{L}_2$, $\bar{J}_1$, and $\bar{J}_2$ are summarized in K. S. Pitzer, J. C. Peiper, and R. H. Busey, "Thermodynamic properties of aqueous sodium chloride solutions", *J. Phys. Chem. Ref. Data*, **13**, 1–102 (1984).
9. L. F. Silvester and K. S. Pitzer, "Thermodynamics of electrolytes. 8. High-temperature properties, including enthalpy and heat capacity, with application to sodium chloride", *J. Phys. Chem.*, **81**, 1822–1828 (1977).
10. D. G. Archer, "Thermodynamic properties of the NaCl + H_2O system. II. Thermodynamic properties of NaCl(aq), NaCl·$2H_2O$(cr), and phase equilibria", *J. Phys. Chem. Ref. Data*, **21**, 793–829 (1992).
11. O. Redlich, "The dissociation of strong electrolytes", *Chem. Rev.*, **39**, 333–356 (1946).
12. C. W. Davies, "Methods of studying ion-pairing", *Ion Association*, Butterworth and Co., Ltd, Washington, 1962.
13. R. E. Mesmer, D. A. Palmer, and J. M. Simonson, "Ion association at high temperatures and pressures", Chapter 8 in *Activity Coefficients in Electrolyte Solutions*, 2nd Edition, K. S. Pitzer, Editor, CRC Press, Boca Raton, Florida, 1991. See also R. E. Mesmer, W. L. Marshall, D. A. Palmer, J. M. Simonson, and H. F. Holmes, "Thermodynamics of aqueous association and ionization reactions at high temperatures and pressures", *J. Solution Chem.*, **17**, 699–718 (1988).
14. X. Chen., J. L. Oscarson, S. E. Gillespie, H. Cao, and R. M. Izatt, "Determination of enthalpy of ionization of water from 250 to 350 °C", *J. Solution Chem.*, **23**, 747–768 (1994).
15. W. L. Marshall and E. U. Franck, "Ion product of water substance, 0–1000 °C, 1–10,000 Bars. New International Formulation and its Background", *J. Phys. Chem. Ref. Data*, **10**, 295–304 (1981).
16. Chia-tsun Liu and W. T. Lindsay, Jr., "Thermodynamics of sodium chloride solutions at high temperatures", *J. Solution Chem.*, **1**, 45–69 (1972).
17. For a description of this system see J. L. Oscarson, R. M. Izatt, P. R. Brown, Z. Pawlak, S. E. Gillespie and J. J. Christensen, "Thermodynamic quantities for the interaction of SO_4^{2-} with H^+ and Na^+ in aqueous solution from 150 to 320 °C", *J. Solution Chem.*, **17**, 841–863, (1988).
18. See R. E. Mesmer, D. A. Palmer, and J. M. Simonson, "Ion association at high temperatures and pressures", Chapter 8 of *Activity Coefficients in Electrolyte Solutions, 2nd Edition*, K. S. Pitzer, Editor, CRC Press, Boca Raton, Florida, 1991, pp. 491–529. Also, see R. E. Mesmer, W. L. Marshall, D. A. Palmer, J. M. Simonson, and H. F. Holmes, Thermodynamics of aqueous association and ionization reactions at high temperatures and pressures, *J. Soln. Chem.*, **17**, 699–718, 1988.
19. The thermodynamic properties at $T = 298.15$ K shown in Figure 18.11 come from S. Causi, R. De Lisi, and S. Milioto, "Thermodynamic properties of N-octyl-, N-decyl- and N-dodecylpyridinium chlorides in water", *J. Solution Chem.*, **20**, 1031–1058 (1991). Results at the other two temperatures are courtesy of K. Ballerat-Busserolles, C. Bizzo, L. Pezzimi, K. Sullivan, and E. M. Woolley, "Apparent molar volumes and heat capacities at aqueous n-dodecyclpyridium chloride at molalities from 0.003 mol·kg^{-1} to 0.15 mol·kg^{-1}, at temperatures from 283.15 K to 393.15 K, and at the pressure 0.35 MPa", *J. Chem. Thermodyn.*, **30**, 971–983 (1998).
20. For a more detailed discussion of the pseudo-phase model, see J. E. Desnoyers and G. Perron, "Thermodynamic methods", Chapter 1 in *Surfactant Solutions: New Methods of Investigation*, R. Zana, Editor, Marcel Dekker, Inc., New York, 1987.

21. Unpublished results shown in Figure 18.16 are courtesy of K. Ballerat-Busserolles of the Institut de Chemie des Surfaces et Interfaces, Mulhouse, France.
22. See T. E. Burchfield and E. M. Woolley, "Model for thermodynamics of ionic surfactant solutions. 1. Osmotic and activity coefficients", *J. Phys. Chem*, **88**, 2149–2155 (1984); and E. M. Woolley and T. E. Burchfield, "Model for Thermodynamics of Ionic Surfactant Solutions 2. Enthalpies, Heat Capacities, and Volumes", *J. Phys. Chem.*, **88**, 2155–2163 (1984).
23. G. Perron, F. Yamashita, P. Martin, and J. Desnoyers, "Heat Capacities and Volumes of Alkyldimethylphosphine and Arsine Oxides in Water at 25 °C", *J. Colloid Interface Sci.*, **144**, 222–235 (1991).

Appendix 5

Thermodynamic Properties of Selected Chemical Substances

Table A5.1 gives the thermodynamic functions $[G° - H°(T_r)]/T$ and the enthalpies of formation $\Delta_f H°(T_r)$ for selected substances. (Enthalpies of formation at T_r are included in this table (as well as in Table A5.2) so that it can be used independently to calculate $\Delta_r G°$.) When a phase change occurs between two of the temperatures given in the table, the nature of the phases to which the value of the free-energy function applies is shown in parentheses at the two temperatures bracketing the phase changes. From this, one can determine the nature of the phases involved at lower and higher temperatures. For example, for Al(cr,l), the (cr) notation on the value at 500 K indicates that all values up to and including this temperature are for the crystal phase. The (l) notation at 1000 K indicates that all values for the free-energy function in the table at this and higher temperatures are for the liquid. (The normal melting temperature of Al is 933.5 K.) When solid-phase transitions occur, the changes are indicated in a similar manner as α, β, γ, I, II. etc., depending upon how the phases are named in the literature. (Note that in some instances, additional phases can form and then disappear in the temperature interval between those shown in the table; indications that this is occurring would not show up in the table.) Values were taken from M. W. Chase Jr., C. A. Davies, J. R. Downey Jr., D. J. Frurip, R. A. McDonald, and A. N. Syverud, "JANAF Thermochemical Tables, Third Edition," *J. Phys. Chem. Ref. Data*, **14** (1995), Supplement No. 1.

Table A5.2 presents standard heat capacities, entropies, enthalpies of formation, and Gibbs free energies of formation for selected substances at $T = 298.15$ K. (Note that for completeness, the enthalpies of formation given in this table are also presented in Table A5.1.) Except as noted the values were taken from M. W. Chase Jr., C. A. Davies, J. R. Downey Jr., D. J. Frurip, R. A. McDonald, and A. N. Syverud, "JANAF Thermochemical Tables, Third Edition," *J. Phys. Chem. Ref. Data* **14**, (1995), Supplement No.1.

Table A5.3 presents standard heat capacities, entropies, enthalpies of formation, and Gibbs free energies of formation for selected ions at

$T = 298.15$ K. The values in this table are all relative to the values for H^+ being set equal to zero. The values were taken from D. D. Wagman, W. H. Evans, V. B. Parker, R. H. Schumm, I. Halow, S. M. Bailey, K. L. Churney, and R. L Nuttall, "The NBS Tables of Chemical Thermodynamic Properties. Selected Values for Inorganic and C_1 and C_2 Organic Substances in SI Units", *J. Phys. Chem. Ref. Data*, **11** (1982) Supplement No. 2.

Table A5.4 gives enthalpies and temperatures of fusion and of vaporization for selected chemical compounds. Values were reproduced from a tabulation by J. R. Goates and J. B. Ott in *Chemical Thermodynamics: An Introduction*, Harcourt, Brace, Jovanovich, Inc., New York, 1971, pp. 137–139. References to the original sources for these data are given there.

Table A5.5 gives the coefficients for the heat capacity equation

$$C_p^\circ = a + 10^{-3}b \cdot T + 10^5 c \cdot T^{-2} + 10^{-6}d \cdot T^2.$$

Values were taken from I. Barin and O. Knacke, *Thermophysical Properties of Inorganic Substances*, Springer-Verlag, Berlin, 1973.

Table A5.6 gives selected values for standard reduction potentials at $T = 298.15$ K. The values were taken from W. M. Latimer, *The Oxidation States of the Elements and their Potentials in Aqueous Solutions, Second Edition*, Prentice-Hall, Inc., Engelwood Cliffs, N.J. (1952).

Table A5.1 Thermodynamic functions[a] (T_r = 298.15 K; standard state pressure = 0.1 MPa)

Substance[b]	$-[G° - H°(T_r)]/T/(J·K^{-1}·mol^{-1})$							$\Delta_f H°(T_r)/(kJ·mol^{-1})$
	100 K	200 K	298.15 K	500 K	1000 K	1500 K	2000 K	
Al_1(cr,l)	47.543	30.413	28.275	31.129(cr)	42.594(l)	55.153	64.129	0
Al_1Cl_3(cr,l)	180.962	117.298	109.286(cr)	125.478(l)	205.884	254.579		−705.632
Al_1Cl_3(g)	372.957	320.862	314.494	322.930	353.637	378.084	397.314	−584.588
Al_1F_3(cr,l)	119.836	72.814	66.484	75.781(α)	112.137(β)	141.976	165.864	−1510.424
Al_1F_3(g)	325.981	282.132	276.691	284.170	312.511	335.761	354.309	−1209.322
Al_2Cl_6(g)	602.707	489.094	475.050	493.701	561.522	615.444	657.830	−1295.743
Al_2F_6(g)	487.750	398.728	387.294	403.449	465.329	516.311	557.032	−2633.619
Al_2O_3(cr-α)	101.230	57.381	50.950	61.098	102.245	137.425	166.201	−1675.692
Ar_1(g)	173.325	156.746	154.845	157.200	165.410	171.773	176.719	0
B_1(cr,l)	12.207	6.704	5.834	7.415	14.637	21.296	26.952	0
B_1(g)	171.936	155.338	153.435	155.791	164.003	170.366	175.314	560.000
B_1H_3(g)	218.682	191.116	187.876	192.164	209.123	224.642	238.158	106.692
B_1N_1(cr)	27.183	16.359	14.795	17.480	29.728	41.293	51.171	−250.914
B_1N_1(g)	238.329	215.038	212.358	215.751	228.187	238.383	246.584	476.976
B_2(g)	228.775	204.880	202.072	205.864	220.415	232.262	241.558	829.687
B_2H_6(g)	274.911	237.985	233.170	240.856	276.179	310.832	341.393	41.003
B_2O_3(cr,l)	96.353	59.093	53.953	62.105(cr)	107.241(l)	149.125	181.085	−1271.936
Ba_1(cr,l)	86.220	64.988	62.475	65.997(α)	81.116(γ)	95.935(l)	106.693	0
Ba_1(g)	188.725	172.146	170.245	172.600	180.811	187.190	192.287	179.075
Ba_1Cl_2(cr,l)	187.175	130.426	123.666	132.335	163.643(cr)	195.068(l)	222.874	−858.557
Ba_1Cl_2(g)	373.964	330.820	325.736	332.161	354.802	372.457	386.221	−498.733
$Ba_1H_2O_2$(cr,l)			107.110	119.399(cr)	174.578(l)	220.219	255.018	−946.295
Ba_1O_1(cr)	111.119	76.289	72.069	77.607	98.018	114.704	128.198	−548.104
Ba_1O_1(g)	263.233	238.400	235.457	239.293	253.197	264.267	272.987	−123.846

(continued)

Table A5.1 *Continued*

Substance[b]	$-[G^\circ - H^\circ(T_r)]/T/(J\cdot K^{-1}\cdot mol^{-1})$							$\Delta_f H^\circ(T_r)/(kJ\cdot mol^{-1})$
	100 K	200 K	298.15 K	500 K	1000 K	1500 K	2000 K	
Be_1(cr,l)	19.434	10.751	9.440	11.551	20.119	27.653(α)	36.128(l)	0
Be_1Cl_2(cr,l)	131.942	88.261	82.676	90.566(α)	126.995(l)	161.115	188.489	−490.930
Be_1Cl_2(g)	294.816	256.831	252.232	258.281	280.478	298.347	312.496	−360.242
Be_1O_1(cr-α)	28.539	15.759	13.770	17.235	32.276	45.708	56.922	−608.354
Be_1O_1(g)	223.605	200.307	197.625	201.023	213.490	223.740	232.164	136.398
Br_1(g)	193.497	176.918	175.017	177.372	185.603	192.065	197.180	111.860
Br_1H_1(g)	224.595	201.363	198.699	202.006	213.737	223.228	230.905	−36.443
Br_2(cr,l)	271.009	171.496(cr)	152.206(l)	160.743				0
Br_2(g)	276.306	248.653	245.394	249.526	264.143	275.595	284.569	30.910
C_1(g)	176.684	160.007	158.100	160.459	168.678	175.044	179.996	716.670
C_1(graphite)	10.867	6.407	5.740	6.932	12.662	18.216	23.008	0
C_1Cl_4(g)	374.168	317.054	309.809	319.840	357.595	388.320	412.725	−95.981
C_1F_4(g)	306.188	266.577	261.419	269.120	300.660	328.081	350.563	−933.199
C_1H_1(g)	208.978	185.708	183.040	186.349	198.062	207.595	215.440	594.128
$C_1H_1Cl_3$(g)	345.889	301.259	295.620	303.641	335.240	362.168	384.180	−103.177
$C_1H_1N_1$(g)	230.911	204.966	201.828	206.125	222.619	236.724	248.441	135.143
C_1H_2(g)	223.967	197.055	193.931	197.957	212.971	225.773	236.489	386.392
$C_1H_2Cl_2$(g)	309.694	274.664	270.293	276.654	302.930	326.467	346.317	−95.521
$C_1H_2F_2$(g)	280.603	250.396	246.698	252.114	275.532	297.457	316.355	−450.659
$C_1H_2O_1$(g)	249.156	222.109	218.950	223.220	240.807	257.131	271.275	−115.897
C_1H_3(g)	226.465	197.609	194.170	198.783	216.836	232.885	246.636	145.687
$C_1H_3Cl_1$(g)	266.858	237.889	234.367	239.486	261.432	282.060	300.015	−83.680
$C_1H_3F_1$(g)	253.738	226.124	222.843	227.540	248.097	267.919	285.399	−234.304
C_1H_4(g)	216.485	189.418	186.251	190.614	209.370	227.660	244.057	−74.873
$C_1Na_2O_3$(cr,l)	225.158	148.470	138.797	152.332(I)	208.977(II)	265.143(l)	310.954	−1130.768

Substance[b]	$-[G^\circ - H^\circ(T_r)]/T/(J\cdot K^{-1}\cdot mol^{-1})$							$\Delta_f H^\circ(T_r)/(kJ\cdot mol^{-1})$
	100 K	200 K	298.15 K	500 K	1000 K	1500 K	2000 K	
C_1O_1(g)	223.539	200.317	197.653	200.968	212.848	222.526	230.342	−110.527
C_1O_2(g)	243.568	217.046	213.795	218.290	235.901	251.062	263.574	−393.522
C_1S_1(g)	274.228	241.981	237.977	243.431	264.073	281.170	294.935	116.943
C_1Si_1(cr-α)	32.865	18.613	16.485	20.030	35.019	48.275	59.297	−71.546
C_1Si_1(cr-β)	33.062	18.740	16.610	20.158	35.165	48.442	59.469	−73.220
C_2(g)	235.431	203.335	199.382	204.042	219.054	230.338	239.145	837.737
C_2Cl_6(g)	504.581	409.925	397.880	414.636	478.066	529.983	571.329	−134.223
C_2F_6(g)	409.522	341.306	332.185	345.562	399.823	446.462	484.440	−1343.901
C_2H_1(g)	237.415	210.703	207.444	211.877	228.801	243.180	255.073	476.976
C_2H_2(g)	234.338	204.720	200.958	206.393	227.984	246.853	262.733	226.731
C_2H_4(g)	252.466	222.975	219.330	224.879	249.742	273.827	295.101	52.467
C_3(g)	272.308	240.748	237.246	241.504	256.913	269.739	280.264	820.064
C_3O_2(g)	328.013	281.870	276.071	284.216	316.075	343.406	365.899	−93.638
C_4(g)	265.752	232.603	228.322	234.527	259.285	280.697	298.329	970.688
C_5(g)	285.525	247.105	241.972	249.648	280.772	307.934	330.389	979.056
Ca_1(cr,l)	63.525	43.924	41.588	44.590(α)	56.437(β)	68.822(l)		0
Ca_1(g)	173.366	156.787	154.886	157.241	165.452	171.814	176.762	177.800
Ca_1Cl_2(cr,l)	164.875	111.119	104.602	113.054	143.521(cr)	177.480(l)	203.777	−795.797
Ca_1Cl_2(g)	340.874	295.620	290.265	297.075	321.173	340.014	354.719	−471.537
Ca_1F_2(cr,l)	120.374	74.450	68.572	76.736	106.981(α)	132.774(β)	158.444(l)	−1225.912
Ca_1F_2(g)	315.945	278.356	273.798	279.791	301.486	318.695	332.211	−784.500
$Ca_1H_2O_2$(cr)	147.109	90.862	83.387	94.075	134.768			−986.085
Ca_1O_1(cr,l)	69.166	41.825	38.212	43.305	62.463	78.146	90.754	−635.089
Ca_1O_1(g)	247.175	222.620	219.717	223.508	237.317	248.399	257.378	43.932

(*continued*)

Table A5.1 *Continued*

Substance[b]	$-[G^\circ - H^\circ(T_r)]/T/(J\cdot K^{-1}\cdot mol^{-1})$							$\Delta_f H^\circ(T_r)/(kJ\cdot mol^{-1})$
	100 K	200 K	298.15 K	500 K	1000 K	1500 K	2000 K	
$Ca_2(g)$	291.717	260.663	257.183	261.012	272.539	280.466	286.281	341.637
$Cl_1(g)$	184.104	167.161	165.189	167.708	176.615	183.475	188.749	121.302
$Cl_1Cs_1(cr,l)$	145.996	105.914	101.182	107.277(α)	132.687(l)	159.168	178.984	−442.835
$Cl_1H_1(g)$	212.797	189.566	186.901	190.205	201.857	211.214	218.769	−92.312
$Cl_1H_4N_1(cr)$	163.795	103.140	94.860(II)	106.407(III)	150.517	189.273		−314.553
$Cl_1K_1(cr,l)$	125.871	87.169	82.554	88.494	110.276(cr)	136.664(l)	156.662	−436.684
$Cl_1K_1(g)$	270.564	242.394	239.087	243.263	258.000	269.541	278.579	−214.681
$Cl_1Li_1(cr,l)$	98.646	63.555	59.300	64.948(cr)	88.792(l)	113.194	130.444	−408.266
$Cl_1Na_1(cr,l)$	114.140	76.643	72.115	77.966	99.428(cr)	125.061(l)	144.561	−411.120
$Cl_1Na_1(g)$	260.320	233.022	229.793	233.906	248.503	259.969	268.959	−181.418
$Cl_1O_2(g)$	291.366	260.743	257.229	262.268	281.553	297.596	310.515	104.600
$Cl_2(g)$	251.696	226.120	223.079	227.020	241.203	252.438	261.277	0
$Cl_2Mg_1(cr,l)$	146.771	95.923	89.629	98.022(cr)	129.341(l)	169.087	196.780	−641.616
$Cl_2Mg_1(g)$	325.112	282.150	277.027	283.635	307.278	325.902	340.486	−392.459
$Cl_2O_1(g)$	306.542	272.170	267.959	273.626	294.565	311.406	324.713	87.864
$Cl_3P_1(g)$	368.917	317.995	311.682	320.107	350.828	375.290	394.530	−288.696
$Cl_4Si_1(g)$	402.620	338.877	330.945	341.632	380.943	412.437	437.276	−662.746
$Cl_4Ti_1(cr,l)$	345.052	236.897(cr)	221.925(l)	238.447	296.617			−804.165
$Cl_4Ti_1(g)$	432.828	363.378	354.889	366.065	406.482	438.507	463.644	−763.162
$Cl_5P_1(g)$	451.647	374.087	364.288	377.544	426.223	465.142	495.804	−360.184
$Co_1(cr,l)$	50.176	32.287	30.067	32.996(α)	44.396(β)	54.688	64.490(l)	0
$Co_1(g)$	198.942	181.570	179.518	182.229	192.159	200.053	206.262	426.676
$Cr_1(cr,l)$	41.746	25.680	23.618	26.398	36.901	45.931	53.905	0
$Cr_1(g)$	192.791	176.212	174.311	176.666	184.877	191.256	196.299	397.480
$Cr_2O_3(cr)$	155.642	90.567	81.154	93.829	140.091	177.518	207.459	−1134.701

Substance[b]	$-[G^\circ - H^\circ(T_r)]/T/(J\cdot K^{-1}\cdot mol^{-1})$							$\Delta_f H^\circ(T_r)/(kJ\cdot mol^{-1})$
	100 K	200 K	298.15 K	500 K	1000 K	1500 K	2000 K	
Cs_1(cr,l)	110.635	87.892	85.147(cr)	91.506(l)				0
Cs_1(g)	194.080	177.501	175.599	177.955	186.165	192.528	197.482	76.500
Cu_1(cr,1)	53.414	35.354	33.164	35.997	46.261(cr)	55.599(l)	64.747	0
Cu_1(g)	184.877	168.298	166.397	168.752	176.963	183.325	188.281	337.600
Cu_1O_1(cr)	74.176	46.256	42.594	47.703	67.011	82.991	96.006	−156.063
Cu_2O_1(cr,1)	141.510	97.826	92.360	99.809	127.769	151.186(cr)	181.227(l)	−170.707
D_1(g)	141.830	125.251	123.350	125.705	133.916	140.278	145.225	221.720
D_1H_1(g)	169.759	146.473	143.803	147.114	158.719	167.926	175.326	0.320
$D_1H_1O_1$(g)	229.267	202.590	199.511	203.406	217.805	230.023	240.261	−245.371
D_2(g)	170.973	147.630	144.960	148.272	159.943	169.311	176.885	0
F_1(g)	178.805	160.833	158.750	161.307	170.038	176.673	181.778	79.390
F_1H_1(g)	199.679	176.445	173.780	177.082	188.631	197.733	205.011	−272.546
F_2(g)	229.549	205.596	202.789	206.452	219.930	230.839	239.531	0
F_2H_2(g)	275.181	242.789	238.849	244.265	265.357	283.444	298.461	−572.664
F_2O_1(g)	282.348	251.252	247.457	252.659	272.411	288.642	301.600	24.518
F_6S_1(g)	358.027	299.562	291.535	303.873	353.670	395.948	430.134	−1220.473
H_1(g)	133.197	116.618	114.716	117.072	125.282	131.644	136.591	217.999
$H_1K_1O_1$(cr,1)	130.178	84.784	78.907	86.721(α)	126.848(l)	156.289	178.070	−424.718
$H_1Li_1O_1$(cr,l)	77.138	46.982	42.821	49.032(cr)	81.732(l)	111.888	134.365	−484.926
$H_1N_1O_3$(g)	306.248	270.926	266.400	273.121	300.937	325.627	346.243	−134.306
$H_1Na_1O_1$(cr,l)	109.879	69.615	64.445	71.595(I)	110.931(l)	139.992	161.401	−425.931
H_1O_1(g)	210.980	186.471	183.708	187.082	198.801	208.043	215.446	38.987
H_2(g)	155.408	133.284	130.680	133.973	145.536	154.652	161.943	0
$H_2Mg_1O_2$(cr)	116.934	69.736	63.242	72.994	111.658			−924.664

(*continued*)

Table A5.1 *Continued*

Substance[b]	$-[G° - H°(T_r)]/T/(J·K^{-1}·mol^{-1})$							$\Delta_f H°(T_r)/(kJ·mol^{-1})$
	100 K	200 K	298.15 K	500 K	1000 K	1500 K	2000 K	
H_2O_1(g)	218.534	191.896	188.834	192.685	206.738	218.520	228.374	−241.826
H_2O_1(l,g)			69.950(l)	104.712(g)	162.736	189.184		−285.830
H_2O_2(g)	261.768	228.978	232.991	238.243	258.884	276.558		−136.106
$H_2O_4S_1$(g)	360.452	305.914	298.796	309.259	351.592	388.416	418.890	−735.129
$H_2O_4S_1$(cr,l)	300.474	181.887(cr)	156.895(l)	173.938	245.666			−813.989
H_2S_1(g)	235.330	208.586	205.757	209.726	224.599	237.375	248.098	−20.502
H_3N_1(g)	223.211	195.962	192.774	197.021	213.849	229.054	242.244	−45.898
$H_3O_4P_1$(cr,l)	183.578	119.270	110.544(cr)	143.882(l)	240.332			−1284.375
H_3P_1(g)	241.134	213.516	210.243	214.764	233.348	250.411	265.068	22.886
H_4N_2(g)	277.002	243.020	238.719	245.221	273.004	298.616	320.698	95.353
H_4N_2(l)	205.395	130.399	121.544	133.305				50.626
H_4Si_1(g)	237.899	208.310	204.653	210.096	233.614	255.706	274.785	34.309
He_1(g)	144.632	128.053	126.152	128.507	136.718	143.080	148.027	0
Hg_1(cr,l)	113.592	80.284(cr)	76.028(l)	79.158				0
Hg_1(g)	193.450	176.871	174.970	177.325	185.536	191.898	196.845	61.380
Hg_1O_1(cr)	105.148	74.128	70.270	75.556	95.855			−90.789
I_1(g)	199.267	182.688	180.786	183.142	191.352	197.717	202.679	106.762
I_2(cr)	162.472	121.036	116.142					0
I_2(g)	292.808	264.038	260.685	264.891	279.680	291.251	300.396	62.421
K_1(cr,l)	89.101	67.270	64.670(cr)	70.482(l)	84.939			0
K_1(g)	178.820	162.241	160.340	162.695	170.905	177.268	182.217	89.000
K_2(g)	283.115	253.150	249.690	254.018	269.222	280.637	288.960	123.683
K_1O_2(cr)	188.849	129.436	122.499	131.719	166.067	193.932		−284.512
K_2O_1(cr)			94.140	104.161	141.627	173.601	200.854	−363.171
K_2O_2(cr)			112.968	124.802	170.527	210.876	245.937	−495.804

Substance[b]	$-[G^\circ - H^\circ(T_r)]/T/(J\cdot K^{-1}\cdot mol^{-1})$							$\Delta_f H^\circ(T_r)/(kJ\cdot mol^{-1})$
	100 K	200 K	298.15 K	500 K	1000 K	1500 K	2000 K	
$Kr_1(g)$	182.565	165.986	164.084	166.440	174.650	181.012	185.959	0
$Li_1(cr,l)$	48.615	31.255	29.085(cr)	32.684(l)	46.946	56.741		0
$Li_1(g)$	157.261	140.682	138.781	141.136	149.346	155.709	160.656	159.300
$Li_2(g)$	227.785	200.255	196.998	201.151	215.949	227.612	236.644	215.900
$Mg_1O_1(cr)$	52.212	30.037	26.924	31.513	49.262	64.017	75.942	−601.241
$N_1(g)$	171.780	155.201	153.300	155.655	163.866	170.228	175.175	472.683
$N_1O_1(g)$	237.757	213.501	210.758	214.145	226.307	236.217	244.199	90.291
$N_1O_2(g)$	271.168	243.325	240.034	244.440	261.545	276.175	288.158	33.095
$N_2(g)$	217.490	194.272	191.609	194.917	206.708	216.277	224.006	0
$N_2O_1(g)$	250.829	223.335	219.957	224.613	242.694	258.120	270.769	82.048
$N_2O_3(g)$	360.299	314.268	308.539	316.466	347.364	373.706	395.230	82.843
$N_2O_4(cr,l)$	392.476	237.881(cr)	209.198(l)	226.598				−19.564
$N_2O_4(g)$	363.098	311.015	304.376	313.907	352.127	385.251	412.484	9.079
$N_2O_5(g)$		354.795	346.548	358.466	405.784	445.871	478.290	11.297
$N_3(g)$	259.348	230.051	226.469	231.358	250.229	266.206	279.220	414.216
$Na_1(cr,l)$	74.885	53.954	51.455(cr)	56.675(l)	71.179			0
$Na_1(g)$	172.147	155.568	153.667	156.002	164.232	170.595	175.542	107.300
$Na_1O_2(cr)$	194.891	118.679	115.897	124.354	156.431	184.421	208.620	−260.663
$Na_2(g)$	263.127	233.663	230.243	234.529	249.687	261.548	270.595	142.070
$Na_2O_1(cr,l)$	128.981	81.114	75.042	83.332	115.355(γ)	146.700(l)	179.117	−417.982
$Na_2O_2(cr)$	163.515	102.600	94.801	105.495(α)	147.833(β)	183.065	210.332	−513.209
$Ne_1(g)$	164.808	148.229	146.327	148.683	156.893	163.255	168.202	0
$O_1(g)$	181.131	163.085	161.058	163.511	171.930	178.390	183.391	249.173
$O_2(g)$	231.094	207.823	205.147	208.524	220.875	231.002	239.160	0

(*continued*)

Table A5.1 *Continued*

Substance[b]	$-[G^\circ - H^\circ(T_r)]/T/(J\cdot K^{-1}\cdot mol^{-1})$							$\Delta_f H^\circ(T_r)/(kJ\cdot mol^{-1})$
	100 K	200 K	298.15 K	500 K	1000 K	1500 K	2000 K	
O_2S_1(g)	281.199	251.714	248.212	252.979	271.339	286.816	299.383	−296.842
O_2Ti_1(cr)	89.638	54.969	50.292	57.077	83.253	104.906	122.286	−944.747
O_3(g)	271.040	242.401	238.932	243.688	262.228	277.866	290.533	142.674
O_3S_1(g)	295.976	261.145	256.769	262.992	287.768	309.041	326.421	−395.765
P_1(cr-red IV)	39.017	25.028	23.197	25.742	35.530			−12.439
P_1(cr-red V)	38.578	24.675	22.853	25.390	35.359			−17.460
P_1(cr-white,l)	62.415(α)	43.173(β)	41.077(β)	43.889(l)	54.115			0
P_4(g)	331.278	285.819	279.992	288.032	317.923	341.996	361.020	58.907
Rb_1(cr,l)	101.811	79.458	76.778(cr)	83.020(l)				0
Rb_1(g)	188.573	171.994	170.093	172.448	180.659	187.021	191.971	80.900
Rb_2(g)	304.707	274.542	271.067	275.407	290.495	301.561	309.536	113.290
S_2(g)	255.684	231.072	228.165	231.958	245.760	256.832	265.657	128.600
S_3(g)			269.517	275.192	296.125	313.063	326.618	141.461
S_4(g)			310.646	318.749	348.788	373.017	392.278	145.771
S_5(g)			308.638	319.351	358.883	390.537	415.514	109.370
S_6(g)			354.076	367.381	416.262	455.276	485.994	101.922
S_7(g)			407.673	423.525	481.600	527.976	564.566	113.679
S_8(g)	552.531	444.003	430.311	448.745	516.162	569.910	612.203	100.416
Si_1(cr,l)	33.351	20.531	18.820	21.237	30.387	37.982(cr)	48.846(l)	0
Xe_1(g)	188.164	171.585	169.684	172.039	180.249	186.612	191.559	0
Zn_1(cr,l)	63.224	44.005	41.717	44.660(cr)	58.892(l)			0

[a] Enthalpies of formation are included in Table A5.1 so that this table can be used independently to calculate $\Delta_r G^\circ$.
[b] The JANAF table representation of the formula for the chemical species has been followed.

Table A5.2 Standard heat capacities, entropies, enthalpies, and Gibbs free energies of formation of selected substances at $T = 298.15$ K

Substance[a]	$C^\circ_{p,m}$/ ($J \cdot K^{-1} \cdot mol^{-1}$)	S°_m/ ($J \cdot K^{-1} \cdot mol^{-1}$)	$\Delta_f H^\circ_m$/ ($kJ \cdot mol^{-1}$)	$\Delta_f G^\circ_m$/ ($kJ \cdot mol^{-1}$)
Al_1(cr)	24.209	28.275	0	0
Al_1Cl_3(cr)	91.128	109.286	−705.632	−630.018
Al_1Cl_3(g)	71.876	314.494	−584.588	−570.158
Al_1F_3(cr)	75.132	66.484	−1510.424	−1431.123
Al_1F_3(g)	62.239	276.691	−1209.322	−1192.695
Al_2Cl_6(g)	158.858	475.050	−1295.743	−1220.985
Al_2F_6(g)	132.744	387.294	−2633.619	−2550.845
Al_2O_3(cr-α)	79.015	50.950	−1675.692	−1582.275
Ar_1(g)	20.786	154.845	0	0
B_1(cr)	11.315	5.834	0	0
B_1(g)	20.796	153.435	560.000	515.993
B_1H_3(g)	36.221	187.876	106.692	110.859
B_1N_1(cr)	19.719	14.795	−250.914	−225.022
B_1N_1(g)	29.450	212.358	476.976	443.965
B_2(g)	31.594	202.072	829.687	772.918
B_2H_6(g)	58.100	233.170	41.003	91.849
B_2O_3(cr)	62.588	53.953	− 1271.936	− 1192.796
Ba_1(cr)	28.096	62.475	0	0
Ba_1(g)	20.786	170.245	179.075	146.944
Ba_1Cl_2(cr)	75.140	123.666	−858.557	−810.290
Ba_1Cl_2(g)	56.160	325.736	−498.733	−510.713
$Ba_1H_2O_2$(cr)	101.629	107.110	−946.295	−859.476
Ba_1O_1(cr)	47.279	72.069	−548.104	−520.382
Ba_1O_1(g)	32.897	235.457	−123.846	−144.839
Be_1(cr)	16.380	9.440	0	0
Be_1Cl_2(cr)	64.852	82.676	−490.930	−446.254
Be_1Cl_2(g)	51.622	252.232	−360.242	−366.120
Be_1O_1(cr)	25.560	13.770	−608.354	−579.062
Be_1O_1(g)	29.481	197.625	136.398	110.873
Br_1(g)	20.786	175.017	111.860	82.369
Br_1H_1(g)	29.141	198.699	−36.443	−53.513
Br_2(l)	75.674	152.206	0	0
Br_2(g)	30.048	245.394	30.910	3.126
C_1(g)	20.838	158.100	716.670	671.244
C_1(graphite)	8.517	5.740	0	0
C_1(diamond)	6.113	2.377	1.895	2.900
C_1Cl_4(g)	83.401	309.809	−95.981	−53.617
C_1F_4(g)	61.054	261.419	−933.199	−888.507

(*continued*)

Table A5.2 *Continued*

Substance[a]	$C^\circ_{p,m}$/ (J·K^{-1}·mol^{-1})	S°_m/ (J·K^{-1}·mol^{-1})	$\Delta_f H^\circ_m$/ (kJ·mol^{-1})	$\Delta_f G^\circ_m$/ (kJ·mol^{-1})
$C_1H_1(g)$	29.171	183.040	594.128	560.747
$C_1H_1Cl_3(g)$	65.383	295.620	−103.177	−70.357
$C_1H_1N_1(g)$	35.857	201.828	135.143	124.725
$C_1H_2(g)$	34.600	193.931	386.392	369.245
$C_1H_2Cl_2(g)$	50.896	270.293	−95.521	−68.924
$C_1H_2F_2(g)$	42.859	246.698	−450.659	−423.076
$C_1H_2O_1(g)$	35.402	218.950	−115.897	−109.921
$C_1H_3(g)$	38.693	194.170	145.687	147.950
$C_1H_3Cl_1(g)$	40.731	234.367	−83.680	−60.146
$C_1H_3F_1(g)$	37.500	222.843	−234.304	−210.359
$C_1H_4(g)$	35.639	186.251	−74.873	−50.768
$C_1Na_2O_3(cr)$	111.003	138.797	−1130.768	−1048.009
$C_1O_1(g)$	29.142	197.653	−110.527	−137.163
$C_1O_2(g)$	37.129	213.795	−393.522	−394.389
$C_1S_2(g)$	45.664	237.977	116.943	66.816
$C_1Si_1(cr)$	26.840	16.610	−73.220	−70.850
$C_2(g)$	43.145	199.382	837.737	781.714
$C_2Cl_6(g)$	138.934	397.880	−134.223	−49.894
$C_2F_6(g)$	106.407	332.185	−1343.901	−1258.134
$C_2H_1(g)$	37.104	207.444	476.976	438.031
$C_2H_2(g)$	44.095	200.958	226.731	248.163
$C_2H_4(g)$	42.886	219.330	52.467	68.421
$C_3(g)$	37.740	237.246	820.064	754.464
$C_3O_2(g)$	66.989	276.071	−93.638	−109.649
$C_4(g)$	50.176	228.322	970.688	909.460
$C_5(g)$	61.135	241.972	979.056	915.470
$Ca_1(cr)$	25.929	41.588	0	0
$Ca_1(g)$	20.786	154.886	177.800	144.020
$Ca_1Cl_2(cr)$	72.856	104.602	−795.797	−748.073
$Ca_1Cl_2(g)$	59.325	290.265	−471.537	−479.169
$Ca_1F_2(cr)$	68.588	68.572	−1225.912	−1173.496
$Ca_1F_2(g)$	51.267	273.798	−784.500	−793.272
$Ca_1H_2O_2(cr)$	87.487	83.387	−986.085	−898.421
$Ca_1O_1(cr)$	42.120	38.212	−635.089	−603.501
$Ca_1O_1(g)$	32.455	219.717	43.932	21.405
$Ca_2(g)$	36.577	257.183	341.637	289.757
$Cl_1(g)$	21.838	165.189	121.302	105.306
$Cl_1Cs_1(cr)$	52.442	101.182	−442.835	−414.360
$Cl_1H_1(g)$	29.136	186.901	−92.312	−95.300
$Cl_1H_4N_1(cr)$	86.441	94.860	−314.553	−203.092

Table A5.2 *Continued*

Substance[a]	$C^\circ_{p,m}$/ ($J \cdot K^{-1} \cdot mol^{-1}$)	S°_m/ ($J \cdot K^{-1} \cdot mol^{-1}$)	$\Delta_f H^\circ_m$/ ($kJ \cdot mol^{-1}$)	$\Delta_f G^\circ_m$/ ($kJ \cdot mol^{-1}$)
Cl_1K_1(cr)	51.287	82.554	−436.684	−408.761
Cl_1K_1(g)	36.496	239.087	−214.681	−233.428
Cl_1Li_1(cr)	48.028	59.300	−408.266	−384.019
Cl_1Na_1(cr)	50.509	72.115	−411.120	−384.024
Cl_1Na_1(g)	35.786	229.793	−181.418	−201.334
Cl_1O_2(g)	41.995	257.229	104.600	122.327
Cl_2(g)	33.949	223.079	0	0
Cl_2Mg_1(cr)	71.379	89.629	−641.616	−592.087
Cl_2Mg_1(g)	57.097	277.027	−392.459	−398.803
Cl_2O_1(g)	47.810	267.959	87.864	105.065
Cl_3P_1(g)	71.581	311.682	−288.696	−269.610
Cl_4Si_1(g)	90.261	330.945	−662.746	−622.784
Cl_4Ti_1(l)	145.205	221.925	−804.165	−728.139
Cl_4Ti_1(g)	95.614	354.889	−763.162	−726.779
Cl_5P_1(g)	111.890	364.288	−360.184	−290.271
Co_1(cr,1)	24.802	30.067	0	0
Co_1(g)	23.024	179.518	426.676	382.117
Cr_1(cr)	23.434	23.618	0	0
Cr_1(g)	20.786	174.311	397.480	352.551
Cr_2O_3(cr)	120.366	81.154	−1134.701	−1053.066
Cs_1(cr,1)	32.195	85.147	0	0
Cs_1(g)	20.786	175.599	76.500	49.532
Cu_1(cr)	24.442	33.164	0	0
Cu_1(g)	20.786	166.397	337.600	297.877
Cu_1O_1(cr)	42.246	42.594	−156.063	−128.292
Cu_2O_1(cr)	62.543	92.360	−170.707	−147.886
D_1(g)	20.786	123.350	221.720	206.553
D_1H_1(g)	29.200	143.803	0.320	−1.463
$D_1H_1O_1$(g)	33.786	199.511	−245.371	−233.181
D_2(g)	29.194	144.960	0	0
F_1(g)	22.746	158.750	79.390	62.289
F_1H_1(g)	29.138	173.780	−272.546	−274.646
F_2(g)	31.302	202.789	0	0
F_2H_2(g)	44.874	238.849	−572.664	−544.453
F_2O_1(g)	43.301	247.457	24.518	41.783
F_6S_1(g)	96.960	291.535	−1220.473	−1116.451
H_1(g)	20.786	114.716	217.999	203.278
$H_1K_1O_1$(cr)	64.894	78.907	−424.718	−378.899
$H_1Li_1O_1$(cr)	49.591	42.821	−484.926	−438.958
$H_1N_1O_3$(g)	53.336	266.400	−134.306	−73.941

(*continued*)

Table A5.2 *Continued*

Substance[a]	$C^\circ_{p,m}$/ (J·K^{-1}·mol^{-1})	S°_m/ (J·K^{-1}·mol^{-1})	$\Delta_f H^\circ_m$/ (kJ·mol^{-1})	$\Delta_f G^\circ_m$/ (kJ·mol^{-1})
$H_1Na_1O_1$(cr)	59.530	64.445	−425.931	−379.741
H_1O_1(g)	29.986	183.708	38.987	34.277
H_2(g)	28.836	130.680	0	0
$H_2Mg_1O_2$(cr)	77.249	63.242	−924.664	−833.652
H_2O_1(l)	75.351	69.950	−285.830	−237.141
H_2O_1(g)	33.590	188.834	−241.826	−228.582
H_2O_2(l)	89.1	109.6	−187.78	−120.35
H_2O_2(g)	43.116	232.991	−136.106	−105.445
$H_2O_4S_1$(l)	138.584	156.895	−813.989	−689.918
$H_2O_4S_1$(g)	83.761	298.796	−735.129	−653.366
H_2S_1(g)	34.192	205.757	−20.502	−33.329
H_3N_1(g)	35.652	192.774	−45.898	−16.367
$H_3O_4P_1$(l)	145.047	150.775	−1271.663	−1123.597
$H_3O_4P_1$(cr)	106.064	110.544	−1284.375	−1124.314
H_3P_1(g)	37.102	210.243	22.886	30.893
H_4N_2(g)	50.813	238.719	95.353	159.232
H_4N_2(l)	98.840	121.544	50.626	149.440
H_4Si_1(g)	42.827	204.653	34.309	56.827
He_1(g)	20.786	126.152	0	0
Hg_1(g)	20.786	174.970	61.380	31.880
Hg_1(l)	27.978	76.028	0	0
Hg_1O_1(cr)	44.062	70.270	−90.789	−58.490
I_1(g)	20.786	180.786	106.762	70.174
I_2(cr)	54.436	116.142	0	0
I_2(g)	36.887	260.685	62.421	19.325
K_1(cr)	29.497	64.670	0	0
K_1(g)	20.786	160.340	89.000	60.476
K_2(g)	37.962	249.690	123.683	87.801
K_1O_2(cr)	77.530	122.499	−284.512	−240.589
K_2O_1(cr)	83.680	94.140	−363.171	−322.094
K_2O_2(cr)	100.165	112.968	−495.804	−429.758
Kr_1(g)	20.786	164.084	0	0
Li_1(cr)	24.623	29.085	0	0
Li_1(g)	20.786	138.781	159.300	126.594
Li_2(g)	36.103	196.998	215.900	174.508
Mg_1O_1(cr)	37.106	26.924	−601.241	−568.945
N_1(g)	20.786	153.300	472.683	455.540
N_1O_1(g)	29.845	210.758	90.291	86.600
N_1O_2(g)	36.974	240.034	33.095	51.258
N_2(g)	29.124	191.609	0	0

Table A5.2 *Continued*

Substance[a]	$C^\circ_{p,m}$/ (J·K^{-1}·mol^{-1})	S°_m/ (J·K^{-1}·mol^{-1})	$\Delta_f H^\circ_m$/ (kJ·mol^{-1})	$\Delta_f G^\circ_m$/ (kJ·mol^{-1})
N_2O_1(g)	38.617	219.957	82.048	104.179
N_2O_3(g)	65.615	308.539	82.843	139.727
N_2O_4(l)	142.509	209.198	−19.564	97.521
N_2O_4(g)	77.256	304.376	9.079	97.787
N_2O_5(g)	96.303	346.548	11.297	118.013
N_3(g)	40.762	226.469	414.216	432.387
Na_1(cr)	28.154	51.455	0	0
Na_1(g)	20.786	153.667	107.300	76.825
Na_1O_2(cr)	72.141	115.897	−260.663	−218.712
Na_2(g)	37.577	230.243	142.070	104.105
Na_2O_1(cr)	69.103	75.042	−417.982	−379.090
Na_2O_2(cr)	89.266	94.801	−513.209	−449.627
Ne_1(g)	20.786	146.327	0	0
O_1(g)	21.911	161.058	249.173	231.736
O_1S_1(g)	30.173	221.944	5.007	−21.026
O_2(g)	29.376	205.147	0	0
O_2S_1(g)	39.878	248.212	−296.842	−300.125
O_2Ti_1(cr)	55.103	50.292	−944.747	−889.406
O_3(g)	39.238	238.932	142.674	163.184
O_3S_1(g)	50.661	256.769	−395.765	−371.016
P_1(cr-white)	23.825	41.077	0	0
P_1(cr-red IV)	21.263	23.197	−12.439	−7.108
P_1(cr-red V)	21.187	22.853	−17.460	−12.026
P_1(cr-black)	21.547	22.586	−12.851	−7.338
P_4(g)	67.158	279.992	58.907	24.416
Rb_1(cr)	31.062	76.778	0	0
Rb_1(g)	20.786	170.093	80.900	53.078
Rb_2(g)	38.116	271.067	113.290	78.254
S_1(cr-orthorhombic)	22.698	32.056	0	0
S_1(cr-monoclinic)	23.225	33.028	0.360	0.070
S_2(g)	32.490	228.165	128.600	79.687
S_3(g)	47.764	269.517	141.461	89.777
S_4(g)	67.585	310.646	145.771	91.381
S_5(g)	89.501	308.638	109.370	65.137
S_6(g)	111.571	354.076	101.922	53.699
S_7(g)	133.502	407.673	113.679	59.034
S_8(g)	156.043	430.311	100.416	48.578
Si_1(cr)	20.000	18.820	0	0
Xe_1(g)	20.786	169.684	0	0
Zn_1(cr)	25.387	41.717	0	0

[a] The JANAF table representation of the formula for the chemical species has been followed.

Table A5.3 Standard[a] heat capacities, entropies, enthalpies, and Gibbs free energies of formation of some common ions at $T = 298.15$ K

Substance	$C^\circ_{p,m}$/ ($J \cdot K^{-1} \cdot mol^{-1}$)	S°_m/ ($J \cdot K^{-1} \cdot mol^{-1}$)	$\Delta_f H^\circ_m$/ ($kJ \cdot mol^{-1}$)	$\Delta_f G^\circ_m$/ ($kJ \cdot mol^{-1}$)
Ag^+	21.8	72.68	105.579	77.107
Al^{3+}	–	−321.7	−531	−485
AsO_4^{3-}	–	−162.8	−888.14	−648.41
Ba^{2+}	–	9.6	−537.64	−560.77
Be^{2+}	–	−129.7	−382.8	−379.73
CH_3COO^-	−6.3	86.6	−486.01	−369.31
CN^-	–	94.1	150.6	172.4
CO_3^{2-}	–	−56.9	−677.14	−527.81
Ca^{2+}	–	−53.1	−542.83	−553.58
Ce^{3+}	–	−205	−696.2	−672.0
Ce^{4+}	–	−301	−537.2	−503.8
Cl^-	−136.4	56.5	−167.159	−131.228
ClO_3^-	–	162.3	−103.97	−7.95
ClO_4^-	–	182.0	−129.33	−8.52
CrO_4^{2-}	–	50.21	−881.15	−727.75
$Cr_2O_7^{2-}$	–	261.9	−1490.3	−1301.1
Cs^+	−10.5	133.05	−258.28	−292.02
Cu^+	–	40.6	71.67	49.98
Cu^{2+}	–	−99.6	64.77	65.49
F^-	106.7	−13.8	−332.63	−278.79
Fe^{2+}	–	−137.7	−89.1	−78.90
Fe^{3+}	–	−315.9	−48.5	−4.7
H^+	0	0	0	0
$HCOO^-$	−87.9	92	−425.55	−351.0
HCO_3^-	–	91.2	−691.99	−586.77
Hg^{2+}	–	−32.2	171.1	164.40
Hg_2^{2+}	–	84.5	172.4	153.52
I^-	−142.3	113.3	−55.19	−51.57
K^+	21.8	102.5	−252.38	−283.27
Li^+	68.6	13.4	−278.49	−293.31
Mg^{2+}	–	−138.1	−466.85	−454.8
Mn^{2+}	50	−73.6	−220.75	−228.1
MnO_4^-	−82.0	191.2	−541.4	−447.2
N_3^-	–	107.9	275.14	348.2
NH_4^+	79.9	113.4	−132.51	−79.31
NO_3^-	−86.6	146.4	−205.0	−108.74
NO_2^-	−97.5	123.0	−104.6	−32.2
Na^+	46.4	59.0	−240.12	−261.905
OH^-	−148.5	−10.75	−229.994	−157.244

Table A5.3 *Continued*

Substance	$C^\circ_{p,m}$/ (J·K^{-1}·mol^{-1})	S°_m/ (J·K^{-1}·mol^{-1})	$\Delta_f H^\circ_m$/ (kJ·mol^{-1})	$\Delta_f G^\circ_m$/ (kJ·mol^{-1})
PO_4^{3-}	–	−222	−1277.4	−1018.7
Rb^+	–	121.50	−251.17	−283.98
S^{2-}	–	−14.6	33.1	85.8
SO_4^{2-}	−293	20.1	−909.27	−744.53
SO_3^{2-}	–	−29	−635.5	−486.5
Sr^{2+}	–	−32.6	−545.80	−559.48
Zn^{2+}	46	−112.1	−153.89	−147.06

[a] The standard state is the hypothetical $m = 1$ solution that obeys Henry's law. The values are relative to those for H^+ being equal to zero.

Table A5.4 Enthalpies and temperatures of fusion and vaporization (normal melting and boiling points and enthalpies of fusion and vaporization are tabulated by type of compound)

Compound	T^*_m/(K)	$\Delta_{fus}H_m$/(J·mol^{-1})	T^*_b/(K)	$\Delta_{vap}H_m$/(J·mol^{-1})
Elements				
He	–	–	4.216	84
Ne	24.57	335.1	27.07	1766
Ar	83.85	1176	87.29	6519
Kr	115.95	1636	119.93	9029
Xe	161.3	2298	165.1	12640
Rn	202	2900	211	16401
H_2	13.96	117	20.39	902.9
F_2	55.20	1556	85.24	6318
Cl_2	172.18	6406	239.11	20410
Br_2	265.95	10544	331.4	29999
I_2	386.8	15648	456	41714
O_2	54.39	444.8	90.19	6820
S_8 (equilibrium S)	392	1226	717.76	10460
N_2	63.15	720	77.36	5577
P_4 (white)	317.4	628	553	12426
Hg	234.29	2295.3	629.88	59149
Li	453.70	3024.1	1604	134683
Na	370.97	2601.6	1163	89036
K	336.4	2318	1039	77530
Rb	312.0	2343	974	69203
Cs	301.8	2134	958	65898

(*continued*)

Table A5.4 *Continued*

Compound	$T_m^*/(K)$	$\Delta_{fus}H_m/(J \cdot mol^{-1})$	$T_b^*/(K)$	$\Delta_{vap}H_m/(J \cdot mol^{-1})$
Carbon Compounds				
CH_4	90.68	941	111.67	8180
C_2H_6	89.88	2859.3	184.52	14715
C_3H_8	85.46	3523.8	231.08	18774
n-C_4H_{10}	134.80	4661.0	272.65	22393
n-C_5H_{12}	143.43	8393.1	309.22	25773
n-C_6H_{14}	177.80	13029.0	341.89	28853
n-C_7H_{16}	182.54	14033.1	371.58	31604
C_6H_{12} (cyclohexane)	279.70	2665.2	353.89	30083
$C(CH_3)_4$	256.60	3256.0	282.65	22753
C_2H_4	103.97	3350.5	169.45	13544
C_2H_2	–	–	189.2	21338
C_6H_6	278.683	9832	353.25	30765
$C_6H_5CH_3$	178.16	6619	383.78	33459
1,2-$C_6H_4(CH_3)_2$	247.97	13598	417.56	36823
1,3-$C_6H_4(CH_3)_2$	225.28	11565	412.25	36443
1,4-$C_6H_4(CH_3)_2$	286.41	17113	411.50	36066
$C_{10}H_8$ (naphthalene)	353.36	18054	491.11	42173
CH_3OH	175.26	3167	337.9	35271
C_2H_5OH	158.6	5021	351.7	38576
HCHO	154.9		253.9	24476
CH_3CHO	155	3222	293.3	27196

Table A5.4 *Continued*

Compound	$T_m^*/(K)$	$\Delta_{fus}H_m/(J\cdot mol^{-1})$	$T_b^*/(K)$	$\Delta_{vap}H_m/(J\cdot mol^{-1})$
Hydrides				
HF	189.39	4577	292.67	6732
HCl	158.97	1991.6	188.13	16150
HBr	186.30	2406.2	206.44	17615
HI	222.37	2871.5	237.81	19765
H_2O	273.150	6009.5	373.150	40656
H_2S	187.63	2377.3	212.85	18673
H_2Se	207.43	2515	231.9	19330
H_2Te	222	4184	270.9	23221
NH_3	195.42	5653	239.76	23351
PH_3	139.41	1130	185.44	14602
AsH_3	156.9	2343	210.7	17489

[a] Normal sublimation point.

Table A5.5 Coefficients at $p = 0.1$ MPa for the heat capacity equation: $C_p^\circ/(J\cdot K^{-1}\cdot mol^{-1}) = a + 10^{-3}b\cdot T + 10^5 c\cdot T^{-2} + 10^{-6}d\cdot T^2$

Substance	State	Temperature range/(K)	a	b	c	d^*
Ag	solid	298–1234	21.30	8.54	1.51	
Ag	liquid	1234–1600	30.54			
Al	solid	298–932	20.67	12.38		
Al	liquid	932–1650	31.8			
Al_2O_3	solid	298–1800	114.77	12.80	−35.44	
Au	solid	298–1336	23.68	5.113	0.142	
Au	liquid	1336–3081	29.3			
Br_2	liquid	273–334	71.5			
Br_2	gas	298–2000	37.359	0.464	−1.293	
Br	gas	298–2000	19.874	1.490	0.423	
C	graphite	298–1100	0.109	38.940	−1.481	−17.385
C	graphite	1100–4073	24.439	0.435	−31.627	
C	diamond	298–1200	9.12	13.22	−6.19	
CH_4	gas	298–2000	12.447	76.689	1.448	− 18.004
C_4H_{10}	gas	298–1500	40.250	265.077	−12.661	−76.362
CO	gas	298–2500	28.41	4.10	−0.46	
CO_2	gas	298–2500	44.14	9.04	−8.54	

(continued)

Table A5.5 *Continued*

Substance	State	Temperature range/(K)	*a*	*b*	*c*	*d**
Cl_2	gas	298–3000	36.90	0.25	−2.85	
Cl	gas	298–3000	23.033	−0.749	−0.695	
Cu	solid	298–1357	22.64	6.28		
Cu	liquid	1357–2846	31.38			
F_2	gas	298–2000	34.69	1.84	−3.35	
F	gas	298–2000	21.686	−0.444	1.159	
H_2	gas	298–3000	27.28	3.26	0.50	
H	gas	298–6000	20.786			
HF	gas	298–2000	26.90	3.43	1.09	
HCl	gas	298–2000	26.53	4.60	1.09	
HBr	gas	298–1600	26.15	5.86	1.09	
HI	gas	298–2000	26.32	5.94	0.92	
H_2O	gas	298–2500	30.00	10.71	0.33	
H_2SO_4	liquid	298–553	156.90	28.30	−23.46	
Hg	liquid	298–630	30.38	−11.46		10.155
Hg	gas	298–3000	20.786			
I_2	solid	298–387	−50.647	246.906	27.974	
I_2	liquid	387–458	80.672			
I_2	gas	298–2000	37.405	0.569	−0.619	
I	gas	290–2000	20.393	0.402	0.280	
K	solid	298–336	7.837	71.915		
K	liquid	336–1037	37.179	−19.12		12.318
KCl	solid	298–1044	40.016	25.468	3.648	
KCl	liquid	1044–1710	73.60			
Mg	solid	298–923	22.30	10.25	−0.431	
Mg	liquid	923–1378	31.8			
MgO	solid	298–3098	48.982	3.142	−11.439	
N_2	gas	298–2500	27.87	4.27		
N	gas	298–1800	20.786			
NH_3	gas	298–1800	29.75	25.10	−1.55	
N_2O*	gas	298–3000	58.099	1.385	−54.116	10.920
NO	gas	298–3000	27.681	7.439	−0.151	−1.431
NO_2	gas	298–1500	35.685	22.907	−4.703	−6.335
NO_2	gas	1500–3000	53.756	1.276		
N_2O_4*	gas	298–3000	128.323	1.598	−128.633	24.782
Na	solid	298–371	14.790	44.229		
Na	liquid	371–1156	37.468	−19.154		10.636
NaCl	solid	298–1074	45.94	16.32		
NaCl	liquid	1074–1500	77.764	−7.531		
NaCl	gas	298–2000	37.334	0.736	−1.586	

Table A5.5 *Continued*

Substance	State	Temperature range/(K)	a	b	c	d^*
O_2	gas	298–3000	29.96	4.18	−1.67	
O	gas	298–2000	20.874	−0.050	0.975	
O_3	gas	298–2000	44.346	15.594	−8.611	−4.347
P	red (solid)	298–870	16.949	14.891		
P	white (solid)	298–317	19.12	15.82		
P	white (liquid)	317–870	26.326			
P	gas	298–2000	20.669	0.172		
P_2	gas	298–2000	36.296	0.799	−4.159	
P_4	gas	298–2000	81.847	0.678	−13.443	
Pt	solid	298–2043	24.250	5.376		
S	rhombic	298–369	14.98	26.11		
S	monoclinic	369–388	14.90	29.12		
S	liquid	388–718	449.734	−959.973	−208.844	607.140
S	gas	298–2000	21.916	−0.460	1.862	
S_2	gas	298–2000	35.73	1.17	−3.31	
S_8	gas	298–2000	181.263	0.870	−22.907	
SF_6	gas	298–2000	133.047	27.886	−39.104	−8.192
SO_2	gas	298–1800	43.43	10.63	−5.94	
SO_3	gas	298–2000	57.145	27.347	−12.912	−7.728
Si	solid	298–1685	22.824	3.858	−3.540	
Si	liquid	1685–3492	27.2			

* For N_2O(g) and N_2O_4(g), the last term of the heat capacity equation is $10^8 d \cdot T^{-3}$ (instead of $10^{-6} d \cdot T^2$).

Table A5.6 *Continued*

Table A5.6 Standard reduction potentials at $T = 298.15$ K

Half-reaction	$E°$/(V)	Half-reaction	$E°$/(V)
$Li^+(aq) + e^- = Li(s)$	−3.045	$H_2SO_3(aq) + 4H^+(aq) + 4e^- = S(s) + 3H_2O$	0.45
$K^+(aq) + e^- = K(s)$	−2.925	$Cu^+(aq) + e^- = Cu(s)$	0.521
$Ba^{2+}(aq) + 2e^- = Ba(s)$	−2.90	$I_2(s) + 2e^- = 2I^-(aq)$	0.535
$Sr^{2+}(aq) + 2e^- = Sr(s)$	−2.89	$I_3^-(aq) + 2e^- = 3I^-(aq)$	0.536
$Ca^{2+}(aq) + 2e^- = Ca(s)$	−2.87	$Cu^{2+}(aq) + Cl^-(aq) + e^- = CuCl(s)$	0.538
$Na^+(aq) + e^- = Na(s)$	−2.714	$MnO_4^-(aq) + e^- = MnO_4^{2-}(aq)$	0.564
$Mg^{2+}(aq) + 2e^- = Mg(s)$	−2.37	$Cu^{2+}(aq) + Br^-(aq) + e^- = CuBr(s)$	0.640
$\frac{1}{2}H_2(g) + e^- = H^-(aq)$	−2.25	$O_2(g) + 2H^+(aq) + 2e^- = H_2O_2(aq)$	0.682
$Be^{2+}(aq) + 2e^- = Be(s)$	−1.85	$Fe^{3+}(aq) + e^- = Fe^{2+}(aq)$	0.771
$Al^{3+}(aq) + 3e^- = Al(s)$	−1.66	$Hg_2^{2+}(aq) + 2e^- = 2Hg(l)$	0.789
$Mn^{2+}(aq) + 2e^- = Mn(s)$	−1.18	$Ag^+(aq) + e^- = Ag(s)$	0.799
$V^{2+}(aq) + 2e^- = V(s)$	−1.18	$Cu^{2+}(aq) + I^-(aq) + e^- = CuI(s)$	0.86
$TiO^{2+}(aq) + 2H^+(aq) + 4e^- = Ti(s) + H_2O$	−0.89	$2Hg^{2+} + 2e^-(aq) = Hg_2^{2+}(aq)$	0.920
$H_3BO_3(aq) + 3H^+(aq) + 3e^- = B(s) + 3H_2O$	−0.87	$NO_3^-(aq) + 4H^+(aq) + 3e^- = NO(g) + 2H_2O$	0.96
$SiO_2(s) + 4H^+(aq) + 4e^- = Si(s) + 2H_2O$	−0.86	$HNO_2(aq) + H^+(aq) + e^- = NO(g) + H_2O$	1.00
$Zn^{2+}(aq) + 2e^- = Zn(s)$	−0.763	$Br_2(l) + 2e^- = 2Br^-$	1.065
$Cr^{3+}(aq) + 3e^- = Cr(s)$	−0.74	$N_2O_4(g) + 2H^+(aq) + 2e^- = 2HNO_2(aq)$	1.07
$H_3PO_2(aq) + H^+(aq) + e^- = P(s) + 2H_2O$	−0.51	$ClO_4^-(aq) + 2H^+(aq) + 2e^- = ClO_3^-(aq) + H_2O$	1.19
$H_3PO_3(aq) + 2H^+(aq) + 2e^- = H_3PO_2(aq) + H_2O$	−0.50	$IO_3^-(aq) + 6H^+(aq) + 5e^- = \frac{1}{2}I_2(s) + 3H_2O$	1.195
$Fe^{2+}(aq) + 2e^- = Fe(s)$	−0.440	$ClO_3^-(aq) + 3H^+(aq) + 2e^- = HClO_2(aq) + H_2O$	1.21
$Cr^{3+}(aq) + e^- = Cr^{2+}(aq)$	−0.41	$O_2(g) + 4H^+(aq) + 4e^- = 2H_2O$	1.229
$Cd^{2+}(aq) + 2e^- = Cd(s)$	−0.403	$MnO_2(s) + 4H^+(aq) + 2e^- = Mn^{2+}(aq) + 2H_2O$	1.23
$PbI_2(s) + 2e^- = Pb(s) + 2I^-(aq)$	−0.365	$Cr_2O_7^{2-}(aq) + 14H^+(aq) + 6e^- = 2Cr^{3+}(aq) + 7H_2O$	1.33
$PbSO_4(s) + H^+(aq) + 2e^- = Pb(s) + HSO_4^-(aq)$	−0.356	$Cl_2(g) + 2e^- = 2Cl^-(aq)$	1.3595

Half-reaction	$E°$/(V)	Half-reaction	$E°$/(V)
$Co^{2+}(aq) + 2e^- = Co(s)$	−0.277	$HIO(aq) + H^+(aq) + e^- = \frac{1}{2}I_2(s) + H_2O$	1.45
$H_3PO_4(aq) + 2H^+(aq) + 2e^- = H_3PO_3(aq) + H_2O$	−0.276	$PbO_2(s) + 4H^+(aq) + 2e^- = Pb^{2+}(aq) + 2H_2O$	1.455
$Ni_1^{2+}(aq) + 2e^- = Ni(s)$	−0.250	$Au^{3+}(aq) + 3e^- = Au(s)$	1.50
$CuI(s) + e^- = Cu(s) + I^-(aq)$	−0.185	$MnO_4^-(aq) + 8H^+(aq) + 5e^- = Mn^{2+}(aq) + 4H_2O$	1.51
$AgI(s) + e^- = Ag(s) + I^-(aq)$	−0.151	$BrO_3^-(aq) + 6H^+(aq) + 5e^- = \frac{1}{2}Br_2(l) + H_2O$	1.52
$Sn^{2+}(aq) + 2e^- = Sn(s)$	−0.136	$HBrO(aq) + H^+(aq) + e^- = \frac{1}{2}Br_2(l) + H_2O$	1.59
$Pb^{2+}(aq) + 2e^- = Pb(s)$	−0.126	$H_5IO_6(aq) + H^+(aq) + 2e^- = IO_3^-(aq) + 3H_2O$	1.6
$2H^+(aq) + 2e^- = H_2(g)$	0.000	$Ce^{4+}(aq) + e^- = Ce^{3+}(aq)$	1.61
$P(s) + 3H^+(aq) + 3e^- = PH_3(g)$	0.06	$HClO(aq) + H^+(aq) + e^- = \frac{1}{2}Cl_2(g) + H_2O$	1.63
$AgBr(s) + e^- = Ag(s) + Br^-(aq)$	0.095	$HClO_2(aq) + 2H^+(aq) + 2e^- = HClO(aq) + H_2O$	1.64
$CuCl(s) + e^- = Cu(s) + Cl^-(aq)$	0.137	$Au^+(aq) + e^- = Au(s)$	1.68
$S(s) + 2H^+(aq) + 2e^- = H_2S(g)$	0.141	$NiO_2(s) + 4H^+(aq) + 2e^- = Ni^{2+}(aq) + 2H_2O$	1.68
$Sn^{4+}(aq) + 2e^- = Sn^{2+}(aq)$	0.15	$PbO_2(s) + HSO_4^-(aq) + 3H^+(aq) + 2e^- = PbSO_4(s) + 2H_2O$	1.685
$Cu^{2+}(aq) + e^- = Cu^+(aq)$	0.153	$MnO_4^-(aq) + 4H^+(aq) + 3e^- = MnO_2(s) + 2H_2O$	1.695
$HSO_4^-(aq) + 3H^+(aq) + 2e^- = H_2SO_3(aq) + H_2O$	0.17	$H_2O_2(aq) + 2H^+(aq) + 2e^- = 2H_2O$	1.77
$AgCl(s) + e^- = Ag(s) + Cl^-(aq)$	0.222	$Co^{3+}(aq) + e^- = Co^{2+}(aq)$	1.82
$Cu^{2+}(aq) + 2e^- = Cu(s)$	0.337	$O_3(g) + 2H^+(aq) + 2e^- = O_2(g) + H_2O$	2.07
$Fe(CN)_6^{3-}(aq) + e^- = Fe(CN)_6^{4-}(aq)$	0.36	$F_2(g) + 2e^- = 2F^-(aq)$	2.87
		$F_2(g) + 2H^+(aq) + 2e^- = 2HF(aq)$	3.06

Table A5.6 is obtained from the extensive tabulation by W. M. Latimer, *The Oxidation States of the Elements and their Potentials in Aqueous Solutions, Second Edition*, Prentice-Hall, Inc., Engelwood Cliffs, N.J. (1952). His tabulation was published at the time when $p = 1$ atm was the standard state for gases. His results should be corrected to the $p = 1$ bar standard state for comparison with other modern standard state thermodynamic data. The correction is given by $(RT/F)\ln(1.01325)$, which has a value of 0.0003 volts at $T = 298.15$ K. The correction is small and probably negligible for all except the most precise work. ($E°$ values measured to better than 10^{-3} volts are unusual.)

Appendix 6

Calculations from Statistical Thermodynamics

The calculation of the thermodynamic functions of a substance is based upon the **Boltzmann distribution equation**, which predicts the most probable distribution[a] of molecules (or atoms) among a set of energy levels. The equation is

$$\frac{n_i}{g_i} = \frac{n_0}{g_0} \exp\left(-\frac{\epsilon_i}{kT}\right), \tag{A6.1}$$

where n_i is the number of molecules in the energy level ϵ_i that has a statistical weight factor (degeneracy) g_i, while n_0 and g_0 are equivalent quantities in the ground (lowest energy) state. In this equation, T is the temperature and k is the Boltzman constant.

A6.1 Atomic and Molecular Energy Levels

Translational and electronic energy levels are present in the ideal monatomic gas. For the molecular gas, rotational and vibrational energy levels are added. The equations that relate these energy levels to the mass, moments of inertia, and vibrational frequencies follow.

A6.1a Translational Energy Levels

Translational energy levels are obtained by confining the molecule to a rectangular box with sides L_x, L_y, and L_z, in which case, the energy levels in the x direction are given by

$$\epsilon_{\text{trans},x} = \frac{n_x^2 h^2}{8mL_x^2}, \tag{A6.2}$$

[a] For Avogadro's number of molecules, fluctuations from the most probable distribution are very small, and the Boltzmann distribution equation can be relied upon to predict the correct distribution.

where h is Planck's constant, m is the mass of the particle, and n_x is a quantum number with values

$$n_x = 1, 2, 3, \ldots \tag{A6.3}$$

Similar expressions can be written for $\epsilon_{\text{trans},y}$ and $\epsilon_{\text{trans},z}$, the energies in the y and z directions. The total translational energy is the sum of the contributions in the three directions. For a cubic box with sides $L = L_x = L_y = L_3$,

$$\epsilon_{\text{trans}} = \frac{h^2}{8mL^2}(n_x^2 + n_y^2 + n_z^2) \tag{A6.4}$$

or

$$\epsilon_{\text{trans}} = \frac{h^2}{8mV^{2/3}}(n_x^2 + n_y^2 + n_z^2), \tag{A6.5}$$

where V is the volume of the container.

A6.1b Rotational Energy Levels

Rotational energy levels depend upon the geometry of the molecule. For a linear molecule acting as a rigid rotator, the energy levels are given by

$$\epsilon_{\text{rot}} = \frac{h^2}{8\pi^2 I} J(J+1), \tag{A6.6}$$

where h is Planck's constant, I is the moment of inertia along an axis perpendicular to the axis of the molecule and through the center of mass, and

$$J = 0, 1, 2, \ldots \tag{A6.7}$$

is the quantum number that sets the energy level. The rotational energy levels have a degeneracy g_J given by

$$g_J = 2J + 1. \tag{A6.8}$$

For a nonlinear molecule, the rotational energy levels are a function of three principal moments of inertia I_A, I_B and I_C. These are moments of inertia around

three mutually orthogonal axes that have their origin (or intersection) at the center of mass of the molecule. They are oriented so that the products of inertia are zero. The relationship between the three moments of inertia, and hence the energy levels, depends upon the geometry of the molecules. For the rigid rotator the equations are as follows:

In a spherical top, $I_A = I_B = I_C$. Examples are CH_4 and SF_6. For a spherical top, the energy levels are given by the same equation as for the linear molecule {equations (A6.6) and (A6.7)} and the degeneracy is given by equation (A6.8).

In a symmetrical top, $I_A \neq I_B = I_C$. Examples are NH_3 and $CHCl_3$. The energy levels for a symmetrical top are given by

$$\epsilon_r = \frac{h^2}{8\pi^2 I_B} J(J+1) + \frac{h^2}{8\pi^2}\left(\frac{1}{I_A} - \frac{1}{I_B}\right) K^2, \tag{A6.9}$$

where

$$J = 0, 1, 2, \ldots \tag{A6.10}$$

$$K = 0, \pm 1, \pm 2, \ldots \pm J. \tag{A6.11}$$

Symmetrical tops are of two types. A prolate spheroid (football shape) in which $I_A < I_B$, and an oblate spheroid (pancake shape) in which $I_A > I_B$. Again, there are $2J + 1$ sets of energy levels for each J, but they are no longer degenerate, as can be seen from equation (A6.9), which includes both the J and K quantum number.

Finally, an asymmetric top is one in which all three principal moments of inertia are different. The energy levels are given by

$$\epsilon_r = J(J+1)\frac{(a+c)}{2} + \frac{(a-c)}{2}\epsilon'(\kappa), \tag{A6.12}$$

where

$$a = \frac{h^2}{8\pi^2 I_A}, \tag{A6.13}$$

$$b = \frac{h^2}{8\pi^2 I_B}, \tag{A6.14}$$

and

$$c = \frac{h^2}{8\pi^2 I_C}, \tag{A6.15}$$

with $I_A < I_B < I_C$, and κ is the parameter of asymmetry defined as

$$\kappa = \frac{2b - a - c}{a - c}. \tag{A6.16}$$

The quantity $\epsilon'(\kappa)$ is a separate function of κ for each energy level. Tabulations showing the form of this function can be found in the literature.[b] Again, $2J + 1$ energy levels are present for each value of J.

A6.1c Vibrational Energy Levels

Vibrational energy levels can be approximated by the harmonic oscillator. For a diatomic molecule the relationship is

$$\epsilon_{vib} = h\nu(v + 1/2), \tag{A6.17}$$

where ν, the **fundamental vibrational frequency**, is related to the force constant k and the reduced mass μ by

$$\nu = \frac{1}{2\pi}\sqrt{\frac{k}{\mu}}. \tag{A6.18}$$

The vibrational quantum number, v, has values

$$v = 0, 1, 2, \ldots \tag{A6.19}$$

For a polyatomic molecule, the complex vibrational motion of the atoms can be resolved into a set of fundamental vibrations. Each fundamental vibration, called a normal mode, describes how the atoms move relative to each other. Every normal mode has its own set of energy levels that can be

[b] See for example, C. H. Townes and A. L. Schawlow, *Microwave Spectroscopy*, McGraw-Hill Book Company, Inc., New York, 1955, pp. 83–110, and T. M. Sugden and C. N. Kenney, *Microwave Spectroscopy of Gases*, D. Van Nostrand Company Ltd., London, 1965, pp. 46–64.

represented by equation (A6.17). A linear molecule has $(3\eta - 5)$ such fundamental vibrations, where η is the number of atoms in the molecule. For a nonlinear molecule, the number of fundamental vibrations is $(3\eta - 6)$.

A6.1d Internal Rotational Energy Levels

Internal rotational energy levels are present in some (nonlinear) molecules, in which rotation about a bond in the molecule replaces a vibrational motion. The contribution of the internal rotation to the thermodynamic functions is determined by the magnitude of kT, the energy available to thermally excite the molecule, relative to V_0, the height of the potential barrier. For free rotation ($kT \gg V_0$) the energy levels are given by

$$\epsilon_f = \frac{h^2}{8\pi^2 I_r} K^2 \tag{A6.20}$$

where $K = 0, \pm 1, \pm 2, \pm 3, \ldots$, and I_r is a reduced moment of inertia for the internal rotation. When the molecular rotation involves a pair of symmetrical tops, the reduced moment of inertia is given by

$$I_r = \frac{I_A I_B}{I_A + I_B} \tag{A6.21}$$

where I_A and I_B are the moments of inertia of the individual tops about the axis of rotation. Internal rotations involving more complicated (usually less symmetric) motions can be found, but they are correspondingly more difficult to represent. Starting with equation (A6.20), a partition function (that we will define in the next section) can be written and the contribution to the thermodynamic functions can be calculated.

For restricted rotation, the thermodynamic functions can be calculated as a function of V_0. Pitzer has assumed a potential barrier of the form

$$V_r = \tfrac{1}{2} V_0(1 - \cos n_f \phi), \tag{A6.22}$$

where ϕ is the rotational angle, V_0 is the height of the potential barrier, and n_f is the number of equivalent orientations. The resulting energy levels and hence, the partition function, are complex, but can be evaluated. Pitzer tabulated results for the various thermodynamic quantities as a function of two variables: V_0/RT and $1/z_f$, where z_f is the value the partition function would have as a free rotator.

For large V_0, the rotation becomes a torsional motion and is treated as a vibration.

A6.1e Electronic Energy Levels

Excited electronic energy levels are sometimes occupied, especially when unpaired electrons are present. A set of quantum numbers describe the electronic levels, but because of the unique nature of these levels for each type of atom or molecule, it is not possible to write general expressions similar to those given earlier for translational, rotational, or vibrational levels.

A6.2 The Partition Function

The partition function for a set of energy levels in an atom or molecule is given by

$$z = \sum_i g_i \exp\left(-\frac{\epsilon_i}{kT}\right). \tag{A6.23}$$

It is a measure of the extent to which energy is partitioned among the different states.

Combining equation (A6.23) with (A6.1) gives

$$\frac{n_i}{N} = \frac{g_i \exp\left(-\dfrac{\epsilon_i}{kT}\right)}{z} \tag{A6.24}$$

where N is the total number of molecules and n_i is the number of molecules in energy level ϵ_i. From the partition function we can get the fraction, n_i/N, of the molecules that are in energy level ϵ_i.

When the total energy of a system is the sum of the energies from the different degrees of freedom, for example, translation, rotation, vibration, and electronic, then the partition function for a combination of the energy levels is the product of the partition functions for each type. Thus,

$$z = z_{\text{trans}} \cdot z_{\text{rot}} \cdot z_{\text{vib}} \cdot z_{\text{elect}} \tag{A6.25}$$

with

$$z_{\text{trans}} = z_{\text{trans},x} \cdot z_{\text{trans},y} \cdot z_{\text{trans},z}. \tag{A6.26}$$

In a similar manner, the partition function for a collection of molecules is the product of the partition function for each molecule. For N identical molecules, the partition function Z is

$$Z = z^N. \tag{A6.27}$$

Equation (A6.27) assumes that each molecule is distinguishable. For gas molecules, this is not the case, so that Z must be decreased by a factor of $1/N!$, and equation (A6.27) becomes

$$Z = \frac{1}{N!} z^N. \tag{A6.28}$$

The molar partition function Z_m is given by equation (A6.28) with N equal to Avogadro's number N_A, so that

$$Z_m = \frac{1}{N_A!} z^{N_A} \tag{A6.29}$$

with $$Z_m = Z_{m,\,trans} \cdot Z_{m,\,rot} \cdot Z_{m,\,vib} \cdot Z_{m,\,elect}. \tag{A6.30}$$

and

$$Z_{m,\,trans} = \frac{1}{N_A!} z_{m,\,trans}^{N_A} \tag{A6.31}$$

$$Z_{m,\,rot} = z_{m,\,rot}^{N_A} \tag{A6.32}$$

$$Z_{m,\,vib} = z_{m,\,vib}^{N_A} \tag{A6.33}$$

$$Z_{m,\,elect} = z_{m,\,elect}^{N_A}. \tag{A6.34}$$

Note that the $1/N!$ term is assigned to the translational partition function, since all gases have translational motion, but only molecular gases have rotational and vibrational degrees of freedom. The electronic partition function is usually equal to one unless unpaired electrons are present in the atom or molecule.

A6.3 Relationship Between the Partition Function and the Thermodynamic Functions for the Ideal Gas

The partition function Z_m for the ideal gas is related to the thermodynamic properties U_m, H_m, $C_{V,m}$, $C_{p,m}$, S_m, A_m, and G_m. The relationships are

summarized by the equations[c]

$$U_m - U_{0,m} = kT^2 \left(\frac{\partial \ln Z_m}{\partial T} \right)_{V_m}, \tag{A6.35}$$

$$H_m - H_{0,m} = kT^2 \left(\frac{\partial \ln Z_m}{\partial T} \right)_{V_m} + RT, \tag{A6.36}$$

$$C_{V,m} = 2kT \left(\frac{\partial \ln Z_m}{\partial T} \right)_{V_m} + kT^2 \left(\frac{\partial^2 \ln Z_m}{\partial T^2} \right)_{V_m}, \tag{A6.37}$$

$$C_{p,m} = C_{V,m} + R, \tag{A6.38}$$

$$S_m = k \ln Z_m + kT \left(\frac{\partial \ln Z_m}{\partial T} \right)_{V_m}, \tag{A6.39}$$

$$A_m - H_{0,m} = -kT \ln Z_m, \tag{A6.40}$$

and

$$G_m - H_{0,m} = -kT \ln Z_m + RT. \tag{A6.41}$$

In equations (A6.35) to (A6.41), k and R are the Boltzmann and gas constants and $U_{0,m} = H_{0,m,} = A_{0,m} = G_{0,m}$ is the value at the absolute zero of temperature T.

A6.4 Partition Functions for the Ideal Gas

The translational, rotational, and vibrational partition functions for the ideal gas, assuming a rigid rotator and a harmonic oscillator approximation, are as

---

[c] The derivation of the equation for entropy uses the Boltzmann relationship

$$S_m = k \ln W_m,$$

where k is the Boltzmann constant and W is the thermodynamic probability, given by

$$W_m = N_A! \prod_i \frac{g_i^{n_i}}{n_i!}.$$

follows (N_A is Avogadro's number, k is the Boltzmann constant, and h is Planck's constant):

$$Z_{m,\,trans} = \frac{1}{N_A!}\left[\frac{(2\pi mkT)^{3/2}V_m}{h^3}\right]^{N_A}, \tag{A6.42}$$

where m is the mass of the molecule and V_m is the molar volume.

For a linear molecule

$$Z_{m,\,rot} = \left[\frac{8\pi^2 IkT}{\sigma h^2}\right]^{N_A}, \tag{A6.43}$$

with I as the moment of inertia around the center of mass of the molecule and σ is the symmetry number. For a nonlinear molecule

$$Z_{m,\,rot} = \left[\frac{8\pi^2(8\pi^3 I_A I_B I_C)^{1/2}(kT)^{3/2}}{\sigma h^3}\right]^{N_A}, \tag{A6.44}$$

where I_A, I_B, and I_C are the principal moments of inertia.

For a diatomic molecule

$$Z_{m,\,vib} = \left[\frac{1}{1-\exp\left(-\dfrac{h\nu}{kT}\right)}\right]^{N_A}, \tag{A6.45}$$

with ν as the fundamental vibrational frequency. For a molecule containing η atoms

$$Z_{m,\,vib} = \left[\prod_i \left(\frac{1}{1-\exp(-h\nu_i/kT)}\right)\right]^{N_A}, \tag{A6.46}$$

where the product is over $(3\eta - 5)$ terms for a linear molecule and $(3\eta - 6)$ terms for a nonlinear molecule.

For atoms or molecules without unpaired electrons, one can usually assume that $Z_{m,\,elect} = 1$ so that the electronic contribution is zero. Electronic energy

level information is given in Table A6.4 for atoms or molecules with unpaired electrons, from which the electronic partition function and hence, the electronic contribution to the thermodynamic functions, can be obtained.

A6.5 Calculation of the Thermodynamic Properties from the Energy Levels

Table A6.1 summarizes the equations needed to calculate the contributions to the thermodynamic functions of an ideal gas arising from the translational, rotational, and vibrational degrees of freedom. The equations assume that the rigid rotator and harmonic oscillator approximations are valid.

For most atomic gases, only the translational contribution is used. For molecules, the contributions from rotations and vibrations must be included. If unpaired electrons are present in either the atomic or molecular species so that degenerate electronic energy levels occur, electronic contributions may also be significant. In molecules where internal rotation is present, such as those containing a methyl group, the internal rotation contribution replaces a vibrational contribution.

Tables A6.2 and A6.3 summarize moments of inertia and fundamental vibrational frequencies of some common molecules, while Table A6.4 gives electronic energy levels for some common molecules or atoms with unpaired electrons. These values can be used to calculate rotational, vibrational, and electronic contributions to the thermodynamic functions.

Table A6.5 summarizes the equations for calculating anharmonicity and nonrigid rotator corrections for diatomic molecules. These corrections are to be added to the thermodynamic properties calculated from the equations given in Table A6.1 (which assume harmonic oscillator and rigid rotator approximations).

Table A6.6 gives the internal rotation contributions to the heat capacity, enthalpy and Gibbs free energy as a function of the rotational barrier V. It is convenient to tabulate the contributions in terms of V/RT against $1/z_f$, where z_f is the partition function for free rotation.

Table A6.7 summarizes the thermodynamic properties of monatomic solids as calculated by the Debye model. The values are expressed in terms of θ_D/T, where θ_D is the Debye temperature. Tables A6.5 to A6.7 are adapted from K. S. Pitzer, *Thermodynamics*, McGraw-Hill, New York, 1995.

Table A6.1 Thermodynamic functions of an ideal gas (use $R = 8.314510\ \text{J·K}^{-1}\text{·mol}^{-1}$ and SI units for pressure, temperature, and all molecular data)

TRANSLATION

$$S_{\text{m, trans}} = \frac{3}{2} R \ln M + \frac{5}{2} R \ln T - R \ln p + \underbrace{\left[\frac{5}{2} R + R \ln \left(\frac{(2\pi k)^{3/2}}{h^3 N_{\text{A}}^{5/2}}\right) + R \ln R\right]}_{+172.3005}$$

$$\left(\frac{G_{\text{m}} - H_{0,\text{m}}}{T}\right)_{\text{trans}} = -\frac{3}{2} R \ln M - \frac{5}{2} R \ln T + R \ln p + \underbrace{\left[-R \ln \left(\frac{(2\pi k)^{3/2}}{h^3 N_{\text{A}}^{5/2}}\right) - R \ln R\right]}_{-151.5142}$$

$$\left(\frac{U_{\text{m}} - U_{0,\text{m}}}{T}\right)_{\text{trans}} = \frac{3}{2} R = (C_{V,\text{m}})_{\text{trans}}$$

$$\left(\frac{H_{\text{m}} - H_{0,\text{m}}}{T}\right)_{\text{trans}} = \frac{5}{2} R = (C_{p,\text{m}})_{\text{trans}}$$

ROTATION (Rigid Molecule Approximations)
Linear Polyatomic or Diatomic Molecules:

$$S_{\text{m, rot}} = R \ln T + R \ln I - R \ln \sigma + \underbrace{\left[R \ln \left(\frac{8\pi^2 k}{h^2}\right) + R\right]}_{+877.3950}$$

$$\left(\frac{G_{\text{m}} - H_{0,\text{m}}}{T}\right)_{\text{rot}} = -R \ln T - R \ln I + R \ln \sigma + \underbrace{\left[-R \ln \frac{8\pi^2 k}{h^2}\right]}_{-869.0805}$$

$$\left(\frac{U_{\text{m}} - U_{0,\text{m}}}{T}\right)_{\text{rot}} = \left(\frac{H_{\text{m}} - H_{0,\text{m}}}{T}\right)_{\text{rot}} = (C_{\text{m}})_{\text{rot}} = R$$

(*continued*)

Table A6.1 *Continued*

Nonlinear Polyatomic Molecules:

$$S_{m,\,rot} = \frac{3}{2} R \ln T + \frac{1}{2} R \ln I_A I_B I_C - R \ln \sigma + \underbrace{\left[R \ln \frac{8\pi^2 (2\pi k)^{3/2}}{h^3} + \frac{3}{2} R \right]}_{+1320.8515}$$

$$\left(\frac{U_m - U_{0,m}}{T} \right)_{rot} = \left(\frac{H_m - H_{0,m}}{T} \right)_{rot} = (C)_{rot} = \frac{3}{2} R$$

$$\left(\frac{G_m - H_{0,m}}{T} \right)_{rot} = -\frac{3}{2} R \ln T - \frac{1}{2} R \ln I_A I_B I_C + R \ln \sigma + \underbrace{\left[-R \ln \frac{8\pi^2 (2\pi k)^{3/2}}{h^3} \right]}_{-1308.3797}$$

VIBRATION (Harmonic Oscillator Approximation)

$$S_{m,\,vib} = R \sum_i^n \left[\frac{x_i}{e^{x_i} - 1} - \ln(1 - \exp(-x_i)) \right]; \quad x_i = \frac{hc\tilde{\omega}_i}{kT} = 1.43877 \frac{\tilde{\omega}_i}{T} \text{ (use } \tilde{\omega}_i \text{ in cm}^{-1})$$

$$\left(\frac{G_m - H_{0,m}}{T} \right)_{vib} = \sum_i^n R \ln (1 - \exp(-x_i)) \approx \sum_{\nu_1}^{\nu_n} - R \ln \frac{kT}{hc\omega_i} \text{ (high temp. approx.)}$$

$$\left(\frac{U_m - U_{0,m}}{T} \right)_{vib} = \left(\frac{H_m - H_{0,m}}{T} \right)_{vib} = R \sum_i^n \frac{x_i}{\exp(x_i) - 1}$$

$$(C_m)_{vib} = R \sum_i^n \frac{x_i^2 \exp(x_i)}{(\exp(x_i) - 1)^2}$$

where $n = (3\eta - 6)$ or $(3\eta - 5)$, with η equal to the number of atoms in the molecule

Table A6.2 Moments of inertia and rotational constants of some common molecules

The values given are for a molecule that corresponds to the natural abundance of each isotope since these "average values" will give the thermodynamic properties of a mole of the naturally occurring substance.[1]

For diatomic molecules, $\tilde{B}_0$ and $\tilde{B}_e$ are rotational constants related by $\tilde{B}_0 = \tilde{B}_e - \frac{1}{2}\tilde{\alpha}$. The moment of inertia $I_0/(\text{kg·m}^2)$ is related to $B_0/(\text{cm}^{-1})$ through the relationship $I_0 = h/(8 \times 10^{-2}\pi^2 B_0 c)$, with h and c expressed in SI units. For polyatomic molecules, I_A, I_B, and I_C are the moments of inertia to use with Table A6.1 where the rigid rotator approximation is assumed. For diatomic molecules, I_0 is used with Table A6.1 to calculate the thermodynamic properties assuming the rigid rotator approximation. The anharmonicity and nonrigid rotator corrections are added to this value.

Table A6.2a Diatomic molecules

Molecule	$\tilde{B}_0/(\text{cm}^{-1})$	$I_0/(10^{-47}\ \text{kg·m}^2)$	$\tilde{B}_e/(\text{cm}^{-1})$	$10^3\tilde{\alpha}/(10^{-3}\,\text{cm}^{-1})$
Br_2	0.081948	341.59	0.082107	0.31873
CO	1.9215	14.568	1.9302	17.46
Cl_2	0.24339	115.01	0.24415	1.5163
H_2	(59.304)	0.47203	(60.800)	(2993)
HBr	8.34954	3.3526	8.46620	233.33
HCl	10.4326	2.6832	10.5844	303.7
HF	20.5577	1.3617	20.9555	795.8
HI	6.426	4.356	6.512	171.5
ICl	0.11272	248.34	0.11298	0.5275
I_2	0.037333	749.81	0.037395	0.12435
N_2	2.001	14.00	(2.010)	(18.7)
NO	1.6953	16.512	1.7042	17.8
NaCl	0.21611	129.53	0.21691	1.598
OH	18.514	1.5120	18.871	714
O_2	1.43765	19.471	1.44562	15.933

(*continued*)

Table A6.2b Polyatomic molecules

Linear molecules

Molecule	$I_A/(10^{-47}\ kg{\cdot}m^2)$	Molecule	$I_A/(10^{-47}\ kg{\cdot}m^2)$
HCN	18.8585	CS_2	256.42
N_2O	66.4882	C_2H_2	23.7864
CO_2	71.4988		

Nonlinear molecules

Molecule	$I_A I_B I_C/(10^{-138}\ kg^3{\cdot}m^6)$	Molecule	$I_A I_B I_C/(10^{-138}\ kg^3{\cdot}m^6)$
CH_4	0.1499	NH_3	0.0348
CCl_4	115003	$POCl_3$	10184.1
H_2O	(0.0058577)	$CFCl_3$	57360.2
SO_2	107.0	NO_2	15.423

[1] Most values were taken from M. W. Chase Jr., C. A. Davies, J. R. Downey, Jr., D. J. Frurip, R. A. McDonald, and A. N. Syverud, "JANAF Thermochemical Tables, Third Edition", *J. Phys. Chem. Eng. Data*, **14**, Supplement No. 1, 1985. For the diatomic molecules, a few values (in parentheses) came from G. Hertzberg, *Molecular Spectra and Molecular Structure, I. Spectra of Diatomic Molecules*, and *II. Infrared and Raman Spectra of Polyatomic Molecules*, Van Nostrand Reinhold Co., New York, 1950 and 1945.

Table A6.3 Fundamental vibrational frequencies of some common molecules

The values given are for a molecule that corresponds to the natural abundance of each isotope since these "average values" will give the thermodynamic properties of a mole of the naturally occurring substance.[2]

For diatomic molecules, $\tilde{\omega}_0$ is the vibrational constant to use with the equations in Table A6.1 to calculate the thermodynamic values for a diatomic molecule, assuming the rigid rotator and harmonic oscillator approximations are valid. The vibrational constants $\tilde{\omega}_e$ and $\tilde{\omega}_e x_e$ are the values to use with the equations in Table A6.5 to calculate the anharmonicity and non-rigid rotator corrections. They are related to $\tilde{\omega}_0$ by $\tilde{\omega}_0 = \tilde{\omega}_e - 2\tilde{\omega}_e x_e$.

For polyatomic molecules, $\tilde{\omega}$ is the vibrational constant to use when making calculations for polyatomic molecules with the equations in Table A6.1.

Table A6.3a Diatomic molecules

Molecule	$\tilde{\omega}_0/(\text{cm}^{-1})$	$\tilde{\omega}_e/(\text{cm}^{-1})$	$\tilde{\omega}_e x_e/(\text{cm}^{-1})$
Br_2	323.166	325.321	1.07742
CO	2142.61	2169.52	13.453
Cl_2	554.362	559.751	2.6943
H_2	4159.44	(4395.24)	(117.90)
HBr	2558.73	2649.182	45.225
HCl	2785.47	2889.59	52.06
HF	3958.63	4138.73	90.05
HI	2229.60	2309.06	39.73
ICl	379.28	382.18	1.450
I_2	213.316	214.5481	0.616259
N_2	(2330.70)	(2359.61)	(14.456)
NO	1875.66	1903.60	13.97
NaCl	360.18	363.62	1.72
OH	3569.59	3735.21	82.81
O_2	1556.231	1580.193	11.981

(*continued*)

Table 6.3b Polyatomic molecules
The numbers in parentheses designate the number of normal modes that have this frequency

Molecule	$\tilde{\omega}/(\text{cm}^{-1})$	Molecule	$\tilde{\omega}/(\text{cm}^{-1})$
	Linear molecules		
HCN	713.5(2), 2096.3, 3311.5	CS_2	396.7(2), 656.6, 1523
N_2O	589.2(2), 1276.5, 2223.7	C_2H_2	611.6(2), 729.3(2), 1973.8, 3281.9, 3373.7
CO_2	667.30(2), 1384.86, 2349.30		
	Nonlinear molecules		
CH_4	1306(3), 1534.0(2), 2916.5, 3018.7(3)	NH_3	1022, 1691(2), 3506, 3577(2)
CCl_4	218(2), 314(3), 458, 776(3)	NO_2	756.8, 1357.8, 1665.5
H_2O	1594.7, 3651.1, 3755.9	$POCl_3$	193(2), 267(2), 337, 486, 581(2), 1290
SO_2	517.69, 1151.38, 1361.76	$CFCl_3$	241(2), 349.5, 398(2), 535.3, 847(2), 1085

[2] Most values were taken from M. W. Chase Jr., C. A. Davies, J. R. Downey, Jr., D. J. Frurip, R. A. McDonald, and A. N. Syverud, "JANAF Thermochemical Tables, Third Edition", *J. Phys. Chem. Eng. Data*, **14**, Supplement No. 1, 1985. For the diatomic molecules a few values (in parentheses) came from G. Hertzberg, *Molecular Spectra and Molecular Structure, I. Spectra of Diatomic Molecules*, and *II. Infrared and Raman Spectra of Polyatomic Molecules*, Van Nostrand Reinhold Co., New York, 1950 and 1945.

Table A6.4 Electronic energy levels of some common molecules or atoms with unpaired electrons[3]

Atom or molecule	g_i	$\epsilon_i/(c_m^{-1})$	Atom or molecule	g_i	$\epsilon_i/(c_m^{-1})$
O_2	3	0	I	4	0
	2	7882.39		2	7603.15
	1	13120.91	Cl	4	0
O	5	0		2	882.36
	3	158.265	Na	2	0
	1	226.977		2	16956.172
	5	15867.862		4	16973.368
	1	33792.583		2	25739.991
NO_2	2	0	H	2	0
NO	2	0			
	2	121.1			

[3] Values were taken from M. W. Chase Jr., C. A. Davies, J. R. Downey, Jr., D. J. Frurip, R. A. McDonald, and A. N. Syverud, "JANAF Thermochemical Tables, Third Edition", *J. Phys. Chem. Eng. Data*, **14**, Supplement No. 1, 1985.

Table A6.5 Anharmonic oscillator and nonrigid rotator corrections

The following equations are used to calculate the anharmonicity and nonrigid rotator corrections to the thermodynamic properties of diatomic molecules.

$$\left(\frac{H_m - H_{0,m}}{T}\right)_{corr} = \left(\frac{R}{u}\right)\left\{2x\left[\frac{u^2\{2u\exp(u) - \exp(u) + 1\}}{\{\exp(u) - 1\}^3}\right] + \delta\left[\frac{u^2\exp(u)}{\{\exp(u) - 1\}^2}\right] + 8\gamma\right\}$$

$$-\left(\frac{G_m - H_{0,m}}{T}\right)_{corr} = \left(\frac{R}{u}\right)\left\{2x\left[\frac{u^2}{\{\exp(u) - 1\}^2}\right] + \delta\left[\frac{u}{\exp(u) - 1}\right] + 8\gamma\right\}$$

$$(S_m)_{corr} = \frac{(H_m - H_{0,m})_{corr}}{T} - \frac{(G_m - H_{0,m})_{corr}}{T}$$

(continued)

Table A6.5 *Continued*

and

$$(C_m)_{corr}) = \left(\frac{R}{u}\right)\left\{4x\left[\frac{\{u^3\exp(u)\}\{2u\exp(u) - 2\exp(u) + u + 2\}}{\{\exp(u) - 1\}^4}\right]\right\}$$
$$+ \left(\frac{R}{u}\right)\left\{\delta\left[\frac{\{u^3\exp(u)\}\{\exp(u) + 1\}}{\{\exp(u) - 1\}^3}\right] + 16\gamma\right\},$$

where

$$u = \frac{hc\tilde{\omega}_0}{kT}, \quad y = \frac{hc\tilde{B}_0}{kT}, \quad x = \frac{x_e}{1 - 2x_e} \approx \frac{x_e\tilde{\omega}_e}{\tilde{\omega}_e}, \quad \delta = \frac{\tilde{\alpha}}{\tilde{B}_0}, \quad \text{and} \quad \gamma = \frac{\tilde{B}_e}{\tilde{\omega}_e}.$$

The above equations can be simplified for calculation of the corrections by first defining and calculating the functions ν and w given

$$\nu = \exp(u) - 1 \qquad \text{and} \qquad w = \exp(u) = \nu + 1.$$

Substitution of these quantities into the above equations gives

$$-\left(\frac{G_m - G_{0,m}}{T}\right)_{corr} = \left(\frac{R}{u}\right)\left\{\left[\frac{2u^2}{\nu^2}\right]x + \left[\frac{u}{\nu}\right]\delta + 8\gamma\right\}$$

$$\left(\frac{H_m - H_{0,m}}{T}\right)_{corr} = \left(\frac{R}{u}\right)\left\{\left[\left(\frac{2u^2}{\nu^3}\right)(2uw - \nu)\right]x + \left[\frac{u^2w}{\nu^2}\right]\delta + 8\gamma\right\}$$

$$(S_m)_{corr} = \frac{(H_m - H_{0,m})_{corr}}{T} - \frac{(G_m - H_{0,m})_{corr}}{T}$$

$$(C_m)_{corr} = \left(\frac{R}{u}\right)\left\{\left[\left(\frac{4u^3}{\nu^4}\right)(2uw^2 + uw - 2\nu w)\right]x\right.$$
$$\left. + \left[\left(\frac{u^3}{\nu^3}\right)(w^2 + w)\right]\delta + 16\gamma\right\}$$

With modern high-speed computers, the corrections can easily be calculated from either set of equations.

Table A6.6 Contributions to the thermodynamic properties due to internal rotation as a function of V, the rotational barrier, and z_f, the partition function for free rotation*

Heat capacity $[C_m]/(J \cdot K^{-1} \cdot mol^{-1})$

	$1/z_f$																			
V/RT	0	0.05	0.1	0.15	0.2	0.25	0.3	0.35	0.4	0.45	0.5	0.55	0.6	0.65	0.7	0.75	0.8	0.85	0.9	0.95
0.0	4.159	4.159	4.159	4.159	4.159	4.159	4.159	4.159	4.159	4.159	4.159	4.159	4.159	4.159	4.159	4.159	4.159	4.159	4.159	4.159
0.2	4.1986	4.197	4.197	4.192	4.188	4.184	4.180	4.176	4.176	4.176	4.184	4.184	4.184	4.184	4.184	4.184	4.184	4.180	4.180	4.180
0.4	4.3212	4.322	4.318	4.310	4.301	4.289	4.284	4.272	4.263	4.255	4.259	4.255	4.247	4.238	4.234	4.226	4.217	4.213	4.205	4.201
0.6	4.5191	4.519	4.515	4.502	4.489	4.469	4.456	4.435	4.418	4.397	4.389	4.376	4.356	4.335	4.314	4.293	4.272	4.255	4.243	4.230
0.8	4.7844	4.782	4.774	4.761	4.740	4.720	4.690	4.661	4.628	4.598	4.569	4.535	4.498	4.464	4.427	4.389	4.351	4.314	4.289	4.268
1.0	5.1057	5.100	5.092	5.071	5.046	5.017	4.979	4.937	4.891	4.841	4.786	4.732	4.678	4.623	4.565	4.510	4.456	4.402	4.351	4.314
1.5	6.0701	6.063	6.042	6.004	5.954	5.891	5.820	5.732	5.640	5.540	5.435	5.326	5.217	5.096	4.987	4.874	4.774	4.665	4.561	4.477
2.0	7.0199	7.092	7.058	7.000	6.925	6.828	6.720	6.586	6.448	6.297	6.130	5.958	5.782	5.611	5.439	5.263	5.096	4.937	4.795	4.657
2.5	8.0387	8.021	7.983	7.899	7.807	7.699	7.535	7.347	7.184	6.987	6.774	6.535	6.293	6.058	5.828	5.611	5.393	5.180	4.979	4.795
3.0	8.7818	8.765	8.711	8.627	8.506	8.351	8.167	7.950	7.724	7.506	7.247	6.958	6.682	6.410	6.134	5.862	5.594	5.339	5.092	4.870
3.5	9.2994	9.280	9.222	9.121	8.979	8.812	8.594	8.347	8.092	7.820	7.544	7.226	6.920	6.611	6.301	5.991	5.694	5.410	5.130	4.874
4.0	9.6186	9.598	9.523	9.410	9.259	9.071	8.828	8.569	8.284	7.979	7.673	7.339	7.004	6.665	6.330	6.004	5.686	5.381	5.084	4.803
4.5	9.7730	9.749	9.673	9.540	9.364	9.163	8.908	8.627	8.326	7.996	7.665	7.318	6.962	6.602	6.259	5.912	5.577	5.268	4.958	4.665
5.0	9.8102	9.782	9.699	9.560	9.376	9.146	8.870	8.602	8.251	7.908	7.565	7.188	6.824	6.456	6.096	5.745	5.406	5.079	4.770	4.469
6.0	9.6893	9.652	9.552	9.393	9.171	8.912	8.615	8.280	7.920	7.544	7.159	6.753	6.360	5.979	5.615	5.251	4.908	4.586	4.276	3.992
7.0	9.4768	9.439	9.322	9.142	8.895	8.598	8.255	7.878	7.477	7.063	6.644	6.222	5.816	5.422	5.050	4.686	4.351	4.025	3.724	3.456
8.0	9.2717	9.226	9.096	8.891	8.611	8.280	7.899	7.481	7.046	6.594	6.142	5.715	5.280	4.870	4.494	4.134	3.799	3.489	3.201	2.946
9.0	9.1052	9.054	8.912	8.678	8.364	7.987	7.565	7.109	6.640	6.167	5.699	5.230	4.786	4.385	4.000	3.636	3.301	3.000	2.728	2.481
10.0	8.9776	8.924	8.761	8.506	8.163	7.757	7.301	6.820	6.305	5.782	5.280	4.816	4.372	3.946	3.556	3.201	2.879	2.586	2.326	2.088
12.0	8.8086	8.740	8.548	8.251	7.853	7.376	6.845	6.284	5.711	5.159	4.632	4.138	3.669	3.238	2.853	2.510	2.209	1.937	1.703	1.498
14.0	8.7082	8.632	8.406	8.046	7.590	7.054	6.468	5.858	5.247	4.653	4.092	3.577	3.113	2.694	2.318	2.004	1.720	1.473	1.268	1.096
16.0	8.6429	8.552	8.297	7.895	7.381	6.786	6.142	5.485	4.837	4.222	3.653	3.134	2.674	2.268	1.912	1.619	1.356	1.138	0.958	0.812
18.0	8.5969	8.498	8.205	7.753	7.184	6.535	5.845	5.155	4.477	3.845	3.264	2.749	2.297	1.908	1.582	1.305	1.084	0.900	0.732	0.602
20.0	8.5626	8.452	8.134	7.644	7.021	6.318	5.577	4.845	4.146	3.502	2.933	2.427	1.996	1.628	1.322	1.071	0.870	0.703	0.565	0.456

(*continued*)

Table A6.6 *Continued*

Enthalpy $[H_m/T]/(J \cdot K^{-1} \cdot mol^{-1})$

	$1/z_f$																			
V/RT	0	0.05	0.1	0.15	0.2	0.25	0.3	0.35	0.4	0.45	0.5	0.55	0.6	0.65	0.7	0.75	0.8	0.85	0.9	0.95
0.0	4.159	4.159	4.159	4.159	4.159	4.159	4.159	4.159	4.159	4.159	4.159	4.159	4.159	4.159	4.159	4.159	4.159	4.159	4.159	4.159
0.2	4.9472	4.778	4.628	4.494	4.393	4.318	4.276	4.247	4.217	4.201	4.184	4.167	4.159	4.159	4.159	4.151	4.151	4.146	4.142	4.138
0.4	5.6547	5.439	5.226	5.021	4.816	4.628	4.489	4.397	4.335	4.289	4.247	4.209	4.180	4.159	4.151	4.142	4.134	4.134	4.125	4.121
0.6	6.2814	6.012	5.749	5.485	5.234	4.979	4.761	4.598	4.485	4.389	4.310	4.243	4.201	4.163	4.142	4.130	4.117	4.109	4.100	4.096
0.8	6.8308	6.510	6.201	5.904	5.607	5.322	5.067	4.841	4.661	4.506	4.385	4.293	4.222	4.167	4.117	4.100	4.084	4.075	4.067	4.063
1.0	7.3065	6.945	6.594	6.255	5.933	5.623	5.335	5.067	4.833	4.628	4.456	4.343	4.243	4.167	4.109	4.067	4.038	4.025	4.017	4.012
1.5	8.2048	7.766	7.335	6.920	6.531	6.159	5.795	5.464	5.146	4.870	4.615	4.431	4.263	4.130	4.025	3.954	3.899	3.858	3.833	3.828
2.0	8.7600	8.247	7.757	7.289	6.845	6.427	6.025	5.648	5.293	4.979	4.686	4.422	4.205	4.025	3.883	3.782	3.707	3.653	3.615	3.598
2.5	9.0625	8.498	7.950	7.443	6.954	6.485	6.058	5.653	5.272	4.933	4.619	4.318	4.067	3.858	3.690	3.556	3.460	3.393	3.351	3.330
3.0	9.1939	8.573	7.987	7.435	6.908	6.422	5.966	5.527	5.121	4.770	4.435	4.134	3.866	3.640	3.464	3.310	3.192	3.113	3.063	3.046
3.5	9.2186	8.548	7.920	7.335	6.782	6.263	5.782	5.335	4.920	4.552	4.209	3.904	3.632	3.393	3.201	3.042	2.916	2.828	2.774	2.757
4.0	9.1826	8.468	7.799	7.176	6.598	6.058	5.561	5.109	4.690	4.310	3.962	3.648	3.372	3.134	2.933	2.766	2.636	2.548	2.489	2.469
4.5	9.1174	8.360	7.653	7.000	6.397	5.832	5.326	4.862	4.439	4.050	3.699	3.389	3.113	2.874	2.669	2.506	2.372	2.280	2.222	2.201
5.0	9.0416	8.247	7.506	6.824	6.197	5.623	5.096	4.619	4.192	3.803	3.448	3.138	2.866	2.628	2.427	2.259	2.125	2.029	1.966	1.946
6.0	8.8969	8.025	7.226	6.494	5.824	5.217	4.665	4.180	3.736	3.343	2.987	2.694	2.427	2.188	1.992	1.828	1.699	1.602	1.540	1.510
7.0	8.7810	7.845	6.987	6.209	5.502	4.870	4.305	3.799	3.356	2.962	2.611	2.318	2.054	1.828	1.640	1.481	1.356	1.264	1.197	1.167
8.0	8.6960	7.699	6.791	5.971	5.234	4.581	3.996	3.485	3.033	2.640	2.297	2.008	1.757	1.540	1.364	1.213	1.092	1.000	0.933	0.900
9.0	8.6345	7.577	6.623	5.770	5.004	4.330	3.732	3.213	2.766	2.381	2.042	1.761	1.519	1.305	1.142	1.004	0.883	0.799	0.736	0.703
10.0	8.5893	7.477	6.477	5.586	4.799	4.109	3.506	2.992	2.544	2.155	1.828	1.548	1.314	1.125	0.967	0.837	0.728	0.644	0.586	0.552
12.0	8.5291	7.318	6.243	5.289	4.464	3.749	3.117	2.611	2.171	1.803	1.490	1.238	1.021	0.845	0.711	0.598	0.506	0.435	0.381	0.351
14.0	8.4914	7.184	6.029	5.029	4.171	3.443	2.812	2.305	1.883	1.527	1.243	1.004	0.816	0.661	0.531	0.431	0.351	0.301	0.259	0.234
16.0	8.4651	7.071	5.862	4.812	3.920	3.180	2.565	2.063	1.648	1.314	1.042	0.828	0.657	0.531	0.410	0.318	0.255	0.213	0.184	0.159
18.0	8.4454	6.971	5.703	4.611	3.707	2.958	2.347	1.854	1.452	1.134	0.883	0.686	0.536	0.414	0.322	0.251	0.197	0.151	0.121	0.109
20.0	8.4308	6.887	5.561	4.439	3.519	2.761	2.155	1.669	1.284	0.987	0.757	0.577	0.439	0.335	0.255	0.197	0.151	0.117	0.092	0.075

Gibbs free energy $[-G_m/T]/(J \cdot K^{-1} \cdot mol^{-1})$

	$1/z_f$														
V/RT	0.25	0.3	0.35	0.4	0.45	0.5	0.55	0.6	0.65	0.7	0.75	0.8	0.85	0.9	0.95
0.0	11.523	10.008	8.728	7.619	6.640	5.761	4.979	4.243	3.582	2.971	2.406	1.854	1.351	0.870	0.427
0.2	11.339	9.870	8.623	7.544	6.586	5.724	4.945	4.222	3.565	2.958	2.385	1.845	1.343	0.866	0.423
0.4	10.975	9.606	8.427	7.385	6.456	5.615	4.870	4.171	3.523	2.925	2.364	1.833	1.331	0.862	0.414
0.6	10.535	9.238	8.134	7.146	6.268	5.477	4.753	4.075	3.456	2.874	2.322	1.803	1.318	0.854	0.406
0.8	10.067	8.812	7.766	6.845	6.033	5.297	4.598	3.962	3.364	2.803	2.272	1.774	1.297	0.837	0.402
1.0	9.606	8.385	7.381	6.523	5.770	5.079	4.418	3.816	3.251	2.707	2.201	1.720	1.264	0.816	0.393
1.5	8.535	7.406	6.477	5.732	5.063	4.473	3.920	3.410	2.929	2.460	2.013	1.586	1.159	0.745	0.351
2.0	7.611	6.540	5.690	4.992	4.402	3.879	3.418	2.983	2.573	2.180	1.791	1.414	1.042	0.669	0.310
2.5	6.820	5.812	5.008	4.364	3.816	3.356	2.950	2.577	2.234	1.900	1.569	1.247	0.916	0.590	0.264
3.0	6.163	5.188	4.431	3.824	3.318	2.908	2.544	2.218	1.916	1.632	1.356	1.079	0.799	0.510	0.222
3.5	5.607	4.674	3.946	3.356	2.904	2.523	2.197	1.912	1.653	1.406	1.163	0.929	0.690	0.439	0.176
4.0	5.125	4.238	3.544	2.983	2.565	2.205	1.904	1.644	1.418	1.205	1.000	0.795	0.586	0.368	0.142
4.5	4.740	3.870	3.197	2.665	2.272	1.937	1.665	1.423	1.213	1.033	0.858	0.678	0.490	0.310	0.113
5.0	4.406	3.552	2.912	2.414	2.021	1.707	1.452	1.243	1.059	0.895	0.741	0.582	0.427	0.264	0.084
6.0	3.845	3.046	2.452	1.996	1.644	1.360	1.142	0.962	0.808	0.674	0.548	0.431	0.310	0.188	0.050
7.0	3.427	2.661	2.105	1.682	1.360	1.117	0.912	0.757	0.623	0.515	0.418	0.326	0.234	0.134	0.033
8.0	3.075	2.360	1.841	1.448	1.151	0.925	0.749	0.607	0.494	0.402	0.326	0.251	0.176	0.100	0.021
9.0	2.791	2.109	1.623	1.255	0.983	0.778	0.623	0.502	0.397	0.326	0.259	0.197	0.134	0.079	0.017
10.0	2.552	1.908	1.443	1.105	0.849	0.665	0.519	0.418	0.331	0.264	0.205	0.155	0.109	0.063	0.008
12.0	2.180	1.590	1.172	0.874	0.657	0.502	0.385	0.297	0.226	0.176	0.138	0.105	0.075	0.042	0.004
14.0	1.891	1.343	0.971	0.707	0.519	0.385	0.289	0.218	0.159	0.126	0.096	0.067	0.050	0.029	0.000
16.0	1.657	1.155	0.816	0.582	0.418	0.301	0.222	0.163	0.117	0.088	0.067	0.050	0.033	0.017	0.000
18.0	1.469	1.004	0.695	0.490	0.343	0.243	0.176	0.126	0.092	0.067	0.050	0.033	0.025	0.013	0.000
20.0	1.318	0.883	0.602	0.410	0.285	0.197	0.138	0.096	0.071	0.050	0.038	0.025	0.017	0.008	0.000

*G. N. Lewis, M. Randall, K. S. Pitzer and L. Brewer, *Thermodynamics*, 2nd Edition, McGraw-Hill Book Co., New York, 1961, p. 441–446.

Table A6.7 The Debye thermodynamic functions expressed in terms of θ_D/T^*

Debye heat capacity $C_{V,m}/3R$ as a function of θ_D/T when $\frac{\theta_D}{T} \geqslant 16$, $\frac{C_{V,m}}{3R} = 77.927\left(\frac{T}{\theta_D}\right)^3$

θ_D/T	0.0	0.1	0.2	0.3	0.4	0.5	0.6	0.7	0.8	0.9	1.0
0.0	1.0000	0.9995	0.9980	0.9955	0.9920	0.9876	0.9822	0.9759	0.9687	0.9606	0.9517
1.0	0.9517	0.9420	0.9315	0.9203	0.9085	0.8960	0.8828	0.8692	0.8550	0.8404	0.8254
2.0	0.8254	0.8100	0.7943	0.7784	0.7622	0.7459	0.7294	0.7128	0.6961	0.6794	0.6628
3.0	0.6628	0.6461	0.6296	0.6132	0.5968	0.5807	0.5647	0.5490	0.5334	0.5181	0.5031
4.0	0.5031	0.4883	0.4738	0.4595	0.4456	0.4320	0.4187	0.4057	0.3930	0.3807	0.3686
5.0	0.3686	0.3569	0.3455	0.3345	0.3237	0.3133	0.3031	0.2933	0.2838	0.2745	0.2656
6.0	0.2656	0.2569	0.2486	0.2405	0.2326	0.2251	0.2177	0.2107	0.2038	0.1972	0.1909
7.0	0.1909	0.1847	0.1788	0.1730	0.1675	0.1622	0.1570	0.1521	0.1473	0.1426	0.1382
8.0	0.1382	0.1339	0.1297	0.1257	0.1219	0.1182	0.1146	0.1111	0.1078	0.1046	0.1015
9.0	0.1015	0.09847	0.09558	0.09280	0.09011	0.08751	0.08500	0.08259	0.08025	0.07800	0.07582
10.0	0.07582	0.07372	0.07169	0.06973	0.06783	0.06600	0.06424	0.06253	0.06087	0.05928	0.05773
11.0	0.05773	0.05624	0.05479	0.05339	0.05204	0.05073	0.04946	0.04823	0.04705	0.04590	0.04478
12.0	0.04478	0.04370	0.04265	0.04164	0.04066	0.03970	0.03878	0.03788	0.03701	0.03617	0.03535
13.0	0.03535	0.03455	0.03378	0.03303	0.03230	0.03160	0.03091	0.03024	0.02959	0.02896	0.02835
14.0	0.02835	0.02776	0.02718	0.02661	0.02607	0.02553	0.02501	0.02451	0.02402	0.02354	0.02307
15.0	0.02307	0.02262	0.02218	0.02174	0.02132	0.02092	0.02052	0.02013	0.01975	0.01938	0.01902

Debye energy content $(U_m - U_{0,m})/3RT$ as a function of θ_D/T when $\frac{\theta_D}{T} \geqslant 16$, $\frac{U_m - U_{0,m}}{3RT} = 19.482\left(\frac{T}{\theta_D}\right)^3$

θ_D/T	0.0	0.1	0.2	0.3	0.4	0.5	0.6	0.7	0.8	0.9	1.0
0.0	1.0000	0.9630	0.9270	0.8920	0.8580	0.8250	0.7929	0.7619	0.7318	0.7026	0.6744
1.0	0.6744	0.6471	0.6208	0.5954	0.5708	0.5471	0.5243	0.5023	0.4811	0.4607	0.4411
2.0	0.4411	0.4223	0.4042	0.3868	0.3701	0.3541	0.3388	0.3241	0.3100	0.2965	0.2836
3.0	0.2836	0.2712	0.2594	0.2481	0.2373	0.2269	0.2170	0.2076	0.1986	0.1900	0.1817
4.0	0.1817	0.1739	0.1664	0.1592	0.1524	0.1459	0.1397	0.1338	0.1281	0.1227	0.1176
5.0	0.1176	0.1127	0.1080	0.1036	0.09930	0.09524	0.09137	0.08768	0.08415	0.08079	0.07758
6.0	0.07758	0.07452	0.07160	0.06881	0.06615	0.06360	0.06118	0.05886	0.05664	0.05453	0.05251
7.0	0.05251	0.05057	0.04873	0.04696	0.04527	0.04366	0.04211	0.04063	0.03921	0.03786	0.03656
8.0	0.03656	0.03532	0.03413	0.03298	0.03189	0.03084	0.02983	0.02887	0.02794	0.02705	0.02620
9.0	0.02620	0.02538	0.02459	0.02384	0.02311	0.02241	0.02174	0.02109	0.02047	0.01987	0.01930
10.0	0.01930	0.01874	0.01821	0.01769	0.01720	0.01672	0.01626	0.01581	0.01538	0.01497	0.01457
11.0	0.01457	0.01418	0.01381	0.01345	0.01311	0.01277	0.01245	0.01213	0.01183	0.01153	0.01125
12.0	0.01125	0.01098	0.01071	0.01045	0.01020	0.00996	0.00973	0.00950	0.00928	0.00907	0.00886
13.0	0.00886	0.00866	0.00846	0.00827	0.00809	0.00791	0.00774	0.00757	0.00741	0.00725	0.00710
14.0	0.00710	0.00695	0.00680	0.00666	0.00652	0.00639	0.00626	0.00613	0.00601	0.00589	0.00577
15.0	0.00577	0.00566	0.00555	0.00544	0.00533	0.00523	0.00513	0.00503	0.00494	0.00485	0.00476

(*continued*)

Table A6.7 *Continued*

Debye-Helmholtz free energy $(A_m - U_{0,m})/3RT$ as a function of θ_D/T. When $\frac{\theta_D}{T} \geqslant 16$, $\frac{A_m - U_{0,m}}{3RT} = 6.494\left(\frac{T}{\theta_D}\right)^3$

θ_D/T	0.0	0.1	0.2	0.3	0.4	0.5	0.6	0.7	0.8	0.9	1.0
0.0	∞	2.6732	2.0168	1.6476	1.3956	1.2077	1.0602	0.9403	0.8405	0.7560	0.6835
1.0	0.6835	0.6205	0.5653	0.5166	0.4734	0.4349	0.4003	0.3692	0.3410	0.3156	0.2925
2.0	0.2925	0.2714	0.2522	0.2346	0.2185	0.2037	0.1901	0.1776	0.1661	0.1554	0.1456
3.0	0.1456	0.1365	0.1281	0.1203	0.1130	0.1063	0.1000	0.09423	0.08882	0.08377	0.07906
4.0	0.07906	0.07467	0.07057	0.06674	0.06316	0.05981	0.05667	0.05373	0.05097	0.04839	0.04596
5.0	0.04596	0.04368	0.04154	0.03952	0.03763	0.03584	0.03416	0.03258	0.03108	0.02967	0.02834
6.0	0.02834	0.02709	0.02590	0.02477	0.02371	0.02271	0.02175	0.02085	0.02000	0.01918	0.01841
7.0	0.01841	0.01768	0.01699	0.01633	0.01570	0.01510	0.01454	0.01400	0.01348	0.01299	0.01252
8.0	0.01252	0.01208	0.01165	0.01124	0.01085	0.01048	0.01013	0.00979	0.00946	0.00915	0.00886
9.0	0.00886	0.00857	0.00830	0.00804	0.00779	0.00755	0.00731	0.00709	0.00688	0.00667	0.00648
10.0	0.00648	0.00629	0.00611	0.00593	0.00576	0.00560	0.00544	0.00529	0.00515	0.00501	0.00487
11.0	0.00487	0.00474	0.00462	0.00450	0.00438	0.00427	0.00416	0.00405	0.00395	0.00385	0.00376
12.0	0.00376	0.00366	0.00357	0.00349	0.00340	0.00332	0.00325	0.00317	0.00310	0.00302	0.00296
13.0	0.00296	0.00289	0.00282	0.00276	0.00270	0.00264	0.00258	0.00253	0.00247	0.00242	0.00237
14.0	0.00237	0.00232	0.00227	0.00222	0.00217	0.00213	0.00209	0.00204	0.00200	0.00196	0.00192
15.0	0.00192	0.00189	0.00185	0.00181	0.00178	0.00174	0.00171	0.00168	0.00165	0.00162	0.00159

Debye entropy $S_m/3R$ as a function of θ_D/T. When $\frac{\theta_D}{T} \geqslant 16$, $\frac{S_m}{3R} = 25.976\left(\frac{T}{\theta_D}\right)^3$

θ_D/T	0.0	0.1	0.2	0.3	0.4	0.5	0.6	0.7	0.8	0.9	1.0
0.0	∞	3.6362	2.9438	2.5396	2.2536	2.0327	1.8531	1.7022	1.5723	1.4587	1.3579
1.0	1.3579	1.2676	1.1861	1.1120	1.0442	0.9820	0.9246	0.8714	0.8222	0.7763	0.7336
2.0	0.7336	0.6937	0.6564	0.6214	0.5886	0.5578	0.5289	0.5017	0.4761	0.4519	0.4292
3.0	0.4292	0.4077	0.3875	0.3683	0.3503	0.3332	0.3171	0.3018	0.2874	0.2737	0.2608
4.0	0.2608	0.2486	0.2370	0.2260	0.2156	0.2057	0.1964	0.1875	0.1791	0.1711	0.1636
5.0	0.1636	0.1564	0.1496	0.1431	0.1369	0.1311	0.1255	0.1203	0.1152	0.1105	0.1059
6.0	0.1059	0.1016	0.09750	0.09358	0.08986	0.08631	0.08293	0.07971	0.07664	0.07371	0.07092
7.0	0.07092	0.06826	0.06572	0.06329	0.06097	0.05876	0.05665	0.05463	0.05270	0.05085	0.04908
8.0	0.04908	0.04739	0.04578	0.04423	0.04274	0.04132	0.03996	0.03866	0.03741	0.03621	0.03506
9.0	0.03506	0.03395	0.03289	0.03187	0.03090	0.02996	0.02905	0.02818	0.02735	0.02655	0.02577
10.0	0.02577	0.02503	0.02431	0.02362	0.02296	0.02232	0.02170	0.02111	0.02053	0.01998	0.01944
11.0	0.01944	0.01893	0.01843	0.01795	0.01749	0.01704	0.01660	0.01618	0.01578	0.01539	0.01501
12.0	0.01501	0.01464	0.01428	0.01394	0.01361	0.01328	0.01297	0.01267	0.01237	0.01209	0.01181
13.0	0.01181	0.01155	0.01129	0.01103	0.01079	0.01055	0.01032	0.01010	0.00988	0.00967	0.00946
14.0	0.00946	0.00926	0.00907	0.00888	0.00870	0.00852	0.00834	0.00818	0.00801	0.00785	0.00770
15.0	0.00770	0.00754	0.00740	0.00725	0.00711	0.00697	0.00684	0.00671	0.00659	0.00646	0.00634

* From K. S. Pitzer, *Thermodynamics*, McGraw-Hill, New York, 1995, pp. 371–374 and Appendix 12.

Appendix 7

Coefficients for Pitzer's Equations

In this appendix, we summarize the coefficients needed to calculate the thermodynamic properties for a number of solutes in an electrolyte solution from Pitzer's equations.[a] Table A7.1 summarizes the Debye–Hückel parameters for water solutions as a function of temperature. They provide the leading terms for Pitzer's equations, and can also be used to calculate the Debye–Hückel limiting law values from the equations

$$\ln \gamma_{\pm} = -C_{\gamma} \mid z_{+}z_{-} \mid I^{1/2}$$

$$1 - \phi = C_{\phi} \mid z_{+}z_{-} \mid I^{1/2}$$

$$C_{\gamma} = 3C_{\phi}$$

$$\bar{L}_2 = C_H \left(\frac{\nu}{2}\right) \mid z_{+}z_{-} \mid I^{1/2}$$

$$\bar{J}_2 = C_J \left(\frac{\nu}{2}\right) \mid z_{+}z_{-} \mid I^{1/2}$$

$$\bar{V}_2 - \bar{V}_2^{\circ} = C_{\mathrm{v}} \left(\frac{\nu}{2}\right) \mid z_{+}z_{-} \mid I^{1/2}$$

---

[a] The equations and coefficients given in this appendix were obtained primarily from K. S. Pitzer, "Ion Interaction Approach: Theory and Data Correlation," Chapter 3 in *Activity Coefficients in Electrolyte Solutions, 2nd Edition*, K. S. Pitzer, Editor, CRC Press, Boca Raton, Florida, (1991). The equations for calculating $\bar{L}_1$, $\bar{L}_2$, $\bar{J}_1$, and $\bar{J}_2$ are summarized in K. S. Pitzer, J. C. Peiper, and R. H. Busey, "Thermodynamic Properties of Aqueous Sodium Chloride Solutions," *J. Phys. Chem. Ref. Data*, **13**, 1–102 (1984), and were taken from that source.

Table A7.1 Debye-Hückel parameters for the osmotic coefficient, volume, enthalpy, and heat capacity

$(T-273.15)/$ (K)	$A_\phi = C_\phi = A_\gamma/3$ ($kg^{1/2}\cdot mol^{-1/2}$)	$A_v = \frac{2}{3} C_v$ ($cm^3\cdot kg^{1/2}\cdot mol^{-3/2}$)	$A_L/RT = \frac{2}{3} C_H/RT$ ($kg^{1/2}\cdot mol^{-1/2}$)	$A_J/R = \frac{2}{3} C_J/R$ ($kg^{1/2}\cdot mol^{-1/2}$)
0.0	0.3767	1.504	0.556	2.95
10.0	0.3821	1.643	0.649	3.39
20.0	0.3882	1.793	0.749	3.76
25.0	0.3915	1.875	0.801	3.94
30.0	0.3949	1.962	0.854	4.13
40.0	0.4023	2.153	0.965	4.51
50.0	0.4103	2.372	1.081	4.92
60.0	0.4190	2.622	1.203	5.37
70.0	0.4283	2.909	1.331	5.86
80.0	0.4384	3.238	1.467	6.40
90.0	0.4491	3.615	1.611	7.00
100.0	0.4606	4.050	1.764	7.66
110.0	0.4727	4.550	1.927	8.40
120.0	0.4857	5.127	2.102	9.24
130.0	0.4994	5.795	2.290	10.17
140.0	0.5140	6.572	2.492	11.23
150.0	0.5295	7.477	2.712	12.45
160.0	0.5460	8.536	2.951	13.84
170.0	0.5634	9.779	3.213	15.47
180.0	0.5820	11.25	3.500	17.38
190.0	0.6017	12.99	3.819	19.65
200.0	0.6228	15.07	4.175	22.38
210.0	0.6453	17.6	4.576	25.72
220.0	0.6694	20.6	5.032	29.85
230.0	0.6953	24.3	5.556	35.05
240.0	0.7232	28.8	6.165	41.73
250.0	0.7535	34.4	6.885	50.46
260.0	0.7865	41.5	7.749	62.15
270.0	0.823	50.5	8.806	78.18
280.0	0.863	62.3	10.13	100.8
290.0	0.908	77.8	11.82	133.7
300.0	0.960	98.7	14.05	183.4
310.0	1.02	127	17.1	261
320.0	1.09	169	21.4	391
330.0	1.18	231	28.0	622
340.0	1.29	330	38.6	1060
350.0	1.44	493	57.3	1920

where $\gamma_\pm$ is the mean ionic activity coefficient and ϕ is the osmotic coefficient given by

$$\phi = -\frac{\ln a_1}{M_1 \sum_k \nu_k m_k},$$

with m as the molatility of the solution and m_1 as the molecular weight of the solvent.

For a single electrolyte, ϕ becomes

$$\phi = -\frac{\ln a_1}{M_1 \nu m}.$$

In these equations I is the molal-based ionic strength given by

$$I = \frac{1}{2} \sum_i m_i z_i^2,$$

z_+ and z_- are the ionic charges, and $\nu = \nu_+ + \nu_-$ is the total number of ions per molecular unit. The coefficients A_γ, A_ϕ, A_H, A_J and A_v are related to fundamental constants and properties of the solvent. The relationships are given in Chapter 11.

In Chapter 11, we saw that $\gamma_\pm$ could be calculated over a larger concentration range by using the extended form of the Debye–Hückel equation

$$\ln \gamma_\pm = -C_\gamma \mid z_+ z_- \mid \frac{I^{1/2}}{1 + I_{1/2}},$$

Similar equations can be written for other thermodynamic functions. For example,

$$1 - \phi = C_\phi \mid z_+ z_- \mid \frac{I^{1/2}}{1 + I^{1/2}},$$

but equations of this type are still limited to low concentrations.

Tables A7.2 to A7.6 summarize other coefficients needed to apply Pitzer's equations for the calculation of $\gamma_\pm$ and ϕ for various 1:1, 2:1, 3:1, 4:1, 5:1, and 2:2 electrolytes. The equations for calculating the osmotic coefficient are

$$\phi - 1 = \mid z_M z_X \mid f^\phi + m(2\nu_M \nu_X / \nu) B^\phi_{MX} + m^2 [2(\nu_M \nu_X)^{3/2} / \nu] C^\phi_{MX}$$

Table A7.2 Pitzer coefficients for 1 : 1 electrolytes

Max m is the maximum molality at which the coefficients will give reliable values. σ is the standard deviation over this molality range. The letter a indicates that data of several types were simultaneously fitted, leading to higher precision for those coefficients than for the ones designated by b and c where only limited data were available.

Compound	$\beta^{(0)}$	$\beta^{(1)}$	$C^{\phi} = 2C$	Max m	σ
	Inorganic acids, bases, and salts of 1:1 type				
HCl	0.1775	0.2945	0.00080	6	a
HBr	0.2085	0.3477	0.00152	6.2	0.003
HI	0.2211	0.4907	0.00482	6	b
$HClO_4$	0.1747	0.2931	0.00819	5.5	0.002
HNO_3	0.1168	0.3546	−0.00539	6	a
$H(HSO_4)$	0.2065	0.5556			
LiCl	0.1494	0.3074	0.00359	6	0.001
LiBr	0.1748	0.2547	0.0053	2.5	0.002
LiI	0.2104	0.373		1.4	0.006
LiOH	0.015	0.14		4	c
$LiClO_3$	0.1705	0.2294	−0.00524	4.2	0.002
$LiClO_4$	0.1973	0.3996	0.0008	3.5	0.002
$LiBrO_3$	0.0893	0.2157	0.0000	5	0.001
$LiNO_2$	0.1336	0.325	−0.0053	6	0.003
$LiNO_3$	0.1420	0.2780	−0.00551	6	0.001
NaF	0.0215	0.2107		1	0.001
NaCl	0.0765	0.2664	0.00127	6	0.001
NaBr	0.0973	0.2791	0.00116	4	0.001
NaI	0.1195	0.3439	0.0018	3.5	0.001
NaOH	0.0864	0.253	0.0044	6	b
$NaClO_3$	0.0249	0.2455	0.004	3.5	0.001
$NaClO_4$	0.0554	0.2755	−0.00118	6	0.001
$NaBrO_3$	−0.0205	0.1910	0.0059	2.5	0.001
NaCNS	0.1005	0.3582	−0.00303	4	0.001
$NaNO_2$	0.0641	0.1015	−0.0049	5	0.005
$NaNO_3$	0.0068	0.1783	−0.00072	6	0.001
NaHSe	0.040	(0.253)		2	c
$NaHCO_3$	0.028	0.044			
$NaHSO_4$	0.0454	0.398			
NaH_2PO_4	−0.0533	0.0396	0.00795	6	0.003
NaH_2AsO_4	−0.0442	0.2895		1.2	0.001
$NaB(OH)_4$	−0.0526	0.1104	0.0154	4.5	0.004
$NaBF_4$	−0.0252	0.1824	0.0021	6	0.006
KF	0.08089	0.2021	0.00093	2	0.001

Table A7.2 *Continued*

Compound	$\beta^{(0)}$	$\beta^{(1)}$	$C^{\phi} = 2C$	Max m	σ
KCl	0.04835	0.2122	−0.00084	4.8	0.0005
KBr	0.0569	0.2212	−0.00180	5.5	0.001
KI	0.0746	0.2517	−0.00414	4.5	0.001
KOH	0.1298	0.320	0.0041	5.5	b
$KClO_3$	−0.0960	0.2481		0.7	0.001
$KBrO_3$	−0.1290	0.2565		0.5	0.001
KCNS	0.0416	0.2302	−0.00252	5	0.001
KNO_2	0.0151	0.015	0.0007	5	0.003
KNO_3	−0.0816	0.0494	0.00660	3.8	0.001
$KHCO_3$	−0.0107	0.0478			
$KHSO_4$	−0.0003	0.1735			
KH_2PO_4	−0.0678	−0.1042		1.8	0.003
KH_2AsO_4	−0.0584	0.0626		1.2	0.003
KSCN	0.0389	0.2536	−0.00192	5	0.001
KPF_6	−0.163	−0.282		0.5	0.001
RbF	0.1141	0.2842	−0.0105	3.5	0.002
RbCl	0.0432	0.1540	−0.0011	7.8	0.003
RbBr	0.0396	0.1530	−0.00144	5	0.001
RbI	0.0397	0.1330	−0.00108	5	0.001
$RbNO_2$	0.0269	−0.1553	−0.00366	5	0.002
$RbNO_3$	−0.0789	−0.0172	0.00529	4.5	0.001
CsF	0.1306	0.2570	−0.0043	3.2	0.002
CsCl	0.0348	0.0397	−0.00050	7.4	0.002
CsBr	0.0279	0.0139	0.00004	5	0.002
CsI	0.0244	0.0262	−0.00365	3	0.001
CsOH	0.150	0.30			b
$CsNO_2$	0.0427	0.060	−0.0051	6	0.004
$CsNO_3$	−0.0758	−0.0669		1.4	0.002
$AgNO_3$	−0.0856	0.0025	0.00591	6	0.001
$TlClO_4$	−0.087	−0.023		0.5	0.001
$TlNO_3$	−0.105	−0.378		0.4	0.001
NH_4Cl	0.0522	0.1918	−0.00301	6	0.001
NH_4Br	0.0624	0.1947	−0.00436	2.5	0.001
NH_4I	0.0570	0.3157	−0.00308	7.5	0.002
NH_4HCO_3	−0.038	0.070		0.7	—
$NH_4H_2PO_4$	−0.0704	−0.4156	0.00669	3.5	0.003
NH_4ClO_4	−0.0103	−0.0194		2	0.004
NH_4NO_3	−0.0154	0.1120	−0.00003	6	0.001
(MgOH)Cl	−0.10	1.658	—	—	—

(*continued*)

Table A7.2 *Continued*

Compound	$\beta^{(0)}$	$\beta^{(1)}$	$C^{\phi} = 2C$	Max m	σ
Salts of carboxylic acids (1 : 1 type)					
Li acetate	0.1124	0.2483	−0.00525	4	0.001
Na formate	0.0820	0.2872	−0.00523	3.5	0.001
Na acetate	0.1426	0.3237	−0.00629	3.5	0.001
Na propionate	0.1875	0.2789	−0.01277	3	0.001
NaH malonate	0.0229	0.1600	−0.00106	5	0.002
NaH succinate	0.0354	0.1606	0.00040	5	0.001
NaH adipate	0.0472	0.3168		0.7	0.001
K acetate	0.1587	0.3251	−0.00660	3.5	0.001
KH malonate	−0.0095	0.1423	0.00167	5	0.004
KH succinate	0.0111	0.1564	0.00274	4.5	0.002
KH adipate	0.0419	0.2523		1	0.001
Rb acetate	0.1622	0.3353	−0.00551	3.5	0.001
Cs acetate	0.1628	0.3605	−0.00555	3.5	0.001
Tl acetate	0.0082	0.0131	−0.00127	6	0.001
Tetraalkylammonium halides					
Me_4NF	0.2677	0.2265	0.0013	3	0.002
Et_4NF	0.3113	0.6155	0.0349	2	0.002
Pr_4NF	0.4463	0.4090	0.0537	2	0.002
Bu_4NF	0.6092	0.402	−0.0281	1.7	0.005
Me_4NCl	0.0430	−0.029	0.0078	3.4	0.005
Et_4NCl	0.0617	−0.099	0.0105	3	0.002
Pr_4NCl	0.1346	−0.300	0.0119	2.5	0.002
Bu_4NCl	0.2339	−0.410	−0.0567	2.5	0.001
Me_4NBr	−0.0082	−0.147	0.0105	3.5	0.004
Et_4NBr	−0.0176	−0.394	0.0156	4	0.001
Pr_4NBr	0.0390	−0.772	0.0099	3.5	0.003
Bu_4NBr	−0.0277	−0.525	0.0011	4.5	0.007
Me_4NI	0.0345	−0.585		0.3	0.003
Et_4NI	−0.179	−0.571	0.0412	2	0.007
Pr_4NI	−0.2839	−0.863		0.5	0.005

Table A7.3 Pitzer coefficients for 2:1 electrolytes

Compound	$\frac{4}{3}\beta^{(0)}$	$\frac{4}{3}\beta^{(1)}$	$\frac{1}{3}2^{5/2}C^{\phi} = \frac{16}{3}C$	Max m	σ
Inorganic electrolytes					
$MgCl_2$	0.4698	2.242	0.00979	4.5	0.003
$MgBr_2$	0.5769	2.337	0.00589	5	0.004
MgI_2	0.6536	2.4055	0.01496	5	0.003
$Mg(ClO_4)_2$	0.6615	2.678	0.01806	2	0.002
$Mg(NO_3)_2$	0.4895	2.113	−0.03889	2	0.003
$Mg(HCO_3)_2$	0.044	1.133			
$Mg(HSO_4)_2$	0.6328	2.305			
$CaCl_2$	0.4071	2.278	0.00406	4.3	0.003
$CaBr_2$	0.5088	2.151	−0.00485	2	0.002
CaI_2	0.5839	2.409	−0.00158	2	0.001
$Ca(ClO_4)_2$	0.6015	2.342	−0.00943	2	0.005
$Ca(NO_3)_2$	0.2811	1.879	−0.03798	2	0.002
$Ca(HCO_3)_2$	0.533	3.97			
$Ca(HSO_4)_2$	0.286	3.37			
$SrCl_2$	0.3779	2.167	−0.00168	3.8	0.002
$SrBr_2$	0.4415	2.282	0.00231	2	0.001
SrI_2	0.5350	2.480	0.00501	2	0.001
$Sr(ClO_4)_2$	0.5692	2.089	−0.02472	2.5	0.003
$Sr(NO_3)_2$	0.1795	1.840	−0.03757	2	0.002
$BaCl_2$	0.3504	1.995	−0.03654	1.8	0.001
$BaBr_2$	0.4194	2.093	−0.03009	2	0.001
BaI_2	0.5625	2.249	−0.03286	1.8	0.003
$Ba(OH)_2$	0.229	1.60		0.1	
$Ba(ClO_4)_2$	0.4819	2.101	−0.05894	2	0.003
$Ba(NO_3)_2$	−0.043	1.07		0.4	0.001
$MnCl_2$	0.4429	2.019	−0.04278	4	0.003
$FeCl_2$	0.4479	2.043	−0.01623	2	0.002
$Fe(HSO_4)_2$	0.5697	4.64			
$CoCl_2$	0.4857	1.967	−0.02869	3	0.004
$CoBr_2$	0.5693	2.213	−0.00127	2	0.002
CoI_2	0.695	2.23	−0.0088	2	0.01
$Co(NO_3)_2$	0.4159	2.254	−0.01436	5.5	0.003
$NiCl_2$	0.4665	2.040	−0.00888	2.5	0.002
$CuCl_2$	0.3955	1.855	−0.06792	2	0.002
$Cu(NO_3)_2$	0.4224	1.907	−0.04136	2	0.002
$ZnCl_2$	0.3043	2.308	−0.1235	1.5	0.007
$ZnBr_2$	0.6213	2.179	−0.2035	1.6	0.007
ZnI_2	0.6428	2.594	−0.0269	0.8	0.002

(*continued*)

Table A7.3 *Continued*

Compound	$\frac{4}{3}\beta^{(0)}$	$\frac{4}{3}\beta^{(1)}$	$\frac{1}{3}2^{5/2}C^{\phi} = \frac{16}{3}C$	Max m	σ
$Zn(ClO_4)_2$	0.6747	2.396	0.02134	2	0.003
$Zn(NO_3)_2$	0.4641	2.255	−0.02955	2	0.001
$Cd(NO_3)_2$	0.3820	2.224	−0.04836	2.5	0.002
$Pb(ClO_4)_2$	0.4443	2.296	−0.01667	6	0.004
$Pb(NO_3)_2$	−0.0482	0.380	0.01005	2	0.002
UO_2Cl_2	0.5698	2.192	−0.06951	2	0.001
$UO_2(ClO_4)_2$	0.8151	2.859	0.04089	2.5	0.003
$UO_2(NO_3)_2$	0.6143	2.151	−0.05948	2	0.002
Li_2SO_4	0.1817	1.694	−0.00753	3	0.002
Na_2SO_4	0.0249	1.466	0.010463	4	0.003
$Na_2S_2O_3$	0.0882	1.701	0.00705	3.5	0.002
Na_2CrO_4	0.1250	1.826	−0.00407	2	0.002
Na_2CO_3	0.0483	2.013	0.0098		
Na_2HPO_4	−0.0777	1.954	0.0554	1	0.002
Na_2HAsO_4	0.0407	2.173	0.0034	1	0.001
K_2SO_4	0.0666	1.039		0.7	0.002
K_2CrO_4	0.1011	1.652	−0.00147	3.5	0.003
K_2CO_3	0.1717	1.911	0.00094		
$K_2Pt(CN)_4$	0.0881	3.164	0.0247	1	0.005
K_2HPO_4	0.0330	1.699	0.0309	1	0.002
K_2HAsO_4	0.1728	2.198	−0.0336	1	0.001
Rb_2SO_4	0.0772	1.481	−0.00019	1.8	0.001
Cs_2SO_4	0.1184	1.481	−0.01131	1.8	0.001
$(NH_4)_2SO_4$	0.0521	0.8851	−0.00156	5.8	0.002
Organic electrolytes of 2 : 1 type (SA = sulfonic acid; S = sulfonate)					
m-Benzenedi SA	0.5611	2.637	−0.0463	1.6	0.004
Li_2 *m*-Benzenedi S	0.5464	2.564	−0.0622	2.5	0.004
Na_2 *m*-Benzenedi S	0.3411	2.698	−0.0419	3	0.004
4,4′-Bibenzyldi SA	0.1136	2.432	0.0705	2	0.01
Li_2 4,4-bibenzyldi S	0.1810	1.755	0.0462	1.2	0.007
Na_2 4,4′-bibenzyldi S	0.0251	1.969	–	0.4	0.01
Na_2 fumarate	0.3082	1.203	−0.0378	2	0.003
Na_2 maleate	0.1860	0.575	−0.0170	3	0.004
Na_2 succinate	0.4175	2.3915	−0.0924	1.4	0.004
K_2 succinate	0.1673	2.1851	–	1.5	0.003

Table A7.4 Pitzer coefficients for 3 : 1 electrolytes

Compound	$\frac{3}{2}\beta^{(0)}$	$\frac{3}{2}\beta^{(1)}$	$\frac{3\sqrt{3}}{2}C^{\phi} = 9C$	Max m	σ
$AlCl_3$	1.0490	8.767	0.0071	1.6	0.005
$ScCl_3$	1.0500	7.978	−0.0840	1.8	0.005
YCl_3	0.939	8.40	−0.040	4.1	0.006
$LaCl_3$	0.883	8.40	−0.061	3.9	0.006
$CeCl_3$	0.907	8.40	−0.074	1.8	0.007
$PrCl_3$	0.883	8.40	−0.054	3.9	0.006
$NdCl_3$	0.878	8.40	−0.049	3.9	0.006
$SmCl_3$	0.900	8.40	−0.053	3.6	0.007
$EuCl_3$	0.911	8.40	−0.054	3.6	0.006
$GdCl_3$	0.913	8.40	−0.049	3.6	0.006
$TbCl_3$	0.922	8.40	−0.046	3.6	0.004
$DyCl_3$	0.929	8.40	−0.045	3.6	0.005
$HoCl_3$	0.937	8.40	−0.045	3.7	0.006
$ErCl_3$	0.928	8.40	−0.038	3.7	0.006
$TmCl_3$	0.926	8.40	−0.036	3.7	0.005
$YbCl_3$	0.923	8.40	−0.033	3.7	0.005
$LuCl_3$	0.922	8.40	−0.033	4.1	0.005
$CrCl_3$	1.1046	7.883	−0.1172	1.2	0.005
$Cr(NO_3)_3$	1.0560	7.777	−0.1533	1.4	0.004
$Ga(ClO_4)_3$	1.2381	9.794	0.0904	2	0.008
$InCl_3$	−1.68	−3.85		0.01	
$Y(NO_3)_3$	0.915	7.70	−0.189	2.0	0.008
$La(NO_3)_3$	0.737	7.70	−0.198	1.5	0.007
$Pr(NO_3)_3$	0.724	7.70	−0.173	1.5	0.005
$Nd(NO_3)_3$	0.702	7.70	−0.142	2.0	0.008
$Sm(NO_3)_3$	0.701	7.70	−0.131	1.5	0.007
$Eu(NO_3)_3$	0.713	7.70	−0.125	2.0	0.007
$Gd(NO_3)_3$	0.776	7.70	−0.170	1.4	0.005
$Tb(NO_3)_3$	0.838	7.70	−0.202	1.4	0.005
$Dy(NO_3)_3$	0.848	7.70	−0.1809	2.0	0.008
$Ho(NO_3)_3$	0.876	7.70	−0.1852	2.0	0.009
$Er(NO_3)_3$	0.938	7.70	−0.226	1.5	0.006
$Tm(NO_3)_3$	0.952	7.70	−0.222	1.5	0.006
$Yb(NO_3)_3$	0.948	7.70	−0.208	1.5	0.006
$Lu(NO_3)_3$	0.926	7.70	−0.174	2.0	0.008
$La(ClO_4)_3$	1.15	9.80	0.001	2.0	0.009
$Pr(ClO_4)_3$	1.13	9.80	0.016	2.0	0.006
$Nd(ClO_4)_3$	1.13	9.80	0.019	2.0	0.007
$Sm(ClO_4)_3$	1.14	9.80	0.014	2.0	0.005

(*continued*)

Table A7.4 *Continued*

Compound	$\frac{3}{2}\beta^{(0)}$	$\frac{3}{2}\beta^{(1)}$	$\frac{3\sqrt{3}}{2}C^{\phi} = 9C$	Max m	σ
$Gd(ClO_4)_3$	1.17	9.80	0.014	2.0	0.007
$Tb(ClO_4)_3$	1.19	9.80	0.012	2.0	0.006
$Dy(ClO_4)_3$	1.20	9.80	0.014	2.0	0.006
$Ho(ClO_4)_3$	1.19	9.80	0.013	2.0	0.004
$Er(ClO_4)_3$	1.20	9.80	0.014	1.8	0.004
$Tm(ClO_4)_3$	1.19	9.80	0.024	2.0	0.005
$Yb(ClO_4)_3$	1.20	9.80	0.013	1.8	0.004
$Lu(ClO_4)_3$	1.18	9.80	0.029	2.0	0.006
Na_3PO_4	0.2672	5.777	−0.1339	0.7	0.003
Na_3AsO_4	0.3582	5.895	−0.1240	0.7	0.001
K_3PO_4	0.5594	5.958	−0.2255	0.7	0.001
$K_3P_3O_9$	0.4867	8.349	−0.0886	0.8	0.004
K_3AsO_4	0.7491	6.511	−0.3376	0.7	0.001
$K_3Fe(CN)_6$	0.5035	7.121	−0.1176	1.4	0.003
$K_3Co(CN)_6$	0.5603	5.815	−0.1603	1.4	0.008

Table A7.5 Pitzer coefficients for 4 : 1 and 5 : 1 electrolytes

4 : 1 Electrolytes

	$\frac{8}{5}\beta^{(0)}$	$\frac{8}{5}\beta^{(1)}$	$\frac{16}{5}C^{\phi} = \frac{64}{5}C$	Max m	σ
$Na_4P_2O_7$	0.699	17.16		0.2	0.01
$K_4P_2O_7$	0.977	17.88	−0.2418	0.5	0.01
$K_4Fe(CN)_6$	1.021	16.23	−0.5579	0.9	0.008
$K_4Mo(CN)_8$	0.854	18.53	−0.3499	0.8	0.01
$K_4W(CN)_8$	1.032	18.49	−0.4937	1	0.005
$(Me_4N)_4Mo(CN)_8$	0.938	15.91	−0.3330	1.4	0.01

5 : 1 Electrolytes

	$\frac{5}{3}\beta^{(0)}$	$\frac{5}{3}\beta^{(1)}$	$\frac{5\sqrt{3}}{3}C^{\phi} = \frac{50}{3}C$	Max m	σ
$Na_5P_3O_{10}$	1.869	36.10	−1.630	0.4	0.01
$K_5P_3O_{10}$	1.939	39.64	−1.055	0.5	0.015

Table A7.6 Pitzer coefficients for 2:2 electrolytes ($\alpha_1 = 1.4$ kg$^{1/2}$·mol$^{-1/2}$, $\alpha_2 = 12.0$ kg$^{1/2}$·mol$^{-1/2}$ throughout)

Electrolyte	$\beta^{(0)}$	$\beta^{(1)}$	$\beta^{(2)}$	$C^{\phi} = 4C$	Range	σ
$MgSO_4$	0.2150	3.365	−32.74	0.0280	0.006–3.6	0.004
$NiSO_4$	0.1702	2.907	−40.06	0.0366	0.005–2.5	0.005
$MnSO_4$	0.213	2.938	−41.91	0.0155	0.1–5.0	0.005
$FeSO_4$	0.2568	3.063	(−42)	0.0209	0.1–2.0	—
$CoSO_4$	0.1631	3.346	−30.7	0.03704	0.2–2.4	0.001
$CuSO_4$	0.2340	2.527	−48.33	0.0044	0.005–1.4	0.003
$ZnSO_4$	0.1949	2.883	−32.81	0.0290	0.005–3.5	0.004
$CdSO_4$	0.2053	2.617	−48.07	0.0114	0.005–3.5	0.002
$CaSO_4$	0.20	3.197	−54.24	—	0.004–0.011	0.003
$SrSO_4$	0.220	2.88	−41.8	0.019	—	—

Table A7.7 Temperature derivatives of Pitzer coefficients for 1:1 electrolytes

Compound	$10^4\beta^{(0)L}$	$10^4\beta^{(1)L}$	$10^5C^{\phi L} = 2 \times 10^5C^L$	Max m
HCl	−3.08	1.41	−6.21	4.5
HBr	−2.04	4.46	−5.68	6
HI	−0.23	8.86	−7.32	6
$HClO_4$	4.90	19.3	−11.7	6
LiCl	−1.68	5.36	−4.52	6.4
LiBr	−1.81	6.63	−2.81	6
$LiClO_4$	0.38	7.00	−7.71	4
NaF	5.36	8.70	–	0.7
NaCl	7.15	7.00	−10.5	6
NaBr	7.69	10.7	−9.30	9
NaI	8.35	8.28	−8.35	6
NaOH	7.00	1.34	−18.9	4.2
$NaClO_3$	10.35	19.0	−9.29	6.4
$NaClO_4$	12.96	22.9	−16.2	6
$NaBrO_3$	5.59	34.3	—	0.1
$NaIO_3$	20.6	60.5	—	0.1
NaCNS	7.80	20.0	—	0.1
$NaNO_3$	12.66	20.6	−23.1	2.2

(*continued*)

Table A7.7 *Continued*

Compound	$10^4\beta^{(0)L}$	$10^4\beta^{(1)L}$	$10^5C^{\phi L} = 2 \times 10^5C^L$	Max m
KF	2.14	5.44	−5.9	5.9
KCl	5.79	10.71	−5.09	4.5
KBr	7.39	17.4	−7.00	5.2
KI	9.91	11.86	−9.44	7
$KClO_3$	19.8	31.8	—	0.1
$KClO_4$	0.6	100.7	—	0.1
KCNS	6.87	37.0	0.43	3.1
KNO_3	2.06	64.5	39.7	2.4
KH_2PO_4	6.04	28	−10.1	1.8
RbF	−0.76	14.7	—	1.0
RbCl	5.52	15.0	—	0.8
RbBr	6.78	20.3	—	1.0
RbI	8.57	23.8	—	0.7
CsF	0.95	5.9	—	1.1
CsCl	8.28	15.0	−12.2	3.0
CsBr	7.80	28.4	—	1.0
CsI	9.75	34.7	—	0.7
NH_4Cl	0.77	12.5	2.1	4
$NH_4H_2PO_4$	1.51	22.8	−2.8	3.4
Me_4NF	−0.82	16.0	−9.2	3
Et_4NF	−16.4	43.4	—	0.5
Pr_4NF	−39.1	41.6	—	0.8
Bu_4NF	−117	105	43.5	1.9
MeH_3NCl	1.1	10.8	—	0.5
Me_2H_2NCl	0.2	18	—	0.5
Me_3HNCl	0.2	35.3	—	0.5
Me_4NCl	5.93	49.0	−7.66	8.1
Et_4NCl	2.0	61.4	−13.1	5.3
Pr_4NCl	−32.2	85.1	11.3	4.4
Bu_4NCl	−122	163	258	2.5
Me_4NBr	6.9	60.2	−6.69	5.5
Et_4NBr	3.8	73.4	−11.3	4.6
Pr_4NBr	−31.0	109.0	26.5	3.0
Bu_4NBr	−116	167	284	3.0
Me_4NI	−7.0	100	—	0.3
Et_4NI	−1.9	92	−36	2
Pr_4NI	−23.4	107	—	0.5

Table A7.8 Temperature derivatives of Pitzer coefficients for 2:1 and 1:2 electrolytes[a]

Compound	$10^3\beta^{(0)L}$	$10^3\beta^{(1)L}$	10^4C^L	Max m
$MgCl_2$	−0.19	2.78	−0.58	2.0
$MgBr_2$	−0.05	3.8	–	0.1
$Mg(ClO_4)_2$	0.52	4.5	−1.25	3.2
$Mg(NO_3)_2$	0.51	4.4	–	0.1
$CaCl_2$	−0.56	2.6	−0.72	6
$CaBr_2$	−0.52	6.0	–	0.6
$Ca(NO_3)_2$	0.53	9.1	–	0.1
$Ca(ClO_4)_2$	0.83	5.0	−1.09	4
$SrCl_2$	0.71	2.8	–	0.1
$SrBr_2$	−0.32	6.5	–	0.1
$Sr(NO_3)_2$	0.17	12.4	–	0.2
$Sr(ClO_4)_2$	1.14	5.3	−1.10	3
$BaCl_2$	0.64	3.2	−0.5	1.8
$BaBr_2$	−0.33	6.7	–	0.1
$Ba(NO_3)_2$	−2.91	29.1	–	0.1
$Mn(ClO_4)_2$	0.39	5.0	−1.18	4
$Co(ClO_4)_2$	0.54	5.3	−1.27	4
$Ni(ClO_4)_2$	0.66	4.7	−1.35	4
$CuCl_2$	−2.7	8.5	–	0.6
$Zn(ClO_4)_2$	0.59	5.0	−1.36	4
Li_2SO_4	0.50	1.41	−0.82	3.0
Na_2SO_4	2.36	5.63	−1.72	3.0
K_2SO_4	1.44	6.7	–	0.1
Rb_2SO_4	0.94	8.6	–	0.1
Cs_2SO_4	−0.89	14.4	–	0.1

[a] $C\phi^L = 2^{3/2}C^L$.

Table A7.9 Temperature derivatives of Pitzer coefficients for 3:1, 2:2, 3:2 and 4:2 electrolytes[a]

3:1 and 2:2 electrolytes[a]

	$10^3\beta^{(0)L}$	$10^2\beta^{(1)L}$	$10\beta^{(2)L}$	10^3C^L	Max m
$LaCl_3$	0.25	0.79	–	−0.10	3.6
$La(ClO_4)_3$	0.15	1.50	–	−0.19	2.1
$La(NO_3)_3$	0.17	1.09	–	−0.13	2.2
$Na_3Fe(CN)_6$	3.05	1.52	–	–	0.1
$K_3Fe(CN)_6$	−0.87	3.15	–	–	0.1
$K_4Fe(CN)_6$	4.74	3.92	–	–	0.2
$MgSO_4$	−0.69	1.53[b]	−2.53	0.13	2.0
$CaSO_4$	–	5.46[b]	−5.16	–	0.02
$CuSO_4$	−4.4	2.3[b]	−4.7	1.2	1.0
$ZnSO_4$	−3.6	2.3[b]	−3.3	0.9	1.0
$CdSO_4$	−2.7	1.7[b]	−5.2	0.6	1.0

[a] For 3:1 electrolytes $C^{\phi L} = 2\sqrt{3}C^L$; for 2:2 electrolytes $C^{\phi L} = 4C^L$.
[b] The parameter α_1 is 1.4 and $\alpha_2 = 12.0$ for these electrolytes; for all others, $\alpha_1 = 2.0$ and $\alpha_2 = 0$.

3:2 and 4:2 electrolytes[a]

	$\beta^{(0)L}$	$\beta^{(1)L}$	$\beta^{(2)L}$	Max m
$Ca_3(Fe(CN)_6)_2$	−0.0052	0.087	−2.13	0.04
$Ba_3(Fe(CN)_6)_2$	0.0008	0.065	−3.54	0.04
$La_2(SO_4)_3$	0.082	−0.202	−51.3	0.024
$Mg_2Fe(CN)_6$	0.016	0.041	−23.9	0.04
$Ca_2Fe(CN)_6$	0.0016	0.158	−7.47	0.04
$Sr_2Fe(CN)_6$	0.0052	0.118	−19.5	0.04

[a] $\alpha_1 = 2.0$; $\alpha_2 = 50$ throughout.

Table A7.10 Volumetric properties and the pressure derivatives of Pitzer coefficients.[a]

Parameter	NaCl	Na_2SO_4	$MgCl_2$	$MgSO_4$
$\bar{V}_2^\circ$ ($cm^3 \cdot mol^{-1}$)	16.68	11.48	14.40	−7.48
$10^5\beta^{(0)V}$ ($kg \cdot mol^{-1} \cdot bar^{-1}$)	1.255	4.466	1.843	5.137
$10^4\beta^{(1)V}$ ($kg \cdot mol^{-1} \cdot bar^{-1}$)	–	1.802	−0.846	1.319
$10^2\beta^{(2)V}$ ($kg \cdot mol^{-1} \cdot bar^{-1}$)	–	–	–	1.49
$10^6C^{\phi V}$ ($kg^2 \cdot mol^{-2} \cdot bar^{-1}$)	−1.376	−3.71	−1.948	–

[a] $C^{\phi V} = 2C^V$.

where

$$f^{\phi} = -A_{\phi} I^{1/2}/(1 + bI^{1/2})$$

$$B^{\phi}_{MX} = \beta^{(0)}_{MX} + \beta^{(1)}_{MX} \exp(-\alpha I^{1/2}).$$

In applying these equations to a range of electrolytes, it is found that a satisfactory fit can be obtained using the values $b = 1.2\ \text{kg}^{1/2}\cdot\text{mol}^{-1/2}$ and $\alpha = 2.0\ \text{kg}^{1/2}\cdot\text{mol}^{-1/2}$ for all electrolytes. The 2:2 salts (such as $MgSO_4$, $ZnSO_4$ ...) are an exception, presumably due to ion pairing. For 2:2 salts, an extra term must be included in B^{ϕ}_{MX} to give

$$B^{\phi}_{MX} = \beta^{(0)}_{MX} + \beta^{(1)}_{MX} \exp(-\alpha_1 I^{1/2}) + \beta^{(2)}_{MX} \exp(-\alpha_2 I^{1/2})$$

with $\alpha_1 = 1.4\ \text{kg}^{1/2}\cdot\text{mol}^{-1/2}$ and $\alpha_2 = 12\ \text{kg}^{1/2}\cdot\text{mol}^{-1/2}$. A_{ϕ} is the Debye–Hückel constant given in Table A7.1 and $\nu = \nu_+ + \nu_-$ is the total number of ions in the formula. Although these equations are not simple expressions, they do an exceptional job of fitting ϕ for a large number of electrolytes with only three parameters ($\beta^{(0)}$, $\beta^{(1)}$, and C^{ϕ}) that are specific to the electrolyte.[b] Furthermore, the equation reduces to the correct limiting law expression at low ionic strengths.

The above equations can be transformed through the Gibbs–Duhem equation to obtain a comparable set for $\ln \gamma_{\pm}$. The results are as follows:

$$\ln \gamma_{\pm} = |z_M z_X| f^{\gamma} + m(2\nu_M \nu_X/\nu) B^{\gamma}_{MX} + m^2 [2(\nu_M \nu_X)^{3/2}/\nu] C^{\gamma}_{MX}$$

where

$$f^{\gamma} = -A_{\phi}\left[I^{1/2}/(1 + bI^{1/2}) + \left(\frac{2}{b}\right)\ln(1 + bI^{1/2})\right]$$

$$B^{\gamma}_{MX} = B_{MX} + B^{\phi}_{MX}$$

$$C^{\gamma}_{MX} = \tfrac{3}{2} C^{\phi}_{MX}$$

with

$$B_{MX} = \beta^{(0)}_{MX} + \beta^{(1)}_{MX} g(\alpha_1 I^{1/2}) + \beta^{(2)}_{MX} g(\alpha_2 I^{1/2}),$$

[b] Four parameters are required for the 2:2 electrolytes.

where the $\beta^{(2)}_{MX}$ is included only for 2:2 electrolytes. The term $g(\alpha I^{(1/2)})$ is of the form

$$g(x) = 2[1 - (1 + x)\exp(-x)]/x^2$$

with

$$x = \alpha I^{1/2}.$$

The values of b and α are the same as were used earlier. That is, $\alpha_1 = 2.0\ \text{kg}^{1/2}\cdot\text{mol}^{-1/2}$ and $\alpha_2 = 0$ for all except the 2:2 electrolyte, where $\alpha_1 = 1.4\ \text{kg}^{1/2}\cdot\text{mol}^{-1/2}$ and $\alpha_2 = 12\ \text{kg}^{1/2}\cdot\text{mol}^{-1/2}$. Note that the same set of three (or four) parameters give the values for $\ln\gamma_\pm$, as well as ϕ.

Equations can be obtained for calculating ϕL, $\bar{L}_1$ $\bar{L}_2$, ϕC_p, $\bar{J}_1$, and $\bar{J}_2$ from Pitzer's equations for $\ln\gamma_\pm$ and ϕ by taking derivatives. For example, $\bar{L}_2$ and $\bar{J}_2$ are obtained from

$$\bar{L}_2 = -\nu RT^2\left(\frac{\partial \ln\gamma_\pm}{\partial T}\right)_p$$

$$\bar{J}_2 = \left(\frac{\partial \bar{L}_2}{\partial T}\right)_p.$$

The resulting equations for ϕL and ϕC_p are

$$\phi L = \nu\,|\,z_M z_X\,|\left(\frac{A_L}{2b}\right)\ln(1 + bI^{1/2})$$

$$- 2\nu_M\nu_X RT^2[mB^L_{MX} + m^2(\nu_M z_M)C^L_{MX}]$$

where

$$B^L_{MX} = \left(\frac{\partial B_{MX}}{\partial T}\right)_{p,I}$$

$$= \beta^{(0)L} + \beta^{(1)L}g(\alpha_1 I^{1/2}) + \beta^{(2)L}g(\alpha_2 I^{1/2})$$

with

$$\beta^{(i)L} = \left(\frac{\partial \beta^{(i)}}{\partial T}\right)_p, \qquad i = 0, 1, 2$$

and

$$C^L_{MX} = \frac{|z_M z_X|^{1/2}}{2}\left(\frac{\partial C^{\phi}_{MX}}{\partial T}\right)_p.$$

In a similar manner

$$\phi C_p - \bar{C}^{\circ}_{p,2} = \left(\frac{\partial \phi L}{\partial T}\right)_{p,I}$$

$$= \nu |z_M z_X| \left(\frac{A_J}{2b}\right) \ln(1 + bI^{1/2})$$

$$- 2\nu_M \nu_X RT^2 [mB^J_{MX} + m^2(\nu_M z_M) C^J_{MX}]$$

where

$$B^J_{MX} = \left(\frac{\partial^2 B_{MX}}{\partial T^2}\right)_{p,I} + \frac{2}{T}\left(\frac{\partial B_{MX}}{\partial T}\right)_{p,I}$$

$$C^J_{MX} = \left(\frac{\partial^2 C_{MX}}{\partial T^2}\right)_p + \frac{2}{T}\left(\frac{\partial C_{MX}}{\partial T}\right)_p.$$

The relative partial molar enthalpy and relative partial molar heat capacity are obtained from

$$\frac{\bar{L}_1}{RT} = M_w \left\{ -\frac{A_H}{2RT}\left[\frac{I^{3/2}}{1 + bI^{1/2}}\right] \right.$$

$$\left. + 2\nu_M \nu_X Tm^2 [\beta^{(0)L}_{MX} + \beta^{(1)L}_{MX} \exp(-\alpha I^{1/2}) + 2\nu_M z_M m C^L_{MX}] \right\},$$

$$\frac{\bar{L}_2}{RT} = \frac{\nu \mid z_M z_X \mid A_H}{4RT}\left[\frac{I^{1/2}}{1+bI^{1/2}} + \left(\frac{2}{b}\right)\ln(1+bI^{1/2})\right]$$

$$-2\nu_M\nu_X Tm\left[2\beta_{MX}^{(0)L} + \frac{2\beta_{MX}^{(1)L}}{\alpha^2 I}\right.$$

$$\times\left\{1-\left(1+\alpha I^{1/2}-\frac{\alpha^2 I}{2}\right)\exp(-\alpha I^{1/2})\right\}$$

$$\left.+3\nu_M z_M m C_{MX}^{L}\right],$$

$$\frac{\bar{J}_1}{R} = M_w\left\{-\frac{A_J}{2R}\left[\frac{I^{3/2}}{1+bI^{1/2}}\right]\right.$$

$$\left.+2\nu_M\nu_X T^2 m^2[\beta_{MX}^{(0)J}+\beta_{MX}^{(1)J}\exp(-\alpha I^{1/2})+2\nu_M z_M m C_{MX}^{J}]\right\},$$

and

$$\frac{\bar{J}_2}{R} = \frac{\nu \mid z_M z_X \mid A_J}{4R}\left[\frac{I^{1/2}}{1+bI^{1/2}} + \frac{2}{b}\ln(1+bI^{1/2})\right]$$

$$-2\nu_M\nu_X T^2 m\left[2\beta_{MX}^{(0)J} + \frac{2\beta_{MX}^{(1)J}}{\alpha^2 I}\right.$$

$$\times\left\{1-\left(1+\alpha I^{1/2}-\frac{\alpha^2 I}{2}\right)\exp(-\alpha I^{1/2})\right\}$$

$$\left.+3\nu_M z_M m C_{MX}^{J}\right].$$

Equations for ϕV, the apparent molar volume, are as follows:

$$\phi V = \bar{V}_2^\circ + \nu \mid z_M z_X \mid \left(\frac{A_v}{2b}\right) \ln(1 + bI^{1/2})$$

$$+ 2\nu_M \nu_X RT[mB^v_{MX} + m^2(\nu_m z_m)C^v_{MX}]$$

where

$$B^v_{MX} = \beta^{(0)v} + \beta^{(1)v} g(\alpha_1 I^{1/2}) + \beta^{(2)v} g(\alpha_2 I^{1/2})$$

$$\beta^{(i)v} = \left(\frac{\partial \beta^{(i)}}{\partial p}\right)_T, \qquad i = 0, 1, 2$$

$$C^v_{MX} = \frac{\mid z_M z_X \mid^{1/2}}{2} \left(\frac{\partial C^\phi_{MX}}{\partial p}\right)_T.$$

Again, the coefficients are the same as defined earlier, with A_H, A_J, and A_v as the Debye–Hückel parameters, and T as the temperature and M_w as the molecular weight of the solvent (water) in kg·mol^{-1}. Values for the thermal coefficients for a number of electrolytes are given in Tables A7.8 to A7.10.

Index

acetone
  thermodynamic properties
    acetonitrile mixture 287
    dimethylsulfoxide mixture 287
  in trichoromethane mixture 118
acetonitrile
  phase equilibria
    dimethylbenzene mixture 137–8
    tetrachoromethane mixture 118–19
    water mixture 140–2
  thermodynamic properties
    acetone mixture 287
    cyclohexane mixture 291–2
    dichoromethane mixture 284–5
    nitromethane mixture 287
    tetrachoromethane mixture 283, 285
    trichoromethane mixture 283–5
activity 13–20
  in electrolyte solutions 317–19
  effect of pressure on 14
  effect of temperature on 14
adenine in DNA 247, 248, 249
adenosine diphosphate (ADP) 216, 217–21
adenosine monophosphate (AMP) 227
adenosine triphosphate (ATP)
  free energy of hydrolysis 227–8
  in glycolysis 217–21
  hydrolysis of 225–6
  in metabolism 216
alkane, thermodynamic properties
  alkane mixture 280
  cyclohexane mixture 281
alkylamines 341
aluminium, superconductor transition in 100
ammonia, synthesis of 161–74
anabolic proccesses 214–15
antiparallel structure of oligonucleotides 249
Archer, D. G. 325–6
atmospheric pressure, effects of 47–8
azeotropy in vapor + liquid equilibria 118–19

barometric formula 48
base pairs in DNA 248
base-stacking oligonucleotides 249
Bence–Jones proteins 242
benzene, phase equilibria of
  dimethylbenzene mixture 135–7
  hexafluorbenzene mixture 119–20, 153–4
  mesitylene mixture 144–5
binary fluid critical points of phase transitions 104
biological processes 213–69
  metabolism and work 214–30
    and phosphate compounds 226–30
biopolymer stability 230–67
  of proteins 239–46
    van't Hoff enthalpy 240–6
  synthetic oligonucleotides 246–50
    database for melting parameters 261–3
      ligand binding of cisplatin 263–7
    duplex melting 250–7
    energetics of structural features 257–61
      wobble base pairs 260–1
    equilibria between two oligonucleotide conformations 255–7
  two-state model 233–9
    calorimetric methods 237–9
    optical methods 235–6
Boltzmann constant 18
Boltzmann distribution law 31
Bradshaw, J. S. 194
ß-brass, phase transition 86–8
Breslauer, K. 247, 253, 259, 261, 262–3, 265–7
Brewer, L. 315, 316
Brewer tabulations on electrolyte solutions 315–16
Brönsted, J. N. 313
Bundy, F. P. 178
Burchfield, T. E. 349
butyl alcohol + water mixture, phase equilibria 123, 125

calcite, effect of temperature on solubility of 181–4
calcium chloride
  activity coefficients 312, 315
  osmotic coefficients 318–19

calorimetric methods in two-state model of biopolymer stability 237–9
van't Hoff enthalpy 240–6
carbon dioxide
heat capacity 87
phase diagram 80
centrifugal fields, effects of 51–3
density-gradient centrifugation 52–3
cesium chloride
activity coefficients 315
concentration gradient of 52–3
first order phase transition 82
Gibbs free energy 83
phase diagram 84
chemical composition
gravitational fields, effects of 48–51
chemical equilibrium 24–9
equilibrium constant 25
alternate forms 25–7
effects of pressure on 27
effects of temperature on 27–8
chemical potential
and surface effects 15
and activity 13
and phase equilibria 7
and chemical equilibrium 25
Christensen, J. J. 278
cisplatin, ligand binding of 263–7
Clapeyron equation 8, 9
Clausius–Clapeyron equation 8–9
coarse-graining transformations in phase transitions 110
concentrated electrolyte solutions, thermodynamics of 312–13
conductor-superconductor transitions for pure substances 96–102
pressure, effect of 100–2
continuous transitions for pure substances 85–102
correlation length in phase transitions 108
critical micelle concentration (CMC) of surfactant solutions 341–3, 345, 348, 349
crown ethers 194–5, 197
curvature of surfaces, effect of 59–62
cycloheptane, thermodynamic properties 275, 277–8
cyclohexane
phase equilibria of
methylcyclohexane mixture 116–17
hexafluorobenzene mixture 128–9
methanol mixture 139–40
thermodynamic properties 277–8
acetonitrile mixture 291–2
n-alkane mixtures 281
2,3-dimethylbutane mixture 275–6
1,4-dioxane mixture 285–6
hexane mixture 278–80, 281–2
methanol mixture 296
methylcyclohexane mixture 275–6
oxane mixture 285–6
cyclooctane, thermodynamic properties 275, 277–8
cyclopentane, thermodynamic properties 275, 277–8

Debye energy content, internal rotation, thermodynamic properties 405
Debye entropy, internal rotation, thermodynamic properties 407
Debye heat capacity
equation 35–6
Debye–Hückel parameters of electrolyte solutions 311, 410
Debye–Hückel theory
and crown ethers 196
and strong electrolyte solutions 16–20
n-decylpyridinium chloride, as a surfactant 342–3
denaturation of proteins 231–2
density-gradient centrifugation 52–3
deoxyribonucleic acid (DNA), thermodynamic and spectroscopic studies 246–50
duplex melting 250–7, 258
equilibria between two conformations 255–7
diamond, synthesis of 174–80
diatomic molecules
inertia, moments of 395
vibrational frequencies of 397
1,4-dichlorobutane, thermodynamic properties 285
1,2-dichloroethane, thermodynamic properties 285
differential relationships from Gibbs equations 4–7
differential scanning calorimetric (DSC) techniques in biopolymer stability 237, 242–3
in duplex melting 250–1
dimethylbenzene, phase equilibria of
acetonitrile mixture 137–8
benzene mixture 135–7
tetrachloromethane mixture 144, 146
1,4-dioxane, thermodynamic properties
of cyclohexane mixture 285–6
of tetrachloromethane mixture 288, 289
DNA, concentration gradient of 52–3
n-dodecylpyridinium chloride, as a surfactant 242–3

electrochemical cells 29–30
electrolyte solutions, thermodynamics of 309–58
  Pitzer coefficients for 408–17
  concentrated solutions 312–13
  Debye–Hückel parameters 311
  generalized equations 325–30
  Guggenheim's equations 313–14
  Guggenheim's constants 314
  ion association 331–40
    from flow calorimetry 337–40
    at high temperatures 335–7
  Pitzer and Brewer tabulations 315–16
  Pitzer equations 316–24
    at elevated temperatures 324–5
    osmotic and activity coefficient 317–19
    thermal properties 319–23
    volumetric properties 324
electronic energy levels 388
  and unpaired electrons 399
endergonic proccesses 215
enthalpy 3
  of formation 29
  Debye–Hückel parameters for electrolyte solutions 311, 410
  change in diamond synthesis 176
  differential relationships 5
  duplex melting, of DNA 262–3
  excess molar *see* excess molar enthalpy
  of formation, selected substances 361–8
  of fusion and vaporization, selected compounds 375–7
  change in Haber cycle 163
  of metal oxides
  of formation from the oxides 187
  of molten solution 191–2
    and silica systems 189–91
  in surfaces of mixtures 64–5, 66
  of ternary oxides 187–8
  van't Hoff *see* van't Hoff enthalpy
entropy 2
  of cesium chloride 83
  change in diamond synthesis 176
  differential relationships 5
  of formation in Haber cycle 163
  selected ions 374–5
  selected substances 369–73
  of formation from the oxides 188–9
equilibrium constant 25
  alternate forms 25–7
  calcite, solubility of 183
  effect of pressure on 27
  effect of temperature on 27–8
ethanol
  ethane mixture, thermodynamic properties 299–300
  surface concentration of 71
  surface tension of 70–1
Euler's theorem 68
excess enthalpy of transition 78
excess molar enthalpy
  acetone + acetonitrile mixture 287
  cyclohexane + acetonitrile mixture 291–2
  cyclohexane + 2,3-dimethylbutane mixture 275–6
  cyclohexane + 1,4-dioxane mixture 285–6
  cyclohexane + hexane mixture 278–80, 281–2
  cyclohexane + methylcyclohexane mixture 275–6
  cyclohexane + oxane mixture 285–6
  dimethylsulfoxide + acetone mixture 287
  ethanol + ethane mixture 299–300
  nitrogen and oxygen mixture 275–6
  nitromethane + acetonitrile mixture 287
excess thermodynamic properties of nonelectrolyte solutions 272–301
  and (fluid + fluid) phase equilibrium 299–301
  ideal solutions 272–3
  and (liquid + liquid) phase equilibrium 291–9
  real solutions 278–91
    complex formations 288–9
    hydrogen-bonded systems 289–91
    nonpolar + nonpolar mixtures 278–83
    polar + nonpolar mixtures 283–7
    polar + polar mixtures 287
  regular solutions 274–8
exergonic proccesses 215

fermentation and metabolism 215–16
first order transitions for pure substances 76–85
fixed nitrogen 162
flow calorimetry, ion association from 337–40
fluid + fluid equilibria, phase transitions for 125–34
  in nonelectrolyte solutions 299–301
  retrograde condensation 128–30
  type I 126–30
  type II 130–1
  type III 131–3
  type IV 133–4
  type V 133–4

fugacity 10–13
  and Henry's law 12–13
  of ideal solution 13
  effect of pressure on 10–12
  and Raoult's law 12–13
  effect of temperature on 10–12

gas + gas immiscibility 128
Gast, A. P. 57
Gaw, W. J. 119
geological systems 181–93
  calcite, effect of temperature on solubility of 181–4
  ternary oxides, energetics of 184–93
    formation of 185–9
      enthalpies of formation 187–8
      entropies of formation 188–9
    metal oxides in molten solution, enthalpies of mixing 191–2
    metal oxide + silica systems, enthalpies of mixing 189–91
    orthosilicates, enthalpies of formation 189
Giauque, W. F. 53
Gibbs equations 3–4
Gibbs free energy 3
  of formation 29
  differential relationships 5
  of formation 29
Gibbs free energy change
  in Haber cycle 163, 165
  in magnetic system 108
  and metabolism 214–15, 227–9
  in nonelectrolyte solutions 272
  of formation of selected ions 374–5
  of formation of selected substances 369–73
  in surfaces of mixtures 64–5
  of surfactants 346
Gibbs phase rule
  for first order transitions 77
  in vapor + liquid equilibria 116
Gibbs–Duhem equation 6–7, 68, 292
glucose
  phosphorylation of 217–18
  in respiration 215
glucose-6-phosphate, isomerization of 218–19, 228
glyceraldehyde-3-phosphate, oxidative phosphorylation of 219–20
glycolysis 217–21
  phosphorylation of glucose 217–18
  isomerization of glucose-6-phosphate 218–19
  phosphorylation of fructose-6-phosphate 219
  cleavage of fructose-1, 6-diphosphate 219–20
  oxidative phosphorylation of glyceraldehyde-3-phosphate 219–20
Goates, J. R. 117
Gokcen, N. A. 85
gold + silver system, phase equilibria 151–2
gravitational fields, effects of 47–51
  on chemical composition 48–51
  height and atmospheric pressure 47–8
Guggenheim, E. A. 314
Guggenheim's equations for electrolyte solutions 313–14

Haber, F. 169–72
Haber cycle 161–74
Hall, H. T. 175
hard ligands, complexation of 205–6
hard metal ions, complexation of 204
heat capacity
  for cesium chloride 83
  coefficients, selected substances 377–9
  Debye–Hückel parameters for electrolyte solutions 311, 410
  in first order phase transition 79
  of selected ions 374–5
  of selected substances 369–73
height, effects of 47–8
helium-3 phase properties 93–5
  molar heat capacity 95
helium-4 normal-superfluid transition 90–3
  heat capacity 92
Helmholtz free energy 3
  differential relationships 5
  and surface tension 55
  and surfaces of mixtures 64–5
Henry's law 12–13
hexafluorobenzene, phase equilibria of
  benzene mixture, 119–20, 153–4
  cyclohexane mixture 128–9
hexane
  cyclohexane mixture, thermodynamic properties 278–80, 281–2
  decane mixture, thermodynamic properties 280
  methanol mixture, phase equilibria 120, 123, 125
Hildebrand, J. H. 274
Huffman, H. 229
hydrogen-bonded solutions, thermodynamic properties of 289–91
hypercritical pressure in liquid + liquid equilibria 123
hypercritical temperature in liquid + liquid equilibria 123

ideal enthalpy of vaporization 11
ideal gas
  partition function for 390–2
    thermodynamic properties of 389–90
  statistical thermodynamics of 32
    internal rotation 32–5
ideal solubility 22
ideal solutions
  fugacity in 13
  nonelectrolyte, thermodynamic properties of 272–3
  thermodynamics of 21–2
internal energy 2
  differential relationships 5
  in surfaces of mixtures 64–5, 66
ion association in electrolyte solutions 331–40
  from flow calorimetry 337–40
  at high temperatures 335–7
isothermal latent heat 78
Izatt, R. M. 194, 195, 197, 278

Kelvin, Lord W. 60

lanthanum chloride
  activity coefficients 312
  osmotic coefficients 318–19
Lewis, G. N. 12, 229, 316
ligand binding of cisplatin 263–7
linear molecules, moments of inertia 396
Lipmann, F. 227, 229–30
liquid + gas critical phase transition 85, 104
liquid + liquid equilibria, phase transitions for 120–5
  in nonelectrolyte solutions 291–9
  and vapor + liquid equilibria 123–5
liquidus line in solid + liquid equilibria 151
lower critical end point (LCEP) 294–5
lower critical solution pressure (LCSP)
  and phase equilibria 121
  and thermodynamic properties 292
lower critical solution temperature (LCST)
  and phase equilibria 121, 133
  and thermodynamic properties 292
lysozyme
  calorimetric enthalpy 242
  free energy of denaturation 246

macrocyclic ligands, complexation of 193–207
  hard and soft ligands 205–6
  hard metal ions 204
  soft ion+soft ligand complexes 206–7
  soft metal ions 205
  thermodynamic properties 197–204
    heteroatoms other than oxygen 200–4
    oxygen macrocycles 197–200
magnesium sulfate, ion association of 335
magnetic effects 89–90
Marshall–Frank equation 337
mass action model of surfactant solutions 349–53
Maxwell relations 65
McGlashan, M. L. 129–30
mean field theories of phase transitions 106
Meissner effect 96
Mesmer, R. E. 335, 340
metabolism and work 214–30
  and phosphate compounds 226–30
metal oxides, enthalpies of
  in molten solution 191–2
  and silica systems 189–91
methane
  heat capacity 90
  rotational disorder phase transition 88
methanol
  cyclohexane mixture, thermodynamic properties 296
  phase equilibria of
    cyclohexane mixture 139–40
    hexane mixture 120, 123, 125
    water mixture 117–18, 148–50
mixtures 20–4
  nonelectrolyte 20–3
    excess functions 22–3
    ideal solutions 21
    see also nonelectrolyte solutions
  phase transitions for 115–16
    fluid + fluid equilibria 125–34
      retrograde condensation 128–30
      type I 126–30
      type II 130–1
      type III 131–3
      type IV 133–4
      type V 133–4
    liquid + liquid equilibria 120–5
      and vapor + liquid equilibria 123–5
    solid + liquid equilibria 134–55
      liquid + liquid equilibria with 138–42
      quadruple point 140
      simple eutectic systems 137–8
      solid + solid with solid + liquid equilibria 142–4
      complete miscibility 151
      congruently melting compounds 144–7
      in congruently melting compounds 147–50
      curve for dissociable solute 153–5

mixtures (*continued*)
metastable equilibrium 144
solid solution formation 150–3
variable composition 152
vapor + liquid equilibria 116–20
relative apparent molar properties 24
relative partial molar thermal properties 23
surfaces, thermodynamics of 62–71
properties of 64–71
[illegible]
energetics of structural features 257–61
wobble base pairs 260–1
equilibria between two oligonucleotide conformations 255–7
optical methods in two-state model of biopolymer stability 235–6
order parameter in phase transitions 87
order-disorder phase transition 86–90
critical points 104
[illegible]
muscle cells, and metabolism 222
contraction, process 224–5

Navrotsky, A. 185, 192
Nernst, W. 166–71
Nernst equation in electrochemical cells 30
nitric acid, activity coefficient 332
nitrogen
fixed 162
and oxygen, enthalpy and Gibbs free energy for 275–6
nonelectrolyte mixtures 20–3, 271–308
excess functions 22–3
ideal solutions 21
and (fluid + fluid) phase equilibrium 299–301
ideal solutions 272–3
and (liquid + liquid) phase equilibrium 291–9
real solutions 278–91
complex formation 288–9
[illegible]
osmotic coefficients, Debye–Hückel parameters for electrolyte solutions 311, 410
Ott, J. B. 117
oxidative phosphorylation of glyceraldehyde-3-phosphate 219–20
oxygen + nitrogen mixture, enthalpy and Gibbs free energy for 275–6

papain proteins 242
partition function 31–2, 388–9
for ideal gas 390–2
and ideal gas thermodynamics 389–90
Patterson, D. 285, 286
Pedersen, C. J. 193, 194
phase equilibria relationships 7–9
phase transitions
for mixtures 115–16
fluid + fluid equilibria 125–34
retrograde condensation 128–30
type I 126–30
[illegible]

continuous 85–102
first order 76–85
helium-3 phase properties 93–5
helium-4 normal-superfluid transition 90–3
liquid + gas critical transition 85, 104
magnetic effects 89–90
order-disorder transition 86–90
position disorder transition 86–8
rotational disorder transition 88–9
second order 76–80
theories of 102–11
Pitzer, K. S. 35, 311, 315, 316, 324, 325
Pitzer and Brewer tabulations on electrolyte solutions 315–16
Pitzer equations for electrolyte solutions 316–24
coefficients for 409–27
at elevated temperatures 324–5
osmotic efficiency and activity 317–19
thermal properties 319–23
volumetric properties 324
polar + nonpolar mixtures, thermodynamic properties of 283–7
polar + polar mixtures, thermodynamic properties of 287
polyatomic molecules, vibrational frequencies 398
position disorder phase transition 86–8
potassium chloride
activity coefficients 312, 315
osmotic coefficients 318–19
power-law relationships in phase transition 102–3, 105
pressure 2
effect on activity 14
effect on equilibrium in ideal solution 21–2
effect on fugacity 10–12
Privalov, P. L. 231, 239–40, 242–6
proteins, stability of 239–46
denaturation 231–2
van't Hoff enthalpy 240–6
pseudo-phase model of surfactant solutions 343–9
pure substances, phase transitions of 75–114
conductor-superconductor transition 96–102
pressure, effect of 100–2
continuous 85–102
first order 76–85
helium-3 phase properties 93–5
helium-4 normal-superfluid transition 90–3
liquid + gas critical transition 85, 104
magnetic effects 89–90
modern theories of 102–11
order-disorder transition 86–90
position disorder transition 86–8
rotational disorder transition 88–9
second order 76–80

Raman spectroscopy on nitric acid 332–3
Randall, M. 12, 316
Raoult's law 12–13
real solutions, thermodynamic properties of 278–91
complex formation 288–9
hydrogen-bonded systems 289–91
nonpolar + nonpolar mixtures 278–83
polar + nonpolar mixtures 283–7
polar + polar mixtures 287
regular solutions, thermodynamic properties 274–8
relative apparent molar properties 24
relative partial molar enthalpy 14
relative partial molar thermal properties 23
respiration and metabolism 215
ribonuclease
calorimetric enthalpy 242, 245
free energy of denaturation 246
ribonucleic acid (RNA) 247
rotation
constants, selected molecules 395–6
in ideal gas 33, 393–4
internal, thermodynamic properties 401–7
nonrigid corrections 399–400
rotational disorder phase transition 88–9
rotational energy levels 384–6
internal 387
rubber band, thermodynamics of 43–6

Schneider, G. M. 124, 141
Scott, R. L. 126–7, 274
second order phase transition 76–80
self complementary oligonucleotides 248, 251, 253
Shedlovsky equation for electrolyte solutions 335
silver, phase equilibria of
with copper 150–1
with gold 151–2
sodium chloride
activity coefficients 326–8, 339
ion association 335–6
sodium dodecylsulfate, CMC for 348
soft metal ions, complexation of 205
and hard ligands 205–6
and soft ligand complexes 206–7

solid + liquid equilibria, phase transitions for 134–55
  complete miscibility 151
  congruently melting compounds 144–50
  curve for dissociable solute 153–5
  liquid + liquid equilibria with 138–42
  metastable equilibrium 144
  quadruple point 140
  simple eutectic systems 137–8
  solid solution formation 150–3
  with solid + solid equilibria 142–4
  variable composition 152
solid + solid equilibria 142–4
solidus line in solid + liquid equilibria 151
standard reduction potentials, selected substances 380–1
standard states 13–20
  choice of 14–16
  for strong electrolyte solutes 16
statistical thermodynamics 31–6
  atomic and molecular energy levels 383–8
    electronic energy levels 388
    rotational energy levels 384–6
      internal 387
    transitional energy levels 383–4
    vibrational energy levels 386–7
  Boltzmann distribution law 31
  energy levels, calculations from 392–407
  of ideal gas 32
    internal rotation 32–5
  partition function 31–2, 388–9
    for ideal gas 390–2
    and ideal gas thermodynamics 389–90
Streett, W. B. 126, 131–2, 134
Strong, H. M. 178, 179
strong electrolyte solutes 16
strong electrolyte solutions 17
sublimation 11
sulfuric acid, ion association from flow calorimetry 337–8
superconductor transitions 96–102
  for selected substances 101
superfluid transitions 90–3
  critical points 104
surface concentration of mixtures 62–4
surface energy of mixtures 68
surface enthalpy 56, 68
surface entropy 56, 69
surface heat capacity 57
surface tension 55, 65–6, 69
surfaces, thermodynamics of 53–71
  curvature, effect of 59–62
  mixtures 62–71
    properties of 64–71
    surface concentration 62–4
  one-component system 54–9
surfactant solutions, thermodynamics of 341–53
  theoretical descriptions 343–53
    mass action model 349–53
    pseudo-phase model 343–9
  thermodynamic properties of 341–3
  database for melting parameters 261–3
    enthalpy 262–3
    ligand binding of cisplatin 263–7
  duplex melting 250–7
  energetics of structural features 257–61
    wobble base pairs 260–1
  equilibria between two oligonucleotide conformations 255–7

temperature 2
  effect on activity 14
  effect on equilibrium in ideal solution 21–2
  effect on fugacity 10–12
  of fusion and vaporization, selected compounds 375–7
ternary oxides, energetics of 184–93
  acid/base scales 186
  formation of 185–9
    enthalpies of 187–8
    entropies of 188–9
  metal oxides in molten solution, enthalpies of 191–2
  metal oxide + silica systems, enthalpies of mixing 189–91
  orthosilicates, enthalpies of formation 189
tetrachloromethane
  phase equilibria
    acetonitrile mixture 118–19
    dimethylbenzene mixture 144, 146
    octane mixture 142–3
    pyridine mixture 152–3
  thermodynamic properties
    acetonitrile mixture 283, 285
    N,N-dimethylformamide mixture 288, 289
    1,4-dioxane mixture 288, 289
thermal properties of electrolyte solutions 319–23
thermodynamic functions, selected substances 361–8
thermodynamic relationships 2–7
three-carbon phosphates 219–20
tin, phase diagram for 81
translational energy levels 383–4
translation in ideal gas 33, 393

trichoromethane
  phase equilibria of
    acetone mixture 118
    dimethoxyethane mixture 146–7
    pyridine mixture 117–18
  thermodynamic properties
    acetonitrile mixture 283–5
trioxanonane, thermodynamic properties 285
tropomyosin, and metabolism 224
trypsin, free energy of denaturation 246
two-state model of biopolymer stability 233–9
  calorimetric methods 237–9
  optical methods 235–6

ultraviolet absorption of biopolymers
  van't Hoff enthalpy 235–6
universality classes of phase transitions 106
upper critical end point (UCEP)
  and phase equilibria 121, 124
  and thermodynamic properties 292, 294–5
upper critical solution temperature (UCST)
  and phase equilibria 121, 123, 133, 140
  in thermodynamic properties 292

van Konynenburg, P. H. 126–7
van't Hoff enthalpy 234, 250
  calorimetrically obtained 240–6
  cisplatin, ligand binding of 264
  in DNA 253–4, 259, 260
  and optical methods 235–5
  in proteins 240–6
vapor fugacity
  of mixtures 69–70
  surface curvature and 61
vapor + liquid equilibria, phase transitions for 116–20
vibration in ideal gas 34, 394
vibrational energy levels 386–7
vibrational frequencies, selected molecules 397–8
volume coefficients, Debye–Hückel parameters for electrolyte solutions 311, 410
volumetric properties of electrolyte solutions 324
vortex state in superconductor transitions 97

water
  phase diagram 84–5
  phase equilibria of
    acetonitrile mixture 140–2
    butyl alcohol mixture 123, 125
    $(C_3H_7)_2NH$ mixture 121–2
    methanol mixture 117–18, 148–50
    tetrahydrofuran mixture 121–2
  triethylamine mixture, thermodynamic properties 297
Watson–Crick base pairs in DNA 260, 262
Wilhelm, E. 286
wobble base pairs in synthetic oligonucleotides 260–1
Woolley, E. M. 326, 342, 34